



*atmosphere*

# Ambient Air Quality in the Czech Republic

---

Edited by  
Iva Hůnová

Printed Edition of the Special Issue Published in *Atmosphere*

# **Ambient Air Quality in the Czech Republic**



# Ambient Air Quality in the Czech Republic

Editor

**Iva Hůnová**

MDPI • Basel • Beijing • Wuhan • Barcelona • Belgrade • Manchester • Tokyo • Cluj • Tianjin



*Editor*

Iva Hůnová  
Ambient Air Quality Department  
Czech Hydrometeorological Institute  
Prague  
Czech Republic

*Editorial Office*

MDPI  
St. Alban-Anlage 66  
4052 Basel, Switzerland

This is a reprint of articles from the Special Issue published online in the open access journal *Atmosphere* (ISSN 2073-4433) (available at: [www.mdpi.com/journal/atmosphere/special\\_issues/Air\\_CS](http://www.mdpi.com/journal/atmosphere/special_issues/Air_CS)).

For citation purposes, cite each article independently as indicated on the article page online and as indicated below:

|  |
|--|
| LastName, A.A.; LastName, B.B.; LastName, C.C. Article Title. <i>Journal Name</i> <b>Year</b> , <i>Volume Number</i> , Page Range. |
|--|

**ISBN 978-3-0365-1762-9 (Hbk)**

**ISBN 978-3-0365-1761-2 (PDF)**

© 2021 by the authors. Articles in this book are Open Access and distributed under the Creative Commons Attribution (CC BY) license, which allows users to download, copy and build upon published articles, as long as the author and publisher are properly credited, which ensures maximum dissemination and a wider impact of our publications.

The book as a whole is distributed by MDPI under the terms and conditions of the Creative Commons license CC BY-NC-ND.

# Contents

|   |     |
|---|-----|
| <b>About the Editor</b> . . . . .   | vii |
| <b>Iva Hůnová</b><br>Ambient Air Quality in the Czech Republic<br>Reprinted from: <i>Atmosphere</i> <b>2021</b> , 12, 770, doi:10.3390/atmos12060770 . . . . .  | 1   |
| <b>Iva Hůnová</b><br>Ambient Air Quality in the Czech Republic: Past and Present<br>Reprinted from: <i>Atmosphere</i> <b>2020</b> , 11, 214, doi:10.3390/atmos11020214 . . . . .  | 5   |
| <b>Vladimíra Volná and Daniel Hladký</b><br>Detailed Assessment of the Effects of Meteorological Conditions on PM <sub>10</sub> Concentrations in the<br>Northeastern Part of the Czech Republic<br>Reprinted from: <i>Atmosphere</i> <b>2020</b> , 11, 497, doi:10.3390/atmos11050497 . . . . .  | 31  |
| <b>Radim Seibert, Irina Nikolova, Vladimíra Volná, Blanka Krejčí and Daniel Hladký</b><br>Air Pollution Sources' Contribution to PM <sub>2.5</sub> Concentration in the Northeastern Part of the<br>Czech Republic<br>Reprinted from: <i>Atmosphere</i> <b>2020</b> , 11, 522, doi:10.3390/atmos11050522 . . . . .  | 53  |
| <b>Irena Pavlíková, Daniel Hladký, Oldřich Motyka, Konstantin N. Vergel, Ludmila P.<br/>Strelkova and Margarita S. Shvetsova</b><br>Characterization of PM <sub>10</sub> Sampled on the Top of a Former Mining Tower by the High-Volume<br>Wind Direction-Dependent Sampler Using INNA<br>Reprinted from: <i>Atmosphere</i> <b>2020</b> , 12, 29, doi:10.3390/atmos12010029 . . . . .   | 81  |
| <b>Jiří Pospisil, Jiří Huzlík, Roman Licbinský and Michal Spiláček</b><br>Dispersion Characteristics of PM <sub>10</sub> Particles Identified by Numerical Simulation in the Vicinity<br>of Roads Passing through Various Types of Urban Areas<br>Reprinted from: <i>Atmosphere</i> <b>2020</b> , 11, 454, doi:10.3390/atmos11050454 . . . . .  | 101 |
| <b>Jiří Neubauer, Jaroslav Michálek, Karel Šilinger and Petr Firbas</b><br>Impacts of Built-Up Area Geometry on PM <sub>10</sub> Levels: A Case Study in Brno, Czech Republic<br>Reprinted from: <i>Atmosphere</i> <b>2020</b> , 11, 1042, doi:10.3390/atmos11101042 . . . . .  | 117 |
| <b>Jana Ďoubalová, Peter Huszár, Kryštof Eben, Nina Benešová, Michal Belda, Ondřej Vlček,<br/>Jan Karlický, Jan Geletič and Tomáš Halenka</b><br>High Resolution Air Quality Forecasting over Prague within the URBI PRAGENSI Project:<br>Model Performance during the Winter Period and the Effect of Urban Parameterization on PM<br>Reprinted from: <i>Atmosphere</i> <b>2020</b> , 11, 625, doi:10.3390/atmos11060625 . . . . . | 137 |
| <b>Michal Vojtisek-Lom, Jonáš Jirků and Martin Pechout</b><br>Real-World Exhaust Emissions of Diesel Locomotives and Motorized Railcars during Scheduled<br>Passenger Train Runs on Czech Railroads<br>Reprinted from: <i>Atmosphere</i> <b>2020</b> , 11, 582, doi:10.3390/atmos11060582 . . . . .   | 161 |
| <b>Pavel Mikuška, Martin Vojtěšek, Kamil Křůmal, Martina Mikušková-Čampulová, Jaroslav<br/>Michálek and Zbyněk Večeřa</b><br>Characterization and Source Identification of Elements and Water-Soluble Ions in<br>Submicrometre Aerosols in Brno and Šlapanice (Czech Republic)<br>Reprinted from: <i>Atmosphere</i> <b>2020</b> , 11, 688, doi:10.3390/atmos11070688 . . . . .  | 187 |

|   |            |
|---|------------|
| <b>Jáchym Brzezina, Klaudia Köbölová and Vladimír Adamec</b><br>Nanoparticle Number Concentration in the Air in Relation to the Time of the Year and Time of the Day<br>Reprinted from: <i>Atmosphere</i> <b>2020</b> , <i>11</i> , 523, doi:10.3390/atmos11050523 . . . . .  | <b>211</b> |
| <b>Markéta Schreiberová, Leona Vlasáková, Ondřej Vlček, Jana Šmejdiřová, Jan Horálek and Johannes Bieser</b><br>Benzo[a]pyrene in the Ambient Air in the Czech Republic: Emission Sources, Current and Long-Term Monitoring Analysis and Human Exposure<br>Reprinted from: <i>Atmosphere</i> <b>2020</b> , <i>11</i> , 955, doi:10.3390/atmos11090955 . . . . .         | <b>225</b> |
| <b>Michal Vojtisek-Lom, Miroslav Suta, Jitka Sikorova and Radim J. Sram</b><br>High NO <sub>2</sub> Concentrations Measured by Passive Samplers in Czech Cities: Unresolved Aftermath of Dieselgate?<br>Reprinted from: <i>Atmosphere</i> <b>2021</b> , <i>12</i> , 649, doi:10.3390/atmos12050649 . . . . .  | <b>255</b> |
| <b>Petra Bauerová, Adriana Šindelářová, Štěpán Rychlík, Zbyněk Novák and Josef Keder</b><br>Low-Cost Air Quality Sensors: One-Year Field Comparative Measurement of Different Gas Sensors and Particle Counters with Reference Monitors at Tušimice Observatory<br>Reprinted from: <i>Atmosphere</i> <b>2020</b> , <i>11</i> , 492, doi:10.3390/atmos11050492 . . . . . | <b>283</b> |
| <b>Milan Váňa, Adéla Holubová Smejkalová, Jaroslava Svobodová and Pavel Machálek</b><br>Long-Term Trends of Air Pollution at National Atmospheric Observatory Košetice (ACTRIS, EMEP, GAW)<br>Reprinted from: <i>Atmosphere</i> <b>2020</b> , <i>11</i> , 537, doi:10.3390/atmos11050537 . . . . .  | <b>299</b> |
| <b>Jiří Huzlík, Jitka Hegrová, Karel Effenberger, Roman Ličbinský and Martin Brtnický</b><br>Air Quality in Brno City Parks<br>Reprinted from: <i>Atmosphere</i> <b>2020</b> , <i>11</i> , 510, doi:10.3390/atmos11050510 . . . . .   | <b>309</b> |
| <b>Markéta Müllerová, Eva Krtková and Zuzana Rošková</b><br>F-Gases: Trends, Applications and Newly Applied Gases in the Czech Republic<br>Reprinted from: <i>Atmosphere</i> <b>2020</b> , <i>11</i> , 455, doi:10.3390/atmos11050455 . . . . .   | <b>329</b> |

# About the Editor

## **Iva Hůnová**

Associate Professor Iva Hůnová is currently affiliated with the Czech Hydrometeorological Institute, Ambient Air Quality Department, and Institute for Environmental Studies, Faculty of Science, Charles University in Prague. Her research interest is ambient air quality assessment with major activities in atmospheric deposition and ground level ozone. She has been involved in numerous national and international projects and activities. She has authored or co-authored more than 50 scientific papers and reviewed for 30 international journals, including *Environmental Pollution*, *Science of the Total Environment*, and *Atmospheric Environment*.



# Ambient Air Quality in the Czech Republic

Iva Hůnová 

Ambient Air Quality Department, Czech Hydrometeorological Institute, Na Šabatce 17,  
14306 Prague 4, Czech Republic; iva.hunova@chmi.cz

## 1. Introduction

Ambient air quality in the present-day Czech Republic (CR), one of the two succession countries of Czechoslovakia post-1993, was perceived as a major problem with severe human health and environmental consequences, particularly between the 1970s and 1990s [1]. Since that time, the ambient air quality in the CR has improved substantially, due to newly introduced stringent legislation and technical countermeasures. Nevertheless, there are still activities which represent significant emission sources, such as local heating and increased vehicle travel through communities. After a substantial decrease in emissions in both the CR and its neighbouring countries, the levels of some ambient air pollutants from the 2000s are still not satisfactory [2]. In this respect, aerosol, ground-level ozone and benzo[a]pyrene remain major problems, as they do elsewhere in Europe [3].

This Special Issue of *Atmosphere* includes one review and 15 original research papers highlighting the progress achieved both in monitoring and modelling air pollution as an important supporting tool for improving of our living environment. Most of the contributions included are aerosol-focused. This editorial provides a short introduction to these interesting papers and presents them in a broader context.

## 2. Summary of This Special Issue

### 2.1. Review on the Time Trends and Spatial Changes in Ambient Air Pollution

In a detailed review, Hůnová [4] provides an overview of ambient air quality development in the present-day Czech Republic over the past seven decades, i.e., from the 1950s to present day. Major air pollution problems are highlighted, main hotspots and air pollutants are indicated, and air pollution impacts on both human health and the environment are discussed. This review provides a broader context for further contributions focussing more specifically on individual ambient air pollutants and issues.

### 2.2. Aerosol Papers

Most papers in this SI are devoted to one of the major ambient air pollutants, i.e., aerosol, by examining it from different perspectives. Volná and Hladký [5] studied the links between ambient  $PM_{10}$  concentrations and meteorological conditions over the Czech-Polish border area, a hot spot region not only in the CR but for the whole of Europe. The analysis of ultrafine particles,  $PM_{2.5}$ , from the same region is provided by Seibert et al. [6], who used the Positive Matrix Factorization approach to identify sources of local air pollution. Their results indicated that the major factors to be blamed for pollution are emissions from residential heating and the burning of solid fuels, followed by the regional primary and secondary aerosol sources, whereas long-range transport and heavy industry appeared to be of only minor importance. Pavlíková et al. [7] measured 34 elements in  $PM_{10}$  sampled in the centre of Ostravsko-karvinská agglomeration at the top of a former mining tower at a height of 90 m above ground to investigate regional air pollution. The elemental composition was found to be seasonal-dependent, and it varied due to sampling conditions. Three large industrial sources were identified as major contributors to regional ambient air pollution, though these were not detected by conventional ground-level air monitoring.



**Citation:** Hůnová, I. Ambient Air Quality in the Czech Republic. *Atmosphere* **2021**, *12*, 770. <https://doi.org/10.3390/atmos12060770>

Received: 1 June 2021

Accepted: 9 June 2021

Published: 15 June 2021

**Publisher's Note:** MDPI stays neutral with regard to jurisdictional claims in published maps and institutional affiliations.



**Copyright:** © 2021 by the author. Licensee MDPI, Basel, Switzerland. This article is an open access article distributed under the terms and conditions of the Creative Commons Attribution (CC BY) license (<https://creativecommons.org/licenses/by/4.0/>).

Furthermore, PM<sub>10</sub> trans-boundary transport from Polish emission sources was indicated to play a major role in winter, contributing substantially to air pollution in the studied region.

Using numerical modelling, Pospisil et al. [8] studied dispersion characteristics of PM<sub>10</sub> in the vicinity of roads passing different types of urban areas. The authors pointed out that major parameters influencing the final shape of the PM<sub>10</sub> mass concentration field are wind direction and velocity, and the built-up area's geometry substantially modifies air flow velocity at the ground-level layers of the atmosphere. That the geometry of built-up areas is important for ambient PM<sub>10</sub> levels in cities is also supported by Neubauer et al. [9], who studied hourly parallel records from two stations in Brno, one located in a park, the other one in a built-up area. The authors concluded that, apart from meteorology, this factor should definitely be accounted for in assessment of PM<sub>10</sub> pollution in densely populated urban areas with high levels of traffic.

Ďoubalová et al. [10] used a high-resolution weather and air-quality forecast system to simulate a typical winter air pollution episode in January–February 2017 in the capital, Prague. Their results confirmed previous findings about urbanisation's effect on ambient air quality in winter, indicating the general behaviour of air pollution in cities in the winter period, regardless of the region or specific air pollution situation. Unique measurements of exhaust PM<sub>10</sub> emissions from two diesel–electric locomotives and one diesel–hydraulic railcar, carried by Vojtisek-Lom et al. [11] during scheduled passenger service, revealed that, despite the fact that these engines were approaching the end of their lives, their emissions were substantially lower compared to cars. These data are very valuable, as information on train emissions is practically non-existent.

Mikuška et al. [12] sampled submicron PM<sub>1</sub> aerosol particles in two Czech urbanized areas: a large city, Brno, and a small town, Šlapanice. They did so through campaigns during heating and non-heating seasons in 2009–2010. Whereas the mean PM<sub>1</sub> concentrations were nearly identical in summer, the mean PM<sub>1</sub> concentrations in winter were 1.6 times higher in the small town. Based on analysis of 14 elements and 12 water-soluble ions, the principal aerosol emission sources were identified. Brzezina et al. [13] studied nanoparticle number concentrations of 61 size fractions (ranging between ca. 200 nm and 15 µm in aerodynamic diameter) in the air at a traffic site in Ústí nad Labem to compare the behaviour of various size fractions within a day, a week, and a year. They attributed the differences in variability of individual size fractions to pollution sources, physical properties of particles, and to meteorological and dispersion conditions.

### 2.3. Benzo[a]pyrene in Ambient Air

A thorough analysis on ambient benzo[a]pyrene (BaP) concentrations is provided by Schreiberová et al. [14]. They pointed out that, during the period of 2012–2018, a full 35–58% of the urban population in the CR were exposed to BaP concentrations above the target value. According to the data from 48 Czech measuring sites, the mean ambient BaP levels ranged from 0.4 ng·m<sup>-3</sup> at a rural regional station to 7.7 ng·m<sup>-3</sup> at an industrial station. Furthermore, short-term campaign measurements in small settlements revealed high values of daily BaP concentrations in winter seasons related to local heating.

### 2.4. Nitrogen Oxides in Ambient Air

Though exhibiting spatially limited ambient air quality levels, nitrogen oxides (NO<sub>x</sub>) emitted by traffic represent a major problem at busy roads in many urbanized areas. In their work, Vojtisek-Lom et al. [15] examined the effects of two problematic recent trends related to increasing use of diesel passenger cars: (i) increasing ambient NO<sub>2</sub>/NO<sub>x</sub> ratio resulting from conversion of NO into NO<sub>2</sub> in catalysts, and (ii) disparity between vehicle emission limits and real emission impacts on ambient air quality due to everyday driving in Prague. They concluded that decreases in NO<sub>x</sub> emission limits for vehicles, introduced in recent decades, have apparently failed to sufficiently reduce ambient NO<sub>2</sub> levels in Prague.

### 2.5. Low-Cost Air Quality Sensors

With an ever-increasing need to control ambient air pollution in cities and industrial areas, we have recently witnessed a boom in demand for low-cost air quality sensors. Bauerová et al. [16] presented the results of almost a one-year field experiment comparing the results of different low-cost sensors and co-located measurements by reference methods used in the Czech nation-wide ambient air quality monitoring network. The authors pointed out the importance of long-term comparison studies through which scientific recommendations are transferred to the general public, providing valuable assistance in decision-making processes when buying suitable types of sensors and eliminating of possible flaws in their application; these revelations also help producers in further enhancing their own products.

### 2.6. Regional and Urban Background Ambient Air Pollution

The ambient air concentrations from regional stations are important as reference sites, providing ambient air quality levels for comparison to impact areas, such as cities and industrial regions. For the CR, the National Atmospheric Observatory Košetice operated by the Czech Hydrometeorological Institute, established in 1988, which participates in numerous international programs, projects, and activities, serves as an important monitoring site by providing data describing the air pollution at a regional scale. Váňa et al. [17] summarized the long-term time trends in principle ambient air pollutants at the Košetice Observatory in the context of air pollutant emission changes.

Huzlík et al. [18] examined the ambient air quality in park areas in Brno, the second largest city of the CR. In spite of a general belief that green urban areas provide the best air quality within the city, the measurements supporting this claim are mostly lacking. Based on four 14-day campaigns measuring NO, NO<sub>2</sub>, PM<sub>10</sub>, and O<sub>3</sub> levels, Huzlík et al. [18] concluded that the air quality in the parks approached that of the urban background sites, except for Koliště park, where similar ambient air pollution levels as at the traffic site were measured.

### 2.7. Emissions

The only emission-oriented paper of this SI focuses on fluorinated greenhouse gases (F-gases) that have been developed to replace stratospheric ozone-depleting substances, and which are used in refrigeration and air-conditioning systems. Although not harmful to the ozone layer, F-gases contribute substantially to the greenhouse effect and global climate change; hence, they are deserving of world-wide attention. Müllerová et al. [19] provided information on changes in the composition of F-gases used in the CR.

## 3. Concluding Remark

To conclude, the papers presented in this SI provide a valuable update both on time trends and spatial changes in ambient air quality, and highlight the recent activities in both monitoring and modelling of principle ambient air pollutants in the CR.

**Funding:** This research received no external funding.

**Institutional Review Board Statement:** Not applicable.

**Informed Consent Statement:** Not applicable.

**Conflicts of Interest:** The author declares no conflict of interest.

## References

1. Moldan, B.; Schnoor, J.L. Czechoslovakia-Examining a Critically Ill Environment. *Environ. Sci. Technol.* **1992**, *26*, 14–21. [[CrossRef](#)]
2. CHMI. *Air Pollution in the Czech Republic in 2018*; Graphical Yearbook (Czech/English); Czech Hydrometeorological Institute: Prague, Czech Republic, 2019.

3. EEA. *Air Quality in Europe—2019 Report*; EEA Report No. 10/2019; EEA: Copenhagen, Denmark, 2019. Available online: <https://www.eea.europa.eu/publications/air-quality-in-europe-2019/air-quality-in-europe-2019/viewfile#pdfjs.action=download> (accessed on 30 February 2020).
4. Hůnová, I. Ambient Air Quality in the Czech Republic: Past and Present. *Atmosphere* **2020**, *11*, 214. [[CrossRef](#)]
5. Volná, V.; Hladký, D. Detailed Assessment of the Effects of Meteorological Conditions on PM<sub>10</sub> Concentrations in the Northeastern Part of the Czech Republic. *Atmosphere* **2020**, *11*, 497. [[CrossRef](#)]
6. Seibert, R.; Nikolova, I.; Volná, V.; Krejčí, B.; Hladký, D. Air Pollution Sources' Contribution to PM<sub>2.5</sub> Concentration in the Northeastern Part of the Czech Republic. *Atmosphere* **2020**, *11*, 522. [[CrossRef](#)]
7. Pavlíková, I.; Hladký, D.; Motyka, O.; Vergel, K.N.; Strelkova, L.P.; Shvetsova, M.S. Characterization of PM<sub>10</sub> Sampled on the Top of a Former Mining Tower by the High-Volume Wind Direction-Dependent Sampler Using INNA. *Atmosphere* **2021**, *12*, 29. [[CrossRef](#)]
8. Pospisil, J.; Huzlík, J.; Licbinsky, R.; Spilacek, M. Dispersion Characteristics of PM<sub>10</sub> Particles Identified by Numerical Simulation in the Vicinity of Roads Passing through Various Types of Urban Areas. *Atmosphere* **2020**, *11*, 454. [[CrossRef](#)]
9. Neubauer, J.; Michálek, J.; Šilinger, K.; Firbas, P. Impacts of Built-Up Area Geometry on PM<sub>10</sub> Levels: A Case Study in Brno, Czech Republic. *Atmosphere* **2020**, *11*, 1042. [[CrossRef](#)]
10. Dóubalová, J.; Huszár, P.; Eben, K.; Benešová, N.; Belda, M.; Vlček, O.; Karlický, J.; Geletič, J.; Halenka, T. High Resolution Air Quality Forecasting over Prague within the URBI PRAGENSI Project: Model Performance during the Winter Period and the Effect of Urban Parameterization on PM. *Atmosphere* **2020**, *11*, 625. [[CrossRef](#)]
11. Vojtisek-Lom, M.; Jirků, J.; Pechout, M. Real-World Exhaust Emissions of Diesel Locomotives and Motorized Railcars during Scheduled Passenger Train Runs on Czech Railroads. *Atmosphere* **2020**, *11*, 582. [[CrossRef](#)]
12. Mikuška, P.; Vojtěšek, M.; Křůmal, K.; Mikušková-Čampulová, M.; Michálek, J.; Večeřa, Z. Characterization and Source Identification of Elements and Water-Soluble Ions in Submicrometre Aerosols in Brno and Šlapanice (Czech Republic). *Atmosphere* **2020**, *11*, 688. [[CrossRef](#)]
13. Brzezina, J.; Köbölóvá, K.; Adamec, V. Nanoparticle Number Concentration in the Air in Relation to the Time of the Year and Time of the Day. *Atmosphere* **2020**, *11*, 523. [[CrossRef](#)]
14. Schreiberová, M.; Vlasáková, L.; Vlček, O.; Šmejdiřová, J.; Horálek, J.; Bieser, J. Benzo[a]pyrene in the Ambient Air in the Czech Republic: Emission Sources, Current and Long-Term Monitoring Analysis and Human Exposure. *Atmosphere* **2020**, *11*, 955. [[CrossRef](#)]
15. Vojtisek-Lom, M.; Suta, M.; Sikorova, J.; Sram, R.J. High NO<sub>2</sub> Concentrations Measured by Passive Samplers in Czech Cities: Unresolved Aftermath of Dieselgate? *Atmosphere* **2021**, *12*, 649. [[CrossRef](#)]
16. Bauerová, P.; Šindelářová, A.; Rychlík, Š.; Novák, Z.; Keder, J. Low-Cost Air Quality Sensors: One-Year Field Comparative Measurement of Different Gas Sensor and Particle Counters with Reference Monitors at Tušimice Observatory. *Atmosphere* **2020**, *11*, 492. [[CrossRef](#)]
17. Váňa, M.; Holubová-Šmejkalová, A.; Svobodová, J.; Machálek, P. Long-Term Trends of Air Pollution at National Atmospheric Observatory Košetice (ACTRIS, EMEP, GAW). *Atmosphere* **2020**, *11*, 537. [[CrossRef](#)]
18. Huzlík, J.; Hegrová, J.; Effenberger, K.; Ličbinský, R.; Brtnický, M. Air Quality in Brno City Parks. *Atmosphere* **2020**, *11*, 510. [[CrossRef](#)]
19. Müllerová, M.; Krtková, E.; Rošková, Z. F-Gases: Trends, Applications and Newly Applied Gases in the Czech Republic. *Atmosphere* **2020**, *11*, 455. [[CrossRef](#)]

Review

# Ambient Air Quality in the Czech Republic: Past and Present

Iva Hůnová 

Ambient Air Quality Department, Czech Hydrometeorological Institute, Na Šabatce 17,  
143 06 Praha 4, Czech Republic; iva.hunova@chmi.cz

Received: 7 January 2020; Accepted: 14 February 2020; Published: 20 February 2020



**Abstract:** Based on an analysis of related core papers and reports, this review presents a historical perspective on ambient air pollution and ambient air quality development in the modern-day Czech Republic (CR) over the past seven decades, i.e., from the 1950s to the present. It offers insights into major air pollution problems, reveals the main hot spots and problematic regions and indicates the principal air pollutants in the CR. Air pollution is not presented as a stand-alone problem, but in the wider context of air pollution impacts both on human health and the environment in the CR. The review is arranged into three main parts: (1) the time period until the Velvet Revolution of 1989, (2) the transition period of the 1990s and (3) the modern period after 2000. Obviously, a major improvement in ambient air quality has been achieved since the 1970s and 1980s, when air pollution in the former Czechoslovakia culminated. Nevertheless, new challenges including fine aerosol, benzo[a]pyrene and ground-level ozone, of which the limit values are still vastly exceeded, have emerged. Furthermore, in spite of a significant reduction in overall emissions, the atmospheric deposition of nitrogen, in particular, remains high in some regions.

**Keywords:** air pollution; air quality; 1950–2018; Czechoslovakia; emissions; aerosol; ground-level ozone; atmospheric deposition; health outcomes; environmental issues

---

## 1. Introduction

The modern-day Czech Republic (CR), one of the two succession countries of the former Czechoslovakia post 1993, is a Central European country with an infamous environmental pollution history, including heavy air pollution with serious impacts in the past. These were mostly due to emissions from burning poor-quality lignite of local provenience with very high contents of sulphur used both for coal-powered thermal power plants and local, domestic heating systems. Extremely high SO<sub>2</sub> emissions affected the health of the inhabitants adversely and resulted in serious environmental damage, including the decline of spruce forests. Furthermore, emissions from high stacks of large power plants added substantially, due to long-range transport, to acid rain and the acidification of ecosystems in other European regions, such as Scandinavia. The infamous ‘Black Triangle’, a border region situated between the former Czechoslovakia, East Germany and Poland, belonged to the most polluted areas of Europe at that time.

As a consequence of fundamental socioeconomic changes triggered by the Velvet Revolution of 1989, the introduction of new legislation, application of effective countermeasures in emission reduction and modernisation of energy production and industry, alongside extensive gasification of local heating systems, the overall situation in ambient air quality has improved substantially. An unprecedented reduction in SO<sub>2</sub> emissions of some 90% has been recorded, accompanied by reductions in TSP (total suspended particles) and NO<sub>x</sub> (nitrogen oxides). Nevertheless, new challenges have emerged in air pollution, such as fine aerosol particles, ground-level ozone, and benzo[a]pyrene (BaP), pollutants of which the ambient air concentration currently extensively exceeds the legal limit values, affecting

a substantial part of the population and vast geographical regions, and the concentrations of which seem to be very difficult to decrease.

This review paper aims to address ambient air pollution in the CR in its historical perspective, collating and summarising the essential information on ambient air pollution and changes thereto, in context with its relevant negative impacts on the environment and human health over the last 70 years, i.e., from the 1950s to the present. The review consists in three main parts covering the three principal time periods: (1) the period until the Velvet Revolution of 1989, (2) the transition period between 1989 and 2000 and (3) the modern period after 2000.

## 2. Air Pollution in the Former Czechoslovakia (Prior to 1989)

### 2.1. Emission Sources and Source Areas

Czechoslovakia's economy from the Second World War through the early 1980s grew at the expense of severe degradation of its natural sources and environment [1–3]. At that time, Czechoslovakia was a centrally planned economy under communist rule, with an emphasis on the massive development of heavy industries [4]. Ambient air pollution has been considered a major environmental threat since the 1950s. At this very time, large coal-combustion power plants were put into operation [5,6], emitting large quantities of sulphur dioxide (SO<sub>2</sub>), TSP, NO<sub>x</sub> and other pollutants [7]. These large emission sources with high stacks (Figure 1) were concentrated in the northwest region of Bohemia (NWR, location in map in Figure 2), in the Podkrusnohori region, adjacent to the German and Polish borders in particular, where their operation was driven by local poor-quality lignite coal with extremely high sulphur and ash content [8–10].



Figure 1. Prunerov coal power plant (photo by the author).

The sulphur content in the local coal varied widely according to the individual coal deposits. Coal mined in the North Bohemian Lignite Basin averaged about 1.2–3.5%, with a maximum total sulphur content as high as 15.8% and an ash content ranging between 2.6% and 69.9% [11]. Some 50–95% of sulphur compounds in the coal were emitted into the air [12]. The emissions were highly dependent on the applied technology and leading of the burning process [13–15]. Moreover, other trace elements potentially harmful for the environment, such as As, Be, Pb, V, F, Cr, Cu and Se were found in elevated concentrations in North Bohemian coal and released into the atmosphere while burning. The highest concentrations of As (387 ppm), Sb (7.5 ppm) and W (108.5 ppm) were reported from the Czechoslovak Army Mine (abbreviated ČSA in Czech) quarry [11]. This coal was mined in open cast mines, the

operation of which devastated the originally scenic landscape and caused the end of numerous small settlements as well as the environmental, social and moral decline of the entire region [16–18].

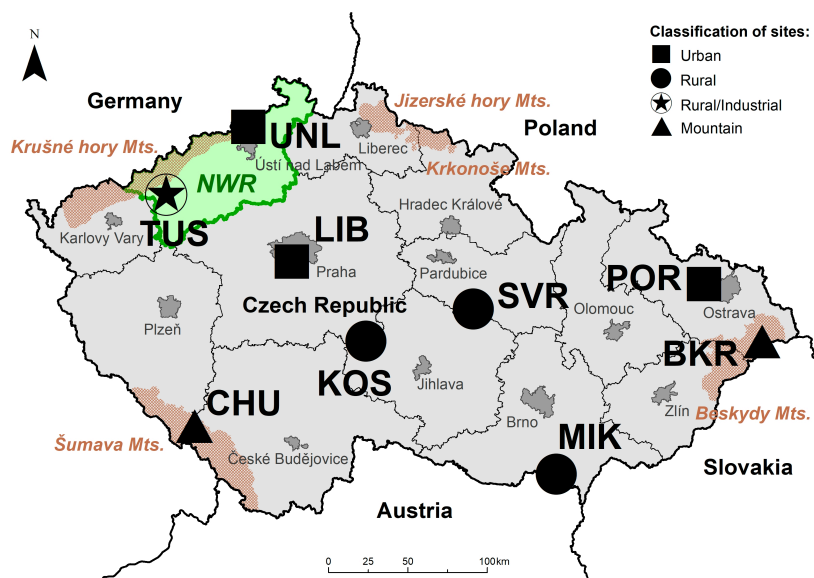
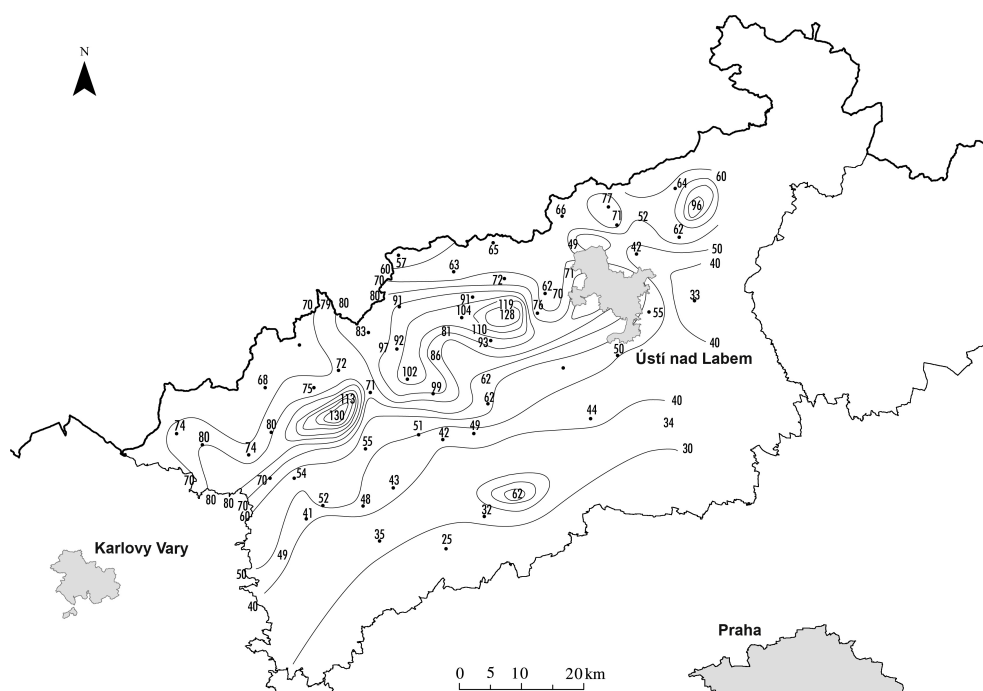


Figure 2. Map showing the areas and places mentioned in this review.

Furthermore, other industries, such as chemical, metallurgical, textile, cellulose paper mills, and glass and ceramic manufacture, added to the overall emissions [19]. The accumulation of numerous large emission sources in the poorly ventilated Podkrusnohori valley in Northwest Bohemia resulted in a poisonous air mixture, in particular during winter thermal inversions, when the ambient air pollutant levels reached extremely high values [20]. Under the communist regime, however, information on environmental, including ambient air, pollution was not available to the general population, and half-classified materials were intended exclusively as reports for experts [21]. The SO<sub>2</sub> annual mean concentrations ranged in the order of hundreds of μg m<sup>-3</sup>, whereas the SO<sub>2</sub> daily mean concentrations ranged in the order of thousands of μg m<sup>-3</sup>. The measurements at that time recorded in the unpublished internal reports of the Czech Hydrometeorological Institute (CHMI) in the above region, in particular in the adjacent Krušné hory (Mts.) (Erzgebirge, the Ore Mts.) reached up to 130 μg m<sup>-3</sup> of SO<sub>2</sub> in annual means during the 1970s (Figure 3). A daily mean of 1590 μg m<sup>-3</sup> of SO<sub>2</sub> (Figure 4) was recorded on 16 January 1982 [20]. For comparison, current ambient SO<sub>2</sub> concentrations measured in the same region are up to 10 μg m<sup>-3</sup> of SO<sub>2</sub> in the annual mean [22]. The Podkrusnohori region ranked amongst the most polluted parts of the entire country [19]. Apart from the North Bohemia region, other emission source regions included the major urban areas, such as Prague (the capital), Ostrava, Pilsen, Hradec Králové and Brno, with numerous industrial enterprises and local heating systems operating on brown coal and lignite, deteriorating the ambient air quality.



**Figure 3.** Map of Northwest Bohemia (NWR in Figure 2), showing the SO<sub>2</sub> annual means in µg m<sup>-3</sup> in 1971–1980, the lines represent the isoconcentrations (redrawn according to [20]).

With 3150 kilotons in 1985, i.e., a full 203 kg per person per year in 1985, SO<sub>2</sub> emissions in the Czech-Slovak Federal Republic (CSFR) were the highest in Europe, 2.48 times higher than in Western Europe per unit of gross national product (GNP) [23]. Further, the total NO<sub>x</sub> emissions (expressed as NO<sub>2</sub>) were estimated to be 1200 kilotons annually, i.e., 57 kg per person per year; hence Czechoslovakia took an infamous first place in NO<sub>2</sub> emissions in Europe [23].

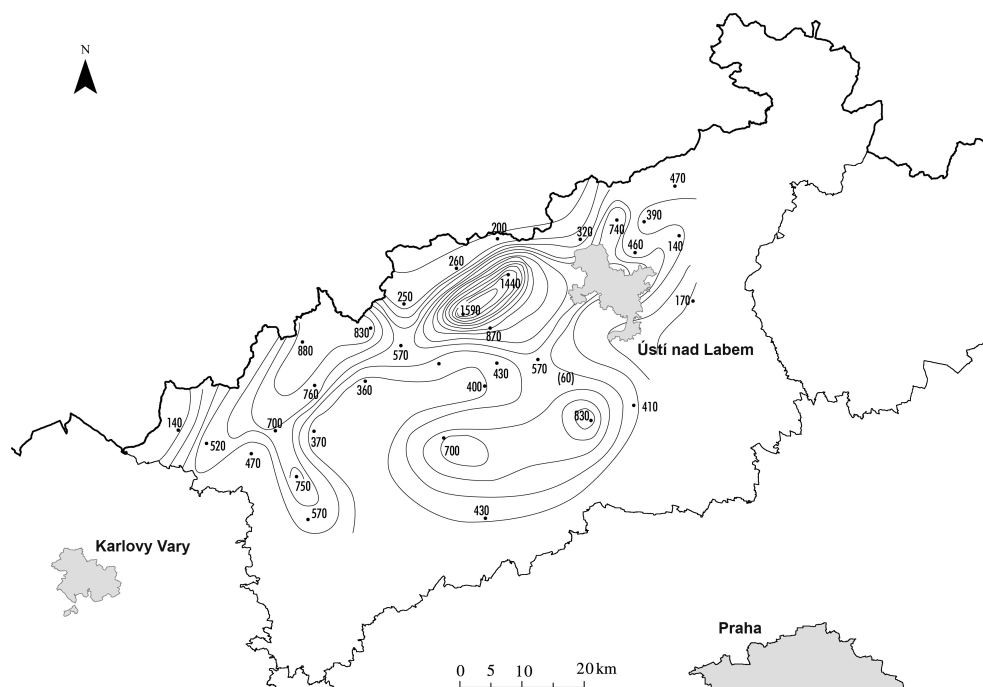


**Figure 4.** Map of Northwest Bohemia (NWR in Figure 2), showing the SO<sub>2</sub> daily mean in µg m<sup>-3</sup> on 16 January 1982, the lines represent the isoconcentrations (redrawn according to [20]).

## 2.2. Ambient Air Quality Monitoring

The first measurements of ambient air pollution addressed sulphur dioxide (SO<sub>2</sub>) and total suspended particles (TSP)—the then measured total sample of aerosol without particle fraction distinction—and date back to the 1950s. The measurement activities at that time focussed on industrial and highly populated areas and ambient air pollution was observed by the Public Health Service with respect to serious human health impacts [24,25].

Regular ambient air quality monitoring has been in operation since the 1960s and individual networks were aimed at the most polluted areas. The Czech Hydrometeorological Institute (CHMI) has been responsible for nationwide ambient air quality monitoring since 1964. The first monitoring sites were situated in the Podkrusnohori region in 1968. In 1969, the network expanded to the Ostrava region and in 1970, to the Brno region [26]. Gradually, a fairly dense network was set up for monitoring SO<sub>2</sub> in particular. Smog regulation and warning systems were built, the first was put in operation in North Bohemia in 1973 [27].

After covering the most heavily impacted regions, measurements also began in relatively unpolluted areas, far from the major emission sources, in order to gain information on regional background air pollution. The Svratouch site in the Czech-Moravian Highlands has supplied data on air quality to the worldwide Background Air Pollution Monitoring Network (BAPMON) since 1972 and to the EMEP (European Monitoring and Evaluation Programme) since 1977 [28]. In the 1980s, the Košetice site (KOS in Figure 2) was set up for environmental monitoring on a regional scale [29,30]. The air quality monitoring was supplemented by observations of precipitation chemistry, with the first site established at Hrádek u Pacova in 1974 [31].

Apart from the CHMI, several other organisations were involved in ambient air quality measurements for their own purposes, such as the Public Health Service (abbreviated in Czech as HS), Organization for the Rationalization of Power Plants (abbreviated in Czech as ORGREZ), Czech Geological Survey (abbreviated in Czech as ČGÚ, and later as ČGS), Forestry and Game Management Research Institute (abbreviated in Czech as VÚLHM), Water Management Research Institute (abbreviated in Czech as VÚV) and the Research Institute of Plant Production (abbreviated in Czech as VÚRV).

Air pollution in Czechoslovakia culminated in the 1970s and 1980s. The monitoring results from 1971–1982 for the eight most heavily impacted regions defined by the then government (i.e., North Bohemia, Mělnicko-Neratovicko, City of Prague, Hradecko-Pardubicko, Brno, West Bohemia and Pilsen) were collated by the CHMI's internal reports [20,32–38]. The incorporation of a certain area into the impacted regions was based on the annual SO<sub>2</sub> mean concentration above 30 µg m<sup>-3</sup> (Figure 5). Based on monitoring and dispersion modelling results, the above regions were categorised into three different air pollution levels: (1) the most polluted, which were the North Bohemia and Prague regions, (2) medium air pollution level—the West Bohemia, Ostravsko-Karvinsko and Mělnicko-Neratovicko regions and (3) the lowest air pollution level—the Hradecko-Pardubicko and Brno regions. Interestingly, the two most polluted regions, i.e., North Bohemia and Prague, showed similar air pollution levels, though these originated from completely different emission sources. In North Bohemia, the problem arose from large emission sources, whereas in Prague the local heating systems were the culprit. Furthermore, with respect to distinct geomorphology, both Prague and the Podkrusnohori region have been prone to frequent thermal inversion occurrence preventing pollutant dispersion [39–41].



**Figure 5.** Map indicating the formerly impacted regions (in the 1970s and 1980s) with respect to air pollution delimited by annual  $\text{SO}_2$  mean concentration above  $30 \mu\text{g m}^{-3}$  (redrawn according to [41]).

### 2.3. Human Health Outcomes

The first information on measured ambient air pollutant concentrations in the then Czechoslovakia, available only in Czech, originate from as early as the 1950s. They cover some industrial regions and are related to local inhabitant health outcomes [24,25]. Children living in areas with high air pollution were somewhat retarded in growth. Furthermore, they evinced significant changes in their red blood cell counts. It was recognised that children responded to elevated  $\text{SO}_2$  concentrations in similar way as to rather lower  $\text{O}_2$  pressure, such as in the high mountains: an increase in the total surface of erythrocytes ensured the transfer of  $\text{O}_2$  to tissues easier [42]. It was demonstrated that a stay of 1–3 months in a clean atmosphere had favourable effects on such children, especially with respect to the haemoglobin, and that this reaction continued for about three months after the children returned to the region with polluted air. Hence children used to be sent to an open-air school, where the air was relatively clean [42]. Air pollution belonged amongst the factors not only impairing human health but contributing even to all-cause mortality. According to Bobak and Marmot [43], an estimated 2–3% of the total mortality could be attributed to air pollution in the CR in 1987. Bobak and Leon [44], in a study examining infant mortality and air pollution in 1986–1988 for 46 of the 85 districts of Czechoslovakia, reported a weakly positive association between neonatal mortality and ambient TSP and  $\text{SO}_2$  concentrations.

A comprehensive Teplice programme aimed at a thorough study of the impacts on human health caused by ambient air pollution, including aerosol, genotoxic organic compounds and toxic trace elements in one of most heavily impacted districts of North Bohemia [45]. A significantly higher prevalence of adverse respiratory symptoms and decreased lung function were indicated as compared to the relatively clean Prachatice district in South Bohemia [46]. Moreover, a study of the effects of exposure on pregnancy and birth revealed an excess prevalence of low birth weight and premature births [47]. Furthermore, within this study, it was indicated that air pollution may alter early childhood susceptibility to infections [48]. Exposure to intermittent air pollution in the North Bohemian Teplice district was shown to cause sperm DNA damage resulting in an increase in rates of male-mediated infertility, miscarriage, and other adverse reproductive outcomes [49].

### 2.4. Environmental Issues

Severe air pollution affected both human health and the environment. Mismanaged forest ecosystems were susceptible to additional stresses [50–57]. A substantial part of forest areas (more

than 60%) were damaged in various degrees by air pollution, namely SO<sub>2</sub> acting either directly or indirectly via acid deposition and subsequent soil changes. The outcomes included increased mortality and decreased increments in forests, loss of valuable ecotypes, impact on water management and overall decrease in stability of the landscape [58–60]. Damaged forests were the most visible and best-known symptoms of acid rain [61,62]. Losses on forest wood attributable to air pollution in the then Czechoslovakia were estimated at 9.5 million m<sup>3</sup> year<sup>-1</sup> by the International Institute for Applied Systems Analysis (IIASA); this estimate being reckoned conservative, as exclusively SO<sub>2</sub> was accounted for, whereas NO<sub>x</sub> and NH<sub>3</sub> were not considered [63]. Unprecedented forest decline, namely in the Krušné hory Mts., Jizerské hory Mts. and Krkonoše Mts., in the 1970s and 1980s were of major concern for the then foresters and forest management [64] and attracted infamous attention from scientists all over the world. The Krkonoše National Park (KRNAP) was cited—together with the adjacent Polski Park Narodowy—by the International Union for Conservation of Nature and Natural Resources (IUCN) as the world's most threatened protected natural area [65].

Though Czech environmental studies at that time were practically non-existent [21], some papers on ambient air pollution impacts on the environment can still be mentioned. Air pollution was reported to influence the nesting ecology of the house martin (*Delichon urbica*) in 141 villages and towns in Czechoslovakia, including a significant reduction in nesting density, colony size and occupancy [66]. Fluoride pollution in wild deer assessed in North Bohemia showed significantly decreasing exposures from the mid-1990s, attributed largely to the implementation of emission control devices on coal-fired power plants [67].

Emissions were also blamed for the contamination of crops. Ustyak and Petrikova [68] reported that the results of their study for North Bohemia in 1987–1992 indicated very high contamination of agricultural crops by heavy metals and As. Specifically, 3–16% of fodder crop samples and 49–86% of food crop samples were contaminated (i.e., they showed higher heavy metal contents than was permissible at that time) in spite of a low degree of soil contamination. The main pollutants of fodder crops were Hg, Cd, Pb and Co, whereas the main pollutants of food crops were Cd, Cr, Hg, As, Pb, Ni and Zn [68].

Air pollution also affected precipitation chemistry, and consequent atmospheric deposition and stream water chemistry was observed [69]. The long-term effects of atmospheric pollution by metals and acids were documented even on sediment cores from Čertovo Lake in the Šumava Mts., situated in a relatively unpolluted region [70].

### 2.5. Air Pollution in the Context of the Former Communist Countries

The problem of severe ambient air pollution and consequent human health and environmental impacts was not limited exclusively to the former Czechoslovakia, but involved other Central European communist countries, such as the former GDR (Eastern Germany or the Democratic Republic of Germany) and Poland [71–73]. These three countries ranked among the worst polluters due to emissions from the power generation systems as well as heat production both for industry and municipalities. These sources accounted for about 90% of total SO<sub>2</sub> emissions and about 60–70% of emissions of dust and NO<sub>x</sub> [74]. Fly-ash emission in Eastern Europe was greater than in any other industrial region in the world [65]. The heavily industrialised 'Black Triangle' (sometimes also called the 'Dirty Triangle') region encompassing Northern Bohemia, Silesia and adjacent portions of Eastern Germany was infamous for its heavily impacted environment and the high frequency of winter smog occurrence causing an adverse effect on the health of local inhabitants and on the environment [74].

### 2.6. Long-Range Transport

A few decades ago, air pollution was considered entirely a local problem. The acceptable solution seemed to be building high stacks to disperse the emissions and thus reduce ground-level air pollutant concentrations. Due to long-range transport, however, the previously local-scale problem developed into a regional-scale issue [75]. Consequently, towards the end of the 1960s, due to the long-range transport of air pollutants, namely SO<sub>2</sub> and NO<sub>x</sub>, a substantial decrease in pH of precipitation and subsequent acidification of both terrestrial and aquatic ecosystems was observed over large portions of

Europe, including areas distant from major emissions sources, such as Norway and Sweden [76]. The problem, popularly called ‘acid rain’, resulted in important negative changes in chemistry and biota in lakes, running water and forests and triggered hot debates among both scientists and the general population [77–80]. The then Czechoslovakia, as a major emitter country, also contributed substantially and was blamed for air pollution export and consequent acidification problems elsewhere [23,81].

### 3. The Period after the Velvet Revolution, the 1990s

Some positive trends, such as a decrease in ambient air pollution by several pollutants can be tracked back as far as the 1980s [82]. The improvement in the state of the environment, including the ambient air quality, however, has been clearly visible only since the transition from the communist past triggered by the Velvet Revolution in November 1989. In the beginning, this was due mainly to industrial decline, then later as a result of economic restructuring and privatisation [62,83]. In fact, the environmental issues, including the vast dissatisfaction of a considerable part of the population over the then ambient air pollution, contributed substantially to the collapse of the old regime in Czechoslovakia [84–87]. From the very beginning, a strong emphasis was therefore placed on solving environmental problems, including air pollution and the adoption of relevant countermeasures to improve the poor state of the environment [88].

As for the emissions, an unprecedented reduction in  $\text{SO}_2$  of some 90% was achieved via a combination of newly adopted strict legislation measures, considerable investments into desulphurisation remedies installed at large emission sources and a transfer from burning lignite to gas in residential heating. For comparison, the reduction in  $\text{SO}_2$  emissions in most European countries at the same time accounted for approximately 60% [89]. At the same time, TSP emissions also decreased substantially [90], whereas  $\text{NO}_x$  emissions decreased considerably less [91]. An important motivation for improvements was also the preparation of the CR for accession to the EU [92]. The CR became a candidate for accession in 1993 and made all efforts to implement the EU legislation, including the Air Quality Law, well in advance.

The most pronounced improvement in a dynamic decrease in air pollutant emissions was seen in the period between 1989 and 1998 [93–95], the impetus to this favourable development being the newly set up strict emission limits to be met in 1998 (Figures 6 and 7). The existing major emission sources were forced to modernise or close up, without the exceptions abundantly permitted so far. Residential heating systems switched from burning coal to gas in many places, including Prague. A substantial reduction of residential coal consumption in the CR from 1990 to 2014 was achieved, by a factor of 6.2 [96].

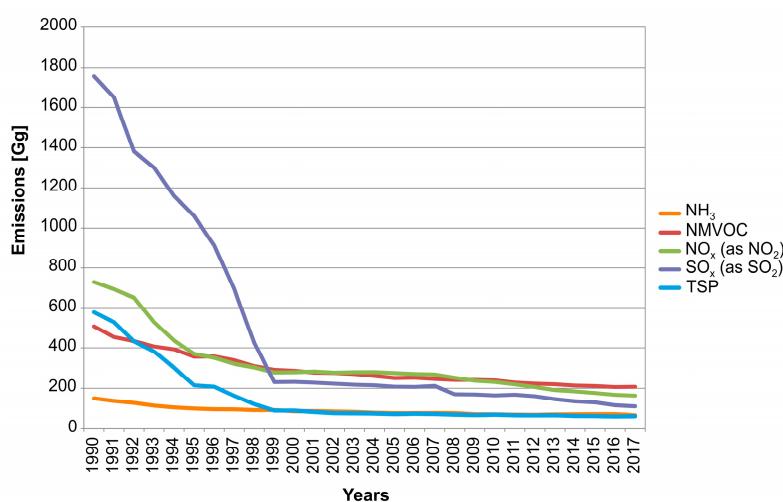


**Figure 6.** Overall emissions of  $\text{SO}_2$ ,  $\text{NO}_x$ ,  $\text{NH}_3$ , NM VOC and TSP in the Czech Republic (CR), according to European Monitoring and Evaluation Programme (EMEP) data [97].

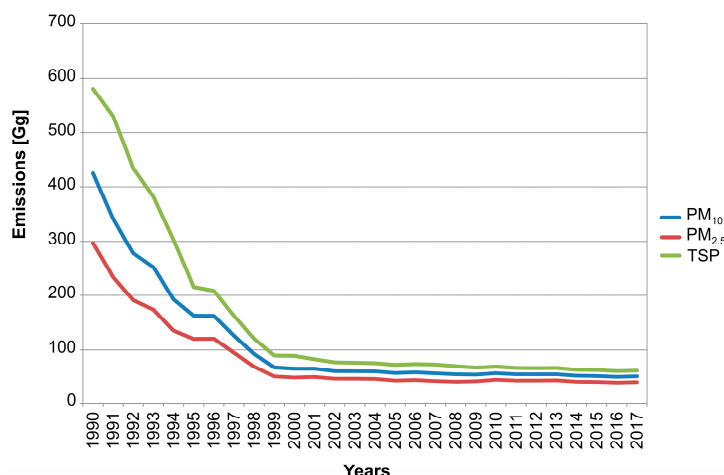


Figure 7. Overall emissions of TSP, PM<sub>10</sub> and PM<sub>2.5</sub> in the CR, according to EMEP data [97].

The extent to which the changes in emissions were reflected in changes in ambient air quality is shown for several sites representing different environments, altitudes and geographical regions (Table 1, location in map in Figure 2). The trends in annual mean concentrations of SO<sub>2</sub>, NO<sub>x</sub>, PM<sub>10</sub> and O<sub>3</sub> from the 1990s to the present time are presented in Figures 8–11. The individual annual means are missing in cases where the requirement of a sufficient number of measured values was not fulfilled [22]. The most impressive decreases, most obvious in the presented diagram for the UNL and TUS sites (both in NWR) and the Prague site LIB were recorded for SO<sub>2</sub> (Figure 8). The ambient NO<sub>x</sub> concentrations (Figure 9) show decreasing trends, though much milder than for SO<sub>2</sub>, with the highest concentrations for the LIB site reflecting clearly the impact of a nearby main road, and somewhat lower concentrations for the NWR sites (UNL and TUS) under influence of large thermal power plants. Fairly large differences (as compared to SO<sub>2</sub> and PM<sub>10</sub>) between NO<sub>x</sub> concentrations at different types of sites are evident. Ambient PM<sub>10</sub> concentrations (Figure 10) also show overall decreasing trends with peaks at the beginning of the 2000s. Annual means of ambient O<sub>3</sub> concentrations (Figure 11) are not decreasing and show contrasting patterns to the above pollutants (Figures 8–10). In accordance with the general assumption, the highest values were recorded at the CHU and BKR mountain sites, whereas the lowest values were measured at the Prague LIB site.

Table 1. Measuring sites (location in map in Figure 2), the long-term records of which are presented in Figures 8–11.

| Station          | Code | Altitude [m a.s.l.] | Classification <sup>1</sup> | Region           |
|------------------|------|---------------------|-----------------------------|------------------|
| Ostrava-Poruba   | POR  | 242                 | B/S/R                       | Ostrava          |
| Mikulov-Sedlec   | MIK  | 245                 | B/R/A-REG                   | South Moravia    |
| Praha4-Libuš     | LIB  | 301                 | B/S/R                       | Prague           |
| Tušimice         | TUS  | 322                 | B/R/IA-NCI                  | NWR <sup>2</sup> |
| Ústí n.L.-Kočkov | UNL  | 367                 | B/S/RN                      | NWR <sup>2</sup> |
| Svratouch        | SVR  | 735                 | B/R/N-REG                   | C-M Uplands      |
| Bílý Kříž        | BKR  | 890                 | B/R/N-REG                   | Beskydy Mts.     |
| Churáňov         | CHU  | 1118                | B/R/N-REG                   | Šumava Mts.      |

<sup>1</sup> Classification according to the European Commission EC Decision EoI 97/101/EC: B/S/R—background/suburban/residential, B/S/RN—background/suburban/residential, natural, B/R/IA/NCI—background/rural/industrial, agricultural/near city, B/R/A-REG—background/rural/agricultural-regional, B/R/N-REG—background/rural/natural-regional, <sup>2</sup> NWR—Northwest region.

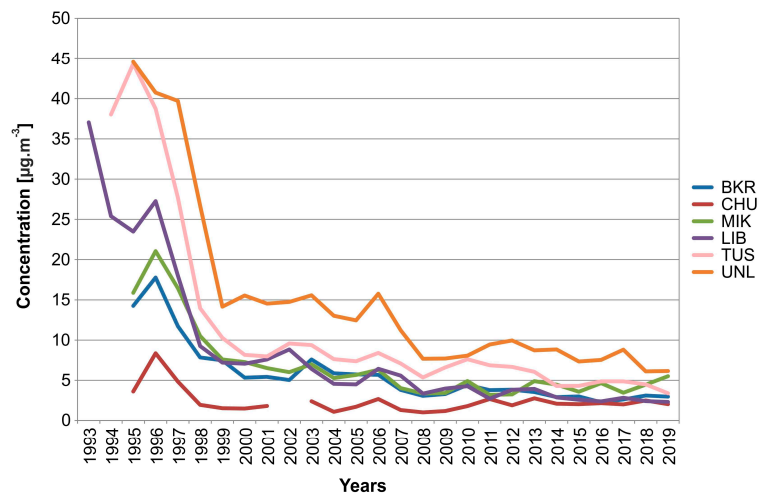


**Figure 8.** Trends in ambient annual mean SO<sub>2</sub> concentrations at selected sites (see Table 1, Figure 2), 1993–2019, based on Czech Hydrometeorological Institute (CHMI) data.

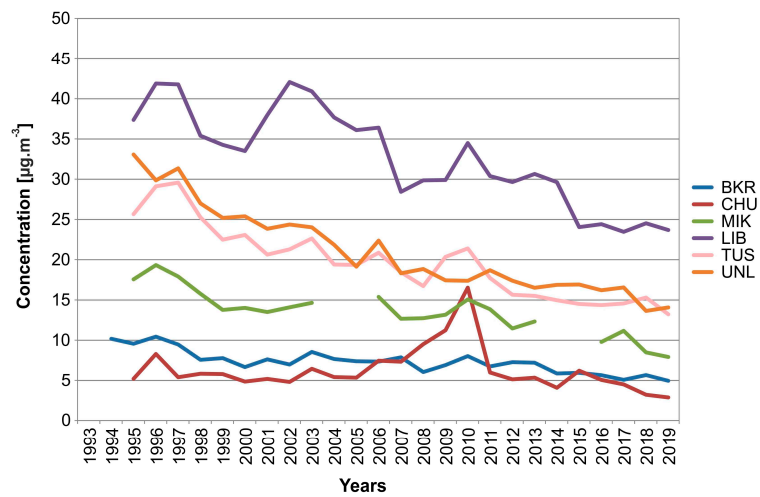


**Figure 9.** Trends in ambient annual mean NO<sub>x</sub> concentrations at selected sites (see Table 1, Figure 2), 1993–2019, based on CHMI data.

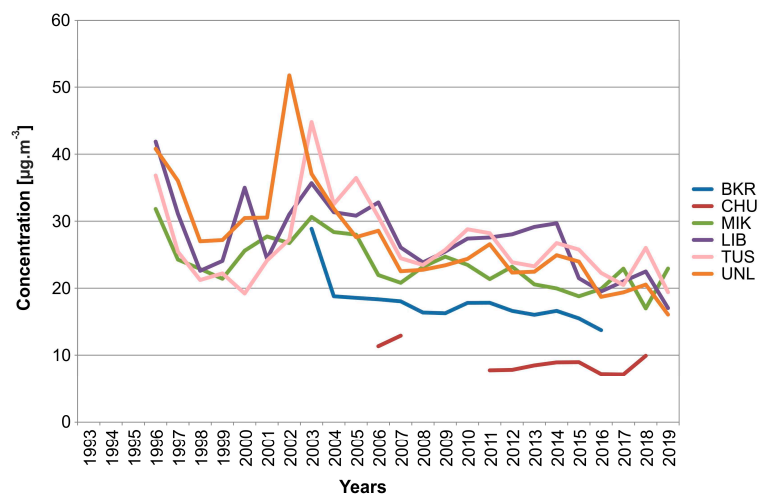


**Figure 10.** Trends in ambient annual mean PM<sub>10</sub> concentrations at selected sites (see Table 1, Figure 2), 1993–2019, based on CHMI data.

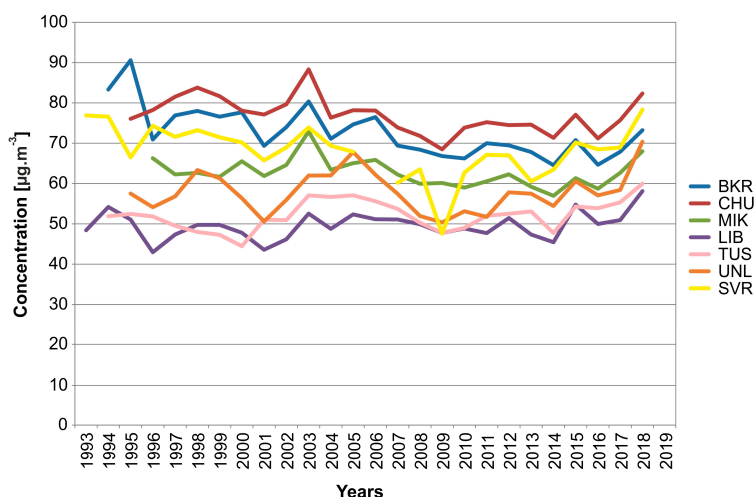


**Figure 11.** Trends in ambient annual mean O<sub>3</sub> concentrations at selected sites (see Table 1, Figure 2), 1993–2018, based on CHMI data.

During the 1990s, Czechoslovakia started to be involved in various international activities, including individual studies, projects and programmes bringing numerous interesting results (e.g., [98–103]). For example, within a CAESAR (Central European Study on Air pollution and Respiratory health) study encompassing 25 study areas in six Central and Eastern European countries (Bulgaria, the Czech Republic, Hungary, Poland, Romania and the Slovak Republic), high PM<sub>10</sub> and PM<sub>2.5</sub> levels were indicated, with large changes between seasons, likely due to local heating. The measured PM levels were hypothesised to contribute to the observed reduced life expectancy in the region [104]. For the first time, the environment including ambient air pollution of the Czech Republic was assessed in the context of Europe’s environment in the comprehensive report published by the European Environmental Agency (EEA) [105].

#### 4. Air Pollution in the Modern-Day Czech Republic (after 2000)

The number of ambient air quality monitoring sites has changed continuously since 1969, the highest number of stations was in operation in the 1980s and 1990s. The optimisation of the monitoring network in the 2000s resulted in a reduction in the number of sites and the replacement of others. Currently, 198 stations in the Czech Republic monitor the air quality, 127 of which are operated by the CHMI. Of these 127 stations, 80 are automated [22].

Even though Czech ambient air quality improved substantially after 2000, the levels for some ambient air pollutants are still not satisfactory [22]. Aerosol/suspended particles, ground-level ozone and benzo[a]pyrene are considered the major problems, similarly to elsewhere in Europe [106].

The national legislation on air quality management evaluation in the Czech Republic is based on European legislation. The basic legislative norm in the CR is Act No. 201/2012 Coll., on air protection as amended (‘Air Protection Act’). The ambient air quality is observed and monitored by a nationwide long-term monitoring network operated by the Czech Hydrometeorological Institute (CHMI) [22]. CHMI, an institute designated to monitor and assess the ambient air quality in the CR, focusses its activities mainly on covering the criteria pollutants, i.e., the pollutants for which limit values were set up on the basis of WHO recommendations [107,108] by relevant national legislation. In accordance with EU legislation [109], these are in particular SO<sub>2</sub>, NO<sub>x</sub>, PM<sub>10</sub>, PM<sub>2.5</sub>, CO, benzene, benzo[a]pyrene, and toxic metals in aerosol (Pb, Cd, As, Hg), monitored on a regular basis. Currently, due to historic reasons, the CR belongs to the countries with the densest monitoring networks [110]. Nevertheless, in accordance with legislation, the major regular monitoring activities are focused primarily on highly populated major urban agglomerations, whereas monitoring in smaller towns and communities is scarce, in spite of the fact that there are strong indications that they are highly polluted in particular

due to local heating emissions, and in reality they are inhabited by a considerable share of the Czech population [111–113].

CHMI runs two types of stations: automated and manually operated. The automated stations measure continuously and give 1 h mean concentrations, whereas the manually operated stations give 24 h mean concentrations. Precipitation chemistry is sampled on a monthly or weekly basis by automated wet-only samplers. All the measured air quality data are stored in a central nationwide ambient air database, ISKO (the Czech acronym for the Air Quality Information System) [22]. In addition, a supersite observatory, Košetice, is run by the CHMI, participating in numerous international activities, including long-term programmes and scientific projects [114]. The regular annual reports providing detailed information on air quality are available and can be downloaded at the CHMI website [115] in Czech and English versions. The results of continuous monitoring are summarised and presented in user-friendly colour maps indicating the hotspot areas and problem regions. The results are interpreted in the context of both human health and environmental effects. Apart from these annual graphic yearbooks, long-term analyses are also available [116–118].

Furthermore, in addition to the nationwide ambient air quality monitoring run by the CHMI, numerous other measuring activities are operated by other institutes and organisations for different purposes. These include, e.g., the monitoring of persistent organic pollutants (POPs), which are not explicitly included among the criteria pollutants but are widely recognised as extremely harmful substances (due to their persistency and bioaccumulation) on human health [119–123]. In addition to direct measurement, tree needles and mosses were proven to be useful monitors giving similar information on POPs as high-volume air monitoring [124,125].

With regard to aerosol, not only lawful mass concentration, but also particle number concentration (particle number size distribution) is measured, suitable in particular for aerosol dynamics and source apportionment studies [126–128]. In addition, the main fractions of carbonaceous aerosols, i.e., organic carbon (OC) and elemental carbon (EC) are measured in both urban and rural areas [129,130].

#### 4.1. Aerosol

Aerosol, or suspended particles, is considered to be a major air pollution problem in the CR, similarly to elsewhere [106]. According to the latest annual report [22] providing an assessment of ambient air quality based on established limit values [109], in 2018, the daily limit value of  $50 \mu\text{g m}^{-3}$  for  $\text{PM}_{10}$  was exceeded over 3.2% of the entire territory of the CR (in a grid of  $1 \times 1 \text{ km}$ ) inhabited by approximately 14% of the population; the annual limit value of  $40 \mu\text{g m}^{-3}$  for  $\text{PM}_{10}$  was exceeded at 0.1% of the entire territory of the CR with approximately 0.3% of the population. The annual limit value of  $25 \mu\text{g m}^{-3}$  for fine fraction of  $\text{PM}_{2.5}$  was exceeded in 1.2% of the entire territory of the CR inhabited by approximately 6.1% of the population. The annual limit value of  $1 \text{ ng m}^{-3}$  for benzo[a]pyrene, an established human carcinogen [131,132] related to  $\text{PM}_{2.5}$  aerosol fraction and indicator of polycyclic aromatic hydrocarbons (PAHs) exposure, was exceeded in a number of cities and municipalities, on 12.6% of the entire CR territory inhabited by an astounding 35.5% of the country's inhabitants [22]. The trends in BaP based on long-term monitoring by the CHMI at several suburban sites, representing the exposure in residential areas of Czech cities in 2004–2018 are presented in Figure 12.

With respect to PAHs as a group, a study [133] measuring 15 PAHs (including seven which are carcinogenic) in  $\text{PM}_1$  in the winters of 2013 and 2017 in industrial, urban and rural sites indicated values ranging between  $60.8 \text{ ng m}^{-3}$  (in the city of Ostrava) and  $11.7 \text{ ng m}^{-3}$  (in the small town of Čelákovice). The burning of biomass and coal used for residential heating in old-style boilers emits high PaH concentrations in particular [134]. PAH concentrations linked to local heating, as one of the important sources, were also found at the National Atmospheric Observatory Košetice (NAOK), a rural background site in the CR [135]. Particle-bound carcinogenic PAHs concentration may be applied as an indicator for estimation of the biologically active (mutagenic, genotoxic, embryotoxic) components used for epidemiological studies of the effects of air pollution on human health [136].

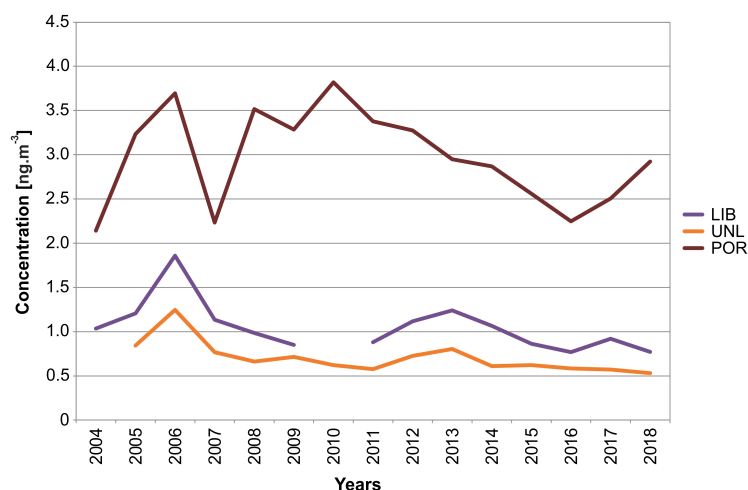


**Figure 12.** Trends in ambient annual mean BaP concentrations at selected sites (see Table 1, Figure 2), 2004–2018, based on CHMI data.

Due to long-term monitoring results, the Moravian-Silesian region/Ostrava region is recognised not only as a Czech hotspot for PM and BaP, but also truly as a European hotspot [22,106]. Ambient BaP concentrations frequently exceed the limit value of  $1 \text{ ng m}^{-3}$  at some sites of this region by seven to nine times [22]. The Ostrava region, with its concentrated heavy industry was in the past nicknamed the steel heart of the country. The heavy air pollution in this region results from several major sources, such as traditional steel and coke plants, local heating (with common burning of waste or coal powder) and traffic and, last but not least, by regional transport of polluted air masses from industrial parts of Poland [137–143]. Industry is apparently the major source of ultrafine particles (UFP) [144,145], the aerosol fraction which is blamed for the strongest effects on human health [146].

The local heating systems in Czech towns and villages burning either coal or wood also contribute substantially to PM exposures [111–113,147–149]. It is estimated that nearly 20% of the households in the CR are heated individually by the combustion of solid fuels [150]. That wood burning might be a dominant source of  $\text{PM}_{10}$  mass followed by coal combustion was somewhat surprisingly demonstrated even for the residential section of Mladá Boleslav, an industrial town famous for its large Skoda automotive factory [151]. Moreover, an incorrectly led combustion process [152], including the co-combustion of fuel with municipal waste, which is a common (though banned) practise in some regions (in particular with low-income residents who use this practise due to economic reasons), adds substantially to both PM and BaP emissions [153]. Currently, a programme subsidising the change of old types of manually operated boilers, which do not meet the emission requirements of European legislation [154] is under way, promoted and supported by the Ministry for the Environment.

All kinds of transport add substantially to this pollution and road vehicles in some places might even be the principal source of aerosol, such as in Prague, with a still unfinished city bypass and the major roads crossing the very centre of the city [155,156]. The hotspots are to be found in particular at places along the main roads, as was shown, e.g., in a study aimed to quantify the UFP exposure in the breathing zone in residential neighbourhoods of streets [157].

Serious health outcomes, including genotoxicity, due to the permanent high ambient PM and BaP exposures were reported for the Ostrava region by several studies conducted recently [158–163]. Furthermore, a moderately strong association between air pollutant concentrations and respiratory difficulties among asthmatic children and adolescents was reported [164]. The association between particle number and  $\text{PM}_{2.5}$  concentrations and daily hospital admissions due to cardiovascular and respiratory diseases was reported for Prague [165]. A long-term study of the health impacts of air pollution on children in heavily polluted parts of the CR revealed that air pollution significantly affected children's health and resulted in increased respiratory morbidity [166,167].

#### 4.2. Ground-Level Ozone

Ground-level O<sub>3</sub>, recognized as an air pollutant only recently, has been monitored in the CR since 1993. Though emissions of O<sub>3</sub> precursors have decreased substantially (NO<sub>x</sub>, VOC and CO by approximately one half and CH<sub>4</sub> by one quarter in the CR and in neighbouring countries), no corresponding decrease in O<sub>3</sub> ambient levels has been observed. In a thorough time trend analysis of continuous data from 26 long-term monitoring sites of various types (urban, mountain, rural) reflecting different environments in 1994–2015, statistically significant decreasing trends were recorded only at about one-half of these [117]. The fact that O<sub>3</sub> concentrations show high year-to-year variability due to their strong dependence on meteorological conditions of the specific year [168–170] was demonstrated also on the Czech data [171]. Both meteorology and air pollution (precursor emissions) are responsible for day-to-day variability in O<sub>3</sub> concentrations. This was shown for five Czech rural sites representing middle-elevated forests in Central Europe, where daily O<sub>3</sub> levels were significantly associated with air temperature, global solar radiation, relative humidity and ambient NO<sub>x</sub> concentrations, the association being highly non-linear [172]. The phytotoxic potential of O<sub>3</sub>, expressed by exposure index for forests AOT40F—a measure of potential effects as used throughout Europe [173]—is high for most of the CR [110,174,175]. The highest AOT40F values observed reached 38–39 ppm h; and the critical level for forest protection of 5 ppm h is usually exceeded early in the growing season, generally in May, at most of the measuring sites [176]. The O<sub>3</sub> spatial exposure pattern correlates strongly with the map showing global solar radiation across the CR [177]. The highest O<sub>3</sub> exposures are found in the relatively unpolluted, with respect to other pollutants, southern portions of the CR [172]. The O<sub>3</sub> concentrations increase with the altitude, whereas the increase of AOT40 with rising altitude is less clear [178].

Apart from long-term monitoring sites, measuring pollution continuously using the reference method as declared by the EU, as well as standard Quality Assurance/Quality Control (QA/QC) procedures (EC, 2008), for developing more detailed O<sub>3</sub> spatial patterns in more detailed scales, diffusive (passive) samplers were used. According to recommendations given by Krupa and Legge [179], these were used for indicative measurements within environmental studies conducted in protected natural areas (the Jizerské hory Mts., Orlické hory Mts., Novohradské hory Mts. and České Švýcarsko National Park), in complex, less accessible terrain in forested mountain areas without electricity available for standard measurements, and proved very successful, offering high precision and accuracy [180–183].

To date, published papers on the O<sub>3</sub> biological effects on Czech forests are ambiguous [183–188]. However, despite the fact that the recorded O<sub>3</sub> concentrations are fairly high, no serious harmful effects attributable to O<sub>3</sub> have been published so far. This conclusion, i.e., that there is no clear field evidence in forests under high O<sub>3</sub> concentrations in the CR, corresponds with similar reports from studies conducted throughout Europe (e.g., [189]).

In contrast to environmental studies, epidemiological studies indicated clear O<sub>3</sub> impacts on human health. In a five-year study (2002–2006) in Prague, including the 2003 and 2006 ozone abundant summer seasons, a statistically significant association between O<sub>3</sub> levels and daily mortality from respiratory diseases was revealed [187]. A relative risk of 1.080 (95% CI: 1.031–1.132) was observed for mortality from respiratory diseases per 10 µg m<sup>-3</sup> increase in 1 day lagged daily mean O<sub>3</sub> concentrations, which acknowledged that O<sub>3</sub> exposure in Prague, though lower when compared to many other European cities, is high enough to influence human health adversely [190]. This factor should be examined more with respect to climate change with an increasing frequency of extreme weather, including heat waves [191].

#### 4.3. Atmospheric Deposition

Atmospheric deposition, as an important self-cleaning process of the atmosphere, removes air pollutants from the air on one hand, while on the other hand it acts as a contamination source for other spheres, such as the hydrosphere, pedosphere and biosphere [170]. The long-term monitoring results have shown a significant decrease in sulphur deposition at most measuring sites [94,116,192]. The spatial pattern of changes in sulphur deposition fluxes between 1995 and 2011 revealed a decrease

over forested areas in a wide range of  $18.1$  to  $0.2 \text{ g m}^{-2} \text{ year}^{-1}$  with the highest improvement in the formerly most heavily impacted areas [116]. In contrast, nitrogen deposition has not improved much, and its spatial patterns are far more complex. The highest decrease in N deposition flux between 1995 and 2011 was a mere  $2.5 \text{ g m}^{-2} \text{ year}^{-1}$  in the formerly most heavily impacted areas, a stagnation in Southern and Northern Moravia and a mild increase of  $0.4 \text{ g m}^{-2} \text{ year}^{-1}$  in the Jizerské Mts., close to the Polish and German borders [116]. The trends in air pollutant emissions are reflected in changes in atmospheric chemistry and deposition, including changing proportions of the ion ratios of  $\text{NO}_3^-/\text{SO}_4^{2-}$ ,  $\text{NH}_4^+/\text{SO}_4^{2-}$  and  $\text{NH}_4^+/\text{NO}_3^-$  in precipitation [94,116,193].

Similarly as in other regions of Europe and US [194,195], it was demonstrated that in the CR, by not considering (1) deposition path via fog and (2) unmeasured constituents of dry deposition, such as  $\text{NH}_3$  and  $\text{HNO}_3(\text{g})$ , the total sulphur and nitrogen depositions are likely to be underestimated substantially [196,197]. Although the chemistry of fog is regularly observed at only a few sites in the CR, and information on fog chemistry is scarce [198,199], it is widely recognised that fog in the CR is enriched as compared to rain, particularly in  $\text{SO}_4^{2-}$  and  $\text{NO}_3^-$  [103,104,200]. Moreover, the hydrological input of fog, namely in forested mountain areas, in the CR above 800 m above sea level might not be negligible [201].  $\text{SO}_2$  and  $\text{NO}_x$ , precursors of  $\text{SO}_4^{2-}$  and  $\text{NO}_3^-$  in fog, were shown to be (apart from the relative humidity) significant explanatory variables modelling the fog probability at Czech sites [202]. The fog pathway should definitely be accounted for in real deposition flux studies, although fog occurrence in the CR has decreased significantly over the last sixty years [203]. The chemistry of rime (as a part of horizontal deposition) has been studied recently at 10 regional mountain-top sites in the CR [204–207], nevertheless the contribution of rime to atmospheric deposition has been unclear thus far.

Improving ambient air quality and decreasing atmospheric deposition have also been demonstrated by long-term nationwide biomonitoring, including analyses of mosses and tree bark [208–213]. Furthermore, peat bogs proved useful for reflecting the history of heavy metal atmospheric deposition. An analysis of historical rates of Pb deposition over the past 150–200 years using  $^{210}\text{Pb}$  dated in sphagnum-derived peat cores peaking in 1965–1992 confirmed a period of the highest production and burning of local lignite [214]. Peaks in Hg accumulation rates in peat cores were indicated between the 1950s and 1980s, reflecting the emissions from intensive coal burning in Central Europe [215]. Moreover, tree rings can be used as an archive for air pollution as was demonstrated for the Pb and  $^{206}\text{Pb}/^{207}\text{Pb}$  ratio [216]. A decrease in arsenic deposition for the Orlické hory Mts. (Adlergebirge) near the Czech–Polish border in the winters of 1984–1986 and 2003–2015 was reported by Doušová et al. [217].

Recovery from acid deposition with respect to changes in soil, stream water and lake water chemistry was reported from numerous places in the CR after the  $\text{SO}_2$  and  $\text{NO}_x$  emission reduction in Central Europe [218–222]. Nevertheless, in spite of a certain N deposition decrease, it was indicated that Czech forest soil horizons up to 20 cm in depth are still affected by a high N input [223], and in some regions elevated N deposition results in soil nutrient imbalances, in particular between nitrogen and phosphorus and nitrogen and magnesium [224]. Consequently, a higher proportion of nitrophilous species was detected in Czech forests during recent decades [225]. It was shown that a high acidic deposition, apart from geographical variables affects the climate–growth association of *Picea abies*, the most important tree species in the CR [226,227].

## 5. Conclusions

This review presents the ambient air quality development over the last 70 years in the territory of the modern-day Czech Republic. Major activities and achievements in ambient air quality management are indicated. The long-term nationwide monitoring results are supplemented by goal-directed one-time studies. Furthermore, apart from the air quality itself, the ambient air pollution impacts on both human health and the environment are collated.

It is obvious that much has been done in air pollution prevention, and that ambient air quality in the CR has improved substantially over the period under review due to newly introduced stringent

legislation and technical countermeasures. Nevertheless, there are still activities which remain significant emission sources, such as local heating and vehicle transport travelling through communities, which are political issues that are hard to manage. The share of the population permanently exposed to PM and BaP concentrations above limit values remains considerable, and O<sub>3</sub> exposure for both humans and the environment is of high concern. Furthermore, despite significant emission reduction, atmospheric deposition, in particular of nitrogen, remains high in some regions.

Long-term ambient air quality monitoring has generated a vast database, which is still, in spite of numerous published studies, largely unexplored. This invaluable source of information should be examined more thoroughly. An association of historical and modern-day results might be one of the interesting goals for future analysis, offering a new perspective. Moreover, the ambient air quality data offer a unique input for large environmental studies and models, exploring in detail how air pollution affects the biosphere and hydrosphere, including forest, agricultural, natural and water ecosystems.

**Funding:** Open Access and Article Processing Charge was funded by the Czech Hydrometeorological Institute research project “Dlouhodobá koncepce rozvoje výzkumné organizace (DKRVO) Český hydrometeorologický ústav na období 2018–2022” financed by the Czech Ministry of Environment.

**Acknowledgments:** I would like to thank Petra Tichá and Jana Schováňková, both from the Czech Hydrometeorological Institute, for preparing Figure 2, Figure 3, Figure 4, Figure 5, Figure 6, Figure 7, Figure 8, Figure 9, Figure 10, Figure 11 and Figure 12 and Erin Naillon for proofreading of this manuscript.

**Conflicts of Interest:** The author declares no conflict of interest.

## References

1. Mejstřík, V. Air pollution and some aspects of the ecotoxicological situation in Czechoslovakia. *Sci. Total Environ.* **1993**, *134* (Suppl. 1), 207–215. [CrossRef]
2. Mikoláš, J. Environment in Czechoslovakia: Today and Tomorrow. In *Strategisches Management Global*; Hammer, R.M., Hinterhuber, H.H., Kutis, P., Turnheim, G., Eds.; Gabler Verlag: Wiesbaden, Germany, 1993; Available online: [http://link.springer.com/chapter/10.1007/978-3-322-89350-5\\_8](http://link.springer.com/chapter/10.1007/978-3-322-89350-5_8) (accessed on 10 September 2019).
3. Kuskova, P.; Gingrich, S.; Krausmann, F. Long term changes in social metabolism and land use in Czechoslovakia, 1830–2000: An energy transition under changing political regimes. *Ecol. Econ.* **2008**, *68*, 394–407. [CrossRef]
4. Kovanda, J.; Hak, T. Historical perspectives of material use in Czechoslovakia in 1855–2007. *Ecol. Indic.* **2011**, *11*, 1375–1384. [CrossRef]
5. Staller, G.J. Czechoslovak Industrial Growth: 1948–1959. *Am. Econ. Rev.* **1962**, *52*, 385–407.
6. Valášek, V.; Chytka, L. *Velká Kronika o Hnědém Uhlí: Minulost, Současnost a Budoucnost Těžby Hnědého Uhlí v Severozápadních Čechách (Large Chronicle on Brown Coal: The Past, Present and Future of Brown Coal Mining in North-West Bohemia)*, 1st ed.; G2 Studio: Plzen, Czech Republic, 2009; In Czech.
7. Rubin, E.S. An International Perspective. *J. Air Pollut. Control Assoc.* **1981**, *31*, 349–360. [CrossRef]
8. Kapička, A.; Petrovský, E.; Ustjak, S.; Macháčková, K. Proxy mapping of fly-ash pollution of soils around a coal-burning power plant: A case study in the Czech Republic. *J. Geochem. Explor.* **1999**, *66*, 291–297. [CrossRef]
9. Bouška, V.; Pešek, J. Quality parameters of lignite of the North Bohemian Basin in the Czech Republic in comparison with the world average lignite. *Coal Geol.* **1999**, *49*, 211–235. [CrossRef]
10. Chow, C.-L. Sulfur in coals: A review of geochemistry and origins. *Int. J. Coal Geol.* **2012**, *100*, 1–13. [CrossRef]
11. Pešek, J.; Sivek, M. *Uhlonosné Pánve a Ložiska Černého a Hnědého Uhlí České Republiky (Coal Basins and Deposits of Black and Brown Coal in the Czech Republic)*; ČGS: Praha, Czech Republic, 2012; In Czech.
12. Kurfürst, J. Reasons and measures for reducing sulfur dioxide emission. *Ochr. Ovzduší* **1986**, *18*, 3–6.
13. Bretschneider, B.; Kurfürst, J. *Air Pollution Control: Technology*; Elsevier: Amsterdam, The Netherlands, 1987.
14. Stehlík, J. Dominantní Příčiny Znečištění ovzduší: Spalovací Procesy. (Principal Reasons for Air Pollution: Combustion Processes). In *Kompendium Ochrany Ovzduší*; Kurfurst, J., Ed.; Ekomonitor: Chrudim, Czech Republic, 2008; In Czech.

15. Kurfürst, J.; Musil, Z. Technické prostředky omezování emisí (Technologies for Emission Abatement). In *Kompendium Ochrany Ovzduší*; Kurfürst, J., Ed.; Ekomonitor: Chrudim, Czech Republic, 2008.
16. Moldan, B.; Schnoor, J.L. Czechoslovakia—Examining a Critically Ill Environment. *Environ. Sci. Technol.* **1992**, *26*, 14–21. [[CrossRef](#)]
17. Říha, M.; Stoklasa, J.; Lafarová, M.; Dejmal, I.; Marek, J.; Pakosta, P. *The Environmental Mining Limits in the North Bohemian Lignite Region*; Společnost Pro Krajinu: Prague, Czech Republic, 2011; p. 64.
18. Frantál, B.; Nováková, E. A Curse of Coal? Exploring Unintended Regional Consequences of Coal Energy in the Czech Republic. *Morav. Geogr. Rep.* **2014**, *22*, 55–65. [[CrossRef](#)]
19. Carter, F.W. Pollution problems in post-war Czechoslovakia. *Trans. Inst. Br. Geogr.* **1985**, *10*, 17–44. [[CrossRef](#)]
20. Hrdá, J. (Ed.) *Znečištění Ovzduší v Severočeské Oblasti (Ambient Air Pollution in North Bohemia)*; Výzkumná Zpráva za Úkol P 16-331-453; ČHMÚ: Praha, Czechoslovakia, 1982; In Czech.
21. Nondek, L. Czechoslovak environment. *Nature* **1991**, *354*, 180. [[CrossRef](#)]
22. CHMI. *Air Pollution in the Czech Republic in 2018*; Graphical Yearbook (Czech/English); Czech Hydrometeorological Institute: Prague, Czech Republic, 2019.
23. Stoklasa, J. Environmental Problems in the CSFR: Solutions Through International Cooperation. In *Coping with Crisis in Eastern Europe's Environment*; Alcamo, J., Ed.; IIASA: Lancs, UK, 1992; Available online: <http://pure.iiasa.ac.at/id/eprint/3585/1/XB-92-005.pdf#page=139> (accessed on 4 November 2019).
24. Krásná, V. Některé poznatky ze studia znečištění pražského ovzduší a jeho vlivu na zdravotní stav obyvatelstva (Some findings from examination of Prague's ambient air and its impact on the human health of Prague's inhabitants). *Československá Hygiena* **1960**, *5*, 77–88. (In Czech)
25. Symon, K. Znečištění ovzduší a jeho vztah ke zdravotnímu stavu obyvatelstva (Ambient air pollution and its relation to human health). *Československá Hygiena* **1960**, *5*, 72–79. (In Czech)
26. Böhm, B. *Znečištění Ovzduší v Podkrušnohoří (Ambient Air Pollution in the Podkrusnohori Region)*; Sborník Prací 20; HMÚ: Praha, Czechoslovakia, 1974; In Czech.
27. Bubník, J.; Keder, J. Prognózní a signální systémy ochrany ovzduší v ČSR (Forecasting and signal systems of air quality protection in the CSR). *Meteor. Zpr.* **1986**, *39*, 169–171.
28. Torseth, K.; Aas, W.; Breivik, K.; Fjaeraa, A.M.; Fiebig, M.; Hjelbrekke, A.G.; Myhre, C.L.; Solberg, S.; Yttri, K.E. Introduction to the European Monitoring and Evaluation Programme (EMEP) and observed atmospheric composition change during 1972–2009. *Atmos. Chem. Phys.* **2012**, *12*, 5447–5481. [[CrossRef](#)]
29. Böhm, B. Výzkum regionálního znečištění některých hlavních složek přírodního prostředí (Research of regional pollution of the natural environment). *Meteor. Zpr.* **1986**, *39*, 136–139.
30. Böhm, B.; Gürtlerová, P. Pozorování na regionální stanici GEMS v Košetících (Observations at the GEMS regional station in Košetice). *Meteor. Zpr.* **1986**, *39*, 175–180.
31. Moldan, B.; Veselý, M.; Bartoňová, A. Chemical composition of atmospheric precipitation in Czechoslovakia, 1976–1984-I. Monthly samples. *Atmos. Environ.* **1987**, *21*, 2383–2395. [[CrossRef](#)]
32. Hrdá, J. *Znečištění Ovzduší v Hradecko-Pardubické Oblasti (Ambient Air Pollution in Hradecko-Pardubicko)*; Výzkumná Zpráva za Úkol P 16-331-453; ČHMÚ: Praha, Czechoslovakia, 1982; In Czech.
33. Hrdá, J. (Ed.) *Znečištění Ovzduší v Praze (Ambient Air Pollution in Prague)*; Výzkumná Zpráva za Úkol P 16-331-453; ČHMÚ: Praha, Czechoslovakia, 1983; In Czech.
34. Hrdá, J. *Znečištění Ovzduší v Mělnicko-Neratovické Oblasti (Ambient Air Pollution in Mělnicko-Neratovicko)*; Výzkumná Zpráva za Úkol P 16-331-453; ČHMÚ: Praha, Czechoslovakia, 1983; In Czech.
35. Hrdá, J. *Znečištění Ovzduší v Ostravské Oblasti (Ambient Air Pollution in the Ostrava Region)*; Výzkumná Zpráva za Úkol P 16-331-453; ČHMÚ: Praha, Czechoslovakia, 1984; In Czech.
36. Hrdá, J. *Znečištění Ovzduší v Brně (Ambient Air Pollution in Brno)*; Výzkumná Zpráva za Úkol P 16-331-453; ČHMÚ: Praha, Czechoslovakia, 1984; In Czech.
37. Hrdá, J. *Znečištění Ovzduší v Postižených Oblastech Západočeského Kraje (Ambient Air Pollution in Impacted Areas of West Bohemia)*; Výzkumná Zpráva za Úkol P 16-331-453; ČHMÚ: Praha, Czechoslovakia, 1985; In Czech.
38. Hrdá, J. *Výzkum Znečištění Ovzduší Pro Rozvoj Postižených Oblastí a Vybraných Odvětví Národního Hospodářství (Air Pollution Research for the Development of Contaminated Regions and Selected Branches of the National Economy)*; Závěrečná Zpráva za Úkol P 16-331-453; ČHMÚ: Praha, Czechoslovakia, 1985; In Czech.
39. Bubník, J. Analýza výsledků matematického modelování znečištění ovzduší v postižených oblastech ČSR (Analysis of results of mathematical air pollution modelling in contaminated regions of the CSR). *Meteor. Zpr.* **1986**, *39*, 164–169.

40. Hrdá, J. Výzkum znečištění ovzduší pro rozvoj postižených oblastí a vybraných odvětví národního hospodářství (Air pollution research for the development of contaminated regions and selected branches of the national economy). *Meteor. Zpr.* **1986**, *39*, 134–136.
41. Weiss, K.; Hůnová, I.; Štengl, B. Znečištění ovzduší v postižených oblastech ČSR (Air pollution in infested areas of the CSR). *Meteor. Zpr.* **1986**, *39*, 141–146.
42. Symon, K. Aspects of air pollution—a public health hazard in Czechoslovakia. In Proceedings of the Inter-Regional Symposium on Criteria for Air Quality and Methods of Measurement, Geneva, Switzerland, 6–12 August 1963; World Health Organization: Geneva, Switzerland, 1963.
43. Bobak, M.; Marmot, M. East-west Mortality Divide and its Potential Explanations: Proposed Research Agenda. *BMJ* **1996**, *312*, 421. [[CrossRef](#)] [[PubMed](#)]
44. Bobak, M.; Leon, D.A. Air pollution and infant mortality in the Czech Republic, 1986–1988. *Lancet* **1992**, *340*, 1010–1014. [[CrossRef](#)]
45. Šrám, R. (Ed.) *Impact of Air Pollution on Human Health: Teplice Program*; Academia: Praha, Czech Republic, 2001.
46. Beneš, I.; Novák, J.; Pinto, J.P. Air Pollution in Teplice and Prachatice in 1995 and 2003: A Comparison after 8 Years. In *Environmental Health in Central and Eastern Europe*; Donnelly, K.C., Cizmas, L.H., Eds.; Springer: Dordrecht, The Netherlands, 2006.
47. Šrám, R.J.; Beneš, I.; Binková, B.; Dejmek, J.; Horstman, D.; Kotěšovec, F.; Otto, D.; Perreault, S.D.; Rubeš, J.; Selevan, S.G.; et al. Teplice program—the impact of air pollution on human health. *Environ. Health Perspect.* **1996**, *104*, 699–714.
48. Dostál, M.; Hertz-Picciotto, I.; Keller, J.R.; Dejmek, J.; Selevan, S.; Kotěšovec, F.; Nozicka, J.; Gomez-Caminero, A.; Wegienka, G.; Srám, R. Childhood morbidity and air pollution in the Teplice program. *Casopis Lekarů Českých* **2001**, *140*, 658–661.
49. Rubeš, J.; Selevan, S.G.; Evenson, D.P.; Zudova, D.; Vozdova, M.; Zudova, Z.; Robbins, W.A.; Perreault, S.D. Episodic air pollution is associated with increased DNA fragmentation in human sperm without other changes in semen quality. *Hum. Reprod.* **2005**, *20*, 2776–2783. [[CrossRef](#)]
50. Slovík, S. Early needle senescence and thinning of the crown structure of *Picea abies* as induced by chronic SO<sub>2</sub> pollution. II. Field data basis, model results and tolerance limits. *Glob. Change Biol.* **1996**, *2*, 459–477. [[CrossRef](#)]
51. Vacek, S.; Lepš, J. Changes in the Horizontal Structure in a Spruce Forest over a 9-year Period of Pollutant Exposure in the Krkonoše Mountains, Czechoslovakia. *For. Ecol. Manag.* **1987**, *22*, 291–295. [[CrossRef](#)]
52. Ardö, J. *Remote Sensing of Forest Decline in the Czech Republic*; Lund University Press: Lund, Sweden, 1998; Available online: <http://citeseerx.ist.psu.edu/viewdoc/download?doi=10.1.1.494.2210&rep=rep1&type=pdf> (accessed on 2 November 2019).
53. Emmer, I.M.; Fanta, J.; Kobus, A.T.; Kooijman, A.; Sevink, J. Reversing borealization as a means to restore biodiversity in Central-European mountain forests—An example from the Krkonoše Mountains, Czech Republic. *Biodivers. Conserv.* **1998**, *7*, 229–247. [[CrossRef](#)]
54. Akselsson, C.; Ardö, J.; Sverdrup, H. Critical Loads of Acidity for Forest Soils and Relationship to Forest Decline in the Northern Czech Republic. *Environ. Monit. Assess.* **2004**, *98*, 363–379. [[CrossRef](#)] [[PubMed](#)]
55. Hofmeister, J.; Oulehle, F.; Krám, P.; Hruška, J. Loss of nutrients due to litter raking compared to the effect of acidic deposition in two spruce stands, Czech Republic. *Biogeochemistry* **2008**, *88*, 139–151. [[CrossRef](#)]
56. Vacek, S.; Hůnová, I.; Vacek, Z.; Hejčmanová, P.; Podrázský, V.; Král, J.; Putalová, T.; Keith Moser, W. Effects of air pollution and climatic factors on Norway spruce forests in the Orlické hory Mts. (Czech Republic) 1979–2014. *Eur. J. For. Res.* **2015**, *134*, 1127–1142. [[CrossRef](#)]
57. Vacek, S.; Vacek, Z.; Remeš, J.; Bílek, L.; Hůnová, I.; Bulušek, D.; Putalová, T.; Král, J.; Simon, J. Sensitivity of unmanaged relict pine forest in the Czech Republic to climate change and air pollution. *Trees* **2017**, *31*, 1599–1617. [[CrossRef](#)]
58. Stoklasa, J.; Duinker, P. *Social and Economic Consequences of Forest Decline in Czechoslovakia*; IIASA Working Paper WP-88-028; IIASA: Laxenburg, Austria, 1988; Available online: <http://pure.iiasa.ac.at/id/eprint/3177/1/WP-88-028.pdf> (accessed on 10 October 2019).
59. Materna, J. Air pollution and forestry in Czechoslovakia. *Environ. Monit. Assess.* **1989**, *12*, 227–235. [[CrossRef](#)]
60. Kubíková, J. Forest dieback in Czechoslovakia. *Vegetatio* **1991**, *93*, 101–108. [[CrossRef](#)]

61. Fanta, J. Rehabilitating degraded forests in Central Europe into self-sustaining forest ecosystems. *Ecol. Eng.* **1997**, *8*, 289–297. [[CrossRef](#)]
62. Moldan, B.; Hak, T. Environment in the Czech Republic: A Positive and Rapid Change. *Environ. Sci. Technol.* **2007**, *41*, 358–362. [[CrossRef](#)]
63. Carrier, J.-G.; Krippel, E. Comprehensive Study of European Forests Assess Damage and Economic Losses from Air Pollution. *Environ. Conserv. J.* **1990**, *17*, 365–366. [[CrossRef](#)]
64. Lomský, B.; Materna, J.; Pfanz, H. (Eds.) *SO<sub>2</sub>-Pollution and Forests Decline in the Ore Mountains*; VÚLHM: Praha, Czech Republic, 2002; p. 342.
65. Mazurski, K.R. Communism and the Environment. *Forum Appl. Res. Policy* **1991**, *5*, 39–44.
66. Newman, J.R.; Novakova, E.; McClave, J.T. The influence of industrial air emissions on the nesting ecology of the house martin *Delichon urbica* in Czechoslovakia. *Biol. Conserv.* **1985**, *31*, 229–248. [[CrossRef](#)]
67. Kierdorf, U.; Bahelková, P.; Sedláček, F.; Kierdorf, H. Pronounced reduction of fluoride exposure in free-ranging deer in North Bohemia (Czech Republic) as indicated by the biomarkers skeletal fluoride content and dental fluorosis. *Sci. Total Environ.* **2012**, *414*, 686–695. [[CrossRef](#)] [[PubMed](#)]
68. Ustýak, S.; Petrikova, V. Heavy metal pollution of soils and crops in Northern Bohemia. *Appl. Geochem.* **1996**, *11*, 77–80. [[CrossRef](#)]
69. Peters, N.E.; Cerny, J.; Havel, M.; Krejci, R. Temporal trends of bulk precipitation and stream waterchemistry in a small forested area, Krusnehořy, northern Bohemia, Czech Republic. *Hydrol. Process.* **1999**, *13*, 2721–2741. [[CrossRef](#)]
70. Vesely, J.; Almquist-Jacobson, H.; Miller, L.M.; Norton, S.A.; Appleby, P.; Dixit, A.S.; Smol, J.P. The history and impact of air pollution at Čertovo Lake, southwestern Czech Republic. *J. Paleolimnol.* **1993**, *8*, 211–231. [[CrossRef](#)]
71. Kramer, J. The Environmental Crisis in Eastern Europe: The Price for Progress. *Slav. Rev.* **1983**, *42*, 204–220. [[CrossRef](#)]
72. Godzik, S. Air Pollution Problems in Some Central European Countries—Czechoslovakia, the German Democratic Republic and Poland. In *Gaseous Air Pollutants and Plant Metabolism*; Koziol, M.J., Whatley, F.R., Eds.; Butterworth: London, UK, 1984.
73. Turnock, D. Environmental problems and policies in East Central Europe: A changing agenda. *GeoJournal* **2001**, *54*, 485–505. [[CrossRef](#)]
74. Jedrychowski, W. Review of Recent Studies from Central and Eastern Europe Associating Respiratory Health Effects with High Levels of Exposure to “Traditional” Air Pollutants. *Environ. Health Perspect.* **1995**, *103*, 15–21.
75. Rao, S.T.; Hogrefe, C.; Holloway, T.; Kallos, G. Long-Range Transport of Atmospheric Pollutants and Transboundary Pollution. In *World Atlas of Atmospheric Pollution*; Sokhi, R.S., Ed.; Anthem Press: London, UK, 2008.
76. Dovland, H. Monitoring European Transboundary Air Pollution. *Environ. Sci. Policy Sustain. Dev.* **1987**, *29*, 10–28. [[CrossRef](#)]
77. Hendrey, G.R.; Baalsrud, K.; Traaen, T.S.; Laake, M.; Raddum, G. Acid Precipitation: Some Hydrobiological Changes. *Ambio* **1976**, *5*, 224–227.
78. Tamm, C.O. Acid Precipitation: Biological Effects in Soil and on Forest Vegetation. *Ambio* **1976**, *5*, 235–238.
79. Bengtsson, B.; Dickson, W.; Nyberg, P. Liming Acid Lakes in Sweden. *Ambio* **1980**, *9*, 34–36.
80. Binkley, D.; Hogberg, P. Tamm Review: Revisiting the influence of nitrogen on Swedish forests. *For. Ecol. Manag.* **2016**, *368*, 222–239. [[CrossRef](#)]
81. Vrablik, P.; Wildova, E.; Vrablikova, J. The Effect of Brown Coal Mining on the Environment and Health of the Population in Northern Bohemia (Czech Republic). *Int. J. Clean Coal Energy* **2017**, *6*, 1–13. [[CrossRef](#)]
82. Šauer, P.; Mádr, M. Economic growth and air pollution in the Czech Republic: Decoupling curves. *IJEF* **2012**, *4*, 205–213.
83. Fagin, A. Environmental Capacity Building in the Czech Republic. *Environ. Plan. A* **2001**, *33*, 589–606. [[CrossRef](#)]
84. Kára, J. Geopolitics and the Environment: The Case of Central Europe. *Environ. Polit.* **1992**, *1*, 186–195. [[CrossRef](#)]
85. Waller, M.; Millard, F. Environmental politics in Eastern Europe. *Environ. Polit.* **1992**, *1*, 159–185. [[CrossRef](#)]

86. Fagin, A. The development of civil society in the Czech Republic: The environmental sector as a measure of associational activity. *J. Eur. Area Stud.* **1999**, *7*, 91–108. [CrossRef]
87. Shriver, T.E.; Adams, A.E. Cycles of Repression and Tactical Innovation: The Evolution of Environmental Dissidence in Communist Czechoslovakia. *Sociol. Q.* **2010**, *51*, 329–354. [CrossRef]
88. Vavroušek, J. Environmental management in Czechoslovakia and succession states. *Environ. Impact Assess. Rev.* **1994**, *14*, 103–110. [CrossRef]
89. Vestreng, V.; Myhre, G.; Fagerli, H.; Reis, S.; Tarrasón, L. Twenty-five years of continuous sulphur dioxide emission reduction in Europe. *Atmos. Chem. Phys.* **2007**, *7*, 3663–3681. [CrossRef]
90. Braniš, M. Particulate Emission Inventory and Trends in Ambient Particulate Matter Concentrations in the Czech Republic between 1993 and 1999. *Environ. Monit. Assess.* **2003**, *87*, 123–132. [CrossRef]
91. CHMI. *Air Pollution in the Czech Republic in 2012*; Graphical Yearbook (Czech/English); Czech Hydrometeorological Institute: Prague, Czech Republic, 2013.
92. Pavlínek, P.; Pickles, J. Environmental Pasts/Environmental Futures in Post-socialist Europe. *Environ. Polit.* **2004**, *13*, 237–265. [CrossRef]
93. Fiala, J.; Rieder, M.; Dvořáková, M.; Livorová, H. Trends in the atmospheric and hydrological cycle of sulphur at catchments in the Czech Republic. *Atmos. Environ.* **2001**, *35* (Suppl. 1), S55–S62. [CrossRef]
94. Hůnová, I.; Šantroch, J.; Ostatnická, J. Ambient Air Quality and Deposition Trends at Rural Stations in the Czech Republic during 1993–2001. *Atmos. Environ.* **2004**, *38*, 887–898. [CrossRef]
95. Kopáček, J.; Veselý, J. Sulfur and nitrogen emissions in the Czech Republic and Slovakia from 1850 till 2000. *Atmos. Environ.* **2005**, *39*, 2179–2188. [CrossRef]
96. Kerimray, A.; Rojas-Solórzano, L.; Torkmahalleh, M.A.; Hopke, P.K.; Gallachoir, B.P.O. Coal use for residential heating: Patterns, health implications and lessons learned. *Energy Sustain. Dev.* **2017**, *40*, 19–30. [CrossRef]
97. EMEP. 2019. Available online: <https://www.ceip.at/webdab-emission-database> (accessed on 20 September 2019).
98. Watts, R.; Lewtas, J.; Stevens, R.; Haerlage, T.; Pinto, J.; Williams, R.; Hattaway, K.; Míšková, I.; Beneš, I.; Kotěšovec, F.; et al. Czech-U.S. EPA Health Study: Assessment of Personal and Ambient Air Exposures to Pah and Organic Mutagens in the Teplice District of Northern Bohemia. *Int. J. Environ. Anal. Chem.* **1994**, *56*, 271–287. [CrossRef]
99. Pinto, J.P.; Stevens, R.K.; Willis, R.D.; Kellogg, R.; Mamane, Y.; Novak, J.; Šantroch, J.; Benes, I.; Lenicek, J.; Bures, V. Czech Air Quality Monitoring and Receptor Modeling Study. *Environ. Sci. Technol.* **1998**, *32*, 843–854. [CrossRef]
100. Grønskei, K.E.; Bartonova, A.; Brechler, J.; Walker, S.E.; Larssen, S.J. Air pollution exposure monitoring and estimation VII. Estimation of population exposure in a central European airshed. *Environ. Monit.* **2000**, *2*, 344–350. [CrossRef] [PubMed]
101. Prechtel, A.; Alewell, C.; Armbruster, M.; Bittersohl, J.; Cullen, J.M.; Evans, C.D.; Helliwell, R.; Kopáček, J.; Marchetto, A.; Matzner, E.; et al. Response of sulphur dynamics in European catchments to decreasing sulphate deposition. *Hydrol. Earth Syst. Sci.* **2001**, *5*, 311–325. [CrossRef]
102. Bridges, K.S.; Jickells, T.D.; Davies, T.D.; Zeman, Z.; Hůnová, I. Aerosol, precipitation and cloud water observations on the Czech Krusne Hory plateau adjacent to a heavily industrialised valley. *Atmos. Environ.* **2002**, *36*, 353–360. [CrossRef]
103. Bridgman, H.A.; Davies, T.D.; Jickells, T.; Hůnová, I.; Tovey, K.; Bridges, K.; Surapipith, V. Air pollution in the Krusne hory region, Czech Republic during the 1990s. *Atmos. Environ.* **2002**, *36*, 3375–3389. [CrossRef]
104. Houthuis, D.; Breugelmans, O.; Hoek, G.; Vaskovi, E.; Miháliková, E.; Pastuszka, J.S.; Jirik, V.; Sachelarescu, S.; Lolova, D.; Meliefste, K.; et al. PM<sub>10</sub> and PM<sub>2.5</sub> concentrations in Central and Eastern Europe: Results from the Cesar study. *Atmos. Environ.* **2001**, *35*, 2757–2771. [CrossRef]
105. Stanners, D.; Bourdeau, P. *Europe's Environment: The Dobris Assessment*; EEA: Copenhagen, Denmark, 1995.
106. EEA. *Air Quality in Europe—2019 Report*; EEA Report No. 10/2019; EEA: Copenhagen, Denmark, 2019; Available online: <https://www.eea.europa.eu/publications/air-quality-in-europe-2019/air-quality-in-europe-2019/viewfile#pdfjs.action=download> (accessed on 30 November 2019).
107. WHO. *Air Quality Guidelines for Europe*; World Health Organization: Geneva, Switzerland, 1987.
108. WHO. *WHO Air Quality Guidelines for Particulate Matter, Ozone, Nitrogen Dioxide and Sulfur Dioxide*; Global Update 2005; World Health Organization: Geneva, Switzerland, 2006.

109. EC. *Directive 2008/50/EC of the European Parliament and of the Council of 21 May 2008 on Ambient Air Quality and Cleaner Air for Europe*; OJEC L 152; EC: Brussel, Belgium, 2008.
110. Hůnová, I. Spatial Interpretation of ambient air quality for the territory of the Czech Republic. *Environ. Pollut.* **2001**, *112*, 107–119. [[CrossRef](#)]
111. Braniš, M.; Domasová, M. PM10 and black smoke in a small settlement: Case study from the Czech Republic. *Atmos. Environ.* **2003**, *37*, 83–92. [[CrossRef](#)]
112. Braniš, M.; Domasová, M.; Řezáčová, P. Particulate air pollution in a small settlement: The effect of local heating. *Appl. Geochem.* **2007**, *22*, 1255–1264. [[CrossRef](#)]
113. Pokorná, P.; Hovorka, J.; Kroužek, J.; Hopke, P.K. Particulate matter source apportionment in a village situated in industrial region of Central Europe. *J. Air Waste Manag.* **2013**, *63*, 1412–1421. [[CrossRef](#)]
114. Váňa, M.; Holoubek, I.; Pacl, A.; Pekárek, J.; Smrčková, V.; Machálek, P.; Helešic, J.; Šeda, Z.; Adamec, V.; Janouch, M.; et al. *Quality of the Natural Environment in the Czech Republic at the Regional Level; Results of the Kosetice Observatory*; ČHMÚ: Praha, Czechoslovakia, 2001.
115. CHMI Website. Available online: [http://portal.chmi.cz/files/portal/docs/uoco/isko/grafroc/grafroc\\_GB.html](http://portal.chmi.cz/files/portal/docs/uoco/isko/grafroc/grafroc_GB.html) (accessed on 7 January 2020).
116. Hůnová, I.; Maznová, J.; Kurfürst, P. Trends in atmospheric deposition fluxes of sulphur and nitrogen in Czech forests. *Environ. Pollut.* **2014**, *184*, 668–675. [[CrossRef](#)] [[PubMed](#)]
117. Hůnová, I.; Baumelt, V. Observation-based trends in ambient ozone in the Czech Republic over the past two decades. *Atmos. Environ.* **2018**, *172*, 157–167. [[CrossRef](#)]
118. Hůnová, I.; Baumelt, V.; Modlík, M. Long-term trends in nitrogen oxides at different types of monitoring stations in the Czech Republic. *Sci. Total Environ.* **2020**. [[CrossRef](#)]
119. Holoubek, I.; Klánová, J.; Jarkovský, J.; Kohoutek, J. Trends in background levels of persistent organic pollutants at Kosetice observatory, Czech Republic. Part I. Ambient air and wet deposition 1996–2005. *J. Environ. Monit.* **2007**, *9*, 557–563. [[CrossRef](#)] [[PubMed](#)]
120. Holoubek, I.; Houšková, L.; Šeda, L.; Holoubková, I.; Korínek, P.; Boháček, Z.; Čáslavský, J. Project TOCOEN. The fate of selected organic pollutants in the environment II. Air and rainwater 1988. *Toxicol. Environ. Chem.* **1990**, *29*, 19–27. [[CrossRef](#)]
121. Dvorská, A.; Lammel, G.; Klanova, J.; Holoubek, I. Kosetice, Czech Republic—Ten years of air pollution monitoring and four years of evaluating the origin of persistent organic pollutants. *Environ. Pollut.* **2008**, *156*, 403–408. [[CrossRef](#)]
122. Dvorská, A.; Lammel, G.; Holoubek, I. Recent trends of persistent organic pollutants in air in central Europe—Air monitoring in combination with air mass trajectory statistics as a tool to study the effectivity of regional chemical policy. *Atmos. Environ.* **2009**, *43*, 1280–1287. [[CrossRef](#)]
123. Degrendele, C.; Okonski, K.; Melymuk, L.; Landlová, L.; Kukučka, P.; Čupr, P.; Klánová, J. Size specific distribution of the atmospheric particulate PCDD/Fs, dl-PCBs and PAHs on a seasonal scale: Implications for cancer risks from inhalation. *Atmos. Environ.* **2014**, *98*, 410–416. [[CrossRef](#)]
124. Holoubek, I.; Kořínek, P.; Šeda, Z.; Schneiderová, E.; Holoubková, I.; Pacl, A.; Triska, J.; Cudlín, P.; Čáslavský, J. The use of mosses and pine needles to detect persistent organic pollutants at local and regional scales. *Environ. Pollut.* **2000**, *109*, 283–292. [[CrossRef](#)]
125. Klánová, J.; Čupr, P.; Baráková, D.; Šeda, Z.; Anděl, P.; Holoubek, I. Can pine needles indicate trends in the air pollution levels at remote sites? *Environ. Pollut.* **2009**, *157*, 3248–3254. [[CrossRef](#)]
126. Thimmaiah, D.; Hovorka, J.; Hopke, P.K. Source Apportionment of Winter Submicron Prague Aerosols from Combined Particle Number Size Distribution and Gaseous Composition Data. *Aerosol Air Qual. Res.* **2009**, *9*, 209–236. [[CrossRef](#)]
127. Římnáčová, D.; Ždímal, V.; Schwarz, J.; Smolík, J.; Římnáč, M. Atmospheric aerosols in suburb of Prague: The dynamics of particle size distributions. *Atmos. Res.* **2011**, *101*, 539–552. [[CrossRef](#)]
128. Zíková, N.; Ždímal, V. Long-Term Measurement of Aerosol Number Size Distributions at Rural Background Station Košetice. *Aerosol Air Qual. Res.* **2013**, *13*, 1464–1474. [[CrossRef](#)]
129. Schwarz, J.; Chi, X.; Maenhaut, W.; Civiš, M.; Hovorka, J.; Smolík, J. Elemental and organic carbon in atmospheric aerosols at downtown and suburban sites in Prague. *Atmos. Res.* **2008**, *90*, 287–302. [[CrossRef](#)]
130. Vodička, P.; Schwarz, J.; Cusack, M.; Ždímal, V. Detailed comparison of OC/EC aerosol at an urban and a rural Czech background site during summer and winter. *Sci. Total Environ.* **2015**, *518*, 424–433. [[CrossRef](#)]

131. Collins, J.F.; Brown, J.P.; Dawson, S.V.; Marty, M.A. Risk assessment for benzo[a]pyrene. *Regul. Toxicol. Pharm.* **1991**, *13*, 170–184. [[CrossRef](#)]
132. Kim, K.-H.; Jahan, S.A.; Kabir, E.; Brown, R.J.C. A review of airborne polycyclic aromatic hydrocarbons (PAHs) and their human health effects. *Environ. Int.* **2013**, *60*, 71–80. [[CrossRef](#)]
133. Křůmal, K.; Mikuška, P. Mass concentrations and lung cancer risk assessment of PAHs bound to PM<sub>1</sub> aerosol in six industrial, urban and rural areas in the Czech Republic, Central Europe. *Atmos. Pollut. Res.* **2020**, *11*, 401–408. [[CrossRef](#)]
134. Křůmal, K.; Mikuška, P.; Horák, J.; Hopan, F.; Krpec, K. Comparison of emissions of gaseous and particulate pollutants from the combustion of biomass and coal in modern and old-type boilers used for residential heating in the Czech Republic, Central Europe. *Chemosphere* **2019**, *229*, 51–59. [[CrossRef](#)]
135. Lhotka, R.; Pokorná, P.; Zíková, N. Long-Term Trends in PAH Concentrations and Sources at Rural Background Site in Central Europe. *Atmosphere* **2019**, *10*, 687. [[CrossRef](#)]
136. Binková, B.; Černá, M.; Pastorková, A.; Jelínek, R.; Beneš, I.; Novák, J.; Šrám, R. Biological activities of organic compounds adsorbed onto ambient air particles: Comparison between the cities of Teplice and Prague during the summer and winter seasons 2000–2001. *Mutat. Res.* **2003**, *525*, 43–59. [[CrossRef](#)]
137. Pokorná, P.; Hovorka, J.; Klán, M.; Hopke, P.K. Source apportionment of size resolved particulate matter at a European air pollution hot spot. *Sci. Total Environ.* **2015**, *502*, 172–183. [[CrossRef](#)] [[PubMed](#)]
138. Mikuška, P.; Křůmal, K.; Večeřa, Z. Characterization of organic compounds in the PM<sub>2.5</sub> aerosol in winter in an industrial urban area. *Atmos. Environ.* **2015**, *105*, 97–108. [[CrossRef](#)]
139. Vossler, T.; Cernikovský, L.; Novak, J.; Placha, H.; Krejci, B.; Nikolova, I.; Chalupnickova, E.; Williams, R. An investigation of local and regional sources of fine particulate matter in Ostrava, the Czech Republic. *Atmos. Pollut. Res.* **2015**, *6*, 454–463.
140. Černikovský, L.; Krejčí, B.; Blažek, Z.; Volná, V. Transboundary air-pollution transport in the Czech-Polish border region between the cities of Ostrava and Katowice. *Cent. Eur. J. Public Health* **2016**, *24*, S45–S50. [[CrossRef](#)]
141. Pokorná, P.; Hovorka, J.; Hopke, P.K. Elemental composition and source identification of very fine aerosol particles in a European air pollution hot-spot. *Atmos. Pollut. Res.* **2016**, *7*, 671–679. [[CrossRef](#)]
142. Horak, J.; Kubonova, L.; Krpec, K.; Hopan, F.; Kubesa, P.; Motyka, O.; Laciok, V.; Dej, M.; Ochodek, T.; Placha, D. PAH emissions from old and new types of domestic hot water boilers. *Environ. Pollut.* **2017**, *225*, 31–39. [[CrossRef](#)]
143. Kozáková, J.; Pokorná, P.; Vodička, P.; Ondráčková, L.; Ondráček, J.; Křůmal, K.; Mikuška, P.; Hovorka, J.; Moravec, P.; Swarcz, J. The influence of local emissions and regional air pollution transport on a European air pollution hot spot. *Environ. Sci. Pollut. Res.* **2019**, *26*, 1675–1692. [[CrossRef](#)]
144. Leoni, C.; Hovorka, J.; Dočekalová, V.; Cajthaml, T.; Marvanová, S. Source Impact Determination using Airborne and Ground Measurements of Industrial Plumes. *Environ. Sci. Technol.* **2016**, *50*, 18. [[CrossRef](#)]
145. Leoni, C.; Pokorná, P.; Hovorka, J.; Massiol, M.; Topinka, J.; Zhao, Y.; Křůmal, K.; Cliff, S.; Mikuška, P.; Hopke, P.K. Source apportionment of aerosol particles at a European air pollution hot spot using particle number size distributions and chemical composition. *Environ. Pollut.* **2018**, *234*, 145–154. [[CrossRef](#)]
146. Ohlwein, S.; Kappeler, R.; Joss, M.K.; Künzli, N.; Hoffman, B. Health effects of ultrafine particles: A systematic literature review update of epidemiological evidence. *Int. J. Public Health* **2019**, *64*, 547–559. [[CrossRef](#)] [[PubMed](#)]
147. Schwarz, J.; Cusack, M.; Karban, J.; Chalupníčková, E.; Havránek, V.; Smolík, J.; Ždímal, V. PM<sub>2.5</sub> chemical composition at a rural background site in Central Europe, including correlation and air mass back trajectory analysis. *Atmos. Res.* **2016**, *176*, 108–120. [[CrossRef](#)]
148. Pokorná, P.; Hovorka, J.; Břejcha, J. Impact of Mining Activities on the Air Quality in the Village Nearby a Coal Strip Mine. *IOP Conf. Ser. Earth Environ. Sci.* **2016**, *44*, 032021. [[CrossRef](#)]
149. Schladitz, A.; Leníček, J.; Beneš, I.; Kováč, M.; Skorkovský, J.; Soukup, A.; Jandlová, J.; Poulain, L.; Plachá, H.; Loschau, G.; et al. Air quality in the German-Czech border region: A focus on harmful fractions of PM and ultrafine particles. *Atmos. Environ.* **2015**, *122*, 236–249. [[CrossRef](#)]
150. Horák, J.; Hopan, F.; Šyc, M.; Machálek, P.; Krpec, K.; Ocelka, T.; Tomšej, T. Estimation of selected pollutant emissions from solid-fuel combustion in small heating appliances. *Chem. Listy* **2011**, *105*, 851–855.

151. Hovorka, J.; Pokorná, P.; Hopke, P.K.; Krůmal, K.; Mikuška, P.; Pišová, M. Wood combustion, a dominant source of winter aerosol in residential district in proximity to a large automobile factory in Central Europe. *Atmos. Environ.* **2015**, *113*, 98–107. [[CrossRef](#)]
152. Hezina, F.; Švec, H.; Postlová, H. Emise malých spalovacích zdrojů. (Emissions from small combustion sources). *Ochrana Ovzduší* **2013**, *25*, 6–12.
153. Tomšej, T.; Horak, J.; Tomsejova, S.; Krpec, K.; Klanova, J.; Dej, M.; Hopan, F. The impact of co-combustion of polyethylene plastics and wood in a small residential boiler on emissions of gaseous pollutants, particulate matter, PAHs and 1,3,5- triphenylbenzene. *Chemosphere* **2018**, *196*, 18–24. [[CrossRef](#)]
154. CEN. EN 303–5:2012 Heating Boilers—Part 5: Heating Boilers for Solid Fuels, Manually and Automatically Stoked, Nominal Heat Output of up to 500 KW; CEN: Brussels, Belgium, 2012.
155. Braniš, M. Air quality of Prague: Traffic as a main pollution source. *Environ. Monit. Assess.* **2009**, *156*, 377–390. [[CrossRef](#)]
156. Ondráček, J.; Schwarz, J.; Ždímal, V.; Andělová, L.; Vodička, P.; Bízek, V.; Tsai, C.-J.; Chen, S.-C.; Smolík, J. Contribution of the road traffic to air pollution in the Prague city (busy speedway and suburban crossroads). *Atmos. Environ.* **2011**, *45*, 5090–5100. [[CrossRef](#)]
157. Stolcpartova, J.; Pechout, M.; Dittrich, L.; Mazac, M.; Fenkl, M.; Vrbova, K.; Ondracek, J.; Vojtisek-Lom, M. Internal Combustion Engines as the Main Source of Ultrafine Particles in Residential Neighborhoods: Field Measurements in the Czech Republic. *Atmosphere* **2015**, *6*, 1714–1735. [[CrossRef](#)]
158. Rossner, P., Jr.; Topinka, J.; Hovorka, J.; Milcova, A.; Krouzek, J.; Sram, R.J. An acellular assay to assess the genotoxicity of complex mixtures of organic pollutants bound on size segregated aerosol. Part II: Oxidative damage to DNA. *Toxicol. Lett.* **2010**, *198*, 312–316. [[CrossRef](#)]
159. Šrám, R.J.; Dostál, M.; Libalová, H.; Rossner, P.; Rossnerová, A.; Svecova, V.; Topinka, J.; Bartonova, A. The European hot spot of B[a]P and PM<sub>2.5</sub> exposure—the Ostrava region, Czech Republic: Health research results. *ISRN Public Health* **2013**, *2013*. [[CrossRef](#)]
160. Topinka, J.; Hovorka, J.; Milcova, A.; Schmuczerova, J.; Krouzek, J.; Rossner, P.Jr.; Sram, R.J. An acellular assay to assess the genotoxicity of complex mixtures of organic pollutants bound on size segregated aerosol. Part I: DNA adducts. *Toxicol. Lett.* **2010**, *198*, 304–311. [[CrossRef](#)] [[PubMed](#)]
161. Topinka, J.; Milcova, A.; Schmuczerova, J.; Krouzek, J.; Hovorka, J. Ultrafine particles are not major carriers of carcinogenic PAHs and their genotoxicity in size-segregated aerosols. *Mutat. Res. Genet. Toxicol. Environ. Mutagen.* **2013**, *754*, 1–6. [[CrossRef](#)]
162. Topinka, J.; Rossner, P., Jr.; Milcová, A.; Schmurzerová, J.; Pěničková, K.; Rossnerová, A.; Ambrož, A.; Štolcpartová, J.; Bendl, J.; Hovorka, J.; et al. Day-to-day variability of toxic events induced by organic compounds bound to size segregated atmospheric aerosol. *Environ. Pollut.* **2015**, *202*, 135–145. [[CrossRef](#)]
163. Jiřík, V.; Machaczka, O.; Miturová, H.; Tomášek, I.; Šlachťová, H.; Janoutová, J.; Velická, H.; Janout, V. Air Pollution and Potential health risk in Ostrava Region—a review. *Cent. Eur. J. Public Health* **2016**, *24*, S4–S17. [[CrossRef](#)]
164. Velická, H.; Puklová, V.; Keder, J.; Brabec, M.; Malý, M.; Bobák, M.; Kotlík, B.; Jiřík, V.; Janout, V.; Kazmarová, H. Asthma exacerbations and symptom variability in children due to short-term ambient air pollution changes in Ostrava, Czech Republic. *Cent. Eur. J. Public Health* **2015**, *23*, 292–298.
165. Braniš, M.; Vyškovská, J.; Malý, M.; Hovorka, J. Association of size-resolved number concentrations of particulate matter with cardiovascular and respiratory hospital admissions and mortality in Prague, Czech Republic. *Inhal. Toxicol.* **2010**, *22* (Suppl. 2), 21–28. [[CrossRef](#)]
166. Šrám, R.J.; Binkova, B.; Dostal, M.; Merkerova-Dostalova, M.; Libalova, H.; Milcova, A.; Rossner, P.Jr.; Rossnerova, A.; Schmuczerova, J.; Svecova, V.; et al. Health impact of air pollution to children. *Int. J. Hyg. Environ. Health* **2013**, *216*, 533–540. [[CrossRef](#)]
167. Dostal, M.; Pastorkova, A.; Rychlik, S.; Rychlikova, E.; Svecova, V.; Schallerova, E.; Sram, R.J. Comparison of child morbidity in regions of Ostrava, Czech Republic, with different degrees of pollution: A retrospective cohort study. *Environ. Health* **2013**, *12*, 74. [[CrossRef](#)] [[PubMed](#)]
168. Finlayson-Pitts, B.J.; Pitts, J.N. *Chemistry of the Upper and Lower Atmosphere*; Academia Press: San Diego, CA, USA, 2000.
169. Fiala, J.; Cernikovský, L.; de Leeuw, F.; Kurfürst, P. *Air Pollution by Ozone in Europe in Summer 2003*; EEA Topic Report 3/2003; European Environment Agency: Copenhagen, Denmark, 2003.

170. Seinfeld, J.H.; Pandis, S.N. *Atmospheric Chemistry and Physics: From Air Pollution to Climate Change*, 2nd ed.; John Wiley & Sons Inc.: New York, NY, USA, 2006.
171. Hůnová, I.; Brabec, M.; Malý, M. What are the principal factors affecting ambient ozone concentrations in Czech mountain forests? *Front. For. Glob. Change* **2019**. [[CrossRef](#)]
172. Hůnová, I.; Kurfürst, P.; Baláková, L. Areas under high ozone and nitrogen loads are spatially disjunct in Czech forests. *Sci. Total Environ.* **2019**, *656*, 567–575. [[CrossRef](#)] [[PubMed](#)]
173. UN/ECE. Mapping Manual Revision. UN-ECE Convention on Long-Range Transboundary Air Pollution. Manual on the Methodologies and Criteria for Modelling and Mapping Critical Loads and Levels and Air Pollution Effects, Risks and Trends. 2004. Available online: <http://www.icp-mapping.org> (accessed on 15 September 2019).
174. Hůnová, I. Ambient air quality for the territory of the Czech Republic in 1996–1999 expressed by three essential factors. *Sci. Total Environ.* **2003**, *303*, 245–251. [[CrossRef](#)]
175. Hůnová, I.; Livorová, H.; Ostatnická, J. Potential Ambient Ozone Impact on Ecosystems in the Czech Republic as Indicated by Exposure Index AOT40. *Ecol. Indic.* **2003**, *3*, 35–47. [[CrossRef](#)]
176. Hůnová, I.; Schreiberová, M. Ambient ozone phytotoxic potential over the Czech forests as assessed by AOT40. *IForest* **2012**, *5*, 153–162. [[CrossRef](#)]
177. Tolasz, R.; Miková, T.; Valeriánová, A.; Voženílek, V. *Climate Atlas of Czechia*; CHMI: Praha, Czech Republic, 2007.
178. Hůnová, I.; Horálek, J.; Schreiberová, M.; Zapletal, M. Ambient ozone exposure in Czech forests: A GIS-based approach to spatial distribution assessment. *Sci. World J.* **2012**, *10*. [[CrossRef](#)]
179. Krupa, S.V.; Legge, A.H. Passive sampling of ambient, gaseous air pollutants: An assessment from an ecological perspective. *Environ. Pollut.* **2000**, *107*, 31–45. [[CrossRef](#)]
180. Hůnová, I.; Matoušková, L.; Srněnský, R.; Koželková, K. Ozone influence on native vegetation in the Jizerske hory Mts. of the Czech Republic: Results based on ozone exposure and ozone-induced visible symptoms. *Environ. Monit. Assess.* **2011**, *183*, 501–515. [[CrossRef](#)]
181. Hůnová, I.; Stoklasová, P.; Schovánková, J.; Kulasová, A. Spatial and Temporal Trends of Ozone Distribution in the Jizerské hory Mountains of the Czech Republic. *Environ. Sci. Pollut. Res.* **2016**, *23*, 377–387. [[CrossRef](#)]
182. Hůnová, I. Measurements of ground-level ozone in Czech mountain forests: What we have learnt from using diffusive samplers. *Eur. J. Environ. Sci.* **2017**, *7*, 125–129. [[CrossRef](#)]
183. Vlasáková-Matoušková, L.; Hůnová, I. Stomatal ozone flux and visible leaf injury in native juvenile trees of *Fagus Sylvatica*, L.: A field study from the Jizerske hory Mts., the Czech Republic. *Environ. Sci. Pollut. Res.* **2015**, *22*, 10034–10046. [[CrossRef](#)] [[PubMed](#)]
184. Šrámek, V.; Novotný, R.; Bednářová, M.; Uhlířová, H. Monitoring of ozone risk for forest in the Czech Republic: Preliminary results. *Sci. World J.* **2007**, *7*, 78–83. [[CrossRef](#)] [[PubMed](#)]
185. Šrámek, V.; Novotný, R.; Vejpusťková, M.; Hůnová, I.; Uhlířová, H. Monitoring of ozone effects on the vitality and increment of Norway spruce and European beech in Central European forests. *J. Environ. Monit.* **2012**, *14*, 1696–1702. [[CrossRef](#)]
186. Matoušková, L.; Novotný, R.; Hůnová, I.; Buriánek, V. Visible foliar injury as a tool for the assessment of surface ozone impact on native vegetation: A case study from the Jizerske hory Mts. *J. For. Sci.* **2010**, *56*, 177–182. [[CrossRef](#)]
187. Hůnová, I.; Novotný, R.; Uhlířová, H.; Vráblík, T.; Horálek, J.; Lomský, B.; Šrámek, V. The impact of ambient ozone on mountain spruce forests in the Czech Republic as indicated by malondialdehyde. *Environ. Pollut.* **2010**, *158*, 2393–2401. [[CrossRef](#)]
188. Zapletal, M.; Pretel, J.; Chroust, P.; Cudlín, P.; Edwards-Jonášová, M.; Urban, O.; Pokorný, R.; Czerný, R.; Hůnová, I. The influence of climate change on stomatal ozone flux to forest ecosystem. *Environ. Pollut.* **2012**, *169*, 267–273. [[CrossRef](#)]
189. Cailleret, M.; Ferretti, M.; Gessler, A.; Rigling, A.; Schaub, M. Ozone effects on European forest growth—Towards an integrative approach. *J. Ecol.* **2018**, *106*, 1377–1389. [[CrossRef](#)]
190. Hůnová, I.; Malý, M.; Řezáčová, J.; Braniš, M. Association between Ambient Ozone and Health Outcomes in Prague. *Int. Arch. Occup. Environ. Health* **2013**, *86*, 89–97. [[CrossRef](#)]
191. Hůnová, I.; Brabec, M.; Malý, M.; Knobová, V.; Braniš, M. Major heat waves of 2003 and 2006 and health outcomes in Prague. *Air Qual. Atmos. Health* **2017**, *10*, 183–194. [[CrossRef](#)]

192. Fottová, D. Trends in Sulphur and Nitrogen Deposition Fluxes in the GEOMON Network, Czech Republic, between 1994 and 2000. *Water Air Soil Pollut.* **2003**, *150*, 73–87. [[CrossRef](#)]
193. Hůnová, I.; Kurfürst, P.; Stráník, V.; Modlík, M. Nitrogen deposition to forest ecosystems with focus on its different forms. *Sci. Total Environ.* **2017**, *575*, 791–798. [[CrossRef](#)] [[PubMed](#)]
194. Bytnerowicz, A.; Fenn, M.E. Nitrogen deposition in California forests: A review. *Environ. Pollut.* **1996**, *92*, 127–146. [[CrossRef](#)]
195. Thimonier, A.; Kosonen, Z.; Braun, S.; Rihm, B.; Schleppe, P.; Schmitt, M.; Seidler, E.; Waldner, P.; Thoni, L. Total deposition of nitrogen in Swiss forests: Comparison of assessment methods and evaluation of changes over two decades. *Atmos. Environ.* **2019**, *198*, 335–350. [[CrossRef](#)]
196. Hůnová, I.; Kurfürst, P.; Maznová, J.; Coňková, M. The contribution of occult precipitation to sulphur deposition in the Czech Republic. *Erdkunde* **2011**, *65*, 247–259. [[CrossRef](#)]
197. Hůnová, I.; Kurfürst, P.; Vlček, O.; Stráník, V.; Stoklasová, P.; Schováňková, J.; Srbová, D. Towards a Better Spatial Quantification of Nitrogen Deposition: A Case Study for Czech Forests. *Environ. Pollut.* **2016**, *213*, 1028–1041. [[CrossRef](#)]
198. Elias, V.; Tesar, M.; Buchtele, J. Occult precipitation: Sampling, chemical analysis and process modelling in the Sumava Mts. (Czech Republic) and in the Taunus Mts. (Germany). *J. Hydrol.* **1995**, *166*, 409–420. [[CrossRef](#)]
199. Fisak, J.; Tesar, M.; Rezacova, D.; Elias, V.; Weignerova, V.; Fottova, D. Pollutant concentrations in fog and low cloud water at selected sites of the Czech Republic. *Atmos. Res.* **2002**, *64*, 75–87. [[CrossRef](#)]
200. Křeček, J.; Palán, L.; Stuchlík, E. Acid atmospheric deposition in a forested mountain catchment. *IForest* **2017**, *10*, 680–686. [[CrossRef](#)]
201. Palán, L.; Křeček, J. Interception and Fog Drip Estimates in Fragmented Mountain Forests. *Environ. Process.* **2018**, *5*, 727–742. [[CrossRef](#)]
202. Hůnová, I.; Brabec, M.; Malý, M.; Valeriánová, A. Revisiting fog as an important constituent of the atmosphere. *Sci. Total Environ.* **2018**, *656*, 1490–1499. [[CrossRef](#)] [[PubMed](#)]
203. Hůnová, I.; Brabec, M.; Malý, M.; Valeriánová, A. Long-term trends in fog occurrence in the modern-day Czech Republic, Central Europe. *Sci. Total Environ.* **2019**, in press. [[CrossRef](#)]
204. Bohdalkova, L.; Novak, M.; Voldrichova, P.; Prechova, E.; Veselovsky, F.; Erbanova, L.; Krachler, M.; Komarek, A.; Mikova, J. Atmospheric deposition of beryllium in Central Europe: Comparison of soluble and insoluble fractions in rime and snow across a pollution gradient. *Sci. Total. Environ.* **2012**, *439*, 26–34. [[CrossRef](#)]
205. Voldrichova, P.; Chrastny, V.; Sipkova, A.; Farkas, J.; Novak, M.; Stepanova, M.; Krachler, M.; Veselovsky, F.; Blaha, V.; Prechova, E.; et al. Zinc isotope systematics in snow and ice accretions in Central European mountains. *Chem. Geol.* **2014**, *388*, 130–141. [[CrossRef](#)]
206. Cimova, N.; Novak, M.; Chrastny, V.; Curik, J.; Veselovsky, F.; Blaha, V.; Prechova, E.; Pasava, J.; Houskova, M.; Bohdalkova, L.; et al. Lead fluxes and 206Pb/207Pb isotope ratios in rime and snow collected at remote mountain-top locations (Czech Republic, Central Europe): Patterns and sources. *Atmos. Environ.* **2016**, *143*, 51–59. [[CrossRef](#)]
207. Novak, M.; Sipkova, A.; Chrastny, V.; Stepanova, M.; Voldrichova, P.; Veselovsky, F.; Prechova, E.; Blaha, V.; Curik, J.; Farkas, J.; et al. Cu-Zn isotope constraints on the provenance of air pollution in Central Europe: Using soluble and insoluble particles in snow and rime. *Environ. Pollut.* **2016**, *218*, 1135–1146. [[CrossRef](#)]
208. Suchara, I.; Sucharová, J. Distribution of 36 element deposition rates in a historic mining and smelting area as determined through fine scale biomonitoring techniques, Part II: Relative long-term accumulated atmospheric deposition levels. *Water Air Soil Pollut.* **2004**, *153*, 229–252. [[CrossRef](#)]
209. Sucharova, J.; Suchara, I. Distribution of 36 element deposition rates in a historic mining and smelting area as documented through fine-scale biomonitoring techniques. Part I: Relative and absolute current atmospheric deposition levels detected by moss analyses. *Water Air Soil Pollut.* **2004**, *153*, 205–228. [[CrossRef](#)]
210. Conkova, M.; Kubiznakova, J. Lead isotope ratios in tree bark pockets: An indicator of past air pollution in the Czech Republic. *Sci. Total Environ.* **2008**, *404*, 440–445. [[CrossRef](#)]
211. Suchara, I. Temporal and spatial changes in spruce bark acidity at the scale of the Czech Republic in the last two decades, and the current abundance of epiphytic lichen *Hypogymnia physodes*. *Water Air Soil Pollut.* **2012**, *223*, 1685–1697. [[CrossRef](#)]

212. Suchara, I.; Sucharová, J.; Holá, M. The influence of contrasting ambient SO<sub>2</sub> concentrations in the Czech Republic in 1995 and in 2000 on the characteristics of spruce bark, used as an air quality indicator. *Ecol. Indic.* **2014**, *39*, 144–152. [[CrossRef](#)]
213. Suchara, I.; Sucharová, J.; Holá, M. Spatiotemporal changes in atmospheric deposition rates across the Czech Republic estimated in the selected biomonitoring campaigns. Examples of results available for landscape ecology and land use planning. *J. Landsc. Ecol.* **2015**, *8*, 1–19. [[CrossRef](#)]
214. Vile, M.A.; Wieder, K.; Novák, M. 200 years of Pb deposition throughout the Czech Republic: Patterns and Sources. *Environ. Sci. Technol.* **2000**, *34*, 12–21. [[CrossRef](#)]
215. Zuna, M.; Ettler, V.; Šebek, O.; Mihaljevič, M. Mercury accumulation in peatbogs at Czech sites with contrasting pollution histories. *Sci. Total Environ.* **2012**, *424*, 322–330. [[CrossRef](#)]
216. Zuna, M.; Mihaljevič, M.; Šebek, O.; Ettler, V.; Handley, M.; Navrátil, T.; Goliáš, V. Recent lead deposition trends in the Czech Republic as recorded by peat bogs and tree rings. *Atmos. Environ.* **2011**, *45*, 4950–4958. [[CrossRef](#)]
217. Doušová, B.; Erbanová, L.; Novák, M. Arsenic in atmospheric deposition at the Czech-Polish border: Two sampling campaigns 20 years apart. *Sci. Total Environ.* **2007**, *387*, 185–193. [[CrossRef](#)]
218. Kopáček, J.; Hejzlar, J.; Stuchlík, E.; Fott, J.; Veselý, J. Reversibility of acidification of mountain lakes after reduction in nitrogen and sulphur emissions in Central Europe. *Limnol. Oceanogr.* **1998**, *43*, 357–361. [[CrossRef](#)]
219. Hruška, J.; Moldan, F.; Krám, P. Recovery from acidification in central Europe—observed and predicted changes of soil and streamwater chemistry in the Lysina catchment, Czech Republic. *Environ. Pollut.* **2002**, *120*, 261–274. [[CrossRef](#)]
220. Vrba, J.; Kopáček, J.; Fott, J.; Kohout, L.; Nedbalová, L.; Pražáková, M.; Soldán, T.; Schaumurg, J. Long-term studies (1871–2000) on acidification and recovery of lakes in the Bohemian Forest (central Europe). *Sci. Total Environ.* **2003**, *310*, 73–85. [[CrossRef](#)]
221. Oulehle, F.; Hofmeister, J.; Cudlín, P.; Hruška, J. The effect of reduced atmospheric deposition on soil and soil solution chemistry at a site subjected to long-term acidification, Načetín, Czech Republic. *Sci. Total Environ.* **2006**, *370*, 532–544. [[CrossRef](#)]
222. Oulehle, F.; McDowell, W.H.; Aitkenhead-Peterson, J.A.; Krám, P.; Hruška, J.; Navrátil, T.; Buzek, F.; Fottová, D. Long-Term Trends in Stream Nitrate Concentrations and Losses Across Watersheds Undergoing Recovery from Acidification in the Czech Republic. *Ecosystems* **2008**, *11*, 410–425. [[CrossRef](#)]
223. Novotný, R.; Buriánek, V.; Šrámek, V.; Hůnová, I.; Skořepová, I.; Zapletal, M.; Lomský, M. Nitrogen deposition and its impact on forest ecosystems in the Czech Republic—Change in soil chemistry and ground vegetation. *IFOREST* **2016**, *10*, 48–54. [[CrossRef](#)]
224. Lomský, B.; Šrámek, V.; Novotný, R. Changes in the air pollution load in the Jizera Mts: Effects on the health status and mineral nutrition of the young Norway spruce stands. *Eur. J. For. Res.* **2012**, *131*, 757–771. [[CrossRef](#)]
225. Buriánek, V.; Novotný, R.; Hellebrandová, K.; Šrámek, V. Ground vegetation as an important factor in the biodiversity of forest ecosystems and its evaluation in regard to nitrogen deposition. *J. For. Sci.* **2013**, *59*, 238–252. [[CrossRef](#)]
226. Altman, J.; Fibich, P.; Santruckova, H.; Dolezal, J.; Stepanek, P.; Kopacek, J.; Hunova, I.; Oulehle, F.; Tumajer, J.; Cienciala, E. Environmental factors exert strong control over the climate-growth relationships of *Picea abies* in Central Europe. *Sci. Total Environ.* **2017**, *609*, 506–516. [[CrossRef](#)] [[PubMed](#)]
227. Cienciala, E.; Russ, R.; Šantrůčková, H.; Altman, J.; Kopáček, J.; Altman, J.; Kopáček, J.; Hůnová, I.; Štěpánek, P.; Oulehle, F.; et al. Discerning environmental factors affecting current tree growth in Central Europe. *Sci. Total Environ.* **2016**, *573*, 541–554. [[CrossRef](#)] [[PubMed](#)]



© 2020 by the author. Licensee MDPI, Basel, Switzerland. This article is an open access article distributed under the terms and conditions of the Creative Commons Attribution (CC BY) license (<http://creativecommons.org/licenses/by/4.0/>).

Article

# Detailed Assessment of the Effects of Meteorological Conditions on PM<sub>10</sub> Concentrations in the Northeastern Part of the Czech Republic

Vladimíra Volná<sup>1,2,\*</sup>  and Daniel Hladký<sup>1</sup>

<sup>1</sup> Czech Hydrometeorological Institute, Na Šabatce 17, 143 06 Praha, Czech Republic; daniel.hladky@chmi.cz

<sup>2</sup> University of Ostrava, Faculty of Science, Department of Physical Geography and Geoecology, 30. dubna 22, 701 03 Ostrava, Czech Republic

\* Correspondence: vladimira.volna@chmi.cz

Received: 6 April 2020; Accepted: 9 May 2020; Published: 12 May 2020



**Abstract:** This article assessed the links between PM<sub>10</sub> pollution and meteorological conditions over the Czech-Polish border area at the Třinec-Kosmos and Věřňovice sites often burdened with high air pollution covering the years 2016–2019. For this purpose, the results of the measurements of special systems (ceilometers) that monitor the atmospheric boundary layer were used in the analysis. Meteorological conditions, including the mixing layer height (MLH), undoubtedly influence the air pollution level. Combinations of meteorological conditions and their influence on PM<sub>10</sub> concentrations also vary, depending on the pollution sources of a certain area and the geographical conditions of the monitoring site. Generally, the worst dispersion conditions for the PM<sub>10</sub> air pollution level occur at low air temperatures, low wind speed, and low height of the mixing layer along with a wind direction from areas with a higher accumulation of pollution sources. The average PM<sub>10</sub> concentrations at temperatures below 1 °C reach the highest values on the occurrence of a mixing layer height of up to 400 m at both sites. The influence of a rising height of the mixing layer at temperatures below 1 °C on the average PM<sub>10</sub> concentrations at Třinec-Kosmos site is not as significant as in the case of Věřňovice, where a difference of several tens of  $\mu\text{g}\cdot\text{m}^{-3}$  in the average PM<sub>10</sub> concentrations was observed between levels of up to 200 m and levels of 200–300 m. The average PM<sub>10</sub> hourly concentrations at Třinec-Kosmos were the highest at wind speeds of up to  $0.5\text{ m}\cdot\text{s}^{-1}$ , at MLH levels of up to almost 600 m; at Věřňovice, the influence of wind speeds of up to  $2\text{ m}\cdot\text{s}^{-1}$  was detected. Despite the fact that the most frequent PM<sub>10</sub> contributions come to the Třinec-Kosmos site from the SE direction, the average maximum concentration contributions come from the W–N sectors at low wind speeds and MLHs of up to 400 m. In Věřňovice, regardless of the prevailing SW wind direction, sources in the NE–E sector from the site have a crucial influence on the air pollution level caused by PM<sub>10</sub>.

**Keywords:** mixing layer height; ceilometer; suspended particulate matter; air pollution; Czech-Polish border

## 1. Introduction

PM<sub>10</sub> is a problematic pollutant with a wide spectrum of effects on human health, mostly on the respiratory and cardiovascular systems of the human body. The hazards of this pollutant lie not only in its quantity, thus in high measured concentrations, but also in the morphology of the particles and their qualitative composition. The suspended particulate matter is capable of creating bonds, which may, of course, result in transferring a range of other elements, e.g., heavy metals and polycyclic aromatic hydrocarbons, into the human body. The effects on the human body have clinically proven to be negative, especially in the form of carcinogenesis [1–5], for some of these transported substances.

As for the areas of concern, the areas in Europe most polluted by suspended particulate matter are the Po Valley in northern Italy, the countries of Eastern Europe, including the Balkan Peninsula, and part of Central Europe. The southern rim of the area (of Central Europe) occupies the northeastern part of the Czech Republic, and spreads northwards (in terms of area) to the larger territory of Poland [6,7]. This Czech-Polish region is part of the Upper Silesian Basin, which is a black coal basin of European significance. The first (primitive) black coal mining in the Upper Silesian Basin began as early as 1657 on Polish territory south of Katowice; real industrial mining development started in the Czech part of the basin no earlier than the second half of the 19th century [8]. The mining industry became the basis for the development of other industrial branches. In the entire region of the Upper Silesian Basin, there is an intricately interconnected system of industry, traffic infrastructure, and high density of population with individual solid fuel heating, which is historically related to black coal burning. All of the transborder region of the Silesian Voivodeship in Poland and the Moravian-Silesian Region in the Czech Republic rank among the most urbanized and industrialized regions in Europe [9,10]. All these anthropogenic activities negatively influence all the environmental components, and pronounced changes in these components have been recorded since the 1970s. From the point of view of air quality improvement, there were significant positive changes in the 1990s during the economic restructuring of both post-communist countries (Poland and the then-Czechoslovakia). Another major step forward was the accession of both countries to the European Union and the necessity of adapting their legislation to the EU requirements [11,12]. Owing to the mentioned measures, there has been a decrease in the pollution load of the Czech-Polish region; the problems, however, remain, and the exceedance of the pollution limits is still frequent [13,14]. This especially concerns the suspended particulate matter and benzo(a)pyren [15].

The particular air pollution level in the region of concern does not depend solely on the pollution source characteristics or the amount of discharged pollutants, but also on the physical geography and meteorological conditions of the area in question. It is the meteorological conditions themselves that determine the intensity and manner of the dispersion of contaminants [16]. The wind direction and speed and the vertical atmospheric stability, contingent on the air temperature, are considered the most important and decisive meteorological dispersion conditions. The wind characteristics influence the transport of pollutants in the horizontal direction, the atmospheric stability and the air temperature influence the dispersion of pollutants in the vertical direction. In the most stable situations, the air temperature rises with the height and the conditions for the vertical mixing are the worst. Conversely, at unstable stratification, the temperature drops more quickly than it would under regular conditions in the atmosphere, and the conditions for pollutant dispersion are favorable [17–19].

It is possible to express the dispersion conditions numerically using the ventilation index, which is defined as a product of the mixing layer height and the average wind speed in the mixing layer [20]. A situation with unfavorable dispersion conditions does not always have to mean the occurrence of high contaminant concentrations. It is important to bear in mind the situation duration, the original pollution level, the source distribution, and the emissions into the layer under inversion. It is, however, possible to state that a significant exceedance of the allowed pollution limits occurs mostly in mildly unfavorable and unfavorable dispersion conditions, or due to the concurrence of other meteorological factors. In order to calculate the ventilation index, the ALADIN (Aire Limitée, Adaptation Dynamique, Development International) numerical forecast model is used in the Czech Republic; this model is meant mostly for short-term forecast composition [21]. It is also possible to find out the information about the atmospheric boundary layer and the mixing layer height by means of direct monitoring. Measurements using radiosondes, high masts, and special devices, such as SODARs (Sonic Detection and Ranging), LIDARs (Light Detection and Ranging), and wind profilers, are used. In the presented analysis, mixing layer height measurement results obtained by means of ceilometers were used. The higher the mixing layer height, the more intensive the mixing of air, and thus, the better the conditions are for contaminant dispersion [22,23].

Awareness of the links between PM<sub>10</sub> concentrations and meteorological variables and their mutual combination is an important premise for assessment of the pollution situation and a possible pollutant concentration trend forecast [24–28]. The detection of these dependences is especially important for the assessment of complex situations with the occurrence of smog situations [29,30]. Apart from those pollutant concentrations exceeding the limit value, knowledge of the development of the meteorological situation, weather forecasts, and thus the possibilities for overall improvement or deterioration of the situation due to better or worse air pollutant dispersion, are important aspects for the announcement of smog situations. Improving the knowledge of correlations between the mostly high suspended particulate matter concentrations and the meteorological conditions may be a significant aspect for defining the measures preventing health hazards in the assessed densely populated region [31].

With this article, the authors reassume a similar topic of PM<sub>10</sub> concentration dependences on the mixing layer height in the area of interest [32]. In the mentioned analysis, the measurement results were assessed at the Věřňovice, Třinec-Kosmos, and Mošnov/Studénka sites for the cold parts of the years 2016/2017 and 2017/2018. The differences in the established facts were caused mostly by a different site location (orography) and by the structure of the sources that influence the pollution. Pollutants other than PM<sub>10</sub> and other meteorological variables were not included in the assessment.

The anticipated findings of this analysis shall be an understanding of the combinations of the meteorological conditions, the mixing layer height, and the connection to PM<sub>10</sub> concentrations. The highest PM<sub>10</sub> concentrations are generally reached at a low mixing layer height, low wind speed or calm air, and at a low air temperature. These assumptions correspond to previous results concerning the dependence of pollutant concentration on the mixing layer height in Europe [33–37]. Furthermore, the mixing layer height and its influence on the pollutant concentrations in the air have been written about in articles in Asia, e.g., in India [38] and China [39], which, as far as the comparability of pollution-meteorology correlations is concerned, is hardly transferrable, given these significantly different areas. The reasons are the different climatological conditions between the Czech-Polish border area and Asia, specifically the meteorological and geographical conditions of the selected locations, the air pollution intensity, and the different position and types of air pollution sources with respect to the monitored ambient air quality stations. The wind direction and speed, as well as the mixing layer height, also make it possible, at least in part, to reveal the main air pollution sources in the monitored border locations. With regard to a different area relief in which the monitored locations are situated, it has been assumed that the PM<sub>10</sub> concentration dependences on meteorological variables are bound to differ up to a certain point.

## **2. Experiments**

For the assessment, sites of the Czech Hydrometeorological Institute [40] have been chosen—Třinec-Kosmos [41] and Věřňovice [42], located in the northeastern part of the Moravian-Silesian Region of the Czech Republic (Figure 1). The monitored sites are about 34 km apart in a straight line. Both sites belong to the National Air Quality Monitoring Network of the Czech Republic [43]. At the Třinec-Kosmos and Věřňovice sites, PM<sub>10</sub> concentrations are measured by means of a radiometric method based on the absorption of beta radiation in a sample collected on filter material by means of an Automatic suspended particulate monitor MP101M [44]. The wind direction and speed are measured at a standard height of 10 m by means of a WindSonic machine, based on ultrasound technology. The air temperature is scanned at a height of 2 m above the ground, by means of a Cormet company machine. At both sites, special ceilometer devices are placed that are traditionally used to measure the height of the cloud base and the cloud amount in individual layers, the vertical visibility, and the aerosol concentration in the ground atmospheric layer. These ceilometers contain a presentation module that enables the measurement and display of the structure of the atmospheric boundary layer based on an algorithm that determines the thickness of the mixing layer depending on the aerosol concentration in the atmosphere. In both cases, these are Vaisala CL31 Ceilometers [45].

It is necessary to point out that measurement by means of ceilometers is limited by height. Although the upper measurement limit reaches the height of a few kilometers, it is impossible to regard the Earth's surface level as the bottom limit. In the vicinity of the Earth's surface, the measurement is limited by higher noise that can reach up to a height of 50 m [46].

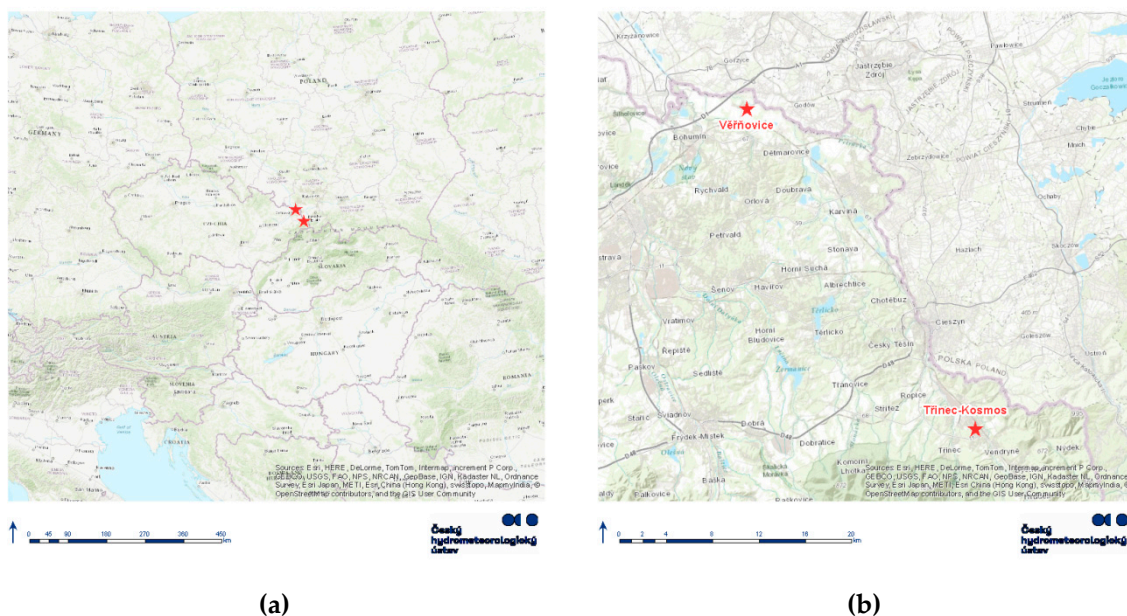


**Figure 1.** The assessed site location: (a) The location within Central Europe; (b) The location within the Czech-Polish border region.

For the purposes of the analysis, the average hourly values of the mixing layer height were used, calculated from the data measured at 16-second intervals from the ceilometers at the Třinec-Kosmos and Věřňovice sites. The output hourly values of  $PM_{10}$ , temperature, wind speed, and direction were also used in the analysis. Due to large diurnal mixing layer height (MLH) variation, the analysis also included the daily averages of the parameters. Correlation coefficients in the analysis are calculated from the hourly and daily data in relation to the MLH, which was divided into 20 intervals and, subsequently, from their arithmetic means and medians. In the case of daily MLH averages, intervals from a height of 150 m are available. The assessed period is from 2016 to 2019. The data utilization rate used for the monitored period was high. In the case of hourly data on  $PM_{10}$  and meteorological variables (air temperature, wind direction, and speed) the average at both sites is 98%; it is 87% from the ceilometers' data for the mixing layer height. In order to assess higher  $PM_{10}$  concentrations and exceedance numbers, a limit value of  $50 \mu\text{g}\cdot\text{m}^{-3}$  was purposefully chosen, which corresponds to the value of the daily pollution limit for  $PM_{10}$  [13]. The term “cold period of the year” is used for the months of January through March and October through December; the term “warm period of the year” is used for the months of April through September.

In the analysis, concentration roses were also used for illustrative purposes, which show average  $PM_{10}$  concentrations for the given wind direction and speed, as well as weighted concentration roses [47]. The difference between a concentration rose and a weighted concentration rose is that the latter provides information about how often a given wind direction and speed combination occurs and states to what extent the concentrations detected for a given wind speed and direction affect the overall average concentration for a given period. The comparison of the two roses may show a significant pollution source located, however, in a sector from which the wind only rarely blows and thus does not contribute significantly to the overall average concentration. The concentration rose reveals what the pollution situation was at maximum concentrations of a given contaminant at a particular site; the weighted concentration rose shows from what wind direction and at what speed the pollution came to the largest extent for the whole period. For the above-described reasons, both rose types for

the same site and period may vary significantly [48]. In the presented roses, there is information about calm air, which is a situation with a wind speed of 0–0.2 m·s<sup>-1</sup>.

The Třinec-Kosmos site is situated in the center of the city of Třinec, in a typical residential development. In the immediate vicinity of the site there are a parking lot as well as a residential development type of road. In the northeastern (NE) direction from the site, the closest pollution line source is a frequented road with an average number of vehicles of more than 9000 every 24 h [49]. The Třinecké železářny a.s. industrial plant premises are situated in the northwestern (NW) sector about 1.5 km from the site. The closest housing development with individual heating is situated in the N–NE direction about 500 m from the site, another is in the S–SW direction about 1 km from the site. The shortest route towards the Polish border is in the NE direction about 3 km from the site. The Třinec-Kosmos site is situated at the end of the Jablunkov Furrow, which starts at Jablunkov Pass and separates the Moravian-Silesian and the Silesian Beskydy mountain ranges. The shortest distance to the foothills of the Beskydy mountains is just 4.5 km southwest of the station. In the furrow is the Olše River basin that drains off the surrounding undulating relief [50,51]. The direction of the furrow also determines the prevailing wind direction along the southeast/northwest axis (Figure 2a) [52]. In the vicinity of the site, at a distance of 40 m in the NE direction, there is a high-rise, a roughly 50-meter-high building that may, with regard to the prevailing wind direction, slightly muffle the wind influence from the northeast.

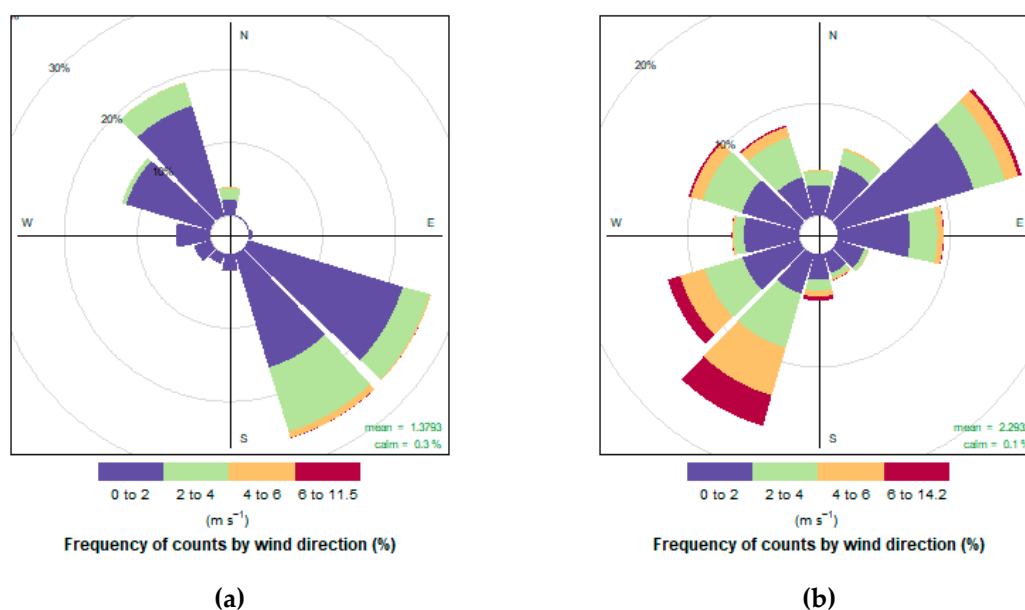


**Figure 2.** Average frequency of counts by wind speed and wind direction, 2016–2019: (a) Třinec-Kosmos; (b) Věřňovice.

According to the existing pollution assessment analyses of the Třinec-Kosmos site, apart from the significant contribution of secondary particles, a combination of sources from abroad and local heating and industry, as well as road traffic, contribute significantly to the PM<sub>10</sub> concentrations [52]. At lower wind speeds of up to 2 m·s<sup>-1</sup>, with a prevailing southeastern (SE) wind direction, a significant influence of dense housing development with individual heating is very likely to be seen at the site. Conversely, in situations with a NW wind direction, a significant influence of the industrial sources of Třinecké železářny is assumed, which includes both high- as well as low-emitting sources. At higher wind speeds, the influence of sources situated north of the site at a greater distance is also apparent here in the cold period of the year, which points at foreign sources from Poland.

The Věřňovice site is situated in the cadastral area of the Dolní Lutyně municipality, about 300 m east of the Věřňovice village and about 1 km south of the Czech-Polish border. In the immediate vicinity of the site, there is an infrequently used and partly paved road flanked by deciduous trees and

fields. Roughly 1.5 km in the NW direction, there is a highway with roughly 11,000 vehicles a day [49]. The closest significant industrial source, Elektrárna Dětmárovice a.s., is situated about 3 km southeast of the site. The Věřňovice site is situated in open terrain in the vicinity of the River Olše. At the site, the prevailing wind direction is along the southwest/northeast axis where the more frequent flow is southwest (Figure 2b). Věřňovice is situated in the area of the Ostrava Basin where the “Moravian Gate” ends; this divides the Podbeskydská hilly area and Nízký Jeseník [50,51]. The shape of the gate along the southwest/northeast axis significantly determines the prevailing wind direction of the region where Věřňovice is situated. It is apparent from the existing analyses that local fireplaces have the greatest contribution to the exceedance of PM<sub>10</sub> pollution limits here among the primary sources, mostly those used on the territory of Poland [52].

### 3. Results

The suspended particulate matter concentrations at both sites are assessed depending on the mixing layer height and other meteorological variables—air temperature, wind speed, and direction.

#### 3.1. Dependence of Suspended Particulate Matter Concentrations on the Mixing Layer Height

Based on the average daily courses of hourly concentrations of PM<sub>10</sub> and MLH in the period between 2016 and 2019 for both stations, it is obvious that the lowest MLH is measured in the evening and night hours and the early morning hours (Figure 3). During this period, the highest PM<sub>10</sub> concentrations were observed at the Věřňovice station. In both cases, higher PM<sub>10</sub> concentrations were observed in the cold part of the year, when the daily variability was also greater than in the warm part of the year.

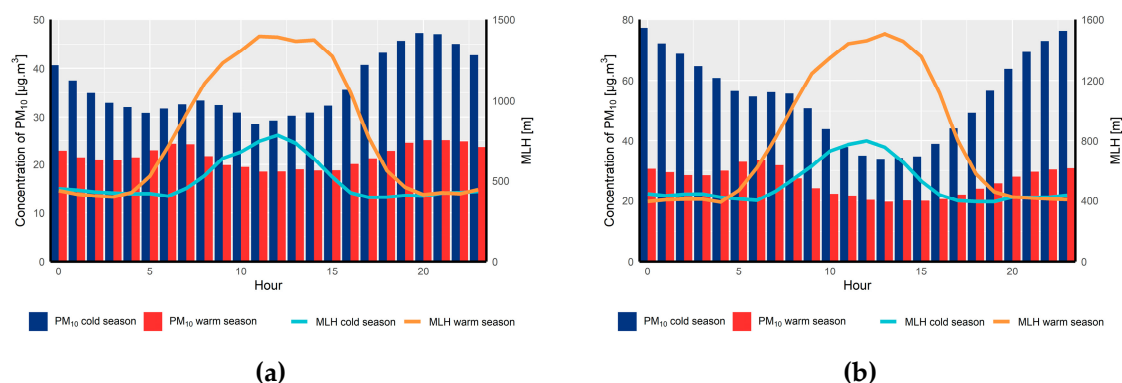


**Figure 3.** Daily course of hourly PM<sub>10</sub> concentrations and mixing layer height (MLH), 2016–2019: (a) Třinec-Kosmos; (b) Věřňovice.

The distribution of the PM<sub>10</sub> and MLH hourly values is depicted in Figure 4.

In order to work out the dependence of PM<sub>10</sub> concentrations on the mixing layer height over the period from 2016 to 2019, correlation coefficients have been calculated for the values of their averages and medians. The median calculations have been added for the purposes of comparison without the influence of extreme values. The highest mean and median hourly PM<sub>10</sub> concentrations at the Třinec-Kosmos station for the entire period between 2016–2019 were observed at MLHs of 150 to 300 m. At the Věřňovice station, the highest hourly concentrations were observed at the lowest MLH, below 200 m. Domestic heating, a low (in terms of height) source of air pollution with the typical chimney height below 15 m, has a significant effect at both locations. The Třinec-Kosmos station is also significantly affected by the large industrial site of Třinecké železářny (Třinec Ironworks), with a chimney height of 100 m or more. At MLHs below 300 m, there is an increase in PM<sub>10</sub> concentrations, due to emissions from both domestic heating and industrial sources. At lower MLHs, the emissions from higher chimneys spread above this height. At higher MLHs (below 300 m), both domestic heating emissions and nearby industrial sources are very significant. After comparing all the levels of MLH,

higher PM<sub>10</sub> concentration values occurred at Věřňovice than in Třinec-Kosmos. On the occurrence of higher levels of the mixing layer, lower PM<sub>10</sub> concentrations were reached at both sites (Figure 5). For the Třinec-Kosmos station, the correlation coefficient for the 2016–2019 period calculated from the mean hourly values of concentrations at increasing MLHs is  $-0.83$ ; from the median values, it is  $-0.84$ . The correlation coefficient from the mean daily values is  $-0.79$ ; from the median values, it is  $-0.77$ . At the Věřňovice station, the correlation coefficient from the mean hourly values for PM<sub>10</sub> in relation to the increasing MLH is  $-0.76$ , and from the median values, it is  $-0.85$ . The correlation coefficient at the Věřňovice station for the entire period from 2016 to 2019 from the mean daily values is  $-0.74$ ; for the median values, it is  $-0.75$ .

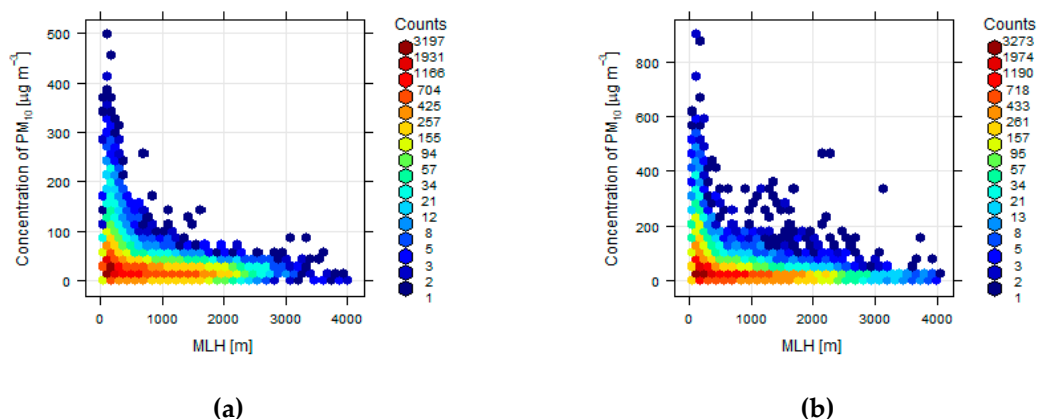


**Figure 4.** Hourly PM<sub>10</sub> concentration variability in relation to MLH, 2016–2019: (a) Třinec-Kosmos; (b) Věřňovice.

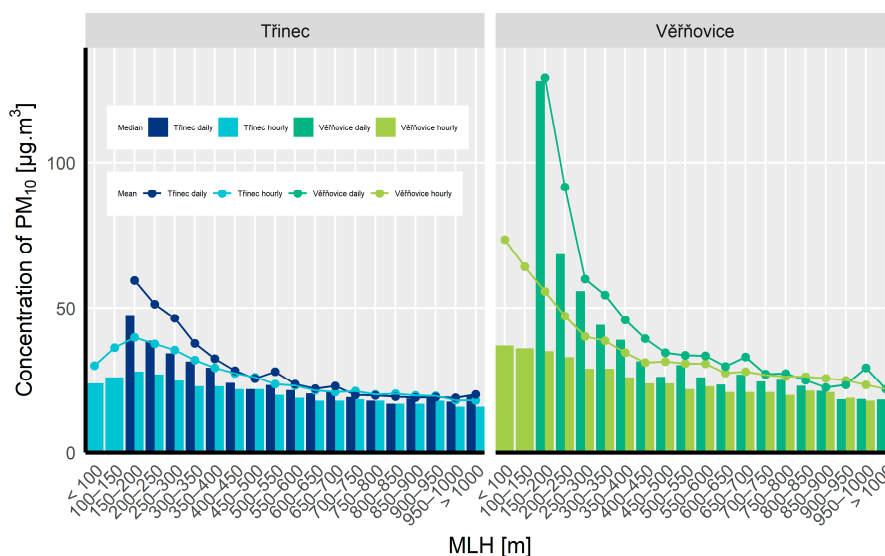


**Figure 5.** Mean and median PM<sub>10</sub> concentration values at mean and median MLH values, Třinec-Kosmos, Věřňovice, 2016–2019.

The correlation coefficients (hourly and daily values) of PM<sub>10</sub> dependences on MLH differ over the period from 2016 to 2019 at both sites; it is, however, possible to state that they are statistically significant dependences in all the cases (Table 1). When comparing the MLH arithmetic and median averages in the individual years, the highest values were reached in 2019 at both sites; they were higher at Věřňovice than at Třinec-Kosmos (Table 2).

**Table 1.** Correlation coefficients of PM<sub>10</sub> concentration dependences on MLH and the mixing layer height values at the Třinec-Kosmos and Věřňovice sites, 2016–2019.

| Year | Třinec-Kosmos     |        |                   |        | Věřňovice         |        |                   |        |
|------|-------------------|--------|-------------------|--------|-------------------|--------|-------------------|--------|
|      | Hour              |        | Day               |        | Hour              |        | Day               |        |
|      | Arithmetical Mean | Median |
| 2016 | −0.85             | −0.83  | −0.81             | −0.78  | −0.76             | −0.84  | −0.70             | −0.66  |
| 2017 | −0.81             | −0.83  | −0.84             | −0.81  | −0.80             | −0.90  | −0.72             | −0.69  |
| 2018 | −0.81             | −0.85  | −0.79             | −0.81  | −0.82             | −0.87  | −0.81             | −0.79  |
| 2019 | −0.84             | −0.84  | −0.72             | −0.69  | −0.64             | −0.78  | −0.73             | −0.85  |

**Table 2.** The mixing layer height values at the Třinec-Kosmos and Věřňovice sites, 2016–2019.

| Year | Třinec-Kosmos         |            | Věřňovice             |            |
|------|-----------------------|------------|-----------------------|------------|
|      | Arithmetical Mean (m) | Median (m) | Arithmetical Mean (m) | Median (m) |
| 2016 | 604                   | 369        | 555                   | 327        |
| 2017 | 659                   | 425        | 628                   | 372        |
| 2018 | 675                   | 450        | 670                   | 408        |
| 2019 | 705                   | 501        | 821                   | 553        |

3.2. Dependence of the Suspended Particulate Matter Concentrations on the Mixing Layer Height and the Air Temperature

The distribution of temperature and MLH hourly values are depicted in Figure 6.

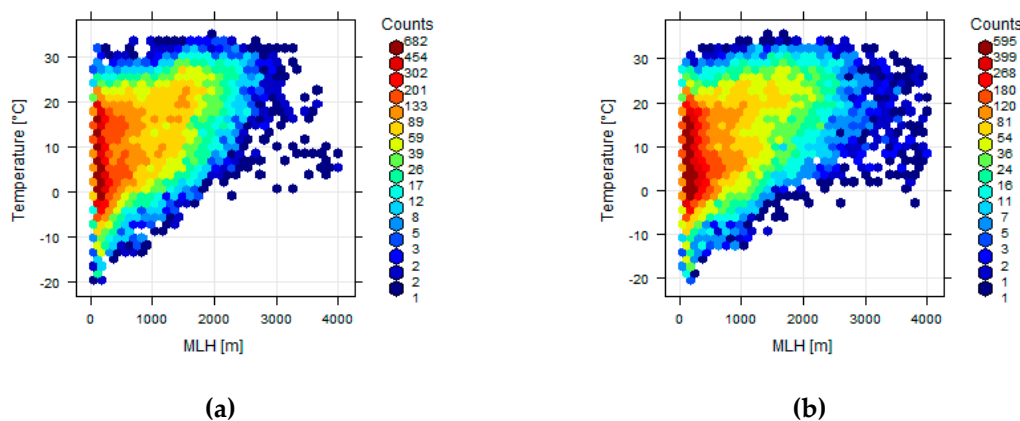


**Figure 6.** Variation of hourly temperature values in relation to MLH, 2016–2019: (a) Třinec-Kosmos; (b) Věřňovice.

The lowest average and median temperature values (hourly and daily values) were reached at both sites over the whole period from 2016 to 2019 on the occurrence of MLHs of 150 up to 300 m. From an MLH of 300 m the mean temperature values rise with increasing MLHs (or range around similar values) and the highest values are observed at an MLH above 800 m (Figure 7). On average, the statistical dependency expressed by a correlation coefficient between the temperature and MLH is significant over the whole period from 2016 to 2019 at both sites. The correlation coefficients calculated from the mean and median values (from the hourly and daily data) range between 0.85 and 0.94 on average for the entire period of analysis for both stations.

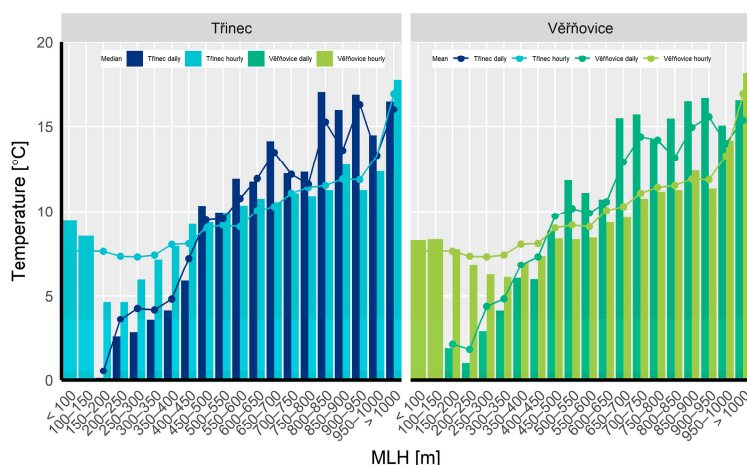


**Figure 7.** Mean and median temperature values at mean and median MLH values, Třinec-Kosmos, Věřňovice, 2016–2019.

The correlation dependences between the temperature and the mixing layer height changed over the years of 2016 to 2019 at both sites. The correlation dependence is significant every year of the monitored period (Table 3).

**Table 3.** Correlation coefficients of dependences of the temperature on the MLH at the Třinec-Kosmos and Věřňovice sites, 2016–2019.

| Year | Třinec-Kosmos   |        |                 |        | Věřňovice       |        |                 |        |
|------|-----------------|--------|-----------------|--------|-----------------|--------|-----------------|--------|
|      | Hour            |        | Day             |        | Hour            |        | Day             |        |
|      | Arithmetic Mean | Median |
| 2016 | 0.95            | 0.88   | 0.89            | 0.81   | 0.94            | 0.87   | 0.89            | 0.90   |
| 2017 | 0.92            | 0.84   | 0.92            | 0.94   | 0.96            | 0.91   | 0.88            | 0.89   |
| 2018 | 0.90            | 0.82   | 0.88            | 0.90   | 0.93            | 0.84   | 0.93            | 0.89   |
| 2019 | 0.96            | 0.92   | 0.85            | 0.82   | 0.91            | 0.79   | 0.86            | 0.75   |

The PM<sub>10</sub> concentrations are significantly dependent on the mixing layer height and temperature in the case of both sites over the entire monitored period from 2016 to 2019. The average PM<sub>10</sub> concentrations reach their highest values at temperatures below 1 °C. At the Třinec-Kosmos location, the highest average daily and hourly PM<sub>10</sub> concentrations were observed at temperatures below 1 °C and a mixing layer height lower than 200 to 300 m. At temperatures above 5 °C, the average daily PM<sub>10</sub> concentrations were highest at an MLH between 200 and 300 m. At a higher MLH the PM<sub>10</sub> concentration values were almost identical. The average daily and hourly PM<sub>10</sub> concentrations at the Věřňovice station reached the highest values during the entire period of analysis in combination with the relationship between the temperature and height of the mixing layer, at temperatures below 1 °C and a mixing layer height below 200 m. At the same temperature, but at an MLH of 200–300 m, the average daily concentrations were lower, but still double the limit value of 50 µg·m<sup>-3</sup>. A more significant PM<sub>10</sub> concentration dependence on temperature as well as MLH was observed at Věřňovice. At Třinec, a lower temperature had a substantial influence on PM<sub>10</sub> concentrations; the mixing layer height influence was shown mostly up to an MLH of 400 m. The combination of a low temperature and low MLH level corresponds to the general assumption about the occurrence of poorer dispersion conditions in the cold period of the year as opposed to the assumed occurrence of better dispersion conditions in the warm period of the year (Figures 8a and 9a). When observing the correlations among the numbers of exceedances of PM<sub>10</sub> daily concentration values of 50 µg·m<sup>-3</sup> and the MLH and temperature (Figures 8b and 9b), a decreasing count of exceedances of this value is apparent with

a rising temperature and increasing MLH. The highest number of  $50 \mu\text{g}\cdot\text{m}^{-3}$  value exceedances for  $\text{PM}_{10}$  daily concentrations is observed at temperatures below  $1^\circ\text{C}$  and MLHs below 300 m. For both sites, a slight increase in the number of 1-hour  $\text{PM}_{10}$  concentrations above  $50 \mu\text{g}\cdot\text{m}^{-3}$  is apparent at an MLH level above 1000 m as opposed to 800 to 1000 m.

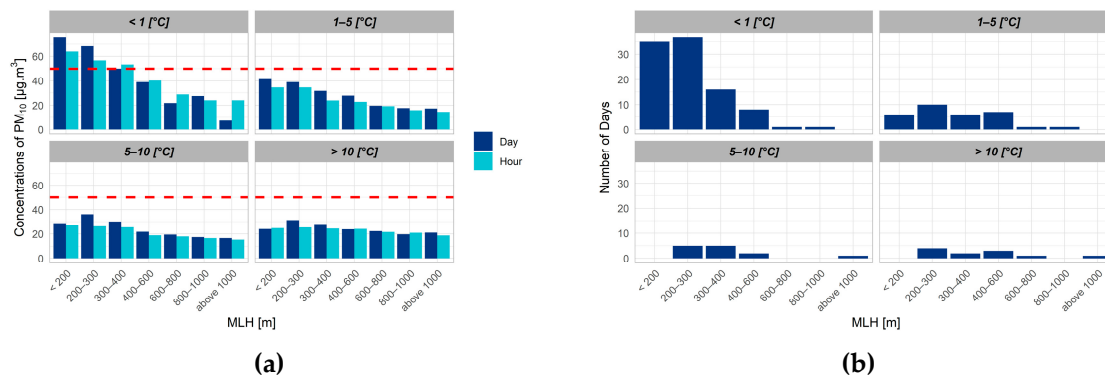


**Figure 8.** The Třinec-Kosmos site, 2016–2019: (a) Average  $\text{PM}_{10}$  concentrations depending on the mixing layer height and temperature; (b) Exceedance count of daily concentrations of  $50 \mu\text{g}\cdot\text{m}^{-3}$  depending on the mixing layer height and temperature.

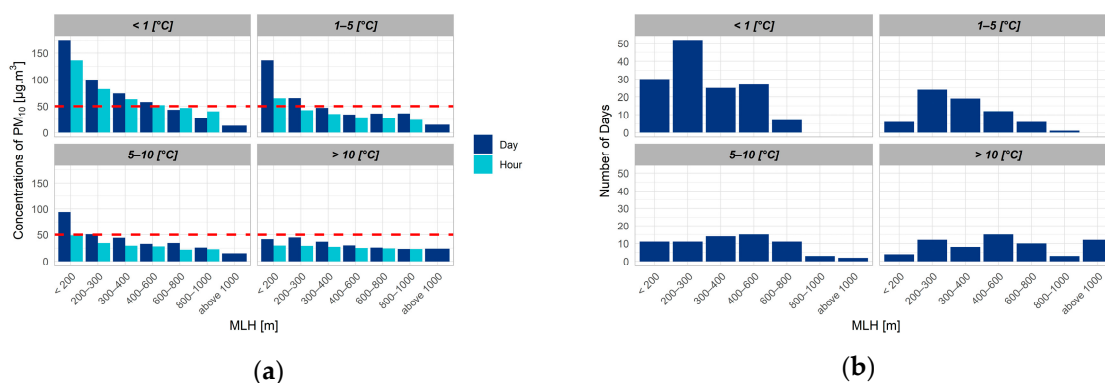


**Figure 9.** The Věřňovice site, 2016–2019: (a) Average  $\text{PM}_{10}$  concentrations depending on the mixing layer height and temperature; (b) Exceedance count of daily concentrations of  $50 \mu\text{g}\cdot\text{m}^{-3}$  depending on the mixing layer height and temperature.

### 3.3. Dependence of Suspended Particulate Matter Concentrations on the Mixing Layer Height, Wind Speed, and Direction

The distribution of wind speed and MLH hourly values are depicted in Figure 10.

At the Třinec-Kosmos site, a wind speed measured at 10 m does not significantly change with a rising MLH. At the Věřňovice site, the wind speed change is more apparent with a rising MLH. Here, the difference of the average values of the wind speed on the occurrence of MLH levels of up to 200 m and above 400 m makes up 1 and more  $\text{m}\cdot\text{s}^{-1}$  (Figure 11). The correlation dependences of the wind speed on MLH are low at the Třinec-Kosmos site; the Věřňovice site shows a statistically more significant dependence than the Třinec-Kosmos site. Higher wind speeds are observed at the Věřňovice station, compared to the Třinec-Kosmos station. The differences are due to the more complex orography of the Třinec region compared to the relatively flat and open region surrounding Věřňovice. The station in Třinec is located in a housing development, at the foothills of the Beskydy Mountains (Chapter 2). This means that the correlation between MLH and wind speed at the Třinec-Kosmos station is much less significant or even insignificant, compared to the station in Věřňovice.

The correlation dependences of the wind speed and MHL also differ from site to site throughout the years of the assessed period. A statistically more significant dependence of the wind speed on the MLH is apparent at the Věřňovice site (Table 4).

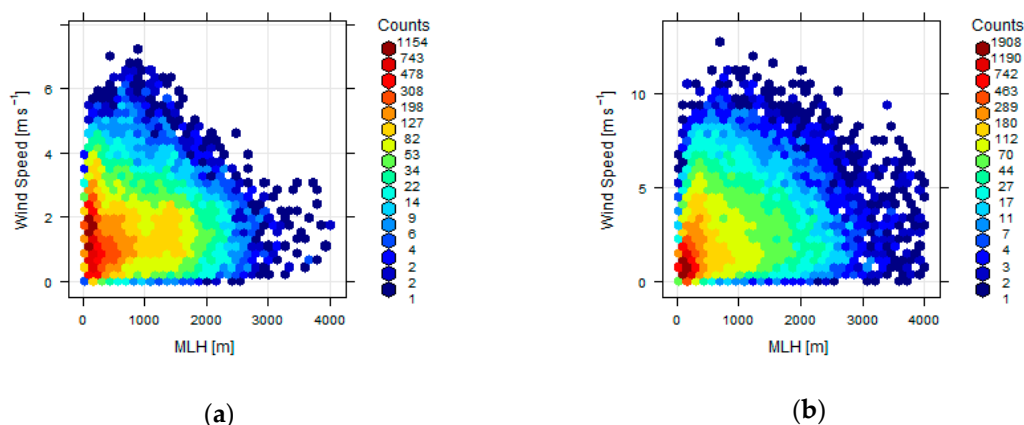


**Figure 10.** Variation of hourly wind speed values in relation to MLH, 2016–2019: (a) Třinec-Kosmos; (b) Věřňovice.

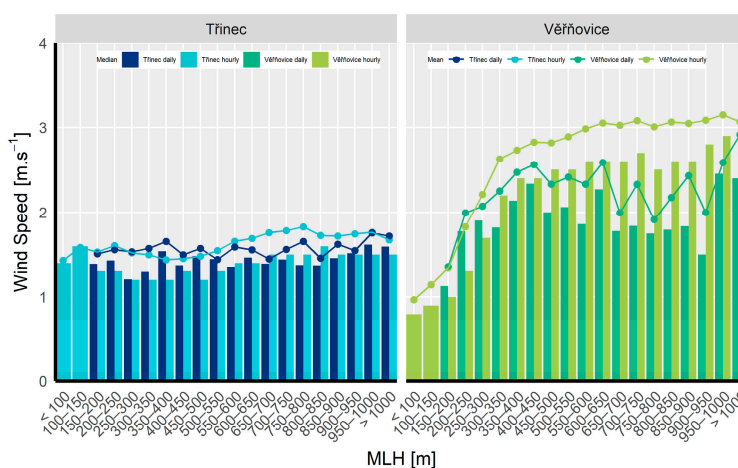


**Figure 11.** Average and median values of the wind speed at average and median MLH values, Třinec-Kosmos, Věřňovice, 2016–2019.

**Table 4.** Correlation coefficients of dependences of the wind speed on the MLH, Třinec-Kosmos and Věřňovice, 2016–2019.

| Year | Třinec-Kosmos   |        |                 |        | Věřňovice       |        |                 |        |
|------|-----------------|--------|-----------------|--------|-----------------|--------|-----------------|--------|
|      | Hour            |        | Day             |        | Hour            |        | Day             |        |
|      | Arithmetic Mean | Median |
| 2016 | 0.53            | 0.45   | 0.28            | 0.32   | 0.69            | 0.69   | 0.07            | 0.32   |
| 2017 | 0.56            | 0.41   | 0.46            | 0.55   | 0.79            | 0.79   | 0.53            | 0.49   |
| 2018 | 0.60            | 0.53   | 0.1             | 0.27   | 0.75            | 0.76   | 0.52            | 0.35   |
| 2019 | 0.51            | 0.34   | 0.01            | 0.2    | 0.63            | 0.71   | 0.43            | 0.37   |

PM<sub>10</sub> concentrations are significantly dependent on the MLH and wind speed. At the Třinec-Kosmos site, situations with calm air and wind speeds of up to 0.5 m·s<sup>-1</sup> had an apparent influence on higher hourly PM<sub>10</sub> concentrations. At wind speeds between 0.5–2 m·s<sup>-1</sup>, the highest average hourly concentrations were observed at MLHs of 200–300 m. The average daily PM<sub>10</sub> concentrations were always the highest at MLHs below 200 m. Average daily wind speeds below 0.5 m·s<sup>-1</sup> were not available for the two stations of interest (Třinec-Kosmos and Věřňovice). The daily average wind speed values were 0.5 m·s<sup>-1</sup> or more. The influence of the wind speed on PM<sub>10</sub> concentrations decreased with the mixing layer height at the Třinec-Kosmos site. At wind speeds above 2 m·s<sup>-1</sup>, the PM<sub>10</sub> concentrations were lowest at the site. During the observation of the occurrence

of the hourly  $PM_{10}$  concentrations above  $50 \mu\text{g}\cdot\text{m}^{-3}$ , the highest count of these higher values was undoubtedly at wind speeds of  $1\text{--}2 \text{ m}\cdot\text{s}^{-1}$  and  $0.5\text{--}1 \text{ m}\cdot\text{s}^{-1}$  and MLHs of up to 300 m. The lowest number of daily  $PM_{10}$  concentrations above  $50 \mu\text{g}\cdot\text{m}^{-3}$  was observed at wind speeds above  $2 \text{ m}\cdot\text{s}^{-1}$  and MLHs above 400 m (Figure 12).

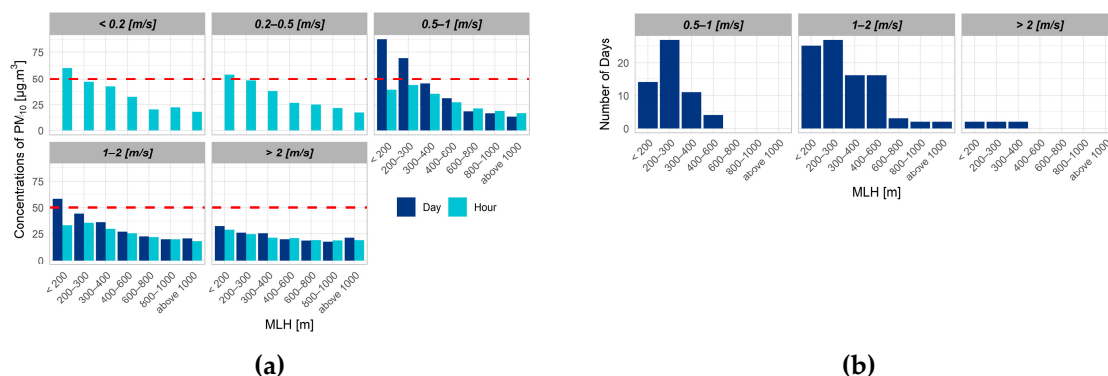


**Figure 12.** The Trinec-Kosmos site, 2016–2019: (a) Average  $PM_{10}$  concentrations depending on the mixing layer height and wind speed; (b) The count of exceedances of daily concentrations of  $50 \mu\text{g}\cdot\text{m}^{-3}$  depending on the mixing layer height and wind speed.

The situation at the Věřňovice site was slightly different. The highest average hourly  $PM_{10}$  concentrations were observed at MLHs below 200 m and wind speeds between  $0.5\text{--}2 \text{ m}\cdot\text{s}^{-1}$ , or under calm conditions and wind speeds below  $0.5 \text{ m}\cdot\text{s}^{-1}$ . The highest average daily  $PM_{10}$  concentrations were observed at MLHs below 200 m and wind speeds below  $2 \text{ m}\cdot\text{s}^{-1}$ . The lowest average  $PM_{10}$  concentrations were reached at all levels with the highest wind speeds above  $2 \text{ m}\cdot\text{s}^{-1}$ . The highest number of  $50 \mu\text{g}\cdot\text{m}^{-3}$  value exceedances for  $PM_{10}$  daily concentrations was observed at wind speeds between 1 and  $2 \text{ m}\cdot\text{s}^{-1}$  and MLHs of 200 to 300 m, at lower wind speeds below  $1 \text{ m}\cdot\text{s}^{-1}$ , and MLHs below 200 m (Figure 13).

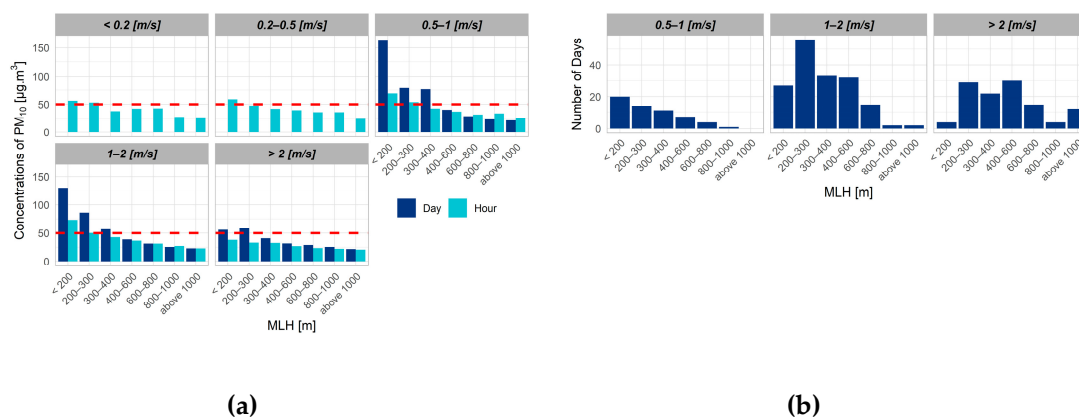


**Figure 13.** The Věřňovice site, 2016–2019: (a) Average  $PM_{10}$  concentration depending on the mixing layer height and wind speed; (b) The count of exceedances of daily concentrations of  $50 \mu\text{g}\cdot\text{m}^{-3}$  depending on the mixing layer height and wind speed.

The prevailing wind directions vary noticeably over the whole period from 2016 to 2019 at both sites (Figure 14). At the Trinec-Kosmos site, the prevailing wind direction is along the southeast/northwest axis, where the SE wind direction prevails. The average relative frequencies of counts of wind directions changed in the individual months throughout the whole period; the prevailing SE wind direction, however, remained. The least frequent wind direction was NE. At the Věřňovice site, the highest frequency of counts of the wind direction is along the southwest/northeast axis; the frequencies of counts of the prevailing wind direction, however, differed throughout the year. On average, the southwestern

(SW) wind direction prevailed in the cold months (October to March). In the warm part of the year, the NE and NW wind directions prevailed. The SE wind direction at the Věřňovice site was the least frequent throughout the whole monitored period.

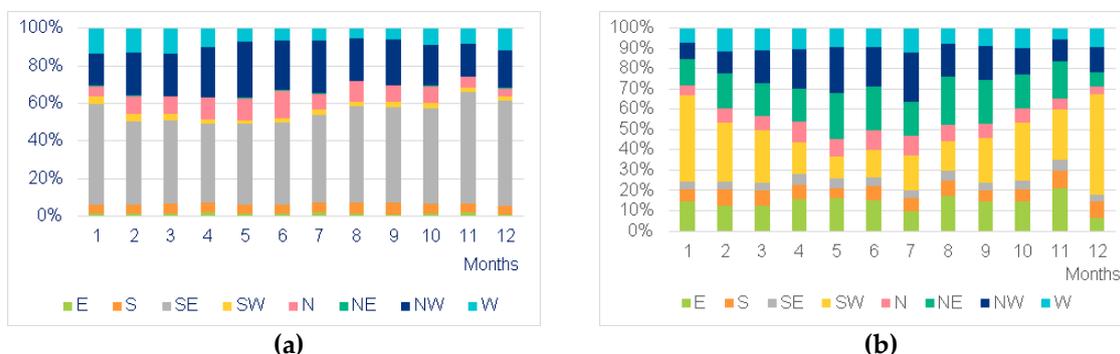


**Figure 14.** Relative frequency of counts of wind direction representation, 2016–2019: (a) the Trinec-Kosmos site; (b) the Věřňovice site.

The average monthly  $PM_{10}$  concentrations reached the highest values at the lowest average MLH in the cold months of the year at all wind directions at Trinec-Kosmos. The lowest average monthly  $PM_{10}$  concentrations were reached during the SE wind direction. During the SE and E wind directions, the MLHs also reached the lowest values of the average monthly heights of the mixing layer. In comparing the years from 2016 to 2019, it is apparent that on average, 2019 showed higher values of the mixing layer height than the preceding years, which is also reflected in the lower average  $PM_{10}$  concentrations (Figure 15).

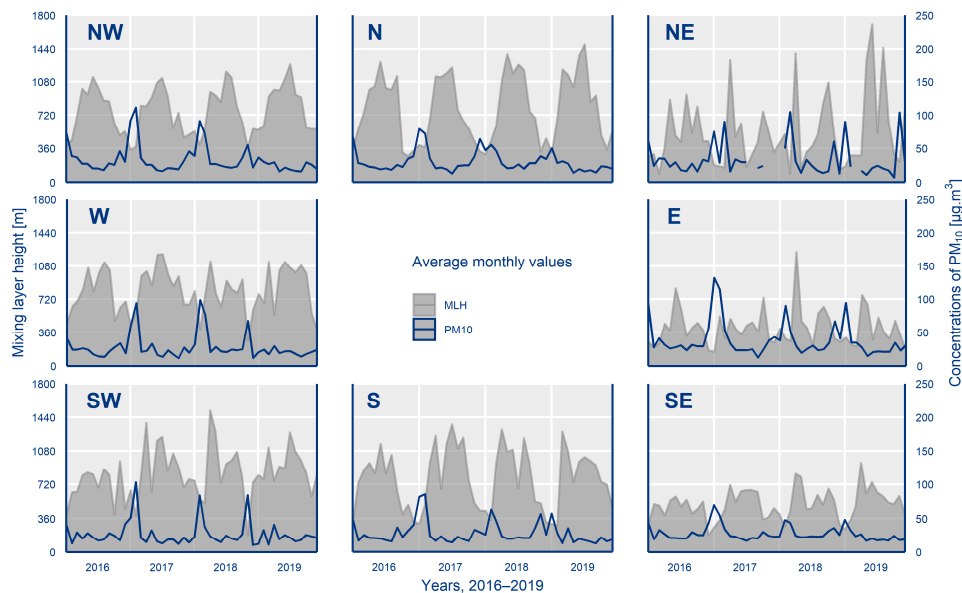


**Figure 15.** Average  $PM_{10}$  concentrations depending on the mixing layer height and wind direction, the Trinec-Kosmos site, 2016–2019.

The weighted concentration roses for  $PM_{10}$  divided according to the mixing layer height (Figure 16) show that the most frequent contribution to the average  $PM_{10}$  concentrations for the period from 2016 to 2019 comes to the Trinec-Kosmos site from a southeasterly direction, which basically corresponds to the described prevailing wind directions at this location. This information, however, does not necessarily mean that the maximum  $PM_{10}$  concentration contributions also come from the same direction; winds from other directions can carry higher concentrations of  $PM_{10}$ , which may lead to the exceedance of the

daily limit of the pollution value for PM<sub>10</sub> of 50 µg·m<sup>-3</sup>. The division of the weighted concentration roses according to the mixing layer height describes the PM<sub>10</sub> concentration at the height of the ground measurement at the site when the mixing layer height reached various levels.

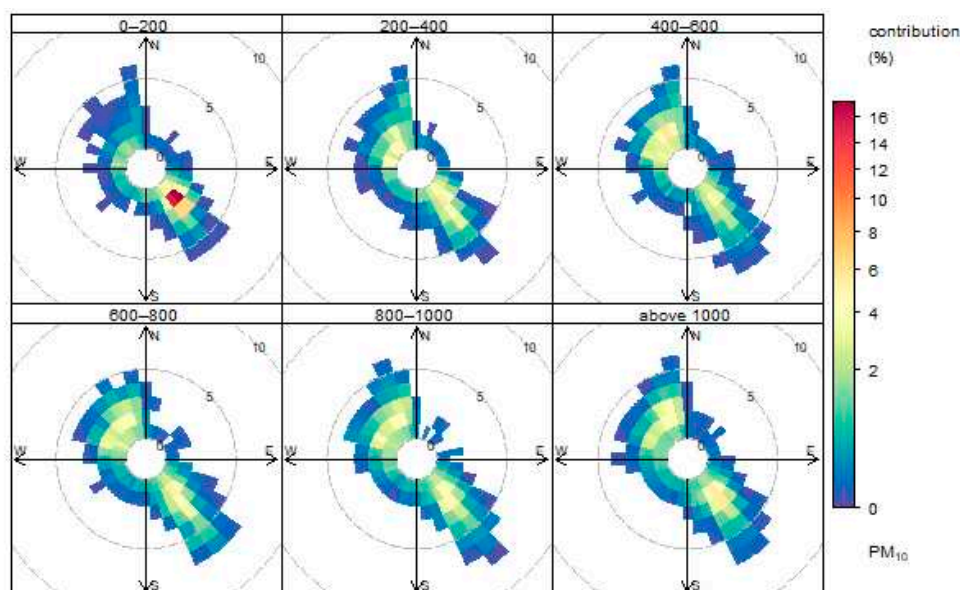


**Figure 16.** PM<sub>10</sub> weighted concentration rose divided according to the mixing layer height (in m), the Třinec-Kosmos site, 2016–2019.

The lowest MLHs at the Věřňovice site are registered for the NE and E wind directions, when the highest average PM<sub>10</sub> concentrations were reached over the entire period from 2016 to 2019. Conversely, the highest MLHs are reached during wind directions from the S to W sectors, when the lowest average monthly PM<sub>10</sub> concentrations occur during the SE and SW wind directions. Having compared the individual years, it becomes apparent that as well as at Třinec-Kosmos, the average MLH in 2019 was, on the whole, the highest, and the average PM<sub>10</sub> concentrations reached the lowest values of the entire monitoring period (Figure 17).

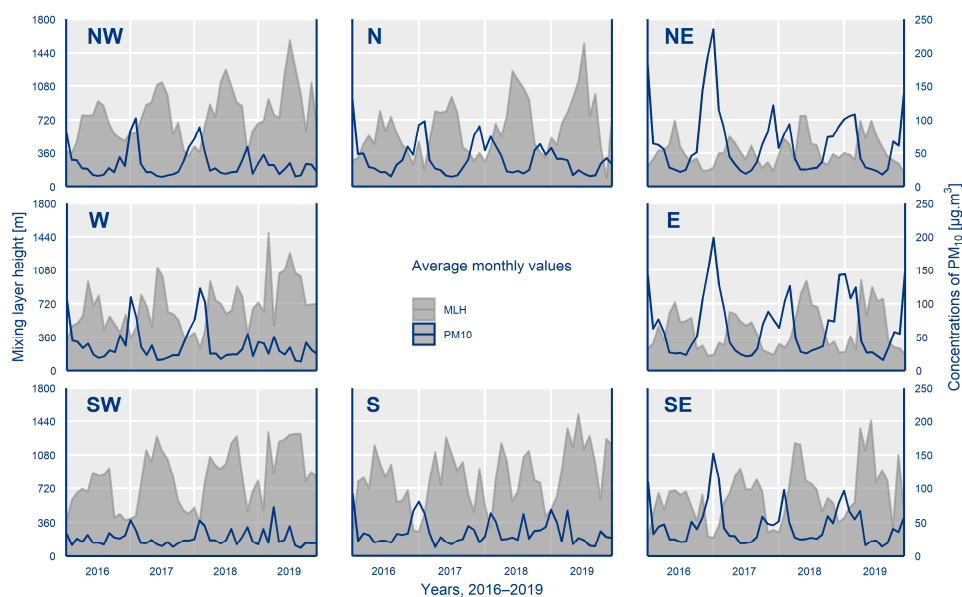


**Figure 17.** Average PM<sub>10</sub> concentrations depending on the mixing layer height and wind direction, the Věřňovice site, 2016–2019.

The weighted concentration roses for  $PM_{10}$ , divided according to the mixing layer height (Figure 18), show that the most frequent contribution to the average  $PM_{10}$  concentrations for the period from 2016 to 2019 come to the Věřňovice site from the NE sector at wind speeds of up to  $2 \text{ m}\cdot\text{s}^{-1}$ , despite the fact that, on the whole, the SW wind direction significantly prevails at the site. The division of the weighted concentration roses according to the mixing layer height does not describe the  $PM_{10}$  concentrations and the wind direction at a certain MLH, but a situation at a ground measurement height at the site and during the time when the mixing layer height reached the described height.

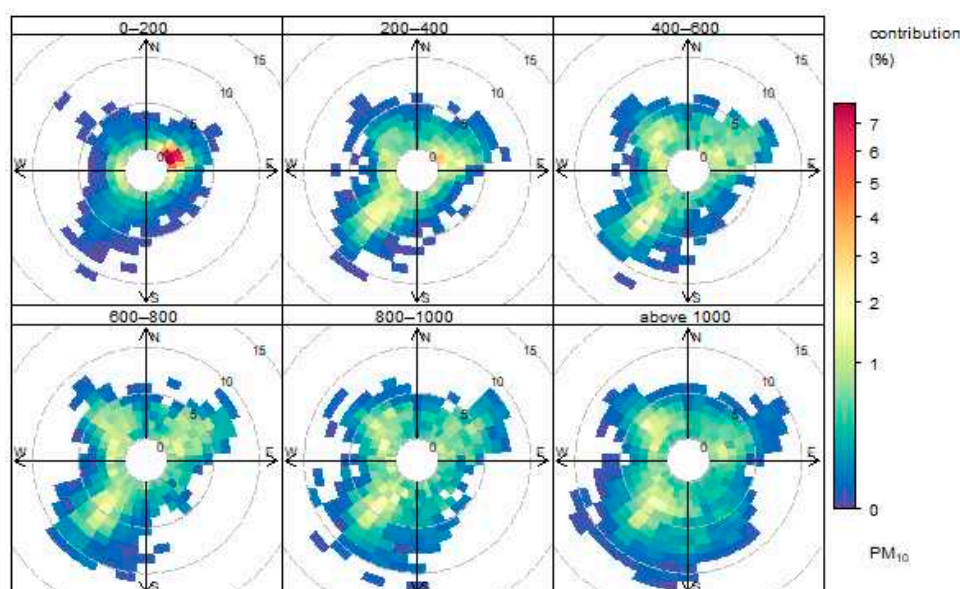


**Figure 18.** A weighted  $PM_{10}$  concentration rose divided according to the mixing layer height, the Věřňovice site, 2016–2019.

When comparing Figures 14, 17 and 18, a difference in the layout of the frequency of counts of wind directions between both sites becomes apparent. While at the Třinec-Kosmos site, a boundary of the prevailing wind direction along the southeast/northwest axis is more sharply visible in the pictures, at Věřňovice, despite the fact that the prevailing wind direction is along the southwest/northeast axis, the frequencies of counts of directions are spread more evenly to the other sectors, as well. This situation corresponds to the information described in Chapters 1 and 2.

The concentration roses (Figure 19) for 2016–2019 show that the maximum  $PM_{10}$  concentration contributions come to the Třinec-Kosmos site at a low MLH level of up to 200 m and low wind speeds of up to  $1 \text{ m}\cdot\text{s}^{-1}$  from the northern (N) to the western (W) sector. For MLHs of 200–400 m, an influence of the wind direction from the E sector is also significantly shown, as well as the influence from the N and W sectors. The average maximum  $PM_{10}$  concentration contributions at the site occur at MLHs of up to 400 m above the ground and at wind speeds of up to  $2 \text{ m}\cdot\text{s}^{-1}$ . On the occurrence of a higher MLH level of up to 600 m, a higher wind speed of above  $4 \text{ m}\cdot\text{s}^{-1}$  from the N and NE directions contributes to the resulting situation more significantly. From the point of view of the  $PM_{10}$  concentration roses divided according to the mixing layer height for the Třinec-Kosmos site, it is possible to regard the SW wind directions as those directions with the lowest  $PM_{10}$  contribution; at higher wind speeds of above  $4 \text{ m}\cdot\text{s}^{-1}$ , the S–SE directions also contribute the lowest amount.

Figure 20 illustrates concentration roses for the Věřňovice site for 2016–2019, which are divided according to the different heights of the mixing layer. The highest  $PM_{10}$  concentration contributions are reached up to the occurrence of MLHs of 200 m above the ground at wind speeds of up to  $2 \text{ m}\cdot\text{s}^{-1}$  from the E–NE. The influence of the wind from these directions is shown in the average maximum  $PM_{10}$  contributions up to the height of 600 m, during which time the influence of a rising wind speed of up to about  $6 \text{ m}\cdot\text{s}^{-1}$  also increases proportionally.

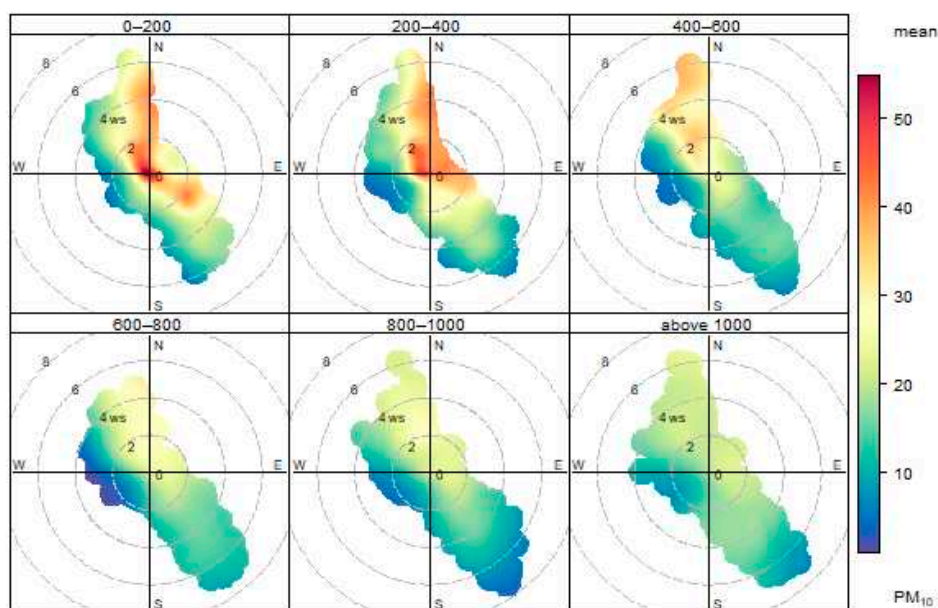


**Figure 19.** Average  $PM_{10}$  concentration roses divided according to the mixing layer height, Třinec-Kosmos site, 2016–2019.

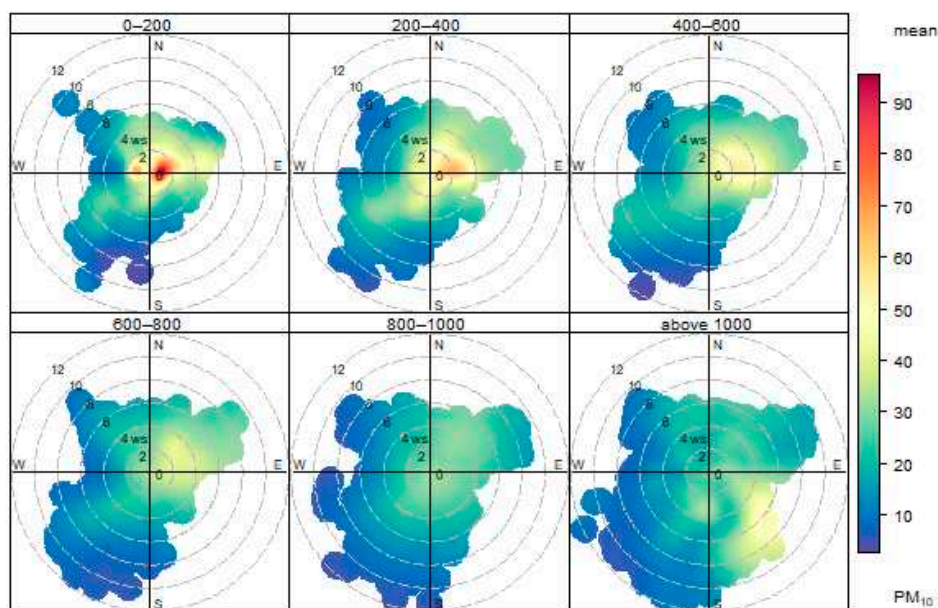


**Figure 20.** Average  $PM_{10}$  concentration roses divided according to the mixing layer height, the Věřňovice site, 2016–2019.

When comparing the  $PM_{10}$  concentration contributions at the sites after the division according to the wind directions and according to the MLH levels (Figures 15–20), it is apparent that at higher MLHs the contributions generally reach lower values for all wind directions.

#### 4. Discussion

The detection of dependences of  $PM_{10}$  concentrations on the mixing layer height may point out at possible pollution sources in the area; it would, however, be necessary to check the exact determination of the source type by other methods used in assessing the field of air quality, e.g., by more detailed air pollutant measurements and by methods for pollution source identification, e.g., Positive Matrix Factorization (PMF) [53] and back trajectories [54]. The high  $PM_{10}$  concentrations in combination with the low mixing layer height provide information about the high influence of low-emitting sources of

air pollution (individual heating) on the air quality at a given site. On the other hand, higher PM<sub>10</sub> concentrations reached at higher MLH levels show the influence of industrial sources, sources with emission release at greater heights. High concentrations combined with a low wind speed, perhaps even with no wind, show the influence of sources in the vicinity of the site. Conversely, higher wind speeds combined with high PM<sub>10</sub> concentrations correspond to the premise of transport from more remote places to the site [16,17,24–26].

The findings of this work correspond to the conclusions of Air Quality Improvement Program [52] elaborated for both sites and areas of interest in which the sites are located and also to the “Air Pollution Sources Contribution to PM<sub>2.5</sub> Concentration in the Northeastern Part of the Czech Republic” analysis [55].

As mentioned before in Section 2, the meteorological variables data used the analysis from the ground measurements of temperature at a height of 2 m above the ground; the wind direction and speed were measured at 10 m above the ground. The values of these variables at various mixing layer heights were not included in the analysis. A vertical wind direction and speed and temperature profile would be a significant addition to the assessment that would, among other things, provide information about the occurrence of temperature inversions. This information could be completed with distant measurement data or from model calculations in a subsequent assessment. It is necessary to point out again that the ceilometer measurement is biased by noise at the lowest level above the ground [46], which interferes up to roughly 50 m according to the existing available sources.

Although the PM<sub>10</sub> concentrations are significantly dependent both on the wind speed and the mixing layer height, the dependence of the wind speed and MLH does not show a significant statistical dependence. The differences are also apparent between both assessed sites with a statistically higher dependence detected at the Věřňovice site. Orography is assumed to play an important role in this aspect (Section 2). While the Věřňovice site is situated in open terrain, the Třinec-Kosmos site is situated in an urban development at the end of Jablunkov Furrow at the foothills of the Moravian-Silesian Beskydy mountains.

Correlation dependences for the wind direction and MLH have not been elaborated. The authors do not consider this aspect important. The prevailing wind direction is different at both sites, the difference lying mostly in the area geomorphology where the sites are situated. The authors find the wind direction and speed assessment sufficiently useful, divided according to the MLHs mentioned in this article. These indicators serve primarily for detection of the origin and location of possible pollution sources that influence the given area.

Another opportunity for analysis is the assessment of other pollutants’ dependence on the mixing layer height. Among the examples are ground-level ozone and processing for the warm part of the year [56], as well as a more detailed assessment of the behavior of pollutants such as sulfur dioxide, nitrogen dioxide, and suspended particles during winter smog situations when there is a low mixing layer height [32].

The disadvantage of an assessment of the relationships between meteorology and ambient air quality with regard to the mixing layer height lies in the fact that there are no available data from a longer sequence of ceilometer measurement. The assessment of the mixing layer height trends from a long-term point of view would surely bring additional information about the development or changes of the dispersion conditions, especially in the areas with poor air quality. The observed information may serve as a basis for the evaluation of current situations with high PM<sub>10</sub> concentrations, for announcing and invalidating smog situations, and model solutions of pollution situation forecasts.

## **5. Conclusions**

The presented analysis provides evidence of the influence of the mixing layer height, combined with other meteorological variables, on PM<sub>10</sub> concentrations in the area of the Czech-Polish border, which faces problems with a complex representation of a substantial number of various pollution

source types. The influence on the pollution situation in combination with meteorological variables at a given site also differs depending on the varied geographical conditions.

The influence of a temperature below 1 °C on the pollution situation is noticeable at both sites. The highest numbers of exceedances of PM<sub>10</sub> daily concentrations of 50 µg·m<sup>-3</sup> occur at low temperatures combined with a mixing layer height of up to 300 m. In the case of Třinec-Kosmos, the average PM<sub>10</sub> concentrations at temperatures below 1 °C reach the highest values on the occurrence of a mixing layer height of up to 300 to 400 m. The decrease in PM<sub>10</sub> concentrations with increasing MLHs at temperatures below 1 °C is not very significant. In this case, the influence of a rising height of the mixing layer at temperatures below 1 °C on the average PM<sub>10</sub> concentrations is not as significant as in the case of Věřňovice, where a difference of several tens of µg·m<sup>-3</sup> in the average PM<sub>10</sub> concentrations is observed between levels of up to 200 m, and levels of 200–300 m.

The influence of the wind speed on the occurrence of various MLHs on PM<sub>10</sub> concentrations is also noticeable. The average PM<sub>10</sub> hourly concentrations at Třinec-Kosmos are the highest at wind speeds of up to 0.2 m·s<sup>-1</sup>, or 0.5 m·s<sup>-1</sup>, at MLH levels of up to almost 600 m, at Věřňovice the influence of wind speeds of up to 2 m·s<sup>-1</sup> is detected. In both cases, throughout the assessment of the number of PM<sub>10</sub> daily concentrations above 50 µg·m<sup>-3</sup>, it is then clear that higher values occur in the case of Třinec at wind speeds of 0.5 up to 2 m·s<sup>-1</sup> and MLHs of 200–300 m. At the Věřňovice station, the highest number of limit value exceedances was observed at wind speeds between 1–2 m·s<sup>-1</sup> and at wind speeds above 2 m·s<sup>-1</sup> and MLHs of 200–300 m.

The influence of the wind direction combined with the MLH is different at both sites; however, it is crucial as well. Despite the fact that the most frequent PM<sub>10</sub> contributions come to the Třinec-Kosmos site from the SE direction, the average maximum concentration contributions come from the W–N sectors at low wind speeds and MLHs of up to 400 m. In Věřňovice, regardless of the prevailing SW wind direction, sources in the NE–E sector from the site have a crucial influence on the air pollution level caused by PM<sub>10</sub>. The maximum PM<sub>10</sub> contributions are reached on the occurrence of MLHs of up to 200 m at Věřňovice station.

**Author Contributions:** Conceptualization, V.V. and D.H.; methodology, V.V. and D.H.; formal analysis, V.V. and D.H.; investigation, V.V. and D.H.; resources, V.V. and D.H.; data curation, D.H. and V.V.; writing—original draft preparation, V.V.; writing—review and editing, D.H. and V.V.; visualization, D.H. and V.V.; supervision, V.V. and D.H.; project administration, V.V. All authors have read and agreed to the published version of the manuscript.

**Funding:** This research received no external funding.

**Acknowledgments:** The data for the analysis were provided by the Czech Hydrometeorological Institute ([www.chmi.cz](http://www.chmi.cz)). The assessment is based on measurements at the sites run by the Czech Hydrometeorological Institute.

**Conflicts of Interest:** The authors declare no conflicts of interest.

## References

1. WHO. *Health Effects of Particulate Matter*, 2nd ed.; Policy Implications for Countries in Eastern Europe, Caucasus and Central Asia; WHO Regional Office for Europe: Copenhagen, Denmark, 2013; ISBN 978-92-890-0001-7.
2. WHO. Ambient (Outdoor) Air Pollution. Available online: [https://www.who.int/en/news-room/fact-sheets/detail/ambient-\(outdoor\)-air-quality-and-health](https://www.who.int/en/news-room/fact-sheets/detail/ambient-(outdoor)-air-quality-and-health) (accessed on 2 February 2020).
3. Kampa, M.; Castanas, E. Human health effects of air pollution. *Environ. Pollut.* **2008**, *151*, 362–367. [[CrossRef](#)] [[PubMed](#)]
4. Schwartz, J. Air Pollution and Blood Markers of Cardiovascular Risk. *Environ. Health Perspect.* **2001**, *109*, 405–409. [[PubMed](#)]
5. Pope, C.A.; Dockery, D.W. Health Effects of Fine Particulate Air Pollution: Lines that Connect. *J. Air Waste Manag. Assoc.* **2006**, *56*, 709–742. [[CrossRef](#)]
6. EEA. *Air quality in Europe—2019 Report*, 1st ed.; Publications Office of the European Union: Copenhagen, Denmark, 2019; ISBN 978-92-9480-088-6.

7. IQ Air. World Most Polluted Cities 2019 (PM2.5). Available online: <https://www.iqair.com/world-most-polluted-cities> (accessed on 30 March 2020).
8. Prášek, J. *Změny Geografického Prostředí v Pohraničních Oblastech Ostravského a Hornoslezského Regionu (Changes in the Geographical Environment in the Border Regions of the Ostrava and Upper Silesian Regions)*; Ostravská Univerzita: Ostrava, Czech, 1998; Volume 1. (In Czech)
9. Prokop, R. Historická hranice Moravy a Slezska ve vývoji ostravské aglomerace (Historical boundary of Moravia and Silesia in the development of the Ostrava agglomeration). *Geogr. Rozhl.* **1996**, *6*, 4–5. (In Czech)
10. Šindler, P. Vývojové tendence sídelní struktury česko-polského pohraničí na příkladu severní Moravy a českého Slezska (Trends in the settlement structure of the Czech-Polish borderland on the example of North Moravia and Czech Silesia). *Geogr. Rozhl.* **1996**, *6*, 11–13. (In Czech)
11. EC. *Directive 2004/107/EC of the European Parliament and of the Council of 15 December 2004 Relating to Arsenic, Cadmium, Mercury, Nickel and Polycyclic Aromatic Hydrocarbons in Ambient Air*; EC: Brusel, Belgium, 2005.
12. EC. *Directive 2008/50/EC of the European Parliament and of the Council of 21 May 2008 on Ambient Air Quality and Cleaner Air for Europe*; EC: Brusel, Belgium, 2008.
13. Zákon č. 201/2012 Sb. ze dne 2. května 2012 o Ochráně Ovzduší (Act No. 201/2012 Coll. of 2 May 2012 on Air Protection); Tiskárna Ministerstva vnitra: Praha, Czech, 2012; pp. 2785–2848. (In Czech)
14. Hůnová, I. Ambient Air Quality in the Czech Republic: Past and Present. *Atmosphere* **2020**, *11*, 214. [[CrossRef](#)]
15. *Znečištění Ovzduší na Území České Republiky v Roce 2018 (Air Pollution in the Territory of the Czech Republic in 2018)*, 1st ed.; Czech Hydrometeorological Institute: Prague, Czech, 2019; ISBN 978-80-87577-95-0. (In Czech)
16. Bednář, J. *Meteorologie (Meteorology)*, 1st ed.; Úvod do Studia Dějů v Zemské Atmosféře (Introduction to the Study of Events in the Earth's Atmosphere); Portál: Praha, Czech, 2003; ISBN 80-7178-653-5. (In Czech)
17. Rein, F. Znečištění ovzduší a mezní vrstva atmosféry z hlediska klimatologie (Air pollution and atmospheric boundary layer in terms of climatology). *Meteorol. Zprávy* **1971**, *24*, 74–79. (In Czech)
18. Novák, M. *Meteorologie a Ochrana Prostředí*, 1st ed.; Úvod do Meteorologie a Klimatologie (Meteorology and Environmental Protection; Introduction to Meteorology and Climatology); Univerzita Jana Evangelisty Purkyně, Fakulta Životního Prostředí: Ústí nad Labem, Czech, 2004; ISBN 80-7044-597-1. (In Czech)
19. Jaňour, Z. *Modelování Mezní Vrstvy Atmosféry (Atmospheric Boundary Layer Modeling)*, 1st ed.; [Učební Text pro Posluchače Matematicko-Fyzikální Fakulty UK] [Textbook for Students of Faculty of Mathematics and Physics of Charles University]; Karolinum: Praha, Czech, 2001; ISBN 80-246-0330-6. (In Czech)
20. Keder, J.; Škáchová, H. *Hodnocení Rozptylových Podmínek pro Šíření Znečišťujících Látek Pomocí Ventilačního Indexu (Evaluation of Dispersion Conditions for the Diffusion of Pollutants Using the Ventilation Index)*; Vodní Zdroje Ekomonitor: Chrudim, Czech, 2011; pp. 19–23. (In Czech)
21. Baláková, L.; Škáchová, H.; Crhová, L. *Kvalita Ovzduší a Rozptylové Podmínky na Území ČR (Air Quality and Dispersion Conditions in the Czech Republic)*; Czech Hydrometeorological Institute: Prague, Czech, 2018. (In Czech)
22. Czernecki, B.; Pótrolniczak, M.; Kolendowicz, L.; Marosz, M.; Kendzierski, S.; Pilgaj, N. Influence of the atmospheric conditions on PM10 concentrations in Poznań, Poland. *J. Atmos. Chem.* **2017**, 115–139. [[CrossRef](#)]
23. Stull, R.B. *An Introduction to Boundary Layer Meteorology*, 1st ed.; Atmospheric and Oceanographic Sciences Library; Springer: Boston, MA, USA, 1988; ISBN 90-277-2769-4.
24. Blažek, Z.; Černikovský, L.; Krajny, E.; Krejčí, B.; Ošrůdka, L.; Volná, V.; Wojtylak, M. *Vliv Meteorologických Podmínek na Kvalitu Ovzduší v Přeshraniční Oblasti Slezska a Moravy (Influence of Meteorological Conditions on Air Quality in the Cross-Border Region of Silesia and Moravia)*, 1st ed.; Český Hydrometeorologický Ústav: Praha, Czech, 2013. (In Czech)
25. Blažek, Z.; Černikovský, L.; Krejčí, B.; Volná, V. Air Silesia—Meteorologicko-imisní vztahy a odhad transhraničního přenosu (Air Silesia—meteorological and air pollution relations and estimation of transboundary transmission). *Ochr. Ovzduší* **2014**, *26*, 53–61. (In Czech)
26. Blažek, Z.; Černikovský, L.; Krejčí, B.; Volná, V. Transboundary Air-Pollution Transport in the Czech-Polish Border Region between the Cities of Ostrava and Katowice. *Cent. Eur. J. Public Health* **2016**, *24*, 45–50.
27. Barmpadimos, I.; Hueglin, C.; Keller, J.; Henne, S.; Prévôt, A.S.H. Influence of meteorology on PM10 trends and variability in Switzerland from 1991 to 2008. *Atmos. Chem. Phys.* **2011**, *11*, 1813–1835. [[CrossRef](#)]
28. Reizer, M.; Juda-Rezler, K. Explaining the high PM<sub>10</sub> concentrations observed in Polish urban areas. *Air Qual. Atmos. Health* **2016**, *9*, 517–531. [[CrossRef](#)]

29. Volná, V.; Blažek, Z.; Krejčí, B. Zimní smogové situace na Ostravsku a Olomoucku v letech 2001–2016 (Winter smog situations in the Ostrava and Olomouc Regions in 2001–2016). *Meteorol. Zprávy* **2018**, *71*, 86–92. (In Czech)
30. Molnár, A.; Bécsi, Z.; Imre, K.; Gácsér, V.; Ferenczi, Z. Characterization of Background Aerosol Properties during a Wintertime Smog Episode. *Aerosol Air Qual. Res.* **2016**, *16*, 1793–1804. [[CrossRef](#)]
31. CHMI. Pravidla Fungování Smogového Varovného a Regulačního Systému (Rules of Operation of Smog Warning and Regulation System). Available online: [http://portal.chmi.cz/files/portal/docs/uoco/smog/SVRS\\_pravidla-fungovani.pdf](http://portal.chmi.cz/files/portal/docs/uoco/smog/SVRS_pravidla-fungovani.pdf) (accessed on 18 February 2020). (In Czech)
32. Volná, V.; Hladký, D. Koncentrace suspendovaných částic PM<sub>10</sub> a výška směšovací vrstvy v Moravskoslezském kraji během chladných sezón 2016/2017 a 2017/2018 (Concentrations of suspended particles PM<sub>10</sub> and mixing layer height in the Moravian-Silesian Region during the cold seasons 2016/2017 and 2017/2018). *Meteorol. Zprávy* **2019**, *72*, 77–87. (In Czech)
33. Oleniacz, R.; Bogacki, M.; Szulecka, A.; Rzeszutek, M.; Mazus, M. Assessing the impact of wind speed and mixing-layer height on air quality in Krakow (Poland) in the years 2014–2015. *JCEEA* **2016**, *33*, 315–342. [[CrossRef](#)]
34. Geiß, A.; Eiegner, M.; Bonn, B.; Schäfer, K.; Forkel, R.; von Schneidmesser, E.; Munkel, C.; Chan, K.L.; Nothard, R. Mixing layer height as an indicator for urban air quality? *Atmos. Meas. Tech.* **2017**, *10*, 2969–2988. [[CrossRef](#)]
35. Schäfer, K.; Emeis, S.; Hoffman, H.; Jahn, C. Influence of mixing layer height upon air pollution in urban and sub-urban areas. *Meteorol. Z.* **2006**, *15*, 647–658. [[CrossRef](#)]
36. Wagner, P.; Schäfer, K. Influence of mixing layer height on air pollutant concentrations in an urban street canyon. *Urban Clim.* **2017**, *22*, 64–79. [[CrossRef](#)]
37. Holst, J.; Mayer, H.; Holst, T. Effect of meteorological exchange conditions on PM<sub>10</sub> concentration. *Meteorol. Z.* **2008**, *17*, 273–282. [[CrossRef](#)]
38. Tiwari, S.; Dumka, U.C.; Gautam, A.S.; Kaskaoutis, D.G.; Srivastava, A.K.; Bisht, D.S.; Chakrabarty, R.K.; Sumlin, B.J.; Solmon, F. Assessment of PM<sub>2.5</sub> and PM<sub>10</sub> over Guwahati in Brahmaputra River Valley. *Atmos. Pollut. Res.* **2017**, *8*, 13–28. [[CrossRef](#)]
39. Zhao, H.; Che, H.; Ma, Y.; Wang, Y.; Yang, H.; Liu, Y.; Wang, Y.; Wang, H.; Zhang, X. The Relationship of PM Variation with Visibility and Mixing-Layer Height under Hazy/Foggy Conditions in the Multi-Cities of Northeast China. *Int. J. Environ. Res. Public Health* **2017**, *14*, 471. [[CrossRef](#)] [[PubMed](#)]
40. Czech Hydrometeorological Institute. Available online: <http://portal.chmi.cz/> (accessed on 18 February 2020).
41. CHMI. Trinec-Kosmos. Available online: [http://portal.chmi.cz/files/portal/docs/uoco/web\\_generator/locality/pollution\\_locality/loc\\_TTRO\\_CZ.html](http://portal.chmi.cz/files/portal/docs/uoco/web_generator/locality/pollution_locality/loc_TTRO_CZ.html) (accessed on 18 February 2020).
42. CHMI. Věřňovice. Available online: [http://portal.chmi.cz/files/portal/docs/uoco/web\\_generator/locality/pollution\\_locality/loc\\_TVER\\_CZ.html](http://portal.chmi.cz/files/portal/docs/uoco/web_generator/locality/pollution_locality/loc_TVER_CZ.html) (accessed on 18 February 2020).
43. MŽP. Sdělení Odboru Ochrany Ovzduší, Kterým se Stanoví Seznam Stanic Zahnutých Do Státní Sítě Imisního Monitoring (Communication from the Air Protection Department, Which Establishes a List of Stations Included in the National Air Pollution Monitoring Network). Available online: [http://portal.chmi.cz/files/portal/docs/uoco/oez/emise/evidence/aktual/Vestnik\\_2016\\_1.pdf](http://portal.chmi.cz/files/portal/docs/uoco/oez/emise/evidence/aktual/Vestnik_2016_1.pdf) (accessed on 22 March 2020). (In Czech)
44. CHMI. Air Pollution and Atmospheric Deposition in Data, the Czech Republic, 2018. Summary Tabular Survey. Available online: [http://portal.chmi.cz/files/portal/docs/uoco/isko/tab\\_roc/2018\\_enh/index\\_CZ.html](http://portal.chmi.cz/files/portal/docs/uoco/isko/tab_roc/2018_enh/index_CZ.html) (accessed on 20 March 2020).
45. Vaisala. Available online: <https://www.vaisala.com/en> (accessed on 11 January 2020).
46. Kotthaus, S.; O'Connor, E.; Munkel, C.; Charlton-Perez, C.; Haefelin, M.; Gabey, A.M.; Grimmond, C.S.B. Recommendations for processing atmospheric attenuated backscatter profiles from Vaisala CL31 ceilometers. *Atmos. Meas. Tech.* **2016**, *9*, 3769–3791. [[CrossRef](#)]
47. Carslaw, D.C.; Ropkins, K. Openair—An R package for air quality data analysis. *Environ. Model. Softw.* **2012**, *27–28*, 52–61. [[CrossRef](#)]
48. CHMI. *Znečištění Ovzduší na Území České Republiky v Roce 2015 (Air Pollution in the Czech Republic in 2015)*, 1st ed.; Český Hydrometeorologický Ústav: Praha, Czech, 2016; ISBN 978-80-87577-60-8. (In Czech)
49. ŘSD ČR. Intenzity Dopravy na Dálnicích a Silnicích I. Třídy v ČR v Roce 2010. Available online: <https://www.rsd.cz/wps/wcm/connect/b63a9557-7496-478a-8ef3-80629d92f954/pentlogram-2010.jpg?MOD=AJPERES> (accessed on 28 March 2020).

50. Czudek, T. *Reliéf Moravy a Slezska v Kvartéru (Relief of Moravia and Silesia in Quaternary)*, 1st ed.; Sursum: Tišnov, Czech, 1997; ISBN 80-85799-27-8. (In Czech)
51. Weissmannová, H. *Ostravsko*, 1st ed.; Agentura Ochrany Přírody a krajiny ČR: Praha, Czech, 2004; ISBN 80-86064-67-0. (In Czech)
52. MŽP. *Air Quality Improvement Program of Agglomeration Ostrava/Karviná/Frýdek-Místek—CZ08A*; MŽP: Praha, Czech, 2016.
53. Norris, G.; Duvall, R.; Brown, S.; Bai, S. *EPA Positive Matrix Factorization (PMF) 5.0 Fundamentals and User Guide*; US EPA: Washington, DC, USA, 2014.
54. Stein, A.F.; Draxler, R.R.; Rolph, G.D.; Stunder, B.J.B.; Cohen, M.D.; Ngan, F. NOAA's HYSPLIT Atmospheric Transport and Dispersion Modeling System. *Bull. Am. Meteorol. Soc.* **2015**, *96*, 2059–2077. [[CrossRef](#)]
55. Seibert, R.; Nikolova, I.; Volná, V.; Krejčí, B.; Hladký, D. Air Pollution Sources Contribution to PM<sub>2.5</sub> Concentration in Northeastern Part of the Czech Republic. *Atmosphere* **2020**. under review.
56. Komínková, K.; Holoubek, I. *Využití Dat z Ceilometru při Interpretaci Vývoje Koncentrací Látek v O vzduší Během Dne (Use of the Ceilometer Data to Explainig Changes in Pollutants Concetration Gradient in the Air during the Day)*; Masarykova Univerzita: Brno, Czech, 2017; pp. 198–202. (In Czech)



© 2020 by the authors. Licensee MDPI, Basel, Switzerland. This article is an open access article distributed under the terms and conditions of the Creative Commons Attribution (CC BY) license (<http://creativecommons.org/licenses/by/4.0/>).



Article

# Air Pollution Sources' Contribution to PM<sub>2.5</sub> Concentration in the Northeastern Part of the Czech Republic

Radim Seibert , Irina Nikolova, Vladimíra Volná , Blanka Krejčí  and Daniel Hladký

Ambient Air Quality Department, Czech Hydrometeorology Institute, 708 00 Ostrava, Czech Republic; irina.nikolova@chmi.cz (I.N.); vladimira.volna@chmi.cz (V.V.); blanka.krejci@chmi.cz (B.K.); daniel.hladky@chmi.cz (D.H.)

\* Correspondence: radim.seibert@chmi.cz

Received: 30 March 2020; Accepted: 15 May 2020; Published: 19 May 2020



**Abstract:** This article focuses on the source apportionment of air pollution in a specific northeastern part of the Czech Republic. The research area, located around the city of Třinec, is significantly affected by a complex spectrum of air pollution sources, including local residential heating (coal and wood burning), heavy industry (mainly iron and steel production), road traffic, and regional and long-range air pollution transport from the nearby cities, Poland, and other countries. The main pollution sources contributing to the total concentration of fine suspended particles (PM<sub>2.5</sub>) were evaluated on the basis of the measurements at three sites and on subsequent positive matrix factorization modeling. The six major air pollution factors were identified, and their relative and absolute contributions were quantified. The result of the study is that the most important current task of air protection is to reduce the residential emissions from solid fuels, which are responsible for approximately 50–60% of PM<sub>2.5</sub> concentration, followed by the regional primary and secondary aerosol sources (up to 40% of the total PM<sub>2.5</sub> aerosol mass). Lower contributions have been identified in the case of resuspended mineral and biogenic particles (15–20%), long-range (trans-European) air pollution transport (up to 10%), and heavy industry (up to 10% in the most affected location). A detailed discussion has been provided considering specific regional EC (elemental carbon)–OC (organic carbon) relations in the region with traditional coal-burning for household heating which complicate the interpretation of the PMF (Positive Matrix Factorization) results, especially due to the interference between the traffic, residential heating, and biogenic aerosol factors.

**Keywords:** source apportionment; PMF (Positive Matrix Factorization); air pollution; PM<sub>2.5</sub>

## 1. Introduction

In the past decades, in the post-socialist countries of Central and Eastern Europe, persistent concentrations of PM<sub>10</sub> and PM<sub>2.5</sub> [1,2] performing the role of carriers of toxicologically significant polycyclic aromatic hydrocarbons (PAH) [3] have been a prominent problem for air quality from the point of view of reaching the limits of pollution and the relevant associated health hazards. The pollution situation regarding these substances has been changing only very slowly, whereas the horizon of reaching air pollution limits in some regions has been impossible to estimate [4,5] (p. 62). One such outstandingly polluted area is the Silesian region, most of which is located in the territory of Poland, but which extends in part into the adjacent northeastern part of the Czech Republic. This is an area with a complex composition of air pollution sources. It has traditionally been a coal-mining region with heavy industry and high area urbanization with relevant vigorous motor vehicle traffic. In the Czech part of the region, there are two areas with different relations between emissions and air pollution. These are

Ostravsko, resembling in its orography the Polish basin part of Silesia, and Třinecko, of which the rugged terrain topography (the Beskydy foothills) leads to varied meteorological relations [6].

The cause of this serious air pollution is the especially high anthropogenic emissions of pollutants [7]. In order to decrease them, it is necessary to intensify measures aimed at the main pollution sources. Although air quality and pollution cause evaluations have been carried out for approximately 50 years, as a result of the gradual development and complexity of the relations between emissions and air pollution no professional consensus regarding the question at what rate the individual air pollution source types influence the air quality here has been agreed thus far; or let us just say that the answer to the question differs depending on the various time periods. The aim of the research has been to provide the source apportionment of the PM<sub>2.5</sub> ambient air concentration in Třinecko using the current procedures of receptor modeling and thus provide the basis for the correct direction of future measures to improve air quality. Identification of the main factor contributions influencing the PM<sub>2.5</sub> concentration has been the primary goal. Part of the research has been to compare the analytical methods ICP-MS (mass spectrometry with inductively coupled plasma) and ED XRF (energy-dispersive X-ray fluorescence spectrometry) from the point of view of their usability for source apportionment by means of receptor modeling. The goal of comparing these datasets was to find whether the results would differ in terms of the types of sources and their contribution to PM<sub>2.5</sub> concentration.

The methodology of the works carried out was based on project activities by the Czech Hydrometeorological Institute in cooperation with an American environmental protection agency (U.S. EPA, United States Environmental Protection Agency) in 2012 [8,9]. It was a pilot air pollution source apportionment in the Czech part of the Moravian-Silesian Region. The realization of the project proved that the methodology approach with the positive matrix factorization model (PMF) used brings credible results even for an area affected by a complex emission mixture.

The research area is located in the eastern part of the Czech Republic, in the Moravian-Silesian Region, in the vicinity of the international border with Poland (Figure 1a,b). The area of interest includes the town of Třinec and its surroundings up to a distance of tens of kilometers. In order to identify the sources by means of PMF, dust aerosol sampling has been carried out at three sites in the town of Třinec and its surrounding areas. These were the local areas of Kosmos, Ropice, and Vrchy (Figure 1c).

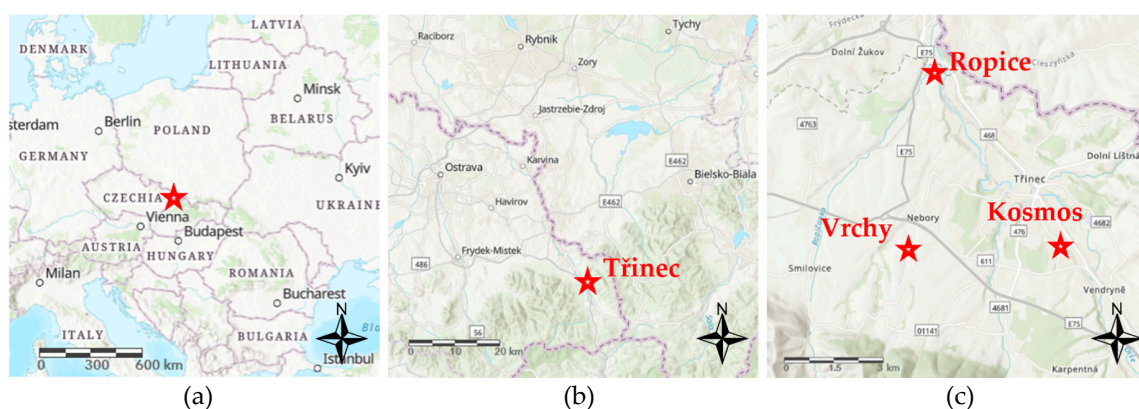


**Figure 1.** The location of the research area: (a) Position within Central Europe; (b) The position of the town of Třinec; (c) Sampling site locations. Topography base: <http://air.discomap.eea.europa.eu>.

The research area is affected by emissions from a number of various air pollution source types. From the Czech sources there is emission abundance, especially as far as iron metallurgy is concerned (TŘINECKÉ ŽELEZÁRNY, a.s. integrated steelworks on the north-northwestern periphery of the town of Třinec, approximately in the middle between the below-described sampling sites of Kosmos and Ropice). The other local industrial works relate mainly to the metallurgical production in Třinec and the regionally strongly developed automotive industry [7].

From the point of view of individual residential heating, the situation here is similar to the wider surrounding area in Silesia. Outside the towns, there is sparse low-floor housing development with the traditional representation of coal in the fuel mixture used for residential heating [10]. The intensity of motor vehicle traffic here does not exceed the usual values in similarly urbanized locations of the Czech Republic. It is localized towards the Třinec city center and international highway corridors towards Poland and Slovakia [11].

The average yearly concentrations of PM<sub>10</sub> and PM<sub>2.5</sub> in the ambient air have generally been decreasing in the direction from the heavily polluted city of Ostrava and its surroundings and the Polish part of Silesia in the north-northeast, to the relatively lightly polluted mountain area of the Beskydy in the south-southwest [12]. Apart from the Beskydy area, the PM<sub>2.5</sub> limit of pollution exceeds the values of 20 µg·m<sup>-3</sup> which is stated as the maximum limit by a regulation that comes into force in 2020 [7] (p. 179), [12]. The increased particulate matter concentrations (PM) bear relation to benzo[*a*]pyrene pollution, the limit of which has been exceeded several times over in the whole of the research area [7] (pp. 171–172).

The population in the research area is concentrated especially in the Olše valley, mainly in the city of Třinec. Our initial analysis, based on the population density, size, and immission concentrations, shows that within the research area, the current air pollution inflicts the highest population health hazards in the city of Třinec and in the villages located in the Jablunkov Furrow (Vendryně, Bystřice).

## 2. Experiments

### 2.1. Sampling Sites

One of the sampling sites marked in Figure 1c is Třinec-Kosmos, which is also the location of the current site of the same name of the National Air Quality Monitoring Network of the Czech Republic. The locality represents background concentrations in the residential zones in an urban environment. In the vicinity, there are a parking, four-lane roads, and residential individual houses with individual residential heating. The main industrial air pollution source in the surrounding area is an integrated steelworks, about 2 km to the north-northeast. With regard to the vicinity of the international border with Poland (about 3.5 km to the northeast), it is possible to presume significant transborder pollution transport.

The Ropice sampling site is situated in the flat valley of the River Olše, between the cities of Třinec and Český Těšín. The air pollution here is composed of industrial activity, especially in Třinec (there is an integrated steelworks in the vicinity of about 1.5 km to the southeast, and about 700 m in the same direction there is a neighboring industrial zone). Motor vehicle traffic in the surrounding areas is represented mainly by the E75 road and its two-level junction with Road II/468 about 300 m to the northwest. There are also local fugitive emissions of PM in the surrounding area (facilities for building-demolition waste use and other kinds of loose material handling), and individual residential heating. With regard to the vicinity of the international border with Poland (about 650 m to the northeast), it is also possible to expect significant transborder pollution transport here.

The Vrchy sampling site is situated in a slightly sloping area at the foothills of the Beskydy Mountains. It represents a background country location in an open, sparsely forested landscape with a diffused settlement of individual houses (the Silesian housing development). The main sources of pollution in the surrounding area are predominantly individual residential heating with solid fuels, and agricultural activities. The surrounding transport sources are mainly the newly built E75 moderately loaded four-lane highway about 850 m away.

### 2.2. Sample Collection

The measured species and the campaign duration followed up the evaluation requirements by means of the PMF model. The sampling campaign was designed to use the data from three sampling sites in the Třinecko area in the PMF model. By this approach, different sources influencing the air

quality in different parts of Trinecko were taken into account and a larger dataset was used, as it allowed to achieve more robust and more representative PMF results than could be provided by modeling of the individual locations. Samples collected at different sites have already been used in many other PMF source apportionment studies and, the approach has proven to increase the statistical significance of the analysis, although it assumes that the chemical profiles of the sources do not vary at the different sites [13] (pp. 134–136). The measurement at the three locations mentioned in Sections 1 and 2.1 was divided into summer and winter sampling. The summer sampling was carried out from 5 June 2018 at 6:00 a.m. to 4 July 2018 at 6:00 p.m. The winter sampling was carried out from 14 December 2018 at 6:00 a.m. to 21 January 2019 at 6:00 p.m. All times in this article are stated in coordinated universal time (UTC). The number of samples collected and subsequently lab processed during the summer campaign was 54 (Ropice) up to 56 (Vrchy), and during the winter campaign, the number ranged from 70 (Kosmos and Vrchy) to 78 (Ropice). In the case of both the ICP-MS (mass spectrometry with inductively coupled plasma) and ED XRF (energy-dispersive X-ray spectroscopy) datasets, the time series of total size from 125 (Kosmos) to 126 (Ropice and Vrchy) samples has been used for the PMF model (sum of the summer and winter samples). The number of samples has been sufficient for reliable source apportionment based on the PMF model, as it is in accordance with its official user guide [14] (PMF is often used on speciated PM<sub>2.5</sub> datasets with a size above 100 samples).

Three sequence automatic samplers (Sven Leckel SEQ, Ingenieurbüro GmbH, Berlin, Germany) and one manual sampler (Sven Leckel MVS, Ingenieurbüro GmbH, Berlin, Germany) have been placed at every sampling site. The samples for PAHs and selected organic molecular tracers were collected simultaneously on 47 mm quartz fiber filters and on polyurethane foam (PUF, density 0.022 g/cm<sup>3</sup>) to collect both solid and gas-phase components of the PAHs. The same quartz fiber filters were used to collect samples for a levoglucosan analysis. The samples for other species analyses were collected on 47 mm glass fiber filters, with the exception of the analysis using the ICP-MS method, which was carried out on cellulose nitrate filters of the same diameter. At the Ropice sampling site, one Leckel SEQ automatic sequence sampler was operated for sampling on 47 mm Teflon filters for subsequent analysis using the ED XRF method.

All the dust aerosol samples were collected continuously for 12 h. For the collection of all the samples, sampling flows and collection heads were used, ensuring representative sampling of PM<sub>2.5</sub> fraction. The measurement of gas pollutants was carried out at the Ropice and Vrchy sites by automatic continuous analyzers placed in the mobile air quality monitoring vehicles. At all the sites, the wind speed and direction were monitored throughout the entire measurement process.

### 2.3. Laboratory Analyses

The lab analyses were performed in the Czech Hydrometeorological Institute, with the exception of determining the Na<sup>+</sup>, K<sup>+</sup>, Ca<sup>2+</sup>, and Mg<sup>2+</sup> concentrations, which was done in the laboratories of the “ALS Czech Republic, s.r.o.” company (Prague, Czechia), and determining levoglucosan, which was done in the laboratories of the Institute of Chemical Process Fundamentals (ICPF) of the Czech Academy of Sciences. In all the collected aerosol samples, the same species were analyzed using the following methods to determine the ambient air concentrations:

- gravimetric analysis: PM<sub>2.5</sub> mass
- thermo-optical transmission: organic and elemental carbon (OC/EC)
- spectrometric analysis: ammonia (NH<sub>4</sub><sup>+</sup>)
- optical emission spectrometry with inductively coupled plasma (ICP-OES): Na<sup>+</sup>, K<sup>+</sup>, Ca<sup>2+</sup>, Mg<sup>2+</sup>
- ion chromatography with conductivity detection (IC-CD): sulfates and nitrates (SO<sub>4</sub><sup>2-</sup>, NO<sub>3</sub><sup>-</sup>)
- gas chromatography with mass detection (GC-MS):

- PAH (anthracene (A), benzo[*a*]anthracene (BaA), benzo[*a*]pyrene (BaP), benzo[*b*]fluoranthene (BbF), benzo[*e*]pyrene (BeP), benzo[*ghi*]perylene (BghiPRL), benzo[*j*]fluoranthene (BjF), benzo[*k*]fluoranthene (BkF), coronene (COR), chrysene (CRY), dibenz[*a,h*]anthracene (DBahA), phenanthrene (FEN), fluorene (Fl), fluoranthene (FLU), indeno[1,2,3-*cd*]pyrene (I123cdP), picene (PIC), perylene (PRL), pyrene (PYR), retene (RET)),
- hopanes (17 $\alpha$ (H)-22,29,30-trisnorhopane, 17 $\alpha$ (H),21 $\beta$ (H)-30-norhopane, 17 $\alpha$ (H),21 $\beta$ (H)-hopane, 17 $\beta$ (H),21 $\alpha$ (H)-hopane, 22S-17 $\alpha$ (H),21 $\beta$ (H)- homohopane, 22R-17 $\alpha$ (H),21 $\beta$ (H)-homohopane),
- steranes ( $\alpha\alpha\alpha$  20S-cholestane,  $\alpha\beta\beta$  (20R)-cholestane,  $\alpha\alpha\alpha$  20R-cholestane,  $\alpha\beta\beta$  20R 24S-methylcholestane,  $\alpha\beta\beta$  20R 24R-ethylcholestane,  $\alpha\alpha\alpha$  20R 24R-ethylcholestane)
- mass spectrometry with inductively coupled plasma (ICP-MS): Li, B, Na, Mg, Al, Si, K, Ca, Ti, V, Cr, Mn, Fe, Co, Ni, Cu, Zn, Ga, Ge, As, Se, Rb, Sr, Mo, Pd, Ag, Cd, In, Sn, Sb, Te, Cs, Ba, La, Ce, Pr, Nd, Sm, Eu, Gd, Tb, Dy, Ho, Er, Tm, Yb, Lu, Hf, Ta, W, Re, Hg, Tl, Pb, Bi, Th, U
- high-performance anion-exchange chromatography with pulsed amperometric detection (IC HPAE-PAD): levoglucosan
- continuous analyzer measurement:
  - UV-fluorescence (Teledyne Advanced Pollution Instrumentation T100): SO<sub>2</sub>
  - chemiluminescence (Teledyne Advanced Pollution Instrumentation T200): nitrogen oxides (NO, NO<sub>2</sub>, NO<sub>x</sub>)
  - optoelectronic method (FIDAS 200): PM<sub>2.5</sub>, PM<sub>10</sub>

At the Ropice site, within the usability of ED XRF testing, species concentrations were also determined by means of this method in the following scale: Na, Mg, Al, Si, S, K, Ca, Ti, V, Cr, Mn, Fe, Ni, Cu, Zn, As, Se, Cd, Sb, Ba, and Pb. A parallel set of results as an alternative to the results of ICP-MS was thus acquired for subsequent receptor modeling.

### 3. Results

#### 3.1. Wind Speed and Direction at the Sampling Sites

The following wind roses (Figure 2) document the situation at the sampling sites during the summer and winter sampling campaigns.

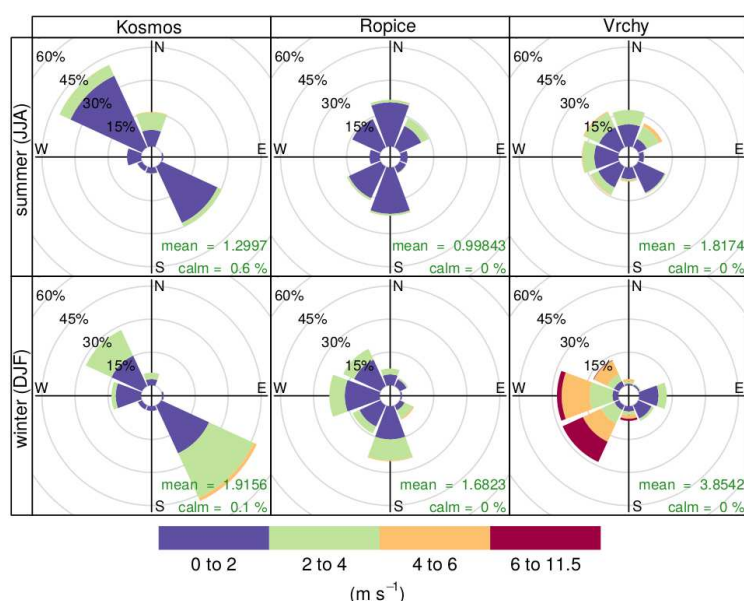


Figure 2. Wind roses structured by season representing the sampling campaign.

In order to interpret the modeling outputs and evaluate the predictive values of the assessment, the wind direction and speed were compared and measured during the sampling campaigns, with the average at the Kosmos site, which is also a site of the National Air Quality Monitoring Network of the Czech Republic, for the years 2009–2018. The prevailing wind direction corresponds to its long-term average. The average wind speed was generally higher (about 1.6 m.s<sup>-1</sup> at the time of sampling) as opposed to its long-term average (about 1.3 m.s<sup>-1</sup>).

### 3.2. Analysis of the Measured Concentrations

The summary Table 1 lists the mean species concentrations, standard deviations, and percentages of missing and below-detection-limit observations. In the case of metals, only the ICP-MS results are listed in the table, as they are available at all three sampling sites, as opposed to the ED XRF results, which were measured at the Ropice site only.

**Table 1.** Species quantified in this study (summary of all 3 sampling sites). Std. Dev.:Standard deviation; BDL: Below detection limit; N/A: no data available.

| Species           | SUMMER                     |                                 |                 |             | WINTER                     |                                 |                 |             |
|-------------------|----------------------------|---------------------------------|-----------------|-------------|----------------------------|---------------------------------|-----------------|-------------|
|                   | Mean (ng.m <sup>-3</sup> ) | Std. Dev. (ng.m <sup>-3</sup> ) | Percent Missing | Percent BDL | Mean (ng.m <sup>-3</sup> ) | Std. Dev. (ng.m <sup>-3</sup> ) | Percent Missing | Percent BDL |
| PM <sub>2.5</sub> | 1.3 × 10 <sup>4</sup>      | 6.0 × 10 <sup>3</sup>           | 0%              | 0%          | 2.8 × 10 <sup>4</sup>      | 3.4 × 10 <sup>4</sup>           | 0%              | 0%          |
| Li (ICP)          | 1.3 × 10 <sup>-1</sup>     | 8.7 × 10 <sup>-2</sup>          | 2%              | 88%         | 1.7 × 10 <sup>-1</sup>     | 2.2 × 10 <sup>-1</sup>          | 7%              | 2%          |
| B (ICP)           | 5.0 × 10 <sup>0</sup>      | 3.2 × 10 <sup>0</sup>           | 2%              | 24%         | 5.2 × 10 <sup>0</sup>      | 6.6 × 10 <sup>0</sup>           | 7%              | 26%         |
| Na (ICP)          | 8.6 × 10 <sup>1</sup>      | 7.3 × 10 <sup>1</sup>           | 2%              | 36%         | 1.1 × 10 <sup>2</sup>      | 1.1 × 10 <sup>2</sup>           | 7%              | 0%          |
| Mg (ICP)          | 2.9 × 10 <sup>1</sup>      | 1.8 × 10 <sup>1</sup>           | 2%              | 4%          | 2.0 × 10 <sup>1</sup>      | 7.0 × 10 <sup>1</sup>           | 7%              | 10%         |
| Al (ICP)          | 5.6 × 10 <sup>1</sup>      | 4.6 × 10 <sup>1</sup>           | 2%              | 10%         | 3.0 × 10 <sup>1</sup>      | 2.0 × 10 <sup>2</sup>           | 7%              | 4%          |
| Si (ICP)          | 1.0 × 10 <sup>2</sup>      | 1.5 × 10 <sup>2</sup>           | 2%              | 42%         | 1.2 × 10 <sup>2</sup>      | 1.9 × 10 <sup>2</sup>           | 7%              | 48%         |
| K (ICP)           | 1.1 × 10 <sup>2</sup>      | 1.3 × 10 <sup>2</sup>           | 2%              | 25%         | 2.8 × 10 <sup>2</sup>      | 9.4 × 10 <sup>2</sup>           | 7%              | 1%          |
| Ca (ICP)          | 9.8 × 10 <sup>1</sup>      | 7.2 × 10 <sup>1</sup>           | 2%              | 9%          | 2.9 × 10 <sup>1</sup>      | 5.4 × 10 <sup>1</sup>           | 7%              | 16%         |
| Ti (ICP)          | 1.3 × 10 <sup>0</sup>      | 8.8 × 10 <sup>-1</sup>          | 2%              | 6%          | 6.8 × 10 <sup>-1</sup>     | 1.3 × 10 <sup>0</sup>           | 7%              | 3%          |
| V (ICP)           | 3.5 × 10 <sup>-1</sup>     | 2.1 × 10 <sup>-1</sup>          | 2%              | 5%          | 1.5 × 10 <sup>-1</sup>     | 1.8 × 10 <sup>-1</sup>          | 7%              | 0%          |
| Cr (ICP)          | 3.6 × 10 <sup>0</sup>      | 2.3 × 10 <sup>0</sup>           | 2%              | 10%         | 1.1 × 10 <sup>0</sup>      | 2.0 × 10 <sup>0</sup>           | 7%              | 26%         |
| Mn (ICP)          | 8.6 × 10 <sup>0</sup>      | 1.3 × 10 <sup>1</sup>           | 2%              | 5%          | 6.4 × 10 <sup>0</sup>      | 1.4 × 10 <sup>1</sup>           | 7%              | 0%          |
| Fe (ICP)          | 2.4 × 10 <sup>2</sup>      | 3.8 × 10 <sup>2</sup>           | 2%              | 5%          | 1.7 × 10 <sup>2</sup>      | 3.7 × 10 <sup>2</sup>           | 7%              | 3%          |
| Co (ICP)          | 4.3 × 10 <sup>-2</sup>     | 3.5 × 10 <sup>-2</sup>          | 2%              | 12%         | 5.2 × 10 <sup>-2</sup>     | 6.7 × 10 <sup>-2</sup>          | 7%              | 0%          |
| Ni (ICP)          | 1.3 × 10 <sup>0</sup>      | 2.1 × 10 <sup>0</sup>           | 2%              | 36%         | 8.1 × 10 <sup>-1</sup>     | 1.6 × 10 <sup>0</sup>           | 7%              | 25%         |
| Cu (ICP)          | 4.6 × 10 <sup>0</sup>      | 3.4 × 10 <sup>0</sup>           | 2%              | 5%          | 4.6 × 10 <sup>0</sup>      | 1.6 × 10 <sup>1</sup>           | 7%              | 15%         |
| Zn (ICP)          | 3.6 × 10 <sup>1</sup>      | 3.7 × 10 <sup>1</sup>           | 2%              | 5%          | 3.4 × 10 <sup>1</sup>      | 8.0 × 10 <sup>1</sup>           | 7%              | 0%          |
| Ga (ICP)          | 1.6 × 10 <sup>-1</sup>     | 1.3 × 10 <sup>-1</sup>          | 2%              | 3%          | 3.5 × 10 <sup>-1</sup>     | 7.6 × 10 <sup>-1</sup>          | 7%              | 0%          |
| Ge (ICP)          | 6.9 × 10 <sup>-2</sup>     | 1.1 × 10 <sup>-1</sup>          | 2%              | 6%          | 1.1 × 10 <sup>-1</sup>     | 1.4 × 10 <sup>-1</sup>          | 7%              | 0%          |
| As (ICP)          | 7.7 × 10 <sup>-1</sup>     | 7.0 × 10 <sup>-1</sup>          | 2%              | 4%          | 1.3 × 10 <sup>0</sup>      | 1.3 × 10 <sup>0</sup>           | 7%              | 0%          |
| Se (ICP)          | 6.6 × 10 <sup>-1</sup>     | 4.2 × 10 <sup>-1</sup>          | 2%              | 18%         | 4.5 × 10 <sup>-1</sup>     | 5.5 × 10 <sup>-1</sup>          | 7%              | 6%          |
| Rb (ICP)          | 4.1 × 10 <sup>-1</sup>     | 5.8 × 10 <sup>-1</sup>          | 2%              | 5%          | 7.2 × 10 <sup>-1</sup>     | 9.3 × 10 <sup>-1</sup>          | 7%              | 0%          |
| Sr (ICP)          | 5.5 × 10 <sup>-1</sup>     | 3.7 × 10 <sup>-1</sup>          | 2%              | 6%          | 1.5 × 10 <sup>0</sup>      | 1.2 × 10 <sup>1</sup>           | 7%              | 6%          |
| Mo (ICP)          | 6.8 × 10 <sup>-1</sup>     | 1.6 × 10 <sup>0</sup>           | 2%              | 3%          | 4.8 × 10 <sup>-1</sup>     | 1.1 × 10 <sup>0</sup>           | 7%              | 0%          |
| Pd (ICP)          | 1.2 × 10 <sup>-3</sup>     | 6.3 × 10 <sup>-4</sup>          | 2%              | 82%         | 1.8 × 10 <sup>-3</sup>     | 7.8 × 10 <sup>-3</sup>          | 7%              | 29%         |
| Ag (ICP)          | 3.6 × 10 <sup>-2</sup>     | 3.4 × 10 <sup>-2</sup>          | 2%              | 7%          | 3.1 × 10 <sup>-2</sup>     | 3.5 × 10 <sup>-2</sup>          | 7%              | 6%          |
| Cd (ICP)          | 2.1 × 10 <sup>-1</sup>     | 2.0 × 10 <sup>-1</sup>          | 2%              | 1%          | 2.6 × 10 <sup>-1</sup>     | 3.1 × 10 <sup>-1</sup>          | 7%              | 3%          |
| In (ICP)          | 7.8 × 10 <sup>-3</sup>     | 7.3 × 10 <sup>-3</sup>          | 2%              | 32%         | 9.0 × 10 <sup>-3</sup>     | 1.2 × 10 <sup>-2</sup>          | 7%              | 1%          |
| Sn (ICP)          | 1.3 × 10 <sup>0</sup>      | 1.1 × 10 <sup>0</sup>           | 2%              | 3%          | 1.0 × 10 <sup>0</sup>      | 1.1 × 10 <sup>0</sup>           | 7%              | 1%          |
| Sb (ICP)          | 8.7 × 10 <sup>-1</sup>     | 6.6 × 10 <sup>-1</sup>          | 2%              | 3%          | 5.8 × 10 <sup>-1</sup>     | 6.6 × 10 <sup>-1</sup>          | 7%              | 0%          |
| Te (ICP)          | 8.2 × 10 <sup>-3</sup>     | 9.4 × 10 <sup>-3</sup>          | 2%              | 14%         | 1.1 × 10 <sup>-2</sup>     | 2.1 × 10 <sup>-2</sup>          | 7%              | 7%          |
| Cs (ICP)          | 7.3 × 10 <sup>-2</sup>     | 1.5 × 10 <sup>-1</sup>          | 2%              | 6%          | 1.1 × 10 <sup>-1</sup>     | 2.1 × 10 <sup>-1</sup>          | 7%              | 0%          |
| Ba (ICP)          | 1.8 × 10 <sup>0</sup>      | 1.1 × 10 <sup>0</sup>           | 2%              | 5%          | 4.1 × 10 <sup>0</sup>      | 3.1 × 10 <sup>1</sup>           | 7%              | 18%         |
| La (ICP)          | 4.0 × 10 <sup>-2</sup>     | 3.0 × 10 <sup>-2</sup>          | 2%              | 12%         | 1.2 × 10 <sup>-2</sup>     | 1.8 × 10 <sup>-2</sup>          | 7%              | 11%         |
| Ce (ICP)          | 7.7 × 10 <sup>-2</sup>     | 5.7 × 10 <sup>-2</sup>          | 2%              | 10%         | 2.2 × 10 <sup>-2</sup>     | 3.7 × 10 <sup>-2</sup>          | 7%              | 8%          |
| Pr (ICP)          | 9.4 × 10 <sup>-3</sup>     | 8.3 × 10 <sup>-3</sup>          | 2%              | 19%         | 2.0 × 10 <sup>-3</sup>     | 2.2 × 10 <sup>-3</sup>          | 7%              | 21%         |
| Nd (ICP)          | 3.4 × 10 <sup>-2</sup>     | 3.0 × 10 <sup>-2</sup>          | 2%              | 9%          | 8.3 × 10 <sup>-3</sup>     | 8.9 × 10 <sup>-3</sup>          | 7%              | 14%         |
| Sm (ICP)          | 6.8 × 10 <sup>-3</sup>     | 5.9 × 10 <sup>-3</sup>          | 2%              | 26%         | 2.0 × 10 <sup>-3</sup>     | 2.2 × 10 <sup>-3</sup>          | 7%              | 16%         |
| Eu (ICP)          | 2.0 × 10 <sup>-3</sup>     | 1.3 × 10 <sup>-3</sup>          | 2%              | 41%         | 2.5 × 10 <sup>-3</sup>     | 1.3 × 10 <sup>-2</sup>          | 7%              | 28%         |
| Gd (ICP)          | 7.3 × 10 <sup>-3</sup>     | 6.2 × 10 <sup>-3</sup>          | 2%              | 19%         | 2.7 × 10 <sup>-3</sup>     | 2.6 × 10 <sup>-3</sup>          | 7%              | 12%         |
| Tb (ICP)          | 1.1 × 10 <sup>-3</sup>     | 7.4 × 10 <sup>-4</sup>          | 2%              | 24%         | 7.6 × 10 <sup>-4</sup>     | 2.9 × 10 <sup>-4</sup>          | 61%             | 4%          |
| Dy (ICP)          | 5.0 × 10 <sup>-3</sup>     | 4.0 × 10 <sup>-3</sup>          | 2%              | 20%         | 1.5 × 10 <sup>-3</sup>     | 1.7 × 10 <sup>-3</sup>          | 7%              | 23%         |

Table 1. Cont.

| Species                       | SUMMER                        |                                    |                    |                | WINTER                        |                                    |                    |                |
|-------------------------------|-------------------------------|------------------------------------|--------------------|----------------|-------------------------------|------------------------------------|--------------------|----------------|
|                               | Mean<br>(ng.m <sup>-3</sup> ) | Std. Dev.<br>(ng.m <sup>-3</sup> ) | Percent<br>Missing | Percent<br>BDL | Mean<br>(ng.m <sup>-3</sup> ) | Std. Dev.<br>(ng.m <sup>-3</sup> ) | Percent<br>Missing | Percent<br>BDL |
| Ho (ICP)                      | 1.1 × 10 <sup>-3</sup>        | 7.4 × 10 <sup>-4</sup>             | 2%                 | 23%            | 8.1 × 10 <sup>-4</sup>        | 3.0 × 10 <sup>-4</sup>             | 57%                | 3%             |
| Er (ICP)                      | 3.0 × 10 <sup>-3</sup>        | 2.2 × 10 <sup>-3</sup>             | 2%                 | 31%            | 1.1 × 10 <sup>-3</sup>        | 7.7 × 10 <sup>-4</sup>             | 7%                 | 68%            |
| Tm (ICP)                      | 6.4 × 10 <sup>-4</sup>        | 3.6 × 10 <sup>-4</sup>             | 2%                 | 54%            | 6.2 × 10 <sup>-4</sup>        | 1.7 × 10 <sup>-4</sup>             | 80%                | 5%             |
| Yb (ICP)                      | 2.8 × 10 <sup>-3</sup>        | 2.1 × 10 <sup>-3</sup>             | 2%                 | 35%            | 1.0 × 10 <sup>-3</sup>        | 1.0 × 10 <sup>-3</sup>             | 7%                 | 30%            |
| Lu (ICP)                      | 5.5 × 10 <sup>-4</sup>        | 3.1 × 10 <sup>-4</sup>             | 2%                 | 67%            | 5.8 × 10 <sup>-4</sup>        | 1.9 × 10 <sup>-4</sup>             | 88%                | 4%             |
| Hf (ICP)                      | 6.0 × 10 <sup>-3</sup>        | 4.5 × 10 <sup>-3</sup>             | 2%                 | 14%            | 2.7 × 10 <sup>-3</sup>        | 4.4 × 10 <sup>-3</sup>             | 7%                 | 12%            |
| Ta (ICP)                      | 1.4 × 10 <sup>-1</sup>        | 2.7 × 10 <sup>-1</sup>             | 2%                 | 64%            | 6.1 × 10 <sup>-2</sup>        | 1.2 × 10 <sup>-1</sup>             | 7%                 | 61%            |
| W (ICP)                       | 6.4 × 10 <sup>-2</sup>        | 7.5 × 10 <sup>-2</sup>             | 2%                 | 6%             | 8.5 × 10 <sup>-2</sup>        | 9.4 × 10 <sup>-2</sup>             | 7%                 | 3%             |
| Re (ICP)                      | 2.3 × 10 <sup>-3</sup>        | 5.2 × 10 <sup>-3</sup>             | 2%                 | 30%            | 1.6 × 10 <sup>-3</sup>        | 1.6 × 10 <sup>-3</sup>             | 26%                | 0%             |
| Hg (ICP)                      | 1.0 × 10 <sup>-1</sup>        | 1.5 × 10 <sup>-1</sup>             | 2%                 | 94%            | 1.7 × 10 <sup>-1</sup>        | 2.6 × 10 <sup>-1</sup>             | 7%                 | 27%            |
| Tl (ICP)                      | 6.0 × 10 <sup>-2</sup>        | 5.2 × 10 <sup>-2</sup>             | 2%                 | 11%            | 1.3 × 10 <sup>-1</sup>        | 2.0 × 10 <sup>-1</sup>             | 7%                 | 0%             |
| Pb (ICP)                      | 8.5 × 10 <sup>0</sup>         | 7.8 × 10 <sup>0</sup>              | 2%                 | 1%             | 1.1 × 10 <sup>1</sup>         | 1.4 × 10 <sup>1</sup>              | 7%                 | 0%             |
| Bi (ICP)                      | 2.4 × 10 <sup>-1</sup>        | 3.0 × 10 <sup>-1</sup>             | 2%                 | 2%             | 7.3 × 10 <sup>-1</sup>        | 5.2 × 10 <sup>0</sup>              | 7%                 | 3%             |
| Th (ICP)                      | 7.4 × 10 <sup>-3</sup>        | 5.9 × 10 <sup>-3</sup>             | 2%                 | 16%            | 1.5 × 10 <sup>-3</sup>        | 1.7 × 10 <sup>-3</sup>             | 7%                 | 27%            |
| U (ICP)                       | 7.1 × 10 <sup>-3</sup>        | 6.8 × 10 <sup>-3</sup>             | 2%                 | 29%            | 7.9 × 10 <sup>-3</sup>        | 1.3 × 10 <sup>-2</sup>             | 7%                 | 55%            |
| OC                            | 4.3 × 10 <sup>3</sup>         | 1.7 × 10 <sup>3</sup>              | 0%                 | 0%             | 1.9 × 10 <sup>3</sup>         | 2.3 × 10 <sup>3</sup>              | 7%                 | 0%             |
| EC                            | 5.2 × 10 <sup>2</sup>         | 3.1 × 10 <sup>2</sup>              | 0%                 | 0%             | 1.1 × 10 <sup>4</sup>         | 1.3 × 10 <sup>4</sup>              | 7%                 | 0%             |
| sulphates                     | 2.7 × 10 <sup>3</sup>         | 1.1 × 10 <sup>3</sup>              | 0%                 | 0%             | 3.2 × 10 <sup>3</sup>         | 2.7 × 10 <sup>3</sup>              | 7%                 | 0%             |
| nitrates                      | 1.3 × 10 <sup>3</sup>         | 7.1 × 10 <sup>2</sup>              | 0%                 | 0%             | 2.2 × 10 <sup>3</sup>         | 2.0 × 10 <sup>3</sup>              | 7%                 | 0%             |
| ammonium ion                  | 5.0 × 10 <sup>2</sup>         | 3.9 × 10 <sup>2</sup>              | 0%                 | 0%             | 1.2 × 10 <sup>3</sup>         | 1.4 × 10 <sup>3</sup>              | 7%                 | 0%             |
| Fluorene                      | 7.5 × 10 <sup>0</sup>         | 5.0 × 10 <sup>0</sup>              | 5%                 | 1%             | 2.4 × 10 <sup>1</sup>         | 1.9 × 10 <sup>1</sup>              | 11%                | 0%             |
| Phenanthrene                  | 1.3 × 10 <sup>1</sup>         | 6.7 × 10 <sup>0</sup>              | 5%                 | 0%             | 4.8 × 10 <sup>1</sup>         | 3.1 × 10 <sup>1</sup>              | 11%                | 0%             |
| Anthracene                    | 3.8 × 10 <sup>-1</sup>        | 3.1 × 10 <sup>-1</sup>             | 5%                 | 0%             | 5.3 × 10 <sup>0</sup>         | 5.5 × 10 <sup>0</sup>              | 11%                | 0%             |
| Fluoranthene                  | 3.1 × 10 <sup>0</sup>         | 1.5 × 10 <sup>0</sup>              | 5%                 | 0%             | 1.9 × 10 <sup>1</sup>         | 1.5 × 10 <sup>1</sup>              | 11%                | 0%             |
| Pyrene                        | 1.5 × 10 <sup>0</sup>         | 7.7 × 10 <sup>-1</sup>             | 5%                 | 0%             | 1.3 × 10 <sup>1</sup>         | 1.2 × 10 <sup>1</sup>              | 11%                | 0%             |
| Benz[a]anthracene             | 3.0 × 10 <sup>-1</sup>        | 2.5 × 10 <sup>-1</sup>             | 5%                 | 1%             | 6.8 × 10 <sup>0</sup>         | 7.9 × 10 <sup>0</sup>              | 11%                | 0%             |
| Chrysene                      | 3.8 × 10 <sup>-1</sup>        | 2.5 × 10 <sup>-1</sup>             | 5%                 | 0%             | 5.0 × 10 <sup>0</sup>         | 5.4 × 10 <sup>0</sup>              | 11%                | 0%             |
| Benzo[b]fluoranthene          | 4.6 × 10 <sup>-1</sup>        | 3.5 × 10 <sup>-1</sup>             | 5%                 | 0%             | 4.0 × 10 <sup>0</sup>         | 3.8 × 10 <sup>0</sup>              | 11%                | 0%             |
| Benzo[k]fluoranthene          | 2.2 × 10 <sup>-1</sup>        | 1.7 × 10 <sup>-1</sup>             | 5%                 | 2%             | 2.1 × 10 <sup>0</sup>         | 2.0 × 10 <sup>0</sup>              | 11%                | 0%             |
| Benzo[j]fluoranthene          | 2.4 × 10 <sup>-1</sup>        | 1.8 × 10 <sup>-1</sup>             | 5%                 | 1%             | 1.9 × 10 <sup>0</sup>         | 1.9 × 10 <sup>0</sup>              | 11%                | 0%             |
| Benzo[a]pyrene                | 3.2 × 10 <sup>-1</sup>        | 2.3 × 10 <sup>-1</sup>             | 5%                 | 1%             | 3.9 × 10 <sup>0</sup>         | 4.3 × 10 <sup>0</sup>              | 11%                | 0%             |
| Indeno[1,2,3-cd]pyrene        | 2.9 × 10 <sup>-1</sup>        | 2.8 × 10 <sup>-1</sup>             | 5%                 | 6%             | 4.4 × 10 <sup>0</sup>         | 4.5 × 10 <sup>0</sup>              | 11%                | 0%             |
| Dibenz[a,h]anthracene         | 1.5 × 10 <sup>-1</sup>        | 1.4 × 10 <sup>-1</sup>             | 5%                 | 6%             | 9.9 × 10 <sup>-1</sup>        | 1.0 × 10 <sup>0</sup>              | 11%                | 0%             |
| Benzo[g,h,i]perylene          | 2.8 × 10 <sup>-1</sup>        | 2.2 × 10 <sup>-1</sup>             | 5%                 | 2%             | 2.9 × 10 <sup>0</sup>         | 3.0 × 10 <sup>0</sup>              | 11%                | 0%             |
| Coronene                      | 9.2 × 10 <sup>-2</sup>        | 6.0 × 10 <sup>-2</sup>             | 5%                 | 11%            | 8.5 × 10 <sup>-1</sup>        | 9.1 × 10 <sup>-1</sup>             | 11%                | 0%             |
| Perylene                      | 6.9 × 10 <sup>-2</sup>        | 5.1 × 10 <sup>-2</sup>             | 5%                 | 26%            | 5.9 × 10 <sup>-1</sup>        | 6.4 × 10 <sup>-1</sup>             | 11%                | 2%             |
| Retene                        | 2.1 × 10 <sup>-1</sup>        | 1.3 × 10 <sup>-1</sup>             | 5%                 | 1%             | 2.5 × 10 <sup>0</sup>         | 2.9 × 10 <sup>0</sup>              | 11%                | 0%             |
| Picene                        | 8.4 × 10 <sup>-2</sup>        | 4.7 × 10 <sup>-2</sup>             | 5%                 | 11%            | 8.3 × 10 <sup>-1</sup>        | 1.0 × 10 <sup>0</sup>              | 11%                | 0%             |
| Benzo[e]pyrene                | 2.9 × 10 <sup>-1</sup>        | 2.3 × 10 <sup>-1</sup>             | 5%                 | 1%             | 2.0 × 10 <sup>0</sup>         | 2.0 × 10 <sup>0</sup>              | 11%                | 0%             |
| Na <sup>+</sup>               | 4.2 × 10 <sup>3</sup>         | 1.4 × 10 <sup>3</sup>              | 0%                 | 0%             | 2.5 × 10 <sup>3</sup>         | 6.4 × 10 <sup>2</sup>              | 7%                 | 0%             |
| K <sup>+</sup>                | 1.7 × 10 <sup>2</sup>         | 1.1 × 10 <sup>2</sup>              | 0%                 | 2%             | 3.3 × 10 <sup>2</sup>         | 1.4 × 10 <sup>3</sup>              | 7%                 | 0%             |
| Ca <sup>2+</sup>              | 5.1 × 10 <sup>3</sup>         | 1.6 × 10 <sup>3</sup>              | 0%                 | 0%             | 3.4 × 10 <sup>3</sup>         | 9.8 × 10 <sup>2</sup>              | 7%                 | 0%             |
| Mg <sup>2+</sup>              | 6.2 × 10 <sup>2</sup>         | 3.1 × 10 <sup>2</sup>              | 0%                 | 0%             | 3.1 × 10 <sup>2</sup>         | 1.4 × 10 <sup>2</sup>              | 7%                 | 0%             |
| levoglucosan                  | 7.8 × 10 <sup>1</sup>         | 7.1 × 10 <sup>1</sup>              | 0%                 | 1%             | 5.8 × 10 <sup>2</sup>         | 5.7 × 10 <sup>2</sup>              | 7%                 | 0%             |
| SO <sub>2</sub>               | 7.1 × 10 <sup>3</sup>         | 3.9 × 10 <sup>3</sup>              | 67%                | 0%             | 8.8 × 10 <sup>3</sup>         | 8.2 × 10 <sup>3</sup>              | 70%                | 0%             |
| NO                            | 1.2 × 10 <sup>3</sup>         | 1.0 × 10 <sup>3</sup>              | 33%                | 0%             | 2.9 × 10 <sup>3</sup>         | 5.1 × 10 <sup>3</sup>              | 36%                | 0%             |
| NO <sub>2</sub>               | 1.1 × 10 <sup>4</sup>         | 6.5 × 10 <sup>3</sup>              | 33%                | 0%             | 1.4 × 10 <sup>4</sup>         | 1.1 × 10 <sup>4</sup>              | 36%                | 0%             |
| CO                            | 2.1 × 10 <sup>5</sup>         | 2.6 × 10 <sup>4</sup>              | 95%                | 0%             | 4.8 × 10 <sup>5</sup>         | 4.8 × 10 <sup>5</sup>              | 36%                | 0%             |
| O <sub>3</sub>                | N/A                           | N/A                                | 100%               | 0%             | 3.9 × 10 <sup>4</sup>         | 1.6 × 10 <sup>4</sup>              | 9%                 | 0%             |
| ααα 20R-Cholestane            | 9.9 × 10 <sup>-2</sup>        | 8.4 × 10 <sup>-2</sup>             | 7%                 | 64%            | 9.5 × 10 <sup>-2</sup>        | 3.1 × 10 <sup>-2</sup>             | 16%                | 82%            |
| ααα 20R 24R-Ethylcholestane   | N/A                           | N/A                                | 100%               | 0%             | 2.3 × 10 <sup>-1</sup>        | 2.4 × 10 <sup>-1</sup>             | 11%                | 49%            |
| 17α(H)-22,29,30-Trisnorhopane | 9.6 × 10 <sup>-2</sup>        | 5.4 × 10 <sup>-2</sup>             | 7%                 | 57%            | 5.7 × 10 <sup>-1</sup>        | 6.7 × 10 <sup>-1</sup>             | 10%                | 2%             |
| 17α(H),21β(H)-30-Norhopane    | 2.0 × 10 <sup>-1</sup>        | 1.1 × 10 <sup>-1</sup>             | 7%                 | 54%            | 7.9 × 10 <sup>-1</sup>        | 7.7 × 10 <sup>-1</sup>             | 10%                | 0%             |
| 17α(H),21β(H)-Hopane          | 2.8 × 10 <sup>-1</sup>        | 1.8 × 10 <sup>-1</sup>             | 7%                 | 77%            | 9.0 × 10 <sup>-1</sup>        | 8.9 × 10 <sup>-1</sup>             | 10%                | 0%             |
| 17β(H),21α(H)-Hopane          | 7.1 × 10 <sup>-2</sup>        | 3.0 × 10 <sup>-2</sup>             | 7%                 | 81%            | 4.1 × 10 <sup>-1</sup>        | 4.5 × 10 <sup>-1</sup>             | 10%                | 3%             |
| 17α(H),21β(H)-22S-Homohopane  | 2.1 × 10 <sup>-1</sup>        | 1.2 × 10 <sup>-1</sup>             | 7%                 | 85%            | 3.7 × 10 <sup>-1</sup>        | 4.7 × 10 <sup>-1</sup>             | 10%                | 2%             |
| 17α(H),21β(H)-22R-Homohopane  | 1.1 × 10 <sup>-1</sup>        | 7.1 × 10 <sup>-2</sup>             | 7%                 | 73%            | 7.0 × 10 <sup>-1</sup>        | 8.3 × 10 <sup>-1</sup>             | 10%                | 0%             |

The measured data show significantly higher concentrations and time variations of heavy PAHs, levoglucosan, retene, picene, and elemental carbon during the winter sampling campaign (about or more than one order of magnitude). On the other hand, most of the typical crustal species, like Mg, Al, Ca, T, and lanthanoides, plus organic carbon, show higher concentrations and variations in the summer. The highest PM<sub>2.5</sub> concentrations were detected at Ropice, somewhat lower concentrations at the Kosmos site and the significantly lowest concentrations at the Vrchy site. In the time series of some metals and hopanes, a sizable percentage of values occurred below the detection limit of the laboratory methods. These cases tended to occur more often in the summer period. The laboratory method sensitivity to detect the concentrations of other analytes was sufficient to reliably quantify its concentrations.

Tables 2 and 3 list the mean species concentrations, standard deviations, and percentages of missing and below-detection-limit observations at the Ropice sampling site provided by ICP-MS and ED XRF methods in the summer and winter samplings, respectively.

**Table 2.** Species concentrations at the Ropice site measured by ICP-MS and ED XRF during the summer sampling period. Std. Dev.: Standard deviation; BDL: Below detection limit.

| Species | ICP-MS                     |                                 |                 |             | ED XRF                     |                                 |                 |             |
|---------|----------------------------|---------------------------------|-----------------|-------------|----------------------------|---------------------------------|-----------------|-------------|
|         | Mean (ng.m <sup>-3</sup> ) | Std. Dev. (ng.m <sup>-3</sup> ) | Percent Missing | Percent BDL | Mean (ng.m <sup>-3</sup> ) | Std. Dev. (ng.m <sup>-3</sup> ) | Percent Missing | Percent BDL |
| Na      | 8.5 × 10 <sup>1</sup>      | 7.4 × 10 <sup>1</sup>           | 5%              | 39%         | 5.3 × 10 <sup>1</sup>      | 3.8 × 10 <sup>1</sup>           | 0%              | 10%         |
| Mg      | 3.1 × 10 <sup>1</sup>      | 2.3 × 10 <sup>1</sup>           | 5%              | 2%          | 1.0 × 10 <sup>2</sup>      | 4.8 × 10 <sup>1</sup>           | 0%              | 0%          |
| K       | 1.2 × 10 <sup>2</sup>      | 1.5 × 10 <sup>2</sup>           | 5%              | 39%         | 1.1 × 10 <sup>2</sup>      | 8.8 × 10 <sup>1</sup>           | 0%              | 19%         |
| Ca      | 1.1 × 10 <sup>2</sup>      | 9.0 × 10 <sup>1</sup>           | 5%              | 4%          | 8.5 × 10 <sup>1</sup>      | 7.4 × 10 <sup>1</sup>           | 0%              | 0%          |
| Ti      | 1.4 × 10 <sup>0</sup>      | 7.1 × 10 <sup>-1</sup>          | 5%              | 0%          | 3.8 × 10 <sup>0</sup>      | 3.0 × 10 <sup>0</sup>           | 0%              | 0%          |
| V       | 3.8 × 10 <sup>-1</sup>     | 2.2 × 10 <sup>-1</sup>          | 5%              | 0%          | 2.4 × 10 <sup>-1</sup>     | 1.2 × 10 <sup>-1</sup>          | 0%              | 0%          |
| Cr      | 4.3 × 10 <sup>0</sup>      | 3.5 × 10 <sup>0</sup>           | 5%              | 9%          | 3.9 × 10 <sup>0</sup>      | 1.4 × 10 <sup>0</sup>           | 0%              | 0%          |
| Mn      | 1.4 × 10 <sup>1</sup>      | 2.2 × 10 <sup>1</sup>           | 5%              | 0%          | 1.4 × 10 <sup>1</sup>      | 2.1 × 10 <sup>1</sup>           | 0%              | 0%          |
| Fe      | 3.9 × 10 <sup>2</sup>      | 6.3 × 10 <sup>2</sup>           | 5%              | 0%          | 3.6 × 10 <sup>2</sup>      | 5.3 × 10 <sup>2</sup>           | 0%              | 0%          |
| Ni      | 2.1 × 10 <sup>0</sup>      | 3.1 × 10 <sup>0</sup>           | 5%              | 27%         | 1.1 × 10 <sup>0</sup>      | 2.6 × 10 <sup>0</sup>           | 0%              | 0%          |
| Cu      | 6.0 × 10 <sup>0</sup>      | 4.8 × 10 <sup>0</sup>           | 5%              | 4%          | 5.0 × 10 <sup>0</sup>      | 4.4 × 10 <sup>0</sup>           | 0%              | 0%          |
| Zn      | 5.1 × 10 <sup>1</sup>      | 4.7 × 10 <sup>1</sup>           | 5%              | 0%          | 5.8 × 10 <sup>1</sup>      | 5.1 × 10 <sup>1</sup>           | 0%              | 2%          |
| As      | 1.0 × 10 <sup>0</sup>      | 9.7 × 10 <sup>-1</sup>          | 5%              | 0%          | 4.1 × 10 <sup>-1</sup>     | 3.9 × 10 <sup>-1</sup>          | 0%              | 0%          |
| Se      | 8.5 × 10 <sup>-1</sup>     | 4.6 × 10 <sup>-1</sup>          | 5%              | 11%         | 1.1 × 10 <sup>0</sup>      | 4.9 × 10 <sup>-1</sup>          | 0%              | 0%          |
| Sb      | 1.1 × 10 <sup>0</sup>      | 7.8 × 10 <sup>-1</sup>          | 5%              | 0%          | -2.3 × 10 <sup>1</sup>     | 1.2 × 10 <sup>1</sup>           | 0%              | 0%          |
| Ba      | 1.8 × 10 <sup>0</sup>      | 8.9 × 10 <sup>-1</sup>          | 5%              | 2%          | 1.6 × 10 <sup>0</sup>      | 9.3 × 10 <sup>-1</sup>          | 0%              | 0%          |
| Pb      | 1.1 × 10 <sup>1</sup>      | 1.1 × 10 <sup>1</sup>           | 5%              | 0%          | 1.2 × 10 <sup>1</sup>      | 1.1 × 10 <sup>1</sup>           | 0%              | 2%          |

**Table 3.** Species concentrations at the Ropice site measured by ICP-MS and ED XRF during the winter sampling period. Std. Dev.: Standard deviation; BDL: Below detection limit.

| Species | ICP-MS                     |                                 |                 |             | ED XRF                     |                                 |                 |             |
|---------|----------------------------|---------------------------------|-----------------|-------------|----------------------------|---------------------------------|-----------------|-------------|
|         | Mean (ng.m <sup>-3</sup> ) | Std. Dev. (ng.m <sup>-3</sup> ) | Percent Missing | Percent BDL | Mean (ng.m <sup>-3</sup> ) | Std. Dev. (ng.m <sup>-3</sup> ) | Percent Missing | Percent BDL |
| Na      | 1.4 × 10 <sup>2</sup>      | 1.4 × 10 <sup>2</sup>           | 0%              | 0%          | 7.2 × 10 <sup>1</sup>      | 5.7 × 10 <sup>1</sup>           | 0%              | 3%          |
| Mg      | 2.5 × 10 <sup>1</sup>      | 6.2 × 10 <sup>1</sup>           | 0%              | 15%         | 8.7 × 10 <sup>1</sup>      | 1.1 × 10 <sup>2</sup>           | 0%              | 3%          |
| K       | 3.0 × 10 <sup>2</sup>      | 4.1 × 10 <sup>2</sup>           | 0%              | 0%          | 4.8 × 10 <sup>2</sup>      | 8.2 × 10 <sup>2</sup>           | 0%              | 1%          |
| Ca      | 5.1 × 10 <sup>1</sup>      | 8.2 × 10 <sup>1</sup>           | 0%              | 6%          | 6.0 × 10 <sup>1</sup>      | 1.3 × 10 <sup>2</sup>           | 0%              | 0%          |
| Ti      | 7.6 × 10 <sup>-1</sup>     | 9.6 × 10 <sup>-1</sup>          | 0%              | 1%          | 2.1 × 10 <sup>0</sup>      | 2.1 × 10 <sup>0</sup>           | 0%              | 0%          |
| V       | 2.0 × 10 <sup>-1</sup>     | 1.9 × 10 <sup>-1</sup>          | 0%              | 0%          | 4.5 × 10 <sup>-1</sup>     | 3.9 × 10 <sup>-1</sup>          | 0%              | 0%          |
| Cr      | 2.1 × 10 <sup>0</sup>      | 2.8 × 10 <sup>0</sup>           | 0%              | 15%         | 4.0 × 10 <sup>0</sup>      | 2.0 × 10 <sup>0</sup>           | 0%              | 1%          |
| Mn      | 1.3 × 10 <sup>1</sup>      | 2.1 × 10 <sup>1</sup>           | 0%              | 0%          | 1.7 × 10 <sup>1</sup>      | 2.7 × 10 <sup>1</sup>           | 0%              | 0%          |
| Fe      | 3.6 × 10 <sup>2</sup>      | 5.6 × 10 <sup>2</sup>           | 0%              | 4%          | 4.8 × 10 <sup>2</sup>      | 7.7 × 10 <sup>2</sup>           | 0%              | 4%          |
| Ni      | 1.1 × 10 <sup>0</sup>      | 2.2 × 10 <sup>0</sup>           | 0%              | 29%         | 1.5 × 10 <sup>0</sup>      | 4.8 × 10 <sup>0</sup>           | 0%              | 0%          |
| Cu      | 6.2 × 10 <sup>0</sup>      | 1.3 × 10 <sup>1</sup>           | 0%              | 14%         | 9.8 × 10 <sup>0</sup>      | 2.3 × 10 <sup>1</sup>           | 0%              | 0%          |
| Zn      | 5.7 × 10 <sup>1</sup>      | 1.3 × 10 <sup>2</sup>           | 0%              | 0%          | 9.0 × 10 <sup>1</sup>      | 1.7 × 10 <sup>2</sup>           | 0%              | 3%          |
| As      | 1.8 × 10 <sup>0</sup>      | 1.8 × 10 <sup>0</sup>           | 0%              | 0%          | 9.8 × 10 <sup>-1</sup>     | 8.8 × 10 <sup>-1</sup>          | 0%              | 0%          |
| Se      | 6.6 × 10 <sup>-1</sup>     | 8.1 × 10 <sup>-1</sup>          | 0%              | 6%          | 1.6 × 10 <sup>0</sup>      | 1.5 × 10 <sup>0</sup>           | 0%              | 0%          |
| Sb      | 7.9 × 10 <sup>-1</sup>     | 9.2 × 10 <sup>-1</sup>          | 0%              | 0%          | 3.5 × 10 <sup>-1</sup>     | 8.0 × 10 <sup>-1</sup>          | 0%              | 0%          |
| Ba      | 4.0 × 10 <sup>0</sup>      | 2.4 × 10 <sup>1</sup>           | 0%              | 5%          | 3.7 × 10 <sup>0</sup>      | 2.1 × 10 <sup>1</sup>           | 0%              | 0%          |
| Pb      | 1.8 × 10 <sup>1</sup>      | 1.9 × 10 <sup>1</sup>           | 0%              | 0%          | 2.4 × 10 <sup>1</sup>      | 2.2 × 10 <sup>1</sup>           | 0%              | 1%          |

Both ICP-MS and ED XRF show a similar seasonal variation of concentrations, as shown in Table 1 (visibly higher crustal species concentrations in summer, and potassium and heavy metals strongly related to biomass and coal combustion in winter). Due to the low reliability of measuring Al, Si, and Cd by the ED XRF, which was found during previous internal measuring tests of this method, this species has been excluded from the comparison of methods in Table 2; Table 3.

The majority of the species showed nearly lognormal distribution. Only in the case of ozone did the dataset come anywhere near normal distribution. Part of the analytes showed bimodal distribution denotative of the influence of at least two different pollution sources. As a significantly larger number of datasets thus affected was detected at the Kosmos and Vrchy sites, it is probably the result of pollution

transport from more remote areas during specific meteorological conditions, while at Ropice, pollution from neighboring sources has a greater impact. At the Kosmos and Ropice sampling sites, the statistical distribution of some species concentrations was more deformed in the area of high values. It is likely to be connected with the occurrence of intensive concentration peaks at these more polluted locations (the result of meteorological situations that rarely occur, but bring high pollution concentrations).

On average, the majority of the measured species has had higher concentrations in the winter period and at night, which goes hand in hand with the series of PM<sub>2.5</sub> concentration. Significantly higher winter concentrations were detected mainly regarding species, the emissions of which are associated with residential heating by solid fuels. They are As, K, K<sup>+</sup>, levoglucosan, retene, picene, EC, and PAH. Apart from these, concentrations several times higher were also detected in the cold half of the year, as opposed to the summer campaign, in the case of nitrogen oxides and nitrates.

In order to evaluate the basic relations among the measured species, correlation matrices have been elaborated, onto which a cluster analysis has been applied by means of the R statistical software. The result of the cluster analysis preliminarily indicated five factors influencing the variability of the measured species concentrations.

### *3.3. Positive Matrix Factorization (PMF) Modeling*

PMF model 5.0 was used in accordance with the U.S. EPA Positive Matrix Factorization (PMF), Fundamentals and User Guide [14]. Based on parallel analyses from Ropice using the ICP-MS and ED XRF methods, an individual PMF model was elaborated for this location for each of the datasets to allow comparison of the PMF results. The results of the other laboratory analyses used in both models (see Section 2.3) were the same. Using the signal/noise ratio, the species were split into the categories of STRONG, WEAK, and BAD. 40 STRONG species were used in the case of the dataset, including the data from ICP-MS, and in the case of the ED XRF dataset, they were 33.

It was necessary to exclude a night sample from 31 December 2018 to 1 January 2019 from the time data series and the following day for the air polluted by a wide spectrum of analytes (especially Ba, Pd, Mg, Al, S, Ti, and Cu) caused by New Year's Eve celebrations. With regard to the fact that the source of this extreme concentration peak was an isolated instance, its influence is unassessable by means of PMF. An isolated value of Zn in the sample from 21 December 2018 (6:00 a.m.–6:00 p.m. UTC), which is about one order of magnitude higher than the average concentration for the rest of the measured period, was also excluded. The missing values were replaced by a median with uncertainty set at quadruple the median value. The values below the detection limit were assigned one-half of the detection limit and their uncertainty, at 5/6 of the detection limit.

Special care for gas species which do not contribute to the total PM<sub>2.5</sub> mass was carried out due to the risk of their possible negative effect on the model solution, e.g., creating redundant unreal factors. Many model runs with different parameters and various gas species have been carried out to test if their use leads to disturbing or complicating model solutions or if they support reasonable interpretation. During the modeling, good usability of gas species was discovered. They have acted not as the main strong markers of specific air pollution sources, but have provided useful supplementary information for profile interpretation. The NO/NO<sub>2</sub> ratio was used successfully when considering the effect of local/distant sources, or of fresh/altered pollution, as complementary information to nitrogen ion concentrations. In a similar way, the SO<sub>2</sub>/sulfate ratio was kept in mind when significant effects of local sources were interpreted (e.g., steelworks and local residential heating clusters). For the mentioned reasons, NO, NO<sub>2</sub>, and SO<sub>2</sub> have been incorporated in the PMF modeling dataset. Due to technical issues, ozone was measured in the winter part of the sampling campaign only. Because of this fact and the complex chemical reactivity of ozone, its role may be confusing rather than beneficial during interpretation of the model. Ozone has thus been excluded from the PMF model of Ropice. Despite the mentioned arguments, during the comprehensive modeling of all three locations ozone has been used with caution. After obtaining a rough stable model solution, ozone has been classified as WEAK and included in the PMF species. The aim of such a controversial use of ozone has been to

test the source profiles in which it tends to be present and to verify if its presence in the profiles is in agreement with the expectation. Using ozone in the comprehensive PMF dataset has been one of the complementary methods to evaluate whether the model corresponds to the real atmospheric relations. Neither the identified factors nor their contributions have been negatively affected by declaring ozone as a WEAK variable.

Using the ICP-MS and ED XRF data, the stable model solution (normal distribution and acceptable residue size in line with the PMF user guide [14], mutual independence of the identified factors, ratio  $Q/Q_{exp}$ , etc.) was established with 5 factors. For the final PMF solution for the Ropice location, 50 model runs have been done using both the ED XRF and ICP-MS datasets. The same number of model runs has been executed within the comprehensive model of all three sampling locations. Based on the bootstrap analysis, the ED XRF and ICP-MS model solution rotations were used with the values of  $F_{peak} = 0.5$  and  $1.0$ , respectively. The coefficient of determination of the predicted and measured concentrations of  $PM_{2.5}$  in the case of the ED XRF and ICP-MS datasets reached the values of  $R^2 = 0.91$  and  $0.93$ , respectively. The Ropice site model was elaborated with 20% extra modeling uncertainty for both the ICP-MS and ED XRF datasets.

Due to the known limitations of ED XRF (see the discussion in the Section 4.2), ICP-MS has been considered to be the main method for the source apportionment whereas ED XRF was the supplementary method for testing its ability in PMF. In order to elaborate a comprehensive PMF model including all three sampling sites (Kosmos, Ropice, Vrchy) only the ICP-MS method element analysis results were used, as it has a wider species composition and lower uncertainty than ED XRF.

For the PMF model, 31 analytes were classified as STRONG. This comprehensive evaluation was elaborated with an 18% extra modeling uncertainty. In other parameters, the modeling methodology was identical to the model of the Ropice site.

### *3.4. Identified Factors and Their Contributions to $PM_{2.5}$ Concentrations Using the All-sites Model*

Within the comprehensive model solution based on the ICP-MS dataset and including all 3 sampling sites, the same factors as those within the PMF model of the Ropice site have been identified. The only difference is the “residential heating” factor differentiation into two independent factors according to the kind of fuel. The chemical composition and factor time series are evident from the graphs in Appendices A and B, respectively.

Residential heating type 1: Dominant representation of polycyclic aromatic hydrocarbons (PAH), elemental carbon (EC), with an increased percentage of levoglucosan and some heavy metals (arsenic, selenium), hopanes, and nitrogen oxides. The daily variation of factor contributions fluctuates a great deal, with its maxima at night. The day/night difference in winter with stable heating operation is in no way as significant as in the summer, when there is only extra heating and hot supply water heating in the evening and the night hours.

Residential heating type 2: These are probably the same sources as in the case of the “local residential heating type 1” factor, but using other fuels or illegal waste combustion. The chemical profile is similar to the case of the “local residential heating type 1” factor, but with a higher representation of a wide spectrum of metals (antimony, cadmium, silver, tin, zinc, lead). The time series fluctuated significantly in the evaluated period, especially in the summer. In the summer as opposed to the winter period, a significantly higher contribution of this factor to the overall  $PM_{2.5}$  mass was detected.

Regional aerosol: A characteristic feature of this factor is the high representation of nitrogen ions ( $NH_4^+$ ,  $NO_3^-$ ) combined with sulfates or/and sulfur, metals (vanadium, selenium, tin, indium, arsenic) and hopanes and an increased contribution of organic carbon. In the signature of the regional aerosol, the influence of coal combustion in individual residential heating sources is evident (sulfur, vanadium, selenium, arsenic), and also, most likely, of motor vehicle traffic (nitrogen ions and nitrogen oxides). Its chemical composition and the factor time series imply that, apart from the primary suspended particles (emitted directly from the pollution sources), it also includes secondary aerosol. The factor contribution time series is marked by somewhat lower variability in the course of the

sampling campaign as opposed to the locally occurring residential heating. In the winter period, several sequences of consecutive days of increased values were detected when the concentrations, as opposed to local source fingerprints, did not decrease to low values as fast as in the case of “Residential heating” factors, which bears evidence of pollution transported from longer distances. During some high pollution episodes in the winter, delayed entrance of this factor after the residential heating factor was noticed, which probably corresponded to the gradual rise of a secondary aerosol in the region during deteriorated dispersion conditions.

**Crustal:** This is, above all, resuspended dust from the Earth’s surface lifted by the wind and road traffic. In its chemical profile, an increased percentage of species abundant in the Earth’s crust is thus prominent (aluminum, barium, strontium, titanium). In comparison with other factor profiles, these elements are accompanied by increased concentrations of ozone, which corresponds to the relatively high contribution of this factor in the period with intense sunshine. The high percentage of organic carbon and, meanwhile, the low percentage of elemental carbon, testify to the presence of an important biogenic component, probably especially pollen and biogenic particles in the summer period of the sampling campaign. This issue is further discussed in Section 4. The factor is typical for its significant daily variation with the maxima during the day. In a yearly course, higher factor contribution in the warm part of the year was discovered; in the course of the winter sampling campaign, the contribution of this factor was close to zero.

**Long-range transport:** The chemical profile contains particles of which the composition is mostly sea salt (ions  $\text{Na}^+$ ,  $\text{Mg}^{2+}$ ,  $\text{Ca}^{2+}$ ), sulfates, nitrates, and ozone with the representation of hopanes. Less significantly, nitrogen oxides demonstrate in its signature. In its chemical profile, a small percentage of coal combustion emissions also demonstrates (arsenic and selenium), probably originating from large industrial energy sources. It is apparent that it is a mixture of sea aerosol with a secondary aerosol that is developed from primary anthropogenic emissions in the course of its long transport time. The factor demonstrates itself by a time series with unremarkable day/night variation and by the relatively lowest difference of the concentration’s contribution out of all the identified factors between the summer and winter parts of the campaign.

**Iron and steelworks:** A factor composed of dominant percentage of iron and manganese accompanied by molybdenum and, relatively less significantly, by a wide spectrum of other metals (lead, indium, thallium, silver, cobalt, zinc, arsenic, selenium, and strontium), which corresponds to the complex production of iron, steel, and relevant productions in the large industrial premises surrounding the TRINECKÉ ŽELEZÁRNY, a.s. plant. The factor time series is extremely variable, depending on the wind direction (very high contribution to  $\text{PM}_{2.5}$  concentration when the emission plume heads towards the sampling site from the metallurgical plant, as opposed to the almost zero influence in other cases). The average size of the factor contribution in the warm and cold parts of the sampling campaign was similar.

The apportioned percentages and  $\text{PM}_{2.5}$  concentrations of the main air pollution sources are illustrated in the following graph (Figure 3).

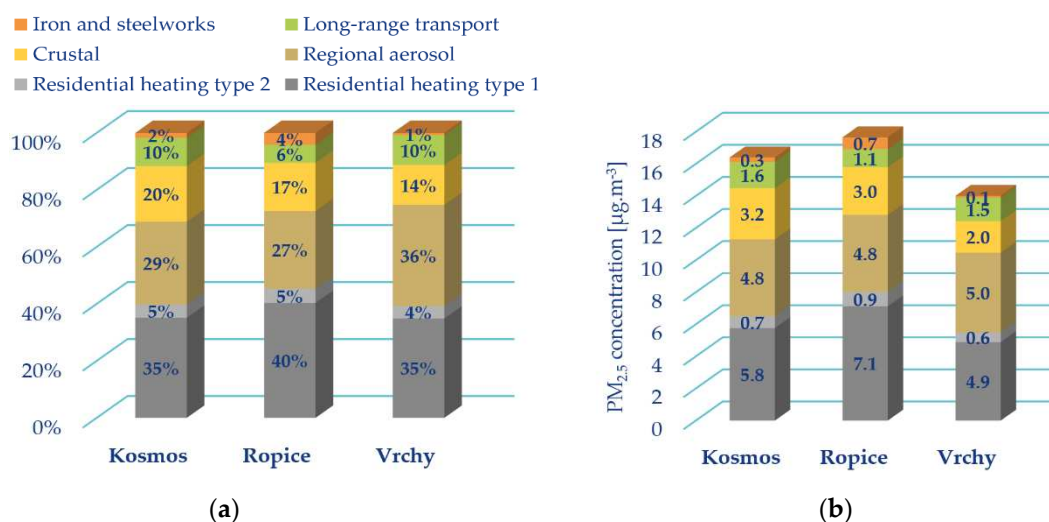


Figure 3. Relative (a) and absolute (b) factor contributions to the average PM<sub>2.5</sub> concentration.

### 3.5. The Conformity of the Identified Factors and Their Contributions to PM<sub>2.5</sub> Concentrations Using ICP-MS and ED XRF Datasets at the Ropice Site

The identified factors at the Ropice site were identical when using both compared analytical methods (ICP-MS and ED XRF): local residential heating, regional aerosol, long-range transport, iron and steelworks, and crustal. Figures 4 and 5 show the chemical profiles of the factors identified by PMF using the ICP-MS and ED XRF datasets.

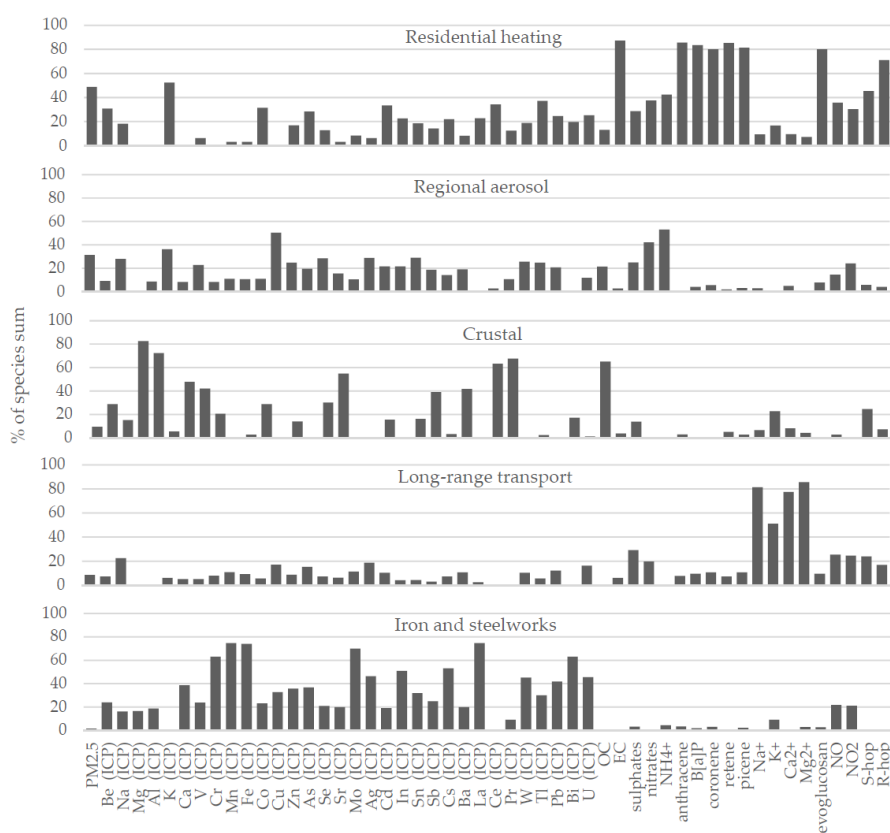
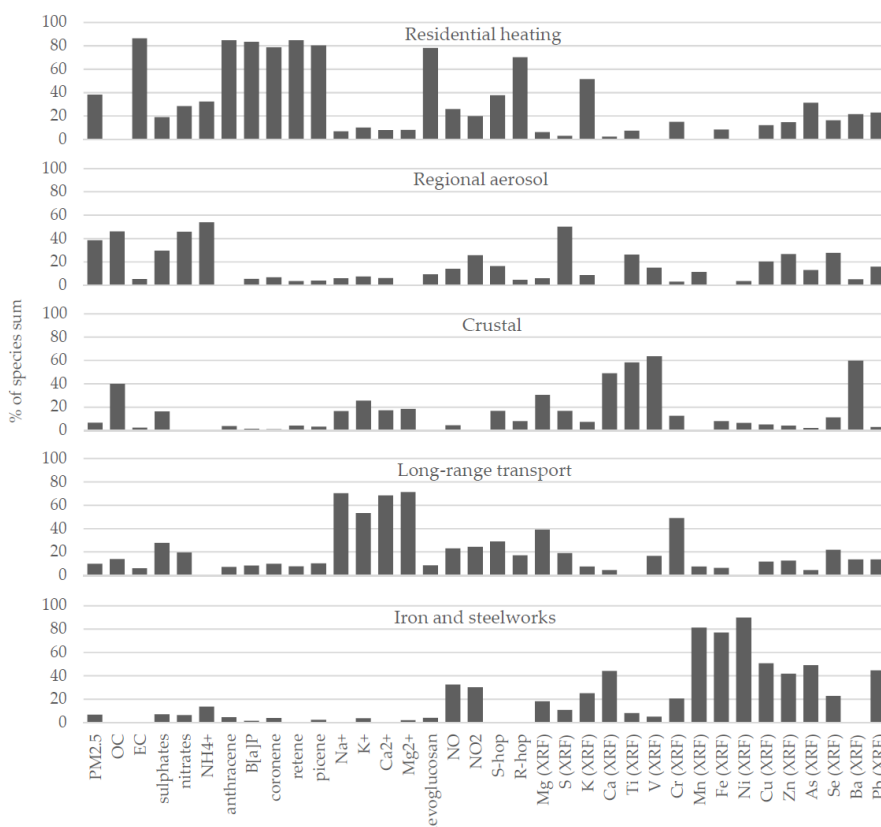


Figure 4. PMF factor profiles at the Ropice sampling site based on the ICP-MS dataset. S-hop: 17α(H),21β(H)-22S-Homohopane; R-hop: 17α(H),21β(H)-22R-Homohopane.



**Figure 5.** PMF factor profiles at the Ropice sampling site based on ED XRF dataset. S-hop: 17 $\alpha$ (H),21 $\beta$ (H)-22S-Homohopane; R-hop: 17 $\alpha$ (H),21 $\beta$ (H)-22R-Homohopane.

The PMF model with the ICP-MS and ED XRF datasets is based on partly different species composition, and, therefore, direct comparison of the model results is impossible. As shown in Figures 4 and 5, with ICP-MS and ED XRF datasets, the same characteristic diagnostic species groups are present in the chemical profiles, which have led to the same identified factors. The final solution is easily interpretable: “Residential heating” stands out by PAHs, elemental carbon, levoglucosan percentage, and relatively high 17 $\alpha$ (H),21 $\beta$ (H)-22R-Homohopane / 17 $\alpha$ (H),21 $\beta$ (H)-22S-Homohopane ratio (due to the frequent burning of low-quality coal). “Regional aerosol” is rich in nitrogen ions and sulfates (in the case of the ED XRF dataset, also in sulfur) as a manifestation of chemical-transformed road traffic and coal-burning emissions. The “crustal” factor contains significant percentages of Mg, Al, Ca, and Ba (ICP-MS dataset), and Ca, Ti, and Ba (ED XRF dataset), respectively. Long-range transport is typical in its high sea-salt percentage with sulfates, nitrates, and a relatively low 17 $\alpha$ (H),21 $\beta$ (H)-22R-Homohopane / 17 $\alpha$ (H),21 $\beta$ (H)-22S-Homohopane ratio. The iron and steelworks chemical profile is characteristic for its dominant percentage of Fe, Mn, and a wide spectrum of heavy metals in combination with nitrogen oxides.

Overall, the PMF factor profiles based on both the ICP-MS and ED XRF datasets are similar and contain the same diagnostic species (further discussion on the specifics of chemical profiles is a part of Section 4). The identified factors at the Ropice site are the same as the comprehensive all-sites PMF model factors, which were explained in more detail in Section 3.4.

### 3.6. Pollution Source Areas

Based on the time series of the factor contributions to PM<sub>2.5</sub> concentrations and hourly values of the wind direction and speed at individual sampling sites, time-weighted concentration roses and CPF (Conditional Probability Function) graphs have been elaborated, based on which it is possible to determine the directions of the main pollution origins. The time-weighted concentration roses include

all the model quantified values; the CPF has been visualized for the contribution values exceeding the 90th percentile. The time-weighted concentration roses of the identified factor contributions form Appendix C. The CPF graphs proved to have little illustrative value and do not contain enough information; that is why they are not part of the article. The determination of the pollution source areas was limited by the amount of data available (about 130 values for each location). Thus, for a more precise source localization, it was inefficient to apply some methods that are more demanding as far as a statistical file size is concerned, e.g., PSCF (potential source contribution function).

**Local residential heating type 1:** At the Kosmos site, the factor acts especially from the direction of the densely populated Jablunkov Furrow (probably the influence of Vendryně, Bystřice, and other villages) and from the north-northwest (probably the influence of the periphery of Třinec). At Ropice the main part of this pollution type is transported from two prevailing directions, north (Olše valley) and south. In both cases, with regard to the high average contributions from these directions, the factor is the influence of the local residential development nearby. The Vrchy site is significantly different in this respect. The factor here acts mainly from the north, and, with respect to the occurrence of both high and low factor contributions, it is probably a combination of the local sources from the Vrchy part as well as the influence from more remote areas, e.g., the Nebory development part.

**Local residential heating type 2:** At the Kosmos site, the most intense concentration peaks of this factor occurred when the wind originated from the northwest (influence of peripheral parts of the city of Třinec in the Olše valley). A significant contribution here occurs both in the warm and cold halves of the year. In winter, however, pollution transport prevails from the southeast. At the Ropice and Vrchy sites, the main source areas are identical to the local residential heating type 1 factor.

**Regional aerosol:** At the Kosmos and Ropice sites, the winter contribution was approximately double as opposed to the summer contribution, and the main pollution origin directions are analogical, as in the case of the residential heating type 1 and 2 factors (from Jablunkov Furrow and sites situated at lower locations in the Olše valley. At Ropice, however, this occurred most significantly from the south). At the Vrchy site, on the contrary, from the point of view of both the maxima and the average contribution values, northwest wind directions dominate, which shows pollution transport not only from the neighboring areas of the city of Třinec, but also from the city of Ostrava and its surroundings or villages situated in this direction.

**Crustal:** At the Kosmos site, factor contributions prevail from the southeast and northwest, and at the Ropice site, from the north and especially the south. At the Vrchy site, although the contribution peaks are connected with a southwest wind direction, probably from the nearby local source (field work), meteorological situations with north and southeast wind directions had a decisive influence on the average factor contribution here.

**Long-range transport:** The main average contribution of long-range transport comes from the north-northwest. The less significant part of the long-range pollution transport was captured at the Kosmos and Vrchy sites in periods with a southeastern wind, thus from the corridor of Jablunkov Furrow. At Ropice, it came from the southern direction.

**Iron and steelworks:** At the Kosmos site, which is situated windward of the integrated metallurgical plant, the high factor contributions occurred during the northwest current. At Ropice, which is situated leeward of the metallurgical sources, there were dominant contributions from the south and southeast. At the background countryside site of Vrchy, the quantified contributions of this factor reached very low values; the determination of the source direction is thus unreliable here. For guidance, the origin is indicated north of the sampling site. All the evaluated directions correspond to both the sampling site location and a presumed source (TŘINECKÉ ŽELEZÁRNY, a.s. steelworks).

## 4. Discussion

### 4.1. Specific Aspects of Identified Factor Profiles

In most aspects, the identified factors and the species percentages in the PMF factor profiles are in line with the expectations based on the chemical composition of the supposed emission sources. Further discussion is needed regarding the road traffic contribution to the concentration of PM<sub>2.5</sub>. As shown in the chemical profiles in Figures 4 and 5, and Appendix A, no standalone chemical profile representing road traffic has been identified by PMF. This applies to all model runs in the case of both the ICP-MS and the ED XRF datasets. The road transport species pattern (especially high contribution of nitrogen oxides and nitrogen ions) is clearly visible in the “Regional aerosol” factor instead, which is a mixed factor combining vehicle emissions and other regionally acting pollution sources. Despite many model runs with testing exclusion/inclusion of many species, road traffic as a standalone PMF factor has never been isolated. Similar problem with the traffic identification in the Moravian-Silesian Region has already been encountered in other study using PMF [15]. This is likely due to the fact that in all sampling locations, road traffic cannot be considered as a significant air pollution factor in comparison with other sources, e.g., residential heating or steelworks. There are no heavily loaded roads near the sampling locations. No significant or even dominant traffic contribution to PM<sub>2.5</sub> concentration is expected here. Based on the results in previous studies [16] (p. 241, 248), it can be assumed that sources with well-defined chemical profiles and seasonal time trends, that make appreciable contributions, can be better quantified by the PMF model than those with low contributions to the PM mass. A relatively low contribution and insignificant seasonal variation leads to the hypothesis that the factor of primary traffic particles has not been identified by the PMF model due to the dominance of other regionally specific source types with partly similar chemical profiles. The complex of metals and NO<sub>x</sub> from traffic is similar as from steelworks and household heating, EC and OC come especially from household heating and, dust resuspended from the roads by vehicles movement contains pattern of crustal species similar to soil and urban dust which is resuspended by the wind. The road traffic emissions influencing the sampling areas are mainly not of local origin and are predominantly transported to the measurement points from longer distances, together with some other sources of emissions in the same time periods. Thus, they cannot be separated by statistical methods including PMF. In addition, due to the expected main road traffic emission origin at distances from several kilometers to one hundred kilometers (agglomeration of Ostrava, the Polish part of Silesia, and the Třinec city center), there is enough time for chemical transformations of road emissions during the atmospheric transport, especially in the presence of complex pollution with many reactive radicals in the heavily polluted northeast part of the Czech Republic. As discussed in large intercomparison studies [16] (p. 249), datasets from areas with complex atmospheric transport and chemistry are likely to be more challenging to quantify the sources (especially secondary and/or distant ones) than areas influenced mainly by local sources. Mixed factors with both residential heating and traffic have been found in several other studies, including the strongly polluted city of Ostrava in the Moravian-Silesian Region [17] (pp. 149–150). Due to the mentioned reasons, we consider the PMF solution, with the road traffic factor mixed with other regionally acting sources in the “Regional aerosol” factor, as reasonable. Based on previous research results [16] (p. 249), the time resolution of the datasets influences the ability of receptor models to capture the time patterns of mobile sources. According to this information, a higher time resolution allowing evaluation of daily variations could be useful for the quantification of the traffic contribution to the PM mass in the specific region of Třinecko.

Due to the complex transformation processes of ozone in the atmosphere, its concentration does not directly correspond to sources of emissions. However, when proceeding with special caution, it provides additional information due to its dependence on meteorological conditions at the time of operation of some source types. Although ozone is only a weak supporting indication for PMF interpretation, its presence in the “Crustal” and “Long-range transport” factors (maximum in dry summer days with strong sunshine), its absence in the “Residential heating” factors (maximum

operation in winter when ozone concentrations are low), and the moderate percentages in the “Iron and steelworks” factor (stable year-round source operation) correspond well with real relations in the atmosphere. It suggests that the model interpretation is reasonable in this respect.

Another interesting aspect demanding an explanation is the content of organic carbon in the chemical profiles factor. As shown in Figures 4 and 5 and in Appendix A, in all model results, ICP-MS and ED XRF datasets, and in Ropice and the comprehensive all-locations model, organic carbon accounts for significant mass percentages in the “Crustal” factor. The PMF model tendency to incorporate the high portion of organic carbon into the “Crustal” chemical profile has been verified repeatedly during the modeling. It is customary and rational to expect its main content rather in factors related to incomplete burning processes like household coal and biomass burning or diesel engine operation. Unlike some other studies [18] (pp. 101–103), the measured organic carbon summer concentrations are more than twice as high as in the winter (the mean concentration varies in the range of 4.0–4.6  $\mu\text{g}\cdot\text{m}^{-3}$  in the summer, depending on the sampling site, and 1.4–1.7  $\mu\text{g}\cdot\text{m}^{-3}$  in the winter, respectively), in spite of the fact that both residential heating and traffic emissions are higher in the winter. The measured data thus surprisingly indicate that the main source of organic carbon is neither road traffic nor household heating in the surveyed area. An analysis of the EC/OC ratio in the warm and cold parts of the sampling campaign (Figure 6) clearly shows that winter concentrations are related, with one dominant source type at all three sites (strong EC/OC correlations with  $R^2 > 0.95$ ), while summer sources are more complex ( $0.29 < R^2 < 0.62$ ). Due to the land use type near the sampling sites (frequent grassy and agricultural areas), and considering the time period of the summer sampling (peak of the flowering season), there is high probability that a significant contribution to the measured summer organic carbon concentrations is of biogenic origin (both primary and secondary aerosols).

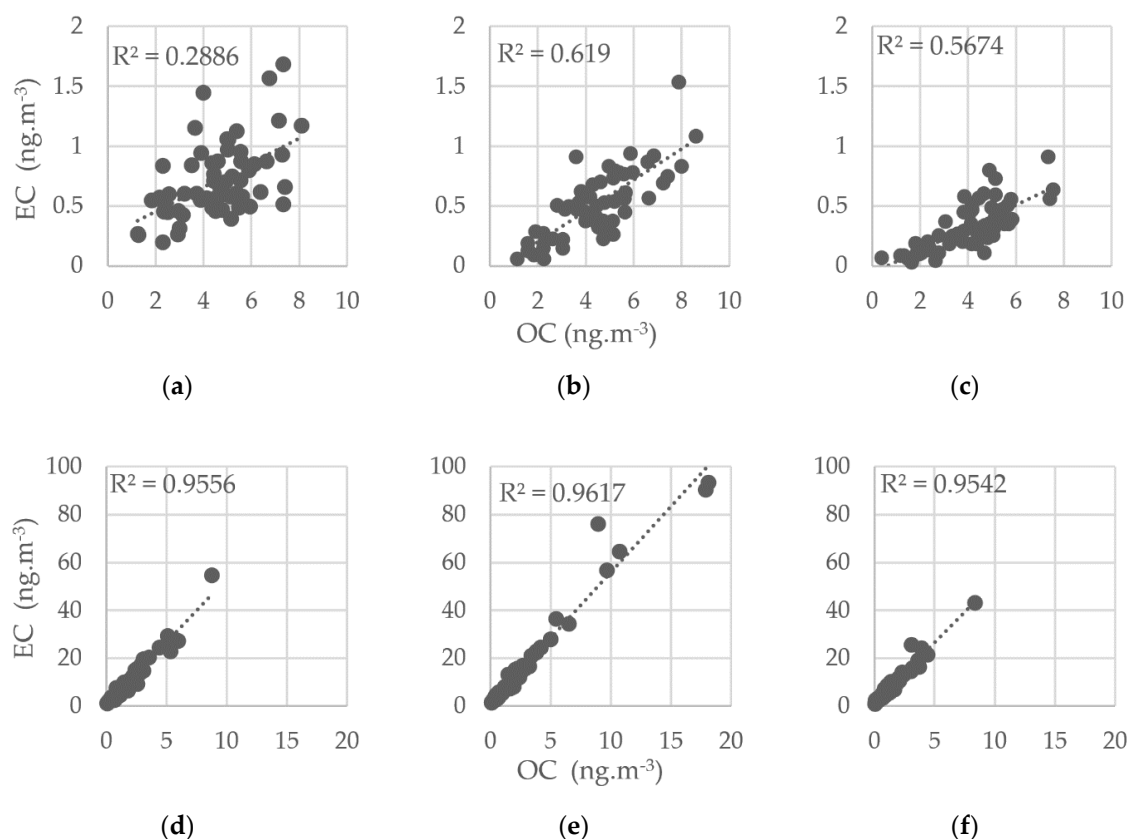


**Figure 6.** Plot of EC and OC concentrations at sampling locations in the summer: (a) Kosmos; (b) Ropice; (c) Vrchy; and the winter: (d) Kosmos; (e) Ropice; (f) Vrchy.

A slight correlation has been discovered between the OC summer concentrations and temperature (Figure 7); the strongest is at the Vrchy site ( $R^2 = 0.36$ ), which is less polluted by both  $PM_{2.5}$  and OC. Conversely, the weakest OC versus temperature correlation has been found at the most polluted site, Ropice ( $R^2 = 0.13$ ).

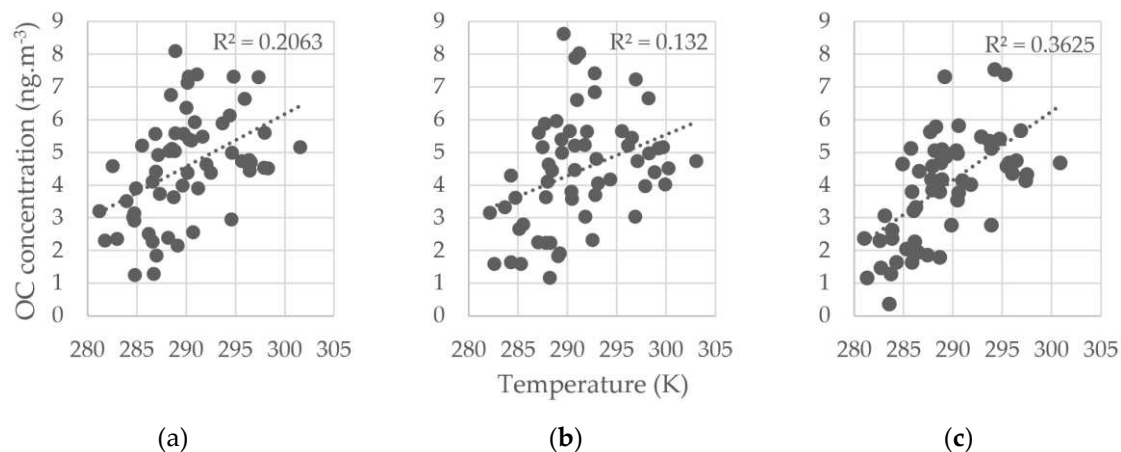


**Figure 7.** Plot of EC concentration and air temperature at: (a) Kosmos; (b) Ropice; (c) Vrchy.

Although the EC versus temperature correlations are rather weak, there is an indication that the summer OC concentrations are related to factors which have an effect in the rural rather than in the urban and suburban areas. Thus, the summer OC concentrations are significantly connected with natural emission sources. The apportioning of most of the OC mass into the “Crustal” factor is likely due to similar source areas and the time periods of high biogenic OC and mineral dust contributions. Typically, those are the warm summer days when the low soil moisture and air humidity lead to easy mineral dust and biogenic primary particle resuspension. Meanwhile, the temperature and sunshine are favorable to the formation of biogenic secondary organic aerosol. Due to the above-mentioned reasons and because the summer OC contributions have caused a dominant effect on the overall OC concentration, there has been no way to separate mineral dust and biogenic organic carbon into standalone source profiles in the survey area.

As shown in Figure 6, measured summer EC concentrations were lower than  $2 \mu\text{g}\cdot\text{m}^{-3}$ , whereas in the winter they reached approx.  $50 \mu\text{g}\cdot\text{m}^{-3}$  and, at Ropice even nearly  $100 \mu\text{g}\cdot\text{m}^{-3}$ . The significant increase of the EC concentration has been detected at all sampling sites. An increase of more than one order of magnitude cannot be explained by the change of weather conditions, especially when considering seasonal wind speed comparison in Section 3.1 (higher wind speed in winter has been discovered). The road traffic emission variation is relatively low during the year and its winter contribution to the EC concentration is thus very likely less than the maximum summer EC concentration ( $<2 \mu\text{g}\cdot\text{m}^{-3}$ ). Based on this fact, it is clear that the relative annual road traffic contribution to the total EC mass in Třinecko is very low (in the winter at most several units of percentage). On the contrary, emissions from the coal burning in the old-technology boilers which are the most common residential heating appliances in the surveyed area varies in a wide range during a year. Signs of an incomplete combustion process with the potential for high EC emissions are manifested by the dominant percentage of PAHs in the “residential heating” source profile, consistently with other studies, e.g. [19] (p. 12). Obsolete household heating boilers emitting a lot of soot are thus very likely to be the dominant sources of EC in this region, at least one order of magnitude higher than the road traffic EC contribution. This fact possibly explains why the EC, which is often used a road traffic marker, has not led to the identification of the individual traffic PMF factor in the surveyed area.

In spite of the high winter correlation between EC and OC, these species are separated by the PMF model to the different PMF source profiles. According to the mentioned findings, it is caused by different EC and OC sources in the summer. In the winter, there were acting OC and EC emissions from

the residential heating (other sources are negligible compared to this source type). On the contrary, a vast majority of primary biogenic and secondary particles (majority of the summer OC mass) and particles likely originating mainly from traffic (contribution to the EC mass) were the most important in the summer.

#### 4.2. Comparison of the Results of the ED XRF and ICP-MS Methods

The ICP-MS is the reference method for heavy metals measurement in PM<sub>2.5</sub> used within the National Air Quality Monitoring Network according to the European and Czech air protection legislation. ED XRF dataset has thus been tested with the aim to verify if it could be a more affordable alternative to the ICP-MS for the source apportionment purposes. Based on the previous comparison of the parallel measurement with ICP-MS (not published in this article), several limitations of ED XRF had been known before its use for PMF modeling. Those are limited species number, significantly higher relative uncertainty and a higher method detection limit of some species compared to ICP-MS. The Table 2; Table 3 show significant concentration differences of some species between ICP-MS and ED XRF dataset, especially in the case of Sb, Ti, V, Cr, and surprisingly, Mg. Based on this and previous comparisons, with caution we have used measured concentrations of the Cd, Cr, Sb, Ti, V, K, Na, S, Si, and Al. Some of these problematic metals has been excluded from the PMF dataset. On the contrary, Cu, Fe, Mn, Pb, Se, and Zn could be considered more reliable.

Despite the mentioned ED XRF limitations, the PMF results based on the two different datasets are similar. In both the ED XRF and ICP-MS datasets, the uncertainties of the elaborated PMF model according to the U.S. EPA [14] guide criteria are acceptable. The solution found with six factors is stable, with good agreement of the predicted and measured values and with the bootstrap (BS), displacement (DISP), and bootstrap-displacement (BS-DISP) stability tests complying with the guide recommendations [14]. The identified air quality factors and their quantified contributions at different wind directions and speeds correspond well to the location of the real pollution sources.

No significant difference has been detected in the predictive ability of the evaluation based on the ICP-MS and ED XRF datasets, i.e., by means of both methods a solution for the sampling site of Ropice has been found that agrees on the substantial aspects (Figure 8).

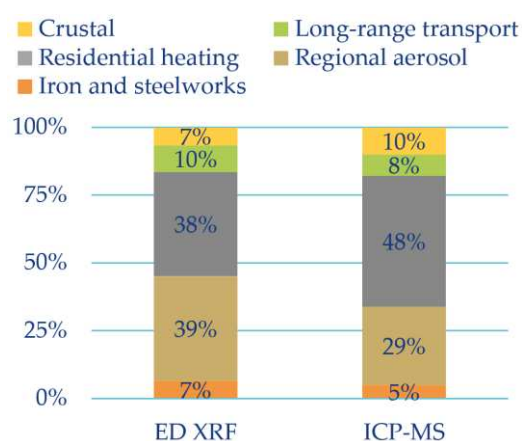


**Figure 8.** Factor contribution to the average PM<sub>2.5</sub> concentration using the ED XRF and ICP-MS datasets.

The model results using ED XRF and ICP-MS differ significantly only in the case of the regional aerosol and the local heating contribution, whereas in total the two factors are quantitatively identical in both datasets (on the whole, they account for approximately  $\frac{3}{4}$  of the total pollution). The split of the pollution origin between these two factors is always disputable, as in regional aerosol there is also a significant pollution contribution from local residential heating. There is no precise boundary between the local and regional residential heating influences. G-Space Plot indicated a partial mutual link, which thus has a rational basis. All the other identified factors were mutually independent, according to

the G-Space Plots analysis. With respect to the goal of the ED XRF and ICP-MS comparison, differences in source contributions up to approximately 5% can be considered as negligible, as they do not change the focus of the main air pollution measures in the research area. It is possible to consider the sensitivity and accuracy of both methods as sufficient for PMF modeling and consecutive recommendations for strategic measures regarding air protection.

#### 4.3. The Use of the Selected Organic Markers

Based on the research information sources mentioned below, some markers have been selected that have proven to be suitable organic molecular tracers for the identification of coal combustion, biomass burning, and vehicular emissions. The concentrations of 19 PAHs, six hopanes, six steranes, and levoglucosan in the PM<sub>2.5</sub> aerosol samples were measured. PAHs are formed mostly from the incomplete combustion of a variety of fuels emitted by different source types, including residential heating, industrial processes, waste incineration, and mobile sources [20,21]. Benzo[*a*]pyrene is the only PAH that has a legislative limit (1 ng.m<sup>-3</sup> annual average concentration), and it was used as a marker for carcinogenic risk assessment [22]. The International Agency for Research on Cancer (IARC) classified BaP as an agent carcinogenic to humans (Group 1). Across all three sites, the BaP concentrations were 12–14 times higher for the winter samples (average 3.95 ng.m<sup>-3</sup>) than for the summer samples (average 0.3 ng.m<sup>-3</sup>). The seasonal differences can be explained by decreased residential heating during the warm months and increased photolysis and dispersion of all PAHs. The rest of the measured PAHs had shown fewer seasonal differences (4–11 times) than BaP, with the exception of BaA (17–21 times), which is highly susceptible to photo-oxidation [20,23].

Concentrations of BaP and BeP are usually similar in fresh emissions [24], but as BaP degrades in the presence of sunlight and strong oxidants in the atmosphere, the BeP/(BeP + BaP) ratio can be used as an index of the aging of aerosol particles [24,25]. During the summer campaign, the ratio BeP/(BeP + BaP) at all three sampling sites was in the range from 0.5 to 0.6, indicating the regional or long-range transport of aerosols. Conversely, in winter, this ratio was less than 0.5 (average 0.4), and that indicates emissions of aerosols from local sources.

Picene was selected as a marker for coal combustion. Furthermore, the diagnostic ratios of the selected hopanes were used to identify the combustion of different types of coal [26]. Hopanes and steranes are present in the lubricating oil used by both gasoline- and diesel-powered motor vehicles. They are considered markers for traffic emissions in the atmosphere [27,28]. On the other hand, only hopanes are present in emissions from coal combustion. The characteristic ratio between concentrations of 22R-17a(H),21b(H)-homohopane and 22S-17a(H),21b(H)-homohopane, known as a homohopane index, can be used for identifying diverse types of coal. For coal combustion, the homohopane index C31 $\alpha\beta$ [S/(S + R)] is in the range from 0.05 to 0.40 and it increases with the maturity of the coal, 0.05 for lignite, 0.08 for brown coal, 0.20 for sub-bituminous coal, and 0.37 for bituminous coal [26]. The homohopane index obtained for gasoline and diesel emissions ranges from 0.45 to 0.60 [29,30]. Hopane concentrations in the samples were quantified by the key ion *m/z* 191, and sterane concentrations were quantified by the key ions *m/z* 217 and 218. Across all three sites, the sterane concentrations were very low or below the detection limit (0.12 ng.m<sup>-3</sup>) in the samples from both the summer and winter campaigns. The most abundant sterane in the summer samples was  $\alpha\alpha\alpha$  20R-Cholestane (average 0.17 ng.m<sup>-3</sup>), and its concentrations within the winter samples were only 2 times higher (average 0.31 ng.m<sup>-3</sup>). Steranes were used as molecular markers for indicating the contribution of vehicular emissions, and their low concentrations indicate a negligible impact of the mobile sources. Like the steranes, the hopane concentrations at all three sites during the summer campaign were exceptionally low, and the homohopane indices were in the range from 0.51 to 0.64, which indicates that hopanes in the summer samples originated mainly from transport emission. During the winter campaign, hopane concentrations were on average 5 times higher than in the summer, and the average homohopane indices for the Kosmos and Ropice sampling sites were 0.36 and 0.34, respectively, which indicates that hopanes in the winter samples were mainly from high-range coal combustion. For the Vrchy site, the homohopane indices were more heterogeneous

than at the other two sites, and were in the range from 0.11 to 0.60 (average 0.40). In three samples, the homohopane indices were below 0.20, which is typical for less mature coal. Conversely, in 27 winter samples (almost 50% of the total samples) from the Vrchy site, the homohopane indices were in the range from 0.45 to 0.60, which, according to literature, corresponds to gasoline and diesel emissions. It has been assumed that these could be emissions from the combustion of waste oil or fuel oil due to exceedingly high concentrations of hopanes and steranes in these samples and relatively low concentrations of the measured PAHs. The trend of PAH production during the combustion of various types of fuels in terms of their chemical composition is in the following order: coal > lignite > wood > waste oil > mazut > fuel oil [31].

#### *4.4. Results in the Context of Current Strategies*

Among the main documents of air protection in the Czech Republic today are the Air Quality Improvement Programmes, which contain measures for individual regional units of NUTS2 (Nomenclature of Units for Territorial Statistics, Level 2). For the Třinecko region, the binding measures are stated in the Air Quality Improvement Programme for the Agglomeration of Ostrava/Karviná/Frýdek-Místek CZ08A [7], the analytical part of which was elaborated using the CAMx chemical transport model.

Based on the established wind direction and speed during the campaigns, it is possible to state that these meteorological conditions, which are one of the main factors influencing the dispersion conditions, correspond well to the long-term average measured at the nearest neighboring sites of the National Air Quality Monitoring Network. It is thus possible to consider that the acquired results are sufficiently representational for a longer period of time and that they can be used for a proposal for strategic measures.

The source apportionment by means of PMF, including an approximate determination of the main source areas of the secondary aerosol, provides new arguments for the prioritization of measures that have so far been missing in the strategic documents relevant to the Třinecko region.

As stated in the previous studies [32] (p. 6), due to the different definition of their sources, comparing the source apportionment output of receptor models and the chemical transport model is not straightforward. Nevertheless, it is evident that the PMF results correspond to the CAMx results in the analytical part of the mentioned strategic document in its main priorities. According to both modeling methods, the main cause of the above-limit pollution by PM<sub>2.5</sub> in Třinecko is individual residential heating, followed by secondary aerosol and transport from abroad. Compared to existing analyses using chemical transport models, the PMF modeling results show a significantly higher influence of local sources (especially residential heating), whereas in the case of the secondary aerosol and transport from abroad, the situation is the opposite. The contribution of transborder pollution is assessed as significant but not high by the PMF model. According to the PMF model, the most significant part of air pollution by PM<sub>2.5</sub> is of local origin, i.e., it comes predominantly from an area within units of km from the assessed sites.

## **5. Conclusions**

The aim of the research documented in the presented article was to contribute to a better understanding of the relations among emissions, pollution transport, and ambient air PM<sub>2.5</sub> concentrations in Třinecko by source apportionment using positive matrix factorization (PMF). At the three assessed sites, six main factors have been identified (two types of residential heating, regional primary and secondary aerosol sources, resuspended dust and biogenic detritus, long-range transport, and iron and steel production). In substantial aspects, the results correspond to earlier analyses carried out for air protection strategic plans. However, they also bring some important corrections. This is true especially when it comes to the discovery that the most significant pollution contribution falls under local sources, whereas pollution transport from more remote areas, including abroad, is less significant.

It is possible to consider a significant decrease of primary emissions of PM, polycyclic aromatic hydrocarbons, and sulfur dioxide from individual residential heating, which create the greatest air

pollution contribution, and the associated health hazards as the main priority of air protection in Třinecko. Directing measures to this source type will support a decrease in the influence of the second most significant pollution type, which is “regional aerosol”.

In this respect, support of traffic measures, from the point of view of air protection, is less important nowadays. Although some interpretation problems with traffic contribution quantification by the PMF have been found, there are no doubts about its minor role, especially considering other source apportionment approaches, including the recent CAMx model which has been provided for planning the strategy measures. Due to the PMF results accordance with the mentioned independent alternative source apportionment method, the traffic measures in Třinecko should have been limited to specific activities at particular locations where it is possible to demonstrably prove an acceptable ratio of costs to air quality improvement. Other factors influencing the air quality at present are not a regional priority in Třinecko now. Measures focusing on them can only be effective locally.

**Author Contributions:** Conceptualization, V.V., B.K. and D.H.; methodology, V.V., B.K., D.H. and R.S.; formal analysis, R.S., I.N.; investigation, R.S., I.N.; resources, R.S., I.N. and D.H.; data curation, R.S. and D.H.; writing—original draft preparation, R.S.; writing—review and editing, I.N., V.V. and B.K.; visualization, R.S.; supervision, B.K.; project administration, R.S. All authors have read and agreed to the published version of the manuscript.

**Funding:** This research was funded by Technology Agency of the Czech Republic, grant number TITSMZP704”.

**Conflicts of Interest:** The authors declare no conflicts of interest. The funders had no role in the design of the study; in the collection, analyses, or interpretation of data; in writing the manuscript; or in the decision to publish the results.

## Appendix A

The following pictures represent the identified air pollution factors. They illustrate the relative species contribution in the PM<sub>2.5</sub> concentration, quantified by the PMF model and the median and the IQR bootstrap test values.

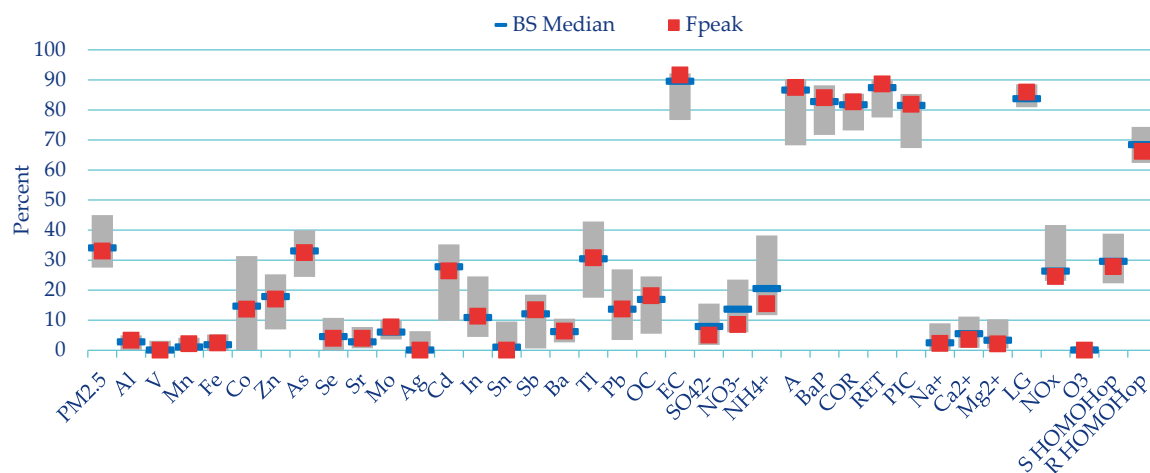


**Figure A1.** Relative species concentration (Fpeak) of the “Residential heating type 1” factor and the result of the BS test (Median and IQR).

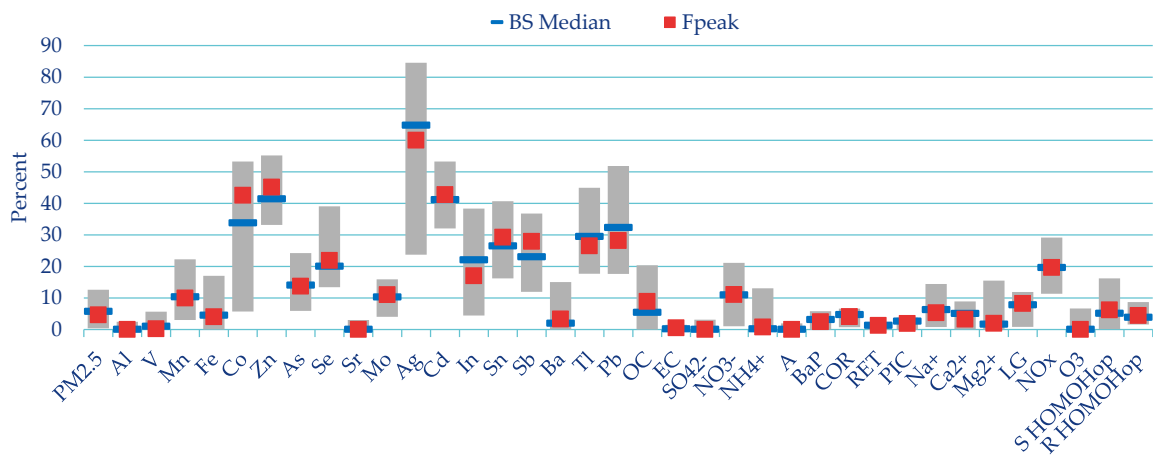


**Figure A2.** Relative species concentration (Fpeak) of the “Residential heating type 2” factor and the result of the BS test (Median and IQR).

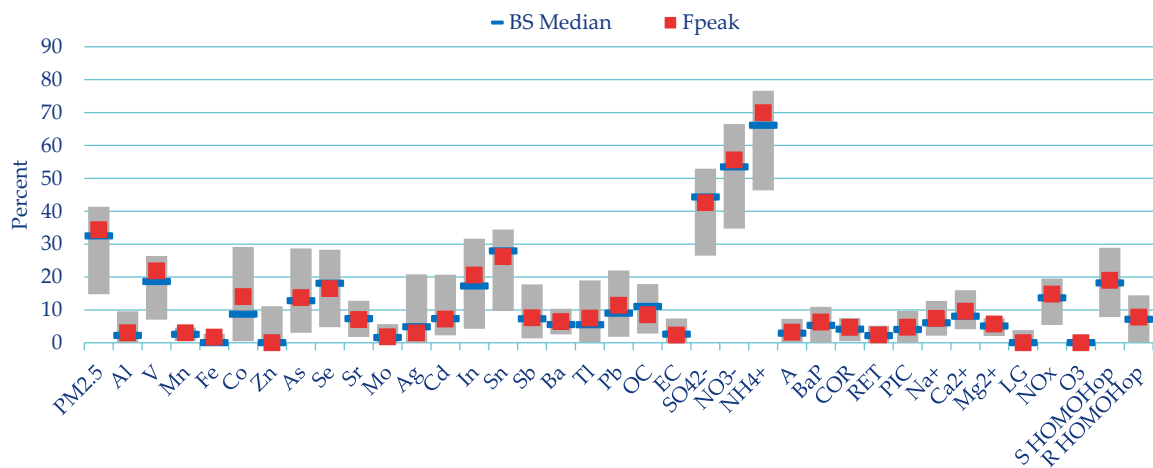


**Figure A3.** Relative species concentration (Fpeak) of the “Regional aerosol” factor and the result of the BS test (Median and IQR).

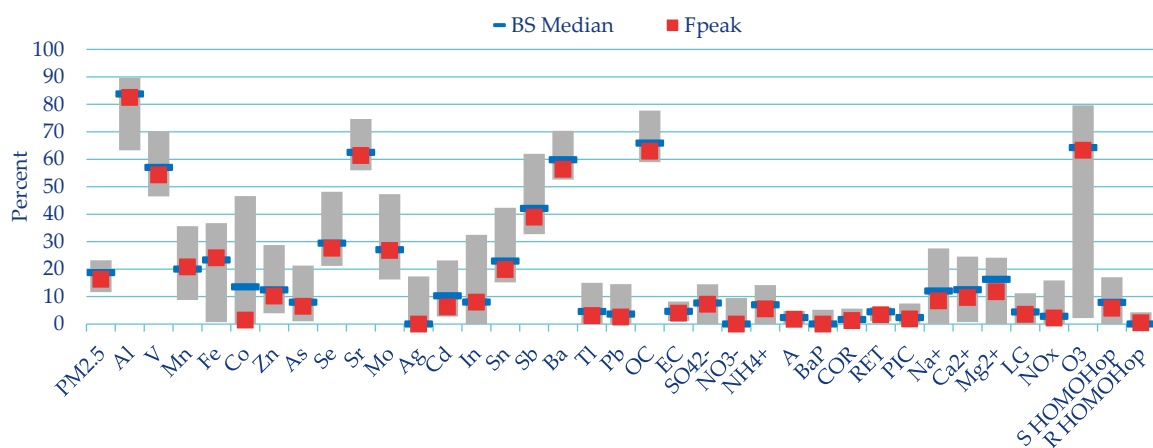


**Figure A4.** Relative species concentration (Fpeak) of the “Crustal” factor and the result of the BS test (Median and IQR).

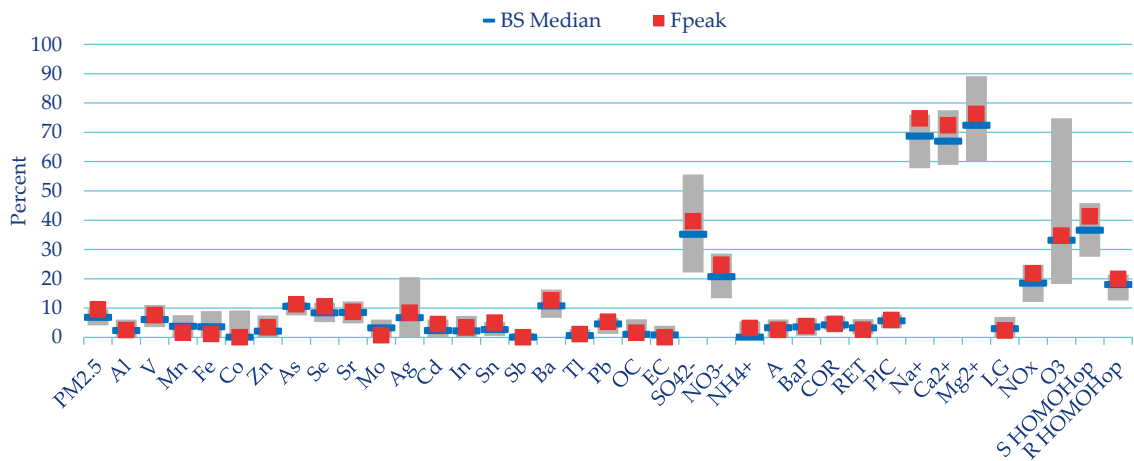


**Figure A5.** Relative species concentration (Fpeak) of the “Long range transport” factor and the result of the BS test (Median and IQR).

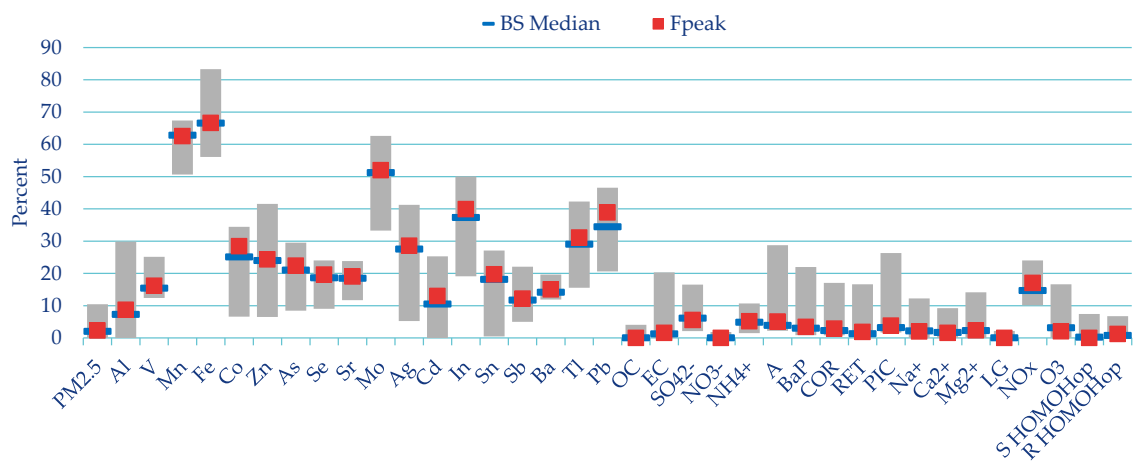


**Figure A6.** Relative species concentration (Fpeak) of the “Iron and steelworks” factor and the result of the BS test (Median and IQR).

## Appendix B

The following pictures illustrate stacked area graphs of the overall PM<sub>2.5</sub> concentration and its apportioning among the identified factors.

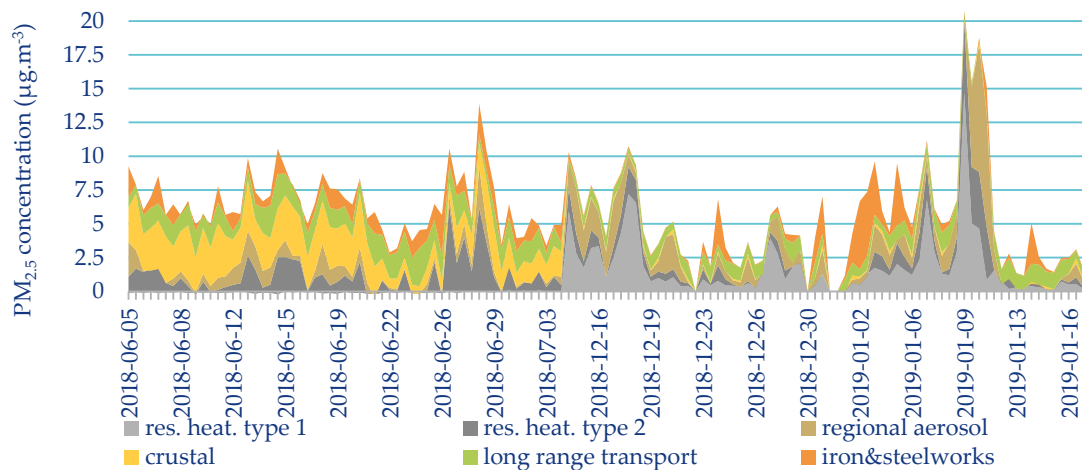


**Figure A7.** Time series of absolute PM<sub>2.5</sub> concentration—“Kosmos” site.

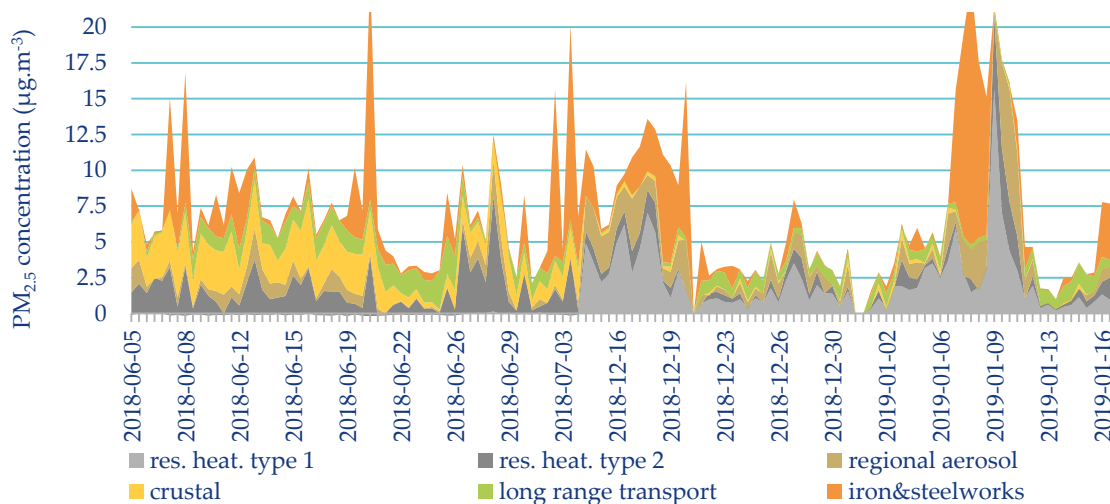


Figure A8. Time series of absolute PM<sub>2.5</sub> concentration—“Ropice” site.

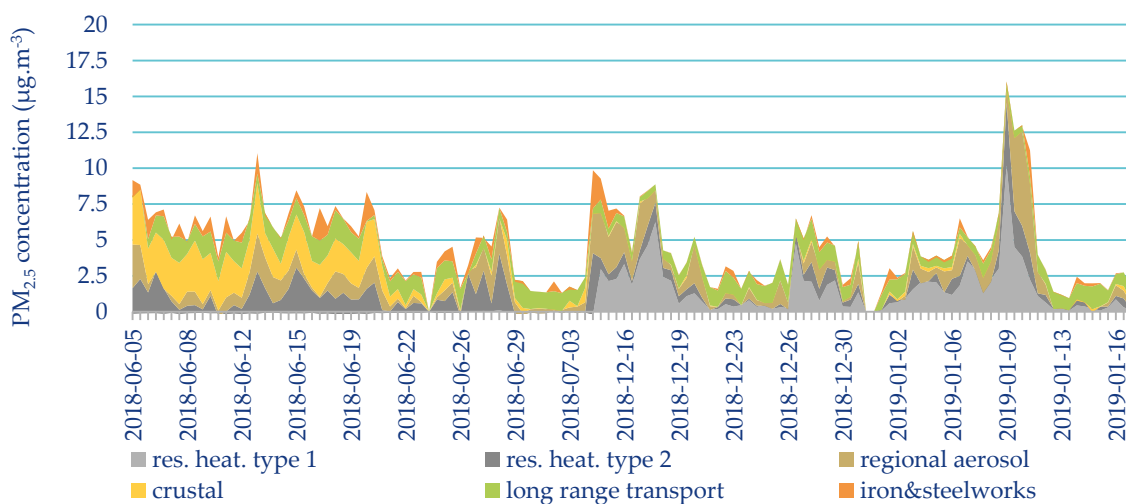


Figure A9. Time series of absolute PM<sub>2.5</sub> concentration—“Vrchy” site.

### Appendix C

The following pictures illustrate the time-weighted concentration roses of the relative PM<sub>2.5</sub> factor contribution to its mean.

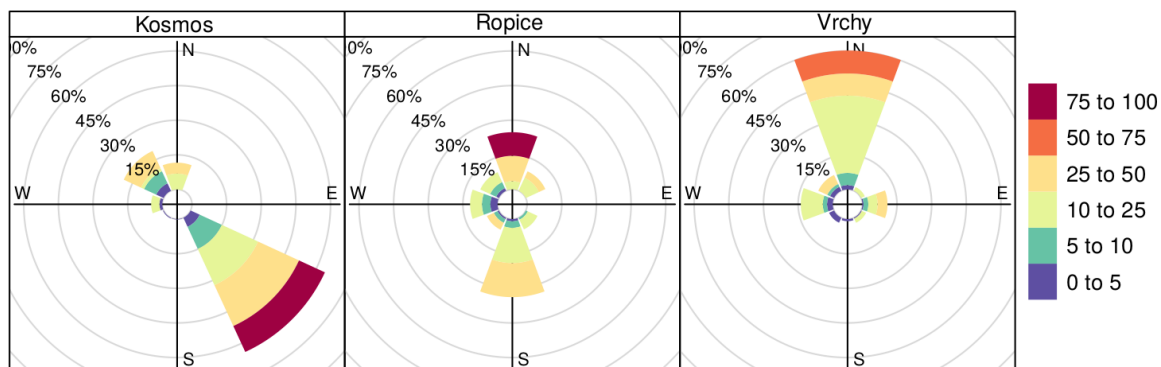


Figure A10. “Residential heating type 1”—proportion of the contribution to the mean (%).

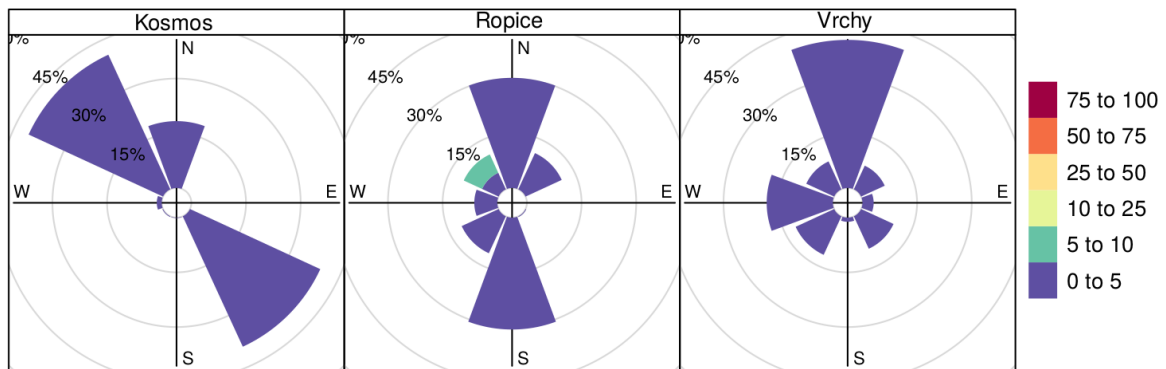


Figure A11. "Residential heating type 2"—proportion of the contribution to the mean (%).

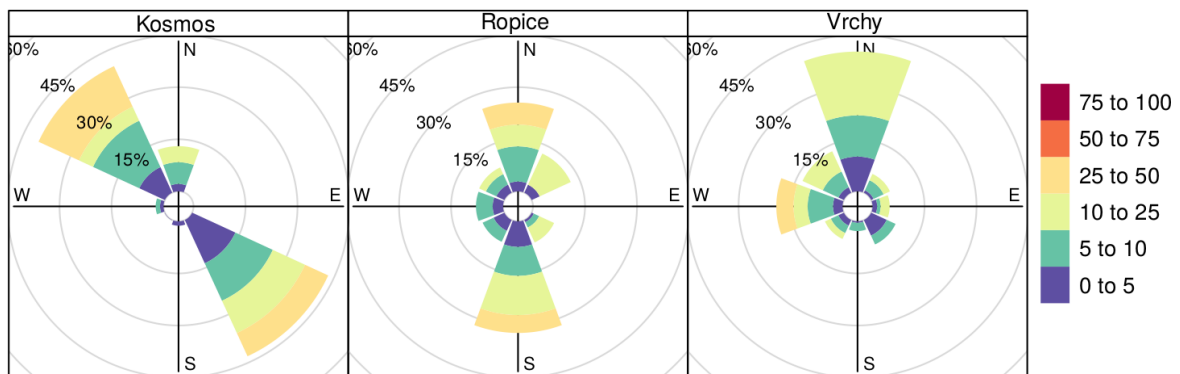


Figure A12. "Regional aerosol"—proportion of the contribution to the mean (%).

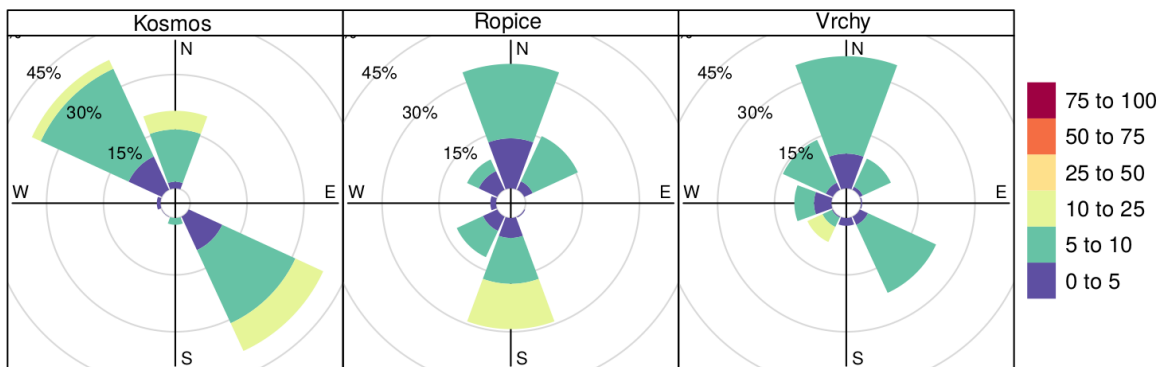


Figure A13. "Crustal"—proportion of the contribution to the mean (%).

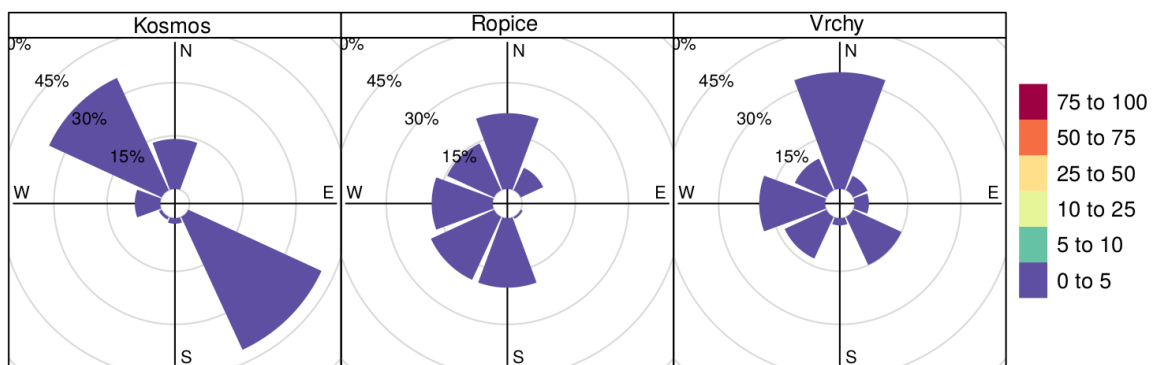


Figure A14. "Long-range transport" - proportion of the contribution to the mean (%).

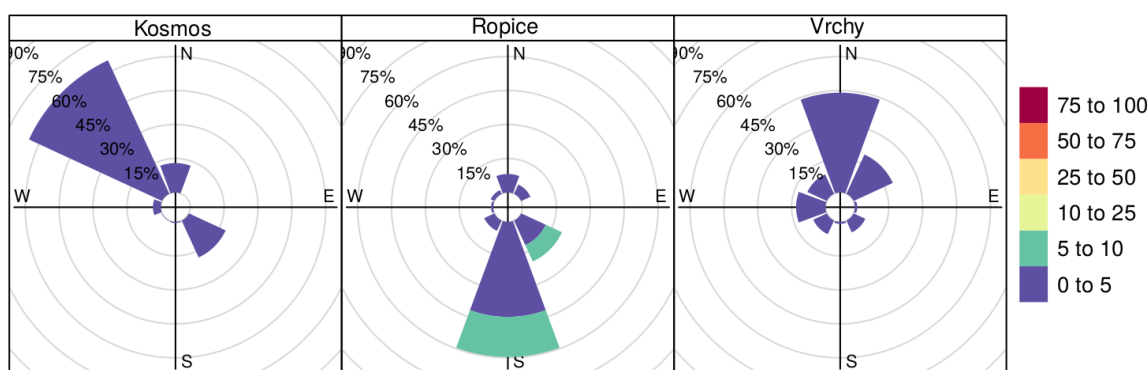


Figure A15. “Iron and steelworks”—proportion of the contribution to the mean (%).

## References

- European Environment Agency. *Air Quality in Europe—2019 Report*; Publications Office of the European Union: Luxembourg, 2019; pp. 26–33. Available online: <https://www.eea.europa.eu/publications/air-quality-in-europe-2019> (accessed on 30 April 2020).
- European Court of Auditors. *Special Report Air Pollution: Our Health Still Insufficiently Protected*; European Union: Luxembourg, 2018; pp. 10–11. Available online: [https://www.eca.europa.eu/Lists/ECADocuments/SR18\\_23/SR\\_AIR\\_QUALITY\\_EN.pdf](https://www.eca.europa.eu/Lists/ECADocuments/SR18_23/SR_AIR_QUALITY_EN.pdf) (accessed on 30 April 2020).
- World Health Organization; Regional Office for Europe. *Health Effects of Particulate Matter*; WHO: Copenhagen, Denmark, 2013; pp. 6–8. Available online: [http://www.euro.who.int/\\_\\_data/assets/pdf\\_file/0006/189051/Health-effects-of-particulate-matter-final-Eng.pdf](http://www.euro.who.int/__data/assets/pdf_file/0006/189051/Health-effects-of-particulate-matter-final-Eng.pdf) (accessed on 30 April 2020).
- Colette, A.; Schucht, S.; Ciarelli, G.; Létinois, L.; Meleux, F.; The Eurodelta-Trends Modelling Team. *ETC/ACM Technical Paper 2017/4, Long-term air quality trends in Europe, Fine Particulate Matter (PM<sub>2.5</sub>) Health Impacts*; ETC/ACM: Bilthoven, The Netherlands, 2018; pp. 16–39. Available online: [https://www.eionet.europa.eu/etcs/etc-atni/products/etc-atni-reports/etcacm\\_tp\\_2017\\_4\\_aqtrendshia](https://www.eionet.europa.eu/etcs/etc-atni/products/etc-atni-reports/etcacm_tp_2017_4_aqtrendshia) (accessed on 30 April 2020).
- Czech Hydrometeorological Institute. *Air Pollution in the Czech Republic in 2018*; Czech Hydrometeorological Institute: Prague, Czech Republic, 2019; Available online: [http://portal.chmi.cz/files/portal/docs/uoco/isko/grafroc/18groc/gr18cz/KO\\_rocenka\\_2018.pdf](http://portal.chmi.cz/files/portal/docs/uoco/isko/grafroc/18groc/gr18cz/KO_rocenka_2018.pdf) (accessed on 30 April 2020).
- Blazek, Z.; Cernikovský, L.; Krejci, B.; Volna, V. *Transboundary Pollution Transport Evaluation within the Air Silesia Project*; Czech Hydrometeorological Institute: Ostrava, Czech Republic, 2013; pp. 5–6.
- Czech Ministry of Environment. *Air Quality Improvement Program of Agglomeration Ostrava/Karviná/Frýdek-Místek-CZ08A*; Czech Ministry of Environment: Prague, Czech Republic, 2016; pp. 87–112. Available online: [https://www.mzp.cz/C1257458002F0DC7/cz/platne\\_programy\\_zlepsovani\\_kvality\\_2016/\\$FILE/OOO-PZKO\\_CZ08A-20190718.pdf](https://www.mzp.cz/C1257458002F0DC7/cz/platne_programy_zlepsovani_kvality_2016/$FILE/OOO-PZKO_CZ08A-20190718.pdf) (accessed on 30 April 2020).
- Vossler, T.; Cernikovský, L.; Novak, J.; Placha, H.; Krejci, B.; Nikolova, I.; Chalupnickova, E.; Williams, R. An Investigation of local and regional sources of fine particulate matter in Ostrava, the Czech Republic. *Atmos. Pollut. Res.* **2015**, *6*, 454–463.
- Vossler, T.; Cernikovský, L.; Novak, J.; Williams, R. Source apportionment with uncertainty estimates of fine particulate matter in Ostrava, Czech Republic using Positive Matrix Factorization. *Atmos. Pollut. Res.* **2016**, *7*, 503–512. [CrossRef]
- Blazek, Z.; Cernikovský, L.; Krejci, B.; Volna, V.; Krajny, E.; Osrodka, L.; Wojtylak, M. *Influences of Meteorological Conditions on Air Quality in the Cross-Border Area of Silesia and Moravia*, 1st ed.; Czech Hydrometeorological Institute, Polish Institute of Meteorology and Water Management-National Research Institute: Warsaw, Poland, 2013; p. 49. Available online: [http://www.airsilesia.eu/files/file/air\\_silesia/publikace\\_.pdf](http://www.airsilesia.eu/files/file/air_silesia/publikace_.pdf) (accessed on 30 April 2020).
- Road and Motorway Directorate of the Czech Republic. *National Traffic Census 2016*. Available online: <http://scitani2016.rsd.cz/pages/informations/default.aspx> (accessed on 30 April 2020).
- Czech Hydrometeorological Institute. *Five-Year Moving Average of Annual Average Concentrations*. Available online: [http://portal.chmi.cz/files/portal/docs/uoco/isko/ozko/ozko\\_CZ.html](http://portal.chmi.cz/files/portal/docs/uoco/isko/ozko/ozko_CZ.html) (accessed on 30 April 2020).

13. Contini, D.; Cesari, D.; Conte, M.; Donato, A. Application of PMF and CMB receptor models for the evaluation of the contribution of a large coal-fired power plant to PM<sub>10</sub> concentrations. *Sci. Total Environ.* **2016**, *560*, 131–140. [[CrossRef](#)] [[PubMed](#)]
14. Norris, G.; Duvall, R.; Brown, S.; Bai, S. *Positive Matrix Factorization (PMF), Fundamentals and User Guide*; U.S. EPA: Washington, DC, USA, 2014. Available online: [https://www.epa.gov/sites/production/files/2015-02/documents/pmf\\_5.0\\_user\\_guide.pdf](https://www.epa.gov/sites/production/files/2015-02/documents/pmf_5.0_user_guide.pdf) (accessed on 30 April 2020).
15. Kozakova, J.; Pokorna, P.; Vodicka, P.; Ondrackova, L.; Ondracek, J.; Krupal, K.; Mikuska, P.; Hovorka, J.; Moravec, P.; Schwarz, J. The influence of local emissions and regional air pollution transport on a European air pollution hot spot. *Environ. Sci. Pollut. Res.* **2019**, *26*, 1675–1692. [[CrossRef](#)] [[PubMed](#)]
16. Belis, C.A.; Karagulian, F.; Amato, F.; Almeida, M.; Artaxo, P.; Beddows, D.C.S.; Bernardoni, V.; Bove, M.C.; Carbone, S.; Cesari, D.; et al. A new methodology to assess the performance and uncertainty of source apportionment models II: The results of two European intercomparison exercises. *Atmos. Environ.* **2015**, *123*, 240–250. [[CrossRef](#)]
17. Leoni, C.; Pokorna, P.; Hovorka, J.; Masiol, M.; Topinka, J.; Zhao, Y.; Krupal, K.; Cliff, S.; Mikuska, P.; Hopke, P.K. Source apportionment of aerosol particles at a European air pollution hot spot using particle number size distributions and chemical composition. *Environ. Pollut.* **2018**, *234*, 145–154. [[CrossRef](#)] [[PubMed](#)]
18. Cesari, D.; Merico, E.; Dinoi, A.; Marinoni, A.; Bonasoni, P.; Contini, D. Seasonal variability of carbonaceous aerosols in an urban background area in Southern Italy. *Atmospheric Research.* **2018**, *200*, 97–108. [[CrossRef](#)]
19. Hůnová, I. Ambient Air Quality in the Czech Republic: Past and Present. *Atmosphere* **2020**, *11*, 214. [[CrossRef](#)]
20. Ravindra, K.; Sokhi, R.; Van Grieken, R. Atmospheric polycyclic aromatic hydrocarbons: Source attribution, emission factors and regulation. *Atmos. Environ.* **2008**, *42*, 2895–2921. [[CrossRef](#)]
21. Dyke, P.H.; Foan, C.; Fiedler, H. PCB and PAH releases from power stations and waste incineration processes in the UK. *Chemosphere* **2003**, *50*, 469–480. [[CrossRef](#)]
22. Directive 2004/107/EC of the European Parliament and of the Council. Available online: <https://eur-lex.europa.eu/legal-content/EN/TXT/?uri=CELEX:32004L0107> (accessed on 30 April 2020).
23. Schauer, C.; Niessner, R.; Poschl, U. Polycyclic aromatic hydrocarbons in urban air particulate matter: Decadal and seasonal trends, chemical degradation, and sampling artifacts. *Environ. Sci. Technol.* **2003**, *37*, 2861–2868. [[CrossRef](#)] [[PubMed](#)]
24. Alves, C.A. Characterisation of solvent extractable organic constituents in atmospheric particulate matter: An overview. *An. Acad. Bras. Cienc.* **2008**, *80*, 21–82. [[CrossRef](#)]
25. Oliveira, C.; Martins, N.; Tavares, J.; Pio, C.; Cerqueira, M.; Matos, M.; Silva, H.; Oliveira, C.; Camões, F. Size distribution of polycyclic aromatic hydrocarbons in a roadway tunnel in Lisbon, Portugal. *Chemosphere* **2011**, *83*, 1588–1596. [[CrossRef](#)] [[PubMed](#)]
26. Oros, D.R.; Simoneit, B.R.T. Identification and emission rates of molecular tracers in coal smoke particulate matter. *Fuel* **2000**, *79*, 515–536. [[CrossRef](#)]
27. Simoneit, B.R.T. A review of biomarker compounds as source indicators and tracers for air pollution. *Environ. Sci. Pollut. Res.* **1999**, *6*, 159–169. [[CrossRef](#)] [[PubMed](#)]
28. Schauer, J.J.; Rogge, W.F.; Hildemann, L.M.; Mazurek, M.A.; Cass, G.R.; Simoneit, B.R.T. Source apportionment of airborne particulate matter using organic compounds as tracers. *Atmos. Environ.* **1996**, *30*, 3837–3855. [[CrossRef](#)]
29. Rogge, W.F.; Hildemann, L.M.; Mazurek, M.; Cass, G.R.; Simoneit, B.R.T. Sources of fine organic aerosol: 2. Noncatalyst and catalyst-equipped automobiles and heavy-duty diesel trucks. *Environ. Sci. Technol.* **1993**, *27*, 636–651. [[CrossRef](#)]
30. Vojtisek-Lom, M.; Beránek, V.; Mikuška, P.; Křůmal, K.; Coufalík, P.; Jitka Sikorová, J.; Topinka, J. Blends of butanol and hydrotreated vegetable oils as drop-in replacement for diesel engines: Effects on combustion and emissions. *Fuel* **2017**, *197*, 407–421. [[CrossRef](#)]

31. Holoubek, I. *Polycyclic Aromatic Hydrocarbons (PAHs) in the Environment*; Český ekologický ústav, Ministry of the Environment of the Czech Republic: Prague, Czech Republic, 1996.
32. Belis, C.A.; Pernigotti, D.; Pirovano, G.; Favez, O.; Jaffrezo, J.L.; Kuenen, J.; Denier van Der Gon, H.; Reizer, M.; Riffault, V.; Alleman, L.Y.; et al. Evaluation of receptor and chemical transport models for PM<sub>10</sub> source apportionment. *Atmos. Environ.* **2020**, *X5*, 100053. [[CrossRef](#)]



© 2020 by the authors. Licensee MDPI, Basel, Switzerland. This article is an open access article distributed under the terms and conditions of the Creative Commons Attribution (CC BY) license (<http://creativecommons.org/licenses/by/4.0/>).

## Article

# Characterization of PM<sub>10</sub> Sampled on the Top of a Former Mining Tower by the High-Volume Wind Direction-Dependent Sampler Using INNA

Irena Pavlíková<sup>1,2,\*</sup> , Daniel Hladký<sup>1,3</sup>, Oldřich Motyka<sup>4</sup> , Konstantin N. Vergel<sup>2</sup>, Ludmila P. Strelkova<sup>2</sup> and Margarita S. Shvetsova<sup>2</sup>

<sup>1</sup> Department of Environmental Protection in Industry, Faculty of Materials Science and Technology, VSB–Technical University of Ostrava, 708 00 Ostrava-Poruba, Czech Republic; daniel.hladky@chmi.cz

<sup>2</sup> Sector of Neutron Activation Analysis and Applied Research, Frank Laboratory of Neutron Physics, Joint Institute for Nuclear Research, 141980 Dubna, Russia; verkn@mail.ru (K.N.V.); lstrel@nf.jinr.ru (L.P.S.); mks@nf.jinr.ru (M.S.S.)

<sup>3</sup> Czech Hydrometeorological Institute, 708 00 Ostrava-Poruba, Czech Republic

<sup>4</sup> Nanotechnology Centre, VSB–Technical University of Ostrava, 708 00 Ostrava-Poruba, Czech Republic; oldrich.motyka@vsb.cz

\* Correspondence: irena.pavlikova@vsb.cz or pavlikova@jinr.ru; Tel.: +420-604-636-041

**Abstract:** The PM<sub>10</sub> concentrations in the studied region (Ostravsko-karvinská agglomeration, Czech Republic) exceed air pollution limit values in the long-term and pose a significant problem for human health, quality of life and the environment. In order to characterize the pollution in the region and identify the pollution origin, Instrumental Neutron Activation Analysis (INAA) was employed for determination of 34 elements in PM<sub>10</sub> samples collected at a height of 90 m above ground level. From April 2018 to March 2019, 111 PM<sub>10</sub> samples from eight basic wind directions and calm and two smog situations were sampled. The elemental composition significantly varied depending on season and sampling conditions. The contribution of three important industrial sources (iron and steelworks, cement works) was identified, and the long-range cross-border transport representing the pollution from the Polish domestic boilers confirmed the most important pollution inflow during the winter season.

**Keywords:** air pollution; PM<sub>10</sub>; tower; high-volume sampler; wind-direction-dependent sampling; neutron activation analysis; elemental composition; cross-border pollution transport; AIR BORDER; Czech-Polish borderlands; Interreg



**Citation:** Pavlíková, I.; Hladký, D.; Motyka, O.; Vergel, K.N.; Strelkova, L.P.; Shvetsova, M.S. Characterization of PM<sub>10</sub> Sampled on the Top of a Former Mining Tower by the High-Volume Wind Direction-Dependent Sampler Using INNA. *Atmosphere* **2021**, *12*, 29. <https://doi.org/10.3390/atmos12010029>

Received: 3 December 2020

Accepted: 23 December 2020

Published: 28 December 2020

**Publisher's Note:** MDPI stays neutral with regard to jurisdictional claims in published maps and institutional affiliations.



**Copyright:** © 2020 by the authors. Licensee MDPI, Basel, Switzerland. This article is an open access article distributed under the terms and conditions of the Creative Commons Attribution (CC BY) license (<https://creativecommons.org/licenses/by/4.0/>).

## 1. Introduction

The studied area—Ostravsko-karvinská agglomeration—is situated in the northeast part of the Czech Republic, in the Moravian-Silesian Region. The region, together with the adjacent cross-border Polish region of Silesia, is historically connected with the accumulation of black coal mining and heavy industry, namely energetics, coking plants and ironworks [1,2]. The particular industrial character of the region along with its topography (basin surrounded by fairly high mountain ranges) and local meteorological conditions [3] causes its specific air pollution problems. The strategic industrial development of the region in the 1950s [4,5] initiated intensive population growth connected with substantial emissions from households. This effect has persisted until the present, as coal is still the most widely used fuel in the Polish border area [6,7]. Thus, the region is one of the most polluted in Europe [8]. The air pollution significantly exceeds the limit values of particulate matter (PM<sub>10</sub>, PM<sub>2.5</sub>), benzo[a]pyrene and ozone [4,8,9] according to European legislation [10] and World Health Organization (WHO) guidelines [11,12]. Both daily and long-term exposure to the substances mentioned above has a number of substantiated

adverse biological effects [5,13]. Airborne particles increase mortality and morbidity, especially of the respiratory system, even at short-term exposures. The population exposed to PM shows a higher incidence of infectious diseases [14–16], and atmospheric pollution and PM pollution are factors classified as proven human carcinogens (category 1) [17]. Being one of the most densely populated regions in the Czech Republic (except its capital city) [18], the air pollution here poses an essential and long-term environmental problem.

Substantial pollution in the region has challenged researchers to identify causes and look for solutions, starting in the 1990s with the US EPA project Silesia [19,20]; later on, the effort continued with projects AIR SILESIA [21,22] and AIR TRITIA [6,23]. Moreover, numerous case studies focused on the pollution origin were performed [24–26] together with the recently published study of the Czech Hydrometeorological Institute (CHMI) [27,28]. All the studies emphasized the role of both the industry and the transboundary pollution from Poland (caused mainly by domestic boilers). According to these studies and state air quality monitoring [9,29], the highest PM concentrations occur near the Czech–Polish border (characterized by more prominent growth in the colder half of the year and during smog events) and also close to important industrial sources where the limit values of PM happened to be reached not only during the winter season. The air quality in the region is significantly influenced by the rate and nature of cross-border pollution transmission along the most frequent wind directions (typically SW/NE), together with the inverse character of the weather with steady atmosphere and subsequently worsened dispersion conditions, which significantly contribute to increased air pollution during the winter. According to the available studies [6,22,27,30], the contribution of the cross-border PM pollution to the annual average values can vary from 20–40% depending on the location in the region, emissions and meteorological conditions in the year.

The air quality monitoring presented in this study was performed within the AIR BORDER project focused on the cross-border pollution transport from Poland to the Ostravsko-karvinská agglomeration (the Czech borderland) and vice versa. The aim of the study was to run a special monitoring campaign in order to characterize the transmission of the PM<sub>10</sub> particles from different groups of air pollution sources specific for the region, excluding the influence of the local sources [31]. This presumption was possible by locating a monitoring device on the top of a tower that reaches a height of over 85 m above the ground level. The device collects the PM<sub>10</sub> particles depending on the wind direction, which enables one to investigate from which directions and from which sources the pollution comes and to more precisely quantify its transfer within the region.

## 2. Experiments

### 2.1. Sampling

The monitoring device was situated on the top of a former mining tower (90 m above ground level) located in Horní Suchá village in the centre of the Ostravsko-karvinská agglomeration.

(World Geodetic System 1984 coordinates 49.805166 N, 18.473954 E). The location of the tower in the region can be seen in Figure 1, the tower in Figure 2.

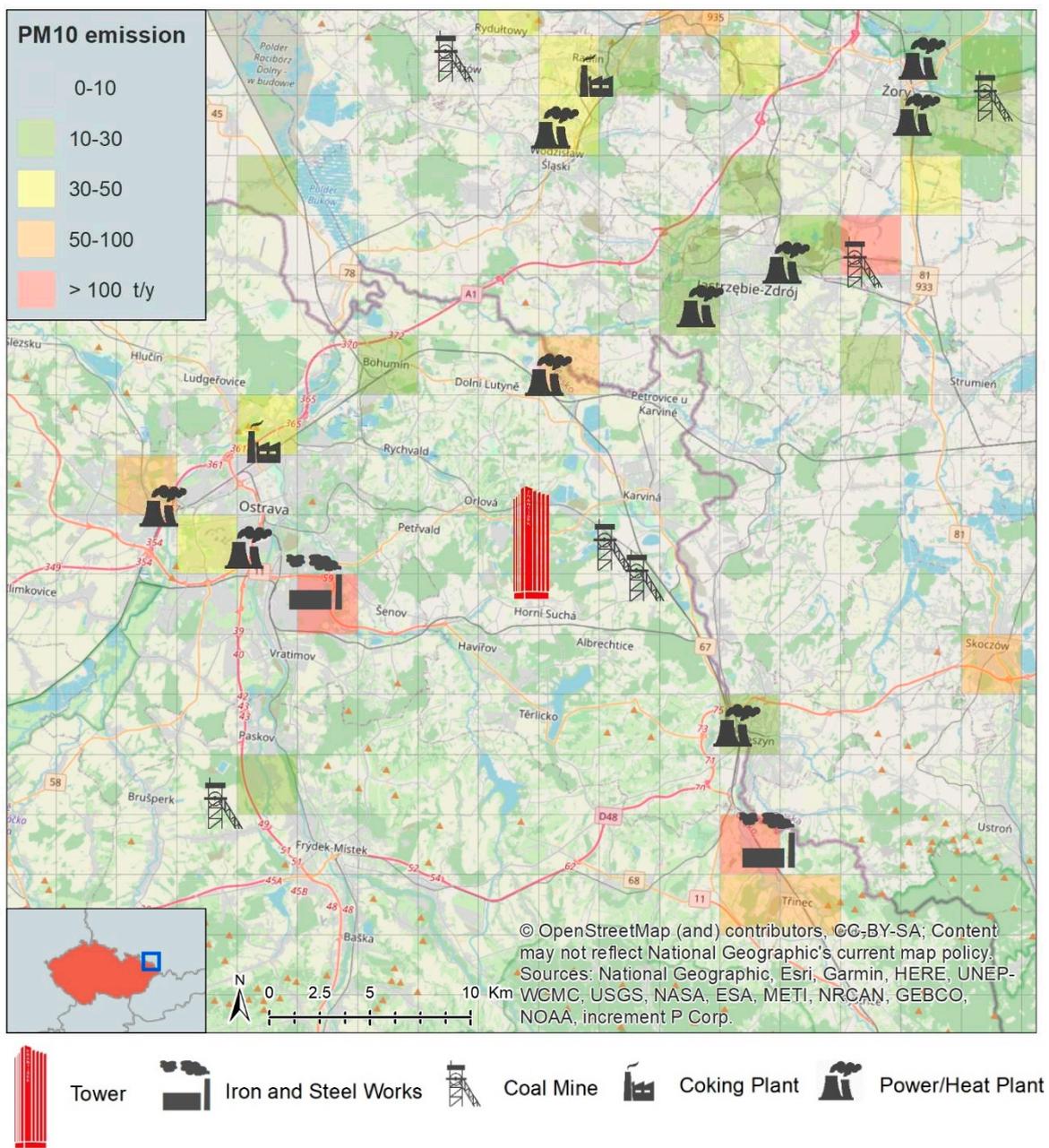


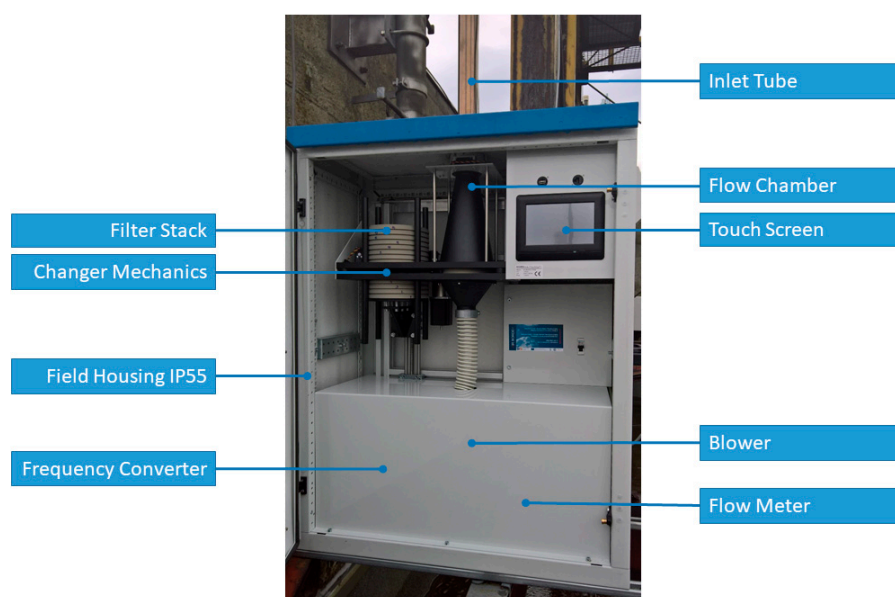
Figure 1. The location of the tower at a regional scale with plotted industrial PM<sub>10</sub> emissions.



Figure 2. The tower in the operation period of the 1980s (a) and presently (b).

For the particulate matter sampling, the high-volume sampler SAM Hi 30 AUTO WIND (Baghirra Ltd., Prague, Czech Republic) was used. The sampler operates respecting the Guidelines on high-volume sampling methods that can be found in the Compendium of Methods for the Determination of Inorganic Compounds in Ambient Air compiled by the United States Environmental Protection Agency (US EPA) [32]; a summary of the research of high-volume samplers performance can be found elsewhere [33].

The SAM Hi 30 AUTO WIND is a fully automatic, remote-controlled sampler intended for gravimetric and chemical analyses of aerosol particles. The device samples particulate matter with a  $<10\ \mu\text{m}$  diameter ( $\text{PM}_{10}$ ) using the DIGITEL DPM10/30/00  $\text{PM}_{10}$  pre-separator for  $30\ \text{m}^3/\text{h}$  according to EN 12341 [34]. The sampler was designed to work depending on wind conditions. It has a magazine of 15 filters (glass microfiber, Whatman GF/A,  $\varnothing 150\ \text{mm}$ ) stretched in filter holders that are automatically changed to the sampling position according to actually evaluated wind conditions. Thus the sampler was able to collect  $\text{PM}_{10}$  particles from eight basic wind directions (N, NE, E, SE, S, SW, W, NW) and CALM (wind speed  $< 0.2\ \text{m}\cdot\text{s}^{-1}$ ). The sampler can be seen in Figure 3. Both wind speed and wind direction were measured via the WindSonic™ SDI-12 anemometer (Gill Instruments Ltd., Lymington, UK). The wind direction and wind speed for selecting a particular sampling filter from the magazine were determined according to one-hour moving averages calculated from 10-min data in accordance with US EPA guidance [35]. Thus, the actual wind may be different. The wind roses representing the measured wind direction in comparison with the sampled sector can be seen in Figure 4. Moreover, a special filter was designed for the episodes with extreme air pollution, defined as three successive average hourly  $\text{PM}_{10}$  concentrations exceeding  $100\ \mu\text{g}\cdot\text{m}^{-3}$ , using 10-min data from continuous ground monitoring.



**Figure 3.** The SAM Hi 30 AUTO WIND sampler.

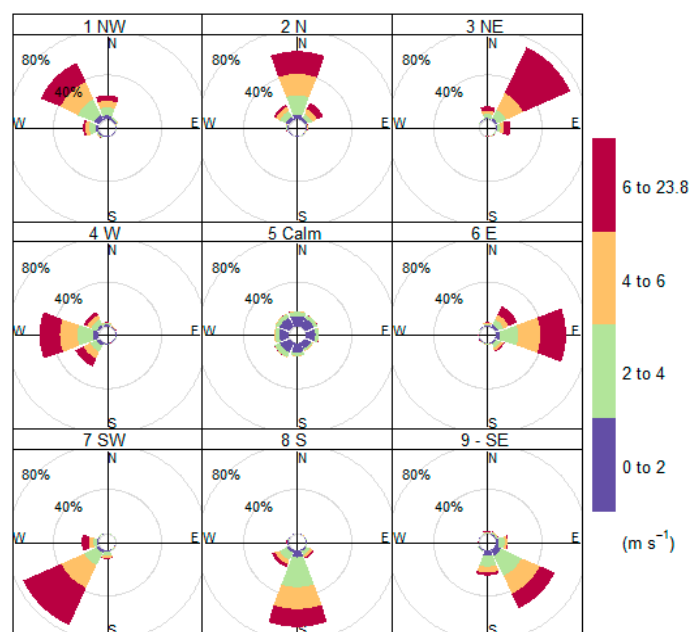


**Figure 4.** Matching of sampled sectors and measured wind directions.

Employing this method, 111  $PM_{10}$  samples from eight wind directions and calm (and extreme air pollution if occurring) were collected for each month from April 2018 to March 2019 (total of 12 months).

### 2.2. Determination of $PM_{10}$ Mass Concentrations

$PM_{10}$  mass concentrations were determined following the guidelines of EN 12341 [34]. Filters were weighed using an analytical balance (Sartorius MC 210P) before and after sampling. The filters were conditioned for  $\geq 48$  h under controlled relative humidity ( $50\% \pm 5\%$ ) and temperature ( $20\text{ }^\circ\text{C} \pm 1\text{ }^\circ\text{C}$ ), then weighed for a first time, followed by a second weighing after additional conditioning for  $\geq 12$  h for filters prior to the sampling and for 24 to 72 h for filters after the sampling. In accordance with the requirements, the difference of weighing results was  $\leq 40\text{ }\mu\text{g}$  for filters prior to the sampling and  $\leq 60\text{ }\mu\text{g}$  for filters after the sampling. The filter weight was calculated as an average of the two results. Weights for the blank filters were also recorded. The collected  $PM_{10}$  mass was calculated by subtracting pre-weight from the post-weight of the filters.

### 2.3. Element Content Determination Using Neutron Activation Analysis

One of the premises of this study was to apply NAA at the IBR-2 reactor of the Joint Institute for Nuclear Research (Russia) for the characterisation of sampled PM. Thus, the testing of filters convenient for the analyses preceded the sampling campaign. Six different filters comprising five different materials were tested (glass microfiber, quartz, PTFE membrane, cellulose and paper). Only glass microfiber filters were determined as being fully suitable; a quartz filter was more problematic for repacking and considering the price, the glass microfiber filters were chosen to be used for the sampling.

Before subjecting the samples to NAA, the preparation of the subsamples of exposed and blank filters was done, as the irradiation capsules of the applied pneumatic transport system have limited volume ( $\text{Ø } 18\text{ mm}$ ) and the whole filter is not able to fit in it. This also allows putting more subsamples in one capsule so the subsamples from one month and the corresponding blank filter can be irradiated all together under the same conditions. For this purpose, a special automatic punching head was designed and made (used materials: stainless steel, Teflon and surface finish synthetic rubber). Prior to cutting, filters were folded in half to avoid the loss of collected material, and then 4 circles ( $\text{Ø } 16\text{ mm}$ ) were cut from the folded filter using the layering of subsamples. This way, one subsample of

each filter (counting eight layers of the filter) was prepared reaching a weight of 0.06–0.07 g depending on the exposure. The preparation of the filters took place under a relative humidity of 50% ( $\pm 5\%$ ) and temperature of 20 °C ( $\pm 1$  °C). After the preparation, each subsample was vacuum-packed to be transported for NAA.

The NAA procedure started with unpacking the subsamples and weighing them under controlled relative humidity and temperature. Then the subsamples were immediately packed in polyethylene and aluminium cups for short-term and long-term irradiation, respectively. Once packed, they were put into irradiation capsules and transported to the reactor.

The employed NAA provides the activation with thermal and epithermal neutrons at low temperatures convenient for this type of samples. Complete information about samples irradiation, measurement and quality can be found elsewhere [36,37].

For short-term irradiation, Channel 2 (epithermal neutrons, flux density  $\varphi_{\text{epi}} = 2.0 \times 10^{11} \text{ cm}^{-2} \cdot \text{s}^{-1}$ ) was used with an irradiation time of about 3 min. Samples were measured with 3–5 min. decay after irradiation for 15 min. Al, Ca, Cl, I, Mg, Mn, Si, Ti and V isotopes were determined in this way. For long-term irradiation, Cd screened Channel 1 (epithermal neutrons, flux density  $\varphi_{\text{epi}} = 2.0 \times 10^{11} \text{ cm}^{-2} \cdot \text{s}^{-1}$ ) was used with an irradiation time of around 4 days. After 4-days cooling, the samples were repacked and measured twice. The first time, they were measured directly after repacking for 30 min to determine As, Br, K, La, Na, Mo, Sm, U and W, and the second time 20 days after the end of irradiation for 1.5 h to determine Ba, Ce, Co, Cr, Cs, Eu, Fe, Hf, Ni, Rb, Sb, Si, Sc, Se, Sr, Ta, Tb, Th, W, Zn and Zr.

Gamma spectra of activated samples were measured on HPGe detectors (resolution of 1.9 keV for the  $^{60}\text{Co}$  1332 keV line, efficiency 40%). The gamma spectra obtained were then processed using GENIE-2K software (CANBERRA) with the verification of the peak fit in an interactive mode. The concentrations of elements were calculated using certified reference materials irradiated simultaneously with samples via “CalcConc” software developed in the Frank Laboratory of Neutron Physics, Joint Institute for Nuclear Research [37]. The element concentrations were calculated by subtracting the corresponding blank filter values from determined values of the element in the subsample and recalculating using the mass concentrations of  $\text{PM}_{10}$ . In cases of values below the detection limit, half of the detection limit was used. In case of missing values (no data) caused by technical problems during the analysis, the data imputation was employed in order to retain the information in the dataset and allow the proper multivariate assessment [38]. The *k*-nearest neighbours algorithm (knn) [39] was applied for the missing non-sub-limit data.

Recommendations of US EPA [40] were kept with respect to the workplace standard operating procedures. The quality control of the NAA results was ensured by triplicating standards per batch of unknown samples and carrying out simultaneous analysis. For filter analyses, standard reference materials were used: 2709a–San Joaquin Soil Baseline Trace Element Concentrations from the National Institute of Standards and Technology (NIST), 2710a–Montana I Soil Highly Elevated Trace Element Concentrations (NIST), 2711a–Montana II Soil Moderately Elevated Trace Element Concentrations (NIST), 1632c Trace Elements in Coal (Bituminous) (NIST), 1633c Trace Elements in Coal Fly Ash (NIST), AGV-2 Andesite from the United States Geological Survey and 433 from the Institute for Reference Materials and Measurements (IRMM). Satisfying agreement between the experimental results and certified material was obtained. The accuracy was formulated as the percentage deviation from the certified value amount up to 10%.

#### 2.4. Statistical Analyses and Visualization

Pearson correlations calculation, Principal Component Analysis (PCA) and the visualizations of the results were performed in the R environment [41], package FactoMineR [42,43], Openair [44] and ggplot2 [45]. Prior to the PCA, the data were transformed according to the compositional data analysis (CoDa) principles [46] using the centred log-ratio (clr) transformation [47]. Only the clr-transformed elemental concentration data were used

for the construction of the model, and the information on the wind direction, calm and inversion situation were added as supplementary variables.

### 3. Results

#### 3.1. PM<sub>10</sub> Mass Concentrations

The values of PM<sub>10</sub> concentrations corresponding to wind directions, calm and inversion situations are shown for year average, warm (from April to September) and cold (from October to March) seasons for the period of observation (04/2018–03/2019) in Table 1 and Figure 5a. The values recorded during inversion events are not included in the calculation of means for respective wind directions considering the set-up function of the sampling device (see Section 2.1). For the PM<sub>10</sub> concentration synopsis, see Table S1 the Supplementary materials.

**Table 1.** Average PM<sub>10</sub> concentrations for the observed period ( $\mu\text{g}\cdot\text{m}^{-3}$ ).

| Wind Conditions | Average <sup>1</sup> | Warm Season Average | Z-Score <sup>2</sup> | Cold Season Average <sup>1</sup> | Z-Score <sup>2</sup> |
|-----------------|----------------------|---------------------|----------------------|----------------------------------|----------------------|
| CALM            | 23.3                 | 19.0                | −0.35                | 27.6                             | 1.16                 |
| N               | 22.9                 | 14.6                | −1.12                | 31.2                             | 1.79                 |
| NE              | 21.7                 | 16.5                | −0.79                | 27.0                             | 1.05                 |
| E               | 25.0                 | 17.8                | −0.56                | 32.3                             | 1.97                 |
| SE              | 21.1                 | 17.5                | −0.60                | 24.6                             | 0.64                 |
| S               | 21.9                 | 16.9                | −0.71                | 27.0                             | 1.05                 |
| SW              | 14.8                 | 14.5                | −1.14                | 15.1                             | −1.04                |
| W               | 21.3                 | 23.6                | 0.45                 | 19.0                             | −0.35                |
| NW              | 16.8                 | 15.9                | −0.89                | 17.8                             | −0.56                |
| Inversion       | -                    | -                   |                      | 59.0                             |                      |

<sup>1</sup> Averages calculated for the concerned period (04/2018–03/2019), the inversion values not included.

<sup>2</sup> Z-score related to the average calculated for the concerned period (04/2018–03/2019).

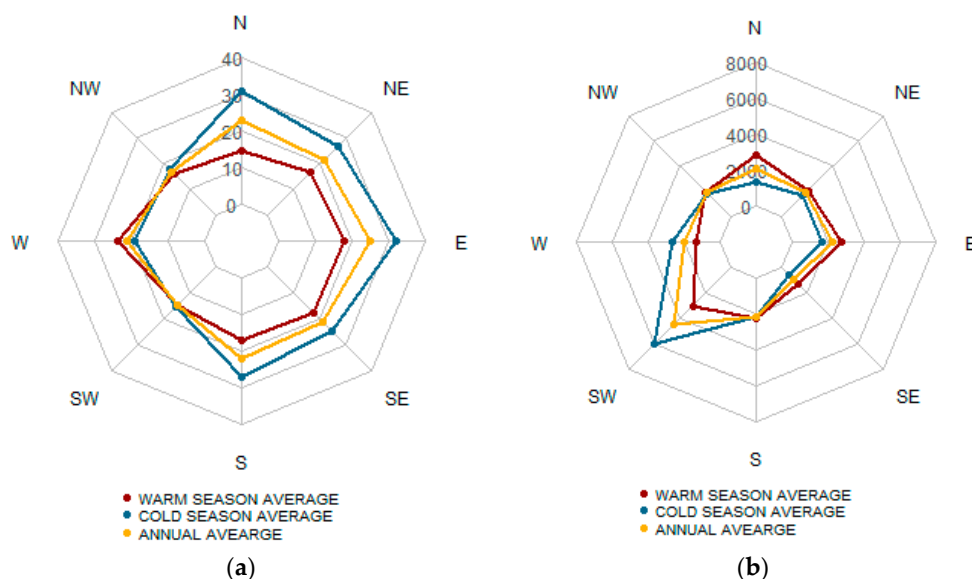


**Figure 5.** The average PM<sub>10</sub> concentrations (a) and wind rose for the observed period (b).

The lowest PM<sub>10</sub> values were observed from the SW and NW directions regardless of the season. The concentrations were below average in the warm part of the year, with the exception of the west direction due to the peak concentration in August 2018 (Figure 6). The highest concentrations were sampled from the east and north during the cold season, though prevailing wind direction in the season was SW Figure 5b. This wind direction in

the cold season was the prevailing wind direction for the whole period of observation, as Figure 5b shows (expressed as a sampled air volume). Calm was recorded for 12% of the sampling time.

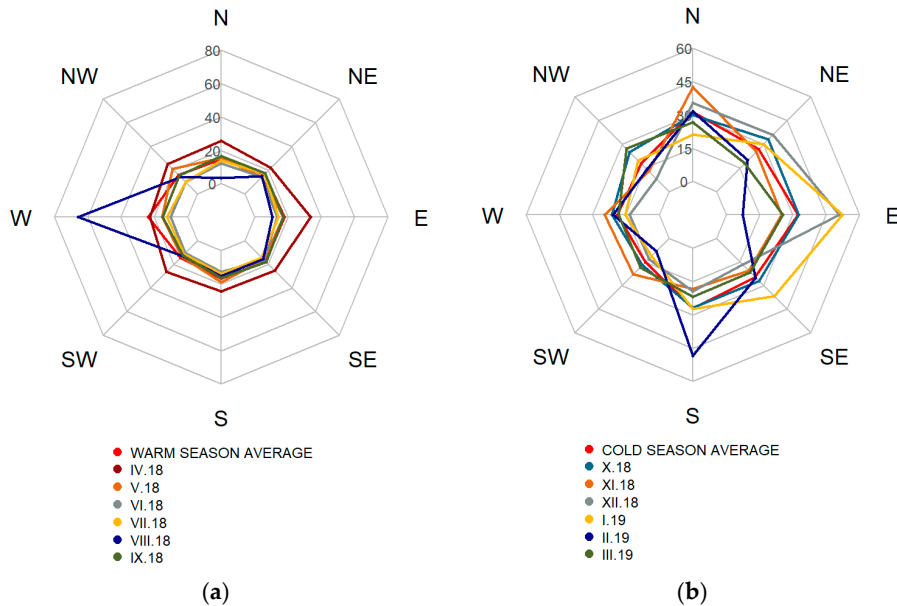


Figure 6. The monthly average PM<sub>10</sub> concentrations for warm (a) and cold (b) season.

Despite the peak concentration in August 2018, there was, in general, no directionality of the pollution in the warm season, as the concentration rose in Figure 6a shows. The peak August concentration originated most likely from the metallurgical complex in the west of the sampling site (see Figure 1), as the elemental composition of this sample also suggests (see Section 3.2). According to the meteorological data, this high concentration occurred in the period of steady cyclonic airflow (wind speed from calm to 2 m/s) preceding an upcoming cold front (see Figure 7). The meteorological situation for this event is illustrated via the ICON EU model data 10 m AGL and the Skew-T diagram as the global model (ICON, NOAA) in this situation was in total disagreement with recorded wind speed and wind direction data on the sampling site.

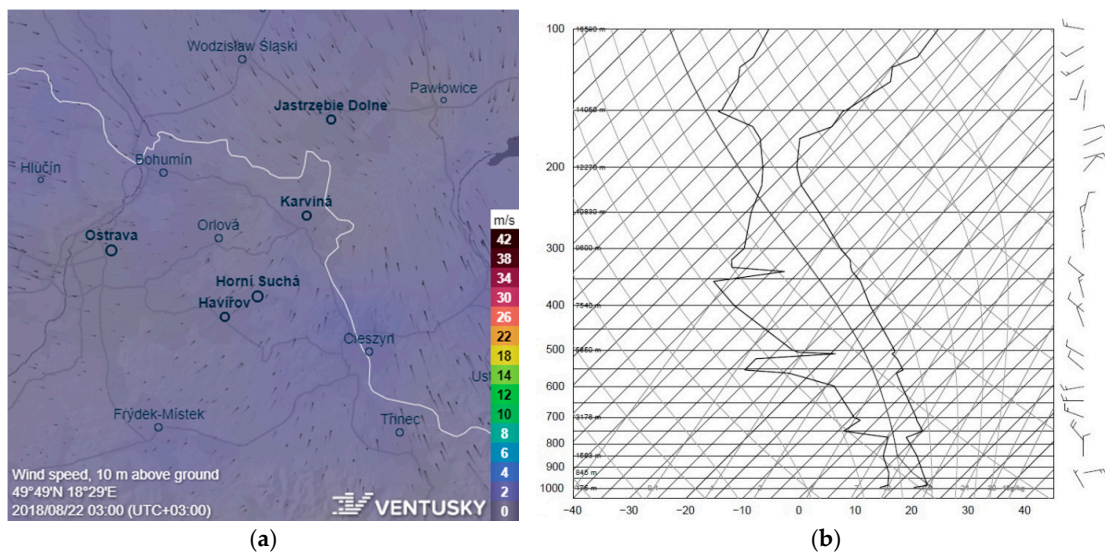
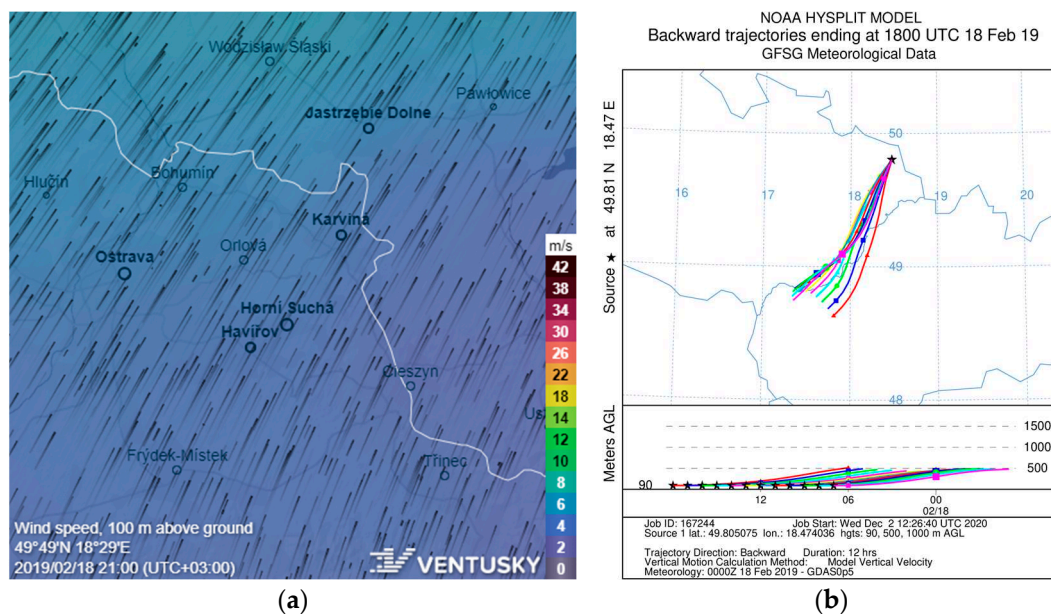


Figure 7. The modelled wind fields (a) and the Skew-T diagram at the Prostějov sounding station (b) for August 2018 peak concentrations [48,49].

The April concentration rose has a similar course to the one for March (Figure 6). Considering the elements found in samples of these two months and the results of PCA (see Section 3.3), a similar origin of the pollution is expected. Thus, the April concentrations should be considered to appertain rather to the cold-season-related pollution sources.

During the winter season, the pollution came predominantly from the north, northeast and east directions, as the monthly average  $PM_{10}$  concentrations show in Figure 6b. This clearly confirms the importance of the PM inflow from the Polish borderland. The increase of  $PM_{10}$  concentrations from these directions in the winter season average  $14 \mu\text{g}\cdot\text{m}^{-3}$  though the prevailing airflow in winter is from the inverse direction (Figure 5b).

High  $PM_{10}$  concentration was sampled in this season also from the south direction in February 2019. As there is no important pollution source in this direction (mountainous rural area), this peak was investigated closer. According to the meteorological data, the airflow was steady (wind speed 1–2 m/s), coming from the southwest via the Moravian Gate for more than one day, accompanied by a radiation inversion (see Figure 8). This indicates that the peak concentration originated from an important pollution source in the south part of the Moravian Gate, directing to the cement works near the city of Hranice (about 50 km from the sampling site), as the elemental composition of this sample confirms (see below in Section 3.2).



**Figure 8.** The modelled wind fields (a) and backward trajectories (b) for February 2019 peak concentrations [48,50,51].

During the winter season, there were two smog events sampled, the first on 19 and 23 November 2018 (sampled on the same filter), with the  $PM_{10}$  concentration reaching  $60.5 \mu\text{g}\cdot\text{m}^{-3}$ , and the second on 23 March 2019, with a  $PM_{10}$  concentration of  $57.4 \mu\text{g}\cdot\text{m}^{-3}$ . In both cases, there was a temperature inversion connected with a steady airflow (measured wind speed  $< 1 \text{ m/s}$ ). In November, the prevailing airflow was from the NE, E and SE directions. Most likely representing the inflow of the pollution from the metallurgical complex on the southeast of the sampling site as confirmed by models (see Figure 9). For the March smog situation, the modelled airflow indicates the direction from the NE and E, suggesting the origin of pollution in the Polish borderland (see Figure 10). The elemental composition of these samples is stated in the next chapter.

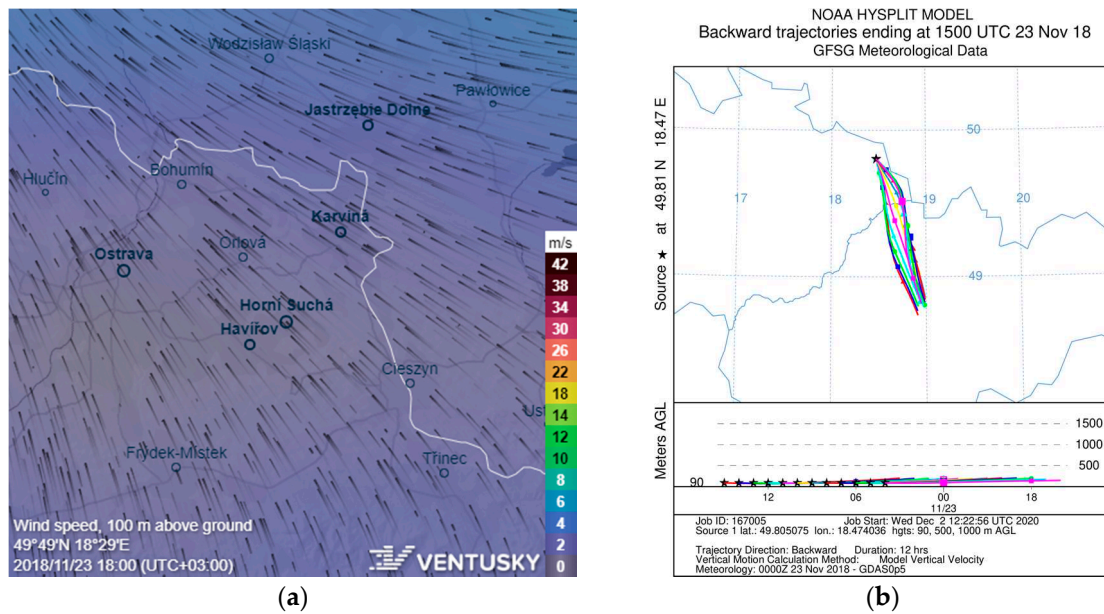


Figure 9. The modelled wind fields (a) and backward trajectories (b) for the smog situations in November 2018 [48,50,51].

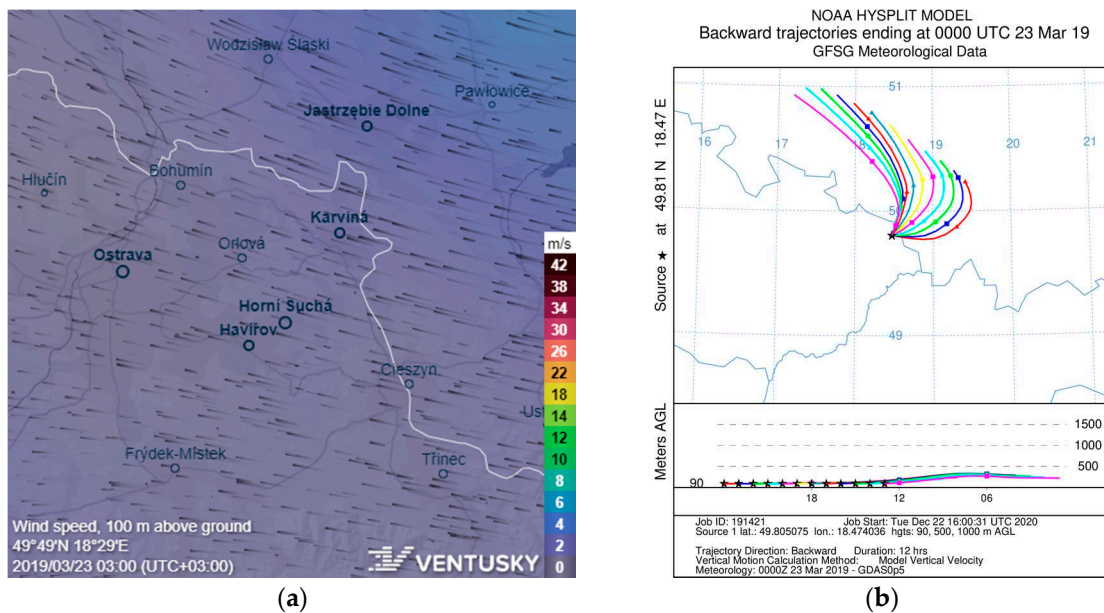


Figure 10. The modelled wind fields (a) and backward trajectories (b) for the smog situations in March 2019 [48,50,51].

### 3.2. Element Content Characterization

The basis of the study was to characterise the sampled PM<sub>10</sub> using NAA. Though this method enables the determination of a wide range of elements, it has specific limitations. Therefore, some of the important markers that would facilitate the source identification are lacking in the obtained dataset of element composition. Thus, the data of Pb (impossible to determine), Cd, Cu, Ni and Ti (determinable only if high concentrations are present) are absent. However, Cd, Ni and Ti were determined in a few samples, but the concentrations were below the minimal detectable concentrations and hence not included in further assessment.

Minimum and maximum levels, mean concentration values, medians and standard deviations of the elements determined in the PM<sub>10</sub> are shown in Table 2; the correlation of

the analysed elements can be found in Table 3. Element contents and concentrations vary depending on the season; thus, the data were investigated separately. To see the element concentrations for the respective directions and seasons, see Table S2 and Figures S1 and S2 in the Supplementary Materials.

The correlation between the analysed element contents was also season-dependent, thus confirming the variability of the sources and the different origin of the pollution. A strong positive correlation ( $R > 0.7$ ) was determined between As and Cr, Mn, Br and I in the warm season, and As correlated with La, Sm, Sr and U in winter. This suggests—together with the directionality of the concentrations of these elements—that As occurrence in the warm season is connected to the metallurgical processes [52–54], while in winter samples, its source appears to be black coal burning [52,55–57].

**Table 2.** Synoptic table (minimum, maximum value, mean, median and standard deviation) of elements concentration ( $\text{ng}\cdot\text{m}^{-3}$ ) determined in the  $\text{PM}_{10}$  using INAA.

| Element | Min                   | Max                   | Mean                  | Median                | Stand. Dev.           |
|---------|-----------------------|-----------------------|-----------------------|-----------------------|-----------------------|
| Al      | $1.15 \times 10^{-2}$ | 873.83                | 15.35                 | 0.73                  | 83.97                 |
| As      | $5.84 \times 10^{-4}$ | 5.17                  | 0.34                  | 0.04                  | 0.94                  |
| Ba      | $4.63 \times 10^{-2}$ | 350.98                | 18.76                 | 0.52                  | 45.96                 |
| Br      | $3.08 \times 10^{-4}$ | 1.72                  | 0.18                  | 0.12                  | 0.22                  |
| Ca      | $8.78 \times 10^{-1}$ | 87.38                 | 13.47                 | 7.33                  | 15.53                 |
| Ce      | $6.47 \times 10^{-3}$ | 1.01                  | 0.12                  | 0.07                  | 0.15                  |
| Cl      | $5.39 \times 10^{-2}$ | 150.66                | 15.73                 | 2.12                  | 29.37                 |
| Co      | $1.71 \times 10^{-4}$ | 0.247                 | 0.019                 | 0.011                 | 0.029                 |
| Cr      | $4.30 \times 10^{-3}$ | 3.22                  | 0.39                  | 0.25                  | 0.49                  |
| Cs      | $9.64 \times 10^{-5}$ | 0.023                 | 0.005                 | 0.003                 | 0.004                 |
| Eu      | $3.39 \times 10^{-5}$ | $1.90 \times 10^{-2}$ | $3.26 \times 10^{-3}$ | $1.60 \times 10^{-3}$ | $3.67 \times 10^{-3}$ |
| Fe      | $2.15 \times 10^{-1}$ | 92.77                 | 19.32                 | 13.42                 | 21.12                 |
| Hf      | $5.49 \times 10^{-4}$ | 0.121                 | 0.013                 | 0.004                 | 0.020                 |
| I       | $7.19 \times 10^{-4}$ | 0.64                  | 0.09                  | 0.05                  | 0.11                  |
| K       | 5.42                  | 524.77                | 74.20                 | 46.06                 | 84.08                 |
| La      | $4.37 \times 10^{-4}$ | 0.67                  | 0.04                  | 0.01                  | 0.12                  |
| Mg      | $3.65 \times 10^{-1}$ | 163.72                | 9.54                  | 5.77                  | 17.61                 |
| Mn      | $1.18 \times 10^{-3}$ | 11.77                 | 1.18                  | 0.62                  | 1.67                  |
| Na      | $1.30 \times 10^{-1}$ | 1074.73               | 62.80                 | 1.58                  | 139.69                |
| Rb      | $3.02 \times 10^{-3}$ | 0.666                 | 0.057                 | 0.028                 | 0.085                 |
| Sb      | $4.73 \times 10^{-5}$ | 0.198                 | 0.050                 | 0.035                 | 0.047                 |
| Sc      | $3.18 \times 10^{-4}$ | 0.021                 | 0.003                 | 0.002                 | 0.004                 |
| Se      | $1.80 \times 10^{-4}$ | 0.176                 | 0.022                 | 0.012                 | 0.027                 |
| Si      | $1.69 \times 10^1$    | 6423.41               | 1529.79               | 1077.04               | 1418.16               |
| Sm      | $2.51 \times 10^{-5}$ | $6.35 \times 10^{-2}$ | $2.65 \times 10^{-3}$ | $7.44 \times 10^{-4}$ | $7.21 \times 10^{-3}$ |
| Sr      | $6.01 \times 10^{-2}$ | 5.428                 | 0.847                 | 0.486                 | 0.967                 |
| Ta      | $1.55 \times 10^{-6}$ | $1.94 \times 10^{-3}$ | $2.36 \times 10^{-4}$ | $1.23 \times 10^{-4}$ | $3.21 \times 10^{-4}$ |
| Tb      | $3.06 \times 10^{-5}$ | $6.54 \times 10^{-3}$ | $8.90 \times 10^{-4}$ | $5.75 \times 10^{-4}$ | $1.03 \times 10^{-3}$ |
| Th      | $2.57 \times 10^{-4}$ | $2.90 \times 10^{-2}$ | $3.67 \times 10^{-3}$ | $1.97 \times 10^{-3}$ | $4.81 \times 10^{-3}$ |
| U       | $9.78 \times 10^{-5}$ | $1.51 \times 10^{-1}$ | $4.96 \times 10^{-3}$ | $7.31 \times 10^{-4}$ | $1.74 \times 10^{-2}$ |
| V       | $2.42 \times 10^{-4}$ | 0.191                 | 0.027                 | 0.018                 | 0.030                 |
| W       | $8.41 \times 10^{-4}$ | 0.202                 | 0.012                 | 0.007                 | 0.022                 |
| Zn      | $1.39 \times 10^{-2}$ | 729.39                | 40.84                 | 0.16                  | 99.27                 |
| Zr      | $2.28 \times 10^{-2}$ | 7.14                  | 1.04                  | 0.80                  | 1.03                  |

**Table 3.** Elements with Pearson correlation coefficients >0.7 determined for the respective seasons.

| Warm Season |    |    |    |    |    | Cold Season |    |    |    |    |    |    |
|-------------|----|----|----|----|----|-------------|----|----|----|----|----|----|
| <b>As</b>   | Cl | Cr | I  | Mg |    | <b>As</b>   | La | Sm | Sr | U  |    |    |
| <b>Ba</b>   | Zn |    |    |    |    | <b>Ba</b>   | Ce | Rb | Sc | Sm | Ta | U  |
| <b>Br</b>   | Fe | La | Mn | Sm | Th | <b>Br</b>   | I  |    |    |    |    |    |
| <b>Ca</b>   | K  |    |    |    |    | <b>Ce</b>   | Rb | Sc | Ta | Th | U  | Zr |
| <b>Ce</b>   | K  | Rb | Th |    |    | <b>Fe</b>   | Sc |    |    |    |    |    |
| <b>Cl</b>   | Cr | I  | Mg |    |    | <b>I</b>    | Sb | Se |    |    |    |    |
| <b>Cr</b>   | I  | Mg |    |    |    | <b>K</b>    | Na |    |    |    |    |    |
| <b>Fe</b>   | Sm | Th |    |    |    | <b>La</b>   | Sr |    |    |    |    |    |
| <b>Hf</b>   | Si |    |    |    |    | <b>Rb</b>   | Sc | Ta | U  |    |    |    |
| <b>I</b>    | Mg |    |    |    |    | <b>Sb</b>   | Se |    |    |    |    |    |
| <b>La</b>   | Sm | Th |    |    |    | <b>Sc</b>   | Ta |    |    |    |    |    |
| <b>Rb</b>   | Sm |    |    |    |    | <b>Sm</b>   | U  |    |    |    |    |    |
| <b>Sm</b>   | Th |    |    |    |    | <b>Ta</b>   | U  |    |    |    |    |    |
| <b>Ta</b>   | V  |    |    |    |    |             |    |    |    |    |    |    |

The element content of coal combustion products, or more precisely, fly ash plays an important role in this study for the determination of pollution origin mainly during the cold season. The distribution of elements during this process is well described in many works [56,58–60], and numerous factors need to be taken into account. First are the element content and its bonding in coal, as well as boiling points of elements and their compounds (in connection to a combustion temperature). Other important factors affecting the resulting emissions are also the type of furnace, rated capacity, combustion temperature, exposure time, the type of separator and its operating temperature, physicochemical reactions with other substances (additives, sulphur or halogens) and others. Depending on these conditions, different elemental compositions of fly ash emission are described in the literature [56,61–64]. The elements presented in bituminous coal fly ash in the majority of information sources are As, Cd, Se, Pb and Hg; other elements vary. Thus, named elements can be considered as strong markers of this process. Regarding the limitations of NAA mentioned above, other less common elements also need to be investigated. Consequently, while determining the main sources of pollution depending on weaker element markers, the element composition of emissions pertaining to particular sources in the region was taken into consideration [52,57]. Thus, a presence or absence of an element can indicate or exclude an origin in a certain source.

In the warm season, Fe was strongly correlated with Br, Sm and Th, while in winter, it was correlated only with Sc. Considering the direction where the highest concentrations of these elements originated (E, NE), it can be assumed that their occurrence is associated with the primary metallurgy [52,53]. Cr correlated with As, I and Mg in the warm season, while in the winter samples, no significant correlation was found. The highest concentrations of these elements in the warm season came from the west direction, suggesting the relation with a steel and iron production [54,65,66] as a relatively high concentration of Br and I was found also in a local coking plant emission [52]. For more correlations, see Table 3. It should be noted that the Rare Earth Element (REE) levels were in good correlation, which is important for both evaluating the data quality and understanding the mass transport events [67,68].

Special attention was paid to the samples with the PM<sub>10</sub> peak concentrations above those mentioned. The sample collected in August 2018 from the west sector was characterized by high concentrations of Cr, Mg and I (the highest of all the set) and relatively high concentrations of Mn and Co. Cr and Co are important solutes for steel alloying in order to obtain special properties of steel; both Cr and Mg form important refractories used as lining in metallurgical facilities [65,69]. Moreover, Mg (with Ca) constitutes a base additive used in almost every step of the steel-making process from agglomeration and blast furnaces (dolomitic limestone, dolomite) to final steel-making (magnesite). Mn is a common element in austenitic steels produced in local steelworks [52,54,65,69]. The presence of iodine can

be also connected with steel alloying as it is used for the production of certain transition metals, among them Co, Cr or Ti. Another possible source is coking [52]. Considering all these facts, the steelworks west of the sampling site are the most likely origin of the peak PM<sub>10</sub> concentration (see Figure 1 above).

The elemental composition of the south sample in February 2019 was characterized by high concentrations of Ca, Se and V (the highest of all the set) and relatively high concentrations of I and Sb. The high concentration of Ca is, in all probability, connected with a cement plant [52,70–72], and regarding the meteorological conditions discussed above, this peak concentration most likely originated from the cement plant quite far (about 50 km) to the southwest of the sampling tower. This hypothesis can be confirmed by the fact that, in this factory, alternative fuels based on waste and tar are used during the process of clinker firing besides coal, explaining the high concentrations of the other elements determined.

The two samples collected during the smog events significantly differed in their elemental composition. The PM<sub>10</sub> sampled in November 2018 was characterized by high concentrations of Ba, Ce, Fe, Hf, Rb, Sc, Ta, Th, U and Zr (the highest of all the set), while the sample in March 2019 by high concentrations of Si, Sr, Zn and Eu. The elemental composition of the first sample indicates two sources of pollution: coal burning and metallurgy [28,52,54,57]. These high concentrations were sampled during steady airflow from the NE, E and SE directions, suggesting the origin of the pollution in the steel plant southeast to the sampling site (see Figure 1 above) together with residential coal burning. The origin of the pollution in the case of the second inversion situation is not as clear; nevertheless, the modelled airflow points to the Polish borderland (see Figure 10) [52,54,65,69].

### 3.3. Principal Component Analysis (PCA)

The samples were investigated using a PCA (see Section 2.4) to understand the variability of the element composition and thus also the pollution origin. The results of PCA performed on the untransformed dataset with the variables *season* and *sector* taken as supplementary qualitative variables indicate that the factor *season* separates the plane and the individual measurements distinctively. This separation of the plane was confirmed by the Wilks test ( $p$ -value of  $9.108346 \times 10^{-11}$ ). Similar separation also occurs when PCA is performed on the whole dataset with the clr-transformed concentration data ( $p$ -value of  $5.219250 \times 10^{-8}$ ), only it is realized alongside the second dimension. Thus, PCA results confirm that the season is a determining factor both for the elemental composition of the entirety of the measurements and for the directionality of the elements expressed as the change in the sectors with similar analysed concentrations. For more details, see Sections 3.3.1 and 3.3.2. According to the analysis (chi-squared goodness-of-fit test), the elements varying the most depending on the season are Sr ( $p < 0.001$ ), Cl ( $p < 0.001$ ), Th ( $p < 0.001$ ), Na ( $p = 0.001$ ), Zn ( $p = 0.01$ ), Cs ( $p = 0.015$ ), Rb ( $p = 0.02$ ) and Co ( $p = 0.04$ ) with higher concentrations in the cold season and Mg ( $p < 0.001$ ), Hf ( $p < 0.001$ ), Sm ( $p < 0.001$ ) and Ba ( $p = 0.015$ ) in the warm season.

#### 3.3.1. PCA of The Warm Season Measurements

According to the PCA results, the first two dimensions express over 81% of the dataset inertia, meaning that the first factor plane represents a major part of the total variability and that no other dimensions need to be considered. Moreover, the first axis itself represents almost 75% of the data; hence, it can be concluded that only this axis carries real information. The variability explained by this axis alone exceeds the reference value of 10.26%; this value is equal to 0.95-quantile of inertia percentages derived from the simulation of 10,000 data tables of equivalent size (normal distribution). The percentages of explained variance of the first five axes were 74.93, 6.52, 4.74, 2.46 and 2.1, respectively. A visualization of the PCA results of the warm season data is presented in Figure 11.

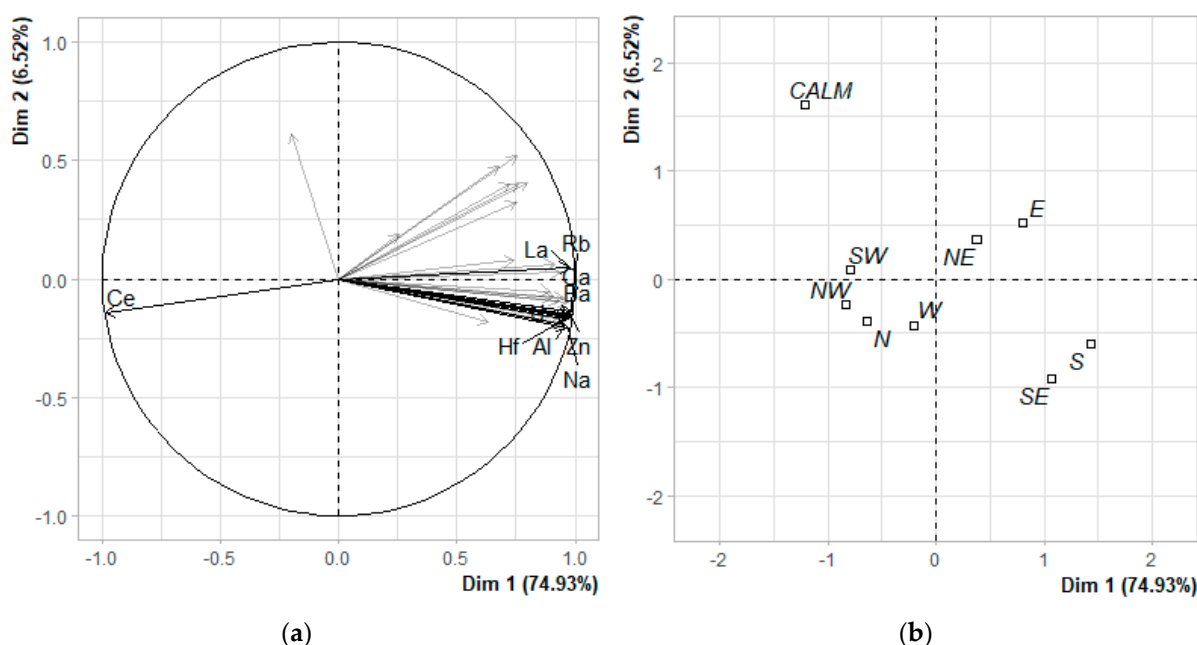


**Figure 11.** The warm season PCA results for the first two dimensions; (a) correlation circle of clr-transformed elemental concentrations; 10 most contributing variables are presented; (b) qualitative factor map of the sectors.

The elements most positively correlated with this dimension were Ba, Zn, Ca, Rb, La, Sm, Na, Hf and Al (Pearson correlation coefficient of 0.98, 0.98, 0.98, 0.98, 0.98, 0.98, 0.97, 0.97 and 0.96, respectively), while Ce was negatively correlated (Pearson correlation coefficient of  $-0.98$ ). Thus, can be assumed that these elements describe this dimension well. Figure 8b shows that the sectors (from where the particulate matter was sampled) are divided alongside this axis mostly to the east and south group on its right and west and north group on its left. The calm has a high score on this axis, while having a high score also on the second axis.

### 3.3.2. PCA of the Cold Season Measurements

In the case of the cold season measurements, the PCA results show that the first dimensions express over 66% of the dataset inertia, meaning that while the first-factor plane represents a significant part of the total variability. The variability explained by this plane is higher than the reference value of 18.75%, and the increase in explained inertia for the second axis is also higher than the reference value for this axis (8.61%); hence, both dimensions carry real information. The percentages of explained variance of the first five axes were 54.87, 11.67, 7.2, 5.8 and 3.3, respectively. A visualization of the PCA results of the cold season data is presented in Figure 12.

The elements most positively correlated with the first dimension are Ca, Al, Sr, Ba, Zn, Rb, Na, Hf and Th (Pearson correlation coefficient of 0.98, 0.98, 0.97, 0.97, 0.96, 0.95, 0.93, 0.92 and 0.84, respectively), while concentrations of Ce are, once again, correlated negatively with this dimension (Pearson correlation coefficient of  $-0.95$ ). As and Sm are the elements most positively correlated with the second dimension (Pearson correlation coefficients of 0.88 and 0.75, respectively). Figure 9b shows that the sectors are divided alongside these axes in a different manner than in the case of the warm season. Samples from the southeast, south, and southwest directions form a cluster with calm on the right of the first axis and the northwest, west, east and northeast located on its left. The inversion event (INV) measurements simultaneously have a high positive score on the first and high negative scores on the second axis.

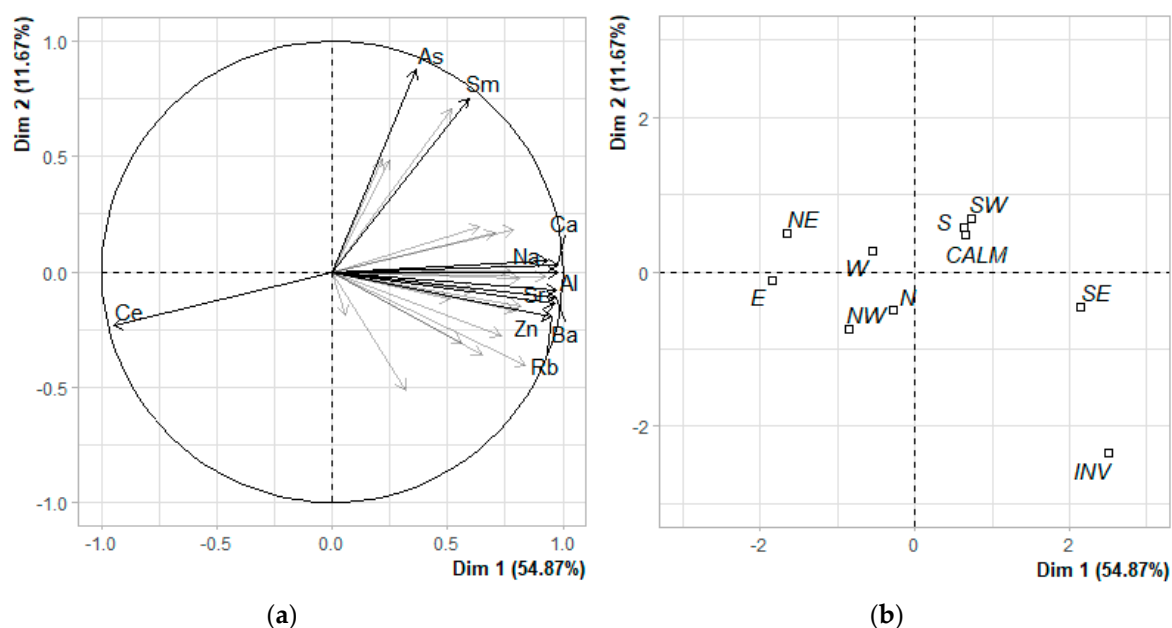


**Figure 12.** The cold season–PCA results for the first two dimensions; (a) correlation circle of clr-transformed elemental concentrations; 10 most contributing variables are presented; (b) qualitative factor map of the sectors.

#### 4. Discussion

Within the study, the elemental composition of sampled  $PM_{10}$  was determined with NAA, and the origin of the pollution was interpreted using specific pollutants as markers of pollution sources, multivariate statistics and meteorological models. More commonly, the pollution origin is investigated by means of receptor modelling [25,28,71,73,74]. However, specifics of the dataset concerned (long sampling period, small number of samples within each sector), an irregular time resolution of samples and a questionable construction of uncertainty matrix (different weights of respective samples) make this method inappropriate.

Despite the limitations of the methods used, the study confirmed that the region has specific types of pollution sources, including two metallurgical complexes (west and southeast to the sampling site), which, in specific meteorological conditions, increase the pollution load in the region and contribute to the pollution transfer in the higher atmospheric levels. However, in certain situations, this transfer is not detected by the ground pollution monitoring stations (in comparison to [9]). This corroborates locating the sampling device at 90 m AGL. By sampling in such height, the contribution of the local sources (residential emission, transport, constructions, autumnal waste biomass burning and others) [28,75] is excluded from the sampling, and the pollution transfer within the region can be more properly investigated.

The other specific type of pollution in the region is the pollution connected to the trans-boundary transfer coming from Poland during the winter season originating from coal burning in domestic boilers. In the cold part of the year, the  $PM_{10}$  concentrations originating in the Polish borderland (the north, northeast and east direction) increased by almost 50%, despite the prevailing wind in this season blowing in the opposite direction. This fact has already been stated in many previous studies [3,21,26,27,29] and confirms once again the importance of the cross-border PM pollution in this region, emphasizing that it is not just a problem of directly adjacent areas but of the region as a whole.

For the determination of elemental content in the samples, neutron activation analysis was applied, and a wide spectrum of elements was analysed. This, on the one hand, brought specific limitations, but on the other hand, helped to identify the origin of element concentrations in samples using data on less commonly determined elements. Though it

should be noted that NAA does not provide information on important elements such as Cd, Cu, Hg or Pb, the obtained information is, in the majority of cases, sufficient to identify the pollution source.

To collect more data on the pollution transfer in the region during meteorologically different years and to render the assessment more precise, the monitoring on the tower continues. In addition to the sampling device used in this study, the PM continual monitoring is now operated both on the top of the tower and on the ground level.

## 5. Conclusions

A specially designed high-volume sampler (SAM Hi 30 AUTO WIND) was used to collect PM<sub>10</sub> samples depending on airflow conditions. The sampler was located on the top of a former mining tower in 90 m AGL. This allowed the elimination of the influence of local sources and investigation of the regional pollution transport. The sampled particulate matter was analysed using the neutron activation analysis, which provided information on the content of 34 elements. This information—together with the PM<sub>10</sub> concentrations and meteorological data (measured and modelled)—was used to characterize the pollution origin in the region. A significant difference in the element composition was observed: elemental concentrations were dependent on both the season and the sampling direction. Contribution of three industrial sources, two ironworks (in the west and in the southeast) and a cement plant (southwest from the sampling site) was identified, showing that—though not detected by ground air pollution monitoring—these sources have a significant impact on the pollution transfer in the region. The measurements also confirmed that the PM<sub>10</sub> cross-border pollution inflow from Poland plays a crucial role during the winter season and contributes significantly to the air pollution in the whole studied region.

Currently, the air quality management and decision-making in the region are performed just on a local level without considering the cross-border impacts. However, to assure that the air quality meets the air pollution limit values, international cooperation and the legitimacy of the joint interregional approach to the air quality management is imperative, as proven herein [9].

**Supplementary Materials:** The following are available online at <https://www.mdpi.com/2073-4433/12/1/29/s1>, Figure S1: The element concentration roses for the warm season ( $\text{ng}\cdot\text{m}^{-3}$ ), Figure S2: The element concentration roses for the cold season ( $\text{ng}\cdot\text{m}^{-3}$ ), Figure S3: The average element concentration according to the wind direction for the warm (plain) and cold seasons (shaded) ( $\text{ng}\cdot\text{m}^{-3}$ ), Figure S4: The average element concentration according to the wind direction for the cold season (plain) and smog events (shaded) ( $\text{ng}\cdot\text{m}^{-3}$ ), Table S1: Synoptic table (minimum, maximum value, mean, median and standard deviation) of elements concentration ( $\text{ng}\cdot\text{m}^{-3}$ ) determined in PM<sub>10</sub> using INAA. Table S2: Synoptic table (minimum, maximum value, mean and standard deviation) of PM<sub>10</sub> concentration ( $\mu\text{g}\cdot\text{m}^{-3}$ ).

**Author Contributions:** Conceptualization, I.P.; validation, I.P., D.H. and O.M.; formal analysis, O.M.; investigation, D.H. and I.P.; data curation, O.M. and D.H.; resources (performing NAA), K.N.V., L.P.S. and M.S.S.; writing—original draft preparation, I.P. and O.M.; writing—review and editing, I.P., O.M. and D.H.; visualization, D.H. and O.M.; supervision, I.P.; project administration, I.P. All authors have read and agreed to the published version of the manuscript.

**Funding:** The research was carried out within the project “AIR BORDER—Joint Czech–Polish Measurements of Cross-border Transmission of Air Pollutants” funded by the cooperation programme Interreg V-A in the Czech Republic and Poland co-financed by European Regional Development Fund (ERDF), grant number CZ.11.4.120/0.0/0.0/15\_006/0000118. The NAA performance was funded within the “3+3 Project” for the cooperation with the Joint Institute for Nuclear Research by Joint Institute for Nuclear Research, grant number 29/209, theme No. 03-4-1128-2017/2019. The work was supported by European Regional Development Fund/European Social Fund—New Composite Materials for Environmental Applications (No. CZ.02.1.01/0.0/0.0/17\_048/0007399).

**Data Availability Statement:** The data presented in this study are available in article and supplementary materials.

**Acknowledgments:** We would like to thank Petr Jančík, the coordinator of the AIR BORDER project (VSB—Technical University of Ostrava, Ostrava, Czech Republic); Marina V. Frontasyeva (Joint Institute of Nuclear Research, Dubna, Russia), the coordinator of the 3 + 3 project on the side of Joint Institute of Nuclear research; Sergey S. Pavlov (Joint Institute of Nuclear Research, Dubna, Russia) for the methodological leadership of the team performing the Neutron Activation Analyses and analysis results processing. Further, we would like to thank Petra Šutarová (VSB—Technical University of Ostrava, Ostrava, Czech Republic) for financial management and administrative support of the projects. The authors also gratefully acknowledge the NOAA Air Resources Laboratory (ARL) for the provision of the HYSPLIT transport and dispersion model and/or READY website (<https://www.ready.noaa.gov>) used in this publication.

**Conflicts of Interest:** The authors declare no conflict of interest. The funders had no role in the design of the study; in the collection, analyses, or interpretation of data; in the writing of the manuscript, or in the decision to publish the results.

## References

1. Klusáček, P. Downsizing of bituminous coal mining and the restructuring of steel works and heavy machine engineering in the Ostrava region. *Morav. Geogr. Rep.* **2005**, *13*, 3–11.
2. Cabala, J.; Cmiel, S.R.; Idziak, A.F. Environmental impact of mining activity in the upper silesian coal basin. *Geol. Belg.* **2004**, *7*, 225–229.
3. Blažek, Z.; Černíkovský, L.; Krejčí, B.; Osrodka, L.; Volna, V.; Wojtylak, M. *Vliv Meteorologických Podmínek Na Kvalitu Ovzduší V Přeshraniční Oblasti Slezska A Moravy—Wpływ Warunków Meteorologicznych Na Jakość Powietrza W Obszarze Przygranicznym Śląska I Moraw [The Influence of Meteorological Conditions on Air Quality in the Border Region of Silesia and Moravia]*, 1st ed.; Český Hydrometeorologický Ústav: Prague, Czech Republic; Instytut Meteorologii i Gospodarki Wodnej, Państwowy Instytut Badawczy: Warsaw, Poland, 2013; ISBN 978-80-87577-15-8. (In Czech/Polish)
4. Hůnová, I. Ambient air quality in the Czech Republic: Past and present. *Atmosphere* **2020**, *11*, 214. [[CrossRef](#)]
5. Kuskova, P.; Gingrich, S.; Krausmann, F. Long term changes in social metabolism and land use in Czechoslovakia, 1830–2000: An energy transition under changing political regimes. *Ecol. Econ.* **2008**, *68*, 394–407. [[CrossRef](#)]
6. Ďurčanská, D.; Drličák, M.; Jandačka, D.; Bitta, J.; Bizek, V.; Foldynová, I.; Hladký, D.; Hrušková, A.; Hruška, L.; Chovanec, P.; et al. *Riadenie Kvality Ovzdušia [Air Quality Management]*; Žilinská Univerzita V Žiline—EDIS—Vydavateľské Centrum ŽU: Žilina, Slovakia, 2020; ISBN 978-80-554-1658-8. (In Czech, Slovaque/Polish)
7. Główny Urząd Statystyczny. *Zużycie Energii w Gospodarstwach Domowych w 2018 Roku [Energy Consumption in Households in 2018]*; Główny Urząd Statystyczny—Statistics Poland: Warsaw, Poland, 2019; Volume 2019.
8. European Environment Agency. *Air Quality in Europe—2019 Report*; Number 10; European Environment Agency: Luxembourg, 2019; ISBN 978-92-9480-088-6.
9. Czech Hydrometeorological Institute. Summary Tabular Survey. 2018. Available online: [http://portal.chmi.cz/files/portal/docs/uoco/isko/tab\\_roc/2018\\_enh/index\\_GB.html](http://portal.chmi.cz/files/portal/docs/uoco/isko/tab_roc/2018_enh/index_GB.html) (accessed on 14 April 2020).
10. European Council. *Directive 2008/50/EC of the European Parliament and of the Council of 21 May 2008 on Ambient Air Quality and Cleaner Air for Europe*; OJEC L 152; European Council: Brussel, Belgium, 2008.
11. World Health Organization. *Air Quality Guidelines: Global Update 2005: Particulate Matter, Ozone, Nitrogen Dioxide, and Sulfur Dioxide*; World Health Organization: Copenhagen, Denmark, 2006; ISBN 978-92-890-2192-0.
12. WHO Regional Office for Europe. *Evolution of WHO Air Quality Guidelines Past, Present and Future*; WHO: Copenhagen, Denmark, 2017; ISBN 978-92-890-5230-6.
13. Jiřík, V.; Hermanová, B.; Dalecká, A.; Pavlíková, I.; Bitta, J.; Jančík, P.; Ošrodka, L.; Krajny, E.; Ślądcezek, F.; Siemiątkowski, G.; et al. *Wpływ Zanieczyszczenia Powietrza Na Zdrowie Ludności W Obszarze Polsko-Czeskiego Pogranicza. Dopad Znečištění Ovzduší Na Zdravotní Stav Obyvatelstva V Česko-Polském Přihraničí [Impact of Air Pollution on the Health Status of the Population in the Czech-Polish Border]*; Sieć Badawcza Łukasiewicz—Instytut Ceramiki i Materiałów Budowlanych Instytut Meteorologii i Gospodarki Wodnej—Państwowy Instytut Badawczy Ostravská Univerzita Vysoká Škola Báňská—Technická Univerzita Ostrava: Ostrava, Czech Republic, 2020; ISBN 978-80-248-4406-0. (In Czech/Polish).
14. World Health Organization. *Ambient Air Pollution: A Global Assessment of Exposure and Burden of Disease*; WHO: Geneva, Switzerland, 2016; ISBN 978-92-4-151135-3.
15. World Health Organization. *Review of Evidence on Health Aspects of Air Pollution—REVIHAAP Project*; Technical Report; World Health Organization: Copenhagen, Denmark, 2013.
16. Jiřík, V.; Machaczka, O.; Miturová, H.; Tomášek, I.; Šlachťová, H.; Janoutová, J.; Velická, H.; Janout, V. Air pollution and potential health risk in Ostrava region—A review. *Cent. Eur. J. Public Health* **2016**, *24*, S4–S17. [[CrossRef](#)] [[PubMed](#)]
17. Cohen, A.; Samet, J.M.; Straif, K. (Eds.) *Air Pollution and Cancer*; International Agency for Research on Cancer: Lyon, France, 2013; Volume 161, ISBN 978-92-832-2161-6.
18. The Czech Statistical Office. *Czech Demographic Handbook—2018*. Available online: <https://www.czso.cz/csu/czso/czech-demographic-handbook> (accessed on 29 June 2020).

19. Pinto, J.P.; Stevens, R.K.; Willis, R.D.; Kellogg, R.; Mamane, Y.; Novak, J.; Šantroch, J.; Beneš, I.; Lenicek, J.; Bureš, V. Czech air quality monitoring and receptor modeling study. *Environ. Sci. Technol.* **1998**, *32*, 843–854. [CrossRef]
20. Čížová, H. Projekt Slezsko/Silesia [The Silesia Project]. *Zprav. Minist. Životn. Prostředí ČR* **1994**, *3*, 6–7. (In Czech)
21. Jančík, P.; Pavlíková, I.; Bitta, J.; Hladký, D. *Atlas Ostravského Ovzduší*; Vysoká Škola Báňská—Technická Univerzita Ostrava: Ostrava, Czech Republic, 2013; ISBN 978-80-248-3006-3.
22. Air TRITIA—Uniform Approach to the Air Pollution Management System for Functional Urban Areas in TRITIA Region. Available online: <http://www.interreg-central.eu/Content.Node/AIR-TRITIA.html> (accessed on 17 April 2020).
23. Mikuška, P.; Křůmal, K.; Večeřa, Z. Characterization of organic compounds in the PM<sub>2.5</sub> aerosols in winter in an industrial urban area. *Atmos. Environ.* **2015**, *105*, 97–108. [CrossRef]
24. Pokorná, P.; Hovorka, J.; Klán, M.; Hopke, P.K. Source apportionment of size resolved particulate matter at a European air pollution hot spot. *Sci. Total Environ.* **2015**, *502*, 172–183. [CrossRef]
25. Leoni, C.; Pokorná, P.; Hovorka, J.; Masiol, M.; Topinka, J.; Zhao, Y.; Křůmal, K.; Cliff, S.; Mikuška, P.; Hopke, P.K. Source apportionment of aerosol particles at a European Air Pollution hot spot using particle number size distributions and chemical composition. *Environ. Pollut. Barking Essex 1987* **2018**, *234*, 145–154. [CrossRef]
26. Aglomerace Ostrava/Karviná/Frýdek-Místek. *Český Hydrometeorologický Ústav Aktualizace Programů Zlepšování Kvality Ovzduší 2020+*; Ministerstvo Životního Prostředí ČR: Prague, Czech Republic, 2019.
27. Seibert, R.; Nikolova, I.; Volná, V.; Krejčí, B.; Hladký, D. Air pollution sources' contribution to PM<sub>2.5</sub> concentration in the northeastern part of the Czech Republic. *Atmosphere* **2020**, *11*, 522. [CrossRef]
28. Czech Hydrometeorological Institute. Summary Tabular Survey. 2015. Available online: [http://portal.chmi.cz/files/portal/docs/uoco/isko/tab\\_roc/2015\\_enh/index\\_GB.html](http://portal.chmi.cz/files/portal/docs/uoco/isko/tab_roc/2015_enh/index_GB.html) (accessed on 23 April 2020).
29. Černíkovský, L.; Krejčí, B.; Blažek, Z.; Volná, V. Transboundary air-pollution transport in the Czech-Polish border region between the cities of Ostrava and Katowice. *Cent. Eur. J. Public Health* **2016**, *24*, S45–S50. [CrossRef] [PubMed]
30. Volná, V.; Hladký, D. Detailed assessment of the effects of meteorological conditions on PM<sub>10</sub> concentrations in the northeastern part of the Czech Republic. *Atmosphere* **2020**, *11*, 497. [CrossRef]
31. U.S. Environmental Protection Agency. *Compendium of Methods for the Determination of Inorganic Compounds in Ambient Air: Sampling of Ambient Air for Total Suspended Particulate Matter (Spm) and PM<sub>10</sub> Using High Volume (Hv) Sampler*; U.S. Environmental Protection Agency: Cincinnati, OH, USA, 1999.
32. Krug, J.D.; Dart, A.; Witherspoon, C.L.; Gilberry, J.; Malloy, Q.; Kaushik, S.; Vanderpool, R.W. Revisiting the size selective performance of EPA's high-volume total suspended particulate matter (Hi-Vol TSP) sampler. *Aerosol. Sci. Technol.* **2017**, *51*, 868–878. [CrossRef]
33. European Committee for Standardization. *Ambient Air. Standard Gravimetric Measurement Method for the Determination of the PM<sub>10</sub> or PM<sub>2.5</sub> Mass Concentration of Suspended Particulate Matter*; EN 12341:2014; NSAI: Dublin, Ireland, 2014.
34. U.S. Environmental Protection Agency. *Office of Air and Radiation. Office of Air Quality Planning and Standards Meteorological Monitoring Guidance for Regulatory Modeling Applications*; U.S. Environmental Protection Agency: Cincinnati, OH, USA, 2000.
35. Frontasyeva, M.V.; Pavlov, S.S.; Shvetsov, V.N. NAA for applied investigations at FLNP JINR: Present and future. *J. Radioanal. Nucl. Chem.* **2010**, *286*, 519–524. [CrossRef]
36. Pavlov, S.; Dmitriev, A.; Frontasyeva, M. Automation system for neutron activation analysis at the reactor IBR-2, Frank Laboratory of Neutron Physics, Joint Institute for Nuclear Research, Dubna, Russia. *J. Radioanal. Nucl. Chem.* **2016**, *309*, 27–38. [CrossRef]
37. Dray, S.; Josse, J. Principal component analysis with missing values: A comparative survey of methods. *Plant. Ecol.* **2015**, *216*, 657–667. [CrossRef]
38. Hron, K.; Templ, M.; Filzmoser, P. Imputation of missing values for compositional data using classical and robust methods. *Comput. Stat. Data Anal.* **2010**, *54*, 3095–3107. [CrossRef]
39. U.S. Environmental Protection Agency. *Compendium Method IO-3.7—Determination of Metals in Ambient Particulate Matter Using Neutron Activation Analysis (NAA) Gamma Spectrometry*; U.S. Environmental Protection Agency: Cincinnati, OH, USA, 1999.
40. The R Foundation. Available online: <https://www.r-project.org/> (accessed on 25 December 2020).
41. Lê, S.; Josse, J.; Husson, F. FactoMineR: An R package for multivariate analysis. *J. Stat. Softw.* **2008**, *25*. [CrossRef]
42. Husson, F.; Josse, J.; Le, S.; Mazet, J. Package 'FactoMineR'—Multivariate Exploratory Data Analysis and Data Mining. Available online: <https://cran.r-project.org/web/packages/FactoMineR/index.html> (accessed on 25 December 2020).
43. Carslaw, D.; Ropkins, K. Package 'Openair'—Tools for the Analysis of Air Pollution Data. Available online: <https://davidcarslaw.github.io/openair/> (accessed on 25 December 2020).
44. Wickham, H.; Chang, W.; Henry, L.; Pedersen, T.L.; Takahashi, K.; Wilke, C.; Woo, K.; Yutani, H.; Dunnington, D. Package 'Ggplot2'—Create Elegant Data Visualisations Using the Grammar of Graphics. Available online: <https://ggplot2.tidyverse.org/reference/ggplot2-package.html> (accessed on 25 December 2020).
45. Pawłowsky-Glahn, V.; Buccianti, A. (Eds.) *Compositional Data Analysis: Theory and Applications*; Wiley: Chichester, UK, 2011; ISBN 978-0-470-71135-4.
46. Aitchison, J. *The Statistical Analysis of Compositional Data*; Blackburn Press: Caldwell, NJ, USA, 2003; ISBN 978-1-930665-78-1.
47. Ventusky. Available online: <https://www.ventusky.com/?p=49.8;18.5;5&l=wind-10m> (accessed on 25 December 2020).
48. University of Wyoming Atmospheric Soundings. Available online: <http://weather.uwyo.edu/upperair/sounding.html> (accessed on 2 December 2020).

49. Stein, A.F.; Draxler, R.R.; Rolph, G.D.; Stunder, B.J.B.; Cohen, M.D.; Ngan, F. NOAA's HYSPLIT atmospheric transport and dispersion modeling system. *Bull. Am. Meteorol. Soc.* **2015**, *96*, 2059–2077. [[CrossRef](#)]
50. Rolph, G.; Stein, A.; Stunder, B. Real-time Environmental Applications and Display System: READY. *Environ. Model. Softw.* **2017**, *95*, 210–228. [[CrossRef](#)]
51. Bureš, V.; Velíšek, J. *Omezování Emisí Znečišťujících Látek Do Ovzduší: II. Etapa, Rok 2005 [Reduction of Emissions of Pollutants into the Air: 2nd Stage, Year 2005]*; TESO: Prague, Czech Republic, 2005. (In Czech)
52. Alleman, L.Y.; Lamaison, L.; Perdrix, E.; Robache, A.; Galloo, J.-C. PM10 metal concentrations and source identification using positive matrix factorization and wind sectoring in a French industrial zone. *Atmos. Res.* **2010**, *96*, 612–625. [[CrossRef](#)]
53. Sylvestre, A.; Mizzi, A.; Mathiot, S.; Masson, F.; Jaffrezo, J.L.; Dron, J.; Mesbah, B.; Wortham, H.; Marchand, N. Comprehensive chemical characterization of industrial PM2.5 from steel industry activities. *Atmos. Environ.* **2017**, *152*, 180–190. [[CrossRef](#)]
54. Hurst, R.W.; Davis, T.E.; Elseewi, A.A. Strontium isotopes as tracers of coal combustion residue in the environment. *Eng. Geol.* **1991**, *30*, 59–77. [[CrossRef](#)]
55. Ritz, M.; Bartoňová, L.; Klika, Z. Emissions of Heavy Metals and Polyaromatic Hydrocarbons During Coal Combustion in Industrial and Small Scale Furnaces. *Sborník Věd. Pr. Vysoké Šk. Báňské Tech. Univerzity Ostrava* **2003**, *49*, 69–82.
56. Horák, J.; Kuboňová, L.; Bajer, S.; Dej, M.; Hopan, F.; Krpec, K.; Ochodek, T. Composition of ashes from the combustion of solid fuels and municipal waste in households. *J. Environ. Manag.* **2019**, *248*, 109269. [[CrossRef](#)] [[PubMed](#)]
57. Ramme, B.W.; Tharaniyil, M.P. *Coal Combustion Products Utilization Handbook*, 3rd ed.; We Energies: Milwaukee, WI, USA, 2013.
58. Robl, T.L.; Oberlink, A.; Jones, R. (Eds.) *Coal Combustion Products (CCPs): Characteristics, Utilization and Beneficiation*; Woodhead Woodhead Publishing: Duxford, UK; Cambridge, MA, USA, 2017; ISBN 978-0-08-100945-1.
59. Juda-Rezler, K.; Kowalczyk, D. Size distribution and trace elements contents of coal fly ash from pulverized boilers. *Pol. J. Environ. Stud.* **2013**, *22*, 25–40.
60. Wang, J.; Yang, Z.; Qin, S.; Panchal, B.; Sun, Y.; Niu, H. Distribution characteristics and migration patterns of hazardous trace elements in coal combustion products of power plants. *Fuel* **2019**, *258*, 116062. [[CrossRef](#)]
61. Bray, C.D.; Strum, M.; Simon, H.; Riddick, L.; Kosusko, M.; Menetrez, M.; Hays, M.D.; Rao, V. An assessment of important SPECIATE profiles in the EPA emissions modeling platform and current data gaps. *Atmos. Environ.* **2019**, *207*, 93–104. [[CrossRef](#)]
62. Pernigotti, D.; Belis, C.A.; Spanò, L. SPECIEUROPE: The European data base for PM source profiles. *Atmos. Pollut. Res.* **2016**, *7*, 307–314. [[CrossRef](#)]
63. Simon, H.; Beck, L.; Bhave, P.V.; Divita, F.; Hsu, Y.; Luecken, D.; Mobley, J.D.; Pouliot, G.A.; Reff, A.; Sarwar, G.; et al. The development and uses of EPA's SPECIATE database. *Atmos. Pollut. Res.* **2010**, *1*, 196–206. [[CrossRef](#)]
64. Ghosh, A.; Chatterjee, A. *Ironmaking and Steelmaking: Theory and Practice*; Eastern Economy 3rd ed.; PHI Learning: New Delhi, India, 2010; ISBN 978-81-203-3289-8.
65. Mohiuddin, K.; Strezov, V.; Nelson, P.F.; Stelcer, E. Characterisation of trace metals in atmospheric particles in the vicinity of iron and steelmaking industries in Australia. *Atmos. Environ.* **2014**, *83*, 72–79. [[CrossRef](#)]
66. Beijer, K.; Jernelov, A. Sources, transport and transformation of metals in the environment. *Environ. Sci.* **1986**, *1*, 68.
67. Avino, P.; Capannesi, G.; Rosada, A. Heavy metal determination in atmospheric particulate matter by instrumental neutron activation analysis. *Microchem. J.* **2008**, *88*, 97–106. [[CrossRef](#)]
68. Bažan, J.; Socha, L. *Základy Teorie a Technologie Výroby Železa a Oceli: Část II—Základy Teorie a Technologie Výroby Oceli*; VŠB—Technická Univerzita Ostrava: Ostrava, Czech Republic, 2013; ISBN 978-80-248-3353-8. (In Czech)
69. Larsen, B.R.; Gilardoni, S.; Stenström, K.; Niedzialek, J.; Jimenez, J.; Belis, C.A. Sources for PM air pollution in the Po Plain, Italy: II. Probabilistic uncertainty characterization and sensitivity analysis of secondary and primary sources. *Atmos. Environ.* **2012**, *50*, 203–213. [[CrossRef](#)]
70. Samara, C.; Kouimtzi, T.; Tsitouridou, R.; Kaniyas, G.; Simeonov, V. Chemical mass balance source apportionment of PM10 in an industrialized urban area of Northern Greece. *Atmos. Environ.* **2003**, *37*, 41–54. [[CrossRef](#)]
71. Yatkin, S.; Bayram, A. Determination of major natural and anthropogenic source profiles for particulate matter and trace elements in Izmir, Turkey. *Chemosphere* **2008**, *71*, 685–696. [[CrossRef](#)]
72. Norris, G.; Duvall, R.; Brown, S.; Bai, S. *Positive Matrix Factorization (PMF) 5.0 Fundamentals and User Guide*; U.S. Environmental Protection Agency: Washington, DC, USA, 2014.
73. European Commission. *European Guide on Air Pollution Source Apportionment with Receptor Models: Revised Version 2019*; JRC Technical Reports; Publications Office of the European Union: Luxembourg, 2019.
74. Bernardoni, V.; Vecchi, R.; Valli, G.; Piazzalunga, A.; Fermo, P. PM10 source apportionment in Milan (Italy) using time-resolved data. *Sci. Total Environ.* **2011**, *409*, 4788–4795. [[CrossRef](#)]
75. Colombi, C.; Gianelle, V.; Belis, C.; Larsen, B. Determination of local source profile for soil dust, brake dust and biomass burning sources. *Chem. Eng. Trans.* **2010**, *22*, 233–238. [[CrossRef](#)]



Article

# Dispersion Characteristics of PM<sub>10</sub> Particles Identified by Numerical Simulation in the Vicinity of Roads Passing through Various Types of Urban Areas

Jiri Pospisil <sup>1,\*</sup>, Jiri Huzlik <sup>2</sup>, Roman Licbinsky <sup>2</sup> and Michal Spilacek <sup>1</sup>

<sup>1</sup> Energy Institute, Faculty of Mechanical Engineering, Brno University of Technology, 61669 Brno, Czech Republic; michal.spilacek@vutbr.cz

<sup>2</sup> Transport and Environment Department, Division of Sustainable Transport and Road Structures Diagnostics, Transport Research Centre, 63600 Brno, Czech Republic; Jiri.Huzlik@cdv.cz (J.H.); roman.licbinsky@cdv.cz (R.L.)

\* Correspondence: pospisil.j@fme.vutbr.cz

Received: 30 March 2020; Accepted: 29 April 2020; Published: 30 April 2020



**Abstract:** The dispersion of particulate matter emitted by road transport to the vicinity of roads is predominantly influenced by the character of the air velocity field. The air flow depends on factors such as the speed and direction of the blowing wind, the movement of cars, and the geometries of the buildings around a road. Numerical modeling based on the control volume method was used in this study to describe the relevant processes closely. Detailed air velocity fields were identified in the vicinity of a straight road surrounded by various patterns of built-up urban land. The evaluation of the results was generalized to exponential expressions, affecting the decrease of the mass concentration of fine particles with the increasing distance from the road. The obtained characteristics of the mass concentration fields express the impact of the building geometries and configurations on the dispersion of particulate matter into the environment. These characteristics are presented for two wind speeds, namely,  $2 \text{ m}\cdot\text{s}^{-1}$  and  $4 \text{ m}\cdot\text{s}^{-1}$ . Furthermore, the characteristics are introduced in relation to three wind directions: perpendicularly, obliquely, and in parallel to the road. The results of the numerical simulations are compared with those obtained via the in-situ measurements, for verification of the validity of the linear emission source calculation.

**Keywords:** particles; traffic; dispersion; PM<sub>10</sub>; pollution

## 1. Introduction

Urban air is significantly polluted by flue gases and fine particulates. The main sources of these pollutants constitute motor vehicle traffic and local furnaces, as well as heating systems [1]. Pollutants produced by motor vehicles are released into the atmosphere in the immediate vicinity to humans present near roads, whether outdoor or in a closed environment such as an adjacent building or a means of transport. Although air pollutant emissions generated by combustion engines have been markedly reduced in recent years, car traffic has remained the most prominent single cause of air pollution in urban centers globally, exerting a critical impact on human health [2]. Such an adverse effect partially stems from long-term persistence of the pollutants in ground-level layers of the air flowing through built-up urban areas; peak mass concentration values are commonly found in close proximity to roads and their intersections [3]. Street canyons receive only limited amounts of fresh air, and this condition progressively leads to rising local ambient concentrations and long pollutant wash-out periods in built-up urban lands. Importantly, there are also certain special scenarios to be considered, including weather with very low or zero air flow velocities. The overall negative health impact of the pollution is exacerbated by the fact that the maximum rates of human presences at

urban roads are reached during rush hours, namely, the time when the highest air pollutant mass concentrations are usually detected [4].

In this context, attention has been paid in recent years to particulate matter emissions with diameters less than 10  $\mu\text{m}$  (PM10). With the development of measurement technology and the state of knowledge, attention was gradually paid to smaller particles. Today, PM2.5 and PM1 mass concentrations are monitored in urban areas as the standard. Czech Hydrometeorological Institute (2018) reported that 61% of fine particles identified in urban areas are generated by road transport.

For descriptive purposes we can point out that combustion-generated particles result from the complex physico-chemical transformations that constitute the combustion process [5]. Such particles then shape and are carried in the flow of waste gases emitted from automobile exhaust pipes. Other instances of particulate matter include relevant products of brake, tire, and roadway abrasion and resuspension of the particulates deposited earlier. In all size categories, the mass concentration of the particles markedly decreases with increasing distance from the road [6]. The dispersion into the environment is influenced particularly by the character of the air velocity field in locations near the roadside. The actual mass concentration is then affected by, among other aspects, the particulate deposition, resuspension, and interaction with solid surfaces and vegetation. By extension, concurrently with these processes there occurs partial physical changes in the particulate matter due to collisions between and growth of the particles; on a lesser scale, the particulates also undergo chemical and photochemical transformations.

Methods suitable for modelling of pollution dispersion were discussed from the beginning [7], while, at present, the individual factors influencing the dispersion of pollutants produced by transport are of more interest. This is caused mainly by the effort to provide the most accurate information about the behavior of pollutants from transport and to more accurately estimate the population exposure in the urban environment. Simulation of traffic induced dispersion at a high resolution using the computational fluid dynamics software, Fluidity and traffic simulation software PTV Vissim was performed to demonstrate how moving vehicles can have a significant effect on street level concentration fields and how large vehicles such as buses can also cause acute high concentration events at the roadside [8]. Influences of vehicle-induced turbulences on pollutant dispersions in a street canyon was discussed as well in [9]. The street morphology relationship with air quality was described by the authors of [10] based on six irregular real-world cases selected from America, Europe, and China using computational fluid dynamic (CFD) simulations to assess the ventilations and pollutant dispersion within street canyons with a parallel approaching wind. The results showed that the street morphology characteristics, including the street width, lateral openings, and intersections, are closely related to the air flows in street canyons. Different types of intersections were assessed as well. The octagon intersections were favorable for air flowing through the lateral openings and improved the channel flows. The oblique intersections can also greatly improve the street ventilations, mainly due to the enhanced air flows through the lateral openings and the increased turbulent diffusion through the street roofs. The effect of buildings with wedge-shaped roofs surrounding urban street canyons on buoyant wind-driven pollutant plume dispersions was presented by Zhang et al. [11]. Miao et al. [12] showed that street canyons' morphology and air humidity were two of the most important factors affecting suspended particulate matter concentrations in urban street canyons. The Meso-NH model (atmospheric non hydrostatic research model) enhanced with an immersed boundary method (IBM) is a promising way to represent flow interactions with buildings (as a 3D shape of buildings) and orography in atmospheric models for urban applications [13].

This paper discusses in detail the dispersion of particles from a road into differently configured urban environments. Modeling via the control volume method (computational fluid dynamics, CFD) embodies the most suitable tool for detailed identification of an air velocity field in urban areas. This software approach enables the computation process to cover geometrically complex zones (such as built-up urban land) and to capture the effect of cars traveling along the road. The vehicles drag with them the air from the immediate vicinity, creating an air flow that moves in their driving direction,

and they generate multiple turbulent vortices that substantially influence the dispersion of particles in the region closely adjacent to the vortices' source [3]. The elevated turbulence then exerts an impact on the air flow and its interaction with solid surfaces (see Figure 1).

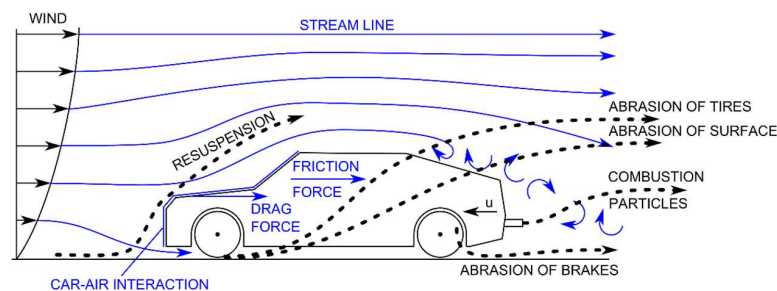


**Figure 1.** The fluxes of traffic-generated fine particulate matter.

Within the article, computational modeling is employed to monitor the dispersion of particles from a straight section of a road passing through five different types of urban environments. In each of these patterns, we conducted a parametric study evaluating the influence of wind speed and wind direction on particle dispersion in the vicinity of the road. The computed mass concentration maps were generalized into 2D-rendered relationships between the PM10 mass concentrations and their distances from the road. These results will enable a quick analytical calculation of the PM10 concentrations in urban areas geometrically close to the tested areas, because the correctness of the inclusion of a linear source of emissions in the numerical model is crucial for the subsequent realistic solution of the dispersion of pollutant particles. The linear emission source calculation will be validated with the results of in-situ measurements at close vicinity to the studied road.

## 2. Numerical Model

### 2.1. Built-Up Area Geometries

In terms of forming the mathematical models, the main criterion defining the actual choice of the areas to be modelled consisted in selecting such regions that, from the perspective of their geometries, are accurately convertible into a computational mesh, with the smallest possible amount of necessary geometrical simplifications. A major complementary criterion was embodied in the steady cruising of vehicles on the roads comprised within the areas of interest; this requirement arises from the stationary character of the developed mathematical model, where the traffic dynamics would introduce undesired inaccuracies.

The research involved converting into specific numerical models five classic types of built-up urban lands adopted from various locations within the city of Brno (CZ); collectively, these sample regions occupy an area of  $1000 \times 1000 \text{ m}^2$ . The real land patterns are substituted with a horizontal surface. The center of each model area is intersected by a straight, four-lane road carrying two-way traffic, with two lanes in each direction. Real geometry-based buildings are assumed to be present in the vicinity of the road, and their positions correspond to the real-world layout obtained through processing the ground plan view contained in the geodetic survey map of the relevant urban district. Progressively, the following numerical models were designed (for the images, see Figure 2):

- Model area #1: An intersection located in an urban center: a crossing of two roads that pass through a built-up area comprising lines of four-story houses (a concrete geometry from the central district of Brno).
- Model area #2: A road passing through a residential area with single-family houses; the 10-m-high units are positioned with a spacing of 15 m, the ground plan of each home equals  $10 \times 15 \text{ m}^2$ , six houses in a row form a regular block of buildings, there is a 15-m-wide aisle (perpendicular to

the main road) separating individual blocks of houses, and 20-m-wide service roads parallel to the main road run through the urban area every two rows of houses.

- Model area #3: A road running between small-size prefabricated houses positioned at regular intervals and having the dimensions of  $20 \times 20 \times 20 \text{ m}^2$ . The buildings are arranged into separate groups, each of which contains three closely neighboring units.
- Model area #4: A road passing through an area containing prefabricated houses configured into longitudinally oriented 15-m-high blocks that are positioned at regular intervals of 50 m and invariably exhibit the ground plan dimensions of  $17 \times 90 \text{ m}^2$ .
- Model area #5: A road in a free space: an almost ideally straight road running through an open landscape, with no barriers in the immediate vicinity. This model item is included to compare the built-up and the open-space pollutant dispersion scenarios.

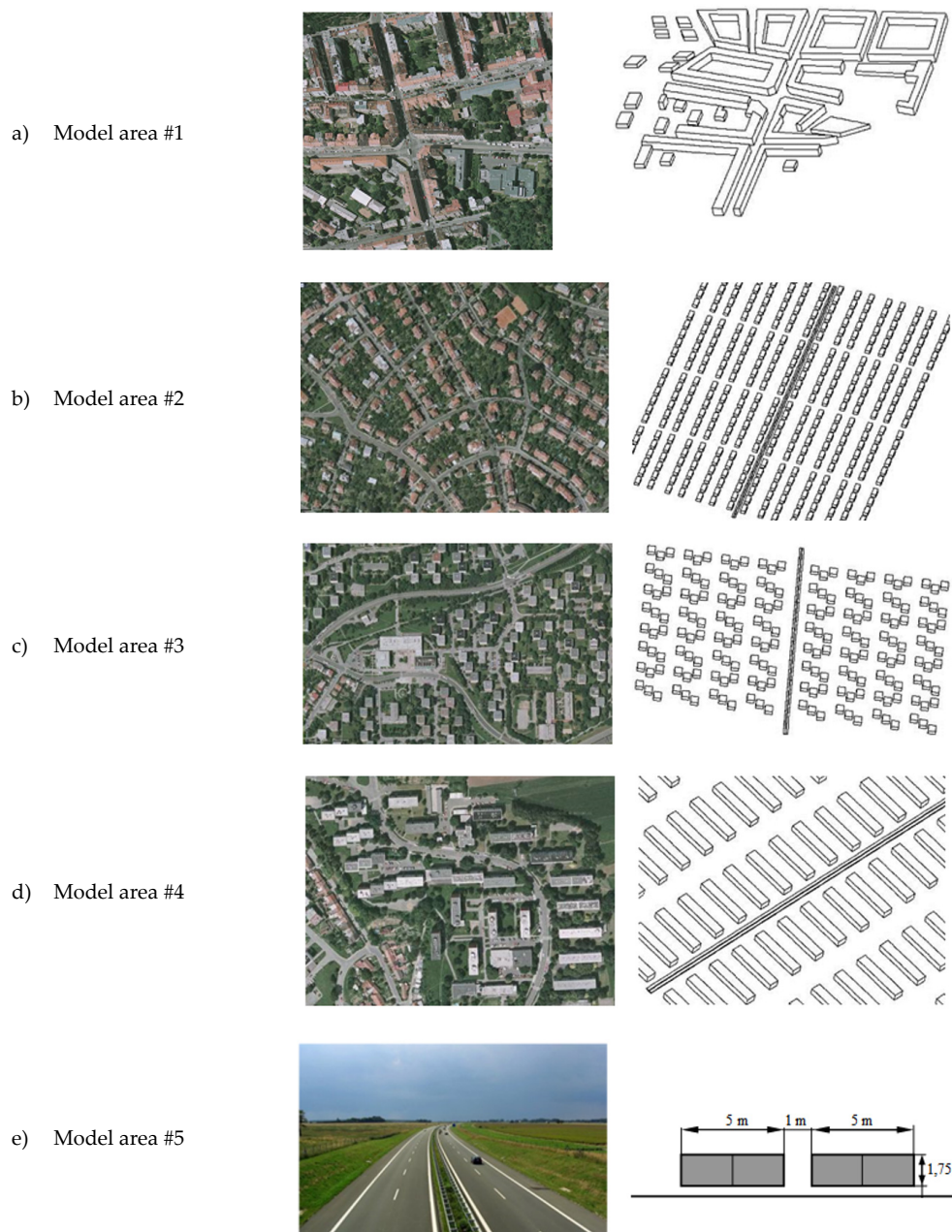


**Figure 2.** Visual representation of the model areas and the building geometries embodied in the relevant numerical models.

## 2.2. Mathematical Description and Boundary Conditions

In a step-by-step, consecutive manner, computational models were created to capture accurately the geometries of the solved model areas. The process involved detailed modeling of the buildings, roads, and their positions. The model area is filled with a computational grid of hexagonal control volumes. The solution domain includes the space above the road and all the space outside the buildings. Volume elements of approximately  $0.25 \text{ m}^3$  with the shortest element side of  $0.5 \text{ m}$  were used at the vicinity of the ground surface. The size of the volume elements filling the space between buildings is in the range of  $1 \text{ m}^3$  to  $3 \text{ m}^3$ . More abundant volume elements are used above the roofs of the buildings. Their size increases with increasing height above the buildings. The canopy layer of the atmosphere with a height of  $200 \text{ m}$  is included in the solution. Control volumes of  $20 \text{ m}^3$  are used in the highest air layer of the model.

In all cases, the straight road simulation encompassed the impact of moving cars, this being a factor that markedly influences the air flow above and on the sides of the road. To facilitate the procedure, we adopted the method proposed by the authors of [3]. The effect of the vehicles was included via setting the resistive force in the volume elements passed through by the vehicles, as shown in Equation (1).

$$F_D = \frac{1}{2} C_D A_{car} \rho_{\infty} (U_{car} - U_{\infty})^2 \quad (1)$$

where  $C_D$  is the aerodynamic characteristic of the car,  $A_{car}$  is car front area,  $\rho_{\infty}$  is the air density,  $U_{car}$  is the car speed, and  $U_{\infty}$  is the air velocity.

Moreover, the same effect was considered within the source term in the formula describing the turbulence kinetic energy production (see Equation (2)). As it is known, moving objects induce a kinetic energy of turbulence that should be added as the additional source  $S_k$  to the k-equation. From different studies [14–16], it follows that turbulence is induced mainly in the wake behind the vehicle. Therefore, the additional source  $S_k$  [7] was added only along the trajectory that cars follow.

$$S_k = C_c (U_{car} - U_{\infty})^2 Q_{car} \quad (2)$$

where  $C_c$  is the model constant,  $U_{car}$  is the car speed,  $U_{\infty}$  is the air velocity, and  $Q_{car}$  is the traffic rate in cars/s.

Such an approach seems to embody one of the most appropriate options for substituting the vehicular motion in a numerical model that exploits a stationary computational mesh.

To perform the actual solution, we utilized the control volume method, where equations expressing the law of conservation of energy, mass, and momentum are solved on predefined volume elements of the computational mesh. The solution was implemented for a steady compressible air flux, exploiting the  $k$ - $\varepsilon$  RNG turbulence model.

At the inlet wall of the computational model, we set the air velocity profile corresponding to the tested wind speed (see Figure 3). The wind velocity for the neutrally stable atmosphere is determined from the equation of the logarithmic wind velocity profile.

$$u = \frac{u_0}{k} \ln\left(\frac{z}{z_0}\right) \quad (3)$$

where  $k$  is the von Karman constant ( $\sim 0.4$ ),  $u_0$  is the specified air velocity at the height  $z_0$ , and  $u$  is the air velocity at the height  $z$ . The velocity profile is taken just from the ground surface.

In all of the areas, the relevant speeds equaled  $2 \text{ m}\cdot\text{s}^{-1}$  and  $4 \text{ m}\cdot\text{s}^{-1}$ , invariably at the height of  $10 \text{ m}$  above the ground. Using these speed values, we progressively directed the wind parallel, perpendicularly, and obliquely ( $45^\circ$ ) to the road. The upper wall of the numerical model was assigned the boundary condition “slip wall”, while the bottom wall, which represented the ground, was assigned “wall with friction”. The same boundary condition was applied to all other solid surfaces (road surface, walls, and roofs of buildings). Due to the roughness of the surfaces, a boundary layer is formed along

each surface. The computational grid is sufficiently detailed and allows to identify air velocity fields in street canyons

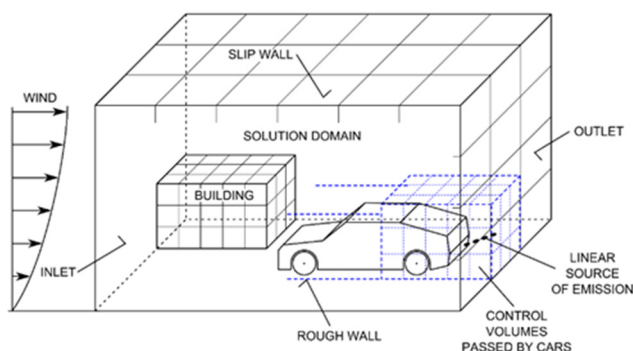


**Figure 3.** Schematic illustration of the modeled area and the assigned boundary conditions.

The side walls of the computational domain, through which the air leaves the model area, were described with “outlet” boundary conditions (see Figure 3).

The physical properties of the air assumed in the computations equaled those of an ideal mixture, namely, one composed of 88% N<sub>2</sub> and 21% O<sub>2</sub>, without considering humidity. At the inlet wall of the model area, a zero concentration of dust particles (particulate matter) was assumed. The computed mass concentration maps indicate how the monitored road contributes to the air pollutant concentration within the area. All of the modeled area’s particulates are generated exclusively by the traffic on the road. The source of the dust particles (particulate matter) was entered as an air pollution line source positioned in the center of the monitored straight road at the height of 0.5 m above its surface. Generally, in a given road, the dust (particulate matter) production intensity depends on the traffic rate, categories and weight of the vehicles, and traveling speeds. For the purposes of the numerical models, the parameters are accounted for within the emission factor. In all of the model areas solved, the emission factor per vehicle corresponded to  $E_f = 0.25387 \text{ g}\cdot\text{km}^{-1}$  (see Table 1), a value computed from the dynamic composition of the sample group of cars observed along road I/42 (Brno, Žabovřeská) [17].

Within the numerical model, the dispersion of fine particulates was solved via the Eulerian approach. In this context, we did not monitor the trajectories of individual particles but followed within balance equations the particle mass percentages in the volume elements of the computational mesh. Such a procedure enables the computations to be executed significantly more quickly and with less intensive hardware requirements. The deposition velocity of fine particles is very small, often smaller than that of Brownian motion; thus, the fine particles in the models were substituted with passive scalars.

### 2.3. Numerical Simulation Results

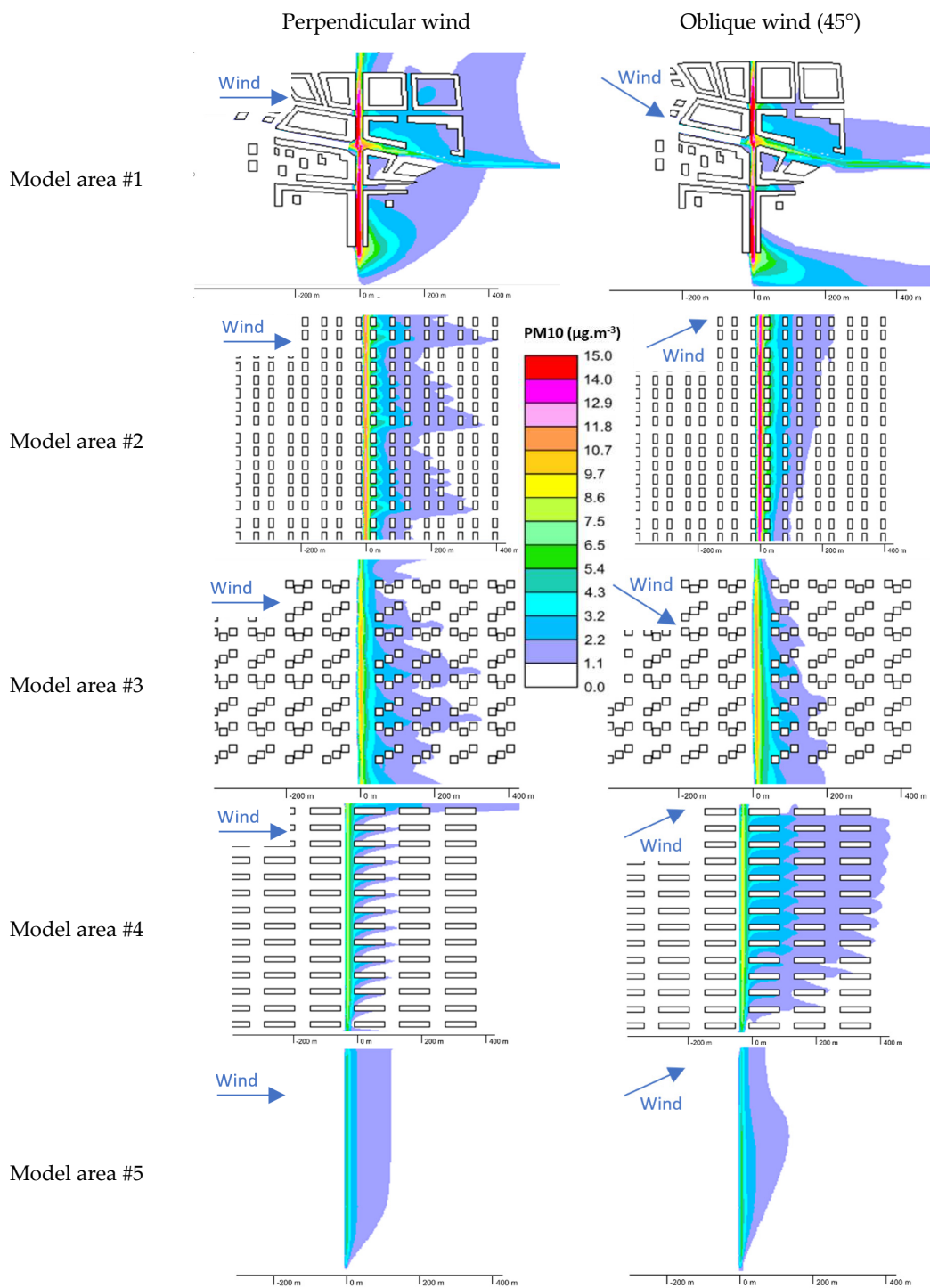
All of the five model areas were solved by using a single computational procedure. In the straight central road, we assumed two-way traffic of vehicles traveling at  $50 \text{ km}\cdot\text{h}^{-1}$ , with the traffic intensity of  $720 \text{ car}\cdot\text{h}^{-1}$  in each direction. Utilizing the StarCD software platform, we obtained the relevant 3D fields of air velocity, static pressure, and PM10 particle mass concentration.

Figure 4 displays the computed PM10 mass concentration fields acquired in a horizontal plane running at 1.5 m above the ground; such a height corresponds to the human breathing level. The mass concentration fields are specified for the perpendicular and oblique (45°) wind directions, assuming the wind speed of  $2 \text{ m}\cdot\text{s}^{-1}$ .

**Table 1.** Determination of the total emission factor of one car by EMEP methodology, according to emission standards and fuel type.

|  | Car Type | PV     |         | LCV    |        | HDV    | UB     | Share of Car Types According to Emission Standards (%) |      |   |      |      |  |
|--|----------|--------|---------|--------|--------|--------|--------|--|------|---|------|------|--|
|  | Fuel     | Petrol | Diesel  | Petrol | Diesel | Diesel | Diesel | NG   | PC   | LCV   | HDV  | UB   |  |
| Emission standards   | PRE ECE  | 0.0032 | 0.2164  | 0.0032 | 0.2493 | 0.5671 | 0.7636 | 0.0200   | 0.9  | 0.3   | 5.5  | 0    |  |
|  | Euro 1   | 0.0032 | 0.0569  | 0.0032 | 0.0903 | 0.4021 | 0.3635 | 0.0100   | 4.1  | 2.9   | 1.3  | 10.5 |  |
|  | Euro 2   | 0.0032 | 0.0467  | 0.0032 | 0.0903 | 0.1772 | 0.1830 | 0.0100   | 9.4  | 4.5   | 6.5  | 15.8 |  |
|  | Euro 3   | 0.0012 | 0.0310  | 0.0012 | 0.0662 | 0.2078 | 0.1817 | 0.0095   | 21.6 | 24.5  | 30.9 | 26.3 |  |
|  | Euro 4   | 0.0012 | 0.0316  | 0.0012 | 0.0356 | 0.0429 | 0.0458 | 0.0095   | 29.1 | 49.7  | 20.9 | 36.8 |  |
|  | Euro 5   | 0.0015 | 0.0027  | 0.0015 | 0.0027 | 0.0527 | 0.0519 | 0.0095   | 29.5 | 15.8  | 24.9 | 5.3  |  |
|  | Euro 6   | 0.0018 | 0.00199 | 0.0018 | 0.0019 | 0.0058 | 0.0051 | 0.0095   | 5.4  | 2.2   | 10   | 5.3  |  |
| Share of cars according to fuel [%]  |          | 45.84  | 54.16   | 13.52  | 86.48  | 100.00 | 46.67  | 53.33  |      |   |      |      |  |
| <b>Emission Factors Weighted with Shares of Fuel and Car Types (g·km<sup>-1</sup>)</b> |          |        |         |        |        |        |        |  |      |   |      |      |  |
| Emission standards   | PRE ECE  | 0.0010 |         | 0.0006 |        | 0.0312 |        | 0.0000   |      |   |      |      |  |
|  | Euro 1   | 0.0013 |         | 0.0022 |        | 0.0052 |        | 0.0183   |      |   |      |      |  |
|  | Euro 2   | 0.0025 |         | 0.0035 |        | 0.0115 |        | 0.0143   |      |   |      |      |  |
|  | Euro 3   | 0.0037 |         | 0.0140 |        | 0.0642 |        | 0.0236   |      |   |      |      |  |
|  | Euro 4   | 0.0051 |         | 0.0154 |        | 0.0089 |        | 0.0097   |      |   |      |      |  |
|  | Euro 5   | 0.0006 |         | 0.0004 |        | 0.0131 |        | 0.0015   |      |   |      |      |  |
|  | Euro 6   | 0.0001 |         | 0.0001 |        | 0.0005 |        | 0.0004   |      | Aggregate Emission factor (g·km <sup>-1</sup> ) |      |      |  |
| Summary emission factors   |          | 0.0146 |         | 0.0364 |        | 0.1349 |        | 0.0680   |      | 0.2538  |      |      |  |

PC—passenger cars, LCV—light commercial vehicles, HDV—heavy-duty vehicles, and UB—urban bus., NG—natural gas, PRE ECE—cars manufactured before 1992.



**Figure 4.** The PM10 mass concentration fields related to the height of 1.5 m above the ground for the wind velocity  $2\text{m}\cdot\text{s}^{-1}$  perpendicular and oblique wind directions.

The maximum particulate mass concentrations are detected immediately above the road; in its near vicinity, the concentration rates drop significantly, but the intensity of the decline weakens with increasing distance from the road. At greater distances, the actual concentration is influenced decisively by advective transport of the particles. Interestingly, the presence of the buildings enables diverse air volumes at the ground-level layers of the atmosphere to blend together, thus helping to reduce the highest particulate mass concentrations; at the same time, however, the houses interfere with and slow down the air flow at the ground levels. Which of the two processes eventually prevails depends on the geometric parameters of particular buildings and land surfaces. As is obvious from the results in Figure 4, smaller-sized houses located within regular intervals from each other (model areas #2 and #3) markedly impair the speed of the air flow above the ground; consequently, higher particulate mass concentrations can be observed even at considerable distances from the road. In long, continuous lines of houses (model area #4), the situation nevertheless differs, because the perpendicularly oriented wind embodies a favorable precondition for fast air motion between the buildings. The particles are then dispersed into the environment more intensively, and the mass concentration decrease intensifies with the growing distance. In the model area #1, the computation result is characterized by difficult predictability of the concentration field shape. It is then apparent that the continuous formations of houses retain highly concentrated particulates in the street canyons; depending on the instantaneous air flow direction, there occur strips of high-particulate concentrations, which, in the urban patterns, disperse only slowly. Moreover, the results for such areas cannot be generalized: Geometrically atypical regions will always require individual geometric modes to facilitate the actual solution procedures. The model area #5 provides results that correspond to the dispersion of particles generated at a straight road in an open landscape.

### 3. Generalizing the Results

The areal mass concentration maps displayed in Figure 4 were utilized as the source data, allowing the results to be generalized for different configurations. The mass concentration maps that correspond to the traffic intensity  $720 \text{ car}\cdot\text{h}^{-1}$  in each direction, denoted as the specific mass concentration of PM10. To yield the real PM10 mass concentrations appropriate to an arbitrary traffic density, the specific concentration of PM10 is multiplied by the ration of real and specific traffic intensity of the line source. The following processing step involves the creation of 2D relationships to express the connection between the ambient mass concentration of the PM10 pollutant and the distance from the road. This purpose was achieved by evaluating the mass concentration in slices perpendicular to the central road. The relationship acquired via the slice with the maximum range of a significant concentration of PM10 is denoted as  $c_{max}$ ; the other relationship was obtained in the slice with the minimum range of the concentration, denoted as  $c_{min}$ . These two relationships then define the region of mass concentrations that will most probably contain the real values of the road's contribution. In Figure 5, the relationships  $c_{max}$  and  $c_{min}$  are expressed for the perpendicular and oblique wind directions. The graphical representation of the relationships is complemented with a relevant mathematical expression, delivered by utilizing the exponential function

$$y = a \cdot e^{bx} \tag{4}$$

where  $x$  is distance from the road, and the factors  $a$  is calculated by Equation (6) and  $b$  are obtained from a line that is a result of the least squared method Equation (5):

$$y = mx + b \tag{5}$$

$$a = e^m \tag{6}$$

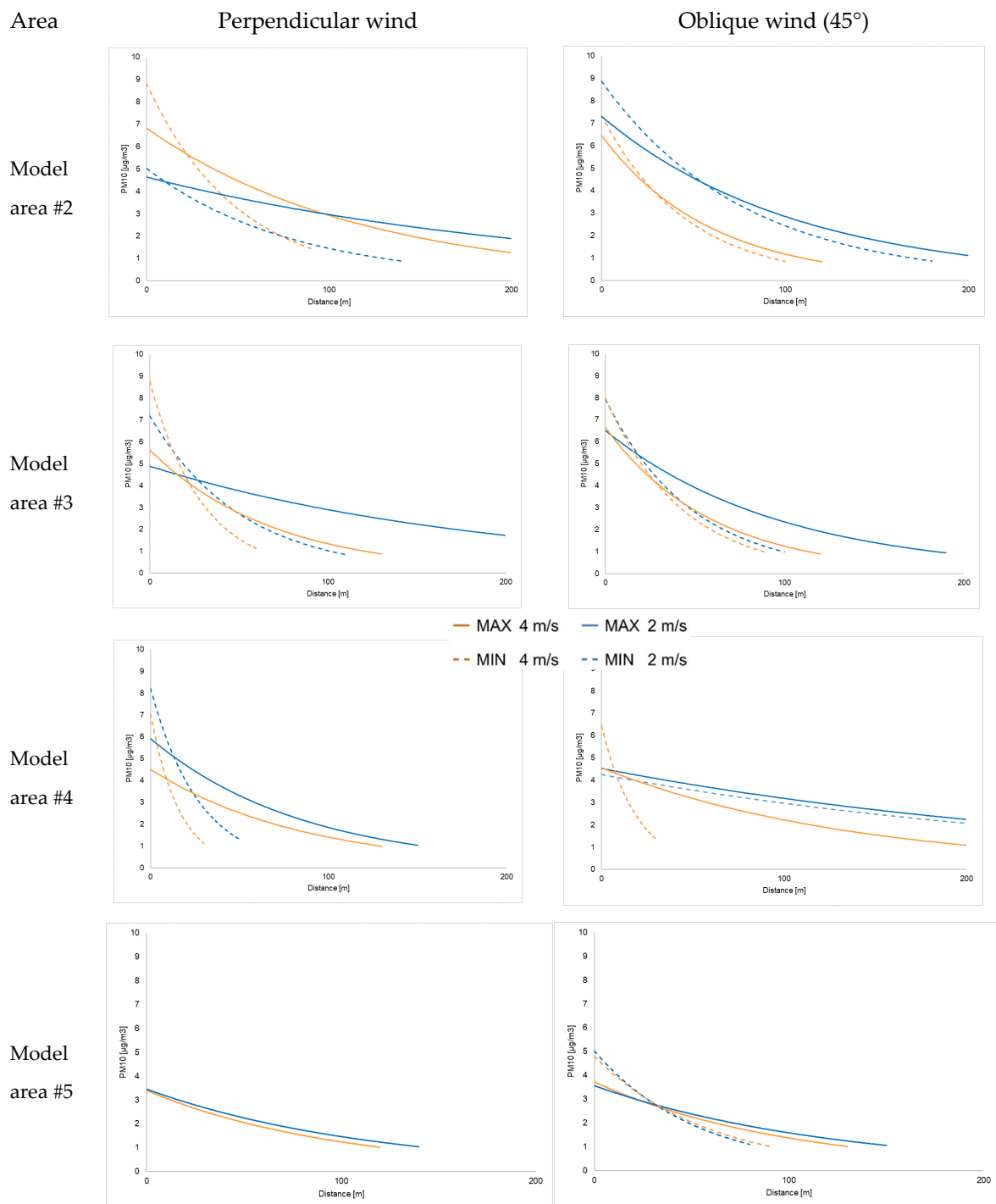


**Figure 5.** The relationship between the specific mass concentration of PM10 and the distance from the road, assuming the perpendicular and oblique (45°) wind directions and traffic intensity  $720 \text{ car}\cdot\text{h}^{-1}$  in each traffic direction.

The calculated factors  $a$  and  $b$  are given in Table 2.

**Table 2.** Coefficients of the exponential expression of PM10 limiting mass concentrations for Equation (4).

| Wind Direction | Area | Velocity (m·s <sup>-1</sup> ) | Range | a      | b      | R <sup>2</sup> |
|----------------|------|-------------------------------|-------|--------|--------|----------------|
| 90°            | #2   | 4                             | MAX   | 6.831  | −0.008 | 0.983          |
|                |      |                               | MIN   | 4.641  | −0.004 | 0.863          |
|                |      | 2                             | MAX   | 8.821  | −0.020 | 0.940          |
|                |      |                               | MIN   | 5.027  | −0.012 | 0.808          |
|                | #3   | 4                             | MAX   | 5.629  | −0.014 | 0.881          |
|                |      |                               | MIN   | 8.773  | −0.034 | 0.979          |
|                |      | 2                             | MAX   | 4.888  | −0.005 | 0.870          |
|                |      |                               | MIN   | 7.201  | −0.019 | 0.905          |
|                | #4   | 4                             | MAX   | 4.516  | −0.012 | 0.932          |
|                |      |                               | MIN   | 7.064  | −0.061 | 0.985          |
|                |      | 2                             | MAX   | 5.922  | −0.012 | 0.981          |
|                |      |                               | MIN   | 8.227  | −0.037 | 0.955          |
|                | #5   | 4                             | MAX   | 3.399  | −0.010 | 0.944          |
|                |      | 2                             | MAX   | 3.455  | −0.009 | 0.872          |
|                | 45°  | #2                            | 4     | MAX    | 6.465  | −0.017         |
| MIN            |      |                               |       | 7.369  | −0.022 | 0.907          |
| 2              |      |                               | MAX   | 7.311  | −0.009 | 0.885          |
|                |      |                               | MIN   | 8.879  | −0.013 | 0.942          |
| #3             |      | 4                             | MAX   | 6.637  | −0.017 | 0.916          |
|                |      |                               | MIN   | 7.987  | −0.024 | 0.969          |
|                |      | 2                             | MAX   | 6.504  | −0.010 | 0.945          |
|                |      |                               | MIN   | 7.931  | −0.021 | 0.958          |
| #4             |      | 4                             | MAX   | 4.555  | −0.007 | 0.989          |
|                |      |                               | MIN   | 6.449  | −0.052 | 0.854          |
|                |      | 2                             | MAX   | 4.525  | −0.004 | 0.950          |
|                |      |                               | MIN   | 4.254  | −0.004 | 0.916          |
| #5             |      | 4                             | MAX   | 3.716  | −0.010 | 0.921          |
|                |      |                               | MIN   | 4.794  | −0.017 | 0.982          |
|                |      | 2                             | MAX   | 3.559  | −0.008 | 0.901          |
|                | MIN  |                               | 5.024 | −0.019 | 0.991  |                |

In the parallel wind, applicable relationships were not formed, as—with respect to the character of the mass concentration fields—their patterns are not representative enough to justify further use.

#### 4. Comparing the Numerical Prediction with the In-Situ Measurements

The correctness of the inclusion of a linear source of PM10 emissions in the numerical model is crucial for the subsequent realistic solution of the particle dispersion. The validity of the emission factor was verified via the results of in-situ measurements at close vicinity of the studied road. To verify the correctness of the linear emission source calculation, the numerical predictions were compared with concentrations acquired via the in-situ measurements performed to determine the concentrations of the PM10 at the central district of Brno. The measurement spot was located in close proximity to a

convenient portion of the city's ring road (see Figure 6). On the side opposite to this spot, the road runs along a continuous formation of five-storey buildings; on the measurement side, however, the main urban element is a city park with lawns, shrubbery, and sparsely planted trees.



**Figure 6.** In-situ measurements of PM10 concentrations in urban roads.

The measurements were conducted between 8 November 2019, 0:00 and 25 November 2019, 23:59:00; the apparatus was an Airpointer (Recordum Messtechnik GmbH, Wiener Neustadt, Austria) whose PM module exploits the nephelometry principle. The obtained mass concentrations of PM10 were calibrated by means of the gravimetric method, following 24-h sampling with a Leckel MVS 6 (Leckel Ingenieurbüro, Berlin, Germany) small filter device and weighing the captured particles on Mettler Toledo MX5/A microbalances. During the measuring cycle, the values of the PM10 pollutant concentration were recorded in the ambient air (at the height of 1.5 m above the road and at the distance of 1 m from its edge), together with the data relating to the traffic intensity and the weather conditions. The subsequent processing phase yielded, for the monitored wind directions (perpendicular and oblique at 45°), the mean values of the PM10 pollutant concentration and the corresponding average traffic intensity. The evaluation used the knowledge of hourly concentrations of PM10. From the set of experimentally obtained data during the measurement, the values corresponding to the monitored wind direction (in the range of ±15°) and the specific wind speed ( $\pm 0.3 \text{ m}\cdot\text{s}^{-1}$ ) were filtered by subsequent processing. From the selected data, the average value of the PM10 concentration was calculated for the studied wind conditions, which was used for comparison with the calculated results. The mass concentration was evaluated when the wind was blowing from the apparatus towards the road; the rate established at that moment was utilized as the road's background concentration. By subtracting the background concentration from the mean concentration in the ambient air, we obtained the measured contribution of the road to the ambient mass concentration of PM10. The background concentration was identified separately for each combination of wind direction and speed. The background concentration value was obtained by filtering and averaging the experimental data corresponding to particular a wind speed and wind direction. The dependence of the background concentration on the wind direction and speed reflects the real conditions in the evaluated area. The numerically computed and in-situ measured contributions of the road are compared in Table 3.

Predicted particle concentration varied in the range of 8.3 until 15.8  $\mu\text{g}\cdot\text{m}^{-3}$  depending on the wind direction and wind speed. The results show that the numerical modeling overestimated the mass concentration of PM10 in the case of a perpendicular wind direction to the road by ca 50%. For the oblique wind direction (45°), numerical predictions and in-situ measurements indicate similar PM10 mass concentration values with fluctuations of deviation in both sides up to 40%. The dispersion of pollutants solved with utilizing computational code StarCD has been verified by numerous authors before [18]. In the framework of this study, it was verified by comparison with real measurements whether the mentioned method of calculating the emission flow from the traffic road corresponds to real conditions because the emission flow from a line source most significantly affects the resulting

concentration field of PM10 emissions. The calculated mass concentration is strongly dependent on the way the line source is entered into the volume elements above the road. Furthermore, in this position, all mathematical simplifications in involving the movement of cars are strongly reflected. The results reached and main commented trends are in accordance with the conclusions of a study [19] that also looked at the dispersion of pollutants from the transport roads in urban areas. The correctness of the inclusion of a linear source of PM10 emissions in the numerical model was confirmed with sufficient accuracy.

**Table 3.** Comparison of the computed and the measured values of the road’s contribution to the concentration of PM10 in the ambient air.

| Wind Direction | Wind Velocity       | PM10 In-Situ Measurement  |                                     |                                     | PM10 Numerical Prediction           |                                     | Comparison<br>Experiment/Prediction<br>Ration |
|----------------|---------------------|---|-------------------------------------|-------------------------------------|-------------------------------------|-------------------------------------|---|
|                |                     | Measured<br>Concentration<br>Recalculated to<br>Specific Traffic<br>Intensity | Background<br>Contribution          | Road<br>Contribution                | Road<br>Contribution<br>MAX         | Road<br>Contribution<br>MIN         |   |
|                |                     | ( $\mu\text{g}\cdot\text{m}^{-3}$ )   | ( $\mu\text{g}\cdot\text{m}^{-3}$ ) | ( $\mu\text{g}\cdot\text{m}^{-3}$ ) | ( $\mu\text{g}\cdot\text{m}^{-3}$ ) | ( $\mu\text{g}\cdot\text{m}^{-3}$ ) |   |
| perpendicular  | 2 m·s <sup>-1</sup> | 53.27   | 48.00                               | 5.27                                | 10.13                               | 8.33                                | 52%   |
| perpendicular  | 4 m·s <sup>-1</sup> | 48.36   | 43.58                               | 4.79                                | 9.20                                | 8.33                                | 55%   |
| oblique (45°)  | 2 m·s <sup>-1</sup> | 55.71   | 42.00                               | 13.71                               | 15.80                               | 10.07                               | 136%  |
| oblique (45°)  | 4 m·s <sup>-1</sup> | 31.13   | 23.47                               | 7.66                                | 12.60                               | 8.60                                | 89%   |

## 5. Conclusions

The computational modeling procedures used in solving the dispersion of polluting substances allowed us to capture in detail most of the relevant physical processes. Despite the marked progress within SW and HW tools, CFD-based modeling still requires a demanding presetting of the mesh and relies on time-intensive computations. Thus, detailed numerical modeling finds use in only a limited number of concrete cases involving mass concentration maps of pollutants. This paper discusses the dispersion of traffic-generated PM10 particulates into the vicinity of a straight road that passes through different types of built-up urban areas; in this context, among other problems, a procedure is presented to generalize a narrow amount of modeling results for further practical analytical applications. The research confirmed that the factors having the greatest impacts on the final shape of the PM10 mass concentration field rest are the wind direction and velocity. Another major parameter is the built-up area geometry, which substantially influences the air flow velocity in the ground-level layers of the atmosphere. Higher numbers of smaller-sized houses positioned in regular intervals apparently do not affect the wind flow direction but slow down considerably the ground-level air layers, resulting in major mass concentrations of pollutants within 200 m from the road. Where the urban pattern consists of long, continuous housing blocks, the air flow direction is altered in a noticeable manner. However, with parallel winds, the ground-level air does not slow down excessively, allowing the emissions to be more diluted and the quantity of PM10 in the ambient air to be reduced. The results acquired from areas characterized by recurring building distribution patterns facilitated the generalization of the outcomes and their confrontation with the in-situ measurements; this generalization then yielded the region of the probable value of the PM10 particulate mass concentration in the direction perpendicular to the road. The region of probable concentrations is limited by the curves of the lowest and the highest PM10 mass concentrations established via the numerical calculations. Urban areas exhibiting random arrangements of the built-up patterns do not allow generalizations of the results but rather necessitate individual solutions and testing of the evaluated configurations. Further refinement of the created analytical tool will require another validation and refinement of the model using a large number of experimental measurements obtained at different distances from the road.

The main result of the presented study is the definition of generalized dependences of PM10 concentrations at a vicinity of direct road passing through five characteristic types of urban areas. These results allow a quick analytical calculation of the PM10 concentrations in urban areas geometrically close to the tested areas. The performed experimental measurements confirmed that the used calculation

of the emission factor and subsequent quantification of the linear source of particles is usable with sufficient accuracy for the needs of dispersion models in the vicinity of direct roads.

Future research activities should focus on a similar examination of other types of typical urban areas and experimental verification numerical predictions at greater distances from the road.

**Author Contributions:** Methodology, J.P., J.H., and R.L.; software, J.P.; validation, J.H. and R.L.; formal analysis, J.P., J.H., and R.L.; investigation, J.P. and J.H.; resources, M.S.; writing—original draft preparation, J.P. and M.S.; visualization, M.S.; and supervision, J.P. All authors have read and agreed to the published version of the manuscript.

**Funding:** This research was supported by the project “Computer Simulations for Effective Low-Emission Energy Engineering” funded as project No. CZ.02.1.01/0.0/0.0/16\_026/0008392 by Operational Programme Research, Development and Education, Priority axis 1: Strengthening capacity for high-quality research. This research was further funded by Ministry of Education, Youth and Sports of Czech Republic within the National Sustainability Programme I, project of Transport R&D Centre (LO1610), on the research infrastructure acquired from the Operation Programme Research and Development for Innovations (CZ.1.05/2.1.00/03.0064).

**Conflicts of Interest:** The authors declare no conflicts of interest. The funders had no role in the design of the study; in the collection, analyses, or interpretation of data; in the writing of the manuscript; or in the decision to publish the results.

## References

1. Santibáñez-Andrade, M.; Quezada-Maldonado, E.M.; Osornio-Vargas, Á.; Sánchez-Pérez, Y.; García-Cuellar, C.M. Air pollution and genomic instability: The role of particulate matter in lung carcinogenesis. *Environ. Pollut.* **2017**, *229*, 412–422. [[CrossRef](#)] [[PubMed](#)]
2. Appel, J.; Bockhorn, H.; Frenklach, M. Kinetic modeling of soot formation with detailed chemistry and physics: Laminar premixed flames of C<sub>2</sub> hydrocarbons. *Combust. Flame* **2000**, *121*, 122–136. [[CrossRef](#)]
3. Jicha, M.; Katolicky, J.; Pospisil, J. Dispersion of pollutants in a street canyon and street intersection under traffic-induced flow and turbulence using a low Re  $\kappa$ - $\epsilon$  model. *Int. J. Environ. Pollut.* **2002**, *18*, 160–170. [[CrossRef](#)]
4. Jiang, Y.-Q.; Ma, P.-J.; Zhou, S.-G. Macroscopic modeling approach to estimate traffic-related emissions in urban areas. *Transp. Res. Part D Transp. Environ.* **2018**, *60*, 41–55. [[CrossRef](#)]
5. Tissari, J.; Hytönen, K.; Sippula, O.; Jokiniemi, J. The effects of operating conditions on emissions from masonry heaters and sauna stoves. *Biomass Bioenergy* **2009**, *33*, 513–520. [[CrossRef](#)]
6. Pospisil, J.; Katolicky, J.; Jicha, M. A comparison of measurements and CFD model predictions for pollutant dispersion in cities. *Sci. Total Environ.* **2004**, *334–335*, 185–195. [[CrossRef](#)] [[PubMed](#)]
7. Holmes, N.S.; Morawska, L. A review of dispersion modelling and its application to the dispersion of particles: An overview of different dispersion models available. *Atmos. Environ.* **2006**, *40*, 5902–5928. [[CrossRef](#)]
8. Woodward, H.; Stettler, M.; Pavlidis, D.; Aristodemou, E.; ApSimon, H.; Pain, C. A large eddy simulation of the dispersion of traffic emissions by moving vehicles at an intersection. *Atmos. Environ.* **2019**, *215*, 116891. [[CrossRef](#)]
9. Zhang, Y.; Gu, Z.; Wah Yu, C. Large eddy simulation of vehicle induced turbulence in an urban street canyon with a new dynamically vehicle-tracking scheme. *Aerosol Air Qual. Res.* **2017**, *17*, 865–874. [[CrossRef](#)]
10. Shen, J.; Gao, Z.; Ding, W.; Yu, Y. An investigation on the effect of street morphology to ambient air quality using six real-world cases. *Atmos. Environ.* **2017**, *164*, 85–101. [[CrossRef](#)]
11. Zhang, X.; Zhang, Z.; Su, G.; Tao, H.; Xu, W.; Hu, L. Buoyant wind-driven pollutant dispersion and recirculation behaviour in wedge-shaped roof urban street canyons. *Environ. Sci. Pollut. Res.* **2019**, *26*, 8289–8302. [[CrossRef](#)] [[PubMed](#)]
12. Miao, C.; Yu, S.; Hu, Y.; Bu, R.; Qi, L.; He, X.; Chen, W. How the morphology of urban street canyons affects suspended particulate matter concentration at the pedestrian level: An in-situ investigation. *Sustain. Cities Soc.* **2020**, *55*, 102042. [[CrossRef](#)]
13. Auguste, F.; Lac, C.; Masson, V.; Cariolle, D. Large-eddy simulations with an immersed boundary method: Pollutant dispersion over urban terrain. *Atmosphere* **2020**, *11*, 113. [[CrossRef](#)]
14. Eskridge, R.E.; Hunt, J.C. Highway modeling. Part I: Prediction of velocity and turbulence fields in the wake of vehicles. *J. Appl. Meteor.* **1979**, *18*, 387–400. [[CrossRef](#)]

15. Sedefian, L.; Trivikrama Rao, S.; Czapski, U. Effects of traffic-generated turbulence on near-field dispersion. *Atmos. Environ.* (1967) **1981**, *15*, 527–536. [[CrossRef](#)]
16. Sini, J.-F.; Mestayer, P.G. Traffic-induced urban pollution: A numerical simulation of street dispersion and net production. In *Air Pollution Modeling and Its Application XII*; Springer: Boston, MA, USA, 1998; pp. 369–377.
17. EMEP/EEA Air Pollutant Emission Inventory Guidebook 2019. Available online: <https://www.eea.europa.eu/publications/emep-eea-guidebook-2019/part-b-sectoral-guidance-chapters/1-energy/1-a-combustion/1-a-3-b-i/view> (accessed on 30 March 2020).
18. Labovský, J.; Jelemenský, L. Verification of CFD pollution dispersion modelling based on experimental data. *J. Loss Prev. Process Ind.* **2011**, *24*, 166–177. [[CrossRef](#)]
19. Tsai, M.Y.; Chen, K.S. Measurement and three-dimensional modeling of air pollutant dispersion in an urban street canyon. *Atmos. Environ.* **2004**, *38*, 5911–5924. [[CrossRef](#)]



© 2020 by the authors. Licensee MDPI, Basel, Switzerland. This article is an open access article distributed under the terms and conditions of the Creative Commons Attribution (CC BY) license (<http://creativecommons.org/licenses/by/4.0/>).



Article

# Impacts of Built-Up Area Geometry on PM<sub>10</sub> Levels: A Case Study in Brno, Czech Republic

Jiří Neubauer <sup>1,\*</sup> , Jaroslav Michálek <sup>1</sup> , Karel Šilinger <sup>2</sup> and Petr Firbas <sup>3</sup> 

<sup>1</sup> Department of Quantitative Methods, Faculty of Military Leadership, University of Defence, Kounicova 65, 662 10 Brno, Czech Republic; jaroslav.michalek@unob.cz

<sup>2</sup> Department of Fire Support, Faculty of Military Leadership, University of Defence, Kounicova 65, 662 10 Brno, Czech Republic; karel.silinger@unob.cz

<sup>3</sup> Institute of Physics of the Earth, Faculty of Science, Masaryk University, Kotlářská 267/2, 611 37 Brno, Czech Republic; Petr.Firbas@ipe.muni.cz

\* Correspondence: jiri.neubauer@unob.cz; Tel.: +42-0973-442-029

Received: 5 August 2020; Accepted: 24 September 2020; Published: 29 September 2020

**Abstract:** This paper presents a statistical comparison of parallel hourly measurements of particulate matter smaller than 10 µm (PM<sub>10</sub>) from two monitoring stations that are located 560 m from each other in the northern part of Brno City. One monitoring station is located in a park, the other in a built-up area. The authors' aim is to describe the influence of a built-up area geometry and nearby traffic intensity on modeling of PM<sub>10</sub> pollution levels in the respective part of Brno. Furthermore, the purpose of this study is also to examine the influence of meteorological factors on the pollution levels; above all, to assess the influence of wind speed and direction, temperature change, and humidity change. In order to evaluate the obtained data, the following methods of mathematical statistics were applied: descriptive statistics, regression analysis, analysis of variance, and robust statistical tests. According to the results of the Passing–Bablok test, it can be stated that the parallel measurements of PM<sub>10</sub> are significantly different. A regression model for PM<sub>10</sub> pollution prediction was created and tested in terms of applicability; subsequently, it was used in order to compare measurements from both stations. It shows that in addition to the monitored meteorological factors, pollution levels are influenced mainly by traffic intensity and the geometry of the monitored built-up area.

**Keywords:** PM<sub>10</sub>; meteorological factors; monitoring stations; Passing–Bablok test; regression analysis; statistical modeling; analysis of variance

## 1. Introduction

Air quality is one of the basic indicators of environment quality. In addition to gaseous pollutants, the air can be polluted by particles (either in a suspension, fluid, or solid state) of divergent composition and size (known as particulate matter (PM)). Air pollution caused by particulate matter smaller than 10 µm (PM<sub>10</sub>) is strongly associated with the occurrence of a number of inflammatory diseases of the respiratory system and has been one of the most common causes of morbidity not only in the Czech Republic, but also across the world. The impact of ambient air pollution on human health, especially on patients suffering from cardiovascular and respiratory diseases, was proven in many studies, for example in [1–3]. On that account, the Council of the European Union decided to set up various programs using legislative instruments, for instance using the respective Council Directive [4].

Specifically, high air pollution levels can be monitored in large cities with a high population density, which is connected to many pollution sources, in particular to heavy traffic. For this reason, a great deal of attention has been paid to PM monitoring in densely populated areas and its evaluation and prediction with respect to accompanying factors (in terms of climate sciences, meteorology, and

urban planning). Moreover, national and international limits have been set in order to protect both human health and various ecosystems.

This topic has been covered in many scientific studies and articles, which gives evidence that a great deal of effort has been made regarding air pollution monitoring in large urban areas. Many scientific papers focus on PM modeling using meteorological variables. The authors in [5,6] described the connection of PM occurrence and meteorological factors affecting Chengdu, China (province of Sichuan), and Hanoi, Vietnam. PM was determined to be the principal pollutant in the Chengdu region. Further, it was stated that in Chengdu, negative correlations, except for average air pressure values, exist between other meteorological parameters and PM. Similarly, in Hanoi, the PM<sub>10</sub> concentration was inversely correlated with most meteorological factors, and the outcome in Hanoi confirmed the importance of meteorological factors in the formation of air pollution. A model for official prediction of PM<sub>10</sub>, which was used in Graz, Austria, was presented in [7,8]. The association between PM levels, morbidity, and mortality from respiratory and cardiovascular diseases in Kuwait was discussed in [9]. The authors found that PM<sub>10</sub> levels significantly correlated with bronchial asthma at a significance level of 0.05. Their study provides good evidence of a consistent relationship between PM<sub>10</sub> levels and respiratory diseases. Furthermore, Reference [10] described the statistical link between short-term exposure to air pollutants (PM and others) and hospitalization for asthma in Ulaanbaatar, Mongolia. Cardiovascular diseases in Europe caused by air pollution were newly evaluated in [11] using the risk ratio function. The authors in [12] explored the economy-wide effects of agriculture on air quality and human health across the EU-28 countries. Uncertainties in estimates of mortality attributable to PM<sub>2.5</sub> in Europe were discussed in [13]. The authors in [14] concluded that 11.3% of the total deaths caused by respiratory and cardiovascular system diseases were attributable to long-term exposure to PM<sub>2.5</sub> pollution in Verona. Child mortality due to ambient air pollution-induced lower respiratory tract infections was analyzed in [15]. The authors in [16] found that fossil fuel-related emissions account for about 65% of the excess mortality rate attributable to air pollution and 70% of the climate cooling caused by anthropogenic aerosols. Last but not least, Reference [17] provided statistical evidence that in the United States, a mere increase in PM of less than 2.5 µm (PM<sub>2.5</sub>) by 1 µg/m<sup>3</sup> is associated with a 15% increase in COVID-19 mortality. The cited studies suggest that the effect of elevated PM levels on the health of the population has been statistically demonstrated. Statistically significant correlations have been found between PM levels and cardiovascular and other diseases in many of the world's major urban areas. It is therefore also important to address the level of PM<sub>10</sub> pollution on a small urban scale with respect to the built-up geometry. That is the aim of this work.

For the purpose of spatio-temporal prediction of PM<sub>10</sub> levels in urban areas, the so-called LUR (land use regression) method was developed and compared to many other methods of statistical prediction [18]. This approach is suitable for high-resolution prediction (spatial resolution < 100 m; temporal resolution ≤ 24 h) [19]. In Oslo, Norway, the monitoring process is focused on PM measuring sensors [20].

Such examples of PM monitoring are merely a fraction of all possible approaches to the evaluation of PM air pollution in selected urban areas. An overview of the results related to PM<sub>10</sub> monitoring, which were published in 2000 and later, also included in the Google Scholar Database, was incorporated in [19] and contained 147 works. Nonetheless, the question remains how to create a model for air quality assessment at a local urban scale using available data (from the fields of meteorology, transportation, and urban planning) obtained from a limited number of monitoring stations. The aim of this paper is to help answer such a question. Its purpose is to compare parallel PM<sub>10</sub> air pollution measurements from two nearby monitoring stations in Brno, Czech Republic, with regard to meteorological factors, traffic intensity, and built-up area geometry.

Brno is a mid-sized city in the Czech Republic with approximately 400,000 inhabitants. It is located in a basin at 190 to 425 m above sea level. There is no heavy industry or mining activities; on that account, the sources of air pollution are rather few and small. The city is, however, crossed by several major international highways. Local road traffic volume is quite high. Assessments of previous

measurements confirmed that the main source of PM<sub>10</sub> air pollution in Brno is intensive road traffic. In [21], a high risk of increase in cardiovascular diseases, premature mortality, and respiratory illnesses for individuals exposed to PM pollution was discussed. The authors' evaluation was based on PM monitoring in four Brno locations with regard to traffic intensity. PM level modeling in Brno City with regard to wind speed and direction and built-up area geometry around roadways in particular was analyzed in [22]. Furthermore, predictions of local PM<sub>10</sub> pollution that take local traffic intensity in Brno into consideration were discussed in [23]. This paper claimed that in urban areas with less intensive traffic, statistical predictions of air pollution using regression models are more accurate. A comparison of statistical prediction models describing air pollution in Brno was presented in [24]. The applicability of the regression model described in [23] was also evaluated using data obtained in Graz, Austria [25], and it was compared with the Austrian prediction model, which is used in Graz for official PM predictions. In the subsequent work [26], this prediction model was adjusted, and only earlier measurements of meteorological variables were used for predictions; on that account, this prediction can be applied in real-world conditions immediately.

In the experiment described and evaluated below, an area rather distant from major international highways was selected with the intention to study local pollution and its variability at short distances. The aim of this paper is to describe differences in PM<sub>10</sub> monitoring in two nearby stations located in Brno, to predict air pollution, and assess its variability regarding meteorological affecting factors, built-up area geometry, and surrounding traffic volume. For this purpose, statistical methods were applied; to be specific, methods of statistical comparison (comparison of relative frequencies, the Passing–Bablok test), regression analysis, and analysis of variance.

## 2. Methodology

### 2.1. Data

PM<sub>10</sub> levels were measured between 2 February and 20 April 2019. The data contained parallel hourly measurements of PM<sub>10</sub> and auxiliary meteorological variables from two monitoring stations located in the city district of Brno-Sever. Parallel measurements obtained at two nearby stations, but different in location, may well illustrate the effect of built-up geometry. In situations where multi-station measurements are available, it is possible to assess the effect of location on PM<sub>10</sub> from multiple perspectives; however, the assessment of this effect is usually performed in pairs of these stations; see, e.g., [21]. The period when parallel measurements took place does not allow for assessment of seasonal variations of the PM<sub>10</sub> level. Nonetheless, to assess the influence of meteorological factors (especially wind direction and speed) and the influence of built-up area geometry on the local level of PM<sub>10</sub>, the above-mentioned parallel measurements are sufficient. Seasonal variations in this part of the city of Brno were discussed in [23,24].

The monitoring station called “Arboretum” is located on top of a hill in the Mendel University botanical garden. East of the Arboretum station lie the premises of the University of Defence in Brno. On its campus, a mobile monitoring station was placed intentionally between the university buildings. Its working title, “Černá Pole”, was based on the name of the surrounding neighborhood. The distance between these two monitoring stations was 560 m; see the left part of Figure 1. Both stations are operated by the Department of Air Protection of the Environmental Protection Division of Brno City Municipality. This organization also provided the data. Between the botanical garden of Mendel University and the University of Defence campus, a busy road called Generála Píky street, which connects the Brno city center with the Brno-Lesná housing estate, runs in a northerly direction. Traffic volumes on individual roads surrounding the monitoring stations are depicted in Figure 1 on the right. The map with data represents the year of 2018 and was provided by Brněnské komunikace (BKOM). Every day, eleven-thousand vehicles use the Generála Píky street, 5 percent of which belong to freight transport. This volume will be denoted 11/5, and such a notation will be used in similar situations further on. Both monitoring stations are located approximately 0.5–1 km (about 1 km east,



variables presented and explained in Table 1 were selected in compliance with previous statistical analyses based on daily mean values described in [23–25]. In this table,  $t$  denotes the hour the measurement was taken;  $t = 1, 2, \dots, 1872$ . (1872 measured hours correspond to 78 measured days). The time series of measurements contain 43 missing observations at the Arboretum station and 2 incomplete observations at the Černá Pole station.

Both stations were equipped with identical devices:

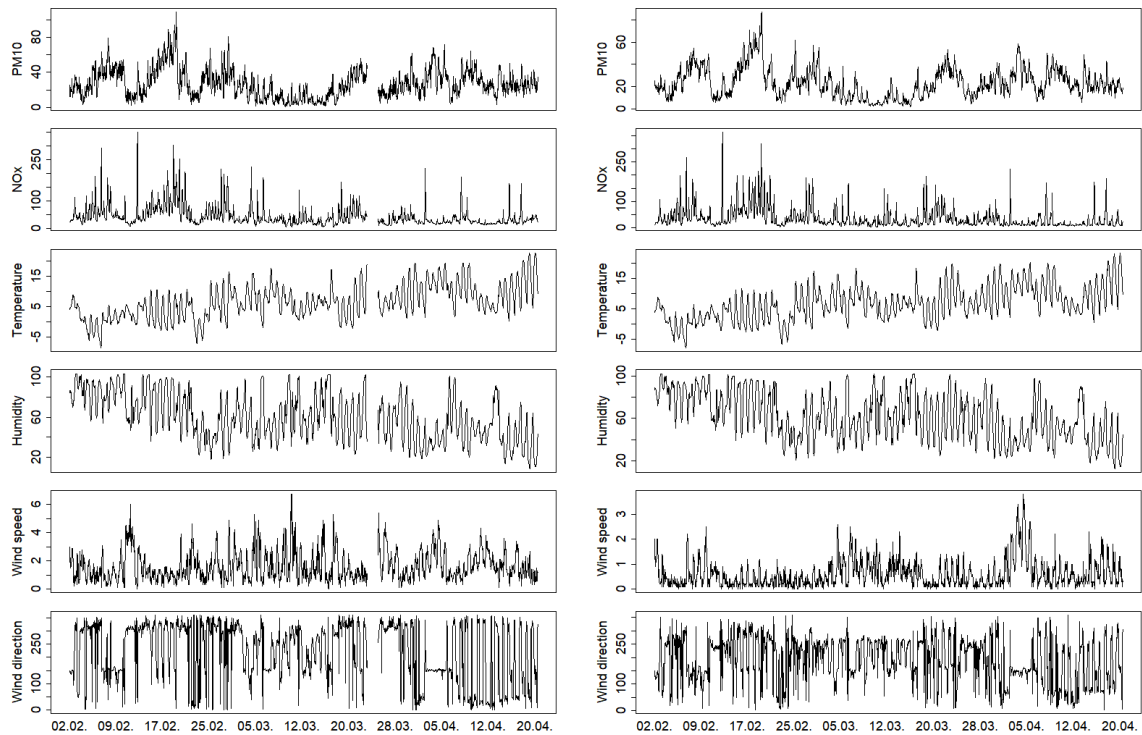
- For measuring concentrations of  $PM_{10}$ : instrument manufactured by Environment SA, Model MP101M (MP101M is the automatic and real-time particulate monitor, compliant with ISO 10473:2000 and for  $PM_{10}$  US-EPA (EQPM-0404-151) and EN 12341 (I-CNR 087/2004, F-LCSQA). It allows the continuous and simultaneous measurement of fine dust, not influenced by the physico-chemical nature, color, or shape of particulates, in measurement ranges up to  $10,000 \mu\text{g}\cdot\text{m}^{-3}$ , with the lowest detectable limit of  $0.5 \mu\text{g}\cdot\text{m}^{-3}$  (24 h average), with fiberglass tape (with 3 years of autonomy for continuous sampling with daily cycles) and with a measurement accuracy of  $\pm 5\%$ ).
- For measuring temperature and humidity: instrument made by Vaisala, Type HMP 155 with radiation shield DTR503 (HMP 155 (Vaisala) is the humidity and temperature probe compliant with the standards EN 61326-1 and EN 550022. Humidity measurement is based on the capacitive thin film HUMICAP® polymer sensor and temperature measurement on the resistive platinum sensors (Pt100). It allows the relative humidity (RH) measurement in the full range (0–100% RH) and with an accuracy in the range from  $-20\text{ }^\circ\text{C}$  to  $+40\text{ }^\circ\text{C} \pm (1.0 + 0.008 \times \text{reading})\%$  RH. The accuracy temperature measurement is in the range from  $-80\text{ }^\circ\text{C}$  to  $+20\text{ }^\circ\text{C} \pm (0.226 - 0.0028 \times \text{temperature})\text{ }^\circ\text{C}$  and in the range from  $+20\text{ }^\circ\text{C}$  to  $+60\text{ }^\circ\text{C} \pm (0.055 + 0.0057 \times \text{temperature})\text{ }^\circ\text{C}$ ).
- For measuring wind direction and speed: instrument manufactured by Gill Instruments Limited, type WindSonic (WindSonic is 2-axis ultrasonic wind sensor for true “fit and forget” wind sensing; it has no moving parts (alternative to conventional cup and vane or propeller wind sensors), compliant with the standard EN 61326:1998. It allows the wind speed measurement up to  $60 \text{ m}\cdot\text{s}^{-1}$  with the accuracy  $\pm 2\%$  (at  $12 \text{ m}\cdot\text{s}^{-1}$ ) and wind direction measurement in the full circle with the accuracy  $\pm 2^\circ$  (at  $12 \text{ m}\cdot\text{s}^{-1}$ ).

Table 1. Notation for the measured variables.

| Variable | Description  |
|----------|--|
| $PM10_t$ | $PM_{10}$ ( $\mu\text{g}\cdot\text{m}^{-3}$ )  |
| $NOx_t$  | $NO_x$ ( $\mu\text{g}\cdot\text{m}^{-3}$ )   |
| $T_t$    | temperature ( $^\circ\text{C}$ )   |
| $H_t$    | humidity (%)   |
| $V_t$    | wind speed ( $\text{m}\cdot\text{s}^{-1}$ )  |
| $D_t$    | wind direction (degrees)   |
| $RH_t$   | rush hours (a dummy variable equal to 1 for 7–10 AM, 3–5 PM; at other times, it is equal to 0) |

Wind direction  $D_t$  was measured as an oriented angle between the vector pointing north of the station and the observed wind direction vector pointing to the station corresponding to the maximum wind speed at hour  $t$ . Rush hour  $RH_t$  is a dummy variable equal to 1 for 7–10 AM, 3–5 PM; at other times, it is equal to 0.

Figure 3 contains graphs with resulting measurements. Similar to [23,25], the previous two variables  $V_t$  and  $D_t$  were transformed into projections  $V_t \sin D_t$  and  $V_t \cos D_t$ . As a result, it was possible to calculate the basic characteristics of wind direction and use them in further statistical analyses. The basic statistical characteristics of the analyzed data (number of observations  $n$ , mean, standard deviation, median, minimal and maximum observations, lower and upper quartiles, skewness, and kurtosis) for the selected variables, including their transformations, are presented in Table 2 for both the Arboretum and Černá Pole stations.



**Figure 3.** Measured variables:  $PM_{10}$  ( $\mu\text{g}\cdot\text{m}^{-3}$ ),  $NO_x$  ( $\mu\text{g}\cdot\text{m}^{-3}$ ), temperature ( $^{\circ}\text{C}$ ), humidity (%), wind speed ( $\text{m}\cdot\text{s}^{-1}$ ), and wind direction (degrees); Arboretum station, left; Černá Pole station, right.

**Table 2.** Descriptive statistics of variables (n—the number of observations; Mean—arithmetic mean; Median—median; St. dev.—standard deviation; Min—minimum value; Max—maximum value;  $Q_{0.25}$ —lower quartile;  $Q_{0.75}$ —upper quartile; Skewness—skewness, Kurtosis—kurtosis).

| Arboretum       | n    | Mean  | Median | St. dev. | Min   | Max   | $Q_{0.25}$ | $Q_{0.75}$ | Skewness | Kurtosis |
|-----------------|------|-------|--------|----------|-------|-------|------------|------------|----------|----------|
| $PM10_t$        | 1830 | 26.9  | 24.8   | 16.6     | 0.9   | 109.5 | 14.7       | 37.0       | 0.89     | 1.00     |
| $NOx_t$         | 1827 | 43.5  | 32.2   | 36.2     | 4.7   | 348.7 | 22.1       | 50.2       | 2.89     | 11.74    |
| $T_t$           | 1830 | 6.4   | 6.1    | 5.5      | −8.6  | 22.5  | 2.5        | 9.8        | 0.30     | −0.11    |
| $H_t$           | 1829 | 59.6  | 58.0   | 23.2     | 9.0   | 103.0 | 41.0       | 77.0       | 0.14     | −0.96    |
| $V_t$           | 1830 | 1.6   | 1.4    | 1.1      | 0.0   | 6.7   | 0.9        | 2.2        | 1.15     | 1.19     |
| $\sqrt{PM10_t}$ | 1830 | 4.9   | 5.0    | 1.6      | 0.9   | 10.5  | 3.8        | 6.1        | 0.04     | −0.32    |
| $V_t \sin D_t$  | 1830 | −0.38 | −0.27  | 1.37     | −6.69 | 3.05  | −0.98      | 0.55       | −0.80    | 0.97     |
| $V_t \cos D_t$  | 1830 | 0.46  | 0.68   | 1.26     | −4.37 | 4.13  | −0.40      | 1.27       | −0.54    | 0.53     |
| Černá Pole      | n    | Mean  | Median | St. dev. | Min   | Max   | $Q_{0.25}$ | $Q_{0.75}$ | Skewness | Kurtosis |
| $PM10_t$        | 1871 | 23.5  | 21.2   | 13.5     | 2.1   | 87.3  | 13.5       | 31.5       | 0.86     | 0.85     |
| $NOx_t$         | 1869 | 36.0  | 22.1   | 38.5     | 2.7   | 361.8 | 12.9       | 43.3       | 2.97     | 12.43    |
| $T_t$           | 1872 | 6.8   | 6.4    | 5.6      | −7.8  | 23.3  | 2.8        | 10.3       | 0.29     | −0.18    |
| $H_t$           | 1871 | 61.4  | 59.0   | 22.0     | 13.0  | 102.0 | 43.5       | 80.0       | 0.09     | −1.03    |
| $V_t$           | 1872 | 0.6   | 0.4    | 0.6      | 0.0   | 3.8   | 0.2        | 0.8        | 1.86     | 4.53     |
| $\sqrt{PM10_t}$ | 1871 | 4.6   | 4.6    | 1.4      | 1.4   | 9.3   | 3.7        | 5.6        | 0.12     | −0.36    |
| $V_t \sin D_t$  | 1872 | 0.05  | −0.01  | 0.56     | −1.98 | 2.22  | −0.27      | 0.36       | 0.32     | 0.85     |
| $V_t \cos D_t$  | 1872 | −0.25 | −0.09  | 0.56     | −3.44 | 1.02  | −0.35      | 0.06       | −2.11    | 5.83     |

### 2.3. Methods

First, let us stress that the statistical data processing described below may resemble the standard procedure as described in Directive 2008/50/EC of the European Parliament and Council on ambient air quality and cleaner air for Europe, but it is a different one. To utilize the measured data more intensively and to get deeper statistical insights into the  $PM_{10}$  pollution level variations both in time and space, we used a finer time-granularity approach. Instead of using the “1 day averaging period” (i.e., one 24 h average per day), based on Annex XI of the European Directive, we used a moving 24 h

average approach applied twenty-four times per day (i.e., every full hour). To bear resemblance to the common approach, the standard  $PM_{10}$  limit value of  $50 \mu\text{g}\cdot\text{m}^{-3}$  was kept for our approach. Please note that with this “fine-granularity approach”, the number of exceedances calculated below cannot be directly compared to the standard national air pollution reports.

A test of equal proportions (see, e.g., [27]) to assess the (non-)equality of the relative frequencies of the moving 24 h average values exceeding the limit level was applied to data collected by the Arboretum and Černá Pole stations.

Parallel measurements of  $PM_{10}$  and  $NO_x$  from both stations were compared using the Passing–Bablok test [28]. It is a robust, nonparametric method for fitting a straight line to two variables  $X$  ( $PM_{10}$ , Arboretum station) and  $Y$  ( $PM_{10}$ , Černá Pole station). This is accomplished by estimating a linear regression line and testing whether the intercept is zero and the slope is one. If the hypothesis that the intercept is zero and the slope is one is not rejected, the measurements can be considered comparable. Otherwise, the measurements are not comparable.

A regression model (see, e.g., [29,30]) for the prediction of pollution by  $PM_{10}$  was created, and regressors were selected using the backward selection method. In statistics, backward selection is a method of fitting regression models in which the choice of regressors is carried out by an automatic procedure. It involves starting with all candidate variables (regressors), testing the deletion of each variable using a chosen model fit criterion, deleting the variable (if any) whose loss gives the most statistically insignificant deterioration of the model fit, and repeating this process until no further variables can be deleted without a statistically significant loss of fit. The common choice of the model fit criterion is the Akaike information criterion (AIC); see, e.g., [29].

With respect to outputs of the regression model, wind direction and speed were analyzed, and mean values of  $PM_{10}$  for various wind directions were compared using the analysis of variance [29].

Hourly measurements of the following variables were crucial for the construction of the regression model:  $PM_{10,t}$ , wind speed  $V_t$ , wind direction  $D_t$ , temperature  $T_t$ , and humidity  $H_t$ . It is clearly visible from Figure 3 that wind speed and wind direction are very different between the stations (their behavior is affected mainly by the built-up area geometry), and the values of these two variables have a great impact on the local  $PM_{10}$  pollution levels.

The details of the statistical methods can be found in [29,30]. All the calculations were carried out in the R environment [31] using the openair [32], forecast [33], mcr [34], MASS [35], and car [36] packages.

### 3. Results

#### 3.1. Frequency of Limit Value Exceedances for a Moving Average

Figure 4 represents hourly averages and 24 h moving averages of  $PM_{10}$  concentrations measured at the Arboretum and Černá Pole stations, together with the limit value.

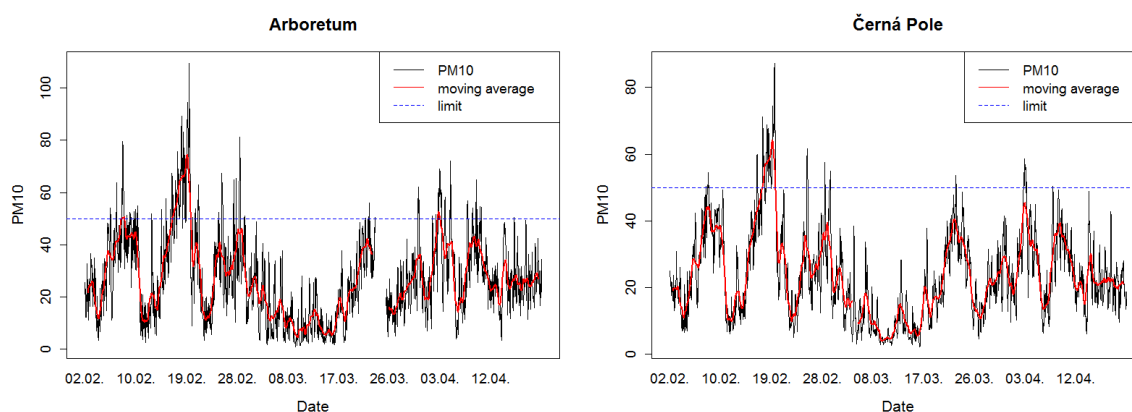


**Figure 4.** PM<sub>10</sub> with a 24 h moving average ( $\mu\text{g}\cdot\text{m}^{-3}$ ) and limit value of  $50\ \mu\text{g}\cdot\text{m}^{-3}$ .

Considering the missing data,  $n = 1757$  measurements were performed at each of the two stations during the monitoring period (only parallel measurements without missing values are considered). At the Arboretum station, the limit value of  $50\ \mu\text{g}\cdot\text{m}^{-3}$  was exceeded by 100 moving average values calculated for every hour of each day, and the relative frequency was equal to 0.0569. At the Černá Pole station, the limit value was exceeded by 53 calculated values, and the relative frequency was equal to 0.0302. The 95% confidence interval for the probability of exceeding the limit value of  $50\ \mu\text{g}\cdot\text{m}^{-3}$  is (0.0514, 0.0624) in the case of the Arboretum station and (0.0260, 0.0342) in the case of the Černá Pole station.

The statistical comparison of relative frequencies of exceeding the limit value at the Arboretum station (0.0569) and at the Černá Pole station (0.0302) shows that the values can be considered different at the significance level of 5%; the corresponding  $p$ -value is 0.0001.

As a side note, it may be of interest to experts dealing with a number of exceedances determined by the “one day averaging period” (i.e., just one 24 h average per day) based on Annex XI of Directive 2008/50/EC that this approach (as applied by the Czech Hydro-meteorological Institute) resulted in only five days with the PM<sub>10</sub> limit of  $50\ \mu\text{g}\cdot\text{m}^{-3}$  exceeded for the processed period. The finer-granularity approach used in this paper results in eight days with one or more 24 h moving averages (of 24 hourly ones calculated daily) exceeding the same limit.

The observational period used in this study is not long enough to draw robust conclusions, but the above stated difference of five and eight exceedances, if projected to the full calendar year, could mean that for a case of a calendar year with 35 exceedances officially reported using the European Directive approach, there could be some 56 days detected with the same limit exceeded if 24 h moving averages calculated hourly are considered in our approach. In another view, the above stated difference in the number of days with detected exceedances could mean that 35 days with the exceeded limit of any of the hourly calculated 24 h moving averages in a day might be reached in a calendar year just when as low as 22 days with the limit exceedance reported based on the current national practice are reported. Without elaborating on the details, it should be noted that a compromise between the two mentioned approaches is needed to fine tune the reporting of exceedances.

It is obvious that our finer-granularity approach exposes a weakness of the official reporting practice. For example, currently, a calendar day with 23 detected exceedances of the 24 h moving average would be neglected in the official reporting if the 24 h average calculated at midnight was not exceeding the limit value. Similarly, a day would not be included in the official reporting in the case that the limit value would be exceeded only once during the day, and this was not the midnight value of the 24 h average. In such a situation, 23 of 24 possible cases would be neglected. Therefore, the current normative situation can be seen as under-representing real pollution levels and therefore to be a breach of the widely accepted precautionary principle used for environment impact assessments.

In conclusion, it can be highlighted that the discrepancy between the two exceedance assessments increases with lowering the  $PM_{10}$  pollution levels. The reason is that the probability of omitting such “exceedance” days in the annual statistics increases with lowering the number of 24 h moving averages exceeding the limit from 23 to one during a single calendar day.

### 3.2. Comparison of $PM_{10}$ Measurements

A comparison of parallel  $PM_{10}$  measurements between the Arboretum and Černá Pole stations can be roughly assessed from the top row graphs in Figure 3. A detailed comparison was carried out using the non-parametric Passing–Bablok test. The robust regression line for  $PM_{10}$  values at Arboretum and Černá Pole stations is defined by the following equation:

$$PM10_t^{\text{Černá Pole}} = 1.754 + 0.802 \cdot PM10_t^{\text{Arboretum}}. \quad (1)$$

Results of the Passing–Bablok test together with the regression line are presented in Figure 5. The 95% confidence intervals for parameters of the regression line are (1.299, 2.215) in the case of the intercept and (0.783, 0.822) in the case of the slope. The null hypothesis that the parallel measurements are not statistically significantly different (the intercept equals zero, and the slope equals one) was rejected at the significance level of 5%. The test revealed a statistically significant difference between both parallel measurements.

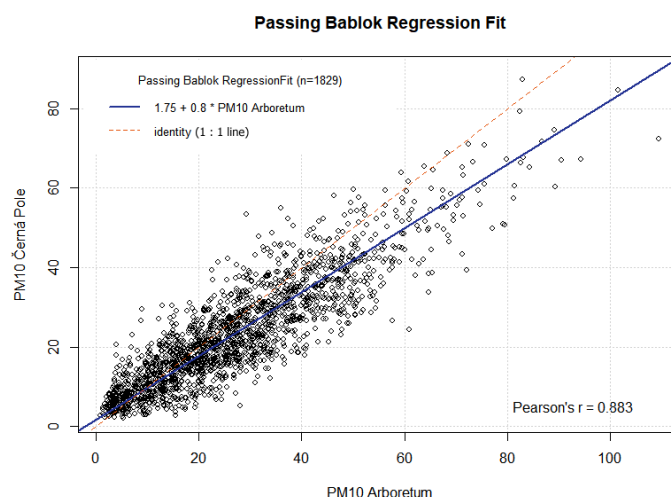


Figure 5. Passing–Bablok regression fit,  $PM_{10}$  in  $\mu\text{g}\cdot\text{m}^{-3}$ .

Furthermore, the correlation coefficients were determined. Pearson’s correlation coefficient between  $PM10_t^{\text{Černá Pole}}$  and  $PM10_t^{\text{Arboretum}}$  is 0.883 ( $p$ -value  $\cong 0$ ), and Spearman’s correlation coefficient is 0.872 ( $p$ -value  $\cong 0$ ). Both correlation coefficients are significantly different from zero. The results show that with a  $10 \mu\text{g}\cdot\text{m}^{-3}$  increase of  $PM_{10}$  pollution level at the Arboretum station, there is on average only an  $8.02 \mu\text{g}\cdot\text{m}^{-3}$  increase at the Černá Pole station. The results obtained by the robust Passing–Bablok test show how the two nearby monitoring stations differ in the level of  $PM_{10}$  pollution.

### 3.3. Comparison of $NO_x$ Measurements

Transport is one of the main sources of nitrogen oxides. The authors in [37] discussed the presence of  $NO_x$  from vehicle exhaust in the composition of PM. Using correlation analysis, we assessed the statistical relationship between  $PM_{10}$  and nitrogen oxides  $NO_x$ . Spearman’s correlation coefficient between  $PM_{10}$  values and  $NO_x$  has a value of 0.478 ( $p$ -value  $\cong 0$ ) for the Arboretum station and 0.372 ( $p$ -value  $\cong 0$ ) for Černá Pole station. From the above values, it is clear that in the case of the Arboretum station, the correlation coefficient is higher ( $p$ -value 0.00017). We will now compare the

NO<sub>x</sub> values for both stations using the Passing–Bablok test, similar to the PM<sub>10</sub> comparison. We get an estimate of the regression function in the form:

$$NOx_t^{\check{C}ern\acute{a} Pole} = -8.212 + 1.014 \cdot NOx_t^{Arboretum}. \tag{2}$$

The 95% confidence intervals for the parameters of the regression line are (−8.898, −7.531) in the case of the intercept and (0.994, 1.034) in the case of the slope. The results of the robust Passing–Bablok test show that the two nearby monitoring stations differ in the level of NO<sub>x</sub>. The difference is due to the non-zero value of the intercept in the estimated regression function Equation (2). The hypothesis that the slope in the regression function has a value of one is not rejected.

Pearson’s correlation coefficient between NO<sub>x</sub><sub>t</sub><sup>Černá Pole</sup> and NO<sub>x</sub><sub>t</sub><sup>Arboretum</sup> is 0.933 (*p*-value ≅ 0), and Spearman’s correlation coefficient is 0.901 (*p*-value ≅ 0). Both correlation coefficients are significantly different from zero.

### 3.4. Regression Models for PM<sub>10</sub> Prediction

The regression model for PM<sub>10</sub> prediction was constructed with respect to the previously published results in [23–25]. The following auxiliary variables were used for the prediction of PM<sub>10</sub><sub>t</sub>: temperature *T*<sub>t</sub>, humidity *H*<sub>t</sub>, wind speed *V*<sub>t</sub>, wind direction *D*<sub>t</sub>, rush hours *RH*<sub>t</sub>, and their transformations: time differences of temperatures *T*<sub>t</sub> − *T*<sub>t−1</sub> and *T*<sub>t−1</sub> − *T*<sub>t−2</sub>, time differences of humidity *H*<sub>t</sub> − *H*<sub>t−1</sub>, and transformations of wind direction and wind speed *V*<sub>t</sub> sin *D*<sub>t</sub>, *V*<sub>t</sub> cos *D*<sub>t</sub>, which made it possible to incorporate wind directions into the regression model.

Since the relation between PM<sub>10</sub> value and atmospheric pressure proved to be statistically insignificant in previous and current analyses, the atmospheric pressure variable was not used in the regression model. Pearson’s correlation coefficient is 0.082, and Spearman’s correlation coefficient is 0.109. Despite the fact that both correlation coefficients are, due to the large number of observations, statistically significant at the significance level of 5%, based on Pearson’s correlation coefficient, it can be concluded that atmospheric pressure explains only 0.68% of the variability of the PM<sub>10</sub><sub>t</sub> variable. On that account, atmospheric pressure is not included in further analyses.

With regard to the article [25], three regression models were studied. There were two generalized autoregressive linear models (GALM) [30]; one with the gamma distribution and canonical link function (which is the reciprocal function for gamma distribution), the other with the gamma distribution and log-link function. The third model was the linear regression model for the √PM<sub>10</sub><sub>t</sub> variable (see [7,25]), and it worked best for the hourly data. All three models were computationally processed, then their comparison was performed using the coefficients of determination; their graphical comparison was performed, and the third model proved to be the most suitable. Due to the scope of the article, the results of the first two models are not presented. One of the reasons why the third model was used was that graphs rendered using Q-Q plots and the Anderson–Darling goodness-of-fit test showed that the distribution of √PM<sub>10</sub><sub>t</sub> is very close to a normal distribution at both stations. The regressors were selected using the backward selection method and the AIC criterion (Akaike information criterion). The final model contained eight parameters β<sub>1</sub>, β<sub>2</sub>, . . . , β<sub>8</sub> and random error ε<sub>t</sub> for observations in time *t* = 1, 2, . . . , *n*, where *n* is the number of hourly observations. It is of the form:

$$\begin{aligned} \sqrt{PM10_t} = & \beta_1 + \beta_2 \sqrt{PM10_{t-1}} + \beta_3(T_t - T_{t-1}) + \beta_4(T_{t-1} - T_{t-2}) + \\ & + \beta_5(H_t - H_{t-1}) + \beta_6 V_{t-1} \sin D_{t-1} + \beta_7 V_{t-1} \cos D_{t-1} + \beta_8 RH_t + \epsilon_t. \end{aligned} \tag{3}$$

The adjusted coefficient of determination *R*<sub>adj</sub><sup>2</sup> was used for assessing the suitability of the statistical relation between the √PM<sub>10</sub><sub>t</sub> response variable and the auxiliary variables incorporated into the model. Its values were high and statistically significant (0.806 for the Arboretum station and 0.918 for the Černá Pole station). Standardized residuals did not show any extreme deviations in comparison to the previous two GALM models.

Estimated coefficients (with their standard errors in parentheses) can be found in Table 3; in the column Arboretum for the Arboretum station and in the column Černá Pole for the Černá Pole station. Moreover, there are the number of observations  $n$  (there were missing observations in the data), the coefficient of determination  $R^2$ , the adjusted coefficient of determination  $R^2_{adj}$ , the residual standard error, the F statistic, and the corresponding degree of freedom  $df = (df1; df2)$ . The statistical significance of the coefficients is denoted by \*, where the number of asterisks indicates the respective  $p$ -values corresponding to the statistical significance of the respective coefficient. It can be seen that the proposed model Equation (3) is suitable for the description of the studied statistical relationship between  $\sqrt{PM10_t}$  and the selected regressors for each of the stations. The coefficient of determination  $R^2$  and the adjusted coefficient of determination  $R^2_{adj}$  are high for both stations, and the value of the F statistic describing the suitability of the model is also statistically significant at the significance level of 1%. Moreover, Table 3 shows that all coefficients of both statistical models are significantly different from zero at least at the significance level of 5% with the exception of coefficients  $\beta_5$  and  $\beta_7$  for the Arboretum station.

Agreement between the prediction model Equation (3) and the data can be visually assessed from Figure 6, where the observed and predicted (fitted)  $PM10_t$  values are in the top row, the corresponding standardized residuals are in the middle row, and graphs of measured and fitted values of  $PM10_t$  are in the bottom row. It is evident from the graphs (especially from the graphs showing the measured values versus the fitted ones) that the estimated models describe the development of  $PM10$  with sufficient accuracy. The model for the Černá Pole station has greater accuracy than the model for the Arboretum station. This conclusion corresponds to the values of  $R^2$  in Table 3, where  $R^2 = 0.919$  for the Černá Pole station and  $R^2 = 0.807$  for the Arboretum station.

Table 3. Estimates of the linear models; standard errors are in parentheses.

| Parameter                | Variable               | Dependent Variable:          |                              |
|--------------------------|------------------------|------------------------------|------------------------------|
|                          |                        | $\sqrt{PM10_t}$              |                              |
|                          |                        | Arboretum                    | Černá Pole                   |
| $\beta_1$                |                        | 0.593 ***<br>(0.060)         | 0.241 ***<br>(0.035)         |
| $\beta_2$                | $\sqrt{PM10_{t-1}}$    | 0.878 ***<br>(0.011)         | 0.946 ***<br>(0.007)         |
| $\beta_3$                | $T_t - T_{t-1}$        | 0.118 ***<br>(0.033)         | 0.117 ***<br>(0.017)         |
| $\beta_4$                | $T_{t-1} - T_{t-2}$    | -0.094 ***<br>(0.024)        | -0.052 ***<br>(0.012)        |
| $\beta_5$                | $H_t - H_{t-1}$        | 0.006<br>(0.005)             | 0.011 ***<br>(0.003)         |
| $\beta_6$                | $V_{t-1} \sin D_{t-1}$ | 0.071 ***<br>(0.014)         | 0.085 ***<br>(0.018)         |
| $\beta_7$                | $V_{t-1} \cos D_{t-1}$ | 0.002<br>(0.015)             | 0.049 ***<br>(0.018)         |
| $\beta_8$                | $RH_t$                 | 0.117 ***<br>(0.040)         | 0.054 **<br>(0.022)          |
| Number of observations n |                        | 1824                         | 1866                         |
| $R^2$                    |                        | 0.807                        | 0.919                        |
| Adjusted $R^2$           |                        | 0.806                        | 0.918                        |
| Residual Std. Error      |                        | 0.722 (df = 1816)            | 0.402 (df = 1858)            |
| F Statistic              |                        | 1,083.102 *** (df = 7; 1816) | 2,993.700 *** (df = 7; 1858) |

Note: \*  $p < 0.1$ ; \*\*  $p < 0.05$ ; \*\*\*  $p < 0.01$ .

Agreement between the estimated parameters of model Equation (3) for Arboretum and Černá Pole stations can be assessed using the regression analysis methods and the F statistic. This statistic can also be modified in order to test the equality of the corresponding regression parameters; see [29]. The value of the F statistics for comparing the two models is  $F = 5.5039$ , and the corresponding  $p$ -value is  $6.193 \times 10^{-7}$ ; i.e., both models are significantly different from each other. A detailed comparison of the parameters of both models from Table 3 can be found in Table 4. It is clear that both models differ

only in parameters  $\beta_1$  (intercept,  $p$ -value  $\cong 0$ ) and  $\beta_2$  ( $p$ -value  $\cong 0$ ), which corresponds to the value of the lagged transformed variable  $\sqrt{PM10_{t-1}}$ ; i.e., the  $PM_{10}$  pollution level from the previous hour.

**Table 4.** Tests of equal parameters and model comparison.

| Parameter      | Variable               | F-Test   | $p$ -Value               |
|----------------|------------------------|----------|--------------------------|
| $\beta_1$      |                        | 25.19828 | $5.41837 \times 10^{-7}$ |
| $\beta_2$      | $\sqrt{PM_{t-1}}$      | 25.51096 | $4.61270 \times 10^{-7}$ |
| $\beta_3$      | $T_t - T_{t-1}$        | 0.00008  | 0.99266                  |
| $\beta_4$      | $T_{t-1} - T_{t-2}$    | 2.65500  | 0.10331                  |
| $\beta_5$      | $H_t - H_{t-1}$        | 0.80706  | 0.36905                  |
| $\beta_6$      | $V_{t-1} \sin D_{t-1}$ | 0.26454  | 0.60705                  |
| $\beta_7$      | $V_{t-1} \cos D_{t-1}$ | 2.56720  | 0.10919                  |
| $\beta_8$      | $RH_t$                 | 1.96325  | 0.16125                  |
| All parameters |                        | 5.5039   | $6.193 \times 10^{-7}$   |

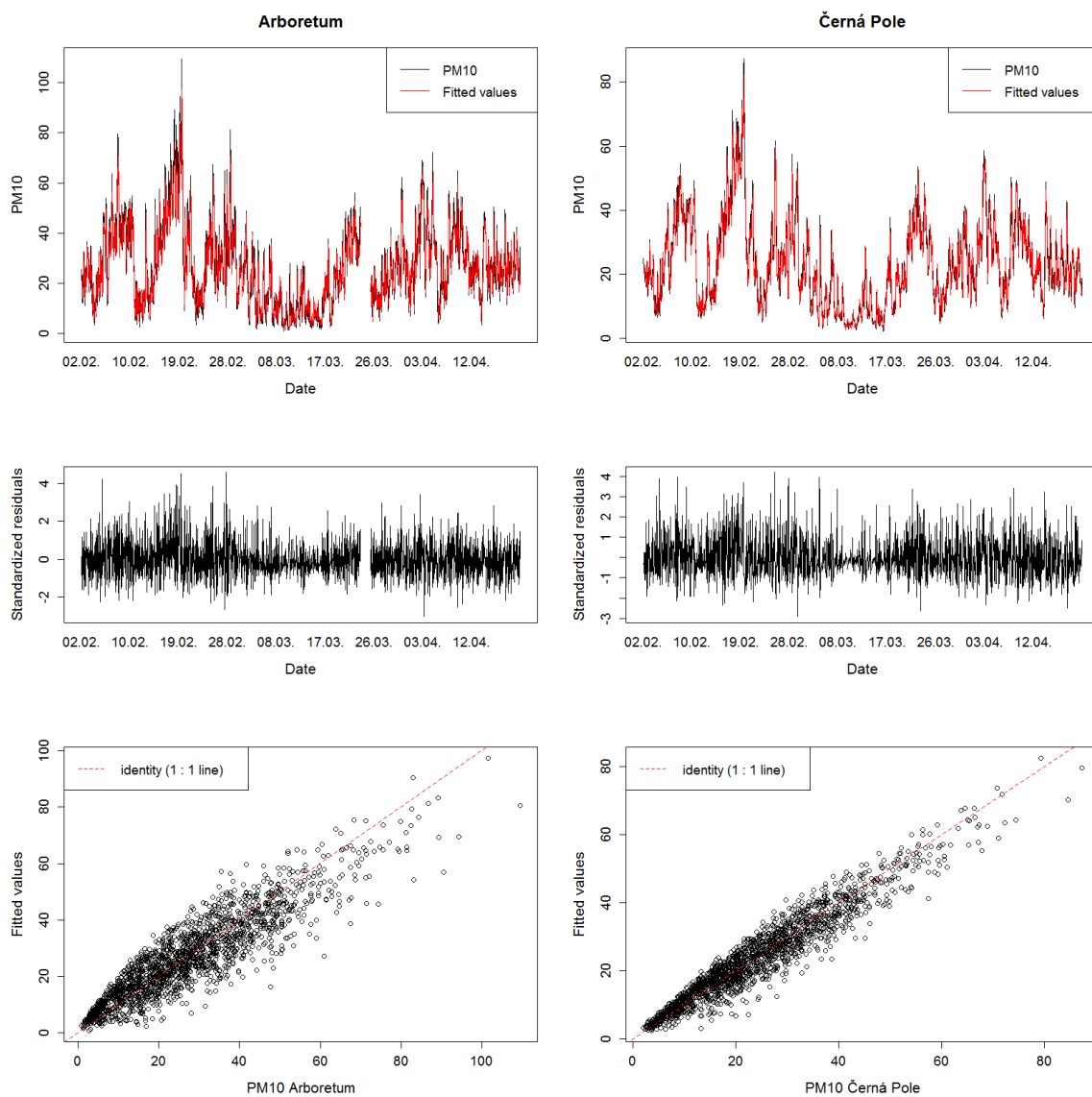


**Figure 6.** Fitted models, standardized residuals, and measured vs. fitted values,  $PM_{10}$  in  $\mu\text{g}\cdot\text{m}^{-3}$ .

### 3.5. Influence of Wind on PM<sub>10</sub> Levels

For the purpose of the statistical analysis of the influence of wind speed  $V_t$  and wind direction  $D_t$  on PM<sub>10</sub> air pollution at both stations, possible wind directions ranging from zero to 360 degrees (clockwise) were divided into 12 sections  $\langle 345, 15 \rangle, \langle 15, 45 \rangle, \langle 45, 75 \rangle, \dots, \langle 315, 345 \rangle$  by 30 degrees. Furthermore, a wind rose representing the frequency of counts by wind direction and wind speed was created. Subsequently, the basic statistical characteristics of PM<sub>10</sub> levels were calculated for each section. One-way analysis of variance was carried out in order to compare mean values of air pollution in individual directions. Wind roses for both the Arboretum and Černá Pole stations are presented in Figure 7. It is clear from the wind rose graphs that the characteristics describing the wind speed and direction are different for both stations. At the Arboretum station located in the open space of the botanical garden, higher wind speeds can be observed, and the northwest and southeast directions predominate. At the Černá Pole station, which is located in a built-up area, the measured wind speeds are lower, and the northeast wind direction is almost absent. Like the Arboretum station, there is a southeast wind direction. These differences are caused by the surrounding built-up area (especially buildings) of the Černá Pole station.

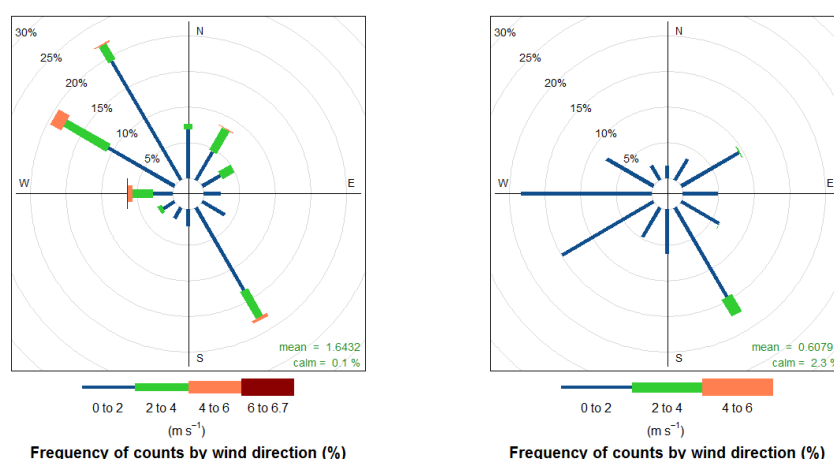


Figure 7. Wind rose (Arboretum, left; Černá Pole, right).

Boxplots comparing pollution levels in individual sections can be found in Figure 8 for both stations. Furthermore, Table 5 contains descriptive statistics for individual sections for the Arboretum station, whereas Table 6 contains the same information from the Černá Pole station. Using one-way analysis of variance, the null hypothesis claiming that the mean level of PM<sub>10</sub> air pollution is the same in all 12 sections was tested against an alternative hypothesis stating that levels of pollution show statistically significant differences due to the effect of various wind directions. The analysis of variance was applied to the  $\sqrt{PM_{10t}}$  variable, which has a normal distribution for data from individual sections. As for the Arboretum station, the value of the test statistics  $F = 17.07$  and  $p$ -value is zero, with degrees of freedom 11 and 1816. For the Černá Pole station, this statistic equals  $F = 22.26$ ; the  $p$ -value is zero, with degrees of freedom 11 and 1858. On that account, it may be argued that each station showed statistically significant differences in the mean values of air pollution in terms of wind direction. Since each station provided evidence on statistically significant differences in the mean values of air pollution caused by PM<sub>10</sub>, Tukey’s honest significance test was performed for each station in order to identify pairs of monitored sections that exhibit substantially different air pollution levels. The test compared 66 section pairs; for the purpose of its interpretation in this paper, only comparisons of sections with the highest and lowest pollution levels were selected.

Regarding the Arboretum station, mean values of pollution levels resulting from measured values and wind directions are presented in Table 5; the corresponding graph can be found in Figure 8 on the left. As can be derived from the table, air pollution with the highest mean value of  $32.2 \mu\text{g}\cdot\text{m}^{-3}$  and the

highest median value of  $31.6 \mu\text{g}\cdot\text{m}^{-3}$  was measured in the direction of 135 to 165 degrees. Another two sections with the mean value of pollution higher than  $28 \mu\text{g}\cdot\text{m}^{-3}$  and the median value higher than  $26 \mu\text{g}\cdot\text{m}^{-3}$  were those of 75–105 degrees and 315–345 degrees. Tukey’s honest significance test did not prove statistically significant differences in the mean values of air pollution between pairs consisting of the above-mentioned three sections with the highest pollution levels. On the contrary, the section with the lowest pollution levels was the one of 225–255 degrees, where the mean value of the pollution level was  $11.9 \mu\text{g}\cdot\text{m}^{-3}$ , and the median was  $7 \mu\text{g}\cdot\text{m}^{-3}$ . Low levels of pollution with the mean value lower than  $23 \mu\text{g}\cdot\text{m}^{-3}$  and the median lower than  $20 \mu\text{g}\cdot\text{m}^{-3}$  were found in four sections between 165 and 285 degrees. Tukey’s honest significance test proved statistically significant differences in the mean value of pollution levels between the section of 135–165 degrees and each of the four sections ranging from 165 to 285 degrees.

**Table 5.** Descriptive statistics for PM<sub>10</sub> by wind direction: Arboretum station (n—the number of observations; Mean—arithmetic mean; Median—median; St. dev.—standard deviation; Min—minimum; Max—maximum; Q<sub>0.25</sub>—lower quartile; Q<sub>0.75</sub>—upper quartile).

| Degrees | n    | Mean | Median | St. dev. | Min | Max   | Q <sub>0.25</sub> | Q <sub>0.75</sub> |
|---------|------|------|--------|----------|-----|-------|-------------------|-------------------|
| all     | 1828 | 27.0 | 24.8   | 16.6     | 0.9 | 109.5 | 14.7              | 37.0              |
| 345–15  | 139  | 27.0 | 24.4   | 14.4     | 3.4 | 109.5 | 17.4              | 33.4              |
| 15–45   | 154  | 27.0 | 25.9   | 11.3     | 6.5 | 79.5  | 19.8              | 33.5              |
| 45–75   | 91   | 26.6 | 25.0   | 13.3     | 4.0 | 90.5  | 19.1              | 32.5              |
| 75–105  | 45   | 31.5 | 28.5   | 16.7     | 3.8 | 71.5  | 18.4              | 43.3              |
| 105–135 | 67   | 28.0 | 23.9   | 17.3     | 1.4 | 79.2  | 15.5              | 40.1              |
| 135–165 | 334  | 32.2 | 31.6   | 18.2     | 2.2 | 94.4  | 17.4              | 45.3              |
| 165–195 | 43   | 22.8 | 19.7   | 19.3     | 1.9 | 84.3  | 6.2               | 34.4              |
| 195–225 | 32   | 19.7 | 14.3   | 19.6     | 0.9 | 89.3  | 4.2               | 31.9              |
| 225–255 | 45   | 11.9 | 7.0    | 11.4     | 2.8 | 50.4  | 4.2               | 12.9              |
| 255–285 | 116  | 18.5 | 12.4   | 17.2     | 1.4 | 81.4  | 5.8               | 27.0              |
| 285–315 | 358  | 24.7 | 20.8   | 16.6     | 1.4 | 83.2  | 12.6              | 34.4              |
| 315–345 | 404  | 29.1 | 27.0   | 15.5     | 2.2 | 101.6 | 18.3              | 37.8              |

**Table 6.** Descriptive statistics for PM<sub>10</sub> by wind direction: Černá Pole station (n—the number of observations; Mean—arithmetic mean; Median—median; St. dev.—standard deviation; Min—minimum; Max—maximum; Q<sub>0.25</sub>—lower quartile; Q<sub>0.75</sub>—upper quartile).

| Degrees | n    | Mean | Median | St. dev. | Min | Max  | Q <sub>0.25</sub> | Q <sub>0.75</sub> |
|---------|------|------|--------|----------|-----|------|-------------------|-------------------|
| all     | 1870 | 23.5 | 21.1   | 13.5     | 2.1 | 87.3 | 13.5              | 31.5              |
| 345–15  | 35   | 25.6 | 21.9   | 13.7     | 7.7 | 67.8 | 16.3              | 33.4              |
| 15–45   | 69   | 22.8 | 21.5   | 10.7     | 6.6 | 67.0 | 15.9              | 29.0              |
| 45–75   | 182  | 24.3 | 21.6   | 11.7     | 5.3 | 72.3 | 16.1              | 30.9              |
| 75–105  | 94   | 25.2 | 23.0   | 10.1     | 6.7 | 49.2 | 17.1              | 31.8              |
| 105–135 | 120  | 24.6 | 21.4   | 12.8     | 5.6 | 52.0 | 14.4              | 34.1              |
| 135–165 | 326  | 28.2 | 27.5   | 14.8     | 2.5 | 74.5 | 17.2              | 37.1              |
| 165–195 | 121  | 19.6 | 19.1   | 12.9     | 2.4 | 65.3 | 8.3               | 29.1              |
| 195–225 | 93   | 20.2 | 18.8   | 9.5      | 3.0 | 55.8 | 14.0              | 26.8              |
| 225–255 | 282  | 17.4 | 16.1   | 9.8      | 2.6 | 54.2 | 9.6               | 23.9              |
| 255–285 | 351  | 20.4 | 18.2   | 13.5     | 2.1 | 65.2 | 8.8               | 29.1              |
| 285–315 | 147  | 32.6 | 29.9   | 15.1     | 6.0 | 87.3 | 23.3              | 40.1              |
| 315–345 | 50   | 29.8 | 26.4   | 14.9     | 8.7 | 84.6 | 18.0              | 38.0              |

Similarly, the mean values of pollution levels measured at the Černá Pole station with regard to the wind direction are presented in Table 6; the corresponding graph is in Figure 8 on the right. This table shows that the air pollution with the highest mean value of  $32.6 \mu\text{g}\cdot\text{m}^{-3}$  and the highest median value of  $29.9 \mu\text{g}\cdot\text{m}^{-3}$  was measured in the direction of 285 to 315 degrees. Another two sections with the mean value of pollution higher than  $28 \mu\text{g}\cdot\text{m}^{-3}$  and the median value higher than  $26 \mu\text{g}\cdot\text{m}^{-3}$  were those of 315–345 degrees and 135–165 degrees. As in the case of the Arboretum station, Tukey’s honest significance test performed for the Černá Pole station did not return statistically significant differences in the mean values of air pollution between pairs consisting of the above-mentioned three sections with the highest pollution levels. On the contrary, the section with the lowest pollution levels was

the one of 225–255 degrees, where the mean value of the pollution level was  $17.4 \mu\text{g}\cdot\text{m}^{-3}$  and the median was  $16.1 \mu\text{g}\cdot\text{m}^{-3}$ . It follows from the above that the section with the lowest pollution levels is the same for both stations. Low pollution levels with the mean value lower than  $23 \mu\text{g}\cdot\text{m}^{-3}$  and the median lower than  $20 \mu\text{g}\cdot\text{m}^{-3}$  were measured again in four sections within the range of 165–285 degrees. Tukey's honest significance test proved statistically significant differences for each pair of these sections; the first section was always selected from the three sections with the highest mean value of air pollution, and the second one was selected among the four sections with the lowest mean value within the range of 165–285 degrees.

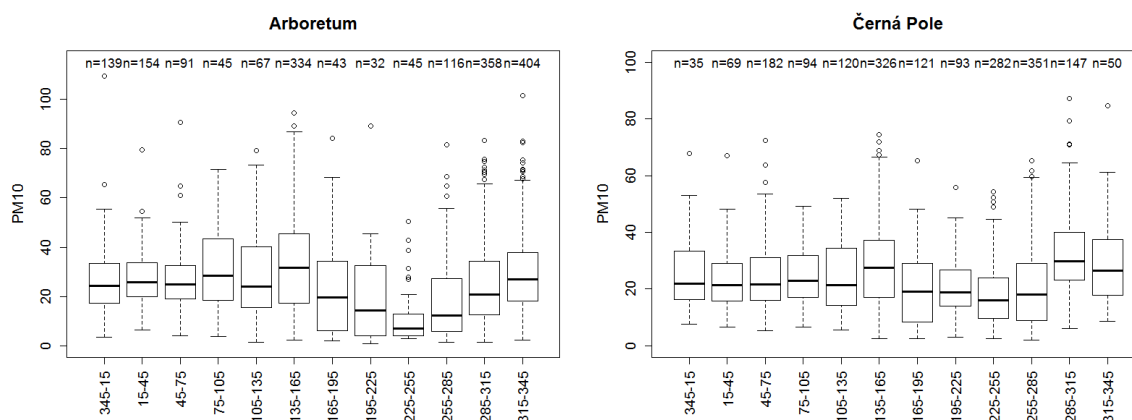


**Figure 8.** Boxplots of  $\text{PM}_{10}$  according to wind directions,  $\text{PM}_{10}$  in  $\mu\text{g}\cdot\text{m}^{-3}$ .  $n$ —the number of observations.

#### 4. Discussion

The analysis of the results of parallel measurements obtained at two stations that are 560 m from each other and located in the northern parts of Brno City showed that the monitored levels of  $\text{PM}_{10}$  vary considerably between the locations; at the Arboretum station, which lies in an open area in a park, as well as at the Černá Pole station, which is placed on a campus and surrounded by low-rise buildings. A comparison of the relative frequencies of exceeding the level of  $50 \mu\text{g}\cdot\text{m}^{-3}$  was performed. From the statistical point of view, these frequencies differed significantly between the stations; at the Černá Pole station, the frequencies of exceeding set limits were significantly lower than at the Arboretum station. Thus, the significant differences between the levels of measurement of PM values at both stations are influenced mainly by the built-up area geometry.

A comparison of parallel measurements using the Passing–Bablok test also showed that the values of air pollution caused by  $\text{PM}_{10}$  measured at the Černá Pole station surrounded by low-rise buildings were lower than those monitored in the open-area of the Arboretum station. Whereas at the Arboretum station,  $\text{PM}_{10}$  pollution levels increased by  $10 \mu\text{g}\cdot\text{m}^{-3}$ , at the Černá Pole station, they grew on average only by  $8.02 \mu\text{g}\cdot\text{m}^{-3}$ .

Based on the results of the correlation analysis between the values of  $\text{PM}_{10}$  and  $\text{NO}_x$ , it can be stated that there is a statistical link between the monitored variables. Spearman's correlation coefficient for the Arboretum station was significantly higher than for the Černá Pole station. The Passing–Bablok test applied to  $\text{NO}_x$  values then showed that the pollution levels for the monitored stations were not the same. The  $\text{NO}_x$  values from the Černá Pole station were lower than at the Arboretum station, by approximately  $8.2 \mu\text{g}\cdot\text{m}^{-3}$ . The results show the effect of built-up geometry on the level of pollution.  $\text{PM}_{10}$  and  $\text{NO}_x$  values were higher for the Arboretum station located in a park near a busy street than for Černá Pole located in a built-up area. The obtained results correspond to the conclusions published, e.g., in [22].

During the analyses of hourly data on air pollution caused by  $\text{PM}_{10}$ , the presented statistical models proved that  $\text{PM}_{10}$  air pollution is influenced, above all, by temperature change; i.e., first, by

its drop with a two hour delay, then by its rise in the next hour. At the Arboretum station, humidity change did not prove to be a statistically significant parameter; however, at the Černá Pole station, quite the contrary was the case. A positive value of the regression parameter 0.011, which was statistically significantly different from zero for the Černá Pole station, indicates an average increase of the  $PM_{10}$  value due to an average hourly increase of humidity. The rush hour influenced the  $PM_{10}$  increase at both stations significantly. From 7 to 10 AM and from 3 to 5 PM, the model identified rising levels of  $PM_{10}$ . When the parameters of both models were compared (see Table 4 and the results of the parameter comparisons), they showed no statistically significant differences, with the exception of the parameter  $\beta_1$ , which was equal to 0.593 for the Arboretum station and only 0.241 for the Černá Pole station, as well as with the exception of the  $\beta_2$  parameter for the lagged square root of  $PM_{10}$  value, which was equal to 0.878 for the Arboretum station and 0.946 for the Černá Pole station. This proves that both models function similarly, but on the campus where the Černá Pole station is located,  $PM_{10}$  levels were lower. Two stations, where the measurements were performed, are located close to each other, at a distance of 560 m. Nevertheless, it was statistically proven that the level of pollution was significantly different at both stations. This evidence was demonstrated by all statistical methods used (robust Passing–Bablok test, regression analysis, statistical test for comparison of frequencies, analysis of variance). Due to the fact that the level of PM values in a given place is influenced by climatic factors (especially the effect of wind speed and direction is significant) and these factors are significantly affected by the built-up area geometry, the effect of built-up area geometry will also affect the level of pollution caused by  $PM_{10}$  particles. Such an influence was studied also in other works, for example in [21,22] or [23], and it should be paid a great deal of attention.

Wind speed and direction with regard to distance from roads with heavy traffic proved to be of paramount importance as far as  $PM_{10}$  air pollution in the studied area is concerned. In the case of the Arboretum station, the heaviest pollution with a mean value of  $32.2 \mu\text{g}\cdot\text{m}^{-3}$  comes from the direction of 135–165 degrees; that is where the thoroughfare with the most intensive traffic is located. The relative frequency of winds coming from this direction is 0.183. The second wind direction that sends the highest pollutant volumes to this station is at 75–105 degrees. In this direction, there is Road No. 42 with the 43/11 traffic volume, part of which is hidden in a tunnel. Nonetheless, the relative frequency of winds coming from this direction is only 0.025, and the mean pollution value resulting from this direction is  $31.5 \mu\text{g}\cdot\text{m}^{-3}$ . The third wind direction, which brings air pollution levels with a mean value of  $29.1 \mu\text{g}\cdot\text{m}^{-3}$ , falls within the range of 315–345 degrees. In this case, the pollution comes from a northwestern traffic hub and Ring Road No. 42. The relative frequency of winds coming from this direction is 0.221, which is the highest value among these three sections. On the contrary, the lowest pollution levels with the mean value of  $18.2 \mu\text{g}\cdot\text{m}^{-3}$  come from the range of 165–285 degrees; the frequency of winds coming from this direction is 0.129. This is a direction with no nearby busy traffic roads; in this specific area, parks and a large football stadium are located.

As far as the Černá Pole mobile station located on the University of Defence campus is concerned, air pollutants get here mainly due to winds coming from the direction falling into the range of 285–315 degrees. In this case, the mean value of  $PM_{10}$  pollution is equal to  $32.6 \mu\text{g}\cdot\text{m}^{-3}$ ; the relative frequency of winds coming from this direction is 0.079. The second highest mean value of air pollution, which amounted to  $29.8 \mu\text{g}\cdot\text{m}^{-3}$ , was found in the direction falling in the range of 315–345 degrees. The relative frequency of winds coming from this direction is only 0.027. It can be concluded that winds coming from these two directions bring air pollutants from a ring road with a 47/12 to 48/12 traffic volume that is located approximately 0.5–0.8 km away from the monitoring station. The third highest amount of air pollutants with the mean value of  $28.2 \mu\text{g}\cdot\text{m}^{-3}$  comes from the section of 135–165 degrees. This is the direction where the thoroughfare with the largest traffic volumes amounting to 40/9 (Road No. 42) and 74/31 (D1-E50 highway) is located. The relative frequency of winds coming from this direction is 0.174. In the case of the open-area Arboretum station, this direction was the source of the highest amount of air pollutants.

On the contrary, the lowest pollution levels with the mean value of  $19.3 \mu\text{g}\cdot\text{m}^{-3}$  come from the range of 165–285 degrees, which is the same for the Arboretum station. The relative frequency of winds coming from this direction is high and equals 0.453. This also explains the lower pollution levels monitored using hourly measurements at this station, because the spaces between buildings are positioned approximately in this direction, which is related to the lowest levels of air pollution. Furthermore, this proves that pollution levels and their variability in urban areas are strongly influenced by built-up area geometry, consequential traffic volume, and the values of local meteorological variables. Parallel measurements carried out for the purpose of this article using two nearby monitoring stations strongly confirmed this fact.

The models of  $\text{PM}_{10}$  described in the articles [23–26] used daily data. As in this article, they were based mainly on meteorological factors. However, the specific regressors and model types used are not completely comparable to the model Equation (3). From the point of view of the accuracy of the predicted  $\text{PM}_{10}$  values, the proposed model Equation (3) shows a higher accuracy. The primary objective of this article was to assess the effect of built-up geometry. The authors in [23–26] did not address this issue. For technical reasons, measurements could only be performed in the period 2 February to 20 April 2019. In view of the fact that for another period, the data could be described by an analogous model (see [23]) as the model Equation (3), the time interval to illustrate the effect of built-up geometry is considered sufficient.

## 5. Conclusions

The authors of this paper showed that when assessing  $\text{PM}_{10}$  air pollution in densely populated urban areas with high traffic volumes, it is necessary to consider built-up area geometry and the related dispersion conditions of the specific area. The results obtained using two nearby monitoring stations serve as a proof of this claim. This line of reasoning works also as the foundation stone for joint research activities carried out by members of the University of Defence in Brno, Czech Republic, and experts who focus on air pollution with regard to built-up area geometry.

In connection with this research, further research activities are expected in order to improve the current methods of evaluating data on measured  $\text{PM}_{10}$  concentrations. The authorities dealing with the issue of air quality in the City of Brno have already shown interest in this research. Existing methods can be innovated in the future by spatio-temporal predictions of air pollution with regard to accompanying factors (meteorological and urban). New methods should take into account the presence of selected organic compounds in the air, which are indicators of toxicity or markers of emission sources. For emission sources, it will be useful to deal with the possibilities of the unambiguous identification and quantification of the impact of the main emission sources in the monitored area.

The above-mentioned results may be applied not only when assessing pollution levels in large urban areas, but also for the purpose of selecting military deployment areas in foreign territory. If it is possible to choose the location of the military base where the military forces are to be deployed, at least the long-term average values of meteorological variables in the area and the location of major pollution sources should be taken into consideration. This way, it may be possible to reduce health risks related to long-term exposure to dust particles.

**Author Contributions:** Conceptualization, J.M. and J.N.; methodology, J.M. and J.N. ; software, J.N.; validation, J.M., J.N., and P.F.; formal analysis, J.N. and J.M.; investigation, K.Š., J.M., and J.N.; resources, K.Š.; data curation, J.N. and K.Š.; writing, original draft preparation, J.M., J.N., P.F., and K.Š.; writing, review and editing, J.M. and J.N.; visualization, J.N. and K.Š.; supervision, J.M. and P.F.; project administration, J.N. and K.Š.; funding acquisition, K.Š. All authors read and agreed to the published version of the manuscript.

**Funding:** This article was supported by the Czech Republic Ministry of Defence—Faculty of Military Leadership of University of Defence development program “Advanced Automated Command and Control System II”.

**Acknowledgments:** The authors would like to thank Brno City Municipality for effective cooperation in terms of setting up the mobile monitoring station and for the provision of the data; namely Ing. Martin Vaněček, head of the Environmental Protection Division of Brno City Municipality, and the staff of this department, Bc. Radek

Kronovet, and Ing. Karel Šplíchal. The authors also appreciate that Brněnské komunikace (BKOM), a municipal organization, monitors yearly traffic volumes, which enabled them to correlate the obtained air pollution data with professionally gathered data on road traffic in Brno City. The authors would also like to thank the anonymous referees for their reviews and constructive comments.

**Conflicts of Interest:** The authors declare no conflict of interest. The funders had no role in the designing of the study; in the collection, analyses, or interpretation of the data; in the writing of the manuscript; nor in the decision to publish the results.

## References

1. Pope, C.A.; Dockery, D.W. Health effects of fine particulate air pollution: Lines that connect. *J. Air Waste Manag. Assoc.* **2006**, *56*, 709–742. [[CrossRef](#)]
2. Abrutzky, R.; Dawidowski, L.; Matus, P.; Lankao, P.R. Health effects of climate and air pollution in Buenos Aires: A first time series analysis. *J. Environ. Prot.* **2012**, *3*, 262–271. [[CrossRef](#)]
3. Restrepo, C.E.; Simonoff, J.S.; Thurston, G.D.; Zimmerman, R. Asthma hospital admissions and ambient air pollutant concentrations in New York City. *J. Environ. Prot.* **2012**, *3*, 1102–1116. [[CrossRef](#)]
4. EC (European Council). 1999/39/EC Directive of 22 April 1999 relating to limit values for sulphur dioxide, nitrogen dioxide and oxides of nitrogen, particulate matter and lead in ambient air. *Off. J. Eur. Communities* **1999**, *L 163*, 0041–0060.
5. Li, Y.; Chen, Q.; Zhao, H.; Wang, L.; Tao, R. Variations in PM<sub>10</sub>, PM<sub>2.5</sub> and PM<sub>1.0</sub> in an Urban Area of the Sichuan Basin and Their Relation to Meteorological Factors. *Atmosphere* **2015**, *6*, 150–163. [[CrossRef](#)]
6. Dung, N.A.; Son, D.H.; Hanh, N.T.D.; Tri, D.Q. Effect of Meteorological Factors on PM<sub>10</sub> Concentration in Hanoi, Vietnam. *J. Geosci. Environ. Prot.* **2019**, *7*, 137–150. [[CrossRef](#)]
7. Hörmann, S.; Pfeiler, B.; Stadlober, E. Analysis and prediction of particulate matter PM<sub>10</sub> for the winter season in Graz. *Austrian J. Stat.* **2005**, *34*, 307–326.
8. Stadlober, E.; Hörmann, S.; Pfeiler, B. Quality and performance of a PM<sub>10</sub> daily forecasting model. *Atmos. Environ.* **2008**, *42*, 1098–1109. [[CrossRef](#)]
9. Al-Hemoud, A.; Al-Dousari, A.; Al-Shatti, A.; Al-Khayat, A.; Behbehani, W.; Malak, M. Health Impact Assessment Associated with Exposure to PM<sub>10</sub> and Dust Storms in Kuwait. *Atmosphere* **2018**, *9*, 6. [[CrossRef](#)]
10. Enkhjargal, A.; Oyun-Erdene, O.; Burmaajav, B.; Tsegmed, S.; Suvd, B.; Norolkhoosuren, B.; Unurbat, D.; Batbayar, J.; Narantuya, D.; Enkhtuya, P. Short Term Impact of Air Pollution on Asthma Admission in Ulaanbaatar. *Occup. Dis. Environ. Med.* **2020**, *8*, 64–78. [[CrossRef](#)]
11. Lelieveld, J.; Klingmüller, K.; Pozzer, A.; Pöschl, U.; Fnais, M.; Daiber, A.; Münzel, T. Cardiovascular disease burden from ambient air pollution in Europe reassessed using novel hazard ratio functions. *Eur. Heart J.* **2019**, *40*, 1590–1596. [[CrossRef](#)]
12. Giannakis, E.; Kushta, J.; Giannadaki, D.; Georgiou, G.K.; Brüggeman, A.; Lelieveld, J. Exploring the economy-wide effects of agriculture on air quality and health: Evidence from Europe. *Sci. Total Environ.* **2019**, *663*, 889–900. [[CrossRef](#)]
13. Kushta, J.; Pozzer, A.; Lelieveld, J. Uncertainties in estimates of mortality attributable to ambient PM<sub>2.5</sub> in Europe. *Environ. Res. Lett.* **2018**, *13*, 064029. [[CrossRef](#)]
14. Pozzer, A.; Bacer, S.; Sappadina, S.D.Z.; Predicatori, F.; Caleffi, A. Longterm concentrations of fine particulate matter and impact on human health in Verona, Italy. *Atmos. Pollut. Res.* **2019**, *10*, 731–738. [[CrossRef](#)]
15. Lelieveld, J.; Haines, A.; Pozzer, A. Age-dependent health risk from ambient air pollution: a modelling and data analysis of childhood mortality in middle-income and low-income countries. *Lancet Planet. Health* **2018**, *2*, 292–300. [[CrossRef](#)]
16. Lelieveld, J.; Klingmüller, K.; Pozzer, A.; Burnett, R.T.; Haines, A.; Ramanathan, V. Effects of fossil fuel and total anthropogenic emission removal on public health and climate. *Proc. Natl. Acad. Sci. USA* **2019**, *116*, 7192–7197. [[CrossRef](#)]
17. Wu, X.; Nethery, R.C.; Sabath, B.M.; Braun, D.; Dominici, F. Exposure to air pollution and COVID-19 mortality in the United States. *medRxiv* **2020**, *42*. [[CrossRef](#)]
18. Alam, M.S.; McNabola, A. Exploring the modeling of spatiotemporal variations in ambient air pollution within the land use regression framework: Estimation of PM<sub>10</sub> concentrations on a daily basis. *J. Air Waste Manag. Assoc.* **2015**, *65*, 628–640. [[CrossRef](#)]

19. Shahraiyini, H.T.; Sodoudi, S. Statistical Modeling Approaches for PM10 Prediction in Urban Areas, A Review of 21st-Century Studies. *Atmosphere* **2016**, *7*, 15. [CrossRef]
20. Liu, H.Y.; Schneider, P.; Haugen, R.; Vogt, M. Performance Assessment of a Low-Cost PM2.5 Sensor for a near Four-Month Period in Oslo, Norway. *Atmosphere* **2019**, *10*, 41. [CrossRef]
21. Bulejko, P.; Adamec, V.; Skeřil, R.; Schüllerová, B.; Bencko, B. Levels and Health Risk Assessment of PM10 Aerosol in Brno, Czech Republic. *Cent. Eur. J. Public Health* **2017**, *25*, 129–134. [CrossRef]
22. Pospisil, P.; Huzlik, J.; Licbinsky, R.; Spilacek, M. Dispersion Characteristics of PM10 Particles Identified by Numerical Simulation in the Vicinity of Roads Passing through Various Types of Urban Areas. *Atmosphere* **2020**, *11*, 454. [CrossRef]
23. Hrdličková, Z.; Michálek, J.; Kolář, M.; Veselý, V. Identification of factors affecting air pollution by dust aerosol PM10 in Brno City, Czech Republic. *Atmos. Environ.* **2008**, *42*, 8661–8673. [CrossRef]
24. Veselý, V.; Tonner, J.; Hrdličková, Z.; Michálek, J.; Kolář, M. Analysis of PM10 air pollution in Brno based on generalized linear model with strongly rank-deficient design matrix. *Environmetrics* **2009**, *20*, 676–698. [CrossRef]
25. Stadlober, E.; Hübnerova, Z.; Michálek, J.; Kolář, M. Forecasting of Daily PM10 Concentrations in Brno and Graz by Different Regression Approaches. *Austrian J. Stat.* **2012**, *41*, 287–310. [CrossRef]
26. Hübnerova, Z.; Michálek, J. Analysis of daily average PM10 prediction by generalized liner model in Brno. Czech Republic. *Atmos. Pollut. Res.* **2014**, *5*, 471–476. [CrossRef]
27. Newcombe, R.G. Two-Sided Confidence Intervals for the Single Proportion: Comparison of Seven Methods. *Stat. Med.* **1998**, *17*, 857–872. [CrossRef]
28. Passing, H.; Bablok, W. A New Biometrical Procedure for Testing the Equality of Measurements from Two Different Analytical Methods. Application of Linear Regression Procedures for Method Comparison Studies in Clinical Chemistry, Part I. *J. Clin. Chem. Clin. Biochem.* **1983**, *21*, 709–720. [CrossRef]
29. Searle, S.R. *Linear Models*; Wiley: New York, NY, USA, 1971.
30. Fahrmeir, L.; Tutz, G. Generalized autoregressive linear model. In *Multivariate Statistical Modelling Based on Generalized Linear Models*; Springer: New York, NY, USA, 1994; pp. 23–24.
31. R Core Team. *R: A Language and Environment for Statistical Computing*; R Foundation for Statistical Computing: Vienna, Austria, 2020. Available online: <https://www.R-project.org/> (accessed on 30 January 2020).
32. Carslaw, D.C.; Ropkins, K. Openair—An R package for air quality data analysis. *Environ. Model. Softw.* **2012**, *27–28*, 52–61. [CrossRef]
33. Hyndman, R.; Athanasopoulos, G.; Bergmeir, C.; Caceres, G.; Chhay, L.; O’Hara-Wild, M.; Petropoulos, F.; Razbash, S.; Wang, E.; Yasmeen, F. Forecast: Forecasting Functions for Time Series and Linear Models. R package Version 8.12, Software, R package. 2020. Available online: <http://pkg.robjhyndman.com/forecast> (accessed on 10 February 2020).
34. Manuilova, E.; Schuetzenmeister, A. mcr: Method Comparison Regression. R Package Version 1.2.1, Software, R Package. 2014. Available online: <https://CRAN.R-project.org/package=mcr> (accessed on 10 February 2020).
35. Venables, W.N.; Ripley, B.D. *Modern Applied Statistics with S*, 4th ed.; Springer: New York, NY, USA, 2002.
36. John Fox, J.; Weisberg, S. *An R Companion to Applied Regression*, 3rd ed.; Sage: Thousand Oaks, CA, USA, 2019. Available online: <https://socialsciences.mcmaster.ca/jfox/Books/Companion/> (accessed on 15 February 2020).
37. Mikuška, P.; Vojtěšek, M.; Křůmal, K.; Mikušková-Čampulová, M.; Michálek, J.; Večeřa, Z. Characterization and Source Identification of Elements and Water-Soluble Ions in Submicrometre Aerosols in Brno and Šlapanice (Czech Republic). *Atmosphere* **2020**, *11*, 688. [CrossRef]



© 2020 by the authors. Licensee MDPI, Basel, Switzerland. This article is an open access article distributed under the terms and conditions of the Creative Commons Attribution (CC BY) license (<http://creativecommons.org/licenses/by/4.0/>).



Article

# High Resolution Air Quality Forecasting Over Prague within the URBI PRAGENSI Project: Model Performance During the Winter Period and the Effect of Urban Parameterization on PM

Jana Ďoubalová <sup>1,2,\*</sup> , Peter Huszár <sup>2</sup>, Kryštof Eben <sup>3</sup>, Nina Benešová <sup>1</sup>, Michal Belda <sup>2</sup>, Ondřej Vlček <sup>1</sup>, Jan Karlický <sup>2,4</sup>, Jan Geletič <sup>3</sup> and Tomáš Halenka <sup>2</sup>

<sup>1</sup> Czech Hydrometeorological Institute, Na Šabatce 17, 14306 Prague 4, Czech Republic; nina.benesova@chmi.cz (N.B.); ondrej.vlcek@chmi.cz (O.V.)

<sup>2</sup> Department of Atmospheric Physics, Faculty of Mathematics and Physics, Charles University, V Holešovičkách 2, 180 00 Prague 8, Czech Republic; peter.huszar@mff.cuni.cz (P.H.); michal.belda@mff.cuni.cz (M.B.); jan.karlicky@mff.cuni.cz (J.K.); tomas.halenka@mff.cuni.cz (T.H.)

<sup>3</sup> Institute of Computer Science of the Czech Academy of Sciences, Department of Complex Systems, Pod Vodárenskou věží 271/2, 182 07 Prague 8, Czech Republic; eben@cs.cas.cz (K.E.); geletic@cs.cas.cz (J.G.)

<sup>4</sup> Institute of Meteorology and Climatology, Department of Water, Atmosphere and Environment, University of Natural Resources and Life Sciences, Vienna, Gregor-Mendel-Straße 33, 1180 Vienna, Austria, jan.karlicky@mff.cuni.cz

\* Correspondence: jana.doubalova@chmi.cz

Received: 30 April 2020; Accepted: 5 June 2020; Published: 12 June 2020



**Abstract:** The overall impact of urban environments on the atmosphere is the result of many different nonlinear processes, and their reproduction requires complex modeling approaches. The parameterization of these processes in the models can have large impacts on the model outputs. In this study, the evaluation of a WRF/Comprehensive Air Quality Model with Extensions (CAMx) forecast modeling system set up for Prague, the Czech Republic, within the project URBI PRAGENSI is presented. To assess the impacts of urban parameterization in WRF, in this case with the BEP+BEM (Building Environment Parameterization linked to Building Energy Model) urban canopy scheme, on Particulate Matter (PM) simulations, a simulation was performed for a winter pollution episode and compared to a non-urbanized run with BULK treatment. The urbanized scheme led to an average increase in temperature at 2 m by 2 °C, a decrease in wind speed by 0.5 m s<sup>-1</sup>, a decrease in relative humidity by 5%, and an increase in planetary boundary layer height by 100 m. Based on the evaluation against observations, the overall model error was reduced. These impacts were propagated to the modeled PM concentrations, reducing them on average by 15–30 µg m<sup>-3</sup> and 10–15 µg m<sup>-3</sup> for PM<sub>10</sub> and PM<sub>2.5</sub>, respectively. In general, the urban parameterization led to a larger underestimation of the PM values, but yielded a better representation of the diurnal variations.

**Keywords:** air pollution; emissions; urban canopy; weather prediction; particulate matter; validation

## 1. Introduction

The increasing urban population worldwide requires elaborate scientific action to estimate the human exposure to different adverse effects that cities cause [1]. It is now well known that probably the most “far-reaching” impact that cities have on the environment is that on the atmosphere [2].

Urban areas impact the atmosphere by two main pathways: they have a strong impact on meteorological conditions, which results in the formation of, e.g., Urban Heat Islands (UHI), and they are, at the same time, intense concentrated emission sources, having great impacts on the local and

regional (and even global) air quality [3,4] with (although minor) consequences even on the regional radiative balance and, hence, temperatures [5]. Given the complexity and non-linear nature of chemical transformations of primary emissions forming secondary species, modeling approaches are essential to describe the city-scale air quality conditions and their footprints over a regional scale. Such modeling approaches have to describe both the local and regional meteorological conditions [6,7], the actual impact of urban emissions and those from surrounding areas on regional air quality [4,8,9], and their mutual interaction [10].

One of the major steps to properly describe the city- and regional-scale weather conditions over cities in regional scale models is the application of urban canopy (sub)models that parameterize the subscale processes that occur on street level or within buildings, but have important feedback to the model-resolvable scales [11,12]. It has been shown in many studies that the way the urban canopy and related meteorological effects are treated in models has important consequences on the concentrations of modeled species (e.g., [13–17]). This is not surprising given the fact that the transport, diffusion, deposition, and chemical transformation of pollutants (driven by the Eulerian continuity equation) are strongly dependent on meteorological conditions [18].

In particular, urban surfaces increase the air temperature, which, in turn, increases the chemical reaction rates and also the dry deposition and leads to a decrease of ozone in urban areas [13,16]. Increased temperatures in the urban canopy layer further decrease the atmospheric stability in urban areas, potentially leading to urban-breeze circulation [19–21]. The decrease of city-scale wind speeds results in limited horizontal dispersion of pollutants, which, alone, leads to elevated concentrations of primary species, especially  $\text{NO}_x$  and primary aerosol [16,17,22,23]. Finally, the drag that causes the decrease of urban winds enhances turbulence, which is further increased by the buoyant forces (due to an increase of near-surface temperature), resulting in a great increase of vertical eddy diffusion. Increased eddy diffusion helps to remove species from the urban canopy and reduces the concentrations of primary species as shown by [16,17,24–27]. The consequences for ozone as a secondary species are however opposite. By removing  $\text{NO}_x$  from the urban canopy by enhanced turbulence, ozone titration is reduced, leading to elevated ozone levels [26]. The large impact of the modifications of vertical turbulent diffusion on ozone levels was assessed also by Tang et al. [28]. In general, turbulence is considered to be the most important component via which the urban canopy meteorological effects act on chemistry. The overall impact, viewed as a combination of temperature, wind, and turbulence changes, is very similar to that of turbulence changes alone [29].

According to the above-mentioned facts, it is very important to analyze the sensitivity of concentrations of the modeled urban species to the numerical representation of urban land use. In two extreme cases, urban areas can either be completely ignored by the model or fully represented by an urban canopy parameterization (as done, e.g., in [16,17]), but many intermediate treatments can be considered, e.g., the BULK approach, which takes urban surfaces into account as any other flat surface with specific physical parameters (e.g., albedo), as done in [7]. The response of urban air chemistry is dependent on the urban parameterizations chosen (e.g., [24,30]) and on the settings of various parameters that describe the urban environment like the albedo of urban surfaces, their heat conductivity, the geometry of the urban setting, etc. [15].

In the Czech Republic, the capital city Prague belongs to a region with worsened air quality. This can be attributed to several factors. One important factor is the topography. The Prague basin, where the city is located, negatively affects the climatic conditions and dispersion of pollutants. During colder periods of the year, temperature inversions are often formed, leading to the accumulation of pollution. The most problematic pollutants, mainly due to heavy traffic in the city and residential heating in the suburban areas, are  $\text{NO}_2$  (nitrogen dioxide),  $\text{PM}_{10}$  (particulate matter of a diameter  $r < 10 \mu\text{m}$ ) and  $\text{PM}_{2.5}$  (particulate matter of a diameter  $r < 2.5 \mu\text{m}$ ), often exceeding the limit values or leading to smog situations [31]. In particular, in January and February 2017, the threshold values of  $\text{PM}_{10}$  for announcing a smog situation were exceeded three times. In the middle of January, even the criteria for announcing a regulation were fulfilled [32]. The ability of models to capture these

extreme pollution episodes correctly is especially important with regards to predicting similar events and proposing effective regulation measures.

Within the URBI PRAGENSI project supported by the Operational Programme Prague–Growth Pole of the Czech Republic (European structural and investment funds), a weather/air quality forecast system for Central Europe was set up at Charles University with high resolution nested predictions for the Czech capital Prague. These forecasts aimed to support fast action of the city council authorities if a significant worsening of air quality is predicted over the city. In order to increase the reliability and quality of the forecasts, multiple configurations have to be tested, and one of the key parts is the numerical treatment of the urbanization-induced meteorological changes (like UHI).

To fulfill this goal, we present here a study that aims to investigate to what extent the urban canopy treatment in the driving meteorological models influences the final species concentrations in the driven chemistry transport model. The basis of this study is a pair of weather prediction configurations of the WRF (Weather Research and Forecasting) Model and the consequent chemistry transport model predictions. Our focus will be a winter period with stagnant conditions, limited mixing, and very strong PM pollution.

## **2. Methods**

### *2.1. Models and Data*

#### **2.1.1. WRF**

Meteorological variables required as inputs of the CAMx (Comprehensive Air Quality Model with Extensions) model or needed for emission pre-processing were obtained from weather forecast simulations performed with the WRF Model. WRF is a non-hydrostatic regional-scale numerical weather prediction and climate model developed to be able to simulate weather phenomena across multiple scales from the global to the city scale [33]. The WRF Model Version 4.0.3 was run in two configurations; here, the common parts are detailed. For radiation calculations, the Rapid Radiative Transfer Model for General Circulation Models (RRTMG [34]) was used. Land-surface processes were solved by the Noah land-surface model [35]. Microphysical transformations of water were treated by the improved BULK Thompson scheme [36]. For the calculation of the Planetary Boundary Layer (PBL) turbulent exchange, the Boulac PBL [37] scheme was used.

The urban canopy effects could be treated with the simple BULK approach that considers urban surfaces as flat ones with prescribed physical parameters like albedo, roughness, etc. A more comprehensive approach is offered by the multi-layer Building Environment Parameterization (BEP; [38]) linked to the Building Energy Model (BEM; [39]), the BEP+BEM method.

#### **2.1.2. CAMx**

Air quality simulations were performed with the Chemistry Transport Model (CTM) CAMx Version 6.50 [40]. As an Eulerian photochemical CTM, CAMx implements multiple gas phase chemistry options (Carbon Bond chemical mechanisms: CB5, CB6; The Statewide Air Pollution Research Center chemical mechanism: SAPRC07TC). In this study, the CB5 scheme [41] was used. The static two-mode approach was used to treat particle matter physics. Dry deposition was solved using the method of Zhang et al. [42], and for wet deposition, the Seinfeld and Pandis [43] scheme was used. To calculate the composition and phase state of the ammonia-sulfate-nitrate-chloride-sodium-water inorganic aerosol system in equilibrium with gas phase precursors, the ISORROPIA thermodynamic equilibrium model was activated [44]. To compute the Secondary Organic Aerosol (SOA) chemistry, the semi-volatile equilibrium scheme SOAP (Secondary Organic Aerosol Processor) [45] was invoked.

CAMx was coupled offline to WRF, meaning that CAMx was run once WRF predictions were ready. To translate the WRF output to CAMx input fields, the WRFCAMx preprocessor which is provided along with the CAMx source code was used (see <http://www.camx.com/download/>

[support-software.aspx](#)). WRF-CAMx takes the WRF output fields and writes them to the CAMx input format. For those CAMx input variables that were not provided in the WRF output, diagnostic methods were used. A key input for CAMx that drives the vertical transport of pollutants is the coefficient of vertical turbulent diffusion ( $K_v$ ).  $K_v$  is of great importance in determining urban air pollution, and it is substantially perturbed by urban land use [29]. In this study, the method used in CMAQ (Community Multiscale Air Quality Modeling System) was adopted to calculate the  $K_v$  values. The “CMAQ” scheme [46] applies the similarity theory for different stability regimes of the boundary layer. The stability regime was determined using the dimensionless ratio of the height above the ground and the Monin–Obukhov length.

Dry deposition velocities in CAMx do not directly depend on the  $K_v$  values provided in CAMx inputs. Instead, for the aerodynamic resistance calculation (used for diffusion through the first model layer to the ground), the Louis [47] scheme was used based on the solar insolation, wind speed, surface roughness, and near-surface temperature lapse rate.

### 2.1.3. Emissions

Anthropogenic emissions corresponding to 2015, if not mentioned otherwise, were used. For the Czech Republic, the high resolution national Register of Emissions and Air Pollution Sources (REZZO—Registr emisí a zdrojů znečištění ovzduší) dataset issued by the Czech Hydrometeorological Institute (<http://www.chmi.cz>) was used. This inventory was completed with unreported fugitive emissions corresponding to 2017: production of coke, iron, and steel (all sources located in the Agglomeration of Ostrava/Karviná/Frýdek-Místek, near the border with Silesia), smelting works (located in the whole territory of the Czech Republic), other fugitive sources in the Agglomeration of Ostrava/Karviná/Frýdek-Místek, and fugitive emissions from quarries (whole territory of the Czech Republic). Detailed road transport emissions based on the traffic census of 2016, as well as emissions from Václav Havel Airport Prague for 2016 were prepared by ATEM (Ateliér ekologických modelů—Studio of ecological models; <http://www.atem.cz>).

For Poland, high-resolution emissions were provided by the authorities of GIOS (Główny Inspektorat Ochrony Środowiska) and KOBiZE (Krajowy Ośrodek Bilansowania i Zarządzania Emisjami) within the LIFE-IP MAŁOPOLSKA project (LIFE14 IPE/PL/000021; <https://powietrze.malopolska.pl/en/life-project/>). For Slovakia, detailed residential heating emissions and point sources that belong to Selected Nomenclature for sources of Air Pollution (SNAP) 2 were provided by the Slovak Hydrometeorological Institute. For remaining regions and sectors, the top-down CAMS (Copernicus Atmosphere Monitoring Service) European anthropogenic emissions (CAMS-REG-AP v1.1; Regional—Atmospheric Pollutants; [48]) were used. The mentioned emission sources contained annual emission totals of the main pollutants, namely nitrogen oxides ( $\text{NO}_x$ ), sulfur dioxide ( $\text{SO}_2$ ), carbon monoxide (CO), ammonia ( $\text{NH}_3$ ), Non-Methane Volatile Organic Compounds (NMVOC), and particulate matter ( $\text{PM}_{10}$  and  $\text{PM}_{2.5}$ ).

The Czech REZZO and ATEM, as well as Polish and Slovak datasets were defined as area, point, and line (for road transportation) shapefiles of irregular shapes corresponding to counties, major sources (e.g., chimney stacks), and roads, while the CAMS data were provided as area and point sources on a regular grid. These raw emissions were processed using the Flexible Universal Processor for Modeling Emissions (FUME) emission model ([49]; <http://fume-ep.org/>). FUME is intended primarily for the preparation of emission files ready-to-use in CTMs. FUME is thus responsible for the preprocessing of the raw input files and the spatial redistribution, chemical speciation, and temporal disaggregation of input emissions. Emissions are provided in 11 SNAP activity sectors. Sector-specific NMVOC speciation was based on Passant [50] and  $\text{PM}_{2.5}$  speciation on country- and sector-specific profiles provided with the CAMS data. For the vertical distribution of emissions from CAMS point sources, typical point source parameters based on the analysis of the data from the Czech database REZZO were used. Time-disaggregation factors [51,52] were applied to the spatially redistributed emissions to derive hourly emission data for CAMx. Biogenic emissions

of hydrocarbons (BVOC—Biogenic Volatile Organic Compounds) and NO were calculated based on WRF meteorological data using the MEGANv2.1 emission model [53].

#### 2.1.4. Air Quality Stations: Meteorology and Pollutants

For the evaluation of the models, validated in situ measurements from air quality stations in Prague were used (Figure 1) [31]. These stations provide measurements of both air pollutant concentrations and meteorological data. In particular, PM<sub>10</sub> and PM<sub>2.5</sub> concentrations, Temperature at 2 m (T2), Wind Speed (WS), and Relative Humidity (RH) were acquired. Eight background urban and background suburban stations were considered for the air pollutants, while the meteorological observations from two available suburban stations were used. All the data were acquired from the Air Quality Information System database of the Czech Hydrometeorological Institute.

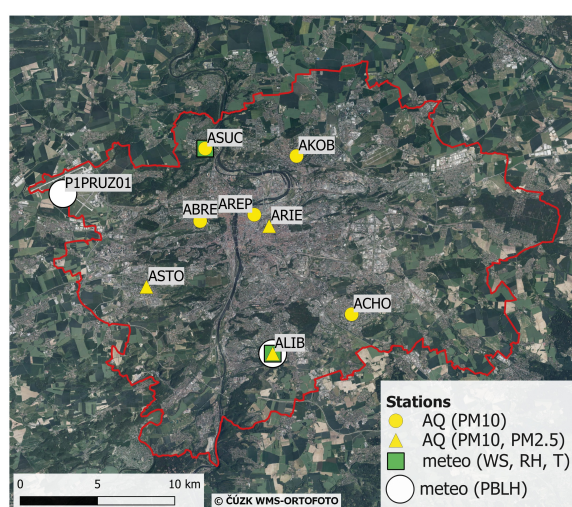


**Figure 1.** The locations of the observation sites in Prague used for evaluation of Air Quality (AQ) and meteorological (meteo) results. The labels show the code name of each station.

#### 2.1.5. PBL Height Retrieval from Ceilometers

The planetary boundary layer heights (PBLHs) were retrieved from ceilometers at two suburban locations in Prague (Figure 1). The instruments used were Vaisala CL31 and CL51 ceilometers, which use pulsed diode laser LIDAR (Light Detection And Ranging) technology [54,55]. The ceilometers give three candidates for the PBLH at 16-s intervals during the entire day. Each candidate is automatically assigned a quality index, ranging from 1 (worst candidate) to 3 (best candidate; for further details, see [56]). For the purpose of this study, the best candidate for the PBL within a certain hour was determined as the candidate with the highest sum of quality indices, and its height was calculated as an arithmetic hourly mean.

## 2.2. Experimental Setup

### 2.2.1. Model Configuration

WRF (Version 4.0.3) was run on three nested domains with horizontal resolutions of 9 km, 3 km, and 1 km, with  $173 \times 153$ ,  $169 \times 151$ , and  $84 \times 84$  grid points, respectively (Figure 2). In the vertical dimension, the model grid had 49 levels. The height of the lowermost level was about 48–50 m (depending on the temperature of the corresponding layer). The model top was at 50 mbar. In order to assess the impact of using an advanced setup of the WRF model on CAMx simulations, when urban canopy meteorological features were calculated more comprehensively (compared to

the default “non-urbanized” case), the WRF model was run in two configurations, which differed both in the parameterizations employed and in the regime in which the forecast was performed (see below). In both regimes, the WRF output data were collected from overlapping runs of 12 h in length, taking initial and boundary conditions from the GFS operational analyses and predictions at synoptic times of 00, 06, 12, and 18 UTC [57]. During the first six hours of each run, grid nudging of global analysis was performed, and this period served as a spin-up. The hourly outputs with prediction horizons of 7–12 of each run (four segments daily) were assembled into 24 hourly outputs per day and used for the generation of inputs for CAMx. In this way, we constructed a surrogate for local analysis and tried to eliminate the drift of WRF model fields from reality. The CAMx-ready meteorological input files were then produced with the WRFCAMx preprocessor.

The two WRF configurations mentioned are:

1. The “non-urbanized” configuration used the “BULK” (or SLAB) treatment of the urban land-surface. In the BULK treatment, the urban land-surface is regarded as any other flat surface with prescribed surface parameters (roughness, albedo, emissivity, etc.) representing zero-order effects of urban surfaces. It is clear that such an approach cannot fully resolve the 3D nature of the urban weather phenomenon (especially turbulence and radiation in street canyons [58]). The term “non-urbanized” here refers to the fact that these urban effects are largely ignored in the BULK approach. In this setup, there was no connection (restart) between any two successive 12 h runs described above, i.e., WRF adopted the so-called cold start concept [59].
2. The “urbanized” configuration of WRF had a more comprehensive treatment of the urban canopy. Instead of the BULK approach, the BEP+BEM urban canopy model was used (cf. 2.1.1). Moreover, significant changes to the land use data were made, resulting in more realistic values of variables describing the urban geometry and physical properties of surfaces (roofs, roads, walls), which influence the exchange between the urban canopy and the atmosphere. Since the state of the urban canopy submodel evolves in time, it was necessary to keep the continuity of its evolution throughout the simulation. Therefore, instead of a cold start as above, a restart was performed each 6 hours with the help of WRF’s restart capability. The restart files produced at the end of a run, needed for the restart of a successive simulation, were enriched with urban variables. Thus, the WRF run mimicked a longer term simulation, driven by analyses and keeping the continuous evolution of the variables that describe the physical state of the urban environment.

For both configurations, land cover information was taken from the high resolution (100 m) CORINE Land Cover (CLC) 2012 data (<https://land.copernicus.eu/pan-european/corine-land-cover>). For the Prague urban area, the values of the urban fraction and other urban parameters used by BEP+BEM were adopted from multiple high resolution data sources. Three land cover sources were combined into one spatially-resolved dataset: the Urban Atlas 2018 (Copernicus Land Monitoring Services, Urban Atlas; <https://land.copernicus.eu/local/urban-atlas/urban-atlas-2018?tab=metadata>), the ZABAGED geodatabase (Základní báze geografických dat České republiky—The Fundamental Base of Geographic Data of the Czech Republic; The Czech Office for Surveying, Mapping and Cadastre; <https://geoportal.cuzk.cz/>), and the digital technical map of Prague provided by GeoPortal Prague (<https://www.geoportalpraha.cz/en>). Further, land cover fractions without natural vegetation were prepared using the European Settlement Map (Release 2017; Copernicus Land Monitoring Services; <https://land.copernicus.eu/pan-european/GHSL/european-settlement-map/esm-2012-release-2017-urban-green?tab=metadata>). For detailed building information, the 3D model of Prague was used (3D model; GeoPortal Prague; <https://www.geoportalpraha.cz/en>), and information about street geometry was based on ZABAGED. Vector data provided by the listed sources were aggregated to gridded data with 333 m spatial resolution. Emissivities of different urban surfaces were based on the ASTER Global Emissivity Dataset with 100 m spatial resolution (ASTER GED; <https://emissivity.jpl.nasa.gov/aster-ged>) and the Land Surface Emissivity algorithm for LANDSAT-8 [60]. In summary, urban parameters were considered as 2D arrays instead of constant

values, i.e., every urban grid point had a unique combination of urban parameters allowing capturing the spatial distribution of urban effects more precisely. An example of street width and vegetation fraction at the original 333 m × 333 m resolution is provided in Figure 3.

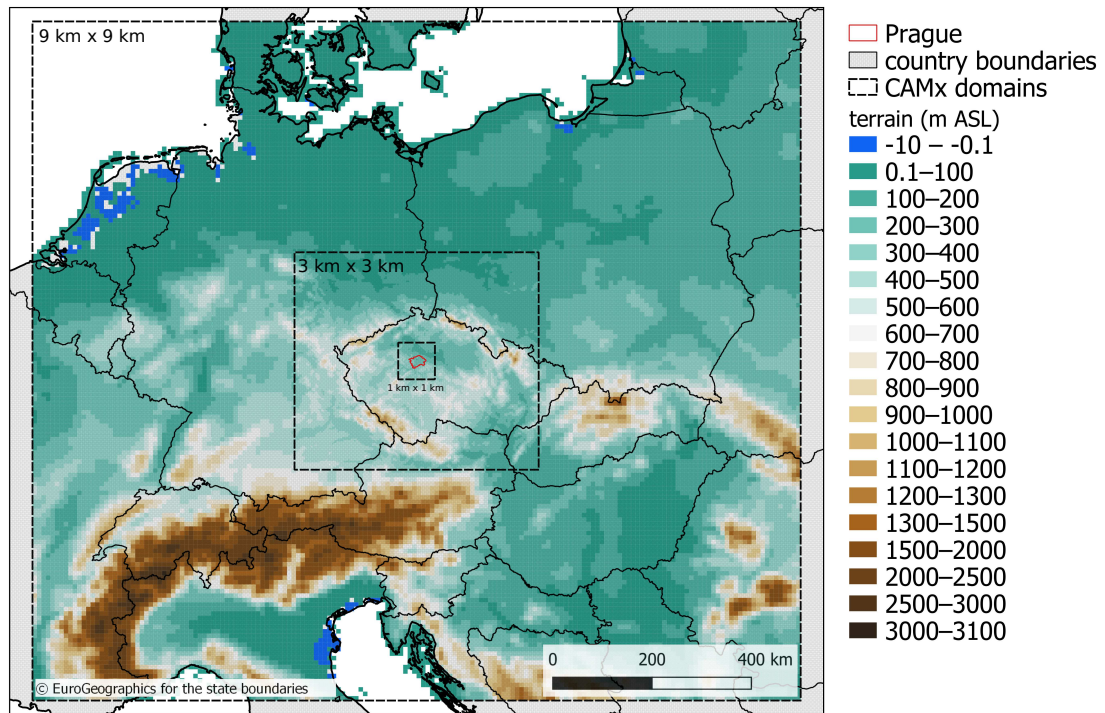


**Figure 2.** The simulation domains of WRF and the Comprehensive Air Quality Model with Extensions (CAMx).

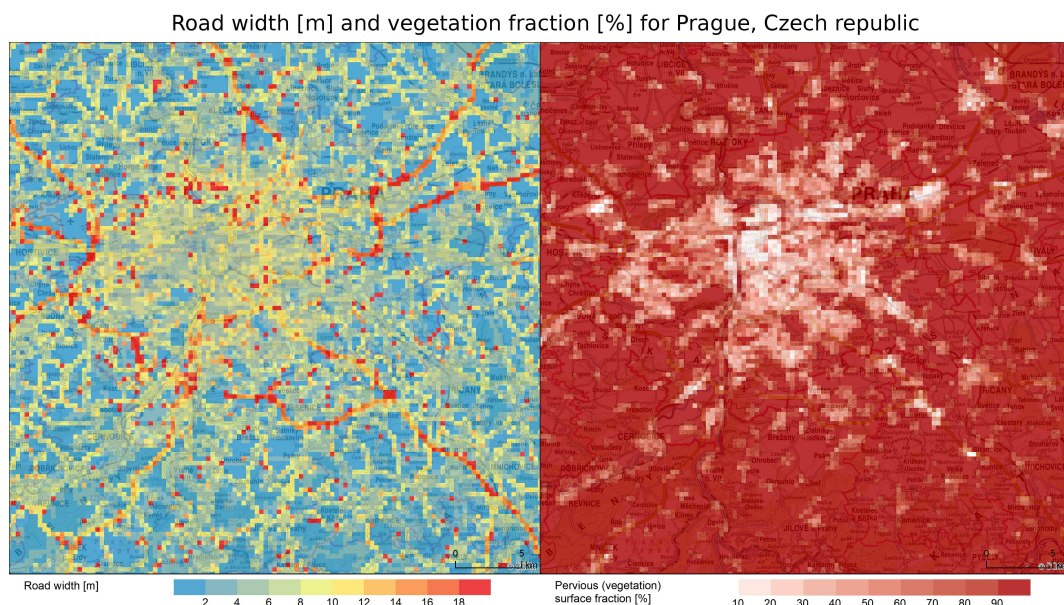


**Figure 3.** The final road width (meters) and vegetation fraction (%) map at the original 333m resolution used to derive the 2D urban input for Prague.

In this validation study, CAMx prediction was performed for each day from 00 UTC to 24 UTC and was restarted from the run of the previous day (using the CAMx restart files for 00 UTC of the actual day). As a first step of the CTM run, the Chemical Boundary Conditions (CHBC) were calculated; in this preliminary setup, they were taken as time- and space-invariant climatological means, so only the effects of the local emissions were taken into account without considering long-range pollution transport. Simultaneously with CHBC, the photolysis rate files were created with the TUV (Tropospheric Ultraviolet-Visible [61]) Model, which were based on Total Ozone Mapping Spectrometer (TOMS) data of the Ozone Monitoring Instrument (OMI) aboard NASA's Aura satellite <https://earthdata.nasa.gov/eosdis/science-system-description/eosdis-components/lance/about-omi-sips>. Besides the boundary conditions and TUV files, the biogenic emissions of isoprene, monoterpenes, and other volatile organic compounds were calculated based on the WRF predicted meteorological data. The start of the CAMx run was conditioned upon the successful execution of all the mentioned preprocessing steps.

The model configuration for both WRF and CAMx runs is summarized in Table 1. Both WRF and CAMx simulations were performed on an Intel Xeon-based HPC (High Performance Computing) cluster at the Faculty of Mathematics and Physics (Charles University, Prague), with parallelization using the OpenMPI (Message Passing Interface) over OmniPath technology and GNU compilers.

**Table 1.** Model configuration for WRF (left) and CAMx (right). CMAQ, Community Multiscale Air Quality Modeling System; RRTMG, Rapid Radiative Transfer Model for General Circulation Models; TUV, Tropospheric Ultraviolet-Visible Model; CB5, Carbon Bond chemical mechanism; SOAP, Secondary Organic Aerosol Processor; BEP + BEM, Building Environment Parameterization linked to Building Energy Model.

| WRF   | CAMx   |
|---|--|
| Geographic Projection   |  |
| Lambert Conformal Conic, Center: 50.075 N 14.44 E, True Latitudes: 50.075 N/50.075 N                    |  |
| Domains (centered on the projection center)   |  |
| 173 × 153 (9 km); 169 × 151 (3 km); 84 × 84 (1 km) as grid points<br>49 vertical levels (up to 50 mbar) | 172 × 152 (9 km); 164 × 146 (3 km); 74 × 74 (1 km) as grid boxes<br>20 vertical layers (up to 12 km) |
| PBL parameterization/vertical diffusivities' calculation  |  |
| Boulac PBL [37]   | CMAQ scheme [46]   |
| Microphysics scheme/wet deposition  |  |
| Thompson scheme [36]  | Seinfeld scheme [43]   |
| Land surface processes/dry deposition   |  |
| Noah [35]   | Zhang scheme [42]  |
| Radiation/UV-photolysis   |  |
| RRTMG [34]  | TUV [61]   |
| Gas phase chemistry   |  |
| -   | CB5 [41]   |
| Inorganic aerosol chemistry   |  |
| -   | ISORROPIA [44]   |
| Organic aerosol chemistry   |  |
| -   | SOAP [45]  |
| Urban canopy model  |  |
| BULK/BEP + BEM[38,39]   | -  |

### 2.2.2. Simulated Period

Our period of interest was 11 January to 20 February 2017. Both January and February were characterized by worsened dispersion conditions. The period was chosen to cover two significant smog episodes with very high PM concentrations largely exceeding the limit values, which occurred 19–24 January and 14–17 February (Figure 4). From the middle of January, the synoptic situation was dominated by anticyclonal weather together with very low temperatures, going down to  $-18$  °C. Since 18 January, the sky was clear, and these conditions led to the formation of a very strong temperature inversion. Based on measurements at Prague-Libuš station (balloon soundings), the inversion layer

reached up to 1 km in height during the period 20–22 January. Together with significantly reduced wind speeds, there was very limited mixing, and these factors caused extensive accumulation of pollutants at the ground level. PM<sub>10</sub> concentrations exceeded the daily limit value (50 µg m<sup>-3</sup>) at all eight Prague background stations. The maximum daily concentrations were reached on 20–21 January when all stations measured over 150 µg m<sup>-3</sup> and up to 180 µg m<sup>-3</sup>. Maximum hourly concentrations were 359 µg m<sup>-3</sup>. The maximum daily value for PM<sub>2.5</sub> was 147 µg m<sup>-3</sup>, and the maximum hourly value was 203 µg m<sup>-3</sup>. During 23–24 January, the Czech Republic was overcast by low clouds, leading to a smaller drop in temperature and improvement of dispersion conditions.

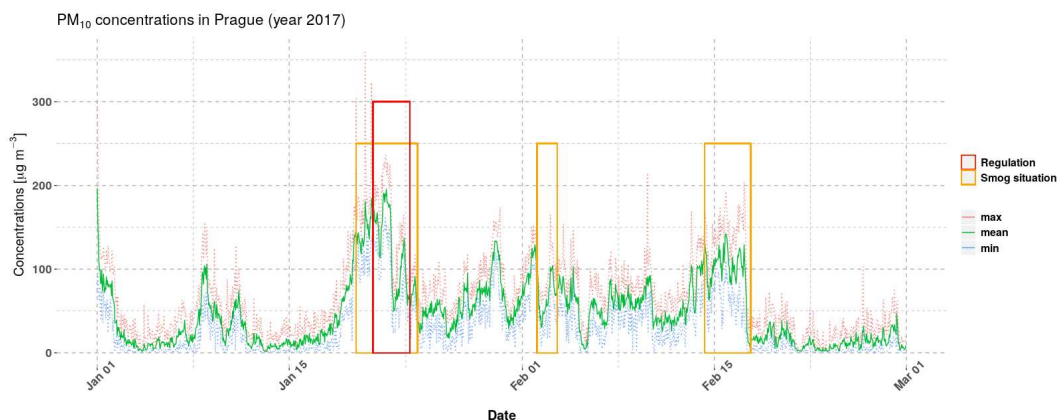


**Figure 4.** Minimum, mean, and maximum hourly PM<sub>10</sub> concentrations from eight background stations in Prague with the indication of the announced smog situations and regulation.

At the beginning of February, several frontal systems passed over the Czech Republic causing a short-term reduction of PM concentrations. In the middle of the month, the weather was influenced by a strong anticyclone, which led to worsening of the dispersion conditions and an increase of PM concentrations. The inversion layer reached several hundreds of meters and was most pronounced from 14 to 16 February. Although the second episode was less severe than the first one, the limit value for PM<sub>10</sub> was also exceeded at all eight background stations, and six of them measured over 100 µg m<sup>-3</sup> on 15–16 February. The maximum hourly value was 215 µg m<sup>-3</sup>. For PM<sub>2.5</sub>, the maximum measured daily value was 98 µg m<sup>-3</sup>, and the maximum hourly value reached 165 µg m<sup>-3</sup>. This episode ended during the night of 17 February when a cold frontal system passed over the Czech Republic. A detailed characterization of the conditions is described in [62].

### 3. Results

The results of the WRF and CAMx simulations with the urbanized (BEP+BEM) scheme and the non-urbanized (BULK) configuration for the period from 11 January to 20 February were compared to observations in order to evaluate the performance of the models and the differences arising from different urban canopy treatment. In this paper, we present the comparison only for the innermost domain with 1 km resolution, as the impact of the urban parameterization turned out to be more pronounced than the change of resolution. We analyzed the spatial differences, as well as the overall agreement with measurements. Hourly data and averaged diurnal profiles of the meteorological conditions and pollutants at the points of measurement have been assessed. For the WRF model, the closest grid point to each measurement site was used, and for CAMx, the values from the grid box that lied above the measurement station were extracted for comparison.

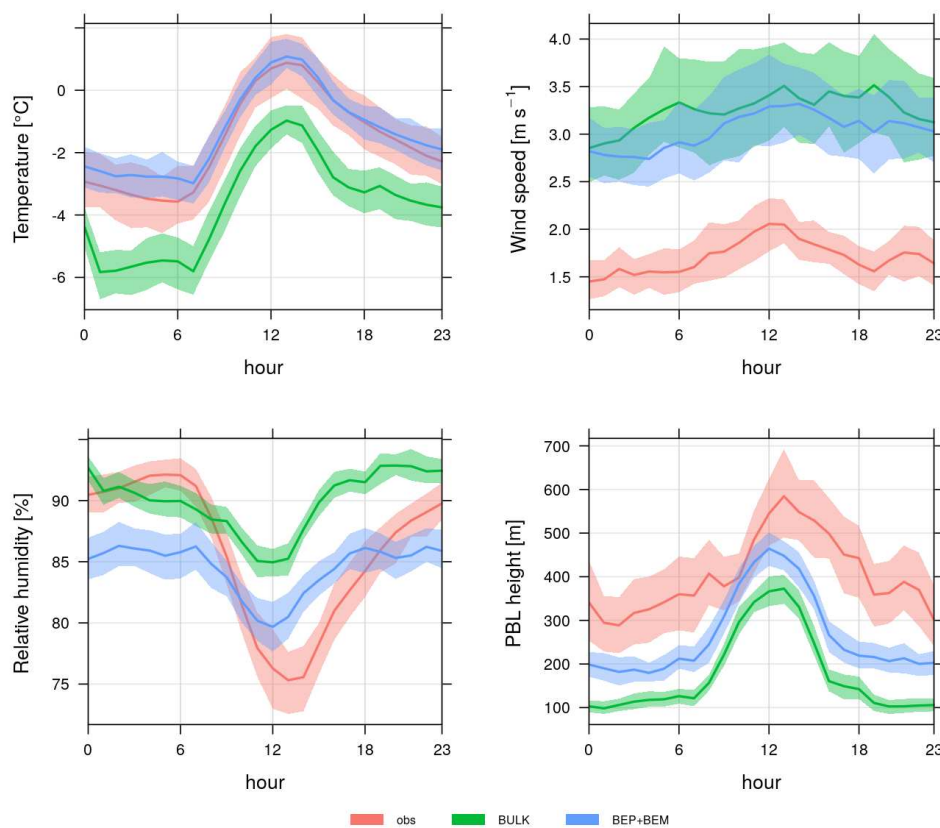
#### 3.1. Meteorology

Table 2 summarizes the values of the bias, the Root Mean Square Error (RMSE), and the correlation coefficient  $r$  (see Appendix A) together with the correlation  $p$ -value for the comparison of meteorological variables with observational data from two stations in Prague. The diurnal profiles for

the modeled and observed air Temperature at 2 m (T2), Wind Speed (WS), Relative Humidity (RH), and Planetary Boundary Layer Height (PBLH) averaged over the modeled period are shown in Figure 5. It can be seen that for T2, the bias was significantly reduced in the urbanized configuration as compared to the BULK configuration. The RMSE was the same in both cases, while the correlation was poorer. As expected, the BULK configuration gave more underestimated temperatures, on some occasions up to 10 °C lower than those predicted with the urbanized configuration. From the averaged diurnal profiles, it could be observed that the daily pattern was captured quite well by the urbanized model, with a small overestimation during the night time. The BULK scheme gave values systematically lower by 2 °C throughout the day.

**Table 2.** Statistical results (bias, RMSE, *r*, correlation *p*-value) of observations and simulations with corresponding units for bias and RMSE: meteorology; hourly averages. T2, Temperature at 2 m; WS, Wind Speed.

| Scheme  |                 | T2 (°C) | WS (m s <sup>-1</sup> ) | RH (%) | PBLH (m) |
|---------|-----------------|---------|-------------------------|--------|----------|
| BULK    | bias            | −1.9    | 1.5                     | 3.3    | −229     |
|         | RMSE            | 2.7     | 2.4                     | 11.5   | 369      |
|         | <i>r</i>        | 0.91    | 0.79                    | 0.34   | 0.5      |
|         | <i>p</i> -value | <0.01   | <0.01                   | <0.01  | <0.01    |
| BEP+BEM | bias            | 0.6     | 1.3                     | −3.2   | −134     |
|         | RMSE            | 2.7     | 2                       | 11.4   | 322      |
|         | <i>r</i>        | 0.82    | 0.75                    | 0.45   | 0.5      |
|         | <i>p</i> -value | <0.01   | <0.01                   | <0.01  | <0.01    |



**Figure 5.** Averaged diurnal profiles of the temperature at 2 m, wind speed, relative humidity, and PBL height for observations (red), BULK simulations (green), and BEP+BEM simulations (blue). Lines represent the mean values and shaded areas the 95% confidence interval in the mean.

Similar results could be observed for wind speed. In this case, the results of both runs were overestimated, the non-urbanized predictions being up to  $6 \text{ m s}^{-1}$  ( $0.5 \text{ m s}^{-1}$  on average) higher than the urbanized ones, which were closer to the observed values. RMSE was better for the BEP+BEM configuration; however, the correlation was somewhat lower in this case.

The relative humidity had a much larger diurnal amplitude in the observed data (almost 17% from 75 to 92%) with an expected maximum in the morning hours and a minimum just after noon. This pattern failed to be captured by either of the configurations: the daily amplitude was slightly over 5% with the urbanized model giving values constantly lower by also about 5%. In both configurations, the biases (in an absolute sense) and RMSE were very similar; however, the correlation for the urbanized version was somewhat higher.

The simulated planetary boundary layer height using the BEP+BEM scheme was improved in terms of bias and RMSE, while both configurations were marked with negative bias compared to measurements. The daily averaged observed heights ranged from 300 m during the night to 600 m around noon; the configuration without urban parameterization predicted heights between 100 m and 400 m; and the urbanized model heights ranged from 200 m to 500 m. The correlation between the two versions and the measurements was almost the same.

A paired *t*-test was performed for all variables, and in all cases, a significant difference between the BULK and BEP+BEM scenarios at a confidence level of 99% was confirmed.

### 3.2. Air Quality

#### 3.2.1. PM<sub>2.5</sub> and PM<sub>10</sub>

As said, the impact of the model treatment of urbanized surfaces propagated to the impact on near-surface PM<sub>2.5</sub> and PM<sub>10</sub> concentrations through modifications in the meteorological conditions driving the transport, diffusion, and chemical transformations of pollutants. It was therefore expected that the differences in meteorological conditions presented above would imply differences in pollutant concentrations. Here, we compare these two configurations in terms of the two aerosol fractions; both their spatial distribution and the agreement with station data are evaluated.

The statistics applied for the comparison of both model setups to observations are summarized in Table 3. Further, we calculated the diurnal profiles averaged over the modeled period (Figure 6). For both pollutants, the bias and RMSE were higher for the urbanized configuration. The correlation for the urbanized version was somewhat lower as well; however, the averaged diurnal profiles showed that the temporal patterns of the urbanized configuration were better correlated with the measurements than the BULK runs, although more underestimated. In particular, the correlation coefficient of the averaged diurnal cycles increased from 0.06 to 0.3 for PM<sub>10</sub> and from 0.55 to 0.69 for PM<sub>2.5</sub>. This could indicate that the day-to-day variability was better captured in the non-urbanized version (unlike the average hourly one, which was better in the urbanized version). Both model outputs showed greater variations during the day than the observed data, especially with a higher peak in the afternoon, which was not present in the measurements. In particular, the average measured concentrations of PM<sub>10</sub> varied from 50–65  $\mu\text{g m}^{-3}$ ; the BULK simulated values ranged from 45–80  $\mu\text{g m}^{-3}$  with two distinct peaks in the morning and evening rush hours; and the BEP+BEM model outputs varied from 30–50  $\mu\text{g m}^{-3}$ , also with two peaks. For PM<sub>2.5</sub>, the concentrations were around 40–55  $\mu\text{g m}^{-3}$ , 35–55  $\mu\text{g m}^{-3}$ , and 25–40  $\mu\text{g m}^{-3}$ , respectively.

The day-to-day variation of the daily average PM<sub>2.5</sub> and PM<sub>10</sub> concentrations (Figure 7) confirmed the diurnal average picture: i.e., systematically lower concentrations in the BEP+BEM case seen on every simulated day; and the differences in both cases could reach 40–50  $\mu\text{g m}^{-3}$ , especially for PM<sub>10</sub>. Another important conclusion was that during days with low measured PM concentrations, the BEP+BEM version had a smaller bias, or in other words, the negative bias in the BEM+BEP case was due to large overestimation of the peak measured values (e.g., during the beginning of the examined period).

Figure 8 shows the surface concentrations of PM<sub>10</sub> and PM<sub>2.5</sub> averaged over the simulated period for the BULK (non-urbanized) and BEP+BEM (urbanized) configurations. A clear decrease of modeled PM<sub>10</sub> concentrations could be observed in the urbanized simulation, not only over the urban areas, but also over a major part of the domain, in agreement with the diurnal cycles and daily averages. The average concentration difference over the area of Prague between the BULK and BEP+BEM results was 12 µg m<sup>-3</sup>. Similar results were obtained for PM<sub>2.5</sub>, where the mean decrease of concentrations in Prague reached 8 µg m<sup>-3</sup>. There was also a visible difference in spatial patterns. In the BULK configuration, the highest PM<sub>10</sub> values were simulated over the urban areas of Prague with a hotspot in the inner part of the city. Elevated concentrations could also be observed in other urban areas north of Prague. However, the simulations with the BEP+BEM configuration gave more evenly mixed concentrations and even a decrease towards the center of the city. The spatial variability of the modeled PM<sub>2.5</sub> concentrations was smaller than that of PM<sub>10</sub>. Similarly to the PM<sub>10</sub> results, the non-urbanized concentration predictions were highest in the central part of the city. The urbanized configuration led to an overall decrease in concentrations over the entire domain, especially in the urban area of Prague. A paired *t*-test was performed for both configurations, and in all cases, a significant difference between the BULK and BEP+BEM scenarios at a confidence level of 99% was confirmed.

**Table 3.** Statistical results (bias, RMSE, *r*, correlation *p*-value) of observations and simulations: air quality; hourly and daily averages. Bias and RMSE units are in µg m<sup>-3</sup>.

| Scheme            |                 | PM <sub>10</sub> | PM <sub>2.5</sub> | PM <sub>10</sub> Diurnal | PM <sub>2.5</sub> Diurnal |
|-------------------|-----------------|------------------|-------------------|--------------------------|---------------------------|
| BULK<br>hourly    | bias            | 0.06             | -6.7              | -1                       | -6.6                      |
|                   | RMSE            | 36.4             | 28.7              | 12.69                    | 8.9                       |
|                   | <i>r</i>        | 0.62             | 0.66              | 0.06                     | 0.55                      |
|                   | <i>p</i> -value | <0.01            | <0.01             | <0.01                    | <0.01                     |
| BEP+BEM<br>hourly | bias            | -20.1            | -18.3             | -20.2                    | -18.3                     |
|                   | RMSE            | 41               | 35.8              | 21.1                     | 18.7                      |
|                   | <i>r</i>        | 0.59             | 0.58              | 0.3                      | 0.69                      |
|                   | <i>p</i> -value | <0.01            | <0.01             | <0.01                    | <0.01                     |
| BULK<br>daily     | bias            | 0.5              | -6.3              |                          |                           |
|                   | RMSE            | 23.1             | 20.9              |                          |                           |
|                   | <i>r</i>        | 0.8              | 0.8               |                          |                           |
|                   | <i>p</i> -value | <0.01            | <0.01             |                          |                           |
| BEP+BEM<br>daily  | bias            | -19.7            | -18               |                          |                           |
|                   | RMSE            | 34.5             | 30.5              |                          |                           |
|                   | <i>r</i>        | 0.7              | 0.7               |                          |                           |
|                   | <i>p</i> -value | <0.01            | <0.01             |                          |                           |

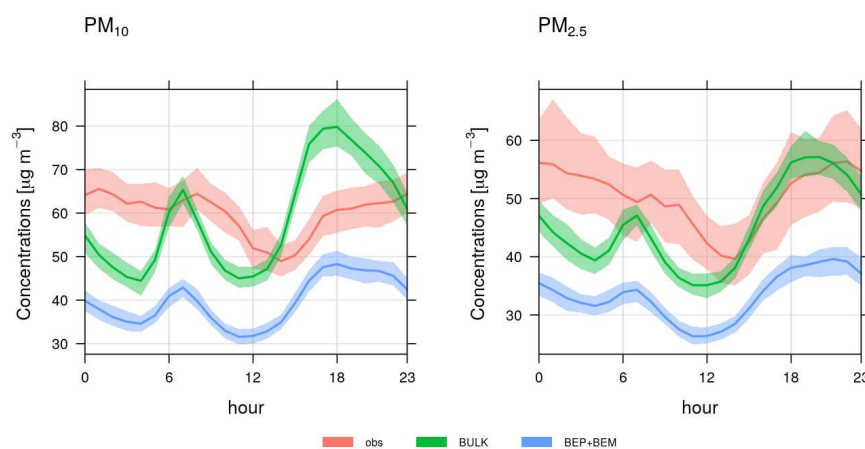


**Figure 6.** Averaged diurnal profiles of PM<sub>10</sub> and PM<sub>2.5</sub> concentrations for observations (red), BULK simulations (green), and BEP+BEM simulations (blue). Lines represent the mean values and shaded areas the 95% confidence interval in the mean.

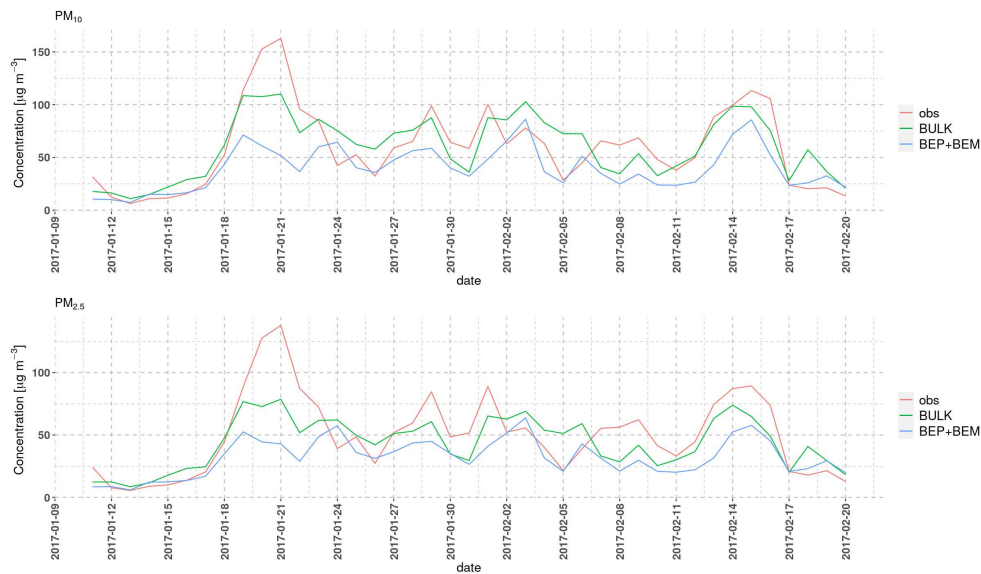


**Figure 7.** Average daily concentrations of PM<sub>10</sub> (top) and PM<sub>2.5</sub> (bottom) for observations (red) and the BULK (green) and BEP+BEM (blue) model configurations.

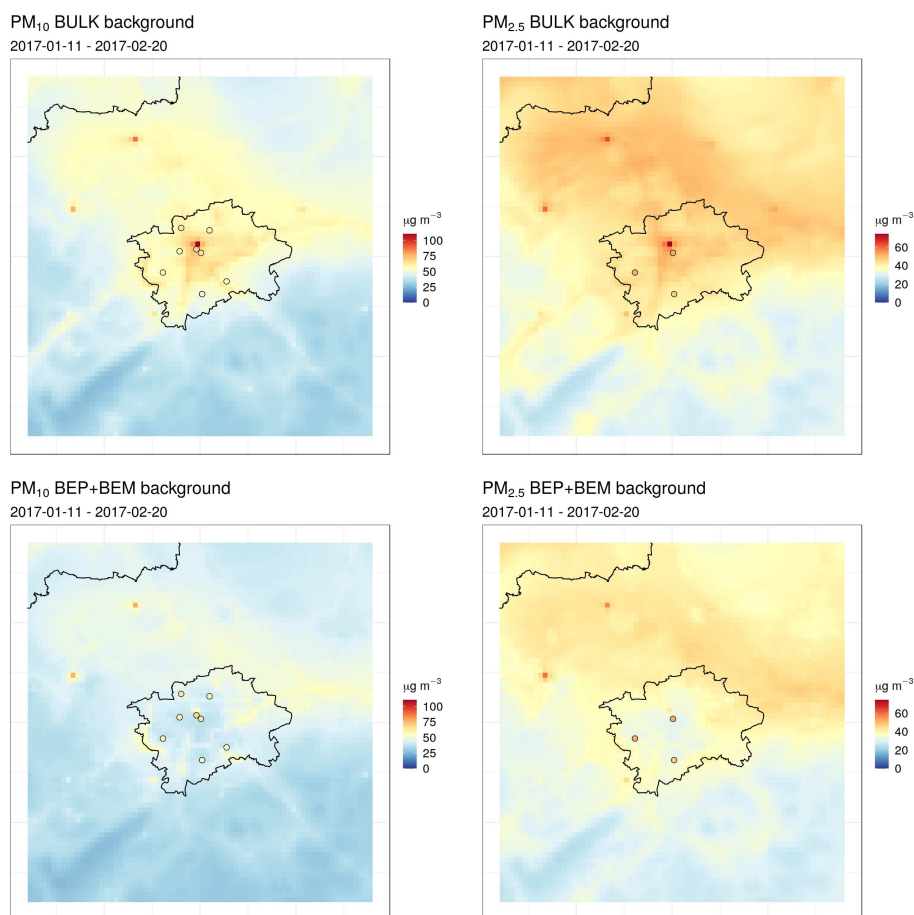


**Figure 8.** Maps of modeled PM<sub>10</sub> (left) and PM<sub>2.5</sub> (right) concentrations averaged over the entire period with the BULK scheme (top) and BEP+BEM scheme (bottom). Circles represent measurement stations and their average concentrations from the same period.

### 3.2.2. Analysis of the Aerosol Components

Huszar et al. [17] showed that different aerosol components contribute to the total urbanization-induced  $PM_{2.5}$  change with a different magnitude. In order to assess this in our simulations, we analyzed the differences in concentrations of both primary and secondary aerosol between the two configurations to evaluate the impact of the urbanized version of the forecast (with respect to the “BULK” approach). The diurnal cycle of the Primary Aerosol (PA) concentrations from the two model versions is presented in Figure 9 and the corresponding day-to-day variations of the average daily values is shown in Figure 10. Figure 11 then presents the case of Secondary Inorganic Aerosol (SIA), nitrates ( $PN_{O_3}$ ), sulfates ( $PSO_4$ ), and ammonium ( $PNH_4$ ) with the respective daily averages in Figure 12. The diurnal cycle for the Secondary Organic Aerosol (SOA) is plotted in Figure 13 and the corresponding day-to-day variations are presented in Figure 14.

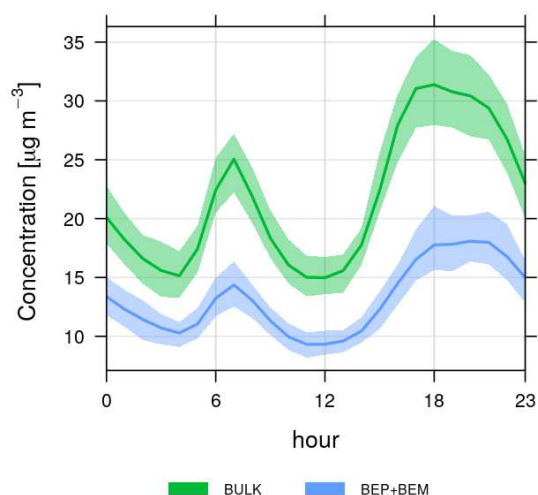


**Figure 9.** Averaged diurnal profiles of PM primary aerosol for BULK simulations (green) and BEP+BEM simulations (blue). Lines represent the mean values and shaded areas the 95% confidence interval in the mean.

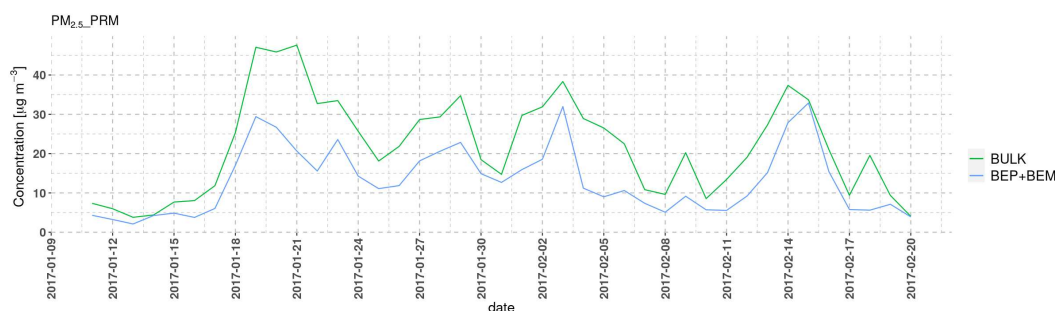


**Figure 10.** Average daily concentrations of PM primary aerosol for BULK simulations (green) and BEP+BEM simulations (blue).

According to Figure 9, primary aerosols exhibited a very similar diurnal cycle to the total  $PM_{2.5}$ , comprising about 50–60% of the total aerosol load. The BEP+BEM version showed lower PA by about 15–25  $\mu g m^{-3}$  compared to the BULK version, and this behavior was systematically seen during every simulated day. This indicated that about half of the difference seen in Figure 6 between the two versions was caused by the differences in primary aerosol.

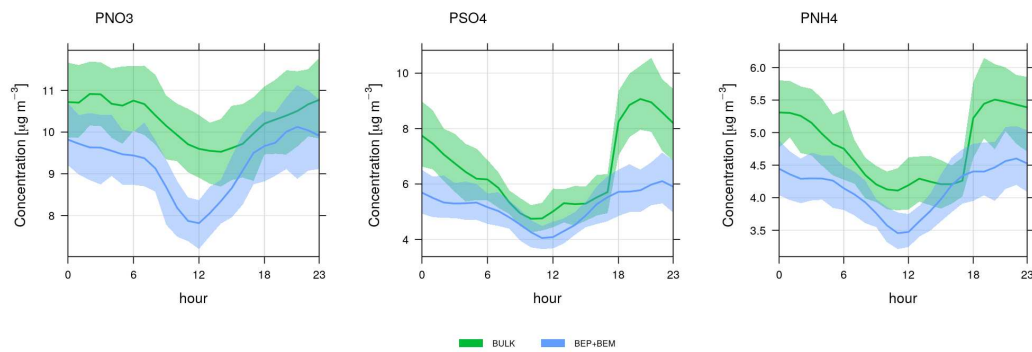


**Figure 11.** Averaged diurnal profiles of PM secondary inorganic aerosol (nitrates-PNO<sub>3</sub>, sulfates-PSO<sub>4</sub>, and ammonium-PNH<sub>4</sub>) for BULK simulations (green) and BEP+BEM simulations (blue). Lines represent the mean values and shaded areas the 95% confidence interval in the mean.



**Figure 12.** Average daily concentrations of PM secondary inorganic aerosol (nitrates-PNO<sub>3</sub>, sulfates-PSO<sub>4</sub>, and ammonium-PNH<sub>4</sub>) for BULK simulations (green) and BEP+BEM simulations (blue).

Regarding secondary inorganic aerosol (Figure 11), in all cases, the BEP+BEM version calculated smaller values; however, the differences were much lower than in the case of PA. For nitrates and sulfates, it showed about 1–2  $\mu\text{g m}^{-3}$  and for ammonium about 1  $\mu\text{g m}^{-3}$ . The diurnal cycle of these components showed a different pattern compared to the primary aerosol with maximum values during the nighttime. The differences were however largest during the daytime for nitrates, while for sulfates and ammonium, the difference peaked rather during the nighttime. The differences were however not uniform during individual days (Figure 12), and under certain conditions, the BEP+BEM configuration could lead to higher aerosol loads. This was the case for 24 January, which ended

the strong inversion period, and the turbulence from the upper layer above the original inversion layer could become of greater importance. Indeed, the turbulence was stronger in the BEP+BEM case, which could explain the slightly higher concentrations. A similar situation was modeled after the second strong inversion period, which ended on 16 February. Here, turbulent transport from upper layers could explain the slightly higher SIA values in the BEP+BEM configuration.

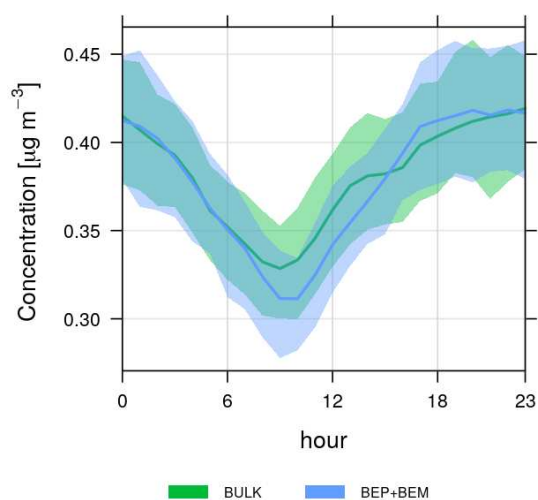


**Figure 13.** Averaged diurnal profiles of PM secondary organic aerosol for BULK simulations (green) and BEP+BEM simulations (blue). Lines represent the mean values and shaded areas the 95% confidence interval in the mean.

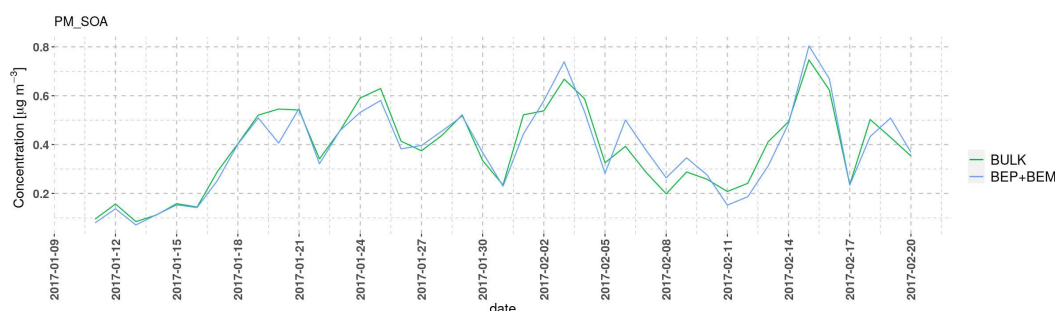


**Figure 14.** Average daily concentrations of PM secondary organic aerosol for BULK simulations (green) and BEP+BEM simulations (blue).

SOA comprised only a small fraction of the total PM<sub>2.5</sub> in our simulations, as seen in Figure 13. The diurnal cycle was similar to that of the SIA with nighttime maxima, while the differences between the two model versions were negligible, less than 0.05 µg m<sup>-3</sup>. This conclusion remained the same also from the day-to-day figure. In summary, the modeled PM<sub>2.5</sub> diurnal cycle was determined mainly by the primary aerosol. The same conclusion could be made for the differences between the BEP+BEM and BULK versions.

#### 4. Discussion

The presented differences between the non-urbanized and urbanized version of the WRF setup showed expected patterns: higher temperatures in the urbanized version as a consequence of accounting for the urban meteorological effects such as radiation trapping and anthropogenic heat release [63]. Indeed, the “BULK” approach could not resolve these effects. Liao et al. [24] also simulated higher temperatures using WRF with the BEP+BEM configuration in comparison with their SLAB scheme (which corresponds to our BULK approach). They however detected smaller

differences between these two approaches. The reason could lie in the fact that in our case, the WRF forecasts with the BULK treatment were cold-started, being systematically closer to the global driving data (GFS), which were apparently negatively biased for urban areas. In the case of [24], the correlations were however slightly worse for the urbanized version, which could suggest that the urban morphology parameters were not entirely realistic in their study. Sharma et al. [58] simulated a smaller temperature bias when using the BEP+BEM instead of the SLAB scheme, especially for nighttime hours. Higher temperatures were simulated for the BEP+BEM compared to the BULK scheme in [7] as well (as a ten-year average); here, however, the differences were smaller, again probably for the same reasons as noted above. Similarly, Wang et al. [30] compared the BULK and SLUCM (Single-Layer Urban Canopy Models) in WRF. SLUCM is a simpler, single-layer approach to describing the urban environment compared to the multilayer BEP+BEM approach presented here. In their study, the SLUCM captured temperature with a smaller bias and RMSE compared to the BULK approach. However, interestingly, their correlation was lower for the more comprehensive approach of SLUCM. This was also true for our case (and also in [24]) and could suggest that the high-frequency variability (hour-by-hour) was less accurately captured with a more advanced urban canopy description as it was always marked with higher number of degrees of freedom (note the large number of urban parameters that needed to be set). This also stressed the need for very careful setting of urban parameters as they have a very large impact on model results and can potentially lead to an increase in model errors.

Regarding wind speed, it was clear that the BEP+BEM configuration accounted for the increased and complex three-dimensional nature of drag in the urban canopy in comparison to the BULK approach, where the urban drag was imposed only by an increased roughness of the surface. This explained why the winds were lower in the BEP+BEM case. This was supported by the findings of Karlicky et al. [7], who simulated long-term winter wind speeds lower by  $2 \text{ m s}^{-1}$ , a larger decrease than in our case. Lower wind speeds were also simulated in [30] by around  $0.5\text{--}1 \text{ m s}^{-1}$ , which was very similar to our result. Improvement in wind speed bias due to the application of an urban canopy model was achieved in [24,58] as well. However, in our case and in all of the mentioned studies, the correlation was higher for the BULK approach, and the reasons were probably similar to the temperature case.

Lower relative humidities in case of the BEP+BEM simulations were clearly a result of higher temperatures, as evaporation of water vapor from the ground was the same in both cases (in the BULK case, surfaces were of urban land use type, so evaporation was also limited). Lower RHs were modeled by [30] as well. It has to be noted however that the main reason for smaller relative humidities in urban areas lies in the limited evaporation and high run-off, as argued by [64].

The increase of the urban PBLH when switching from the BULK approach to BEP+BEM was attributable to better representation and thus stronger turbulence in the urban boundary layer. This was concluded by [24] as well, who simulated higher PBLH by 200–300 m in BEP+BEM simulation compared to the BULK approach. Their differences were larger than our 100 m, but the urban agglomeration they analyzed was much larger with stronger potential impacts. Similarly to our results, Wang et al. [30] simulated improvements in bias and RMSE when applying a more sophisticated urban canopy treatment instead of the BULK approach. About 100 m higher PBLH was modeled in [7,23], using BEP+BEM (BEP in the case of the first study) instead of the BULK approach. The Boulac PBL was used recently by [65] as well, who concluded, in accordance with our results, that urban PBLs were higher and thus much more accurately represented in a multi-layer urban canopy scheme (as BEP) compared to a single-layer approach.

The simulated  $\text{PM}_{10}$  and  $\text{PM}_{2.5}$  concentrations were systematically larger in the BULK case. This was very much in line with the expectations regarding the vertical mixing in the two versions. In BEP+BEM, the PBLH was higher, indicating stronger turbulence and hence larger turbulent transport and removal of pollutants. Huszar et al. [17,29] also showed that turbulence was a primary factor that played a role in the urban-induced meteorological modifications in cities. Liao et al. [24] also showed that the BEP+BEM scheme resulted in lower  $\text{PM}_{10}$  concentrations by about  $15\text{--}20 \mu\text{g m}^{-3}$ .

Although wind speeds were lower in the BEP+BEM scheme in our simulation, the dominance of the enhanced turbulence in this model version was confirmed [29].

Our results were also in line with Kim et al. [26], who simulated lower PM<sub>2.5</sub> concentrations when using a more comprehensive treatment of the urban canopy than a simple BULK approach with differences reaching about 5–10 µg m<sup>-3</sup>. Similar decreases for PM<sub>10</sub> were modeled by Zhu et al. [66], who analyzed the effect of urban expansion, which resulted in increased vertical eddy mixing and therefore lower near-surface pollutant concentrations.

Our PM biases for the BEP+BEM case and the difference between the BEP+BEM and BULK case were larger during peak measured values, and on the other hand, during low PM values, the BEP+BEM tended to perform with a smaller bias. This strongly suggested that the turbulence was somewhat overestimated in BEP+BEM during very stable conditions, while it performed more realistically in other situations.

It must be stressed that although in most of the studies, turbulence had a dominant effect, under certain conditions, wind speed could play a major role as well and change the overall picture regarding the impacts of urban areas. For example, de la Paz et al. [23] calculated higher near-surface concentrations for PM<sub>2.5</sub> when using the BEP (without BEM) approach in WRF instead of the BULK one and concluded the dominant role of decreased wind speeds in urban areas preventing dispersion of primary emissions. In their case, the urbanized approach yielded a much larger difference in wind speed (up to 2 m s<sup>-1</sup>) between the two setups than in our study. Our results showed that if turbulence became dominant, the conclusions could be qualitatively different.

There were striking differences in the shape of the PM diurnal cycles between modeled and observed values, especially in the case of PM<sub>10</sub>. As PBL and wind were simulated with much lower bias and higher correlation, we concluded that the main reason lied in an incorrect representation of the diurnal cycle of the emissions. Our diurnal emission factors were taken from Gon et al. [52], and probably their hourly distribution of vehicle emissions overestimates the rush hour peaks that are not seen in the measured data from Prague.

Our analysis showed that the modeled differences of PM<sub>2.5</sub> concentrations between the two versions were well explained by the primary component of PM<sub>2.5</sub> (primary aerosol), which had an almost identical shape in diurnal variation. Indeed, Huszar et al. [17] showed that the urban induced changes in PM<sub>2.5</sub> were largely determined by the primary aerosol and that the main driver of the primary aerosol decrease was the elevated turbulence that removed material from the urban canopy layer to the mixing layer above. Our largest differences in PA were modeled during early evening hours, which were very in line with the results of [17,29], who showed that turbulence caused the largest impact (decrease) during this period of the day.

The modeled differences for secondary inorganic aerosol had, besides increased turbulence, another cause: the differences in temperatures between the two model versions. Temperature acted as a major driver for secondary aerosol gas-particle partitioning, with increasing temperatures resulting in less secondary aerosol forming [67]. The largest impact of the temperature itself was modeled in [17] during evening hours. Indeed, during these hours, the impact on temperature was the largest in our simulations, and this probably translated to the large impact of the BEP+BEM on SIA during nighttime, especially for ammonium and sulfates.

Apparently, our PM<sub>2.5</sub> model performance was worse for the urbanized version as this decreased the PM<sub>2.5</sub> values, making the negative bias even larger. This however did not mean that urbanization of the prediction system was the wrong step towards a more accurate weather/air-quality forecast system. This meant (and confirmed) that the overall model bias had many sources that caused the model results to deviate in both directions with respect to the observed values. It was likely that the emissions of PM were too low, creating the general negative bias, which was intensified with the introduction of the urbanized model version with BEP+BEM.

## 5. Conclusions

A high resolution weather and air-quality forecast system was set up using the WRF numerical prediction model and CAMx chemistry transport model for the city of Prague, Czech Republic. This system was used to simulate a typical winter pollution episode in January–February 2017 using two distinct setups: BULK configuration using the “BULK” treatment of urban land-surface and the BEP+BEM (Building Environment parameterization linked to Building Energy Model) configuration, taking the urban canopy into account. The effects of the urbanization were compared to the non-urbanized simulations, and both outputs were evaluated against observations.

The results showed that the urbanized runs were able to capture the meteorological conditions better than the non-urbanized simulations. In particular, we observed an average increase in temperature at 2 m by approximately 2 °C, a decrease in wind speed by around 0.5 m s<sup>-1</sup>, a decrease in relative humidity by 5% on average, and an increase of the planetary boundary layer height by around 100 m. When compared to observations, the urbanized simulations performed better for all of the considered meteorological variables.

The modeled concentrations of both evaluated air pollutant species, PM<sub>10</sub> and PM<sub>2.5</sub>, decreased by 35% and 28% on average, respectively, when using the urbanized configuration as compared to the BULK configuration. The main difference was caused by the reduction of primary aerosol. Compared to the measurements, the urbanized model results were underestimated by up to 40%. From the statistical evaluation of both model results, it could be concluded that the urbanized scheme led to an enhancement of the overall model error with an improvement only in the better representation of the diurnal variations. This important conclusion must be, however, considered with caution. It pointed out that there were multiple sources of model-observation disagreement, and besides the accurate representation of the urban canopy, e.g., high quality emission data were also crucial for the modeling of the urban air chemistry. Thus, model improvements aiming at better performance should consider every potential source of model errors. Otherwise, improving only one aspect (like including the urban effects) could lead to some worsening of the model accuracy.

It has to be noted that our conclusions were based on a winter episode, so they cannot be simply extended to other air pollution situations (e.g., occurring during summer); however, they confirmed previous findings about the urbanization effect on air quality during winter, and thus, they revealed some general behavior of winter air pollution in cities regardless of the region or the particular air pollution situation. It also has to be stressed that the “offline” nature of the coupling between WRF and CAMx brought some errors to the air quality predictions, as pointed out by Grell [68], Baklanov [69], especially regarding vertical mass distribution. Indeed, it was largely influenced by the choice of the urban canopy scheme in our study via turbulence. On the other hand, offline coupling here allowed independent development of the coupled components and the implementation of new parameterizations.

**Author Contributions:** Conceptualization, P.H. and K.E.; methodology, P.H., J.K., and J.G.; validation, J.Ď.; formal analysis, J.Ď.; investigation, P.H. and K.E.; data curation, N.B.; writing, original draft preparation, J.Ď., P.H., and K.E.; writing, review and editing, P.H., J.Ď., M.B., J.K., J.G., and O.V.; visualization, J.Ď. and O.V.; supervision, P.H., O.V., and T.H.; project administration, T.H. and O.V.; funding acquisition, T.H. All authors read and agreed to the published version of the manuscript.

**Funding:** This work was done within the project URBI PRAGENSI—“Urban Development of weather forecast, air quality, and climate scenario for Prague” financed by the Operational Programme Prague –Growth Pole of the Czech Republic, Project No. CZ.07.1.02/0.0/0.0/16\_040/0000383, with the partial support of the SVV260581project supported by Charles University.

**Acknowledgments:** The authors would like to thank Petra Bauerová for providing the processed data from ceilometers.

**Conflicts of Interest:** The authors declare no conflict of interest.

## Appendix A. The Definition of the Statistical Scores

Bias (mean bias):

$$bias = \frac{1}{N} \sum_{i=1}^N c_i - o_i$$

RMSE (Root Mean Squared Error):

$$RMSE = \sqrt{\frac{1}{N} \sum_{i=1}^N (c_i - o_i)^2}$$

r (correlation):

$$r = \frac{\sum_{i=1}^N (c_i - \bar{c})(o_i - \bar{o})}{\sqrt{\sum_{i=1}^N (c_i - \bar{c})^2} \sqrt{\sum_{i=1}^N (o_i - \bar{o})^2}}$$

$N$  denotes the number of samples, and  $c$  and  $o$  stand for modeled and observed values.

## References

1. Marlier, M.E.; Jina, A.S.; Kinney, P.L.; DeFries, R.S. Extreme Air Pollution in Global Megacities. *Curr. Clim. Chang. Rep.* **2016**, *2*, 15–27, doi:10.1007/s40641-016-0032-z.
2. Folberth, G.A.; Butler, T.M.; Collins, W.J.; Rumbold, S.T. Megacities and climate change—A brief overview. *Environ. Pollut.* **2015**, *203*, 235–242, doi:10.1016/j.envpol.2014.09.004.
3. Lawrence, M.G.; Butler, T.M.; Steinkamp, J.; Gurjar, B.R.; Lelieveld, J. Regional pollution potentials of megacities and other major population centers. *Atmos. Chem. Phys.* **2007**, *7*, 3969–3987, doi:10.5194/acp-7-3969-2007.
4. Huszár, P.; Belda, M.; Halenka, T. On the long-term impact of emissions from central European cities on regional air quality. *Atmos. Chem. Phys.* **2016a**, *16*, 1331–1352, doi:10.5194/acp-16-1331-2016.
5. Huszár, P.; Belda, M.; Karlický, J.; Pišoft, P.; Halenka, T. The regional impact of urban emissions on climate over central Europe: Present and future emission perspectives. *Atmos. Chem. Phys.* **2016b**, *16*, 12993–13013, doi:10.5194/acp-16-12993-2016.
6. Huszár, P.; Halenka, T.; Belda, M.; Zak, M.; Sindelarova, K.; Mikšovský, J. Regional climate model assessment of the urban land-surface forcing over central Europe. *Atmos. Chem. Phys.* **2014**, *14*, 12393–12413, doi:10.5194/acp-14-12393-2014.
7. Karlický, J.; Huszár, P.; Halenka, T.; Belda, M.; Žák, M.; Pišoft, P.; Mikšovský, J. Multi-model comparison of urban heat island modeling approaches. *Atmos. Chem. Phys.* **2018**, *18*, 10655–10674, doi:10.5194/acp-18-10655-2018.
8. Kanakidou, M.; Mihalopoulos, N.; Kindap, T.; Im, U.; Vrekoussis, M.; Gerasopoulos, E.; Dermizaki, E.; Unal, A.; Kocak, M.; Markakis, K.; et al. Megacities as hot spots of air pollution in the East Mediterranean. *Atmos. Environ.* **2011**, *45*, 1223–1235.
9. Im U.; Kanakidou, M. Impacts of East Mediterranean megacity emissions on air quality. *Atmos. Chem. Phys.* **2012**, *12*, 6335–6355, doi:10.5194/acp-12-6335-2012.
10. Han, W.; Li, Z.; Wu, F.; Zhang, Y.; Guo, J.; Su, T.; Cribb, M.; Chen, T.; Wei, J.; Lee, S.-S. Opposite Effects of Aerosols on Daytime Urban Heat Island Intensity between Summer and Winter. *Atmos. Chem. Phys. Discuss.* **2020**. doi:10.5194/acp-2020-162.
11. Baklanov, A.; Korsholm, U.; Mahura, A.; Petersen, C.; Gross, A. ENVIRO-HIRLAM: On-line coupled modeling of urban meteorology and air pollution. *Adv. Sci. Res.* **2008**, *2*, 41–46, doi:10.5194/asr-2-41-2008.
12. Chen, F.; Kusaka, H.; Bornstein, R.; Ching, J.; Grimmond, C.S.B.; Grossman-Clarke, S.; Loridan, T.; Manning, K.W.; Martilli, A.; Miao, S.; et al. The integrated WRF/urban modeling system: Development, evaluation, and applications to urban environmental problems. *Int. J. Climatol.* **2011**, *31*, 273–288.
13. Sarrat, C.; Lemonsu, A.; Masson, V.; Guedalia, D. Impact of urban heat island on regional atmospheric pollution. *Atmos. Environ.* **2006**, *40*, 1743–1758.

14. Struzewska, J.; Kaminski, J.W. Impact of urban parameterization on high resolution air quality forecast with the GEM—AQ model. *Atmos. Chem. Phys.* **2012**, *12*, 10387–10404, doi:10.5194/acp-12-10387-2012.
15. Fallmann, J.; Forkel, R.; Emeis, S. Secondary effects of urban heat island mitigation measures on air quality. *Atmos. Environ.* **2016**, *25*, 199–211.
16. Huszár, P.; Karlický, J.; Belda, M.; Halenka, T.; Pišoft, P. The impact of urban canopy meteorological forcing on summer photochemistry. *Atmos. Environ.* **2018**, *176*, 209–228, doi:10.1016/j.atmosenv.2017.12.037.
17. Huszár, P.; Belda, M.; Karlický, J.; Bardachova, T.; Halenka, T.; Pišoft, P. Impact of urban canopy meteorological forcing on aerosol concentrations. *Atmos. Chem. Phys.* **2018**, *18*, 14059–14078, doi:10.5194/acp-18-14059-2018.
18. Brasseur, G.; Jacob, D. *Modeling of Atmospheric Chemistry*; Cambridge University Press: Cambridge, UK, 2017, doi:10.1017/9781316544754.
19. Hidalgo, J.; Masson, V.; Gimeno, L. Scaling the Daytime Urban Heat Island and Urban-Breeze Circulation. *J. Appl. Meteorol. Clim.* **2010**, *49*, 889–901.
20. Ryu, Y.-H.; Baik, J.-J.; Kwak, K.-H.; Kim, S.; Moon, N. Impacts of urban land-surface forcing on ozone air quality in the Seoul metropolitan area. *Atmos. Chem. Phys.* **2013**, *13*, 2177–2194, doi:10.5194/acp-13-2177-2013.
21. Ryu, Y.-H.; Baik, J.-J.; Lee, S.-H. Effects of anthropogenic heat on ozone air quality in a megacity. *Atmos. Environ.* **2013**, *80*, Atmos. Environ..
22. Jacobson, M.Z.; Nghiem, S.V.; Sorichetta, A.; Whitney, N. Ring of impact from the mega-urbanization of Beijing between 2000 and 2009. *J. Geophys. Res.* **2015**, *120*, 5740–5756, doi:10.1002/2014JD023008.
23. De la Paz, D.; Borge, R.; Martilli, A. Assessment of a high resolution annual WRF-BEP/CMAQ simulation for the urban area of Madrid (Spain). *Atmos. Environ.* **2016**, *144*, 282–296.
24. Liao, J.; Wang, T.; Wang, X.; Xie, M.; Jiang, Z.; Huang, X.; Zhu, J. Impacts of different urban canopy schemes in WRF/Chem on regional climate and air quality in Yangtze River Delta, China. *Atmos. Res.* **2014**, *145–146*, 226–243, doi:10.1016/j.atmosres.2014.04.005.
25. Chen, B.; Yang, S.; Xu, X.D.; Zhang, W. The impacts of urbanization on air quality over the Pearl River Delta in winter: Roles of urban land use and emission distribution. *Theor. Appl. Climatol.* **2014**, *117*, 29–39.
26. Kim, Y.; Sartelet, K.; Raut, J.-C.; Chazette, P. Influence of an urban canopy model and PBL schemes on vertical mixing for air quality modeling over Greater Paris. *Atmos. Environ.* **2015**, *107*, 289–306, doi:10.1016/j.atmosenv.2015.02.011.
27. Ren, Y.; Zhang, H.; Wei, W.; Wu, B.; Cai, X.; Song, Y. Effects of turbulence structure and urbanization on the heavy haze pollution process. *Atmos. Chem. Phys.* **2019**, *19*, 1041–1057, doi:10.5194/acp-19-1041-2019.
28. Tang, W.; Cohan, D.S.; Morris, G.A.; Byun, D.W.; Luke, W.T. Influence of vertical mixing uncertainties on ozone simulation in CMAQ. *Atmos. Environ.* **2011**, *45*, 2898–2909.
29. Huszár, P.; Karlický, J.; Ďoubalová, J.; Šindelářová, K.; Nováková, T.; Belda, M.; Halenka, T.; Žák, M.; Pišoft, P. Urban canopy meteorological forcing and its impact on ozone and PM<sub>2.5</sub>: Role of vertical turbulent transport. *Atmos. Chem. Phys.* **2020**, *20*, 1977–2016, doi:10.5194/acp-20-1977-2020.
30. Wang, J.; Mao, J.; Zhang, Y.; Cheng, T.; Yu, Q.; Tan, J.; Ma, W. Simulating the Effects of Urban Parameterizations on the Passage of a Cold Front During a Pollution Episode in Megacity Shanghai. *Atmosphere* **2019**, *10*, 79.
31. CHMI: *Air Pollution in the Czech Republic in 2018*; CHMI: Prague, Czech Republic, 2019; ISBN 978-80-87577-95-0.
32. CHMI: *Air Pollution in the Czech Republic in 2017*; CHMI: Prague, Czech Republic, 2018; ISBN 978-80-87577-83-7.
33. Skamarock, W.C.; Klemp, J.B. A time-split nonhydrostatic atmospheric model for weather research and forecasting applications. *J. Comput. Phys.*, **2008**, *227*, 3465–3485.
34. Iacono, M.J.; Delamere, J.S.; Mlawer, E.J.; Shephard, M.W.; Clough, S.A.; Collins, W.D. Radiative forcing by longlived greenhouse gases: Calculations with the AER radiative transfer models. *J. Geophys. Res.* **2008**, *113*, 2–9, doi:10.1029/2008JD009944.
35. Chen, F.; Dudhia, J. Coupling an Advanced Land Surface-Hydrology Model with the Penn State-NCAR MM5 Modeling System. Part I: Model Implementation and Sensitivity. *Mon. Weather Rev.* **2001**, *129*, 569–585.
36. Thompson, G.; Field, P.R.; Rasmussen, R.M.; Hall, W.D. Explicit Forecasts of Winter Precipitation Using an Improved Bulk Microphysics Scheme. Part II: Implementation of a New Snow Parameterization. *Mon. Weather Rev.* **2008**, *136*, 5095–5115, doi:10.1175/2008MWR2387.1.
37. Bougeault, P.; Lacarrere, P. Parameterization of orography-induced turbulence in a mesobeta-scale model. *Mon. Weather Rev.* **1989**, *117*, 1872–1890.

38. Martilli, A.; Clappier, A.; Rotach, M.W. An urban surface exchange parameterisation for mesoscale models. *Bound. Layer Meteorol.* **2002**, *104*, 261–304.
39. Salamanca, F.; Krpo, A.; Martilli, A.; Clappier, A. A new building energy model coupled with an urban canopy parameterization for urban climate simulations—Part I. formulation, verification, and sensitivity analysis of the model. *Theor. Appl. Climatol.* **2009**, *99*, 331.
40. *ENVIRON, CAMx User's Guide, Comprehensive Air Quality Model with Extensions, Version 6.50*; Ramboll: Los Angeles, CA, USA, 2018.
41. Yarwood, G.; Rao, S.; Yocke, M.; Whitten, G.Z. Updates to the Carbon Bond Chemical Mechanism: CB05, Final Report Prepared for US EPA. 2015. Available online: [http://www.camx.com/publ/pdfs/CB05\\_Final\\_Report\\_120805.pdf](http://www.camx.com/publ/pdfs/CB05_Final_Report_120805.pdf) (accessed on 19 May 2020).
42. Zhang, L.; Brook, J.R.; Vet, R. A revised parameterization for gaseous dry deposition in air-quality models. *Atmos. Chem. Phys.* **2003**, *3*, 2067–2082, doi:10.5194/acp-3-2067-2003.
43. Seinfeld, J.H.; Pandis, S.N. *Atmospheric Chemistry and Physics: From Air Pollution to Climate Change*; Wiley: New York, NY, USA, 1998.
44. Nenes, A.; Pilinis, C.; Pandis, S.N. ISORROPIA: A new thermodynamic equilibrium model for multiphase multicomponent inorganic aerosols. *Aquat. Geochem.* **1998**, *4*, 123–152.
45. Strader, R.; Lurmann, F.; Pandis, S.N. Evaluation of secondary organic aerosol formation in winter. *Atmos. Environ.* **1999**, *33*, 4849–4863.
46. Byun, D.W.; Ching, J.K.S. *Science Algorithms of the EPA Model-3 Community Multiscale Air Quality (CMAQ) Modeling System*; Office of Research and Development, U.S. EPA: Washington, DC, USA, 1999.
47. Louis, J.F. A Parametric Model of Vertical Eddy Fluxes in the Atmosphere. *Bound. Lay. Meteor.* **1979**, *17*, 187–202.
48. Granier, C.S.; Darras, H.; Denier van der Gon, J.; Doubalova, N.; Elguindi, B.; Galle, M.; Gauss, M.; Guevara, J.-P.; Jalkanen, J.; Kuenen, C.; et al. *The Copernicus Atmosphere Monitoring Service Global and Regional Emissions*; Report April 2019 version [Research Report]; ECMWF: Reading, UK, 2019; doi:10.24380/d0bn-kx16.
49. Benešová, N.; Belda, M.; Eben, K.; Geletič, J.; Huszár, P.; Juruš, P.; Krč, P.; Resler, J. and Vlček, O.: New open source emission processor for air quality models. In Proceedings of Abstracts 11th International Conference on Air Quality Science and Application, Barcelona, Spain, 12–16 March 2018; Sokhi, R., Tiwari, P.R., Gállego, M.J., Craviotto Arnau, J.M., Castells Guiu, C., Singh, V., Eds.; University of Hertfordshire: Hatfield, UK, 2018; doi: 10.18745/PB.19829.
50. Passant, N. *Speciation of UK Emissions of Non-Methane Volatile Organic Compounds*; DEFRA: Oxon, UK, 2002.
51. Bultjes, P.J.H.; van Loon, M.; Schaap, M.; Teeuwisse, S.; Visschedijk, A.J.H.; Bloos, J.P. *Project on the Modelling and Verification of Ozone Reduction Strategies: Contribution of TNO-MEP*; TNO-report, MEP-R2003/166; TNO: Apeldoorn, The Netherlands, 2003.
52. Van der Gon, H.D.; Hendriks, C.; Kuenen, J.; Segers, A.; Visschedijk, A. Description of Current Temporal Emission Patterns and Sensitivity of Predicted AQ for Temporal Emission Patterns. EU FP7 MACC Deliverable Report D\_D-EMIS\_1.3. 2011. Available online: [http://www.gmes-atmosphere.eu/documents/deliverables/d-emis/MACC\\_TNO\\_del\\_1\\_3\\_v2.pdf](http://www.gmes-atmosphere.eu/documents/deliverables/d-emis/MACC_TNO_del_1_3_v2.pdf) (accessed on 19 May 2020).
53. Guenther, A.B.; Jiang, X.; Heald, C.L.; Sakulyanontvittaya, T.; Duhl, T.; Emmons, L.K.; Wang, X. The Model of Emissions of Gases and Aerosols from Nature version 2.1 (MEGAN2.1): An extended and updated framework for modeling biogenic emissions. *Geosci. Model Dev.* **2012**, *5*, 1471–1492, doi:10.5194/gmd-5-1471-2012.
54. Vaisala's Ceilometer CL31. Available online: <https://www.vaisala.com/en/products/instruments-sensors-and-other-measurement-devices/weather-stations-and-sensors/cl31> (accessed on 19 May 2020).
55. Vaisala's Ceilometer CL51. Available online: <https://www.vaisala.com/en/products/instruments-sensors-and-other-measurement-devices/weather-stations-and-sensors/cl51> (accessed on 19 May 2020).
56. *User's Guide: Vaisala Boundary Layer View Software BL-VIEW*; Vaisala Oyj: Helsinki, Finland, 2010.
57. National Centers for Environmental Prediction/National Weather Service/NOAA/U.S. Department of Commerce. *NCEP GFS 0.25 Degree Global Forecast Grids Historical Archive*; National Center for Atmospheric Research, Computational and Information Systems Laboratory: Boulder, CO, USA, 2015; doi:10.5065/D65D8PWK.
58. Sharma, A.; Fern, H.J.; Hamlet, A.F.; Hellmann, J.J.; Barlage, M.; Chen, F. Urban meteorological modeling using WRF: A sensitivity study. *Int. J. Climatol.* **2017**, *37*, 1885–1900. doi:10.1002/joc.4819.

59. Warner, T.T. *Numerical Weather and Climate, Prediction*; Cambridge University Press: Cambridge, UK, 2011.
60. Gillespie, A. Land Surface Emissivity. In *Encyclopedia of Remote Sensing*; Encyclopedia of Earth Sciences Series; Njoku, E.G., Ed.; Springer: New York, NY, USA, 2014.
61. Madronich, S.; Flocke, S.; Zeng, J.; Petropavlovskikh, I.; Lee-Taylor, J. *Tropospheric Ultraviolet-Visible Model (TUV)*; version 4.1.; National Center for Atmospheric Research: Boulder, CO, USA, 2002.
62. Šopko, F., Vlček, O., Juras, R., and Škáchová, H.: Meteorological analysis of the extensive smog situations in January and February 2017 in the Czech Republic. *Meteorol. Bull.* **2017**, *70*, 107–133.
63. Oke, T.; Mills, G.; Christen, A.; Voogt, J. *Urban Climates*; Cambridge University Press: Cambridge, UK, 2017; doi:10.1017/9781139016476.
64. Richards, K. Observation and simulation of dew in rural and urban environments. *Prog. Phys. Geogr.* **2004**, *28*, 76–94.
65. Teixeira, J.C.; Fallmann, J.; Carvalho, A.C.; Rocha, A. Surface to boundary layer coupling in the urban area of Lisbon comparing different urban canopy models in WRF. *Urban Clim.* **2019**, *28*, 100454, doi:10.1016/j.uclim.2019.100454.
66. Zhu, K.; Xie, M.; Wang, T.; Cai, J.; Li, S.; Feng, W. A modeling study on the effect of urban land surface forcing to regional meteorology and air quality over South China. *Atmos. Environ.* **2017**, *152*, 389–404, doi:10.1016/j.atmosenv.2016.12.053.
67. Dawson, J.P.; Adams, P.J.; Pandis, S.N. Sensitivity of PM 2.5 to climate in the Eastern US: A modeling case study. *Atmos. Chem. Phys.* **2007**, *7*, 4295–4309, doi:10.5194/acp-7-4295-2007.
68. Grell, G.; ; Baklanov, A. Integrated modeling for forecasting weather and air quality: A call for fully coupled approaches. *Atmos. Environ.* **2011**, *45*, 6845–6851.
69. Baklanov, A.; Schlünzen, K.; Suppan, P.; Baldasano, J.; Brunner, D.; Aksoyoglu, S.; Carmichael, G.; Douros, J.; Flemming, J.; Forkel, R.; et al. Online coupled regional meteorology chemistry models in Europe: Current status and prospects. *Atmos. Chem. Phys.* **2014**, *14*, 317–398, doi:10.5194/acp-14-317-2014.



© 2020 by the authors. Licensee MDPI, Basel, Switzerland. This article is an open access article distributed under the terms and conditions of the Creative Commons Attribution (CC BY) license (<http://creativecommons.org/licenses/by/4.0/>).



Article

# Real-World Exhaust Emissions of Diesel Locomotives and Motorized Railcars during Scheduled Passenger Train Runs on Czech Railroads

Michal Vojtisek-Lom <sup>1,2,\*</sup> , Jonáš Jirků <sup>3</sup> and Martin Pechout <sup>4</sup>

<sup>1</sup> Department of Automobile, Combustion Engine and Railway Engineering,

Faculty of Mechanical Engineering, Czech Technical University of Prague, 160 00 Prague, Czech Republic

<sup>2</sup> Department of Vehicles and Engines, Technical University of Liberec, 46117 Liberec, Czech Republic

<sup>3</sup> Department of Vehicle Technology, Faculty of Transportation Sciences, Czech Technical University in Prague, 110 00 Prague, Czech Republic; xjjirku@fd.cvut.cz

<sup>4</sup> Department of Vehicles and Ground Transport, Faculty of Engineering, Czech University of Life Sciences, 165 21 Prague, Czech Republic; pechout@tf.czu.cz

\* Correspondence: michal.vojtisek@tul.cz or Michal.vojtisek@fs.cvut.cz; Tel.: +420-774-262-854

Received: 17 April 2020; Accepted: 28 May 2020; Published: 2 June 2020



**Abstract:** The paper summarizes exhaust emissions measurements on two diesel-electric locomotives and one diesel-hydraulic railcar, each tested for several days during scheduled passenger service. While real driving emissions of buses decrease with fleet turnaround and have been assessed by many studies, there are virtually no realistic emissions data on diesel rail vehicles, many of which are decades old. The engines were fitted with low-power portable online monitoring instruments, including a portable Fourier Transform Infra Red (FTIR) spectrometer, online particle measurement, and in two cases with proportional particle sampling systems, all installed in engine compartments. Due to space constraints and overhead electric traction lines, exhaust flow was computed from engine operating data. Real-world operation was characterized by relatively fast power level transitions during accelerations and interleaved periods of high load and idle, and varied considerably among service type and routes. Spikes in PM emissions during accelerations and storage of PM in the exhaust were observed. Despite all engines approaching the end of their life, the emissions per passenger-km were very low compared to automobiles. Tests were done at very low costs with no disruption of the train service, yielded realistic data, and are also applicable to diesel-hydraulic units, which cannot be tested at standstill.

**Keywords:** locomotives; non-road engines; rail; diesel-electric; emissions; real-world emissions; portable on-board emissions monitoring systems; NO<sub>x</sub>; particulate matter; real driving emissions

## 1. Introduction

The Czech Republic, with 9567 km of active railroad lines [1], has one of the highest density railroad infrastructures in the world, on both per area (over 12 km per 100 km<sup>2</sup>) and per capita (over 9 km per 10,000 inhabitants) bases. Of these, about two thirds (6330 km) have electric traction lines (significant systems 3 kV DC and 25 kV 50 Hz) and one third (3237 km), mostly local lines with minimal traffic, rely on independent traction provided (except for historical trains using steam engines and battery powered locomotives in industrial yards) by diesel locomotives and railcars [1]. In 2018, railroads in the Czech Republic transported 190 million passengers, accounting for 10,292 million (or about 10<sup>10</sup>) passenger-kilometers (pkm) [2], roughly 1000 km per year per capita. There are 104 registered railroad operators [1] for freight and passenger transport; of these, state-run Czech Railways (ČD) account for about 90% of the passenger transport. In 2018, Czech Railways transported

179 million passengers (8225 million pkm), with a 2018 total of 2.58 million dispatched passenger trains and a total distance traveled of 124 million train-kilometers, at a mean train occupancy of 30% [3]. The company had 293 electric locomotives, 309 electric units, 215 diesel locomotives, 696 diesel railcars and units, and 2210 cars in passenger service in 2018, with additional 692 locomotives used in cargo service. The Czech Ministry of Transport register shows a total of 843 electric, 1120 diesel, and 36 steam locomotives, with diesel locomotives representing about one quarter of the total rated power [4]. In 2018, 78,000 t of diesel fuel were consumed on Czech railroads [5] (including passenger and freight services and construction and maintenance work), corresponding, at 30–35% electric power generating efficiency, to 11–13% of the primary energy used on railroads.

Railroads have been both praised for their superior fuel efficiency compared to other means of transport and criticized for using diesel locomotives with several decades old engines, which were not subject to any emissions standard. Rail engine emissions standards were introduced in Europe relatively late in 2004 (Directive 2004/26/EC), and the exhaust emissions from locomotive diesel engines have not been as scrutinized as those of their on-road counterparts. On the other hand, compared to motor vehicle engines, locomotive engines are often conservatively rated, operate at relatively constant load with no abrupt transients, and release their exhaust about 4 m above railroad tracks, allowing for more separation from nearby citizens. With Czech cities, and most other cities in Europe, suffering from high concentrations of nitrogen oxides (NO<sub>x</sub>) and particulate matter (PM), with an annual toll of premature deaths in Europe of about 0.1% of the population [6] and associated economic damages of outdoor air pollution of about 5% of the Gross Domestic Product [7], and with diesel engines being one of the key sources of both NO<sub>x</sub> and PM, the question of emissions is a legitimate one.

Unfortunately, there are very limited data available on the emissions performance of rail vehicles, especially when it comes to their typical operation, which may differ from the test conditions of laboratory and rail yard tests.

Most diesel locomotives use electric power transmission: A diesel engine drives a direct current (DC) generator or an alternator with a semiconductor rectifier. The generated electric power is transmitted to direct (DC) or alternating current (AC) traction motors driving individual axles. In the Czech Republic, DC generators and DC traction motors are used. At higher currents, the torque of a DC traction series motor is approximately proportional to the motor current. The maximum traction motor current is an important locomotive design parameter, as it reflects the maximum torque on the driven wheels, and the maximum force exerted on the train. The current is regulated indirectly by regulating generator voltage, taking into the account the back-induced voltage on the traction motor, which is approximately proportional to the motor speed, and the traction motor impedance. At any given power output, the voltage increases and the current decreases with the rotational speed. On most locomotives, the maximum power output is limited at lower speeds by the maximum traction motor current, and at higher speeds by the rated maximum power.

Typically, the diesel engine rpm and torque and the generator voltage and current are controlled automatically, with the only user-selectable input being the desired power output. While some newer systems allow for continuous regulation of the power output, most traditional systems use eight discrete power levels, called notches (from notches on early control levers).

In theory, the acceleration of a train from a standstill therefore proceeds at maximum traction force up to a certain speed, and, beyond this speed, at maximum power. The engineer typically progresses through higher notches as the train accelerates. This is, however, not always readily apparent, as the control system increases the engine power gradually. The engineers thus often do not wait for the transition to the current notch setting to be completed before selecting a higher notch. The highest notch setting used during the acceleration often depends on the elevation profile of the track, the posted speed of the track, and the total weight of the train. The full locomotive power is utilized on the mainline rail with average or heavier trains, but rarely with short trains or on slower regional lines.

The traditional method of measuring emissions on a diesel-electric locomotive relies on stationary operation of the locomotive, where the diesel engine drives the generator, which is disconnected from

the traction motors, and generated electrical power is directed to a load bank consisting of water-cooled resistors. The engine is then operated at discrete points. For example, the method prescribed by the U.S. Regulations [8,9] mandates operation at low and normal idle, followed by operation at notches 1–8. Emissions are measured during steady-state operation at each of the regimes with instrumentation typically located outside of the locomotive [10–17]. The measured emissions at each point are then aggregated into a weighted average by assigning a weight to each operating point.

This method does not necessarily represent realistic operation due to some simplifications. First, the procedure does not account for transient emissions during simultaneous acceleration of the engine and its transition to a higher load, which were visually observed by the authors on other locomotives, and which can account for a significant fraction of total PM emissions [18]. Second, the prescribed procedure may not properly account for the fraction of particulate matter which is retained in the engine and in the exhaust system at idle [19,20], and thus is not accounted for during idle, and is released after the transition of the engine to higher loads, with the levels gradually decreasing, and since the measurement is not started immediately after the change of the operating regime, it is not fully accounted for at higher loads either. Third, the prescribed procedure is markedly different from the typical operation of a passenger train locomotive, characterized by a relatively fast transition from lower to higher notches during acceleration. Fourth, the load bank procedure cannot be used with a diesel-hydraulic drivetrain, a widely used type of propulsion primarily on diesel rail units both in Czech Republic and in the rest of Europe [16,21].

As an alternative, on-track measurements using simple portable monitoring systems developed by the first author based on repair grade gas analyzers [22] and light scattering particle monitors [23] have been used in the Czech Republic [21,24] and the U.S. [25,26]. Another alternative to detailed tests of a relatively small number of vehicles is the remote sensing approach [27] allowing the measurement of a larger number of locomotives during passage through or near the measurement point [28,29].

This study sought to provide a realistic insight into the exhaust emissions from diesel locomotives and rail vehicles on Czech railroads, reviewing and reanalyzing data from several relevant monitoring campaigns conducted during real operation (analogous to real driving emissions of highway vehicles) with portable on-board emissions monitoring systems mounted on the tested machine.

The primary goal of this study was to characterize the emissions from diesel railcars and locomotives on Czech railroads under conditions relevant to normal, typical operation. This goal was motivated by the need to characterize the operating patterns and emissions of diesel-powered rail vehicles, in order to evaluate the potential for the utilization of advanced fuels, implementation of retrofits, and emissions benefits associated with redirecting a portion of transit long-haul truck traffic to rail.

The secondary goal of this study was to develop a methodology for practical measurement of exhaust emissions of in-use rail vehicles powered by internal combustion engines, preferably during their actual regular operation. This part was, in addition, motivated by the need to develop and demonstrate a suitable approach to measure real-world emissions on larger non-road engines (one possible definition is engines with rated power greater than 560 kW) using simple to install, robust on-board monitoring systems. Finally, the study was also motivated by the desire to demonstrate the suitability of a portable Fourier Transform Infra Red (FTIR) analyzer as a universal instrument for measurement of gaseous pollutants, including greenhouse gases and reactive nitrogen species that could be relevant to modern aftertreatment systems and advanced fuels.

## **2. Experimental**

### *2.1. Rail Vehicles*

The test rail vehicles, shown on a photograph in Figure 1, were a 749 series ČKD diesel-electric locomotive, a 754 series ČKD diesel-electric locomotive (both ČKD Praha, Czechoslovakia), and an

854 series diesel railcar (Vagónka Studénka, Czechoslovakia, now Škoda Vagónka a.s., Studénka, Czech Republic).



(a) ČKD Series 749 locomotive (1968)



(b) Series 854 diesel railcar (1968)



(c) ČKD 754 locomotive (1979)

**Figure 1.** Test vehicles: (a) ČKD Series 749 diesel-electric locomotive, ČKD; (b) Vagónka Sduténka diesel railcar series 854 with hydraulic power transmission; and (c) ČKD 754 Series diesel-electric locomotive.

The 749 series is a four-axle, 75-t diesel-electric locomotive, made at ČKD Praha in 1968. It has one main engine, an inline, four-stroke, six-cylinder turbocharged diesel engine with four valves per cylinder, a bore of 310 mm, stroke of 360 mm, and displacement of 163 dm<sup>3</sup> (liters), with rated power of 1100 kW at 750 rpm. The fuel is delivered by cam-driven unit injectors. The engine is coupled with a direct-current traction generator, a 3000 V direct-current generator for electrical heating of the railcars, a 120 V DC generator for the locomotive electrical system, an air compressor for brakes and accessories, and hydraulic motors for accessories, such as cooling fans. The traction generator supplies electric power to four traction motors, one at each driven axle.

The 754 series is a four-axle, 74-t diesel-electric locomotive, made at ČKD Praha in 1979, with an original twelve-cylinder turbocharged K 12 V 230 DR diesel engine (ČKD Praha) with a displacement of 129.5 dm<sup>3</sup> and a rated power of 1460 kW at 1100 rpm. The fuel is delivered by cam-driven unit injectors. The engine is coupled with a 1100 kW DC traction generator directly feeding four DC traction motors, one at each axle. The engine also powers a 300 kW 3000 V DC auxiliary power generator for passenger car heating, air compressor, and various accessories.

The 854 series is a four-axle, 56-t diesel railcar with a rated capacity of 108 passengers, made at Vagónka Studénka in 1968. The railcar was originally fitted with a ČKD KS 12 V 170 DR engine

coupled with a Praga hydrodynamic transmission with a torque converter. In 2004, the railcar was retrofitted with a Caterpillar 3412 E DI-TA turbocharged twelve-cylinder 29 dm<sup>3</sup> engine, derated to 588 kW at 1460 rpm to maintain compatibility with the original transmission. The railcar is typically coupled with 1–3 non-motorized trailing cars depending on the anticipated travel demand.

## *2.2. Route and Testing Procedures*

All three vehicles were, at the respective time of the tests, based at the depot Praha–Vršovice and used on scheduled service on Praha–Turnov–Tanvald line. The diesel-electric locomotives were used primarily on express service. The 854 railcar was used for both express and local service on Praha–Turnov segment in configurations comprising of none, one, two or three non-motorized trailing cars.

The Tanvald route (depicted in Figure 2 left) features runs from the Prague main station on a main line corridor with 3 kV direct current (DC) traction lines, and after about 7 km, separates from the mainline and steadily climbs from Prague onto a mid-country plateau. From Turnov, the track runs along the Jizera river gorge, and terminates with a steep climb along the Kamenice gorge into Tanvald, a small city in the Jizera mountains. The route is typically served by diesel units with 2–4 cars, with larger five-car trains operated on weekends due to tourist traffic.

The 749 locomotive was also temporarily used on the Praha–České Budějovice line. The Praha–Zdice–Písek–České Budějovice (displayed on map as Figure 2 right) line is a regional line through rolling country, with the first part to Zdice and last part to České Budějovice being part of main-line corridors with 3 kV DC (Prague region) and 25 kV, 50 Hz (České Budějovice region) traction lines [30]. This line is of regional significance; most of the through traffic uses the electrified Praha–Tábor–České Budějovice line.

It should be noted that, on all lines, at the end of the line, the locomotive was decoupled from the train, driven on a parallel track to the other side of the railcars, and coupled on the railcar on the opposite end. This is the normal procedure for nearly all Czech trains, and for this reason, all locomotives and railcars can be driven in either direction from either end of the train. For this reason, both cabins and the passageway through the engine compartment have to remain clear during operation. In addition, the doors between the engine compartment and the cabins need to remain closed for fire safety and noise protection reasons.

The engines were instrumented during scheduled maintenance at the locomotive depot, allowing for about half a day installation time. The instruments were operated continuously during the regular service and were removed several days later during a short refueling and maintenance visit to the depot. During the service, a test engineer was riding either in the momentarily vacant train engineer cabin or as a passenger on the train, periodically checking on the instruments at turnarounds or during longer stops.

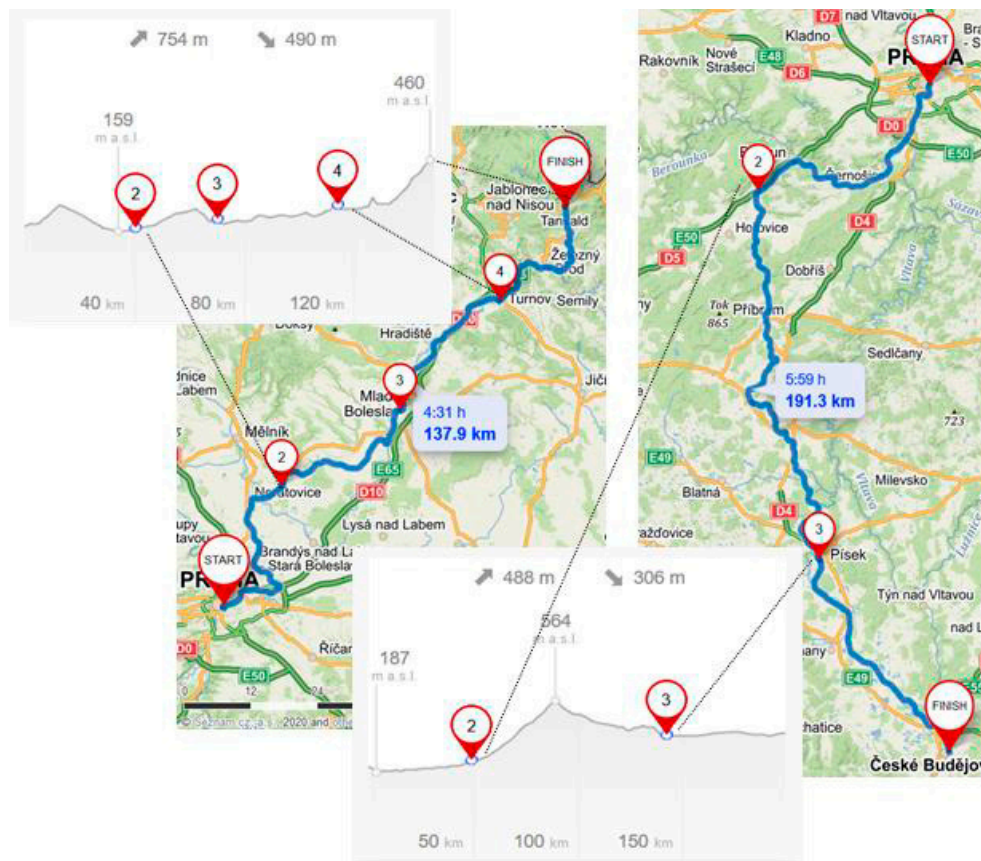
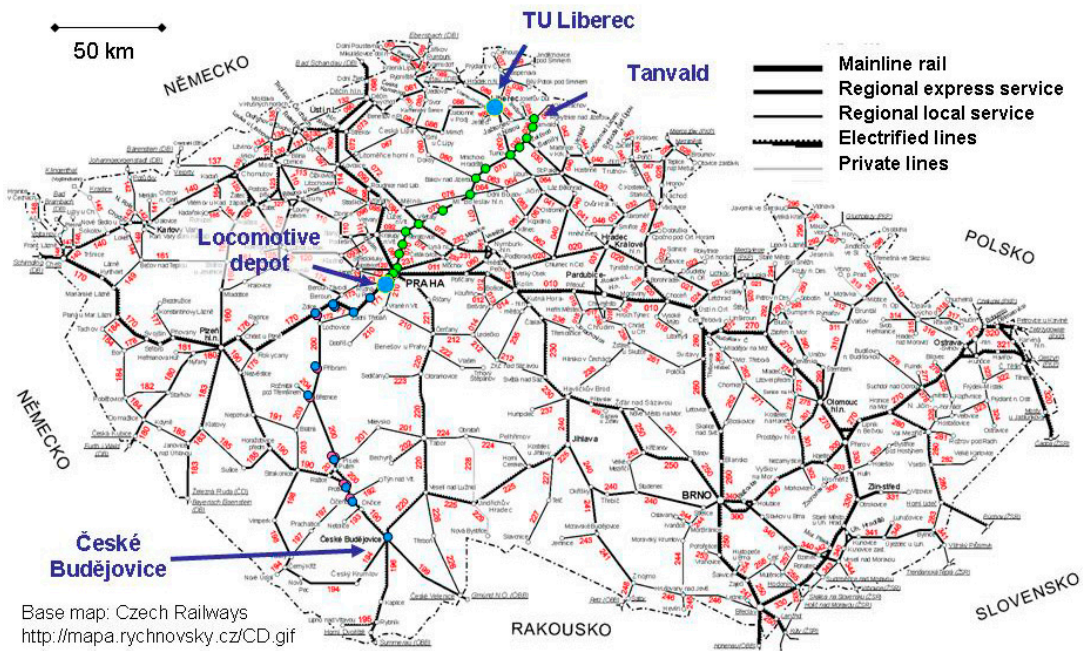


**Figure 2.** Test routes marked on the Czech railroad network (top) [30] and on cartographical maps (bottom) with associated elevation profiles (source: [31]) with highlighted operated routes and marked major points: Praha–Tanvald (left): 2, Vsetaty; 3, Mlada Boleslav; and 4, Turnov; Praha–České Budejovice (right): 2, Zdice; 3, Pisek.

### 2.3. Test Equipment

Emissions were measured with a home-made monitoring system constructed by the first author, utilizing components typical for a BAR 97 standard [32] garage-grade five-gas analyzer and a laser light scattering instrument (modified model 8587A, TSI, St. Paul, MN, USA), sampling raw, undiluted exhaust, reheated prior to its introduction into the analytical part of the instrument to approximately 50 °C to prevent condensation of the water vapor. A parallel line was coupled to an inline heater and a proportional sampling system collecting particles on a filter for gravimetric measurement of total particle mass.

The gas analyzer employed a non-dispersive infra-red (NDIR) cell (modified version of Andros 6500, Lumasense, CA, USA, approved to BAR 97 standard) to measure the concentrations of hydrocarbons (HC, 0–10,000 ppmC), carbon monoxide (CO, 0–10%), and carbon dioxide (CO<sub>2</sub>, 0–16%), and an electrochemical cell to measure nitric oxide (NO, 0–5000 ppm). None of the engines were equipped with any exhaust aftertreatment device; therefore, concentrations of NO<sub>2</sub> in excess of several percent of the total NO<sub>x</sub> were not expected, and not measured. Gas analyzers normally require periodic zeroing and are subject to drifts caused by deposition of organic materials and water in the sample cell and by other factors. For this reason, two analyzers were often used in parallel [10,33]. Advances in analyzer technology, optimization of the warm-up procedure, addition of a reference channel, and extensive characterization of the analyzer in the laboratory have allowed for the use of a single analyzer without zeroing, with verification of the zero level at approximately 3-h intervals at each endpoint of the route.

The intake air mass flow was estimated using the speed-density method from the known engine displacement, the assumed engine volumetric efficiency, the engine rpm from the signal obtained from the locomotive control system (749 series) or directly measured by an optical sensor (754 and 854 series), and temperature and pressure of the charge in the intake manifold were measured by sensors inserted into a spare port in the intake manifold. This method was described in [34] and was reported to have a reasonable accuracy for road vehicle engines [23,33]. None of the engines used exhaust gas recirculation, so no compensation for the volume of the recirculated gas was necessary.

Analogous home-made and commercially produced monitoring systems have been used for on-road studies over the last two decades and have undergone extensive comparison testing. As a part of instrument validation for a California roadside truck study [35], total NO<sub>x</sub> and CO<sub>2</sub> were measured by the portable system (using calculated exhaust flow) and by a laboratory (using a full-flow dilution tunnel) on a light duty diesel truck over multiple transient cycles driven multiple times. The correlation of total emissions per test (for the three monitoring systems, slopes were 1.05–1.06 for NO<sub>x</sub> and 0.94–0.96 for CO<sub>2</sub>, Pearson's R<sup>2</sup> coefficients were 0.991–0.997 for NO<sub>x</sub> and 0.990–0.998 for CO<sub>2</sub>). A similar comparison using three full-size diesel pickup trucks and a greater range of test cycles has shown a greater variance [34], approximately up to 15–20% for NO<sub>x</sub>, and, in most cases, approximately 20–30% for PM (quantitative data not given). As the total mass emissions per cycle are influenced by the concentration measurements, exhaust flow inference, and synchronization between concentration and exhaust flow data, a good agreement between the instruments on mass emissions over a transient cycle was taken as a validation of concentration and exhaust flow computations.

The monitoring system used here was tested at the state certification laboratory TUV-SUD Auto in Prague on a Euro 3 Iveco Tector highway diesel engine during both steady-state and transient tests. The intake air mass flow and the concentrations of CO, CO<sub>2</sub>, and NO<sub>x</sub> were comparable with the laboratory measurements (correlation of second-by-second data over European Transient Cycle: intake air flow, slope 0.986, R<sup>2</sup> = 0.961; CO<sub>2</sub>, slope 0.964, R<sup>2</sup> = 0.956; NO<sub>x</sub>, slope 0.949, R<sup>2</sup> = 0.73; CO, slope 0.932, R<sup>2</sup> = 0.627), except for the slower response for NO<sub>x</sub>, especially during decreasing concentrations, and for CO at very low concentrations (below about 0.02%).

The monitoring system has also undergone extensive comparison testing at the departmental engine laboratory on a Zetor 1505 tractor engine with a mechanically controlled inline injection pump and no aftertreatment, certified to approximately 4 g/kWh NO<sub>x</sub> and 0.3 g/kWh PM. The laser scattering

method, when used with raw, undiluted exhaust, pumped at a relatively fast rate, reheated to prevent condensation of water in the instrument, provided a reading that was, during comparison tests, mostly within 20–25% of PM mass [36] when running on diesel fuel. However, previous experience of the first author [34] as well as of others [37] with this method and theoretical considerations of the density [38] and fractal dimension [38,39] all suggest that the light scattering instrument reading might be reasonably proportional to the mass concentration of PM, but not necessarily at a unity slope. Therefore, the PM measurements were calibrated with parallel gravimetric measurements during steady-state operation. For the 749 series tests, the gravimetric sampling system was analogous to the first part of the field PM measurement system described in CARB Method 5 [40] (without the second part consisting of impingers), working with undiluted exhaust, and was operated at 45–50 °C, a common temperature for diesel particulate measurement, and an allowed temperature under Method 5. Fluorocarbon coated borosilicate glass 47 mm diameter PallFlex T60A20 filters, conditioned and weighted prior to and twice after the testing using standard vehicular PM emissions measurement procedures [41], were used. For subsequent tests, proportional sampling system developed by the authors (description and validation in [42]) was used.

On the 854 series, a portable FTIR analyzer (modified I-series, MIDAC, Irvine, California, USA), was used to measure spectra in mid-infrared region (4000–650  $\text{cm}^{-1}$ ) at 0.5  $\text{cm}^{-1}$  optical resolution. The instrument uses a Michelson interferometer, zinc selenide optics, and mercury cadmium telluride detector cooled by liquid nitrogen, all housed in airtight enclosure, and a custom 6 m path length optical cell heated to 121 °C. The spectra were then interpreted for greenhouse gases  $\text{CO}_2$ ,  $\text{CH}_4$ , and  $\text{N}_2\text{O}$ , as well as CO, NO,  $\text{NO}_2$ , ammonia, and formaldehyde, with quantitative assessment of the presence of additional compounds present at higher concentrations. The analysis was validated during laboratory and on-road tests of passenger cars [43]. In addition, on the 854 series, a commercial portable particle number monitoring instrument (NanoMet3, Matter Engineering, Switzerland), compliant with the EU requirements for solid particle number portable emissions monitoring systems (see [44] for review and uncertainty analysis), was used to measure non-volatile particle number concentrations. The instrument also reported the mean particle diameter and the total particle mass concentration. The FTIR and the NanoMet were supplied with a sample line operated at 150 °C.

On the two diesel-electric locomotives, analog voltage signals of the engine rpm and voltage and current on the traction generator were extracted from the locomotive control system and logged by a galvanically separated analog-to-digital converter. On the 854 series motor car, engine output power was inferred from the fuel consumption, calculated from total carbon exhaust emissions, and from brake-specific fuel consumption data provided by the manufacturer.

The position and speed of the locomotive was measured by a GPS receiver mounted on the side of the roof of the locomotive. The GPS was operational through most of the route, excluding tunnels and deep river gorges.

The overall uncertainty of the measurements (measured emissions vs. actual emissions from the measured unit at the time of the measurement) was estimated to be within 5% for concentrations of  $\text{NO}_x$ , CO, and  $\text{CO}_2$ ; within 20–25% for PM and PN concentrations; within 2% for engine rpm, intake manifold pressure, and temperature; within 5% for measured power output; within 5–10% for the computed exhaust flow; within 10–15% for measured emissions of  $\text{NO}_x$ ,  $\text{CO}_2$ , and fuel consumption; and within 30% for emissions of particulate matter (number and mass).

#### *2.4. Installation and Exhaust Sampling*

Before the tests, several visits to the depot were made to plan the test, consisting of a physical inspection of the locomotive, discussions with the depot personnel including a locomotive control system specialist and a train engineer, securing a permit for up to two researchers to be present on the locomotive, and an introductory trip in the locomotive on both lines by the third author, during which operation and track conditions were noted.

This preparation revealed several severe restrictions placed on the instrumentation, with the most severe one imposed by the presence of 3 kV or 25 kV traction lines directly above the exhaust stack. To prevent damage to the instruments or even a fault current through the locomotive chassis caused by an excessive proximity of the sampling system with the traction line, a well-secured sampling system which does not protrude upwards more than several cm was needed. Another critical condition was that the train service must not be delayed or disrupted.

The locomotives have cabins on both ends, with the rear-facing cabin theoretically offering sufficient room for placement of the instrumentation. The locomotive direction is, however, reversed in both Tanvald and České Budějovice, and during switching of the trailing cars at Praha hl.n. (Prague main station) and at Praha–Vršovice station. In addition, for security reasons, the door between the cabin and the engine compartment has to be closed during the operation, not allowing for easy passage of sample lines or electrical cables between the engine compartment and the cabin. The cabins are connected by a walkway on one side of the main engine, which has to remain passable for the engineer.

Attempts were made to use ports in the exhaust system, but these were well rusted-in, and could not be removed without the danger of breaking the bolt. Combined with the hazards posed by tree branches on the sides of the locomotive, and the absence of a roof opening into the cabin and of a passage between the cabin and the engine room, the conditions mandated a very frugal, simple, and robust installation of the sampling system, and placement of the monitoring system in the corner of the engine room opposite of the passageway, on the alternator side (Figures 3–5).

These conditions dictated the choice of the monitoring system. Raw, undiluted exhaust was sampled by three separate 6 mm internal diameter copper probes, bent during installation to face into the stack, and directed along and grounded to the stack rim, on the roof, through a handle on the roof, and transitioning into 6 mm internal diameter conductive flexible polymer lines, leading through a crack in the partially open and secured engine compartment roof hatch into the engine control room, and along the roof of the control room to the instrument. On the 854 series, the sampling line was heated to 150 °C and heavily insulated.

The choice of electric power supply at the locomotive—110 V DC used in the locomotive electrical system, 3000 V DC for heating, and variable voltage from the traction generator—did not readily offer an option for powering of the instrumentation, which was supplied from two 12 V, 60 Ah absorbed gel mat, starved-electrolyte lead-acid deep-cycle batteries, except for the 854 series tests, where four 13.3 V, 90 Ah LiFeYPO traction batteries and a 2 kW inverter/charger were used due to heated sampling train. Prior to the tests, the power consumption of all components was strictly minimized to allow for 4–8 h of runtime on a single charge, with recharging wherever possible at end stations and overnight.



**Figure 3.** ČKD Series 749 diesel-electric locomotive: ČKD K 6 S 310 DR engine (left); locomotive controls (middle); and portable emissions monitoring system (right).

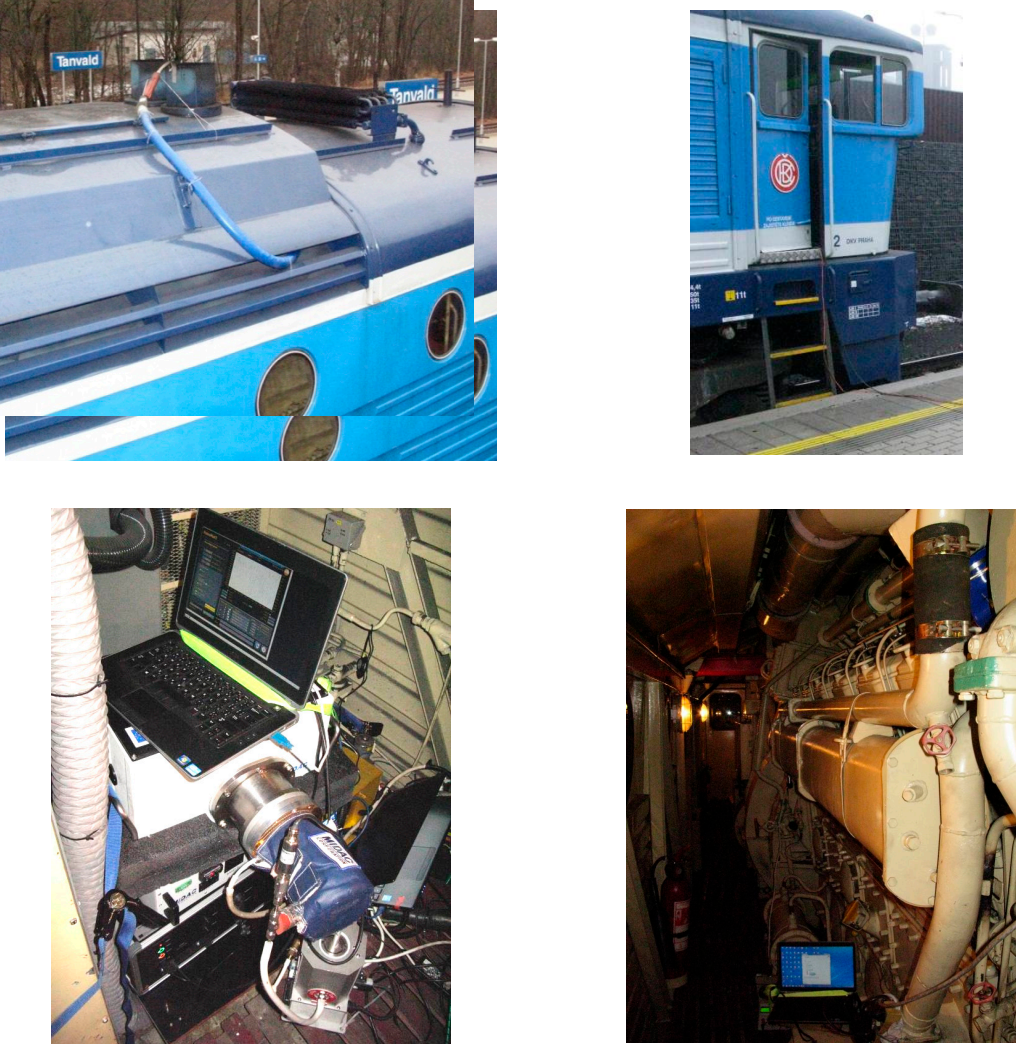


**Figure 4.** ČKD Series 754 diesel-electric locomotive tests: heated sampling line (top left); cabin door detail (top right); portable emissions monitoring system (bottom left); ČKD K 12 V 230 DR engine (bottom right).



**Figure 5.** Series 854 diesel-hydraulic railcar tests: installation of the sampling line (left); sampling probe (middle); and portable emissions monitoring system (right).

The instrumentation was galvanically separated from the locomotive, except for static charges dissipated through the conductive sampling lines ( $<10^6$  Ohm/m) to the probes, which were grounded to the locomotive chassis. This setup was also selected to minimize a possible damage to the instrument from the presence of the traction lines.

### 3. Results

For a representative Praha–Tanvald run of the 749 locomotive, the running speed and power are plotted in the upper part, and the measured concentrations of CO, NO, and PM in the lower part, of Figure 6. Throughout the work, “power” denotes electrical power transmitted from the generator to the traction motors, which was the only kind of power that could be effectively measured.

The verification of the PM measurement by simultaneous gravimetric sampling took place during periods over which steady state operation was anticipated during this run. Nine filters were used: two served as a blank, two were damaged during handling in the moving locomotive, and five used for measurements. The PM concentrations determined from the filter measurements are plotted in Figure 7 and are overlaid on the continuous PM concentrations measurement by the nephelometer. It should be noted that each measurement uses a different axis, with nephelometer measurements being 65% higher than the gravimetric ones. The filter mass was not corrected for background concentrations, as undiluted exhaust was used. The change of the mass of two “blank” filters was within 2 µg.

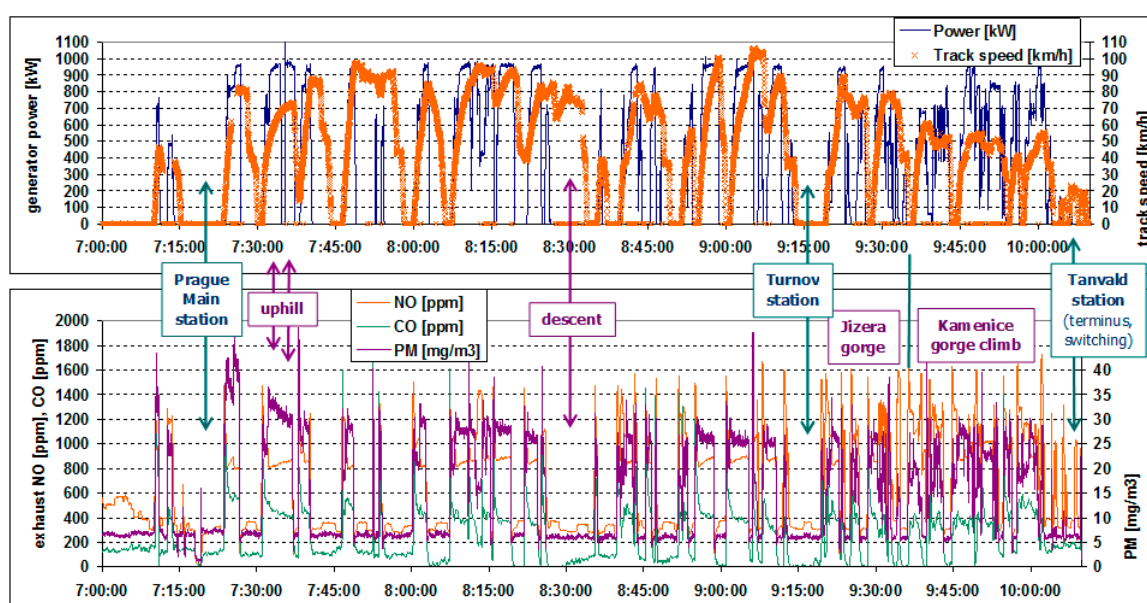


**Figure 6.** Measured values of running speed and generator power output (top); and concentrations of NO<sub>x</sub>, PM, and CO in the exhaust (bottom) of the ČKD 749 diesel-electric locomotive pulling a five-car, 297 t passenger train on the Praha–Tanvald line along a foothills route.

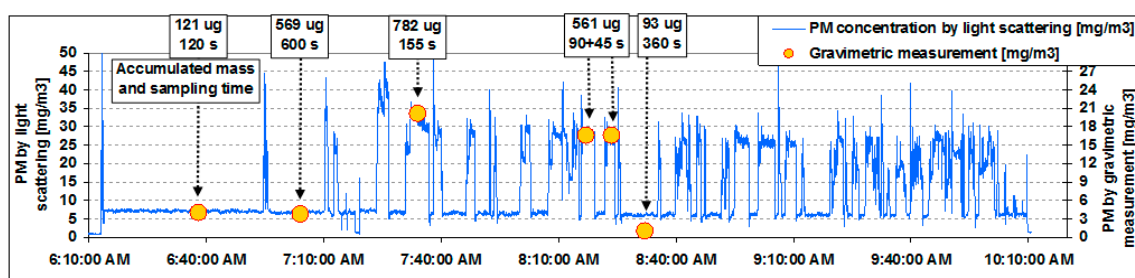


**Figure 7.** Comparison of particulate matter concentrations measured dynamically by light scattering with gravimetric measurements conducted during steady-state operation at idle and high load.

Analogous plots are given for the Praha–České Budějovice run in Figure 8. In Figures 6 and 8, it is apparent that the engine alternates between idle and a higher load level, given by the track profile and the mass of the train. The “higher load level” was higher on the Praha–Tanvald line, a hilly route traveled with a five-car train, and lower on the Praha–České Budějovice line, a nearly level line run with only two cars. The cumulative distributions of the locomotive power for both lines are given in Figure 9.

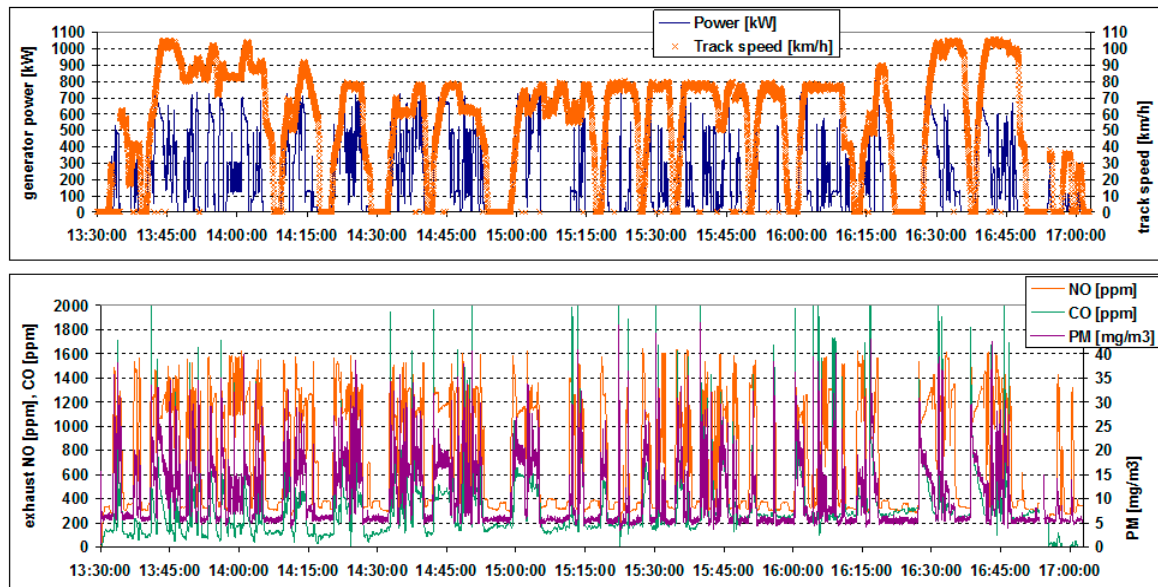


**Figure 8.** Measured values of running speed and generator power output (top); and concentrations of NO<sub>x</sub>, PM, and CO in the exhaust (bottom) of the ČKD 749 diesel-electric locomotive pulling a two-car, 160-t passenger train on the Praha–České Budějovice line.

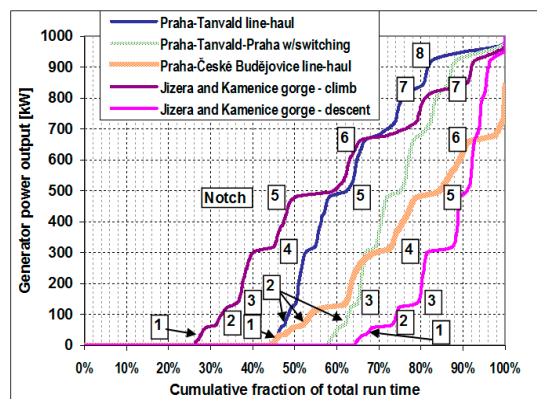


**Figure 9.** Cumulative distribution of locomotive generator output for the Praha–Tanvald line per schedule and with rides to/from depot and shunting cars at endpoints, and for major incline sections of this line along river gorges, and for Praha–České Budějovice line.

The transition from idle to a higher load is in several steps of a relatively short duration, with higher power levels selected as soon as the train speed becomes sufficient to keep the traction motor current below the maximum limit. The transition from a higher load level to idle is instantaneous. The track speed and the traction motor power and current are plotted for a typical acceleration to a higher cruising speed in Figure 10 (left), and to a lower speed in Figure 10 (right). Figure 10 also demonstrates the relationship between track speed and traction motor voltage, current, and power, discussed in the introduction.

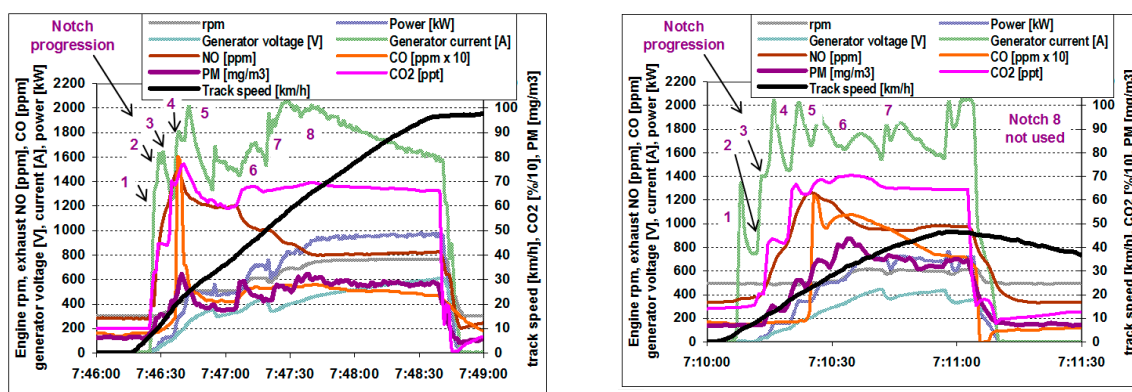


**Figure 10.** Generator voltage, current and power, running speed, and concentrations of NO<sub>x</sub>, CO, and PM during an acceleration of the five-car train from a station to high speed (left) and to a lower speed (right).

As apparent in Figure 6, Figure 8, and Figure 10, the only operating points where the emissions were somewhat stabilized were idle and full-load (notch 8) accelerations of one to several minutes in duration. Even there, the values were far from stable. At idle, the combustion chamber gradually cooled down and the particle concentrations increased, while NO<sub>x</sub> concentrations decreased. The opposite trend was apparent after a transition to notch 8, with additional increases in particle concentration due to the reentrainment of previously deposited semivolatile particulate matter in the exhaust system [20]. For three selected longer uninterrupted accelerations at notch 8, the concentrations of particulate matter and NO<sub>x</sub> are shown in Figure 11. It is apparent that in none of the cases a steady-state value is reached. However, all type approval and in-use tests use steady-state values obtained at stabilized operation at a given notch. For comparison with legislative tests, stabilized values can be reasonably inferred by extrapolation of computed regression lines, as shown in Figure 11 along with regression equations obtained by an iterative process discussed in [45]. Such inference has, however, little relevance to the real world emissions, as it is not apparent that such steady-state values are reached during normal operation. For the same reason, modeling emissions by recording the notch used and assigning a corresponding steady-state emissions factor to the respective time period is of limited relevance.

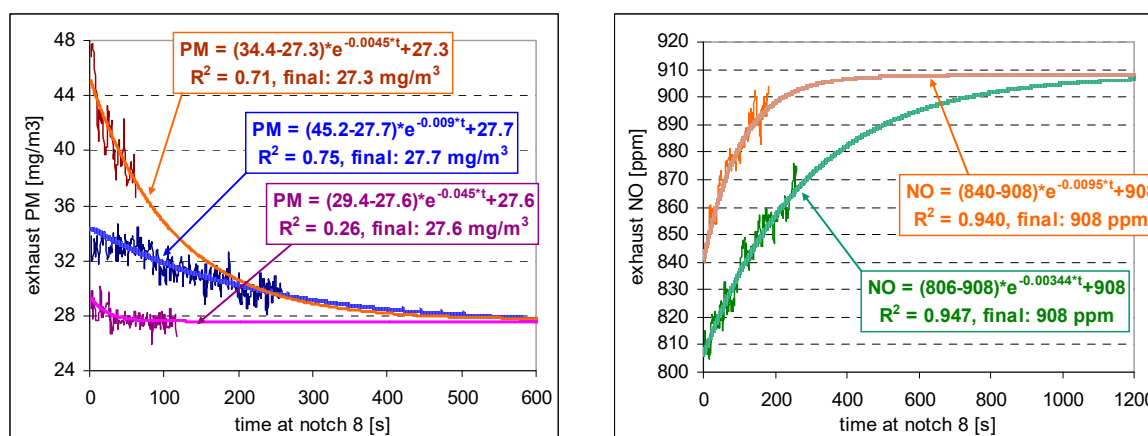
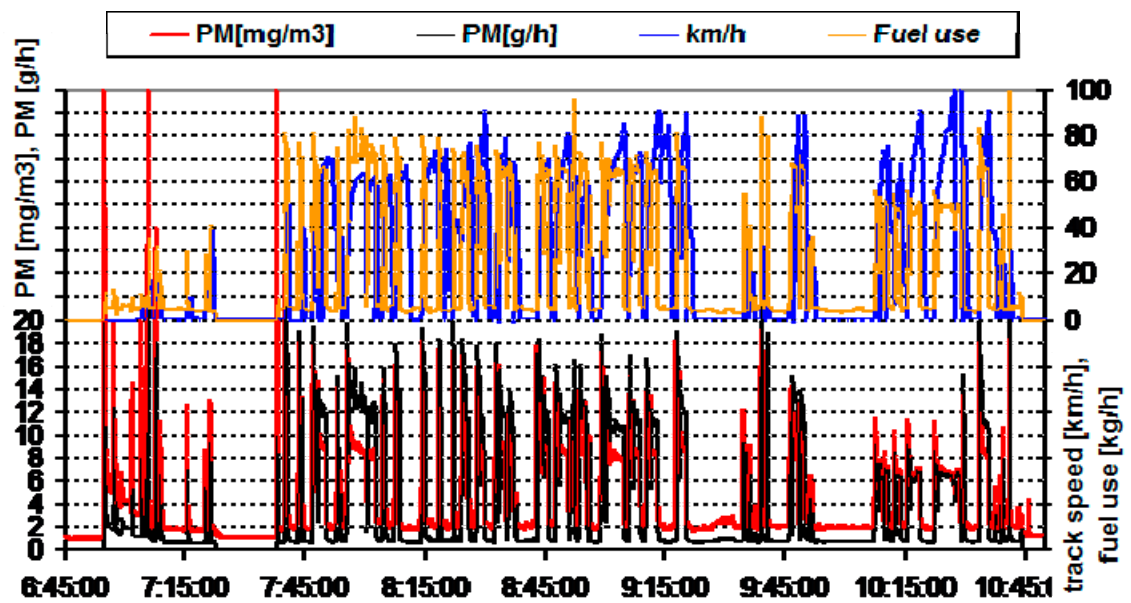


**Figure 11.** Estimate of steady-state notch 8 concentrations of PM (left) and NO (right) by extrapolation (described in [45]) of measured data.

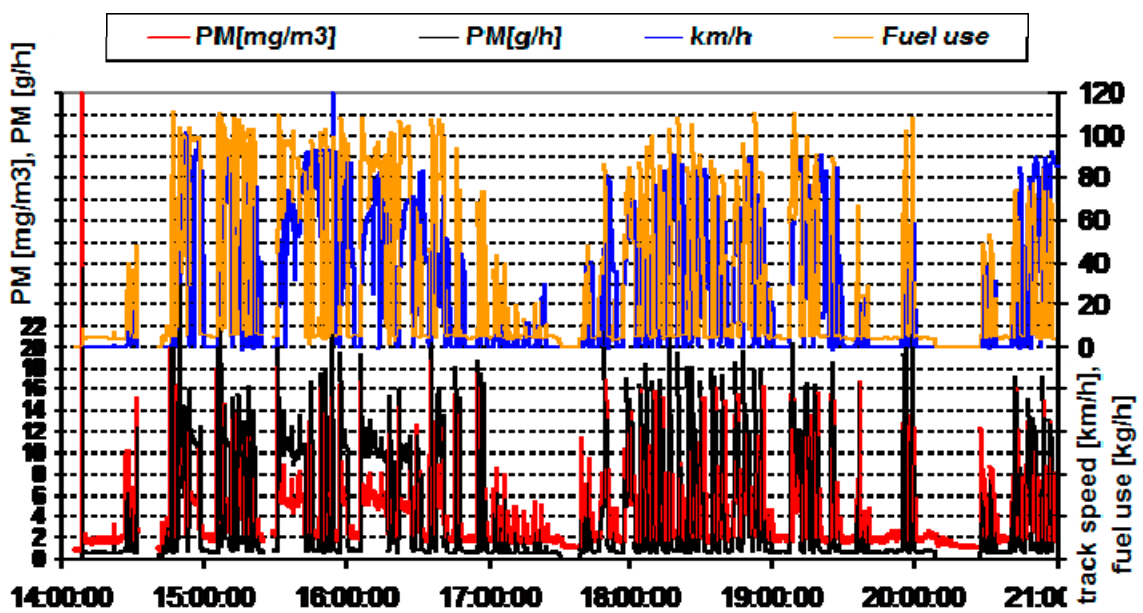
The engine in the diesel-hydraulic railcar showed somewhat different operating characteristics. The control of the power output is continuous, and the engine is either at idle or within a relatively narrow working range of the rpm. Figure 12a shows the morning operation of the 854 railcar, consisting of switching at the depot and traveling to the station at 6:50–7:20, a local service from Praha to Mladá Boleslav from 7:35 to 9:20 in 1 + 1 configuration (854 + 1 trailing car), followed by switching to 1 + 0, a short local run, and a local run to Turnov. Fuel consumption in kg/h and track speed in km/h is shown on the right axis in the upper portion of the graph, while the lower portion of the graph shows particulate matter concentrations in the exhaust and PM mass emissions rates on the left axis.

The same variables are plotted in Figure 12b for the afternoon express service Turnov–Praha in 1 + 3 configuration (854 + 3 trailing cars, 14:30–17:30), followed by a local service from Praha to Mladá Boleslav in a 1 + 2 configuration (17:40–19:40), followed by a short local service there and a return trip, during which the measurements were terminated at an intermediate stop shortly after 21:00.

It is apparent that particulate matter emissions were high after a cold start (details in Figure 13a) and also after a transition to a high load for some period after the cold start or a longer idle, and there were moderate spikes following a transition from idle to a load. The fuel consumption at load was relatively steady, and ranged about 50–110 kg/h depending mostly on the number of trailing cars coupled to the 854 and on the track profile (track speed and incline). This fuel consumption corresponds to an engine-out power of slightly over 200 kWh to slightly over 500 kWh, or about 35–90% of the engine rated power. This pattern of the fuel consumption being more or less the same for most of the periods under load corresponding to the train engineers making a deliberate decision about the target power output depending on the total mass of the train, leading to comparable acceleration rates among train configurations. There is a lack of “steady-state” operation: the train is accelerated at a pre-determined power to the desired speed (either the posted track speed or a speed chosen by the engineer), after which the train coasts down with the engine at idle until either another acceleration is commanded or the train approaches a station (see Figure 13b for detail of a local run). On the 854 railcar, braking is done by pneumatically controlled friction brakes; newer railcars use, in addition, a retarder built into the hydrodynamic transmission. Diesel-electric locomotives and railcars use electrodynamic braking, where electric power generated in traction motors is dissipated in resistor banks on the roof of the locomotive. The avoidance of fractional engine loads at cruise is beneficial to the fuel economy. It should also be noted that the engine is shut off for safety reasons during coupling and decoupling of the railcars, and also for fuel efficiency reasons during longer stops (over tens of minutes), unless the engine has been operated at a high load, in which case it is left idling to allow for removal of the heat from the engine compartment through cooling and active ventilation. The fuel consumption at idle (596–602 rpm) ranged from 3.4 to 5.6 kg/h, with variations attributed to accessory loads (alternator and air compressor supplying the whole train, cooling fan and cooling pumps of the engine).

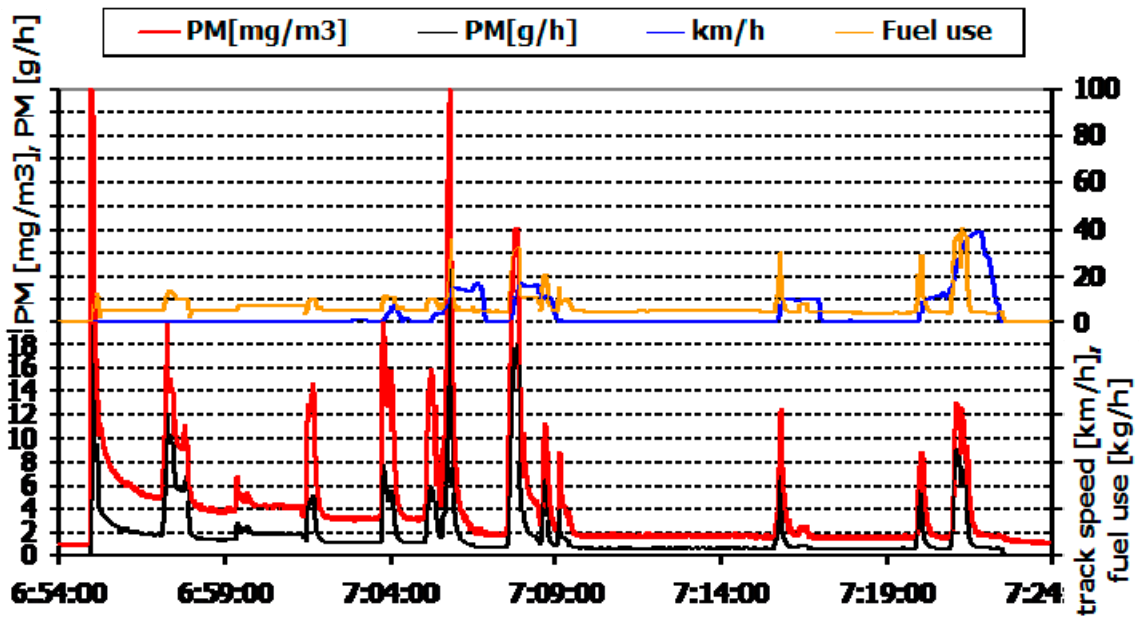


(a)

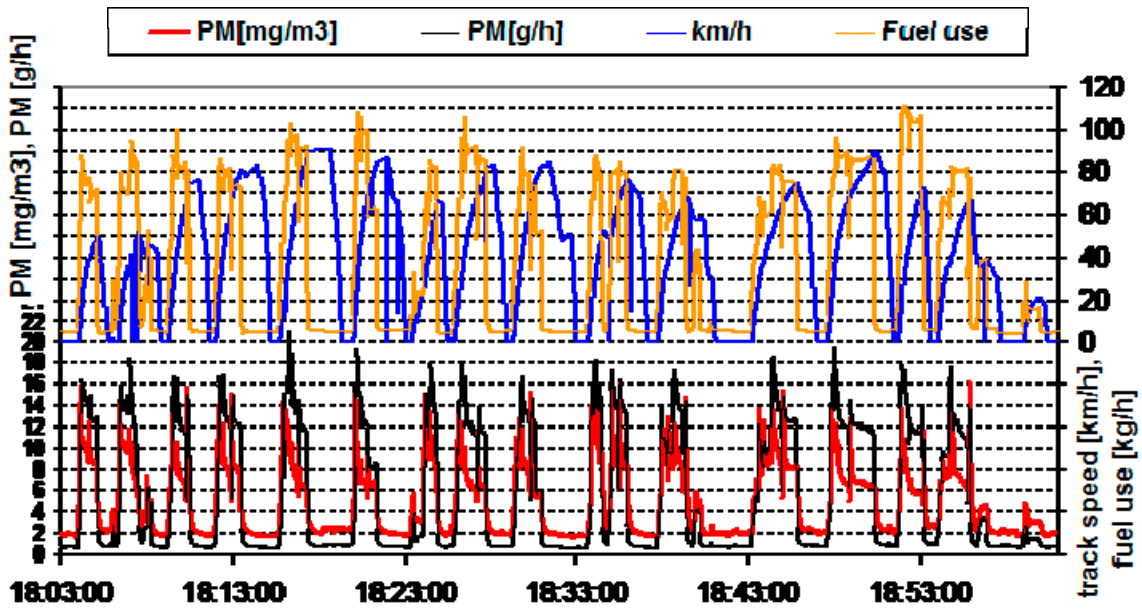


(b)

Figure 12. Track speed, fuel consumption, and particulate matter emissions from an 854 series railcar during (a) morning and (b) afternoon service on local and express trains on the Praha–Turnov line.



(a)



(b)

Figure 13. Track speed, fuel consumption, and particulate matter emissions from an 854 series railcar, showing: (a) cold start and switching at the depot; and (b) local service.

PM and NO<sub>x</sub> emission rates as a function of the instantaneous fuel consumption are plotted in Figure 14. The slope of the graphs represents fuel-specific emissions (in grams per kg fuel). In addition, as engine power is nearly a linear function (with a non-zero offset) of the fuel consumption [46], brake-specific emissions in g/kWh may be inferred from the slope. Unfortunately, the slope is not linear and is not uniform. Higher PM is apparent during cold engine operation and during transients, but also, higher engine loads are characterized by—compared to medium loads—relatively lower PM and relatively higher NO<sub>x</sub>. The simultaneous relative increase in NO<sub>x</sub> and a relative decrease in PM resembles a typical shift along the diesel engine NO<sub>x</sub>–PM curve, and therefore appears to be a result of engine calibration, not necessarily applicable to rail engines in general.

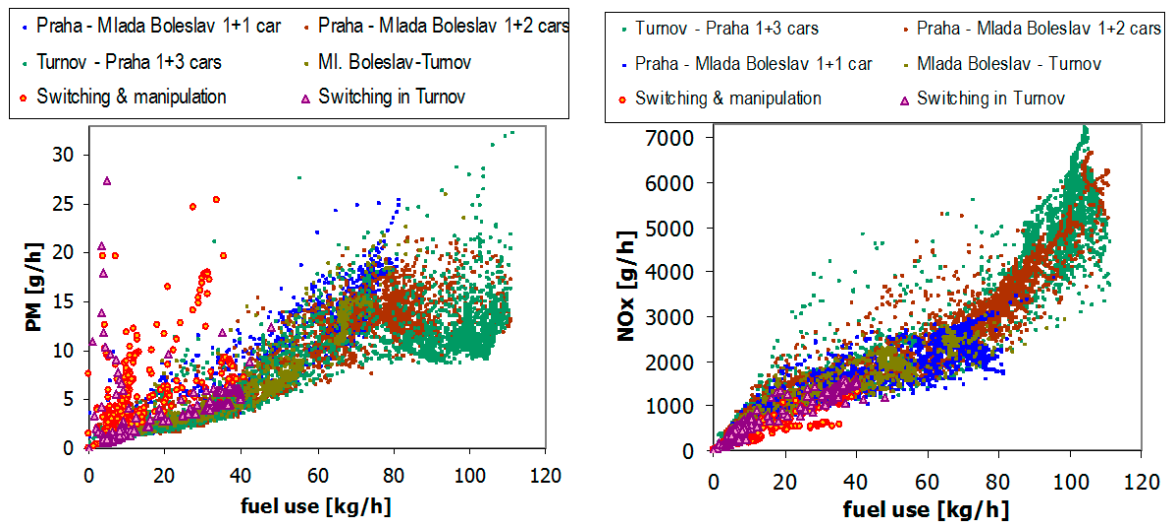


Figure 14. Emission rates from an 854 series railcar: (a) particulate matter; and (b) nitrogen oxides.

The emissions, fuel consumption, and traction power (electric power delivered to traction motors, only available on 749), averaged over a line and expressed per km driven, are provided in Table 1. The 749, on its return to Prague, was stopped in Všetaty (near Prague) due to a temporary track closure, and sent back to Tanvald on another service, changing places with a train scheduled on the same run 2 h earlier, leading to gaps in data due to insufficient battery voltage. For express trains running from Praha to Tanvald, separate sums are shown for the Praha–Turnov segment and for the slow, mountainous Turnov–Tanvald segment. For the 854 railcar, different configurations were separated to allow for an assessment of train weight.

The fuel consumption and emissions at idle are given in Table 2. As the engine provides power for both traction and auxiliary services, which on electric locomotives also includes electric heating of cars (trailing cars for 854 use auxiliary diesel-fired heaters), the auxiliary loads can be considerable. For 749 and 754, electric heating increased, on average, the fuel consumption by 22 kg/h, and NO<sub>x</sub> emissions by 1.5–2.1 kg/h (depending on the engine temperature), calculated as the difference between the idle power consumption during periods with heating and during periods near the end of the run when the heating was not active. Much smaller variations are attributable to automatic operation of the air compressor and the auxiliary cooling fans. It should be noted that, on many mechanically controlled diesel engines with constant static injection timing, NO<sub>x</sub> per kg fuel increases with decreasing engine rpm, due to start of the combustion occurring earlier on a crank angle position basis. The electric heating power consumption is a function of the number of the railcars in the train, the setting of the heaters, and the temperature inside of the railcars.

**Table 1.** Fuel consumption and emissions.

| 749 Praha–Tanvald, 5 cars, 280 t      | Fuel kg/km | NO <sub>x</sub> g/km | PM g/km | CO g/km | Traction kWh/km      |
|---------------------------------------|------------|----------------------|---------|---------|----------------------|
| Praha–Turnov                          | 1.55       | 79                   | 1.05    | 22      | 6.79                 |
| Turnov–Tanvald                        | 2.36       | 142                  | 1.36    | 32      | 10.85                |
| Praha–Tanvald                         | 1.79       | 98                   | 1.15    | 98      | 7.78                 |
| Tanvald–Turnov                        | 0.95       | 75                   | 0.65    | 34      | 5.29                 |
| Turnov–Vsetaty                        | 0.86       | 53                   | 0.55    | 19      | 3.96                 |
| Vsetaty–Turnov                        | 1.06       | 65                   | 0.59    | 21      | 4.37                 |
| Praha–Tanvald–Vsetaty                 | 1.39       | 80                   | 0.90    | 24      | 6.34                 |
| Praha–Ceske Budejovice, 2 cars, 160 t | 0.81       | 61                   | 0.41    | 15      | 3.50                 |
| 754 Praha–Tanvald, 4 cars, 231 t      | Fuel kg/km | NO <sub>x</sub> g/km | PM g/km | CO g/km | PN #/km              |
| Praha–Turnov                          | 1.33       | 83                   | 0.60    | 23      | $7.8 \times 10^{13}$ |
| Turnov–Tanvald                        | 1.74       | 124                  | 0.94    | 30      | $1.0 \times 10^{13}$ |
| Praha–Tanvald                         | 1.44       | 93                   | 0.67    | 25      | $8.4 \times 10^{13}$ |
| Tanvald–Turnov                        | 1.01       | 71                   | 0.44    | 14      | $5.2 \times 10^{13}$ |
| Turnov–Praha                          | 1.02       | 64                   | 0.43    | 14      | $5.6 \times 10^{13}$ |
| Tanvald–Praha                         | 1.01       | 66                   | 0.44    | 14      | $5.6 \times 10^{13}$ |
| Tanvald–Turnov                        | 0.91       | 57                   | 0.32    | 14      | $5.2 \times 10^{13}$ |
| Turnov–Praha                          | 1.11       | 67                   | 0.49    | 16      | $6.3 \times 10^{13}$ |
| Tanvald–Praha                         | 1.07       | 64                   | 0.45    | 16      | $6.0 \times 10^{13}$ |
| Praha–Tanvald–Praha average           | 1.22       | 79                   | 0.56    | 19      | $7.0 \times 10^{13}$ |
| 854 Praha–Turnov, 0–3 cars            | Fuel kg/km | NO <sub>x</sub> g/km | PM g/km | CO g/km |                      |
| Depot operation, switching            | 1.76       | 77                   | 0.53    | 22.4    |                      |
| Praha–Mlada Boleslav local 1+1        | 0.78       | 31                   | 0.15    | 8.9     |                      |
| Mlada Boleslav–Turnov 1+0             | 0.71       | 33                   | 0.11    | 9.7     |                      |
| Turnov–Praha express 1+3              | 1.04       | 55                   | 0.14    | 5.9     |                      |
| Praha–Mlada Boleslav local 1+2        | 0.89       | 42                   | 0.14    | 9.5     |                      |
| 854—average for all operation         | 0.89       | 43                   | 0.14    | 8.2     |                      |

**Table 2.** Fuel consumption and emissions during idling.

| Vehicle and Conditions        | Fuel kg/h | NO <sub>x</sub> g/h | PM g/h | PN #/h               | CO g/h |
|-------------------------------|-----------|---------------------|--------|----------------------|--------|
| 749—cold, with car heating    | 31        | 2238                | 14     |                      | 380    |
| 749—first station (semi-cold) | 8.3       | 733                 | 8.3    |                      | 189    |
| 749—warm                      | 8.2       | 875                 | 7.9    |                      | 21     |
| 754—cold, with car heating    | 34        | 2819                | 5.1    | $1.0 \times 10^{15}$ | 421    |
| 754—warm                      | 12        | 718                 | 1.3    | $1.2 \times 10^{15}$ | 370    |
| 854—average for all operation | 4.0       | 261                 | 0.68   |                      | 101    |

To allow for comparison with other studies and to aid in calculations, the emission totals for each rail vehicle expressed in g/kg fuel are given in Table 3. To allow for comparison on per-ton and per-passenger bases, emissions per kilometer per ton (tkm) and per kilometer per seat (skm) are given in Table 4. The emissions per kilometer per passenger (pkm, not given in the table) can be obtained by dividing skm with the occupancy rate. The mean occupancy rate declared by Czech Railways (ČD) is 30%, which is in agreement with unofficial estimates by train conductors that about 70 people travel on a three-car (railcar plus two trailing cars) train with 168 seats. On regional and local trains, the total train capacity is approximately double the seating capacity. Typically, the minimum train capacity is contracted with the regional or state government, and additional capacity is added based on group reservations and anticipated travel demand.

**Table 3.** Emissions per kg fuel.

| Emissions per kg Fuel      | NO <sub>x</sub> g/kg | PM g/kg | CO g/kg | BSFC g/kWh | PN #/kg                |
|----------------------------|----------------------|---------|---------|------------|------------------------|
| 749 Praha–Tanvald–Vsetaty  | 58                   | 0.65    | 17      | 219        | 5.7 × 10 <sup>13</sup> |
| 749 Praha–Ceske Budejovice | 75                   | 0.51    | 19      | 231        |                        |
| 754 Praha–Tanvald–Praha    | 65                   | 0.46    | 16      |            |                        |
| 854 average all operation  | 48                   | 0.16    | 9       |            |                        |

Note: BSFC, brake-specific fuel consumption.

**Table 4.** Fuel consumption and emissions per ton-km and per seat-km.

| Emissions per ton-km       | Tons  | Fuel g/tkm | NO <sub>x</sub> g/tkm | PM mg/tkm | CO g/tkm | Traction Wh/tkm | PN #/tkm               |
|----------------------------|-------|------------|-----------------------|-----------|----------|-----------------|------------------------|
| 749 Praha–Tanvald–Vsetaty  | 280   | 5.0        | 0.29                  | 3.2       | 0.09     | 23              | 3.0 × 10 <sup>11</sup> |
| 749 Praha–Ceske Budejovice | 160   | 5.1        | 0.38                  | 2.6       | 0.09     | 22              |                        |
| 754 Praha–Tanvald–Praha    | 231   | 5.3        | 0.34                  | 2.4       | 0.08     |                 |                        |
| 854 Praha–Mlada Bol. local | 100   | 7.8        | 0.31                  | 1.5       | 0.09     |                 |                        |
| 854 Mlada Boleslav–Turnov  | 56    | 12.7       | 0.59                  | 2.0       | 0.17     |                 |                        |
| 854 Turnov–Praha express   | 232   | 4.5        | 0.24                  | 0.6       | 0.04     |                 |                        |
| 854 Praha–Mlada Bol. local | 144   | 6.2        | 0.29                  | 1.0       | 0.07     |                 |                        |
| Emissions per seat and km  | Seats | Fuel g/skm | NO <sub>x</sub> g/skm | PM mg/skm | CO g/skm | Traction Wh/skm | PN #/skm               |
| 749 Praha–Tanvald–Vsetaty  | 360   | 3.9        | 0.22                  | 2.5       | 0.07     | 18              | 2.5 × 10 <sup>11</sup> |
| 749 Praha–Ceske Budejovice | 160   | 5.1        | 0.38                  | 2.6       | 0.09     | 22              |                        |
| 754 Praha–Tanvald–Praha    | 280   | 4.4        | 0.28                  | 2.0       | 0.07     |                 |                        |
| 854 Praha–Mlada Bol. local | 108   | 7.2        | 0.29                  | 1.4       | 0.09     |                 |                        |
| 854 Mlada Boleslav–Turnov  | 48    | 14.8       | 0.69                  | 2.3       | 0.20     |                 |                        |
| 854 Turnov–Praha express   | 268   | 3.9        | 0.21                  | 0.5       | 0.02     |                 |                        |
| 854 Praha–Mlada Bol. local | 188   | 2.5        | 0.22                  | 0.7       | 0.05     |                 |                        |

Note: Train mass obtained from the train engineer’s records. Passenger occupancy is not known; mean occupancy on Czech Railways is around 30%, a number not visibly inconsistent with the observations by the authors.

## 4. Discussion

### 4.1. Feasibility of the Approach

The results suggest that, while measurements on a moving locomotive are technically very challenging, they are very feasible, and offer a very realistic image of the actual emissions, which vary greatly depending on the operating patterns of a given locomotive. Calibration of real-time PM measurement via laser light scattering by gravimetric method was found to be useful and can be recommended for applications where steady-state engine operation can be achieved, or with a proportional PM sampling system, as the intake air mass flow can be calculated online. Knowledge and careful consideration of the local operating environment—usual daily routines of the locomotives and train crews, sources of power and data, safety considerations including prohibited or non-feasible locations for instruments, cables or sample lines, the presence of overhead lines and clearance margins overall, and access to the instruments during testing—were found to be essential during the design and implementation of the test.

The PM emissions were found to be remarkably low for the decades old locomotive engines. It is, however, expected that the gradual engine deterioration was somewhat counteracted by improvements in the diesel fuel quality over the last four decades and by good maintenance practices. The engine in the 749 was part of an engine family originally developed as a marine engine with a conservative power rating, was known for its durability and reliability, and has outlived many successor models. Numerous visual observations of opacity levels of locomotives by the first author during regular travel suggest that at least the PM emissions vary among locomotives. The tested locomotive belonged to

the large “cleaner” group, from which visible smoke was seldom observed, as opposed to a relatively small number of “high emitters”. This distribution is analogous to on-road vehicles, where few high emitters are responsible for a disproportionately high fraction of the total emissions. The measured values therefore do not necessarily represent the “average” locomotive, but more likely the emissions levels achieved (and achievable) with good maintenance practices.

The operating patterns were found to vary greatly from the prescribed test cycles. This was not as much the case with the cumulative distribution of engine load, which varied with route and train mass, but showed a good resemblance with the load distribution in stationary tests. On the Prague to Tanvald route, approximately 46% of time was spent at idle and approximately 18% at full load (notch 8), compared to 50.5% at idle and 16.2% at notch 8 specified for line-haul locomotive tests in the U.S. legislation [47]. The major difference was, however, in the sequencing of the operation points. While the test procedures generally start at idle and progress in steps to the full load, the real-world conditions exhibit much faster progressions to a higher load, and relatively short stays, of up to several minutes, at any given load setting. In addition, emission spikes during transients, and artifacts of PM storage during low-load operation during switching prior to the Praha to Tanvald run, were readily observable. It is possible that with a high fraction of organic carbon in the PM due to the introduction of biofuels and/or frequent operation at idle and low loads, the effects of the particle deposition and reentrainment phenomena may be of such magnitude that steady PM levels might seldom be reached during real-world operation.

Given the large difference in test cycle and real-world operating conditions, the test cycles may also be prone to “cycle beating”, a questionable but in recent history not uncommon practice of carelessly or even deliberately “tuning” the engine control unit so that the emissions are higher during real-world operation than during the prescribed test cycles [32,48–53].

The entire testing was accomplished without taking the locomotive out of service, without requesting unscheduled operation, and with minimal extra effort and expenses incurred by Czech Railways (ČD), which were limited primarily to logistics and initial technical advice. The presence of the test apparatus did not interfere with train operation. The locomotive was returned to the depot at the end of each test day, but the test apparatus, weighing less than 14 kg without batteries (FTIR and NanoMet additional 40 kg), could have been removed at any place en route without overhead traction lines. Aside from the gravimetric measurements, it is anticipated that the presence of technicians on the locomotive might not be necessary during routine testing. At the same time, first-hand observations by the authors were found to be quite valuable in understanding the context of the data collected. It is the opinion of the first author that many emissions studies could be greatly improved just by understanding and taking into account the processes involved, which is not an easy task given the highly interdisciplinary nature of the subject.

From the exposure and emissions hot-spots perspective, of highest relative concern appears to be emissions during the departure from the station, although it can be argued that, even there, the exhaust is dispersed well away from people compared to the case of highway vehicles. From the regional emissions perspective, the operation of the train is very efficient, and, due to very conservative engine ratings and relatively infrequent transients compared to road vehicles, the overall emissions can be very low when divided among the number of passengers, and in most cases lower than for cars and buses even with old locomotives. Additional data are, of course, needed to quantify such statements.

The use of FTIR and NanoMet is believed to be of key significance for new technologies and fuels, and was tested here despite higher power consumption and mass compare to the simpler monitoring system, which was capable of providing comparable NO readings. Potent greenhouse gases methane (from gaseous fuels) and nitrous oxide (from NO<sub>x</sub> aftertreatment) and key reactive nitrogen species (including, but not limited to, NO, NO<sub>2</sub>, and ammonia) can be readily measured with FTIR. NanoMet allows for measurement of very small particles at low concentrations. The prime reason these instruments were included was to test their response in the specific conditions of the locomotive engine room. The infrared spectra were additionally evaluated for noise around 4 μm (2500 cm<sup>-1</sup>)

region showing virtually no absorption during exhaust measurements. The operation of both FTIR and NanoMet was flawless, suggesting that this combination can be used in future locomotive studies.

#### 4.2. Comparison with Other Published Data

Graver et al. [54] and Frey et al. [55] (only relative data are reported in [54], figures used here calculated from data given in [55]) reported the fuel consumption of a three-car train on the 278 km Piedmont (Charlotte to Raleigh) route in North Carolina as 531–713 kg, or about 1.5–1.9 g/km. The Piedmont route trains, however, operated at higher average (about 90 km/h) and maximum (127 km/h) speeds, compared to the track speeds of 80 or 100 km/h, and even lower in river gorges and other areas with poor visibility, in this study. The fuel-specific emissions of NO<sub>x</sub> (55–64 g/kg) were comparable to this study (48–75 g/kg), while PM emissions (1.6–1.8 g/kg based on data taken from Table 9.1 in [55]; similar ratio is in Table 8.5 in [55]) were higher than measured here (0.16–0.65 g/kg).

The fuel consumption reported in this study is similar to 3–5 mL (cm<sup>3</sup>) per gross ton-km reported by Johnson et al. [28], while NO<sub>x</sub> emissions are about double (48–75 g/kg) compared to those (28 ± 14 g/kg) measured by Johnson et al., while PM emissions observed here (0.16–0.65 g/kg) are considerably lower than those (1.1 ± 0.5 g/kg) measured in [28]. One possible reason is that the runs here were all on ultra low sulfur diesel fuel, while the authors of [28] reported emissions of SO<sub>2</sub> of (1.4 ± 0.4) g·kg<sup>-1</sup>, corresponding to thousands of ppm of S in the fuel. Another possible reason could be the difference in the combustion timing among the engines. Higher NO<sub>x</sub> and lower PM observed in this study for both ČKD engines may possibly be attributable to earlier start of combustion compared to engines tested in [28], many of which probably were, unlike the old ČKD engines in 749 and 754, subject to U.S. Tier 0–2 standards. This has not been verified as actual injection timing was not found for any of the engines discussed. Another possible reason is the inclusion of high emitters: Graver et al. [54] and this study used several specimens with advance permission of the owner, making an inclusion of a high emitter unlikely, while Johnson et al. [28] tested a higher number of locomotives. A difference between this study and that in [55] could be the calibration of the light scattering sensor for the specific aerosol. In [55], a multiplication factor of five compared to (an undisclosed) calibration of the unit was used. In this study, light scattering measurement used on 749 and 854 was calibrated by the gravimetric method, with differences in both direction (under- and over-statement) on the order of tens of percent.

An older Czech study [56] states the 2004 passenger load and energy consumption of 5030 million passenger-kilometers and 1428 TJ for electric traction and 1560 million pkm and 1171 TJ for diesel traction, corresponding to energy intensity of 79 Wh/pkm for electric traction and 209 Wh/pkm for diesel traction (at 35% mean combined efficiency of diesel engine and generator, this translates to 73 Wh/pkm traction power and fuel consumption of 18 g/pkm). The mean emissions for diesel traction were reported as 1.2 g/tkm NO<sub>x</sub> and 80 mg/tkm PM and 0.60 g/pkm NO<sub>x</sub> and 46 mg/pkm PM. At 30% occupancy, the NO<sub>x</sub> values are in agreement, while the measured PM values are about an order of magnitude lower.

The current emissions factors used in the national inventory, the latest ones dating to 2006, were 33.9 g/kg for NO<sub>x</sub> and 2.62 g/kg for particulate matter (total, not PM<sub>2.5</sub> or PM<sub>10</sub>) [57]. Another source states NO<sub>x</sub> emissions factors of 42.3 g/kg NO<sub>x</sub> [58], a value adopted from heavy-duty highway engines due to lack of data for rail engines. It is apparent, from comparison with Table 2, that the results obtained here show considerably higher NO<sub>x</sub> emissions and considerably lower PM emissions than estimated in the emissions inventory.

The European Environmental Agency, in a recent (2019) document, uses Tier 1 emissions (rail vehicle without closer specification of model, type, and operating conditions) of 52.4 g/NO<sub>x</sub>, 1.52 g/kg total PM, 1.44 g/kg PM<sub>10</sub>, and 1.37 g/kg PM<sub>2.5</sub>. Tier 2 emissions (rail vehicle of known type without close specifications of size, age, and operating conditions) for line-haul locomotives are 63 g/kg NO<sub>x</sub> and 1.1 g/kg PM<sub>2.5</sub>, and those for railcars are 39.9 g/kg NO<sub>x</sub> and 1 g/kg PM<sub>2.5</sub> [59].

### *4.3. Mitigation Options*

It is apparent from the data that a considerable portion of energy is expended to accelerate the train, some of which may be recovered if electrodynamic braking and on-board electric power storage is used. Battery storage may also allow for a smaller engine to be used. Not considering the Ceske Budejovice run where only two railcars were pulled, and excluding switching operation, the average utilization of engine power on the 749 and 754 was (very roughly) around 20% of the rated power. The engines can therefore be replaced with engines analogous to higher-power heavy-duty trucks, in the mid-hundreds of kW range, equipped with standard diesel aftertreatment (oxidation catalyst, particle filter, and NO<sub>x</sub> reduction catalyst), a larger battery bank, and the necessary power electronics. For the North Carolina Dept. of Transportation Piedmont service described in [44], the average engine load was somewhere (very roughly) around 1 MW, or about 40%, not offering much benefit in terms of improved brake-specific efficiency, but possibly in terms of recuperating kinetic energy lost during braking.

The emissions associated with generation of electric power for railcar heating are relatively very high, and could be mitigated by using electric power at the depot and at the end stations, a practice already being implemented over time where feasible.

Due to the passenger loads on non-electrified tracks being relatively low (relative to the mainline rail in the Czech Republic), it is expected that diesel locomotives will be replaced by railcars and units, reducing the mass of the train. The reason the 854 railcar did not show substantial fuel economy benefits over locomotive driven trains is the rather low efficiency of the hydraulic power transmission, causing a higher fuel consumption per ton-km compared to the locomotives, as shown in Table 3.

### *4.4. Are Old Diesel Locomotives Eco-Friendly Compared to Cars?*

At roughly 4 g of fuel per ton-km, the fuel consumption per ton is nearly an order of magnitude lower compared to passenger cars. On the other hand, the vehicle mass per passenger, considering about 30% occupancy rates of both cars and trains, is 2–3 times higher for rail vehicles than for automobiles. However, the train is, overall, several times more fuel efficient than a car. Considering the 30% occupancy of both, cars and trains can be roughly compared on a per-seat basis. The per-seat emissions of NO<sub>x</sub> measured here, about 0.25 g per seat and km, are tens of percent higher compared to an average European diesel automobile, Euro 2–5, with slightly under 1 g/km NO<sub>x</sub>. The PM emissions of about 2 mg per seat and km represent the lower end of the range for diesel engines without a particle filter (which account for about half of the diesel automobiles and for about one third of all automobiles being driven on Prague roads). It should also be noted that, on automobiles, NO<sub>x</sub> and PM emissions typically increase with the severity of congestion, and their exhaust is released in the streets in the immediate vicinity of other people, while many fewer people are expected to receive a “direct hit” by locomotive exhaust. The emissions of some of the oldest rail engines operating in a relatively inefficient regional service can therefore be classified as “not that bad” compared to not-so-old cars when it comes to NO<sub>x</sub> and PM, and superior even to new automobiles on a greenhouse gas emissions basis. Of course, NO<sub>x</sub> and PM can be readily reduced by exhaust aftertreatment, replacement of the engine, or replacement of the whole vehicle. In terms of transition to electric power, replacement of the diesel engine with a MWh-sized battery bank, which would be charged from overhead traction lines or a limited number of fixed charging stations, seems much closer to today’s reality than a similar switch in the general car fleet. Already, the incremental increase in ridership on the electric-powered trains among Prague, Brno, and Ostrava, the three largest Czech cities, by far surpasses the travel by all electric cars in the country.

## 5. Conclusions

Exhaust emissions of particulate matter, nitrogen oxides, and other pollutants from two diesel-electric locomotives and one diesel-hydraulic railcar were measured during regular scheduled passenger service. Low-power portable emissions monitoring instruments were installed during scheduled maintenance into engine compartments and were sampling raw exhaust from the stack. Due to space constraints and overhead electric traction lines, exhaust flow was computed from engine operating data.

The chosen approach was found to be feasible, the instruments worked well, and realistic data was obtained at reasonably cost and at no disruption to the train operation. The use of a NanoMet3 to measure non-volatile particle number concentrations and a portable FTIR capable of measuring a wide range of gaseous pollutants demonstrates that such instrumentation could be used to test newer engines with advanced exhaust aftertreatment. Tests were done at very low costs with no disruption of the train service, yielded realistic data, and are also applicable to diesel-hydraulic units which cannot be tested at standstill.

Real-world operation was characterized by relatively fast power level transitions during accelerations and interleaved periods of high load and idle, and varied considerably among service type and routes. Spikes in PM emissions during accelerations and storage of PM in the exhaust were observed. On all three engines, all near the end of their useful life, NO<sub>x</sub> emissions were 48–75 g per kg fuel and PM emissions were 0.16–0.65 g per kg fuel (averages over several hours of service). Relative to other published data and emission factors used in models, NO<sub>x</sub> emissions were comparable or slightly higher, while PM emissions were considerably lower. Despite all engines approaching the end of their life, NO<sub>x</sub> and PM emissions per passenger-km were very surprisingly low compared to those from European diesel automobiles (Euro 2–5 without a particle filter, but also the Czech “fleet average”).

Similar approach can probably be used on other non-road engines, including large engines over 560 kW used on railroads, inland waterways, construction sites, and in stationary applications. Such engines are difficult and in many cases nearly impossible to test in laboratory or in a stationary mode.

**Author Contributions:** Conceptualization, M.V.-L. and J.J.; methodology, all; software, M.V.-L.; validation, M.V.-L. and M.P.; formal analysis, M.V.-L. and M.P.; investigation, all; instrumentation design, M.V.-L.; installing instruments and running experiments, all; resources, all; data curation, M.V.-L. and M.P.; writing—original draft preparation, M.V.-L.; writing—review and editing, all; visualization, M.V.-L. and M.P.; supervision, all; project administration, all; and funding acquisition, M.V.-L. and J.J. All authors have read and agreed to the published version of the manuscript.

**Funding:** FTIR acquisition and development—EU project MEDETOX—Innovative Methods of Monitoring of Diesel Engine Exhaust Toxicity in Real Urban Traffic (LIFE10 ENV/CZ/651); NanoMet3 acquisition—Czech Ministry of Education CZ.1.05/2.1.00/19.04.08.; 749 tests—no external funding; 854 tests—LIFE10 ENV/CZ/651; 754 tests—Student Grant Competition of the Czech Technical University in Prague, grant number 16/106/OHK2/1T/16; and ex-post validation, new analysis and writing—EU project uCARE, You can also reduce emissions, H2020 project No. 815002.

**Acknowledgments:** The 749 tests were done on a volunteer basis, following up on J.J. request for emissions estimates and M.V. proposal to determine emissions by direct measurements. Jaroslav Opava (Czech Technical University in Prague) was M.S. thesis supervisor of J.J. and arranged for load bank tests (not reported on here), which led to the on-track tests. In addition to all authors performing the measurements, Luboš Dittrich and Michael Fenkl (Technical University of Liberec) helped with 749 and 854 tests, and Vít Beránek (Czech Technical University in Prague) helped with 754 tests. Michal Strapko (Czech Technical University in Prague) helped with electrical wiring of sensors and battery pack. Numerous technicians and train engineers from the Czech Railways (ČD) locomotive depot in Prague provided useful information and help during planning, installation, and measurements.

**Conflicts of Interest:** The authors declare no conflict of interest. The funders had no role in the design of the study; in the collection, analyses, or interpretation of data; in the writing of the manuscript, or in the decision to publish the results.

## References

1. Mašková, K. Economy of Railway Transport from the Point of View of the Client. Master's Thesis, Czech Technical University, Prague, Czech Republic, 2019.
2. Ministry of Transport of the Czech Republic. *Quarterly Rail Transport Report for 2018*; Ministry of Transport of the Czech Republic: Prague, Czech Republic, 2019.
3. Czech Railways. *2018 Annual Report*; Czech Railways: Prague, Czech Republic, 2019. (In Czech)
4. SYDOS (Office of Transport Statistics). *Rail Vehicles*; Czech Ministry of Transport: Prague, Czech Republic, 2019.
5. SYDOS (Office of Transport Statistics). *Energy Consumption in the Rail Sector*; Czech Ministry of Transport: Prague, Czech Republic, 2019.
6. European Environment Agency (EEA). *Air Quality in Europe—2018 Report*; EEA: København, Denmark, 2018; ISBN 978-92-9213-990-2.
7. World Bank and Institute for Health Metrics and Evaluation. *The Cost of Air Pollution: Strengthening the Economic Case for Action*; World Bank and Institute for Health Metrics and Evaluation: Washington, DC, USA, 2016.
8. U.S. Federal Government. Title 40, Part 92, Section 124 and 131, Title 40, Parts 85, 86 and 92, Title 40, Parts 1065 and 1033. In *U.S. Code of Federal Regulation*; Federal Chronicle Office (United States): Washington, DC, USA, 1938.
9. U.S. Locomotive Emissions Standards. Available online: <http://www.dieselnet.com/standards/us/loco.php> (accessed on 17 April 2020).
10. Frey, H.C.; Choi, H.W.; Kim, K. "Measurement of the energy use and emissions of passenger rail locomotives using a portable emission measurement system," paper 2009-A-243-AWMA. In Proceedings of the 102nd Annual Conference and Exhibition, Air & Waste Management Association, Detroit, MI, USA, 16–19 June 2009.
11. Fritz, S.G. Evaluation of Biodiesel Fuel in an EMD GP38-2 Locomotive. Report by Southwest Research Institute for National Renewable Energy Laboratory, Golden, CO, Contract No. DE-AC36-99-GO10337, Document No. NREL/SR-510-33436. 2004. Available online: <http://www.nrel.gov/docs/fy04osti/33436.pdf> (accessed on 17 April 2020).
12. Federal Railroad Administration; U.S. Department of Transportation. Locomotive Exhaust Emissions. Research Results RR 09-18 September 2009. Available online: <http://www.fra.dot.gov/downloads/research/rr0918.pdf> (accessed on 17 April 2020).
13. Transport Canada. Locomotive Emissions Monitoring Program 2007. Available online: <http://www.tc.gc.ca/eng/programs/environment-ecofreight-about-voluntary-racemissions2007-5-341.htm> (accessed on 17 April 2020).
14. BNSF Railway Company; Union Pacific Railroad Company; The Association of American Railroads and California Environmental Associates. An Evaluation of Natural Gas-Fueled Locomotives. Report 2007. Available online: <http://www.arb.ca.gov/railyard/ryagreement/112807ngqa.pdf> (accessed on 17 April 2020).
15. Honc, R.L.; Fritz, S.G.; Osborne, D.T.; Grisier, R.; Carpenter, S. Exhaust emissions and fuel consumption of a railpower RP20BD switcher locomotive. In *Proceedings of the 2009 Spring Technical Conference of the ASME Internal Combustion Engine Division*; ICES: Toronto, ON, Canada, 2009; pp. 379–387.
16. Savant, A.A.; Nigam, A.; Miller, J.W.; Johnson, K.C.; Cocker, D.R. Regulated and non-regulated emissions from in-use diesel-electric locomotives. *Environ. Sci. Technol.* **2007**, *41*, 6074–6083. [CrossRef]
17. Evaluation of Emissions and Performance of NJ Transit Diesel Locomotives with B20 Biodiesel Blends. Available online: [http://www.nj.gov/dep/oce/biodiesel\\_njtransit\\_summary.pdf](http://www.nj.gov/dep/oce/biodiesel_njtransit_summary.pdf) (accessed on 17 April 2020).
18. Yanowitz, J. Particulate matter emissions during transient locomotive operation: Preliminary study. *J. Air Waste Manag. Assoc.* **2003**, *53*, 1241–1247. [CrossRef] [PubMed]
19. Johnson, J.E.; Kittelson, D.B. Deposition, diffusion, and adsorption in the diesel oxidation catalyst. *Appl. Catal. B Environ.* **1996**, *10*, 117–137. [CrossRef]
20. Vojtisek-Lom, M.; Pechout, M.; Dittrich, L.; Beranek, V.; Kotek, M.; Schwarz, J.; Vodicka, P.; Milcova, A.; Rossnerova, A.; Ambroz, A.; et al. Polycyclic aromatic hydrocarbons (PAH) and their genotoxicity in exhaust emissions from a diesel engine during extended low-load operation on diesel and biodiesel fuels. *Atmos. Environ.* **2015**, *109*, 9–18. [CrossRef]
21. Vojtisek-Lom, M.; Jirků, J.; Opava, J. Measurement of exhaust emissions of railroad locomotives using an on-board system. In Proceedings of the 14th ETH Conference on Combustion Generated Nanoparticles, Zurich, Switzerland, 1–4 August 2010.

22. Vojtisek-Lom, M.; Cobb, J.T., Jr. Measurement, variance and reduction of real-world emissions of 20 dedicated CNG vans. In Proceedings of the 1998 91st Annual Meeting & Exposition of the Air & Waste Management Association, San Diego, CA, USA, 14–18 June 1998. Code 49496.
23. Vojtisek-Lom, M.; Allsop, J. *Development of Heavy-Duty Diesel Portable, On-Board Mass Exhaust Emissions Monitoring System with NO<sub>x</sub>, CO<sub>2</sub> and Qualitative PM Capabilities*; SAE Technical Paper 2001-01-3641; SAE International: Warrendale, PA, USA, 2001. [CrossRef]
24. Vojtisek-Lom, M.; Jirků, J. Operating History Artifacts of Large Engine Particulate Matter Emissions Measurement. In Proceedings of the ASME 2012 Internal Combustion Engine Division Spring Technical Conference, ASME 2012 Internal Combustion Engine Division Spring Technical Conference, Torino, Italy, 6–9 May 2012; pp. 101–110.
25. Graver, B.M.; Frey, H.C. Comparison of locomotive emissions measured during dynamometer versus rail yard engine load tests. *Transp. Res. Rec.* **2013**, *2341*, 23–33. [CrossRef]
26. Graver, B.M.; Frey, H.C. Comparison of over-the-rail and rail yard measurements of diesel locomotives. *Environ. Sci. Technol.* **2015**, *49*, 13031–13039. [CrossRef]
27. Popp, P.J.; Bishop, G.A.; Stedman, D.H. *Remote Sensing of Railroad Locomotive Emissions: A Feasibility Study*; The Federal Highway Administration: Washington, DC, USA, 1999.
28. Johnson, G.R.; Jayaratne, E.R.; Lau, J.; Thomas, V.; Juwono, A.M.; Kitchen, B.; Morawska, L. Remote measurement of diesel locomotive emission factors and particle size distributions. *Atmos. Environ.* **2013**, *81*, 148–157. [CrossRef]
29. Krasowsky, T.; Daher, N.; Sioutas, C.; Ban-Weiss, G. Measurement of particulate matter emissions from in-use locomotives. *Atmos. Environ.* **2015**, *113*, 187–196. [CrossRef]
30. Base Map: Czech Republic Railroad Map. Available online: <http://mapa.rychnovsky.cz/CD.gif> (accessed on 17 April 2020).
31. Map Server. Available online: <http://www.mapy.cz> (accessed on 17 April 2020).
32. Bureau of Automotive Repair. Available online: [www.bar.ca.gov](http://www.bar.ca.gov) (accessed on 25 May 2020).
33. Vojtisek-Lom, M.; Fenkl, M.; Dufek, M.; Mares, J. *Off-Cycle, Real-World Emissions of Modern Light-Duty Diesel Vehicles*; SAE Technical Paper Series; Paper No. 2009-24-0148; Society of Automotive Engineers: Warrendale, PA, USA, 2009.
34. Vojtisek-Lom, M.; Cobb, J.T. Vehicle mass emissions measurement using a Portable 5-Gas exhaust analyzer and engine computer data. In *Proceedings of the EPA/A&WMA Emission Inventory Meeting*; IEIC: Research Triangle Park, NC, USA, 1997.
35. Vojtisek-Lom, M.; Lambert, D.; Wilson, P. Real-World Emissions from 40 Heavy-Duty Diesel Trucks Recruited at Tulare, CA Rest Area, SAE Technical Paper 2002-01-2901. Available online: <https://doi.org/10.4271/2002-01-2901> (accessed on 17 April 2020).
36. Vojtisek-Lom, M.; Pechout, M.; Blažek, J.; Moc, L.; Hlavenka, T. Effects of Current and Prior Operating Conditions on Particulate Matter Emissions from a Diesel Engine Operated on Heated Rapeseed Oil, SAE Technical Paper 2009-01-1913. 2009. Available online: <https://doi.org/10.4271/2009-01-1913> (accessed on 17 April 2020).
37. Moosmueller, H.; Arnott, W.P.; Rogers, C.F.; Bowen, J.L.; Gillies, J.A.; Pierson, W.R.; Collins, J.F.; Durbin, T.D.; Norbeck, J.M. Time resolved characterization of diesel particulate emissions. 1. instruments for particle mass measurements. *Environ. Sci. Technol.* **2001**, *35*, 781–787. [CrossRef]
38. Maricq, M.M.; Xu, N. The effective density and fractal dimension of soot particles from premixed flames and motor vehicle exhaust. *Aerosol Sci.* **2004**, *35*, 1251–1274. [CrossRef]
39. Di Stasio, S. Optics of fractal structures. In *Proceedings of the GAeF-Meeting 2008 on Light Scattering: Mie and More*; GAeF: Karlsruhe, Germany, 2008.
40. Determination of Particulate Matter Emissions from Stationary Sources. California Air Resources Board Test Method 5. Available online: [http://www.arb.ca.gov/testmeth/vol1/m\\_5.pdf](http://www.arb.ca.gov/testmeth/vol1/m_5.pdf) (accessed on 17 April 2020).
41. European Parliament. *European Parliament Directives 2004/26/ES and 97/68/ES*; European Parliament: Brussels, Belgium, 2004.
42. Vojtisek, M.; Pechout, M. Assessment of a low-cost portable proportional exhaust sampling system for gravimetric particulate matter emissions measurement. *J. Middle Eur. Constr. Des. Cars* **2013**, *11*, 22–28. [CrossRef]

43. Suarez-Bertoa, R.; Mendoza-Villafuerte, P.; Riccobono, F.; Vojtisek, M.; Pechout, M.; Perujo, A.; Astorga, C. On-road measurement of NH<sub>3</sub> emissions from gasoline and diesel passenger cars during real world driving conditions. *Atmos. Environ.* **2017**, *166*, 488–497. [[CrossRef](#)]
44. Giechaskiel, B.; Bonnel, P.; Perujo, A.; Dilara, P. Solid particle number (SPN) portable emissions measurement systems (PEMS) in the European legislation: A review. *Int. J. Environ. Res. Public Health* **2019**, *16*, 4819. [[CrossRef](#)] [[PubMed](#)]
45. Vojtíšek-Lom, M. Inference of steady-state non-road engine exhaust emissions values from non-stabilized data. *SAE Tech. Pap. Ser.* **2012**. [[CrossRef](#)]
46. Thompson, G.J.; Clark, N.; Gautam, M.; Carder, D.K.; Lyons, D.W. Inference of torque and power from heavy-duty diesel engines for on-road emissions monitoring. *SAE Tech. Pap. Ser.* **2002**. [[CrossRef](#)]
47. U.S. Federal Government. Title 40: Protection of the environment, volume 1033: Control of emissions from locomotives, section 1033.530: Duty cycles and calculations. In *United States Code of Federal Regulation*; Federal Chronicle Office (United States): Washington, DC, USA, 1938.
48. Kågeson, P. *Cycle-Beating and the EU Test Cycle for Cars*; European Federation for Transport and Environment (T&E): Brussels, Belgium, 1998.
49. Kelly, N.A.; Groblicki, P.J. Real-world emissions from a modern production vehicle driven in los angeles. *Air Waste* **1993**, *43*, 1351–1357. [[CrossRef](#)]
50. Weiss, M.; Bonnel, P.; Hummel, R.; Provenza, A.; Manfredi, U. On-road emissions of light-duty vehicles in Europe. *Environ. Sci. Technol.* **2011**, *45*, 8575–8581. [[CrossRef](#)]
51. Weiss, M.; Bonnel, P.; Kühlwein, J.; Provenza, A.; Lambrecht, U.; Alessandrini, S.; Carriero, M.; Colombo, R.; Forni, F.; Lanappe, G.; et al. Will Euro 6 reduce the NO<sub>x</sub> emissions of new diesel cars?—Insights from on-road tests with Portable Emissions Measurement Systems (PEMS). *Atmos. Environ.* **2012**, *62*, 657–665. [[CrossRef](#)]
52. Degraeuwe, B.; Weiss, M. Does the New European Driving Cycle (NEDC) really fail to capture the NO<sub>x</sub> emissions of diesel cars in Europe? *Environ. Pollut.* **2017**, *222*, 234–241. [[CrossRef](#)]
53. Suarez-Bertoa, R.; Valverde, V.; Clairotte, M.; Pavlovic, J.; Giechaskiel, B.; Franco, V.; Kregar, Z.; Astorga, C.; Ricardo, S.-B.; Victor, V.; et al. On-road emissions of passenger cars beyond the boundary conditions of the real-driving emissions test. *Environ. Res.* **2019**, *176*, 108572. [[CrossRef](#)]
54. Graver, B.M.; Frey, H.C.; Hu, J. Effect of biodiesel fuels on real-world emissions of passenger locomotives. *Environ. Sci. Technol.* **2016**, *50*, 12030–12039. [[CrossRef](#)] [[PubMed](#)]
55. Frey, H.C.; Rastogi, N. *Evaluation of Locomotive Emissions Reduction Strategies*; North Carolina Department of Transportation Project No. 2016–20, Report No. FHWA/NC/2016-20; North Carolina State University: Raleigh, NC, USA, 2018.
56. Zeman, J. Energy and environmental performance of transport modes in the Czech Republic. *Vědeckotechnický Sborník ČD* **2007**, *23*, 1–16. (In Czech)
57. Špička, L. (Center for Transport Research, Brno, Czech Republic). Personal Communication, 2020.
58. Dufek, J.; Huzlík, J.; Adamec, V. *Stanovení Emisí Látek Znečišťujících Ovzduší z Dopravy. (Development of Emissions Factors for Air Pollutants from Transport)*; Contract No. CE 801/210/09; Center for Transport Research: Brno, Czech Republic, 2006. (In Czech)
59. Norris, J.; Ntziachristos, L.; Samaras, Z.; Zierock, K.-H. Railways. In *EMEP/EEA Air Pollutant Emission Inventory Guidebook*; European Environmental Agency: København, Denmark, 2019.



© 2020 by the authors. Licensee MDPI, Basel, Switzerland. This article is an open access article distributed under the terms and conditions of the Creative Commons Attribution (CC BY) license (<http://creativecommons.org/licenses/by/4.0/>).

Article

# Characterization and Source Identification of Elements and Water-Soluble Ions in Submicrometre Aerosols in Brno and Šlapanice (Czech Republic)

Pavel Mikuška<sup>1,\*</sup> , Martin Vojtěšek<sup>1</sup>, Kamil Křůmal<sup>1</sup>, Martina Mikušková-Čampulová<sup>2</sup>, Jaroslav Michálek<sup>3</sup> and Zbyněk Večeřa<sup>1</sup>

<sup>1</sup> Institute of Analytical Chemistry, Czech Academy of Sciences, v.v.i., Veveří 97, 602 00 Brno, Czech Republic; vojtkov@seznam.cz (M.V.); krumal@iach.cz (K.K.); vecera@iach.cz (Z.V.)

<sup>2</sup> Faculty of Business and Economics, Department of Statistics and Operation Analysis, Mendel University in Brno, Zemědělská 1, 613 00 Brno, Czech Republic; martina.campulova@mendelu.cz

<sup>3</sup> Faculty of Military Leadership, Department of Quantitative Methods, University of Defence, Kounicova 65, 662 10 Brno, Czech Republic; jaroslav.michalek@unob.cz

\* Correspondence: mikuska@iach.cz

Received: 28 May 2020; Accepted: 24 June 2020; Published: 29 June 2020



**Abstract:** Submicrometre aerosol particles (particulate matter, PM<sub>1</sub>) were collected in two Czech cities (Brno and Šlapanice) during week campaigns in winter and summer of 2009 and 2010. The aerosols were analysed for 14 elements and 12 water-soluble ions using inductively coupled plasma–mass spectrometry and ion chromatography techniques. The average PM<sub>1</sub> mass concentration was 14.4 and 20.4 µg m<sup>-3</sup> in Brno and Šlapanice, respectively. Most of the analysed elements and ions exhibit distinct seasonal variability with higher concentrations in winter in comparison to summer. The determined elements and ions together accounted for about 29% of total PM<sub>1</sub> mass, ranging between 16% and 44%. Ion species were the most abundant components in collected aerosols, accounting for 27.2% of mass of PM<sub>1</sub> aerosols, and elements accounted for 1.8% of mass of PM<sub>1</sub> aerosols. One-day backward trajectories were calculated using the Hysplit model to analyse air masses transported towards the sampling sites. The Pearson correlation coefficients between individual PM<sub>1</sub> components and PM<sub>1</sub> mass and air temperature were calculated. To identify the main aerosol sources, factor analysis was applied. Six factors were identified for each locality. The following sources of PM<sub>1</sub> particles were identified in Brno: a municipal incinerator, vehicle exhausts, secondary sulphate, a cement factory, industry and biomass burning. The identified sources in Šlapanice were as follows: a combustion source, coal combustion, a cement factory, a municipal incinerator, vehicle exhausts and industry.

**Keywords:** PM<sub>1</sub> aerosol; elements; water-soluble ions; factor analysis; source apportionment

## 1. Introduction

Atmospheric aerosol (particulate matter, PM) is an important airborne component with various environmental and health effects. Aerosols can deteriorate air quality, affect global climate, reduce visibility, and are involved in smog production [1]. Epidemiological studies showed an association between the concentration of aerosol particles in ambient air and adverse health effects [2–4]. The environmental and health effects of atmospheric aerosols depend on the particle size, shape and the chemical composition of particles. The atmospheric aerosol consists of a complex mixture of components including carbonaceous species (elemental and organic carbons), inorganic ions and elements in variable amounts, depending on their location and emission sources.

In the last decade, air pollution by atmospheric aerosols has also been a subject to increased interest in the Czech Republic. Numerous studies have reported the chemical composition of PM in the Czech

Republic, focusing on PM<sub>10</sub> [5–10], PM<sub>2.5</sub> particles [6,7,11–17] and also on PM<sub>1</sub> particles [6,8,10,11,18–24] that have greater toxicity compared to PM<sub>2.5</sub> and PM<sub>10</sub>. Due to their small sizes, PM<sub>1</sub> particles can penetrate deep into the alveolar part of the lungs and cause respiratory and cardiovascular diseases [4]. Moreover, ultrafine particles (i.e., particles smaller than 100 nm) are even able to translocate from the lungs into secondary organs [25,26].

A number of individual studies have reported the aerosol chemical speciation and PM levels at specific locations in the Czech Republic, such as Prague [6,7,20], Mladá Boleslav [5,23], Brno [11,15–19,21], background site in Košetice [9,14,27] or the heavily polluted Ostrava region [8,10,12,13,22,24]. However, unlike other sites in the Czech Republic, where all components of PM (i.e., organic compounds, elements or ions) are studied, the studies dealing with aerosol composition in Brno focus almost exclusively on organic compounds [11,15,17–19], whereas particulate ions [16] and elements [21,28] have been measured in PM in Brno only marginally and information on the content of ions and elements in aerosols in this area is still incomplete.

Receptor models based on the statistical evaluation of PM chemical data acquired at receptor sites are used to identify emission sources of aerosols [29]. The chemical mass balance model assumes knowledge of the composition of the emissions for all relevant sources, however, fulfilling this requirement is often problematic [29]. More widespread are two multivariate models, principal component analysis [30–33] and positive matrix factorisation [5,8,22,24,34–36], which apportion the sources on the basis of the ambient data from the receptor site alone.

The aims of the study were to fill the gap in the missing information about the content of elements and water-soluble ions in aerosols in the Brno agglomeration; to obtain comprehensive information on the composition of PM<sub>1</sub> aerosols in Brno and Šlapanice in a combination with other studies in the same area focused on the characterization of organic compounds in PM<sub>1</sub> aerosols in Brno and Šlapanice [11,18,19]; to identify their sources. The paper presents the results of determination of elements and water-soluble ions in submicrometre aerosols (PM<sub>1</sub>, particles with aerodynamic diameter smaller than 1 µm) collected in two cities in the Czech Republic (Brno and Šlapanice) in Central Europe. The seasonal differences (winter vs. summer) were evaluated and the sources of studied aerosol components were analysed.

## **2. Experiments**

### *2.1. Sampling Sites*

The PM<sub>1</sub> aerosols were sampled in Brno and Šlapanice that represent a large city and a small town in the Czech Republic. Brno, the second largest city in the Czech Republic (370,000 inhabitants), is an industrial and administration centre of Moravia, the eastern part of the Czech Republic. There are various local sources of aerosols in Brno, such as traffic (cars and trams on Veverí street), residential heating and large emission sources, such as heating plant, a municipal waste incinerator (on the eastern outskirts of Brno) and industry, including a foundry plant. Regional sources comprise mainly residential heating in the surrounding villages and a cement factory east of Brno. Šlapanice, a small town (6000 inhabitants), is located 3 km southeast from Brno. Overall, the sources of aerosols in Šlapanice are similar to those in Brno, but there is a difference between the composition of local and regional sources in both locations. Local sources of aerosols in Šlapanice include traffic, residential heating, small industrial factories and brickworks. Aerosols can be transported to Šlapanice from various regional sources, such as the nearby motorway between Brno and Šlapanice, Brno airport southwest of Šlapanice, a municipal waste incinerator northwest of Šlapanice, residential heating in the surrounding villages, a cement factory northeast of Šlapanice, etc. In addition, a large power plant in Hodonín that burns coal and biomass is located about 50 km southeast from Brno and Šlapanice. Moreover, a long-range transport of pollutants from distant areas or neighbouring countries to Brno and Šlapanice cannot be ignored.

## 2.2. Aerosol Sampling

Atmospheric aerosols in the size fraction of  $PM_{10}$  were sampled for 24 h every day over one week in winter and one week in summer of 2009 and 2010 in Brno and Šlapanice (Figure 1) to compare the  $PM_{10}$  composition in the large city and a nearby small town. The sampling of aerosols began every day at 9:00 a.m. Aerosol samples in Brno were collected in an urban locality on the balcony on the first floor (at the height of 8.9 m above ground level and at the distance of 15.6 m from the street Veveří) of the Institute of Analytical Chemistry facing northeast toward the street Veveří ( $49^{\circ}12'28.27''N$  and  $16^{\circ}35'28.00''E$ ). In Šlapanice the aerosols were collected in small urban locality in the garden of a family house ( $49^{\circ}09'55.92''N$  and  $16^{\circ}43'26.18''E$ ). Sampling locations are located relatively in the centre of both Brno and Šlapanice, and therefore, the influence of different PM sources is expected, although the sampling site in Brno is situated near the street with traffic.



**Figure 1.** Location of sampling sites (Brno and Šlapanice) on a map of the Czech Republic.

Submicrometre aerosols were collected at each site in parallel using a high-volume (HV) and a low-volume (LV) sampler. The HV sampler (DHA-80, Digitel,  $30 \text{ m}^3 \text{ h}^{-1}$ ) equipped with a  $PM_{10}$  size selective impaction inlet (model DPM01/30/00, Digitel) collected  $PM_{10}$  aerosols on cellulose nitrate filters (150 mm diameter, porosity  $3 \mu\text{m}$ , Sartorius). A total number of 52 samples (24 samples from Brno and 28 samples from Šlapanice) were collected with HV sampler during all campaigns. The LV sampler ( $1 \text{ m}^3 \text{ h}^{-1}$ ), consisting of a Teflon coated aluminium cyclone inlet (cut point diameter of  $1 \mu\text{m}$ , model URG-2000-30EHB), and a NILU filter unit (type 9633) collected  $PM_{10}$  aerosols on 47mm Teflon filters (Zefluor, porosity  $1 \mu\text{m}$ , PALL). To eliminate interference of gaseous pollutants, such as  $\text{SO}_2$ ,  $\text{HNO}_3$ ,  $\text{NH}_3$  and others, an annular diffusion denuder [37] was placed between the cyclone and Teflon filter. A total number of 56 samples (28 samples from Brno and 28 samples from Šlapanice) were collected with the LV sampler during all campaigns.

Meteorological parameters (i.e., temperature and relative humidity) measured by means of a commercial sensor (type T3113, Comet Systems) are given in Table 1. We also present predominant wind directions obtained from one-day backward trajectories calculated using the Hysplit v5.0.0 model. All trajectories are shown in the Supplementary Material (Figures S1–S8) separately for each location and campaign.

**Table 1.** Meteorological parameters in Brno and Šlapanice during campaigns.

| Locality—Season       | Temperature (°C) |             | Relative Humidity (%) |             | Modelled Wind Direction (Predominant) |
|-----------------------|------------------|-------------|-----------------------|-------------|---------------------------------------|
|                       | Average          | (Range)     | Average               | (Range)     |                                       |
| Brno—winter 2009      | −1.9             | (−3.0–0.1)  | 77.6                  | (67.7–89.5) | north, northwest                      |
| Šlapanice—winter 2009 | 0.6              | (−2.4–1.6)  | 81.7                  | (69.6–92.2) | northeast                             |
| Brno—summer 2009      | 21.0             | (18.5–21.8) | 67.1                  | (54.3–80.7) | all directions                        |
| Šlapanice—summer 2009 | 20.0             | (14.3–24.9) | 71.9                  | (67.7–86.7) | northwest                             |
| Brno—winter 2010      | −3.0             | (−6.0–1.0)  | 75.2                  | (69.4–85.0) | all directions                        |
| Šlapanice—winter 2010 | 0.8              | (−1.9–2.5)  | 88.1                  | (82.0–97.2) | south                                 |
| Brno—summer 2010      | 18.0             | (17.2–21.2) | 71.3                  | (65.3–84.8) | west                                  |
| Šlapanice—summer 2010 | 18.2             | (15.1–20.1) | 79.2                  | (65.9–93.4) | north                                 |

### 2.3. Processing and Filter Analysis

Mass concentrations of collected aerosols were determined by weighing filters, using a microbalance M5P ( $\pm 1 \mu\text{g}$ ; Sartorius). Filters were equilibrated before weighing in an air-conditioned room under constant conditions for 48 hrs (temperature  $20 \pm 1 \text{ }^\circ\text{C}$ , relative humidity  $50 \pm 3\%$ ). Static electricity was eliminated with an ionizer prior to weighing (PRX-U, Haug). After weighing, exposed filters were cut, using ceramic scissors, into two equal pieces; each of them was weighted again.

One half of the cellulose-nitrate filters was digested in 4 mL of sub-boiling nitric acid in the UniClever microwave device (Plazmatronika). The decomposed samples were transferred quantitatively along with 4 mL of deionized water into polyethylene scintillation vials (Kartel). The extracts were analysed for the content of 14 selected elements (Al, K, Ca, Fe, Mn, Zn, Cu, Cd, Ba, As, Pb, V, Ni, Sb), employing an inductively coupled plasma–mass spectrometry (model 7500 CE, Agilent). Relative uncertainty of element analysis was in the range of 1 to 3%.

Both halves of the Teflon filters were extracted in 8 mL of deionized water under ultrasonic agitation. The extract of the first half was analysed for the content of seven anions (fluoride, chloride, nitrite, nitrate, sulphate, oxalate, phosphate), while the second half of the filter was analysed for five cations ( $\text{Na}^+$ ,  $\text{K}^+$ ,  $\text{NH}_4^+$ ,  $\text{Ca}^{2+}$ ,  $\text{Mg}^{2+}$ ) by means of ion chromatography (ICS-2100, Dionex). Relative uncertainty of water-soluble ion analysis was in the range of 4 to 7%.

### 2.4. Calculation of Air Trajectories

The analysis of air mass transported towards the sampling sites was performed using the Hysplit model v5.0.0 [38,39], by calculation of one-day backward trajectories at 300, 750 and 1500 m above ground level.

### 2.5. Factor Analysis Model

Measured aerosol components can be grouped by their correlations. The components within a particular group are highly correlated among themselves but have relatively small correlations with aerosol components in a different group. In the factor analysis presented in this paper, it is assumed the observed correlations in a given group of aerosol components are influenced by a factor, which for given group corresponds to a source of pollution (such a pollution source can be, for example, vehicle exhausts, coal combustion and others). Factors are unmeasurable and the number of factors is much smaller than the number of aerosol components. The correlation relationship among aerosol components can be described in terms of a few underlying factors.

Suppose the observed concentrations  $X_1, \dots, X_p$  of elements and ions in PM particles with means (expectations)  $\mu_1, \dots, \mu_p$ . In our study  $p = 16$ . Let  $F_1, \dots, F_m$ , ( $m < p$ ) be considered common factors corresponding to the sources of pollution. We then consider the linear model describing how the

concentrations of elements and ions  $X_1, \dots, X_p$  can be explained using linear combinations of these common factors  $F_1, \dots, F_m$ . The model can be described by equation

$$X_i - \mu_1 = l_{1i}F_1 + \dots + l_{mi}F_m + \varepsilon_i, i = 1, \dots, p \quad (1)$$

where  $l_{ij}$ ,  $i = 1, \dots, p$ ,  $j = 1, \dots, m$ , are the coefficients of linear combinations. They represent the so-called factor loadings indicating how strong is the statistical association between the  $i$ -th aerosol component  $X_i$  and the  $j$ -th factor  $F_j$ . The higher the absolute value of  $l_{ij}$  is, the higher is the statistical association between the aerosol component  $X_i$  and the factor  $F_j$ . The term  $\varepsilon_i$  stands for random errors. Random errors are supposed to be independent with zero mean and variance  $Var(\varepsilon_i) = \psi_i$ , and common factors are assumed to have a zero mean and unit variance. The independence of common factors and random errors ( $Cor(\varepsilon_i, F_j) = 0$  for  $i = 1, \dots, p$ ,  $j = 1, \dots, m$ ) is also considered. From the above assumptions follows  $Var(X_i) = l_{1i}^2 + l_{2i}^2 + \dots + l_{mi}^2 + \psi_i = h_i^2 + \psi_i$ , where  $h_i^2 = l_{1i}^2 + l_{2i}^2 + \dots + l_{mi}^2$  is called the  $i$ -th communality, the proportion of the variance of the variable  $X_i$  contributed by the  $m$  common factors.

Various methods [40] that allow us to estimate the parameters of model (1) exist. Here, the principal component method [41], which does not impose restrictions on distribution of analysed variables, is preferred. A crucial task of the factor analysis is the selection of appropriate number of common factors  $m$ . Since the higher values of  $m$  lead to common factors that are difficult to interpret, the aim is to choose the smallest possible value  $m$ , such that a sufficient proportion of variability in the data is explained. For this problem, Kaiser's criterion and scree plot [41] are considered.

The original factor loads obtained by the principal component method can be difficult to interpret. Thus, the factor rotation is performed for better interpretation of factor loads. A common goal of rotation in this paper is to ensure that each aerosol component loads highly on a single factor and has small-to-moderate loads on the remaining single factors. The factor model with such rotated loads is called the model with a simpler structure. Usually the criterion, which is used to obtain a simpler structure, is the varimax criterion [41].

### 3. Results

#### 3.1. Characterization of Submicrometre Aerosols

Mass concentrations of PM<sub>1</sub> aerosols collected at both sites during all campaigns are given in Table 2. The average measured PM<sub>1</sub> mass concentration was 19.1  $\mu\text{g m}^{-3}$  in winter and 9.65  $\mu\text{g m}^{-3}$  in summer in Brno, and 30.8 and 10.0  $\mu\text{g m}^{-3}$  in winter and in summer, respectively, in Šlapanice. PM<sub>1</sub> samples in both locations were collected at a different time; therefore, we tested if the mass concentrations of PM<sub>1</sub> aerosols in Brno and Šlapanice were similar in the same season. Agreement of mass concentration of PM<sub>1</sub> aerosols collected in Brno and Šlapanice was statistically tested by non-paired t-test for equal means. Probability of equality of mean concentrations (P) smaller than 0.05 indicates disagreement of tested mean values at both sampling sites. P value was 0.0081 for winter 2009; 0.1366 for summer 2009; 0.1339 for winter 2010 and 0.1399 for summer 2010, which indicates that the mean mass concentrations of aerosols in Brno and Šlapanice in the same season were similar in summer 2009, winter 2010 and summer 2010 but different in winter 2009. The difference in the PM<sub>1</sub> concentration in Brno and Šlapanice in winter 2009 was caused by heavy snow during days 2–5 of the campaign in Brno leading to lower concentration of PM<sub>1</sub> in Brno, while in Šlapanice (no snow during the campaign), the PM<sub>1</sub> concentration remained at a normal level for this time of a year. The concentrations of aerosols in winter were higher than in summer both in Brno and Šlapanice, which can be attributed to increased anthropogenic emissions in heating season due to household heating of local residents [11,18,19] and to lower mixing layer height due to the lower dispersive capacity of the lower atmospheric layers in winter, which favours the accumulation of pollutants and prevents air convection and the dispersion of pollutants [42,43]. The strong relationship of the PM<sub>1</sub> concentration with air temperature was confirmed by a significant negative correlation ( $p < 0.01$ ) both

in Šlapanice (a correlation coefficient  $R = -0.71$ , Table S1) and in Brno ( $-0.64$ , Table S2). Calculated one-day backward trajectories (Figures S1–S8) indicate possible transport of not only regional air pollution from surrounding villages but also long-range transport of polluted air from more distant localities, such as heavy polluted areas in the Silesian Voivodeship in southern Poland that has been recently identified as an important PM source in winter [12]. The differences in the concentration of PM<sub>1</sub> aerosols in corresponding seasons in 2009 and 2010 (Table 2) were probably caused mainly by different meteorological and dispersal conditions in those two years.

**Table 2.** Mass concentrations of PM<sub>1</sub> aerosols during the campaigns.

| Locality—Season                             | PM <sub>1</sub> (µg/m <sup>3</sup> ) |             |
|---|--------------------------------------|-------------|
|   | Mean                                 | (Range)     |
| Brno—winter 2009 (10–16 February 2009)      | 12.3                                 | (10.3–20.3) |
| Šlapanice—winter 2009 (25–31 January 2009)  | 28.5                                 | (13.1–47.8) |
| Brno—summer 2009 (3–9 August 2009)          | 8.89                                 | (7.72–10.7) |
| Šlapanice—summer 2009 (25–31 August 2009)   | 12.2                                 | (5.99–18.6) |
| Brno—winter 2010 (1–7 February 2010)        | 25.9                                 | (20.9–32.5) |
| Šlapanice—winter 2010 (16–22 February 2010) | 33.1                                 | (19.1–52.8) |
| Brno—summer 2010 (17–23 August 2010)        | 10.4                                 | (5.77–17.6) |
| Šlapanice—summer 2010 (25–31 July 2010)     | 7.73                                 | (5.88–11.3) |

The mass of determined elements and ions together accounted for about 29% of total PM<sub>1</sub> mass, ranging between 16% and 44%. The rest of the mass probably consists of organic compounds, elemental carbon and water. Previous studies at the same locations showed that organic material and elemental carbon formed on average 37.6% and 7.80% of PM<sub>1</sub> mass [11,18,19].

The concentration of PM<sub>1</sub> aerosols found in Brno and Šlapanice in 2009 and 2010 are similar to those observed in other study from this site [11] as well as in PM<sub>1</sub> from other localities in the Czech Republic [6,23], or from other sites in Europe, such as Birmingham [44], Melpitz [45], Bologna [46], Granada [34], Katowice [47] and Racibórz, whereas the concentration of PM<sub>1</sub> in Zabrze [48] was higher than in Brno and Šlapanice.

Two recent studies [21,49] from the same location in Brno do not show any decrease in air pollution with PM<sub>1</sub> aerosol. The concentration of PM<sub>1</sub> aerosols collected in summer 2014 (i.e., the mean value of 10.8 µg/m<sup>3</sup>) was similar to the concentration found in the presented study, while the concentration found in winter 2015 (i.e., the mean value of 16.5 µg/m<sup>3</sup>) [21] was in the middle of the concentrations found in the present study in winter 2009 and 2010. The sampling of PM<sub>1</sub> aerosols in winter 2017 was accompanied by a few days of smog event, which resulted in an increased PM concentration in Brno and the concentrations of PM<sub>1</sub> aerosols measured in this study (i.e., the mean value of 34.2 µg/m<sup>3</sup>) [49] was thus even higher than the concentrations found in the present study.

### 3.2. Characterization of Elements

We analysed 14 elements in all submicrometre aerosol samples collected in Brno and Šlapanice. The average element concentrations in PM<sub>1</sub> aerosols from both sampling sites are summarized in Table 3 (campaigns of 2009) and Table 4 (campaigns of 2010). In winter 2009, the concentrations of elements in Šlapanice were higher than those in Brno, whereas in all other seasons the concentrations of elements at both localities were comparable. The sum of concentrations of the analysed elements accounted for 1.77% of PM<sub>1</sub> mass. In winter, the contribution of elements to PM<sub>1</sub> mass was 2.17% (1.70–2.76%) and in summer decreased to 1.37% (0.92–1.97%). In winter, lead and potassium were the two most abundant elements accounting for 65–84% of the total element mass in PM<sub>1</sub>, while in summer potassium prevailed (27–40% of the total element mass in PM<sub>1</sub>). The daily changes in element concentrations in 2009 and 2010 are shown in Figures 2 and 3, respectively. As, Cd, Pb and Ni are elements known to be toxic to human health [50,51]. The annual average concentration of these

elements, calculated as the average of summer and winter concentrations, do not exceed the annual limit valid in the Czech Republic [52] in both Brno and in Šlapanice in 2009 and 2010.

**Table 3.** Summary of concentrations of elements and water-soluble ions ( $\text{ng m}^{-3}$ ) in  $\text{PM}_{10}$  aerosols collected during the winter and summer campaigns in Brno and Šlapanice in 2009.

| PM Component                  | Brno                |                      | Šlapanice           |                     |
|-------------------------------|---------------------|----------------------|---------------------|---------------------|
|                               | Winter              | Summer               | Winter              | Summer              |
|                               | Mean<br>(range)     | Mean<br>(range)      | Mean<br>(range)     | Mean<br>(range)     |
| V                             | 0.41<br>(0.29–0.66) | 0.13<br>(nd–0.30)    | 0.51<br>(0.36–0.77) | 0.07<br>(nd–0.27)   |
| Cd                            | 0.09<br>(0.05–0.14) | 0.18<br>(nd–0.35)    | 0.48<br>(0.20–0.93) | 0.20<br>(0.08–0.45) |
| As                            | 0.32<br>(0.15–0.58) | 0.55<br>(nd–1.51)    | 0.74<br>(0.19–1.47) | 0.17<br>(nd–0.42)   |
| Sb                            | 0.24<br>(0.14–0.42) | 0.67<br>(0.20–0.98)  | 1.08<br>(0.41–2.26) | 0.78<br>(0.41–1.35) |
| Cu                            | 0.46<br>(0.25–0.76) | 1.08<br>(nd–1.56)    | 1.33<br>(0.38–3.16) | 0.50<br>(0.23–0.98) |
| Ni                            | 0.37<br>(0.09–0.66) | nd<br>(nd–nd)        | 3.79<br>(0.77–20.7) | nd<br>(nd–nd)       |
| Mn                            | 1.18<br>(0.54–2.23) | 1.38<br>(0.42–2.11)  | 3.10<br>(0.69–6.36) | 1.94<br>(0.39–5.50) |
| Al                            | 9.44<br>(1.82–18.8) | 7.07<br>(nd–18.9)    | 9.32<br>(3.64–14.0) | 9.35<br>(nd–27.8)   |
| Ba                            | 22.1<br>(2.39–63.9) | 11.42<br>(3.15–20.0) | 31.9<br>(0.48–107)  | 10.2<br>(1.99–17.7) |
| Fe                            | 28.8<br>(14.7–45.9) | 5.45<br>(nd–10.9)    | 37.9<br>(10.2–123)  | 4.01<br>(nd–12.6)   |
| Zn                            | 8.49<br>(5.48–15.6) | 8.52<br>(2.60–12.8)  | 35.8<br>(13.6–72.6) | 17.2<br>(5.61–66.1) |
| Ca                            | 30.0<br>(4.12–47.3) | 54.7<br>(19.3–119)   | 31.7<br>(14.8–48.1) | 40.9<br>(29.9–51.2) |
| K                             | 63.3<br>(32.9–127)  | 68.1<br>(34.3–124)   | 201<br>(95.2–326)   | 76.7<br>(24.7–145)  |
| Pb                            | 133<br>(90.5–265)   | 27.3<br>(5.93–44.9)  | 211<br>(83.4–465)   | 42.9<br>(15.5–96.0) |
| F <sup>-</sup>                | 5.87<br>(nd–16.9)   | 5.51<br>(0.99–14.6)  | 29.1<br>(4.46–67.1) | 4.90<br>(1.20–10.2) |
| Cl <sup>-</sup>               | 10.4<br>(nd–36.5)   | 6.59<br>(1.05–17.1)  | 515<br>(47.3–1461)  | 13.1<br>(1.93–26.4) |
| NO <sub>2</sub> <sup>-</sup>  | 3.20<br>(2.11–4.29) | 5.14<br>(0.99–22.5)  | 8.35<br>(5.83–13.7) | 5.97<br>(0.74–12.1) |
| NO <sub>3</sub> <sup>-</sup>  | 2462<br>(969–5224)  | 79.9<br>(8.39–294)   | 3460<br>(1128–6090) | 215<br>(82.9–530)   |
| SO <sub>4</sub> <sup>2-</sup> | 1386<br>(846–1775)  | 1012<br>(262–1535)   | 3516<br>(2328–4731) | 1799<br>(285–3742)  |
| oxalate                       | 55.9<br>(32.2–72.8) | 85.8<br>(19.0–148)   | 91.5<br>(50.2–109)  | 133<br>(28.4–262)   |

Table 3. Cont.

| PM Component                  | Brno                |                     | Šlapanice           |                     |
|-------------------------------|---------------------|---------------------|---------------------|---------------------|
|                               | Winter              | Summer              | Winter              | Summer              |
|                               | Mean<br>(range)     | Mean<br>(range)     | Mean<br>(range)     | Mean<br>(range)     |
| PO <sub>4</sub> <sup>3-</sup> | 3.00<br>(nd–8.84)   | 3.90<br>(1.00–10.7) | 26.2<br>(13.0–48.1) | 5.18<br>(nd–21.1)   |
| Na <sup>+</sup>               | 4.30<br>(nd–11.5)   | 50.1<br>(2.01–166)  | 30.4<br>(nd–148)    | 25.0<br>(1.01–57.1) |
| K <sup>+</sup>                | 39.5<br>(10.5–72.7) | 55.6<br>(17.3–109)  | 84.7<br>(18.7–175)  | 63.3<br>(18.2–119)  |
| NH <sub>4</sub> <sup>+</sup>  | 1140<br>(616–1894)  | 395<br>(121–601)    | 2387<br>(1388–3989) | 733<br>(134–1450)   |
| Ca <sup>2+</sup>              | 5.37<br>(2.11–10.3) | 26.6<br>(15.0–46.3) | 28.0<br>(11.9–43.7) | 35.4<br>(25.9–45.8) |
| Mg <sup>2+</sup>              | nd<br>(nd–nd)       | nd<br>(nd–nd)       | nd<br>(nd–nd)       | 3.52<br>(1.00–6.02) |

nd—not detected.

Table 4. Summary of concentrations of elements and water-soluble ions (ng m<sup>-3</sup>) in PM<sub>1</sub> aerosols collected during winter and summer campaigns in Brno and Šlapanice in 2010.

| PM Component | Brno                |                     | Šlapanice           |                     |
|--------------|---------------------|---------------------|---------------------|---------------------|
|              | Winter              | Summer              | Winter              | Summer              |
|              | Mean<br>(range)     | Mean<br>(range)     | Mean<br>(range)     | Mean<br>(range)     |
| V            | 0.57<br>(0.31–0.97) | nd<br>(nd–nd)       | 0.98<br>(0.37–1.45) | 0.08<br>(nd–0.58)   |
| Cd           | 0.58<br>(0.38–1.17) | 0.15<br>(0.07–0.26) | 0.50<br>(0.42–0.62) | 0.10<br>(0.02–0.32) |
| As           | 1.11<br>(0.54–1.68) | 0.20<br>(nd–0.43)   | 1.06<br>(0.66–1.92) | 0.88<br>(nd–2.44)   |
| Sb           | 1.05<br>(0.67–1.72) | 0.70<br>(0.44–1.13) | 1.93<br>(0.84–4.96) | 0.29<br>(0.09–0.39) |
| Cu           | 1.40<br>(0.45–3.47) | 1.44<br>(1.04–2.15) | 1.09<br>(0.31–3.02) | 0.60<br>(nd–1.14)   |
| Ni           | 1.38<br>(0.40–4.21) | 0.10<br>(0.02–0.23) | 0.72<br>(0.29–1.40) | nd<br>(nd–nd)       |
| Mn           | 5.90<br>(1.71–11.6) | 1.24<br>(0.51–1.83) | 2.14<br>(0.73–5.28) | 2.37<br>(0.78–3.84) |
| Al           | 3.89<br>(0.90–11.1) | 8.63<br>(7.21–11.4) | 1.51<br>(0.45–2.90) | 13.5<br>(nd–27.6)   |
| Ba           | 12.6<br>(nd–69.6)   | 0.10<br>(nd–0.30)   | nd<br>(nd–nd)       | 0.87<br>(nd–4.87)   |
| Fe           | 57.4<br>(20.6–86.0) | 25.1<br>(20.8–31.5) | 20.4<br>(10.6–53.0) | 33.2<br>(7.44–70.1) |
| Zn           | 46.2<br>(19.8–73.7) | 12.5<br>(4.54–19.7) | 40.2<br>(27.4–51.4) | 9.77<br>(4.45–12.9) |

Table 4. Cont.

| PM Component                  | Brno                |                     | Šlapanice           |                     |
|-------------------------------|---------------------|---------------------|---------------------|---------------------|
|                               | Winter              | Summer              | Winter              | Summer              |
|                               | Mean<br>(range)     | Mean<br>(range)     | Mean<br>(range)     | Mean<br>(range)     |
| Ca                            | 20.7<br>(13.6–26.5) | 13.0<br>(10.7–16.8) | 6.87<br>(2.88–13.2) | 6.15<br>(2.45–12.8) |
| K                             | 273<br>(217–377)    | 44.0<br>(8.59–100)  | 353<br>(229–391)    | 25.7<br>(18.2–33.1) |
| Pb                            | 76.7<br>(46.5–109)  | 3.05<br>(1.69–5.04) | 81.1<br>(50.6–135)  | 3.36<br>(nd–7.18)   |
| F <sup>-</sup>                | 14.4<br>(7.65–27.3) | 4.02<br>(nd–7.89)   | 43.4<br>(16.5–141)  | 0.27<br>(nd–1.91)   |
| Cl <sup>-</sup>               | 140<br>(37.8–194)   | 7.65<br>(nd–19.2)   | 315<br>(40.3–1129)  | 10.7<br>(2.61–21.6) |
| NO <sub>2</sub> <sup>-</sup>  | 23.4<br>(3.52–74.8) | 2.06<br>(0.48–3.54) | 16.7<br>(nd–46.5)   | 17.5<br>(0.30–82.6) |
| NO <sub>3</sub> <sup>-</sup>  | 3746<br>(2234–5422) | 105<br>(8.20–519)   | 3156<br>(1727–4315) | 137<br>(25.1–335)   |
| SO <sub>4</sub> <sup>2-</sup> | 1355<br>(518–2770)  | 577<br>(79.0–1315)  | 1591<br>(280–3228)  | 596<br>(178–1009)   |
| oxalate                       | 74.8<br>(51.9–112)  | 78.0<br>(7.29–190)  | 121<br>(2.82–234)   | 23.7<br>(0.50–46.6) |
| PO <sub>4</sub> <sup>3-</sup> | 24.0<br>(5.48–37.2) | 12.3<br>(1.75–44.0) | 30.1<br>(nd–67.0)   | 3.01<br>(0.28–6.59) |
| Na <sup>+</sup>               | 45.1<br>(13.1–70.2) | 4.74<br>(nd–10.2)   | 75.9<br>(6.34–324)  | 2.58<br>(nd–6.68)   |
| K <sup>+</sup>                | 212<br>(171–278)    | 36.8<br>(10.1–105)  | 314<br>(191–352)    | 18.5<br>(12.8–21.7) |
| NH <sub>4</sub> <sup>+</sup>  | 3217<br>(2539–3942) | 701<br>(117–1382)   | 3261<br>(1783–5475) | 716<br>(211–1173)   |
| Ca <sup>2+</sup>              | 6.12<br>(3.35–9.05) | 8.27<br>(4.49–13.7) | 4.93<br>(2.03–9.48) | 4.50<br>(1.85–9.43) |
| Mg <sup>2+</sup>              | 1.00<br>(nd–3.08)   | 0.66<br>(0.06–1.37) | 4.32<br>(nd–27.2)   | 0.10<br>(nd–0.68)   |

nd—not detected.

The concentrations of elements in the PM<sub>1</sub> samples from both the Brno and Šlapanice sites are comparable with those found in Granada [34], Bologna [46] and Frankfurt [53], but lower than those in samples from other European sites, such as Katowice [47] or Tito Scalo [54]. In other Polish cities, Zabrze and Racibórz, the concentrations of several elements (Al, Mn, Fe, Cu, Zn, As) in PM<sub>1</sub> were higher than those in Brno and Šlapanice, while the concentrations of other elements were comparable [48].

A comparison of the concentrations of elements in PM<sub>1</sub> aerosols collected in Brno in 2009 and 2010 with the concentrations of elements collected at the same location in summer 2014 and winter 2015 [21] does not show a marked drop in air pollution with heavy metals in Brno location during this period. Most of the elements measured simultaneously in this and in a later study (i.e., Fe, Mn, V, Ni, Cu, Zn, Cd) show approximately similar concentrations, with the exception of lead, as the concentrations of which in winter 2015 were much lower than the concentrations found in the corresponding season in 2009 and 2010. Similarly, the concentration of lead in summer of 2014 was much lower than in summer of 2009, but practically identical with the concentrations in summer of 2010.

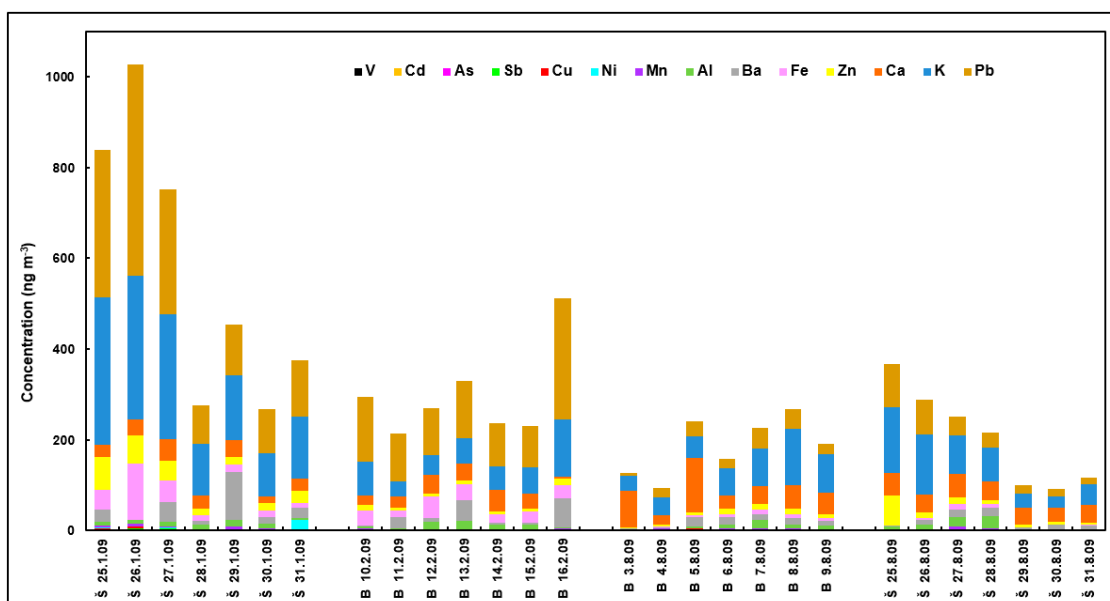


**Figure 2.** Daily variations in the concentrations of elements in the PM<sub>1</sub> aerosols in Brno and Šlapanice in 2009.

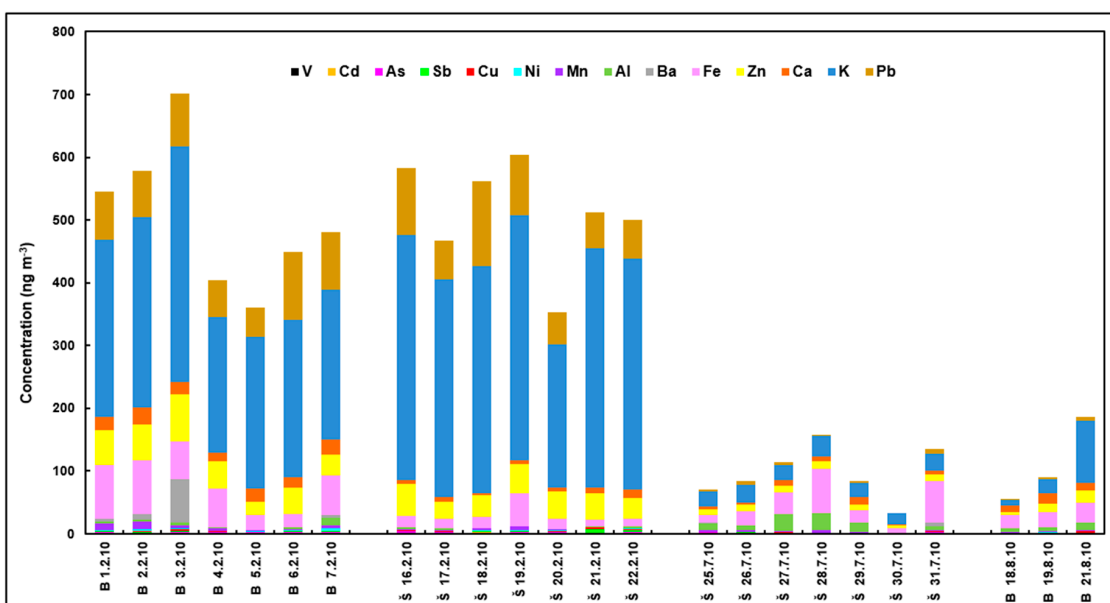


**Figure 3.** Daily variations in the concentrations of elements in the PM<sub>1</sub> aerosols in Brno and Šlapanice in 2010.

The enrichment factors (EFs) of elements in aerosols collected in Brno and Šlapanice were calculated to discriminate the anthropogenic and crustal (i.e., natural) origin of the studied elements. The EFs are defined by the equation

$$EF = (X/R)_{\text{aerosol}} / (X/R)_{\text{crust}} \quad (2)$$

where X represents the considered element and R is the reference element, while the subscripts aerosol and crust indicate concentrations in PM<sub>1</sub> and in the Earth’s crust, respectively [55]. The EFs were calculated for Fe as the reference element [21]. Generally, EF < 5 indicates the crustal soil as the predominant source of the element, while the anthropogenic origin of the element may be considered at EF > 100 [56]. The enrichment factors calculated from the element concentrations determined in

PM<sub>1</sub> aerosols collected in Brno and Šlapanice are shown in Table 5. Pb, Cd and Sb have the highest EFs, with Pb being the most enriched element for PM<sub>1</sub> particles both in Brno and Šlapanice followed by Cd, Sb, Zn and As with EF > 100, which indicates their anthropogenic sources. The EFs of Cu, Ba, Ni, K, Mn and V are within the range of 5–100, which suggests that these elements are of both anthropogenic origin and soil contribution. The EF of Al approaches to unity, which indicates crustal soil as a predominant source [54,57]. The EFs of most elements in the aerosols sampled in Šlapanice are larger than enrichment factors of elements in aerosols collected in Brno. The obtained value of the EFs from both localities are similar to those of the recent study in Brno [21], with the exception of V, Mn and Cd, the values of which in this study are approximately twice higher, and the EF of Pb is approximately 20 times higher.

**Table 5.** Enrichment factors calculated from the element concentrations determined in PM<sub>1</sub> aerosols collected in Brno and Šlapanice.

|           | Fe   | Al   | Ca   | V    | Mn   | K    | Ni   | Ba   | Cu   | As  | Zn   | Sb   | Cd   | Pb     |
|-----------|------|------|------|------|------|------|------|------|------|-----|------|------|------|--------|
| Brno      | 1.00 | 0.24 | 4.57 | 4.82 | 5.65 | 8.94 | 8.59 | 48.2 | 103  | 283 | 462  | 4356 | 5753 | 6393   |
| Šlapanice | 1.00 | 0.37 | 4.41 | 8.11 | 9.39 | 17.9 | 28.2 | 53.4 | 80.8 | 285 | 1096 | 7985 | 9717 | 11,722 |

Most of the elements exhibit distinct seasonal variability when the concentrations of elements in winter were higher than in summer. High seasonal differences were observed especially for K, Pb, Fe, As, V, Cd, Zn, Ni, Sb and Ba, and less for Mn and Cu. Potassium is produced largely during wood combustion [58]. Other metals can originate from several different sources. Arsenic and cadmium originate mainly from coal combustion and partly from industry. Zn, Mn, Cu, Fe or Pb are produced, next to various industrial sources and traffic, mainly by biomass (wood) burning and coal combustion [59–62]. Coal combustion and biomass burning are still frequently used for energy production and for residential heating in many European countries [36,63]. Hence, it is plausible that increased concentration of these elements (with exception of Al and Ca) in heating seasons when compared to the rest of the year is largely caused by wood and coal combustion in residential heating. Recent studies [11,15,18,19] and the results from the last census in the Czech Republic in 2011 [64] indicate that the combustion of coal and wood is used for heating only in a small part of households both in Brno (0.46%) and in Šlapanice (1.36%), but the proportion of households in small villages near Šlapanice and Brno using wood or coal for heating is much higher (up to 11%). In addition, elements, such as Cd, As, Mn, Ni, Pb, V, Cu, Zn, Sb and so on, can also originate from emission of a municipal solid waste incinerator [65,66] located directly on the connecting line between the sampling site in Brno and Šlapanice, or from the incineration of waste in households (Sb, Cu, Pb, Sn, Ti, and Zn) [67]. Another possible source of elements, in particular Ca, Zn, Fe, Mn, Pb, Cd, As, Cu and Ni, is a cement plant [68–70] located north of Šlapanice and east of Brno. To verify this hypothesis, we calculated one-day backward trajectories for all the sampling campaigns in both the Brno and Šlapanice sampling sites (Figures S1–S8). Detailed analysis revealed the transport of air masses from all directions, although during individual campaigns certain wind directions prevailed (Table 1). Moreover, the backward trajectory analysis shows the possibility of a long-range transport of air masses to Brno and Šlapanice from areas as far as several hundred kilometres.

### 3.3. Characterization of Water-Soluble Ions

We analysed 12 water-soluble ions in total (i.e., 5 inorganic cations, 6 inorganic anions and oxalate) in all submicrometre aerosol samples collected in Brno and Šlapanice. Average water-soluble ion concentrations in PM<sub>1</sub> aerosols from both Brno and Šlapanice are summarized in Table 3 (campaigns of 2009) and Table 4 (campaigns of 2010). Ion species were important constituents of submicrometre aerosols both in Brno and Šlapanice, accounting for 27.5% and 26.8% of PM<sub>1</sub> mass in Brno and Šlapanice, respectively. Ion species on average accounted for 27.2% of mass of PM<sub>1</sub> aerosols. Ammonium, nitrate and sulphate were the three major ion species, contributing 32.3%, 36.2% and 23.4% of the total

ion concentrations, respectively.  $\text{SO}_4^{2-}$ ,  $\text{NO}_3^-$  and  $\text{NH}_4^+$  are generally considered as secondary inorganic aerosol components (SIA; [71]). They derive from gas to particle conversion processes when  $\text{SO}_2$  is transformed to  $\text{H}_2\text{SO}_4$  and nitrogen oxides to  $\text{HNO}_3$ , followed by  $\text{NH}_3$  neutralization to form  $(\text{NH}_4)_2\text{SO}_4$  and  $\text{NH}_4\text{NO}_3$ .  $\text{SO}_2$  and  $\text{NO}_x$  are products of combustion processes, whereas  $\text{NH}_3$  originates mainly from anthropogenic sources, such as agricultural activity, industry and traffic [36,72]. The sum of  $\text{SO}_4^{2-}$ ,  $\text{NO}_3^-$  and  $\text{NH}_4^+$  accounted together for 91.9% on average (86.1–97.5%) of total ion concentration and for 25.1% of  $\text{PM}_{10}$  mass. The concentrations of other analysed anions and cations were much lower. The daily changes in the concentrations of ions in 2009 and 2010 are shown in Figures 4 and 5, respectively.

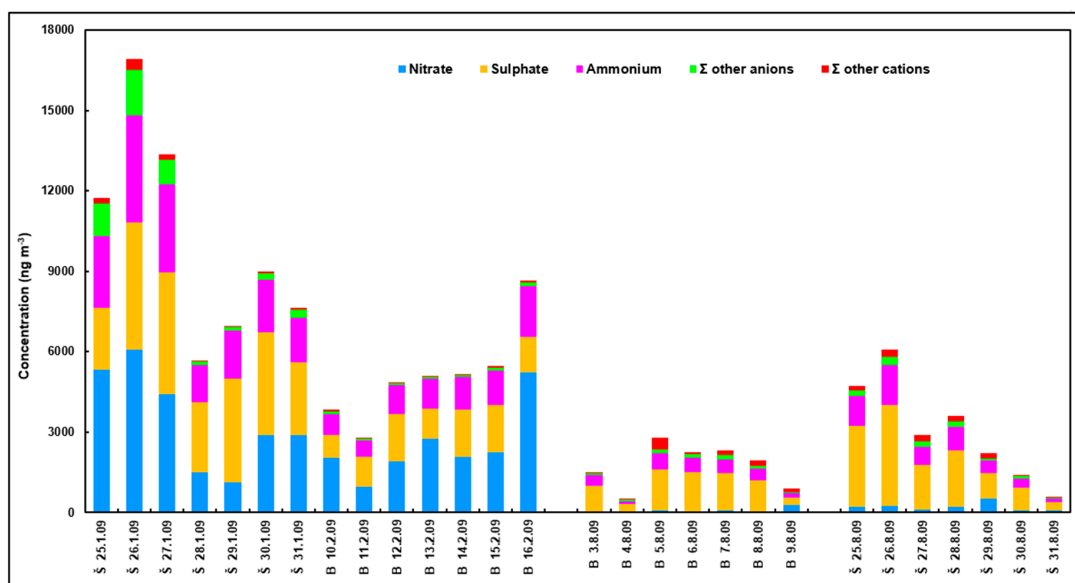


Figure 4. Daily variations in the concentrations of water-soluble ions in the  $\text{PM}_{10}$  aerosols in Brno and Šlapanice in 2009.

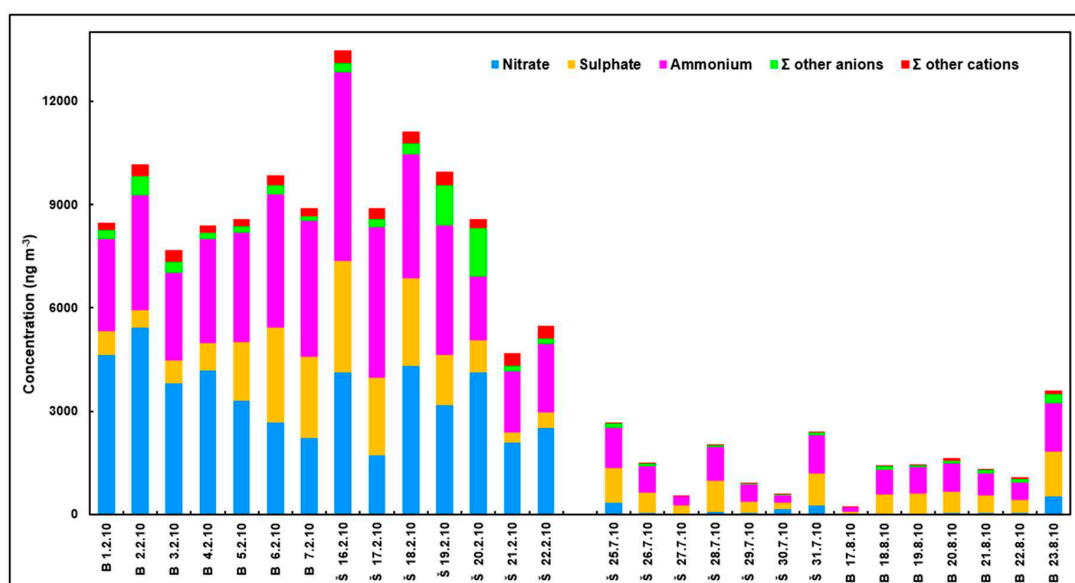


Figure 5. Daily variations in the concentrations of water-soluble ions in the  $\text{PM}_{10}$  aerosols in Brno and Šlapanice in 2010.

The majority of the analysed ions show significant seasonal variability with winter concentrations, significantly exceeding those in the summer (Tables 3 and 4). The SIA contribution decreased from

a share of 32.4% in PM<sub>1</sub> mass in winter to 17.8% in summer. The concentration of NO<sub>3</sub><sup>-</sup> was much higher in winter than in summer, which may be due to the low thermal stability of ammonium nitrate in the summer, favouring the conversion of particulate ammonium nitrate to gaseous nitric acid and ammonia [1,73]. In contrast, the difference between the winter and summer SO<sub>4</sub><sup>2-</sup> concentrations was much smaller compared to that of NO<sub>3</sub><sup>-</sup>, which indicates an active photochemical production of SO<sub>4</sub><sup>2-</sup> in summer [74].

Increased concentrations of F<sup>-</sup>, Cl<sup>-</sup>, NO<sub>2</sub><sup>-</sup>, SO<sub>4</sub><sup>2-</sup>, PO<sub>4</sub><sup>3-</sup>, NO<sub>3</sub><sup>-</sup>, NH<sub>4</sub><sup>+</sup> and K<sup>+</sup> in winter are mostly associated with burning of wood and coal in residential heating [11,18,19,36]. Combustion processes are the main sources of fluoride (i.e., coal), chloride (i.e., wood, coal, solid waste) and phosphate (i.e., coal, wood, traffic). K<sup>+</sup>, considered an inorganic tracer for biomass burning [14,62], formed the majority (i.e., 73.9%) of the total potassium in submicrometre aerosol. Enhanced winter concentrations of Cl<sup>-</sup>, F<sup>-</sup>, PO<sub>4</sub><sup>3-</sup> and K<sup>+</sup> were observed especially in Šlapanice, which is likely associated with local and regional combustion of wood and coal in residential heating [11,18,19]. Moreover, Cl<sup>-</sup> and F<sup>-</sup> may also be emitted from the brickworks [75,76] located directly in Šlapanice. Cl<sup>-</sup> and PO<sub>4</sub><sup>3-</sup> serving as markers of plastic waste combustion may also originate from a large municipal waste incinerator located east of Brno or from the combustion of solid waste by households [67].

The concentrations of oxalate in winter were similar to those during summer campaigns, with the exception of Šlapanice in 2010. Oxalates, considered a major water-soluble organic compound in the aerosols, were reported as both a product of primary emissions from combustion processes (traffic, biomass burning, biogenic activity) and as a secondary product of atmospheric chemistry [77,78]. Oxalate correlated both with sulphate and K<sup>+</sup> (Tables S1 and S2), which suggests that oxalate found in PM<sub>1</sub> aerosols in Brno and Šlapanice originated from both biomass burning and secondary oxidation.

The concentration of ions in PM<sub>1</sub> in Brno and Šlapanice were comparable with those found in Granada [34] and Katowice [47], while in other Polish cities, Zabrze and Racibórz, the concentrations of several ions (Cl<sup>-</sup>, K<sup>+</sup>, Na<sup>+</sup>, Ca<sup>2+</sup>, Mg<sup>2+</sup>) were higher and others (NH<sub>4</sub><sup>+</sup>) were lower [48]. The concentrations of ions at background station in Melpitz were comparable with the exception of a higher concentration of Mg<sup>2+</sup> and a lower concentration of Ca<sup>2+</sup> in comparison with results of this study [45]. A recent study from Prague reported generally higher concentrations of the analysed Cl<sup>-</sup>, SO<sub>4</sub><sup>2-</sup>, NO<sub>3</sub><sup>-</sup> and NH<sub>4</sub><sup>+</sup> in comparison with those from Brno and Šlapanice [20]. Recently, Cl<sup>-</sup>, NO<sub>2</sub><sup>-</sup>, SO<sub>4</sub><sup>2-</sup> and NO<sub>3</sub><sup>-</sup> have been analysed in Brno in PM<sub>2.5</sub> particles, using the continuous aerosol sampler [16]. The concentrations of Cl<sup>-</sup> and SO<sub>4</sub><sup>2-</sup> found by the aerosol sampler were comparable with filter-based concentrations in this study, but the concentrations of NO<sub>2</sub><sup>-</sup> and NO<sub>3</sub><sup>-</sup> from the aerosol sampler were higher. This difference can be explained by the bimodal distribution of nitrate in PM<sub>1</sub> and PM<sub>2.5</sub> [6] and by sampling artefacts observed during the sampling of nitrite on filters [16].

### 3.4. Correlation Analysis

Pearson correlation coefficients provide another way to assess the sources of the analysed components in PM<sub>1</sub> aerosols. The possible sources can be identified from the correlation matrix by analysing the value, which represents the linear coefficient of correlation between the species. The high correlation of two species suggests their identical sources. The results of correlation analysis of the studied elements and water-soluble ions and their relationship to the mass concentration of PM<sub>1</sub> and temperature of air are shown in Table S1 (Šlapanice) and Table S2 (Brno), and are discussed in detail below.

Several elements (V, Cd, As, Fe, Zn, K) and most ions (NO<sub>3</sub><sup>-</sup>, Cl<sup>-</sup>, F<sup>-</sup>, PO<sub>4</sub><sup>3-</sup>, K<sup>+</sup> and NH<sub>4</sub><sup>+</sup>) both in Šlapanice and Brno ( $p < 0.01$ ) significantly positively correlated with PM<sub>1</sub>, but negatively correlated with temperature, which indicates a strong association of the mentioned elements and ions with combustion sources, especially in heating seasons.

Many elements and ions have the same overlapping sources. For example, Zn, Cu, Mn, Pb, As, Cd were found in the emissions from several combustion processes, such as coal combustion, biomass burning, an incinerator or vehicle emissions. The effect of biomass burning on the studied elements

and ions was investigated through the correlation with  $K^+$ , which is used as a marker of biomass (especially wood) burning [14,62].  $K^+$  correlated significantly ( $p < 0.01$ ) in Brno with V, Cd, As, Sb, Cu, Ni, Mn, Fe, Zn, K,  $NO_3^-$ ,  $Cl^-$ ,  $F^-$ ,  $PO_4^{3-}$ ,  $NO_2^-$  and  $NH_4^+$ , and in Šlapanice with V, Cd, Sb, Zn, K,  $NO_3^-$ ,  $F^-$ ,  $NH_4^+$  ( $p < 0.01$ ) and with As and  $PO_4^{3-}$  ( $p < 0.05$ ), which suggests that wood burning was one of the major sources of the  $PM_{10}$  constituents during the campaigns in Brno and Šlapanice. This finding is in good agreement with the list of elements found in the emissions from the combustion of various biomass fuels [61,62]. Other elements (i.e., Zn, Cu, Cd and As) are important markers of coal combustion [60]. Significant cross-correlations among these elements ( $p < 0.01$ ) confirm their common origin in combustion of coal. Moreover, some elements and ions originated from the municipal waste incinerator, such as Sb, Zn, Cd, As, Mn, Ni,  $Cl^-$ ,  $F^-$ , and  $PO_4^{3-}$  correlated significantly with other elements and ions in Brno more than in Šlapanice, which suggests a stronger effect of emissions from the municipal incinerator on the composition of  $PM_{10}$  in Brno than in Šlapanice. Ni did not correlate with any other element or ion in Šlapanice, but in Brno, Ni correlated significantly with V, Mn, Fe, K,  $NH_4^+$ ,  $PO_4^{3-}$  ( $p < 0.01$ ), Cd,  $NO_3^-$  and  $Cl^-$  ( $p < 0.05$ ), which indicates the municipal incinerator as a predominant source of Ni in Brno. A similar difference in the correlations between the Brno and Šlapanice was also observed for Mn. The opposite situation was observed for Pb, which highly correlated with other  $PM_{10}$  components more in Šlapanice (i.e., Cd, Cu, Fe, Zn, K,  $SO_4^{2-}$ ,  $NO_3^-$ ,  $Cl^-$ ,  $F^-$ ,  $PO_4^{3-}$ ,  $NH_4^+$  ( $p < 0.01$ ), Mn,  $F^-$  ( $p < 0.05$ )) than in Brno (Ba,  $NO_3^-$  ( $p < 0.01$ ), V ( $p < 0.05$ )). No apparent correlation with other constituents in the  $PM_{10}$  samples collected in the Brno and Šlapanice sites was observed for Al and Ca, suggesting that Al and Ca have different sources compared to other elements and ions in  $PM_{10}$ , such as soil dust resuspension for Al or emissions from a cement factory for Ca and  $Ca^{2+}$ .

### 3.5. Source Apportionment

The correlation analysis groups the elements and ions on the basis of high pair correlations. The method provides only general information about the possible sources. Moreover, it does not evaluate the relationship between various sources, so overlapping of sources is problematic. To enhance the accuracy of emission source identification and their relative contribution, the method of factor analysis was also applied. The factor analysis belongs to multivariate statistical methods and is commonly used to identify the sources of PM aerosols [29,31,32,79].

In order to identify the aerosol emission sources, the factors were extracted by using the principal component analysis method (PCA) [41] and further rotated by using the varimax criterion, which achieves a simpler structure of the orthogonal factor model and also better interpretable factors. The optimal number of factors was estimated based on the Kaiser criterion and scree plot [41]. All computations were performed by using the software R version 3.6.1.

The principal component analysis was performed on the concentrations of elements and ions in  $PM_{10}$  aerosols collected in Šlapanice and Brno sites. The six extracted factor loadings from PCA analysis in Šlapanice and Brno dataset are given in Tables 6 and 7, and Figures 6 and 7, respectively. Only factor loadings above 0.1 are shown and values greater than 0.5 are in bold. The last lines in the tables (Variance and Cumul. Var., %) show the proportions of the total data variance explained by each individual factor and total explained variance, respectively.

**Table 6.** Principal component analysis results of PM<sub>1</sub> components in Šlapanice.

|                               | F1          | F2          | F3          | F4          | F5          | F6   |
|-------------------------------|-------------|-------------|-------------|-------------|-------------|------|
| V                             | <b>0.79</b> |             |             | 0.24        |             | 0.1  |
| Cd                            | <b>0.7</b>  | 0.46        | 0.14        | 0.33        | 0.3         | 0.16 |
| As                            | 0.32        | 0.49        |             |             |             |      |
| Sb                            | 0.38        |             |             |             | <b>0.88</b> |      |
| Cu                            |             | 0.43        |             | 0.26        | <b>0.84</b> |      |
| Ni                            |             |             |             |             |             | 0.5  |
| Mn                            | 0.1         | <b>0.59</b> | 0.19        | 0.19        |             |      |
| Al                            |             | 0.3         | 0.17        |             |             |      |
| Ba                            |             |             | 0.44        |             |             | 0.42 |
| Fe                            |             | <b>0.84</b> |             | 0.28        | 0.16        |      |
| Zn                            | <b>0.6</b>  | 0.28        | 0.1         | 0.43        | 0.3         | 0.16 |
| Ca                            |             |             |             | <b>0.98</b> |             |      |
| K                             | <b>0.89</b> | 0.11        |             | 0.25        | 0.34        |      |
| Pb                            | 0.34        | 0.59        | 0.31        | 0.4         | 0.27        | 0.39 |
| NO <sub>3</sub> <sup>-</sup>  | <b>0.6</b>  | 0.35        |             | <b>0.51</b> | 0.22        | 0.38 |
| SO <sub>4</sub> <sup>2-</sup> | 0.39        | 0.48        | <b>0.51</b> |             |             | 0.44 |
| Oxalate                       | <b>0.57</b> | 0.1         | 0.45        |             |             |      |
| F <sup>-</sup>                |             | 0.44        | 0.19        |             | <b>0.77</b> |      |
| Cl <sup>-</sup>               | 0.18        | 0.45        |             | <b>0.84</b> | 0.2         | 0.12 |
| NO <sub>2</sub> <sup>-</sup>  | 0.1         |             |             | 0.27        |             |      |
| PO <sub>4</sub> <sup>3-</sup> | 0.41        | 0.25        |             | <b>0.6</b>  |             | 0.12 |
| NH <sub>4</sub> <sup>+</sup>  | <b>0.87</b> | 0.39        |             | 0.14        |             | 0.15 |
| Na <sup>+</sup>               | 0.25        | <b>0.59</b> | 0.28        | 0.41        | 0.18        |      |
| K <sup>+</sup>                | <b>0.89</b> |             |             | 0.15        | 0.31        |      |
| Ca <sup>2+</sup>              |             |             | <b>0.98</b> |             |             |      |
| Variance (%)                  | 23          | 14          | 13          | 12          | 9           | 5    |
| Cumul.Var. (%)                | 23          | 37          | 50          | 62          | 71          | 76   |

**Table 7.** Principal component analysis results of PM<sub>1</sub> components in Brno.

|                               | F1          | F2          | F3          | F4          | F5          | F6          |
|-------------------------------|-------------|-------------|-------------|-------------|-------------|-------------|
| V                             | <b>0.61</b> |             | 0.5         |             | 0.24        |             |
| Cd                            | 0.26        | <b>0.58</b> | <b>0.66</b> | 0.11        |             |             |
| As                            | 0.45        | 0.32        | 0.38        | 0.18        |             |             |
| Sb                            | 0.32        | <b>0.87</b> | 0.16        | 0.16        |             |             |
| Cu                            | 0.26        | <b>0.86</b> |             | 0.2         | 0.11        |             |
| Ni                            | <b>0.59</b> | 0.15        | <b>0.51</b> |             |             |             |
| Mn                            | <b>0.9</b>  | 0.38        |             |             |             |             |
| Al                            |             |             | 0.1         | 0.13        |             |             |
| Ba                            |             | 0.31        |             |             | <b>0.71</b> |             |
| Fe                            | <b>0.88</b> | 0.3         | 0.16        |             | 0.15        |             |
| Zn                            | <b>0.65</b> | <b>0.68</b> | 0.2         |             | 0.14        | 0.15        |
| Ca                            |             |             |             | <b>0.74</b> |             |             |
| K                             | <b>0.61</b> | <b>0.63</b> | 0.35        |             | 0.21        | 0.2         |
| Pb                            | 0.26        |             | 0.27        |             | <b>0.8</b>  |             |
| NO <sub>3</sub> <sup>-</sup>  | <b>0.73</b> | 0.11        | 0.25        |             | <b>0.57</b> | 0.18        |
| SO <sub>4</sub> <sup>2-</sup> |             |             | <b>0.84</b> | 0.28        | 0.19        |             |
| Oxalate                       |             |             | 0.27        | <b>0.52</b> |             | 0.31        |
| F <sup>-</sup>                | 0.27        | <b>0.54</b> | 0.16        |             |             | 0.29        |
| Cl <sup>-</sup>               | <b>0.79</b> | 0.4         |             |             |             | 0.32        |
| NO <sub>2</sub> <sup>-</sup>  | 0.47        | 0.37        |             |             |             | 0.38        |
| PO <sub>4</sub> <sup>3-</sup> | 0.13        | 0.27        | <b>0.6</b>  |             |             | <b>0.51</b> |
| NH <sub>4</sub> <sup>+</sup>  | <b>0.6</b>  | 0.25        | <b>0.69</b> |             | 0.13        | 0.24        |
| Na <sup>+</sup>               | 0.2         | 0.3         | 0.23        | <b>0.75</b> |             |             |
| K <sup>+</sup>                | <b>0.55</b> | <b>0.53</b> | 0.38        |             |             | 0.48        |
| Ca <sup>2+</sup>              |             | 0.1         |             | <b>0.92</b> |             |             |
| Variance (%)                  | 23          | 18          | 13          | 10          | 8           | 7           |
| Cumul.Var. (%)                | 23          | 41          | 54          | 64          | 72          | 79          |

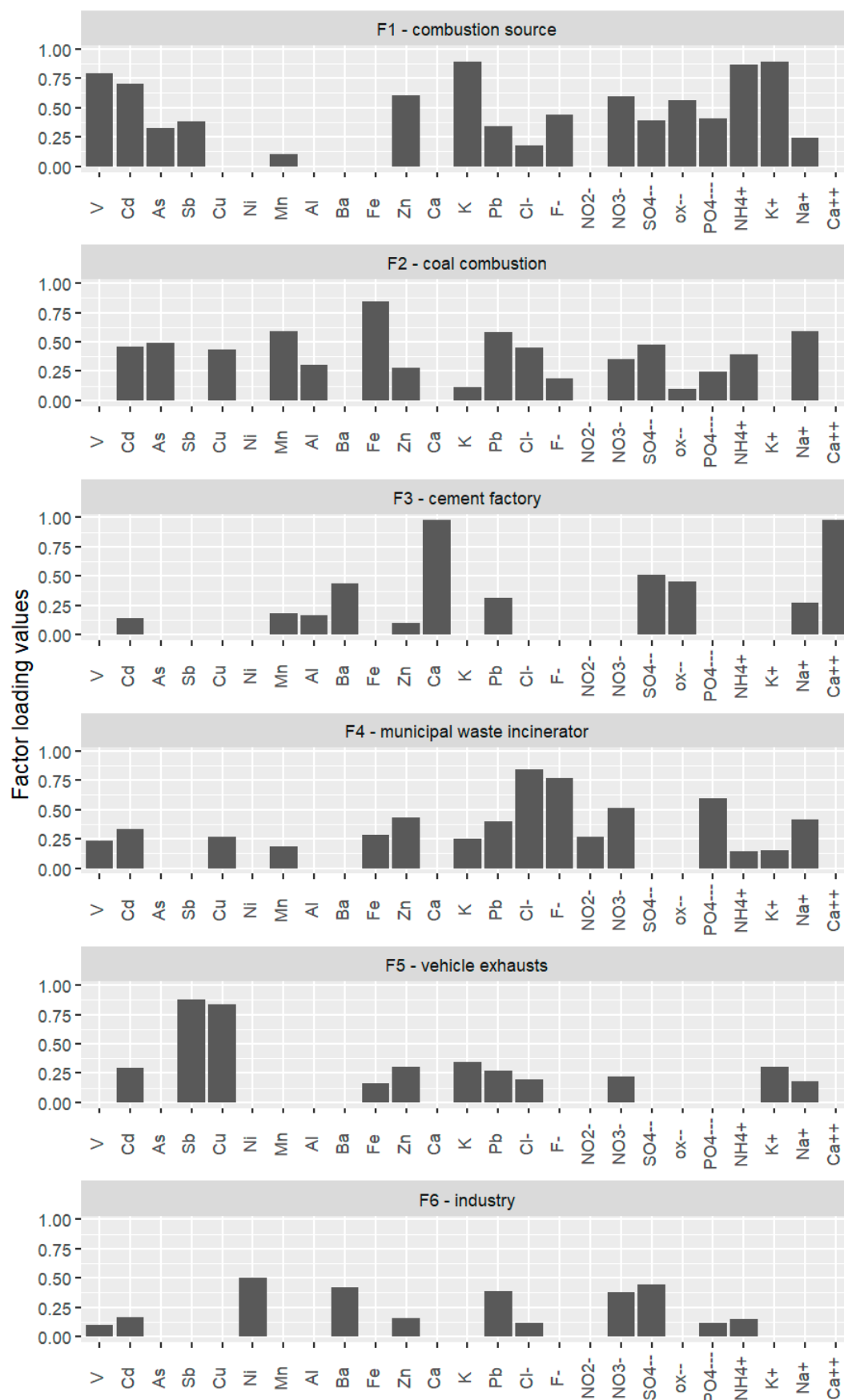


Figure 6. Source profiles for PM<sub>1</sub> in Šlapanice.

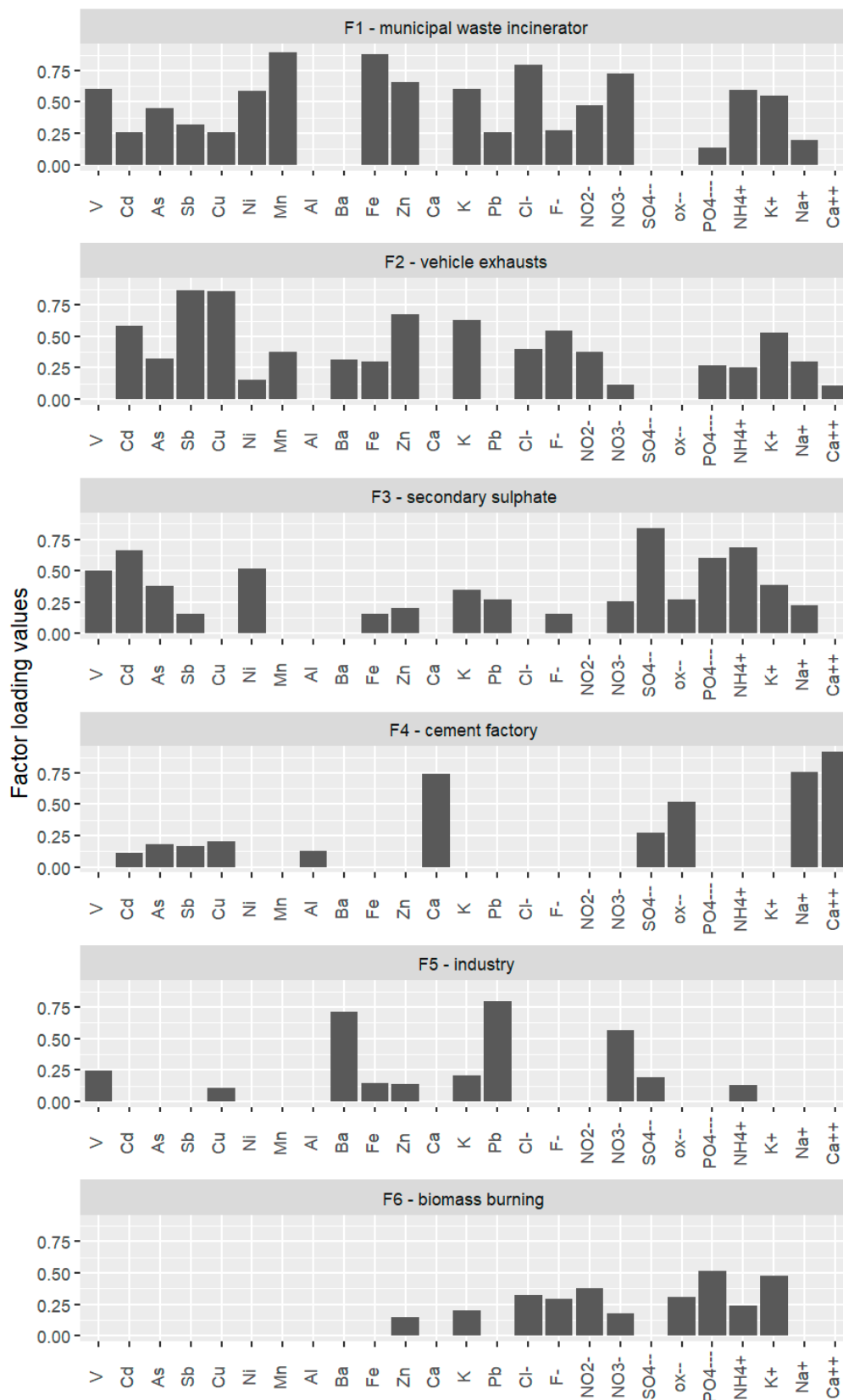


Figure 7. Source profiles for PM<sub>1</sub> in Brno.

### 3.5.1. Analysis for Šlapanice

Six independent sources identified in Šlapanice dataset (F1–F6 in Table 6 and Figure 6) include a combustion source (23%), coal combustion (14%), a cement factory (13%), a municipal waste incinerator (12%), vehicle exhausts (9%) and industry (5%). The identified factors together explained 76% of the total variance.

The first factor was identified as a combustion source. It is dominated by  $K^+$ ,  $K$ ,  $NH_4^+$ ,  $V$  and  $Cd$ , followed by  $NO_3^-$ , oxalate and  $Zn$ . Other identified tracers are  $As$ ,  $Sb$ ,  $Pb$ ,  $PO_4^{3-}$  and  $SO_4^{2-}$ . These can be related to biomass (mainly wood) burning and coal combustion in residential heating [11,18,19,35] or in a power plant burning coal and biomass located 50 km southeast of Šlapanice. The factor may also include local sources, such as engine vehicle emissions ( $Zn$ ,  $Pb$ ,  $Mn$ ) [80] or emissions from brickworks built on a small hill at the north side of Šlapanice.

The second factor was identified as coal combustion. The factor was associated with high loadings of  $Fe$ ,  $Mn$ ,  $Pb$  and  $Na^+$  and moderate loadings of  $Cd$ ,  $As$ ,  $Cu$ ,  $SO_4^{2-}$ ,  $Cl^-$ ,  $NO_3^-$  and  $NH_4^+$ . Coal is used for household heating to some degree in Šlapanice and, in particular, in villages around Šlapanice. Moreover, a coal-fired power plant is located in a distance of 50 km southeast of Šlapanice.

The third factor with high loadings of  $Ca$  and  $Ca^{2+}$  may be explained mainly by emissions from a cement factory [68–70,81]. The cement factory in Mokra is situated in a short distance, about 6.5 km northeast of Šlapanice.

The fourth factor with high loadings of  $Cl^-$ ,  $F^-$ ,  $PO_4^{3-}$  and  $NO_3^-$  and moderate loadings of  $Cd$ ,  $Cu$ ,  $Zn$ ,  $Pb$ ,  $K$  and  $Na^+$  was identified as emissions from a municipal waste incinerator [65,66]. The large municipal waste incinerator, located at the southeast side of Brno and at a distance of 5 km northwest of Šlapanice, is used for the entire agglomeration of Brno. It is also necessary to take into account a partial contribution from waste incineration in households in Šlapanice and surrounding villages [67].

The fifth factor identified as vehicle exhausts was characterized with high loadings of  $Sb$  and  $Cu$  and moderate loadings of  $Cd$ ,  $Zn$ ,  $K$ ,  $Pb$  and  $K^+$ .  $Cu$ ,  $Sb$  and  $Zn$  are used as markers of vehicle-related sources [57]. They generally originate from abrasions of tires or break wear. However,  $Cu$ ,  $Zn$  and  $Sb$  present in  $PM_1$  aerosols, originating probably from the exhaust emissions from diesel and petrol engines as  $Cu$ ,  $Zn$  and  $Sb$ , along with other elements, are present directly in the fuel or lubricating oils [36,57,80,82].

The sixth factor with moderate loadings of  $Ni$ ,  $Ba$ ,  $Pb$ ,  $SO_4^{2-}$  and  $NO_3^-$ , represented emissions from industry. Several small production workshops dealing with the processing of metals are located on the outskirts of Šlapanice or nearby.

### 3.5.2. Analysis for Brno

Six independent sources identified in the Brno dataset (F1–F6 in Table 7 and Figure 7) included a municipal waste incinerator (23%), vehicle exhausts (18%), secondary sulphate (13%), a cement factory (10%), industry (8%) and biomass burning (7%). Identified factors together explained 79% of the total variance.

The first factor was identified as the municipal waste incinerator [65,66] situated about 6 km southeast of the sampling site. The factor is associated with high loadings of  $Mn$ ,  $Fe$ ,  $Cl^-$ ,  $Ni$ ,  $Zn$ ,  $V$ ,  $K$ ,  $NO_3^-$  and  $NH_4^+$  and moderate loadings of  $K^+$ ,  $As$ ,  $Sb$ ,  $Cu$ ,  $Cd$ ,  $Pb$  and  $F^-$ .

The second factor was identified as vehicle exhausts. It is dominated by  $Sb$  and  $Cu$  and by moderate loadings of  $Zn$ ,  $K$ ,  $Cd$ ,  $F^-$ ,  $K^+$ ,  $Mn$ ,  $As$ ,  $Ba$ ,  $Cl^-$  and  $Fe$  [35,36,57]. The intensity of traffic, including cars and trams on the Veveří street, is quite high, with frequent queues of standing cars in front of the sampling site due to a nearby intersection.

The third factor representing the secondary aerosol production was identified as a secondary sulphate with  $SO_4^{2-}$  and  $NH_4^+$  as the two main markers. They derive from gas to particle conversion processes from  $SO_2$  oxidation and  $NH_3$  neutralization [30,57].  $SO_2$  originates largely from coal and

biomass combustion, while  $\text{NH}_3$  results from agricultural and traffic emissions [36,72]. This factor represents regional or long-range transport of aerosols.

The fourth factor was dominated by high loadings of  $\text{Ca}^{2+}$ , Ca and  $\text{Na}^+$ , followed by moderate loadings of oxalate and  $\text{SO}_4^{2-}$ , and represented the emissions from a cement factory [68–70] situated about 14 km east of the Brno sampling site.

The fifth factor was identified as an industry source. It was characterized with high loadings of Pb and Ba and moderate loading of  $\text{NO}_3^-$  [57]. The factor is associated with emissions from various industrial plants around Brno.

The sixth factor with  $\text{PO}_4^{3-}$ ,  $\text{K}^+$ ,  $\text{Cl}^-$ ,  $\text{F}^-$ , oxalate,  $\text{NH}_4^+$  and Zn, as the main indicators, was related to biomass burning [30,35]. The factor relates mainly to the regional transport of emissions from biomass (mainly wood) burning within residential heating in villages near Brno.

### 3.5.3. Comparison of Results for Šlapanice and Brno

The major sources of  $\text{PM}_{10}$  components identified by PCA in both localities are quite similar, but they differ with their contribution. PCA showed that local pollution from the municipal waste incinerator (accounting for 23%) and vehicle exhausts (18%) prevailed in Brno, while Šlapanice was more burdened by the transport of pollution from regional sources, such as the municipal waste incinerator in Brno (12%), the cement factory in Mokra (13%) or coal and wood combustion (14 and 23%) in the nearby villages. This hypothesis was confirmed by one-day backward trajectories (Figures S2, S4, S6 and S8) that indicate possible regional transport of air masses to Šlapanice from all directions, although the transport from east is less frequent. Villages, predominantly south or north of Šlapanice could thus be an important source of air pollution originated from biomass and coal combustion in the frame of residential heating. Moreover, there is a coal and biomass burning power plant located southeast of Šlapanice within a distance of 1 day of transport. Trajectories also confirmed the transport of air masses to Šlapanice from a northeast or northwest direction, where the cement factory and municipal incinerator are located. One-day backward trajectories calculated for Brno location (Figures S1, S3, S5 and S7) also indicated possible regional transport of air masses to Brno from all directions, which confirms findings of the factor analysis which identified the cement factory and biomass burning (i.e., within residential heating in surrounding villages or in a biomass-burning power plant located southeast of Brno) as regional sources of air pollution in Brno. Finally, we cannot neglect the contribution of long-range transport of polluted air from remote areas at distances of as far as several hundred kilometres to the pollution of both locations.

It should be borne in mind that, due to the limited sampling period at both locations, the findings concerning the source apportionment are valid only for the sampling period, while for the rest of the year, the  $\text{PM}_{10}$  sources or their contribution may vary.

## 4. Conclusions

The concentrations of elements and water-soluble ions in  $\text{PM}_{10}$  aerosols in Brno and Šlapanice, representing a large city and a small town in the Czech Republic, were compared in heating and non-heating seasons in 2009 and 2010. The average  $\text{PM}_{10}$  mass concentration was 19.1 and 9.65  $\mu\text{g m}^{-3}$  in winter and summer in Brno, respectively, and 30.8 and 10.0  $\mu\text{g m}^{-3}$  in winter and summer in Šlapanice, respectively. In the winter season, ions formed a significant part of  $\text{PM}_{10}$  mass of aerosols, accounting for 34.6% (26.8–41.6%), while in the summer season the contribution of ions to  $\text{PM}_{10}$  mass decreased to 19.7% (14.8–24.9%). Ammonium, nitrate and sulphate, the three major ion species, accounted for 91.9% of a total ion concentration and 25.1% of  $\text{PM}_{10}$  mass. The contribution of elements to  $\text{PM}_{10}$  mass was much smaller: 2.17% (1.70–2.76%) in winter and 1.37% (0.92–1.97%) in summer. A more recent seasonal studies in Brno and Šlapanice [11,18,19] ascribed the rest of  $\text{PM}_{10}$  mass to other components: organic material and elemental carbon that accounted for 38.8% and 7.00% of  $\text{PM}_{10}$  mass in winter, respectively, and for 36.5% and 8.62% of  $\text{PM}_{10}$  mass in summer, respectively.

The differences in the concentrations of PM<sub>1</sub> aerosols, elements and water-soluble ions in the corresponding seasons (especially winter) in 2009 and 2010 may have mainly been due to different meteorological and dispersal conditions in those two years. The variations in the concentrations of PM<sub>1</sub>, elements and water-soluble ions in Brno and Šlapanice during the same season result from a change in the actual emission and meteorological and dispersal situation at the relevant site.

The backward trajectory analysis confirmed that the concentrations of elements and ions in aerosols collected in Brno or Šlapanice do not depend only on local emission sources but are affected significantly also by regional transport of polluted air from various sources both nearby (e.g., surrounding villages, cement factory etc.) and by a long-range transport of polluted air from sources at larger distances from both the studied locations, such as a power plant southeast of Brno and Šlapanice, or even from more distant areas, such as a heavily polluted region in Ostrava or southern Poland situated north of Brno and Šlapanice.

The source apportionment of the PM<sub>1</sub> samples collected in Brno and Šlapanice was performed using PCA. The six major sources of PM<sub>1</sub> components identified by PCA in both localities are quite similar in composition, although differing in their fractional contribution. Coal and biomass (largely wood) combustion, a municipal waste incinerator, vehicle exhausts, a cement factory and industry were identified as major sources at both localities. Both sampling sites were burdened by both local and regional pollution. The municipal waste incinerator (23%) and vehicle exhausts (17%) identified as the two major sources of PM<sub>1</sub> in Brno indicate a predominant effect of local sources in Brno, while Šlapanice was more burdened by the transport of pollution from regional sources, such as the municipal waste incinerator in Brno (12%) or the combustion of wood and coal in the nearby villages (37%). The transport of aerosols from sources at larger distances from Šlapanice (for example a coal- and biomass-fired power plant near the border with Slovakia) or a long-range transport of PM<sub>1</sub> from neighbouring countries should also be taken into account. However, the short sampling period at both locations restricts the validity of conclusions concerning the sources of PM<sub>1</sub> aerosols at both locations only to the sampling period, while in rest of year, the PM<sub>1</sub> sources or their contribution may vary.

**Supplementary Materials:** The following are available online at <http://www.mdpi.com/2073-4433/11/7/688/s1>, Figure S1: One-day back-trajectories in winter 2009 in Brno; Figure S2: One-day back-trajectories in winter 2009 in Šlapanice; Figure S3: One-day back-trajectories in summer 2009 in Brno; Figure S4: One-day back-trajectories in summer 2009 in Šlapanice; Figure S5: One-day back-trajectories in winter 2010 in Brno; Figure S6: One-day back-trajectories in winter 2010 in Šlapanice; Figure S7: One-day back-trajectories in summer 2010 in Brno; Figure S8: One-day back-trajectories in summer 2010 in Šlapanice; Table S1: Correlation analysis between PM<sub>1</sub>, temperature, elements and ions in Šlapanice; Table S2: Correlation analysis between PM<sub>1</sub>, temperature, elements and ions in Brno.

**Author Contributions:** Conceptualization, P.M.; data curation, M.V., K.K. and Z.V.; methodology, P.M., M.V. and K.K.; project administration, M.V.; software, M.M.-Č. and J.M.; supervision, P.M.; writing—original draft, M.V. and Z.V.; writing—review and editing, P.M., K.K., M.M.-Č. and J.M. All authors have read and agreed to the published version of the manuscript.

**Funding:** This research received no external funding.

**Acknowledgments:** This work was supported by Grant Agency of the Czech Republic under grant No. P104/19/12109S and P503/20/02203S, by the Ministry of the Environment of the Czech Republic under grant No. SP/1a3/148/08, by the Ministry of Defence under project No. PSVŘ II—DZRO K-110 and by the Institute of Analytical Chemistry of CAS under an Institutional research plan No. RVO 68081715. The authors gratefully acknowledge the NOAA Air Resources Laboratory (ARL) for the provision of the HYSPLIT transport and dispersion model and/or READY website (<https://www.ready.noaa.gov/index.php>) used in this publication.

**Conflicts of Interest:** The authors declare no conflict of interest.

## References

- Seinfeld, J.H.; Pandis, S.N. *Atmospheric Chemistry and Physics. From Air Pollution to Climate Change*; Wiley & Sons: New York, NY, USA, 1998.
- Pope, C.A.; Dockery, D.W.; Schwartz, J. Review of epidemiological evidence of health-effects of particulate air-pollution. *Inhal. Toxicol.* **1995**, *7*, 1–18. [[CrossRef](#)]
- Brunekreef, B.; Holgate, S.T. Air pollution and health. *Lancet* **2002**, *360*, 1233–1242. [[CrossRef](#)]
- Kim, K.H.; Kabir, E.; Kabir, S. A review on the human health impact of airborne particulate matter. *Environ. Int.* **2015**, *74*, 136–143. [[CrossRef](#)]
- Hovorka, J.; Pokorná, P.; Hopke, P.K.; Křůmal, K.; Mikuška, P.; Pišová, M. Wood burning as a main source of winter aerosol in residential district in proximity to a large automobile factory in Central Europe. *Atmos. Environ.* **2015**, *113*, 98–107. [[CrossRef](#)]
- Kozáková, J.; Leoni, C.; Klán, M.; Hovorka, J.; Racek, M.; Koštejn, M.; Ondráček, J.; Moravec, P.; Schwarz, J. Chemical Characterization of PM<sub>1-2.5</sub> and its Associations with PM<sub>1</sub>, PM<sub>2.5-10</sub> and Meteorology in Urban and Suburban Environments. *Aerosol Air Qual. Res.* **2018**, *18*, 1684–1697. [[CrossRef](#)]
- Schwarz, J.; Pokorná, P.; Rychlík, Š.; Škáchová, H.; Vlček, O.; Smolík, J.; Ždímal, V.; Hůnová, I. Assessment of air pollution origin based on year-long parallel measurement of PM<sub>2.5</sub> and PM<sub>10</sub> at two suburban sites in Prague, Czech Republic. *Sci. Total Environ.* **2019**, *664*, 1107–1116. [[CrossRef](#)]
- Pokorná, P.; Hovorka, J.; Klán, M.; Hopke, P.K. Source apportionment of size resolved particulate matter at a European air pollution hot spot. *Sci. Total Environ.* **2015**, *502*, 172–183. [[CrossRef](#)]
- Lhotka, R.; Pokorná, P.; Zíková, N. Long-Term Trends in PAH Concentrations and Sources at Rural Background Site in Central Europe. *Atmosphere* **2019**, *10*, 687. [[CrossRef](#)]
- Kozáková, J.; Pokorná, P.; Vodička, P.; Ondráčková, L.; Ondráček, J.; Křůmal, K.; Mikuška, P.; Hovorka, J.; Moravec, P.; Schwarz, J. The influence of local emissions and regional air pollution transport on a European air pollution hot spot. *Environ. Sci. Pollut. R.* **2019**, *26*, 1675–1692. [[CrossRef](#)]
- Křůmal, K.; Mikuška, P.; Vojtěšek, M.; Večeřa, Z. Seasonal variations of monosaccharide anhydrides in PM<sub>1</sub> and PM<sub>2.5</sub> aerosol in urban areas. *Atmos. Environ.* **2010**, *44*, 5148–5155. [[CrossRef](#)]
- Mikuška, P.; Křůmal, K.; Večeřa, Z. Characterization of organic compounds in the PM<sub>2.5</sub> aerosols in winter in an industrial urban area. *Atmos. Environ.* **2015**, *105*, 97–108. [[CrossRef](#)]
- Vossler, T.; Cernikovský, L.; Novak, J.; Placha, H.; Krejci, B.; Nikolova, I.; Chalupnickova, E.; Williams, R. An investigation of local and regional sources of fine particulate matter in Ostrava, the Czech Republic. *Atmos. Pollut. Res.* **2015**, *6*, 454–463.
- Schwarz, J.; Cusack, M.; Karban, J.; Chalupníčková, E.; Havránek, V.; Smolík, J.; Ždímal, V. PM<sub>2.5</sub> chemical composition at a rural background site in Central Europe, including correlation and air mass back trajectory analysis. *Atmos. Res.* **2016**, *176–177*, 108–120. [[CrossRef](#)]
- Mikuška, P.; Kubátková, N.; Křůmal, K.; Večeřa, Z. Seasonal variability of monosaccharide anhydrides, resin acids, methoxyphenols and saccharides in PM<sub>2.5</sub> in Brno, the Czech Republic. *Atmos. Pollut. Res.* **2017**, *8*, 576–586. [[CrossRef](#)]
- Mikuška, P.; Čapka, L.; Večeřa, Z. Aerosol sampler for analysis of fine and ultrafine aerosols. *Anal. Chim. Acta* **2018**, *1020*, 123–133. [[CrossRef](#)] [[PubMed](#)]
- Coufalík, P.; Čmelík, R.; Křůmal, K.; Čapka, L.; Mikuška, P. Determination of short-term changes in levoglucosan and dehydroabietic acid in aerosols with Condensation Growth Unit-Aerosol Counterflow Two-Jets Unit-LC-MS. *Chemosphere* **2018**, *210*, 279–286. [[CrossRef](#)]
- Křůmal, K.; Mikuška, P.; Večeřa, Z. Polycyclic aromatic hydrocarbons and hopanes in PM<sub>1</sub> aerosols in urban areas. *Atmos. Environ.* **2013**, *67*, 27–37. [[CrossRef](#)]
- Křůmal, K.; Mikuška, P.; Večeřa, Z. Monosaccharide anhydrides, monocarboxylic acids and OC/EC in PM<sub>1</sub> aerosols in urban areas in the Czech Republic. *Atmos. Pollut. Res.* **2015**, *6*, 917–927. [[CrossRef](#)]
- Kubelová, L.; Vodička, P.; Schwarz, J.; Cusack, M.; Makeš, O.; Ondráček, J.; Ždímal, V. A study of summer and winter highly time-resolved submicron aerosol composition measured at a suburban site in Prague. *Atmos. Environ.* **2015**, *118*, 45–57. [[CrossRef](#)]
- Coufalík, P.; Mikuška, P.; Matoušek, T.; Večeřa, Z. Determination of bioaccessible fraction of elements in urban aerosol using simulated lung fluids. *Atmos. Environ.* **2016**, *140*, 469–475. [[CrossRef](#)]

22. Pokorná, P.; Hovorka, J.; Hopke, P.K. Elemental composition and source identification of very fine aerosol particles in a European air pollution hot-spot. *Atmos. Pollut. Res.* **2016**, *7*, 671–679. [CrossRef]
23. Křůmal, K.; Mikuška, P.; Večeřa, Z. Characterization of organic compounds in winter PM<sub>1</sub> aerosols in a small industrial town. *Atmos. Pollut. Res.* **2017**, *8*, 930–939. [CrossRef]
24. Leoni, C.; Pokorná, P.; Hovorka, J.; Masiol, M.; Topinka, J.; Zhao, Y.; Křůmal, K.; Cliff, S.; Mikuška, P.; Hopke, P.K. Source apportionment of aerosol particles at a European air pollution hot spot using particle number size distributions and chemical composition. *Environ. Pollut.* **2018**, *234*, 145–154. [CrossRef]
25. Dumková, J.; Vrlíková, L.; Večeřa, Z.; Putnová, B.; Dočekal, B.; Mikuška, P.; Fictum, P.; Hampl, A.; Buchtová, M. Inhaled Cadmium Oxide Nanoparticles: Their in Vivo Fate and Effect on Target Organs. *Int. J. Mol. Sci.* **2016**, *17*, 874. [CrossRef]
26. Dumková, J.; Smutná, T.; Vrlíková, L.; Le Coustumer, P.; Večeřa, Z.; Dočekal, B.; Mikuška, P.; Čapka, L.; Fictum, P.; Hampl, A.; et al. Sub-chronic inhalation of lead oxide nanoparticles revealed their broad distribution and tissue-specific subcellular localization in target organs. *Part. Fibre Toxicol.* **2017**, *14*, 55. [CrossRef]
27. Dvorská, A.; Komprdová, K.; Lammel, G.; Klánová, J.; Plachá, H. Polycyclic aromatic hydrocarbons in background air in central Europe—Seasonal levels and limitations for source apportionment. *Atmos. Environ.* **2012**, *46*, 147–154. [CrossRef]
28. Vojtěšek, M.; Mikuška, P.; Křůmal, K.; Večeřa, Z. Analysis of water-soluble fraction of metals in atmospheric aerosols using Aerosol Counterflow Two-Jets Unit and chemiluminescent detection. *Intern. J. Environ. Anal. Chem.* **2012**, *92*, 432–449. [CrossRef]
29. Viana, M.; Kuhlbusch, T.A.J.; Querol, X.; Alastuey, A.; Harrison, R.M.; Hopke, P.K.; Winiwarter, W.; Vallius, M.; Szidat, S.; Prévôt, A.S.H.; et al. Source apportionment of particulate matter in Europe: A review of methods and results. *J. Aerosol. Sci.* **2008**, *39*, 827–849. [CrossRef]
30. Almeida, S.M.; Pio, C.A.; Freitas, M.C.; Reis, M.A.; Trancoso, M.A. Source apportionment of fine and coarse particulate matter in a sub-urban area at the Western European Coast. *Atmos. Environ.* **2005**, *39*, 3127–3138. [CrossRef]
31. Vallius, M.; Janssen, N.A.H.; Heinrich, J.; Hoek, G.; Ruuskanen, J.; Cyrys, J.; Van Grieken, R.; de Hartog, J.J.; Kreyling, W.G.; Pekkanen, J. Sources and elemental composition of ambient PM<sub>2.5</sub> in three European cities. *Sci. Total Environ.* **2005**, *337*, 147–162. [CrossRef]
32. Viana, M.; Querol, X.; Alastuey, A.; Gil, J.I.; Menéndez, M. Identification of PM sources by principal component analysis (PCA) coupled with wind direction data. *Chemosphere* **2006**, *65*, 2411–2418. [CrossRef]
33. Dai, Q.L.; Bi, X.H.; Wu, J.H.; Zhang, Y.F.; Wang, J.; Xu, H.; Yao, L.; Jiao, L.; Feng, Y.C. Characterization and source identification of heavy metals in ambient PM<sub>10</sub> and PM<sub>2.5</sub> in an integrated iron and steel industry zone compared with a background site. *Aerosol Air Qual. Res.* **2015**, *15*, 875–887. [CrossRef]
34. Titos, G.; Lyamani, H.; Pandolfi, M.; Alastuey, A.; Alados-Arboledas, L. Identification of fine (PM<sub>1</sub>) and coarse (PM<sub>10-1</sub>) sources of particulate matter in an urban environment. *Atmos. Environ.* **2014**, *89*, 593–602. [CrossRef]
35. Samek, L.; Stegowski, Z.; Furman, L.; Styszko, K.; Szramowiat, K.; Fiedor, J. Quantitative Assessment of PM<sub>2.5</sub> Sources and Their Seasonal Variation in Krakow. *Water Air Soil Pollut.* **2017**, *228*, 290. [CrossRef] [PubMed]
36. Juda-Rezler, K.; Reizer, M.; Maciejewska, K.; Blaszczyk, B.; Klejnowski, K. Characterization of atmospheric PM<sub>2.5</sub> sources at a Central European urban background site. *Sci. Total Environ.* **2020**, *713*, 136729. [CrossRef] [PubMed]
37. Mikuška, P.; Večeřa, Z.; Bartošíková, A.; Maenhaut, W. Annular diffusion denuder for simultaneous removal of gaseous organic compounds and air oxidants during sampling of carbonaceous aerosols. *Anal. Chim. Acta* **2012**, *714*, 68–75. [CrossRef]
38. Stein, A.F.; Draxler, R.R.; Rolph, G.D.; Stunder, B.J.B.; Cohen, M.D.; Ngan, F. NOAA's HYSPLIT atmospheric transport and dispersion modeling system. *Bull. Am. Meteorol. Soc.* **2015**, *96*, 2059–2077. [CrossRef]
39. Rolph, G.D. *Real-time Environmental Applications and Display System (READY)*; NOAA Air Resources Laboratory: College Park, MD, USA, 2017. Available online: <http://www.ready.noaa.gov> (accessed on 15 June 2020).
40. Überla, K. *Faktorová Analýza*; Alfa Bratislava: Bratislava, Slovak Republic, 1976.
41. Johnson, R.A.; Wichern, D.W. *Applied Multivariate Statistical Analysis*; Prentice-Hall: New Jersey, NJ, USA, 1992.
42. Miao, Y.; Li, J.; Miao, S.; Che, H.; Wang, Y.; Zhang, X.; Zhu, R.; Liu, S. Interaction between planetary boundary layer and PM<sub>2.5</sub> pollution in megacities in China: A Review. *Curr. Pollut. Rep.* **2019**, *5*, 261–271. [CrossRef]
43. Xiang, Y.; Tianshu Zhang, T.; Liu, J.; Lv, L.; Dong, Y.; Chen, Z. Atmosphere boundary layer height and its effect on air pollutants in Beijing during winter heavy pollution. *Atmos. Res.* **2019**, *215*, 305–316. [CrossRef]

44. Yin, J.; Harrison, R.M. Pragmatic mass closure study for PM<sub>1.0</sub>, PM<sub>2.5</sub> and PM<sub>10</sub> at roadside, urban background and rural sites. *Atmos. Environ.* **2008**, *42*, 980–988. [[CrossRef](#)]
45. Spindler, G.; Brüggemann, E.; Gnauk, T.; Grüner, A.; Müller, K.; Herrmann, H. A four-year size-segregated characterization study of particles PM<sub>10</sub>, PM<sub>2.5</sub> and PM<sub>1</sub> depending on air mass origin at Melpitz. *Atmos. Environ.* **2010**, *44*, 164–173. [[CrossRef](#)]
46. Sarti, E.; Pasti, L.; Rossi, M.; Ascaneli, M.; Pagnoni, A.; Trombini, M.; Remelli, M. The composition of PM<sub>1</sub> and PM<sub>2.5</sub> samples, metals and their water soluble fractions in the Bologna area (Italy). *Atmos. Pollut. Res.* **2015**, *6*, 708–718. [[CrossRef](#)]
47. Rogula-Kozłowska, W. Chemical composition and mass closure of ambient particulate matter at a crossroads and a highway in Katowice, Poland. *Environ. Prot. Eng.* **2015**, *41*, 15–29. [[CrossRef](#)]
48. Rogula-Kozłowska, W.; Klejnowski, K. Submicrometer Aerosol in Rural and Urban Backgrounds in Southern Poland: Primary and Secondary Components of PM<sub>1</sub>. *Bull. Environ. Contam. Toxicol.* **2013**, *90*, 103–109. [[CrossRef](#)] [[PubMed](#)]
49. Křůmal, K.; Mikuška, P. Mass concentrations and lung cancer risk assessment of PAHs bound to PM<sub>1</sub> aerosol in six industrial, urban and rural areas in the Czech Republic, Central Europe. *Atmos. Pollut. Res.* **2020**, *11*, 401–408. [[CrossRef](#)]
50. Tchounwou, P.B.; Yedjou, C.G.; Patlolla, A.K.; Sutton, D.J. Heavy Metal Toxicity and the Environment. In *Molecular, Clinical and Environmental Toxicology. Experientia Supplementum*; Luch, A., Ed.; Springer: Basel, Switzerland, 2012; Volume 101, pp. 133–164.
51. Genchi, G.; Carocci, A.; Lauria, G.; Sinicropi, M.S.; Catalano, A. Nickel: Human Health and Environmental Toxicology. *Int. J. Environ. Res. Public Health* **2020**, *17*, 679. [[CrossRef](#)] [[PubMed](#)]
52. The Czech Republic Act No. 201/2012 Coll., On Air Protection. Available online: [https://www.mzp.cz/www/platnalegislativa.nsf/9F4906381B38F7F6C1257A94002EC4A0/%24file/201\\_2012.pdf](https://www.mzp.cz/www/platnalegislativa.nsf/9F4906381B38F7F6C1257A94002EC4A0/%24file/201_2012.pdf) (accessed on 26 June 2020).
53. Wiseman, C.L.S.; Zereini, F. Characterizing metal(loid) solubility in airborne PM<sub>10</sub>, PM<sub>2.5</sub> and PM<sub>1</sub> in Frankfurt, Germany using simulated lung fluids. *Atmos. Environ.* **2014**, *89*, 282–289. [[CrossRef](#)]
54. Caggiano, R.; Macchiato, M.; Trippetta, S. Levels, chemical composition and sources of fine aerosol particles (PM<sub>1</sub>) in an area of the Mediterranean basin. *Sci. Total Environ.* **2010**, *408*, 884–895. [[CrossRef](#)]
55. Rudnick, R.L.; Gao, S. Composition of the continental crust. In *Treatise on Geochemistry*; Holland, H.D., Turekian, K.K., Eds.; Elsevier: New York, NY, USA, 2003; pp. 1–64.
56. Harrison, R.M.; Tilling, R.; Romero, M.S.C.; Harrad, S.; Jarvis, K. A study of trace metals and polycyclic aromatic hydrocarbons in the roadside environment. *Atmos. Environ.* **2003**, *37*, 2391–2402. [[CrossRef](#)]
57. Gugamsetty, B.; Wei, H.; Liu, C.N.; Awasthi, A.; Hsu, S.C.; Tsai, C.J.; Roam, G.D.; Wu, Y.C.; Chen, C.F. Source characterization and apportionment of PM<sub>10</sub>, PM<sub>2.5</sub> and PM<sub>0.1</sub> by using positive matrix factorization. *Aerosol Air Qual. Res.* **2012**, *12*, 476–491. [[CrossRef](#)]
58. Fine, P.M.; Cass, G.R.; Simoneit, B.R. Chemical characterization of fine particle emissions from fireplace combustion of woods grown in the northeastern United States. *Environ. Sci. Technol.* **2001**, *35*, 2665–2675. [[CrossRef](#)] [[PubMed](#)]
59. Pacyna, J.M.; Pacyna, E.G. An assessment of global and regional emissions of trace metals to the atmosphere from anthropogenic sources worldwide. *Environ. Rev.* **2001**, *9*, 269–298. [[CrossRef](#)]
60. Xu, M.; Yan, R.; Zheng, C.; Qiao, Y.; Han, J.; Sheng, C. Status of trace element emission in a coal combustion process: A review. *Fuel Process. Technol.* **2003**, *85*, 215–237. [[CrossRef](#)]
61. Wiinikka, H.; Grönberg, C.; Boman, C. Emissions of heavy metals during fixed-bed combustion of six biomass fuels. *Energy Fuels* **2013**, *27*, 1073–1080. [[CrossRef](#)]
62. Chen, J.; Li, C.; Ristovski, Z.; Milic, A.; Gu, Y.; Islam, M.S.; Wang, S.; Hao, J.; Zhang, H.; He, C.; et al. A review of biomass burning: Emissions and impacts on air quality, health and climate in China. *Sci. Total Environ.* **2017**, *579*, 1000–1034. [[CrossRef](#)]
63. Křůmal, K.; Mikuška, P.; Horák, J.; Hopan, F.; Krpec, K. Characterization of gaseous and particulate pollutants in emissions from combustion of biomass and coal in modern and old-type boilers during reduced output used for residential heating. *Chemosphere* **2019**, *229*, 51–59. [[CrossRef](#)] [[PubMed](#)]
64. Czech Statistical Office. *Population and Housing Census*; Prague, Czech Republic, 2011; Available online: <https://vdb.czso.cz/vdbvo2/faces/cs/index.jsf?page=vystup-objekt-parametry&pvo=OTOR119&sp=A&z=T&f=TABULKA&katalog=30812&pvokc=65&pvoch=6203> (accessed on 11 October 2017).

65. Hu, C.W.; Chao, M.R.; Wu, K.Y.; Chang-Chien, G.P.; Lee, W.J.; Chang, L.W.; Lee, W.S. Characterization of multiple airborne particulate metals in the surroundings of a municipal waste incinerator in Taiwan. *Atmos. Environ.* **2003**, *37*, 2845–2852. [[CrossRef](#)]
66. Rovira, J.; Nadal, M.; Schuhmacher, M.; Domingo, J.L. Concentrations of trace elements and PCDD/Fs around a municipal solid waste incinerator in Girona (Catalonia, Spain). Human health risks for the population living in the neighborhood. *Sci. Total Environ.* **2018**, *630*, 34–45. [[CrossRef](#)] [[PubMed](#)]
67. Horák, J.; Kuboňová, L.; Bajer, S.; Dej, M.; Hopan, F.; Krpec, K.; Ochodek, T. Composition of ashes from the combustion of solid fuels and municipal waste in households. *J. Environ. Manag.* **2019**, *248*, 109269. [[CrossRef](#)]
68. Conesa, J.A.; Rey, L.; Egea, S.; Rey, M.D. Pollutant formation and emissions from cement kiln stack using a solid recovered fuel from municipal solid waste. *Environ. Sci. Technol.* **2011**, *45*, 5878–5884. [[CrossRef](#)]
69. Gupta, R.K.; Majumdar, D.; Trivedi, J.V.; Bhanarkar, A.D. Particulate matter and elemental emissions from a cement kiln. *Fuel Process. Technol.* **2012**, *104*, 343–351. [[CrossRef](#)]
70. Arfala, Y.; Douch, J.; Assabbane, A.; Kaaouachi, K.; Tian, H.; Hamdani, M. Assessment of heavy metals released into the air from the cement kilns co-burning waste: Case of Oujda cement manufacturing (Northeast Morocco). *Sustain. Environ. Res.* **2018**, *28*, 363–373. [[CrossRef](#)]
71. Zhou, J.; Zhang, R.; Cao, J.; Chow, J.C.; Watson, J.G. Carbonaceous and ionic components of atmospheric fine particles in Beijing and their impact on atmospheric visibility. *Aerosol Air Qual. Res.* **2012**, *12*, 492–502. [[CrossRef](#)]
72. Aneja, V.P.; Roelle, P.A.; Murray, G.C.; Southerland, J.; Erisman, J.W.; Fowler, D.; Asman, W.A.H.; Patni, N. Atmospheric nitrogen compounds II: Emissions, transport, transformation, deposition and assessment. *Atmos. Environ.* **2001**, *35*, 1903–1911. [[CrossRef](#)]
73. Russell, A.G.; McRae, G.J.; Cass, G.R. Mathematical modeling of the formation and transport of ammonium nitrate aerosol. *Atmos. Environ.* **1983**, *17*, 949–964. [[CrossRef](#)]
74. Zhang, F.; Cheng, H.; Wang, Z.; Lv, X.; Zhu, Z.; Zhang, G.; Wang, X. Fine particles (PM<sub>2.5</sub>) at a CAWNET background site in Central China: Chemical compositions, seasonal variations and regional pollution events. *Atmos. Environ.* **2014**, *86*, 193–202. [[CrossRef](#)]
75. Weinstein, L.H.; Davison, A. *Fluorides in the Environment: Effects on Plants and Animals*; CABI Publishing: Wallingford, Oxfordshire, England, 2004.
76. Zavala, M.; Molina, L.T.; Maiz, P.; Monsivais, I.; Chow, J.C.; Watson, J.G.; Munguia, J.L.; Cardenas, B.; Fortner, E.C.; Herndon, S.C.; et al. Black carbon, organic carbon, and co-pollutant emissions and energy efficiency from artisanal brick production in Mexico. *Atmos. Chem. Phys.* **2018**, *18*, 6023–6037. [[CrossRef](#)]
77. Jiang, Y.; Zhuang, G.; Wang, Q.; Liu, T.; Huang, K.; Fu, J.S.; Li, J.; Lin, Y.; Zhang, R.; Deng, C. Characteristics, sources and formation of aerosol oxalate in an Eastern Asia megacity and its implication to haze pollution. *Atmos. Chem. Phys.* **2011**, *11*, 22075–22112. [[CrossRef](#)]
78. Laongsri, B.; Harrison, R.M. Atmospheric behaviour of particulate oxalate at UK urban background and rural sites. *Atmos. Environ.* **2013**, *71*, 319–326. [[CrossRef](#)]
79. Wang, Y.; Zhuang, G.; Tang, A.; Yuan, H.; Sun, Y.; Chen, S.; Zheng, A. The ion chemistry and the source of PM<sub>2.5</sub> aerosol in Beijing. *Atmos. Environ.* **2005**, *39*, 3771–3784. [[CrossRef](#)]
80. Coufalík, P.; Matoušek, T.; Křůmal, K.; Vojtíšek-Lom, M.; Beránek, V.; Mikuška, P. Content of metals in emissions from gasoline, diesel, and alternative biofuels. *Environ. Sci. Pollut. Res.* **2019**, *26*, 29012–29019. [[CrossRef](#)] [[PubMed](#)]
81. Xue, Y.; Wu, J.; Feng, Y.; Dai, L.; Bi, X.; Li, X.; Zhu, T.; Tang, S.; Chen, M. Source characterization and apportionment of PM<sub>10</sub> in Panzhihua, China. *Aerosol Air Qual. Res.* **2010**, *10*, 367–377. [[CrossRef](#)]
82. Huang, X.; Olmez, I.; Aras, N.K.; Gordon, G.E. Emissions of trace elements from motor vehicles: Potential marker elements and source composition profile. *Atmos. Environ.* **1994**, *28*, 1385–1391. [[CrossRef](#)]



© 2020 by the authors. Licensee MDPI, Basel, Switzerland. This article is an open access article distributed under the terms and conditions of the Creative Commons Attribution (CC BY) license (<http://creativecommons.org/licenses/by/4.0/>).

Article

# Nanoparticle Number Concentration in the Air in Relation to the Time of the Year and Time of the Day

Jáchym Brzezina <sup>1,\*</sup>, Klaudia Köbölová <sup>2</sup> and Vladimír Adamec <sup>2</sup>

<sup>1</sup> Air Quality Department, Czech Hydrometeorological Institute, 616 67 Brno, Czech Republic

<sup>2</sup> Institute of Forensic Engineering, Brno University of Technology, 612 00 Brno, Czech Republic; xckobolova@usi.vutbr.cz (K.K.); vladimir.adamec@usi.vutbr.cz (V.A.)

\* Correspondence: jachym.brzezina@chmi.cz; Tel.: +420-541421046

Received: 6 May 2020; Accepted: 15 May 2020; Published: 19 May 2020



**Abstract:** The paper analyzes suspended particles number concentrations of 61 size fractions (184 nm to 17,165 nm) in the air at a traffic location. The average course of the individual fractions was analyzed at various intervals – daily, weekly, monthly and annually, in the period between 2017 and 2019. The data was then used to calculate the arithmetic mean for all the fractions (MS Excel, R) and then using a proprietary web application, heatmaps were constructed. The obtained results showed significant differences in both the annual and daily variation of number concentrations between the individual fractions differing in particle size. In the case of the annual variation, one can see a greater variability of smaller particles, which is most likely due to the source of the actual suspended particles. Meteorological and dispersion conditions are found as important factors for suspended particle concentrations. These can lead to significant differences from year to year. However, a comparison between 2018 and 2019 showed that even though the average absolute number concentrations can differ between years, the actual relative number concentrations, i.e., the ratios between the individual fractions remain very similar. In conclusion it can be said that the difference between the number concentration variation of the size fractions depends on both the actual pollution sources (especially in the long-term, i.e., the annual variation) and the actual size of the particles, which plays a role especially in the short-term (daily, weekly variation).

**Keywords:** PM pollution; seasonality; air quality; meteorological conditions

## 1. Introduction

Air pollution has recently been identified as a major issue in the field of the environment and public health [1]. Suspended particles (PM) can potentially have very undesirable effects on human health [2]. These particles are suspended in the atmosphere and can have a very complex chemical composition and have variable sizes. Sources of fine particles (aerodynamic diameter of  $<2.5 \mu\text{m}$ ) and ultrafine particles (aerodynamic diameter of  $<0.1 \mu\text{m}$ ) include both natural and anthropogenic sources [3]. The increase in concentrations of  $\text{PM}_{2.5}$  and  $\text{PM}_{0.1}$  has recently become a global issue due to their impact on human health, air pollution and the atmospheric and climate system [4–6]. In general, the smaller the particle, the potentially more dangerous it is for human health as it penetrates deeper into the respiratory system or even directly to the bloodstream in the case of the smallest nanoparticles.

The current legislation in the Czech Republic and European Union as a whole specifies only mass concentrations of particles  $\text{PM}_{2.5}$  and  $\text{PM}_{10}$  (aerodynamic diameter  $<10 \mu\text{m}$ ). However, in an urban environment, the ultrafine particles represent more than 90% of particles in terms of their overall count (number concentration), but their mass concentration is negligible in comparison to large particles. There is no exact regulation for air pollution in terms of the  $\text{PM}_1$  fraction [7,8]. This gap in legislation is due to insufficient data available for the  $\text{PM}_1$  effects on the environment and human

health, because measuring smaller particles is demanding financially and technically. Nanotoxicological studies, however, show that particles in the nano range have completely different physio-chemical properties such as lower weight, ultrahigh reactivity, a high ratio between surface area and mass etc. These unique properties can pose more serious consequences for human health compared to particles of a larger size. It is therefore very important to study the PM<sub>1</sub> and PM<sub>0.1</sub> particles and measure and characterize their concentration and distribution [9,10].

Lots of information and studies are available for the PM<sub>10</sub> and partially also the PM<sub>2.5</sub> particles in Europe [11–13], however, data for the PM<sub>1</sub> particles, especially regarding their chemical composition and concentrations [14–16], short-term measurements [17–19] or long term measurements [20–22] are still insufficient.

Significant changes in seasonal variability have been observed for the concentration and size distribution of ultrafine particles. Samek et al. analyzed the seasonality effect on fine and ultrafine particles from various sources. These included combustion processes (fossil fuels, biomass), secondary aerosols, and the category “other”, which included traffic, industry and soil. In winter, the major sources were combustion and secondary aerosols. In the case of combustion, fine particles dominated (53% by mass for PM<sub>2.5</sub>), while ultrafine particles represented 27%. Secondary aerosols in winter were composed of especially PM<sub>1</sub> (approximately 63%). In summer, the contribution from combustion was much smaller, from 3% to 6%. The contribution of secondary aerosols in the summer was approximately 50% for both fractions. The average particle concentration in summer months for PM<sub>1</sub> was  $16.4 \pm 8.3 \mu\text{g}\cdot\text{m}^{-3}$  and for PM<sub>2.5</sub> it was  $27.2 \pm 14.1 \mu\text{g}\cdot\text{m}^{-3}$ . In winter months the concentrations increased to  $58.0 \pm 18.4 \mu\text{g}\cdot\text{m}^{-3}$  for PM<sub>1</sub> and  $58.6 \pm 29.5 \mu\text{g}\cdot\text{m}^{-3}$  for PM<sub>2.5</sub> [17]. Similar correlations between seasons and PM concentrations has also been proved by other studies [23–25].

Some studies studied the effect of traffic on particle number concentration in different seasons of the year. Meteorology and traffic emissions play a significant role in urban air quality, but relationships among them are very complicated [26,27]. Dédelé et al. [28] tried to estimate the inter-seasonal differences in concentration of PM<sub>10</sub> at different site types. The highest mean concentration of PM<sub>10</sub> was determined at sites classified as urban background in the winter season ( $34.8 \mu\text{g}/\text{m}^3$ ), while in spring and summer, the highest concentrations of PM<sub>10</sub> were determined at traffic sites, which were characterized by high traffic intensity (>10,000 vehicles per day). This is a result of the low level of emissions from domestic heating during the warm period of the year, which means that vehicle emissions contribute more to the overall concentrations. The mean PM<sub>10</sub> concentrations measured at traffic sites ranged from  $20.4 \mu\text{g}/\text{m}^3$  in summer to  $41.8 \mu\text{g}/\text{m}^3$  in the winter season. Kamińska [29] analyzed the relationship between pollution, traffic, and meteorological parameters. As for the PM<sub>2.5</sub> concentrations, the meteorological conditions had the largest effect. Only in the summer, the significance of traffic intensity was comparable to that of the meteorological conditions. This can again be explained by the low level of emissions from domestic heating in that part of the year. This finding is in accordance with the analyses performed in other cities [30,31].

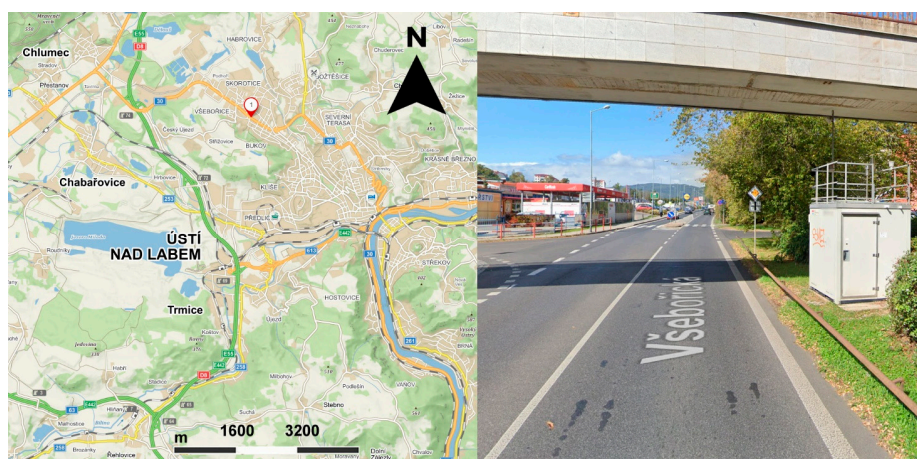
Results presented in this study are based on pilot measurement at the ambient air quality at a monitoring station in Ústí nad Labem, where number concentrations have been measured since mid-2017. The main goal of this analysis was to compare the variation of various size fractions in daily, weekly and annual intervals. The monitored size fractions ranged from approximately 200 nm to particles larger than 15  $\mu\text{m}$  in aerodynamic diameter.

## 2. Experiments

The study used data from continuously measuring automated ambient air quality monitoring station in Ústí nad Labem. The city lies in the northwest of the Czech Republic and is the center of the Ústecký region. The location is in an urban, residential and commercial area. The station is classified as a traffic station as it is located 2 m from a busy road in the direction of Teplice, Prague and Dresden (D8) on the city outskirts. Local domestic heating is an important source of pollution in this location as well. A more detailed characterization of the location is provided in Table 1 and in Figure 1.

**Table 1.** Characterization of ambient air quality monitoring station Ústí nad Labem-Všebořická.

| Basic Characterization        |  |
|-------------------------------|--|
| Station ID                    | UULD                                   |
| Name                          | Ústí nad Labem – Všebořická (hot spot) |
| Country                       | Czech Republic                         |
| Region                        | Ústecký                                |
| District                      | Ústí nad Labem                         |
| Classification                |  |
| Abbreviation                  | T/U/RC                                 |
| EOI – station type            | traffic (T)                            |
| EOI – zone type               | urban (U)                              |
| EOI B/R – zone characteristic | Residential, commercial (RC)           |
| Location                      |  |
| Geographic co-ordinates       | 50°40′59.248″ N 13°59′52.344″ E        |
| Elevation                     | 230 m                                  |
| Further Details               |  |
| Terrain                       | Flat                                   |
| Landscape                     | Multistory housing development         |
| Representativeness            | 100–500 m                              |

**Figure 1.** Photograph of the ambient air quality monitoring station Ústí nad Labem-Všebořická [32,33].

The station is located in the city of Ústí nad Labem near the Všebořická street. It is labeled as a “hot spot” station meaning it is primarily focused on air pollution from traffic. The station is equipped with the Pallas Fidas 200 analyzer (see Table 2), which works in an automated measuring mode including measurements of particle count distribution. The analyzed particles range from 180 nm to 100  $\mu\text{m}$  in aerodynamic diameter and the measuring range is 0–20,000/cm<sup>3</sup>. Volume flow is 4.8 L/min (0.3 m<sup>3</sup>/h). The measurement is based on optical light-scattering. Measurement includes monitoring of PM<sub>1</sub>, PM<sub>2.5</sub>, PM<sub>10</sub> and TSP concentrations, and particle size distribution. This measurement is set to monitor over 60 different particle-size fractions. Data used in this study included the period from 15 June 2017 to 31 December 2019 with an interval of measurement of 10 min. The station is also equipped with a traffic counter. In the period of analysis, the average daily car count was 16,751. The majority of the traffic represented passenger cars (79.99%), then vans (12.15%). Large goods vehicles represented 3.87% and large trucks 3.99%.

**Table 2.** Specification of the Pallas Fidas 200 analyzer.

| Measurement Range (Size)      | 0.18–100 µm (3 Measuring Ranges)  |
|-------------------------------|---|
| Size channels                 | 64 (32/decade)  |
| Measuring principle           | Optical light-scattering  |
| Measurement range (number CN) | 0–20,000 particles/cm <sup>3</sup>  |
| Time resolution               | 1 s - 24 h, 15 min in type approved operation   |
| Volume flow                   | 4.8 L/min ± 0.3 m <sup>3</sup> /h   |
| Data acquisition              | Digital, 20 MHz processor, 256 raw data channels  |
| Power consumption             | Approx. 200 W   |
| User interface                | Touchscreen, 800 × 480 Pixel, 7"  |
| Power supply                  | 115–230 V, 50–60 Hz   |
| Housing                       | Table housing, optionally with mounting brackets for rack-mounting  |
| Dimensions                    | 450 × 320 × 180.5 mm (H × W × D), 19"   |
| Software                      | PDAnalyze Fidas®  |
| Aerosol conditioning          | Thermal with IADS   |
| Measurement range (mass)      | 0–10,000 µg/m <sup>3</sup>  |
| Reported data                 | PM <sub>1</sub> , PM <sub>2.5</sub> , PM <sub>4</sub> , PM <sub>10</sub> , TSP, CN, particle size distribution, pressure, temperature, humidity |
| Sampling head                 | Sigma-2   |

### 3. Results

The period of analysis represented the period from 15 June 2017 to 31 December 2019. Particle number concentrations per cm<sup>3</sup> were monitored in 61 fractions (from 184 nm up to larger than 17,165 µm, see Table 3) in 10-min intervals. The analysis was focused on the average course of the individual fractions for various time intervals – daily, weekly, and annual variations.

**Table 3.** Monitored size fractions.

| Fraction (nm) | Fraction (nm) | Fraction (nm) | Fraction (nm) |
|---------------|---------------|---------------|---------------|
| 184–198       | 583–627       | 2130–2289     | 7239–7779     |
| 198–213       | 627–674       | 2289–2460     | 7779–8359     |
| 213–229       | 674–724       | 2460–2643     | 8359–8983     |
| 229–246       | 724–778       | 2643–2841     | 8983–9653     |
| 246–264       | 778–836       | 2841–3053     | 9653–10,373   |
| 164–284       | 836–898       | 3053–3280     | 10,373–11,147 |
| 284–305       | 898–965       | 3280–3525     | 11,147–11,979 |
| 305–328       | 965–1037      | 3525–3788     | 11,979–12,872 |
| 328–352       | 1037–1198     | 3788–4071     | 12,872–13,833 |
| 352–379       | 1198–1383     | 4071–4374     | 13,833–14,865 |
| 379–407       | 1383–1486     | 4374–4701     | 14,865–15,974 |
| 407–437       | 1486–1597     | 4701–5051     | 15,974–17,165 |
| 437–470       | 1597–1717     | 5051–5833     | >17,165       |
| 470–505       | 1717–1845     | 5833–6268     |               |
| 505–543       | 1845–1982     | 6268–6736     |               |
| 543–583       | 1982–2130     | 6736–7239     |               |

To compare the differences between the individual fractions, the absolute number concentrations of the individual fractions have been converted to relative values, where the overall arithmetic mean

for each fraction has been calculated and the value from each interval (hour, day of the week, month) has been related to this mean value.

The following heatmap (Figure 2) shows the differences in variation of the individual fractions. The X-axis represents the individual size fractions, the Y-axis represents the hours of the day. Data are shown as a relative value of each hour to the overall arithmetic mean of that particular size fraction. The visualization clearly shows that fractions of smaller particles have two obvious peaks correlating with traffic peaks in the morning and in the afternoon. However, larger particles (approximately  $>1.5 \mu\text{m}$ ) show an increase during the day, where the number concentration increases during the morning peak hours and do not go down significantly until the end of the afternoon peak hour. One can also see that the number concentration drops much more significantly during the night in the case of the larger particles. One can, therefore, say that the variability is greater in case of the larger particles. While the 213–229 nm fraction only has a difference between the minimum and the maximum ratio of the individual hours of 0.17, the larger fractions have a difference of even more than 1 (9653–10,373 nm – 1.06; 15,976–17,165 nm – 1.09;  $>17,165 \text{ nm}$  – 1.18).

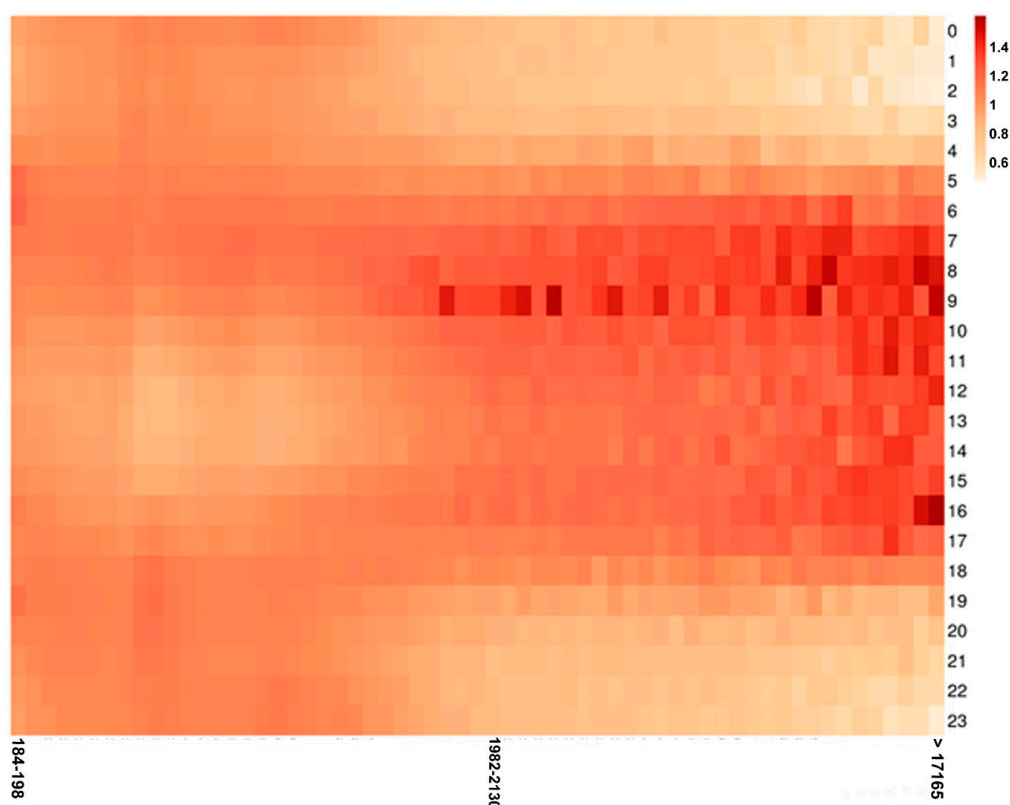


**Figure 2.** Heatmap showing daily variation (hourly average, Y-axis) of all the size fractions (X-axis, in nm) analyzed.

Similarly to the hourly averages, ratios between average number concentrations for weekdays (Monday–Friday) and weekends (Saturday–Sunday) have been calculated for the individual fractions (Figure 3), where the ratio corresponds to the average number concentration of that fraction on the weekend (Saturday–Sunday) divided by the average number concentration of that fraction on weekday (Monday–Friday). The graph clearly shows that the difference between weekdays and weekends is least profound in the case of the smaller fractions around 300 nm, where the ratio between average of weekday and weekend number concentration is close to 1, i.e., same values. In contrast, most significant differences were observed in case of the larger fractions, where the ratio was approximately 0.65 (smallest for 14,865–15,974 nm fraction, 0.642), i.e., the number concentration during the weekend was approximately 65% of those observed during weekdays.

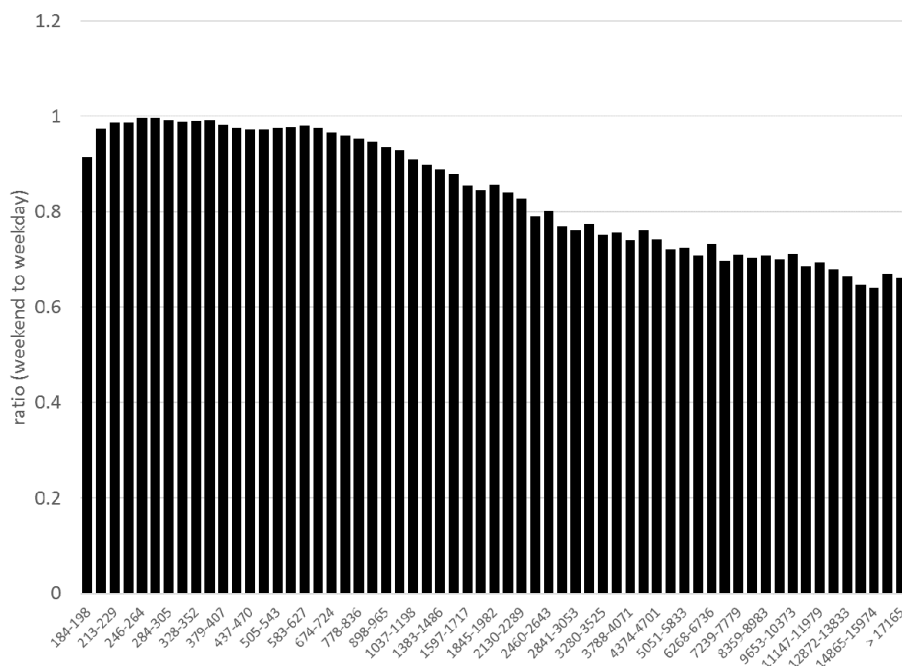


**Figure 3.** Ratio between average number concentration on the weekdays (Monday-Friday) and the weekends (Saturday-Sunday) weekend/weekday.

Analysis of annual variability was also summarized in a heatmap (Figure 4), where the Y-axis represents the individual months and X-axis the various size fractions. The actual value represents the ratio of the particular monthly mean in relation to the overall mean value of that fraction.

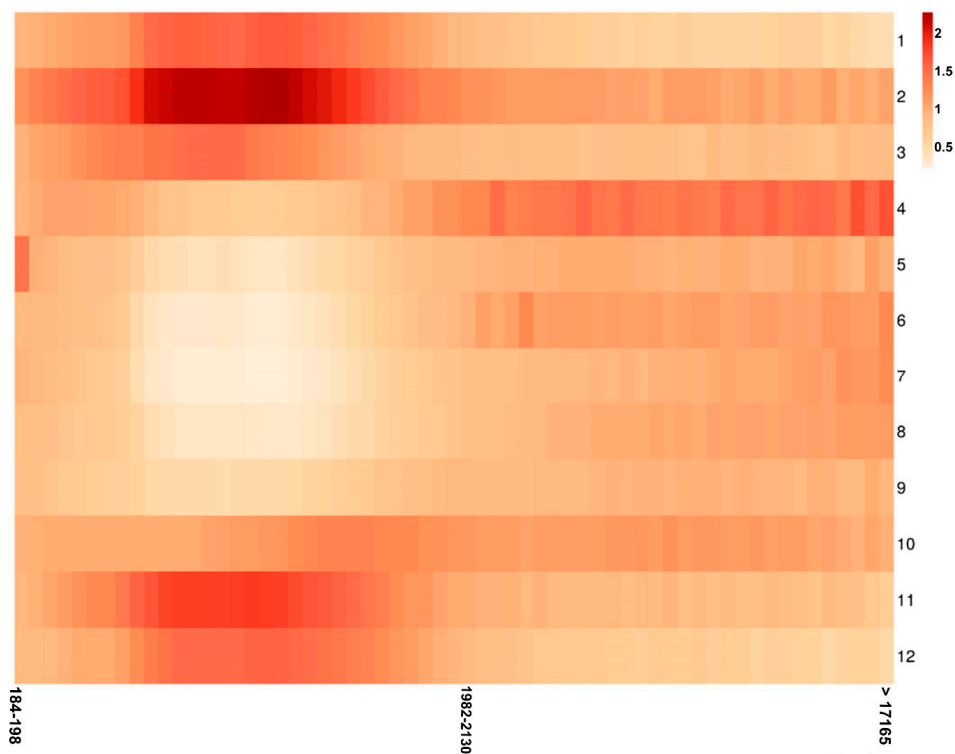


**Figure 4.** Heatmap showing annual variation (monthly average, Y-axis) of all the size fractions (X-axis, in nm) analyzed.

It can be clearly seen that the number concentrations in the case of the smaller particles were high especially in the winter months. In particular, in the case of particles in the range from 320 to 800 nm. In contrast, larger particles had the average number concentrations distributed throughout the year much more evenly.

If we divide the year into two half-years – cold (October–March) and warm (April–September), we can compare the ratio between the average number concentrations for both these half-years (Figure 5), where the ratio corresponds to the average number concentration of a particular fraction during the cold half-year divided by the average number concentration of a particular fraction during the warm half-year. The graph shows the individual size fractions (X-axis) and the ratio between the cold and warm half-years (Y-axis).

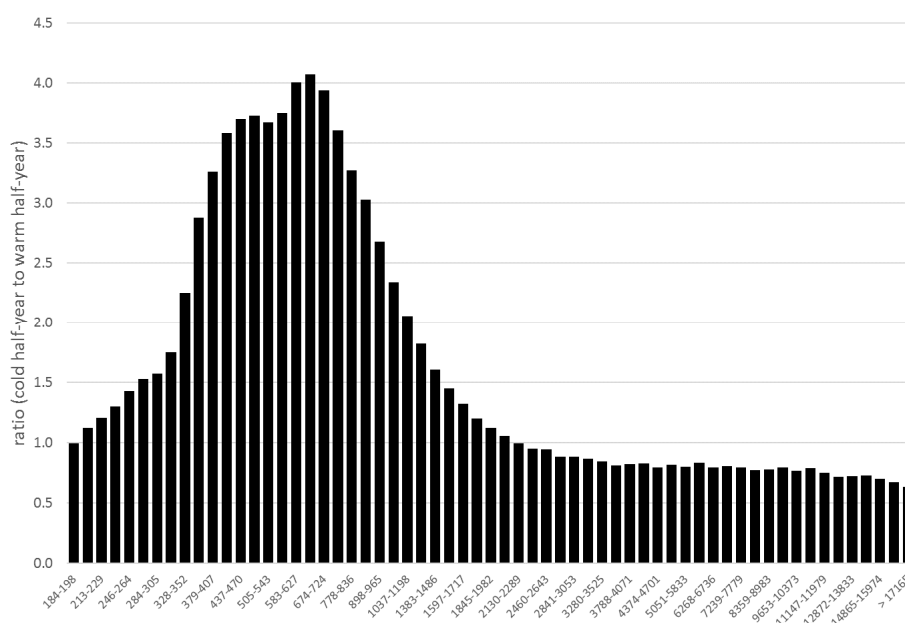


**Figure 5.** Ratio (Y-axis) between average number concentration of all the size fractions (X-axis) between the cold half-year (October–March) and warm half-year (April–September) (cold half-year/warm half-year).

The trends in the ratio show that the fractions can be divided into three groups – the smallest particles (approximately 180–320 nm), which have similar number concentrations during both half-years, medium-sized particles (approximately 320 to 700 nm) where there is a gradual increase in the relative number concentrations in the winter period, with maximum ratio observed in case of the fraction 627–674 nm (4.07). Then as the particles get larger the ratio decreases. The last group of particles, with an aerodynamic larger than approximately 2 μm, has lower number concentrations in the cold half-year than in the warm half-year. In the case of the fraction >17,165 nm, the ratio is 0.63.

To see how the various years compare a comparison was made between the two complete years 2018 and 2019 (Figure 6), in particular, the average number concentrations of the individual size fractions from the entire year were compared.

It is obvious that the two years differ in terms of the absolute values of the average number concentrations, with higher values in 2018 (most likely due to overall better meteorological and dispersion conditions in 2019, which was a very warm year). If, however, we convert the absolute values to relative ones, i.e., calculate the relative ratios between the number concentrations of each fraction and the overall mean number concentration for each year we get the relative contribution of each fraction from the overall particle count. This comparison (Figure 7) then shows that the years 2018 and 2019 were almost identical in terms of the ratios between the average number concentrations of the individual fractions.

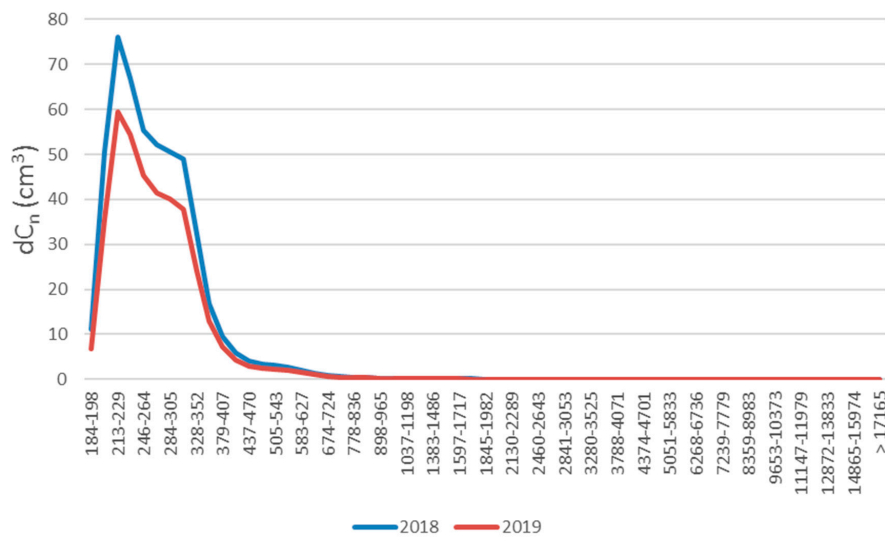


Figure 6. Comparison between average number concentration for all size fractions for 2018 and 2019.

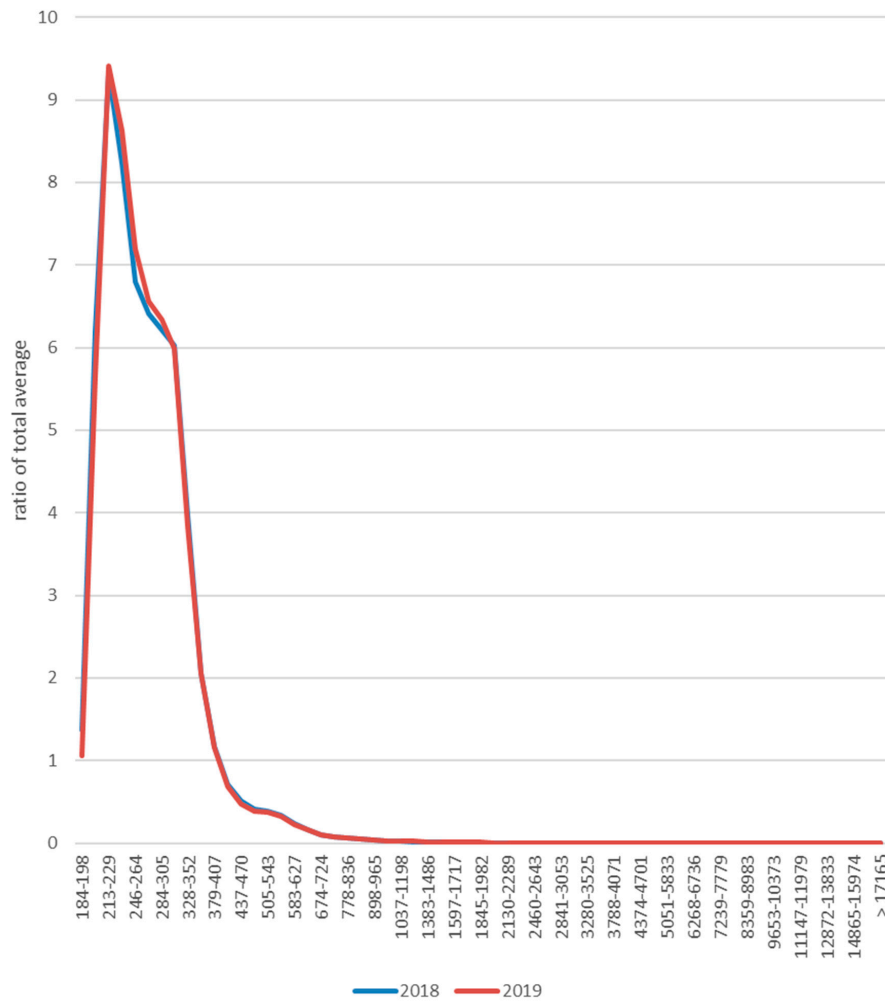


Figure 7. Comparison between the contribution of each average number concentration to the overall total for 2018 and 2019.

#### 4. Discussion

The results of the analysis proved that the annual and daily variation in number concentrations can differ a lot in relation to the particle size. It has been shown that in the case of smaller particles in the range from approximately 200 to 800 nm, there is a significant variability throughout the year, with much higher values, particularly in the winter months. This is most likely due to the variability in particle sources during the year. In cold conditions, the intensity of heating increases significantly (being almost negligible in summer months) and local domestic heating becomes a very significant source of air pollution. Even though traffic is a very important suspended particles source at this location, it is a stable source in that it is relevant both in the summer and in the winter (although meteorological and dispersion conditions [34–36], which are in general worse in the winter – lower wind speed, less precipitation, temperature inversions – can lead to a higher number of particles in the air in winter months).

Higher number concentrations in the winter months compared to the warm months were observed especially in the case of the PM<sub>1</sub> particles. Larger particles did not show such a trend. This is in accordance with other studies. For example Vecchi [17] observed an increase of PM<sub>1</sub> in the winter period by a factor of 2.5 compared to the summer, while in the case of PM<sub>2.5</sub> the increase was only by a factor of approximately 2. A similar conclusion was also made in a study by Triantafyllou et al. [37], which showed a more significant increase of smaller particles in the winter period.

The most significant difference between the winter and summer period has been observed for particles in the range between 300 and 800 nm. Particles of this size can be a product of heating. Zhang et al. [38] analyzed emissions from coal combustion. They concluded that while primary particles generated by coal combustion have a size of approximately 10 to 30 nm, their subsequent coagulation leads to the formation of particles approximately 500 nm large, which is in accordance with the findings of this study.

Apart from heating, low temperature also affects traffic exhaust emissions. This was proved for example by a study by Weilenmanna et al. [39], which showed that a vehicle cold start has a significant negative effect especially on the emissions of CO and HC, but to a lesser extent also suspended particles.

Larger particles show higher number concentrations in the warm period of the year. This could be due to the fact that combustion generally produces smaller particles and some sources of larger particles are significant especially in the warm part of the year. This includes for example resuspension, which is more significant in the summer than in the winter when the surface is cold and soil frozen [40]. Traffic is a significant contributor to resuspension.

When looking at the differences in daily variation of the individual fractions it is obvious that there is a much more significant difference between day and night in the case of the larger particles, which show higher number concentrations during the day. The number of larger particles increases in the morning, in correlation with the morning traffic peak. Vehicles can produce these larger particles by resuspension or abrasion of brake pads, clutch, tires, and the road surface. Number concentration falls significantly in the evening. This is most likely due to the higher mass of these particles, which are therefore more likely to deposit on the ground.

In contrast, the number concentrations of the smaller particles do not differ between day and night to such an extent as the larger particles. As Figure 2 shows, two peaks can also be seen, corresponding to the morning and afternoon traffic peak, but the average number concentration of day and night do not differ as much.

The minimum number concentration is observed around noon and early afternoon hours, not during the night. This is in accordance with other studies focusing on this topic. A study by Zhu [41] showed that even though the traffic intensity at night is 75% lower than during the day, the number of submicron particles only dropped by 20%. Explanation of this could be that the wind speed at night is lower and another possible answer is that there is a weaker atmospheric dilution at night. One other factor is air temperature. Air temperature is on average lower at night and colder ambient temperatures contribute to significantly increased nuclei mode particle formation in vehicle

exhaust [42,43]. Pérez et al. [44] think that the reason for higher concentrations of smaller particles at night compared to the larger ones could also be the decrease of the boundary layer height. Lower air temperature and higher air relative humidity are a favorable factor for condensation and coagulation processes between particles and precursor gases [45].

## 5. Conclusions

In this study, an analysis of number concentrations in 61 size fractions of suspended particles was made focusing on the difference in daily and annual variation. Data comes from ambient air quality monitoring station Ústí nad Labem-Všebořická, an urban traffic station, with data available from mid-June 2017 to the end of 2019.

The results of the study showed that there are significant differences in both the annual and daily number concentration variations depending on the particle size. In the case of the annual variation, a higher variability can be seen for the smaller particles (Figure 4). This is most likely related to the sources of these particles. The most significant source of PM<sub>2.5</sub> particles in the Czech Republic is local domestic heating. This source, however, is almost negligible in the summer months. In contrast, in the case of the daily variation there is a higher variability of the larger particles (Figure 2). This can be explained by the fact that these larger particles deposit quicker to the ground and also by meteorological conditions as explained in the paper. Given that the most significant source of suspended particles at this station is traffic, there are obvious peaks in suspended particle concentrations correlating with morning peak hour and afternoon peak hour. In the evening and at night, there is a rapid decrease in the number of large particles in the air. Smaller particles do not deposit to such an extent so their number concentration remains higher at night. Additionally, a comparison was made between number concentrations on weekdays (Monday-Friday) and weekends (Saturday-Sunday), when the traffic intensity is much lower. The comparison showed that in this case, the variation is very similar to the daily variation in that there is a much more obvious decrease of larger particles number concentrations (Figure 3).

Meteorological and dispersion conditions have a very important effect on air quality. Their variability can cause very significant differences from year to year in terms of absolute values of number concentrations. A comparison between 2018 and 2019, however, showed that the relative ratio between the number concentrations of the various size fractions remain very similar (Figure 7).

It can be concluded that the differences in variation between the various size fractions are determined by both the actual pollution sources (especially in the long-term, i.e., annual variation) and by the actual physical properties of the particles and their behavior in the atmosphere, also determined by the meteorological and dispersion conditions.

In the future, it would be ideal to research annual and daily variation of different size fractions at more station types, i.e., not just traffic stations, but also suburban and rural background stations and also repeat the analysis when a longer time-series is available.

**Author Contributions:** Conceptualization, V.A. and J.B.; methodology, J.B. and V.A.; formal analysis, K.K.; investigation, V.A., J.B. and K.K.; resources, J.B. and K.K.; data curation, J.B.; writing—original draft preparation, J.B. and K.K.; writing—review and editing, K.K.; visualization, J.B.; supervision, V.A.; project administration, K.K.; funding acquisition, J.B. All authors have read and agreed to the published version of the manuscript.

**Funding:** This paper is supported by the Czech Hydrometeorological Institute.

**Conflicts of Interest:** The authors declare no conflict of interest.

## References

1. World Health Organization. *Ambient Air Pollution—a Major Threat to Health and Climate*; World Health Organization: Copenhagen, Denmark, 2018.
2. Loxham, M.; Davies, D.E.; Holgate, S.T. The health effects of fine particulate air pollution. *BMJ* **2019**. [CrossRef]
3. Zhang, Y.L.; Cao, F. Fine particulate matter (PM<sub>2.5</sub>) in China at a city level. *Sci. Rep.* **2015**, *5*, 14884. [CrossRef]

4. Kim, K.H.; Kabir, E.; Kabir, S. A review on the human health impact of airborne particulate matter. *Environ. Int.* **2015**, *74*, 136–143. [[CrossRef](#)] [[PubMed](#)]
5. Luo, X.; Bing, H.; Luo, Z.; Wang, Y.; Jin, L. Impacts of atmospheric particulate matter pollution on environmental biogeochemistry of trace metals in soil-plant system: A review. *Environ. Pollut.* **2019**, *255*. [[CrossRef](#)] [[PubMed](#)]
6. Banerjee, T.; Kumar, M.; Singh, N. *Aerosol, Climate, and Sustainability. Encyclopedia of the Anthropocene*; Elsevier: Oxford, UK, 2018; pp. 419–442. ISBN 9780128135761. [[CrossRef](#)]
7. Zhu, Y.; Hinds, W.C.; Shen, S.; Sioutas, C. Seasonal Trends of Concentration and Size Distribution of Ultrafine Particles Near Major Highways in Los Angeles Special Issue of Aerosol Science and Technology on Findings from the Fine Particulate Matter Supersites Program. *Aerosol Sci. Technol.* **2004**, *38* (Suppl. 1), 5–13. [[CrossRef](#)]
8. Baldauf, R.W.; Devlin, R.B.; Gehr, P.; Giannelli, R.; Hassett-Sipple, B.; Jung, H.; Narubum, G.; McDonald, J.; Sacks, J.D.; Walker, K. Ultrafine Particle Metrics and Research Considerations: Review of the 2015 UFP Workshop. *Int. J. Environ. Res. Public Health* **2016**, *13*, 1054. [[CrossRef](#)] [[PubMed](#)]
9. Zhao, Y.; Nalwa, H.S. (Eds.) *Nanotoxicology: Interactions of Nanomaterials with Biological Systems*; American Scientific Publishers: Los Angeles, CA, USA, 2007.
10. Chen, L.Q.; Fang, L.; Ling, J.; Ding, C.Z.; Kang, B.; Huang, C.Z. Nanotoxicity of silver nanoparticles to red blood cells: Size dependent adsorption, uptake, and hemolytic activity. *Chem. Res. Toxicol.* **2015**, *28*, 501–509. [[CrossRef](#)]
11. Gehrig, R.; Brigitte, B. Characterising seasonal variations and spatial distribution of ambient PM10 and PM2.5 concentrations based on long-term Swiss monitoring data. *Atmos. Environ.* **2003**, *37*, 2571–2580. [[CrossRef](#)]
12. Li, J.; Chen, B.; de la Campa, A.M.S.; Alastuey, A.; Querol, X.; Jesus, D. 2005–2014 trends of PM10 source contributions in an industrialized area of southern Spain. *Environ. Pollut.* **2018**, *236*, 570–579. [[CrossRef](#)]
13. Bartzis, J.G.; Kalimeri, K.K.; Sakellaris, I.A. Environmental data treatment to support exposure studies: The statistical behavior for NO2, O3, PM10 and PM2.5 air concentrations in Europe. *Environ. Res.* **2020**, *181*. [[CrossRef](#)]
14. Samek, L.; Stegowski, Z.; Styszko, K.; Furman, L.; Fiedor, J. Seasonal contribution of assessed sources to submicron and fine particulate matter in a Central European urban area. *Environ. Pollut.* **2018**, *241*, 406–411. [[CrossRef](#)] [[PubMed](#)]
15. Křůmal, K.; Mikuška, P.; Vojtěšek, M.; Večeřa, Z. Seasonal variations of monosaccharide anhydrides in PM1 and PM2.5 aerosol in urban areas. *Atmos. Environ.* **2010**, *44*, 5148–5155. [[CrossRef](#)]
16. Asimakopoulou, D.N.; Maggos, T.; Assimakopoulou, V.D.; Bougiatioti, A.; Bairachtari, K.; Vasilakos, C.; Mihalopoulos, N. Chemical characterization, sources and potential health risk of PM2.5 and PM1 pollution across the Greater Athens Area. *Chemosphere* **2020**, *241*. [[CrossRef](#)]
17. Vecchi, R.; Marazzan, G.; Valli, G.; Ceriani, M.; Antoniazzi, C. The role of atmospheric dispersion in the seasonal variation of PM1 and PM2.5 concentration and composition in the urban area of Milan (Italy). *Atmos. Environ.* **2004**, *38*, 4437–4446. [[CrossRef](#)]
18. Samek, L.; Furman, L.; Mikrut, M.; Regiel-Futyra, A.; Macyk, W.; Stochel, G.; van Eldik, R. Chemical composition of submicron and fine particulate matter collected in Krakow, Poland. Consequences for the APARIC project. *Chemosphere* **2017**, *187*, 430–439. [[CrossRef](#)]
19. Gugamsetty, B.; Wei, H.; Liu, C.N.; Awasthi, A.; Hsu, S.C.; Tsai, C.J.; Roam, G.D.; Wu, Y.C.; Chen, C.F. Source Characterization and Apportionment of PM10, PM2.5 and PM0.1 by Using Positive Matrix Factorization. *Aerosol Air Qual. Res.* **2012**, *12*, 476–491. [[CrossRef](#)]
20. Carbone, C.; Decesari, S.; Paglione, M.; Giulianelli, L.; Rinaldi, M.; Marinoni, A.; Cristofanelli, P.; Didonato, A.; Bonasoni, P.; Fuzzi, S.; et al. 3-year chemical composition of free tropospheric PM1 at the Mt. Cimone GAW global station—South Europe—2165 m a.s.l. *Atmos. Environ.* **2014**, *87*, 218–227. [[CrossRef](#)]
21. Spindler, G.; Grüner, A.; Müller, K.; Schlimper, S.; Herrmann, H. Long-term size-segregated particle (PM10, PM2.5, PM1) characterization study at Melpitz—Influence of air mass inflow, weather conditions and season. *J. Atmos. Chem.* **2013**, *70*, 165–195. [[CrossRef](#)]
22. Pitz, M.; Kreyling, W.G.; Hölscher, B.; Cyrus, J.; Wichmann, H.E.; Heinrich, J. Change of the ambient particle size distribution in East Germany between 1993 and 1999. *Atmos. Environ.* **2001**, *35*, 4357–4366. [[CrossRef](#)]
23. Liu, Y.; Fu, B.; Shen, Y.; Yu, Y.; Liu, H.; Zhao, Z.; Zhang, L. Seasonal properties on PM1 and PGEs (Rh, Pd, and Pt) in PM1. *Atmos. Pollut. Res.* **2018**, *9*, 1032–1037. [[CrossRef](#)]

24. Titos, G.; Lyamani, H.; Pandolfi, M.; Alastuey, A.; Alados-Arboledas, L. Identification of fine (PM<sub>1</sub>) and coarse (PM<sub>10-1</sub>) sources of particulate matter in an urban environment. *Atmos. Environ.* **2014**, *48*, 593–602. [[CrossRef](#)]
25. Tao, J.; Shen, Z.; Zhu, C.; Yue, J.; Cao, J.; Liu, S.; Zhu, L.; Zhang, R. Seasonal variations and chemical characteristics of sub-micrometer particles (PM<sub>1</sub>) in Guangzhou, China. *Atmos. Res.* **2012**, *118*, 222–231. [[CrossRef](#)]
26. Pinto, J.A.; Kumar, P.; Alonso, M.F.; Andreão, W.L.; Pedruzzi, R.; dos Santos, F.S.; Moreira, D.M.; de Almeida Albuquerque, T.T. Traffic data in air quality modeling: A review of key variables, improvements in results, open problems and challenges in current research. *Atmos. Pollut. Res.* **2020**, *11*, 454–468. [[CrossRef](#)]
27. Hu, D.; Wu, J.; Tian, K.; Liao, L.; Xu, M.; Du, Y. Urban air quality, meteorology and traffic linkages: Evidence from a sixteen-day particulate matter pollution event in December 2015, Beijing. *J. Environ. Sci.* **2017**, *59*, 30–38. [[CrossRef](#)] [[PubMed](#)]
28. Dėdėlė, A.; Miškinytė, A. Seasonal and site-specific variation in particulate matter pollution in Lithuania. *Atmos. Pollut. Res.* **2019**, *10*, 768–775. [[CrossRef](#)]
29. Kamińska, J.A. The use of random forests in modelling short-term air pollution effects based on traffic and meteorological conditions: A case study in Wrocław. *J. Environ. Manag.* **2018**, *217*, 164–174. [[CrossRef](#)] [[PubMed](#)]
30. Zhang, Z.; Zhang, X.; Gong, D.; Quan, W.; Zhao, X.; Ma, Z.; Kim, S.J. Evolution of surface O<sub>3</sub> and PM<sub>2.5</sub> concentrations and their relationships with meteorological conditions over the last decade in Beijing. *Atmos. Environ.* **2015**, *108*, 67–75. [[CrossRef](#)]
31. Laña, I.; Del Ser, J.; Padró, A.; Vélez, M.; Casanova-Mateo, C. The role of local urban traffic and meteorological conditions in air pollution: A data-based case study in Madrid, Spain. *Atmos. Environ.* **2016**, *145*, 424–438. [[CrossRef](#)]
32. Google Maps Steetview. (28.4.2020). Ústí nad Labem. Available online: <https://goo.gl/maps/inqx7S1vjV94w1DdA> (accessed on 18 May 2020).
33. Seznam. Mapy.cz. (28.4.2020). Ústí nad Labem. Available online: <https://en.mapy.cz/s/kubonunano> (accessed on 18 May 2020).
34. Ramsey, N.R.; Klein, P.M.; Moore, B., III. The impact of meteorological parameters on urban air quality. *Atmos. Environ.* **2014**, *86*, 58–67. [[CrossRef](#)]
35. Fisher, B. Meteorological factors influencing the occurrence of air pollution episodes involving chimney plumes. *Meteorol. Appl.* **2002**, *9*, 199–210. [[CrossRef](#)]
36. Radaideh, J.A. Effect of Meteorological Variables on Air Pollutants Variation in Arid Climates. *J. Environ. Anal. Toxicol.* **2017**, *7*. [[CrossRef](#)]
37. Triantafyllou, E.; Diapouli, E.; Korras-Carraca, M.B.; Manousakas, M.; Psanis, C.; Floutsi, A.A.; Spyrou, C.; Eleftheriadis, K.; Biskos, G. Contribution of locally-produced and transported air pollution to particulate matter in a small insular coastal city. *Atmos. Pollut. Res.* **2020**, *11*, 667–678. [[CrossRef](#)]
38. Zhang, L.; Ninomiya, Y.; Yamashita, T. Formation of submicron particulate matter (PM<sub>1</sub>) during coal combustion and influence of reaction temperature. *Fuel* **2006**, *85*, 1446–1457. [[CrossRef](#)]
39. Weilenmann, M.; Favez, J.Y.; Alvarez, R. Cold-start emissions of modern passenger cars at different low ambient temperatures and their evolution over vehicle legislation categories. *Atmos. Environ.* **2009**, *43*, 2419–2429. [[CrossRef](#)]
40. Keramat, A.; Marivani, B.; Samsami, M. Climatic Change, Drought and Dust Crisis in Iran. *World Academy of Science. Environ. Eng.* **2011**, *6*, 10–13. [[CrossRef](#)]
41. Zhu, Y.; Kuhn, T.; Mayo, P.; Hinds, W.C.; HINDS. Comparison of Daytime and Nighttime Concentration Profiles and Size Distributions of Ultrafine Particles near a Major Highway. *Environ. Sci. Technol.* **2006**, *40*, 2531–2536. [[CrossRef](#)] [[PubMed](#)]
42. Wei, Q.; Kittelson, D.B.; Watts, W.F. Single-Stage Dilution Tunnel Performance. SAE Transaction: Warrendale, PA, USA, 2001. [[CrossRef](#)]
43. Kittelson, D.; Johnson, J.; Watts, W.; Wei, Q.; Drayton, M.; Paulsen, D.; Bukowiecki, N. Diesel Aerosol Sampling in the Atmosphere. In *SAE Transactions Journal of Fuels and Lubricants*; SAE Paper No. 2000-01-2212; SAE: Warrendale, PA, USA, 2000.

44. Pérez, N.; Pey, J.; Cusack, M.; Reche, C.; Querol, X.; Alastuey, A.; Viana, M. Variability of Particle Number, Black Carbon, and PM 10, PM 2.5, and PM 1 Levels and Speciation: Influence of Road Traffic Emissions on Urban Air Quality. *Aerosol Sci. Technol.* **2010**, *44*, 487–499. [[CrossRef](#)]
45. Jamriska, M.; Morawska, L.; Mergersen, K. The effect of temperature and humidity on size segregated traffic exhaust particle emissions. *Atmos. Environ.* **2008**, *42*, 2369–2382. [[CrossRef](#)]



© 2020 by the authors. Licensee MDPI, Basel, Switzerland. This article is an open access article distributed under the terms and conditions of the Creative Commons Attribution (CC BY) license (<http://creativecommons.org/licenses/by/4.0/>).



Article

# Benzo[a]pyrene in the Ambient Air in the Czech Republic: Emission Sources, Current and Long-Term Monitoring Analysis and Human Exposure

Markéta Schreiberová <sup>1,\*</sup>, Leona Vlasáková <sup>1</sup>, Ondřej Vlček <sup>1</sup>, Jana Šmejdiřová <sup>1</sup>, Jan Horálek <sup>1</sup> and Johannes Bieser <sup>2</sup>

<sup>1</sup> Czech Hydrometeorological Institute, Ambient Air Quality Department, Na Šabatce 17, 143 06 Praha, Czech Republic; leona.vlasakova@chmi.cz (L.V.); ondrej.vlcek@chmi.cz (O.V.); jana.smejdirova@chmi.cz (J.Š.); jan.horalek@chmi.cz (J.H.)

<sup>2</sup> Helmholtz-Zentrum Geesthacht (HZG), Institute of Coastal Research, Max-Planck-Str. 1, D-21502 Geesthacht, Germany; johannes.bieser@hzg.de

\* Correspondence: marketa.schreiberova@chmi.cz; Tel.: +420-244-032-406

Received: 3 July 2020; Accepted: 28 August 2020; Published: 7 September 2020



**Abstract:** This paper provides a detailed, thorough analysis of air pollution by benzo[a]pyrene (BaP) in the Czech Republic. The Czech residential sector is responsible for more than 98.8% of BaP, based on the national emission inventory. According to the data from 48 sites of the National Air Quality Monitoring Network, the range of annual average concentration of BaP ranges from 0.4 ng·m<sup>-3</sup> at a rural regional station to 7.7 ng·m<sup>-3</sup> at an industrial station. Additionally, short-term campaign measurements in small settlements have recorded high values of daily benzo[a]pyrene concentrations (0.1–13.6 ng·m<sup>-3</sup>) in winter months linked to local heating of household heating. The transboundary contribution to the annual average concentrations of BaP was estimated by the CAMx model to range from 46% to 70% over most of the country. However, the contribution of Czech sources can exceed 80% in residential heating hot spots. It is likely that the transboundary contribution to BaP concentrations was overestimated by a factor of 1.5 due to limitations of the modeling approach used. During the period of 2012–2018, 35–58% of the urban population in the Czech Republic were exposed to BaP concentrations above target. A significant decreasing trend, estimated by the Mann-Kendall test, was found for annual and winter BaP concentrations between 2008 and 2018.

**Keywords:** benzo(a)pyrene; ambient air concentrations; spatial-temporal; long-term trends; population exposure; transboundary transport; source apportionment

## 1. Introduction

Polycyclic aromatic hydrocarbons (PAHs) are ubiquitously distributed in the environment [1]. They are common by-products of combustion processes of fossil fuels and wood. PAHs represent a group of substances, many of which have toxic teratogenic, mutagenic or carcinogenic properties [2,3]. They affect fetal growth. Prenatal exposure to PAHs is related to markedly lower birth weight [2] and probably also has negative effects on the cognitive development of young children [4]. Due to their physical and chemical properties, all these substances can be transported over long distances and deposited in remote areas [5–7]. PAHs can bioaccumulate, enter the food chain [1] and be toxic to the environment.

Benzo(a)pyrene, occurring in the atmosphere primarily bound to particulate matter, has been set as a suitable marker of ambient air pollution caused by PAHs. A European directive has set a target value of 1 ng·m<sup>-3</sup> for the total content of BaP in the PM<sub>10</sub> fraction, averaged over a calendar year [8], with the aim of avoiding, preventing or reducing harmful effects on human health and/or the

environment as a whole. The WHO has not drafted a guideline for BaP, which is a potent carcinogen. The reference level of  $0.12 \text{ ng}\cdot\text{m}^{-3}$  was estimated assuming the WHO unit risk for lung cancer for PAH mixtures and an acceptable risk of additional lifetime cancer of approximately  $1 \times 10^{-5}$  [9,10].

Residential combustion as an important source of PAHs and other air pollutants are responsible for the majority of anthropogenic emissions of BaP in Europe. Such emissions are linked to adverse health effects, especially in urban and suburban areas where emissions and population densities are higher [11]. A modeling study of Europe [11] stated that it is necessary to assess concentrations of BaP in Europe, as an indicator for PAHs, and quantify their health-related effects. The European Environmental Agency estimates that in 2017, 17% of the EU–28 urban population was exposed to above-target annual mean BaP concentrations; this is the lowest value since 2008. As in previous years, values above  $1 \text{ ng}\cdot\text{m}^{-3}$  are predominantly found in Central and Eastern Europe. The highest concentrations were recorded mainly at stations in Poland and the Czech Republic [12].

Air pollution by BaP is one of the main problems associated with ensuring air quality in the Czech Republic. BaP concentrations exhibit significant intra-annual variation with maxima in winter that are related to emissions from seasonal anthropogenic sources (local heating units) and generally worsened dispersion conditions.

The aim of this study is to assess the current levels and long-term trends of air pollution by benzo(a)pyrene in the Czech Republic, together with their causes. A transboundary contribution to the annual mean concentrations of BaP is also quantified via a modeling-based approach.

## **2. Materials and Methods**

### *2.1. Area Description*

The Czech Republic is located in Central Europe. The topography of the Czech Republic consists predominantly of hills and highlands. More than two thirds of the territory is located below 500 m altitude, with the large majority of the rest between 500 m and 1000 m and only 1% above 1000 m.

The climate in the Czech Republic is mild; it could be classified as somewhere between continental and maritime. It has 4 seasons. Local variations of weather and climate are influenced by ruggedness and altitude. The average annual air temperature in the Czech Republic usually varies from 5.5 to 9.5 °C. The coldest months of the year are December, January and February. The hottest are July and August. Usually, precipitation in the Czech Republic is at a maximum in July and a minimum in February. Currently, about 60% of the population lives in cities with more than 5000 inhabitants [13,14].

### *2.2. Sampling and Analytical Methods*

In the Czech Republic, concentrations of BaP in the  $\text{PM}_{10}$  fraction as measured at manual monitoring stations form the basis for the evaluation of air quality. The monitoring stations are placed mainly in cities and in areas with known high BaP concentrations (Figure 1). In 2018, BaP concentrations were measured at 48 monitoring sites (Table A1). The majority of stations are located in cities, with 28 urban and suburban stations. Transport and industrial contributions to BaP are monitored at six traffic and nine industrial stations. Background levels of BaP concentrations are monitored at 5 rural monitoring stations.

$\text{PM}_{10}$  samples are taken by low or high volume samplers on a quartz filter. The samples are processed in certified chemical laboratories and analyzed by high pressure liquid chromatography (HPLC) or gas chromatography with mass detection (GC/MS). The measured concentrations of BaP are daily averaged value and are collected with a minimum three-day frequency. The concentrations measured at the pollution monitoring stations are stored in the Czech national Air Quality Information System (AQIS) database. The lower detection limit is  $0.04 \text{ ng}\cdot\text{m}^{-3}$  for GC/MS and  $0.10 \text{ ng}\cdot\text{m}^{-3}$  for HPLC. The measurement uncertainty of BaP is up to 25%.

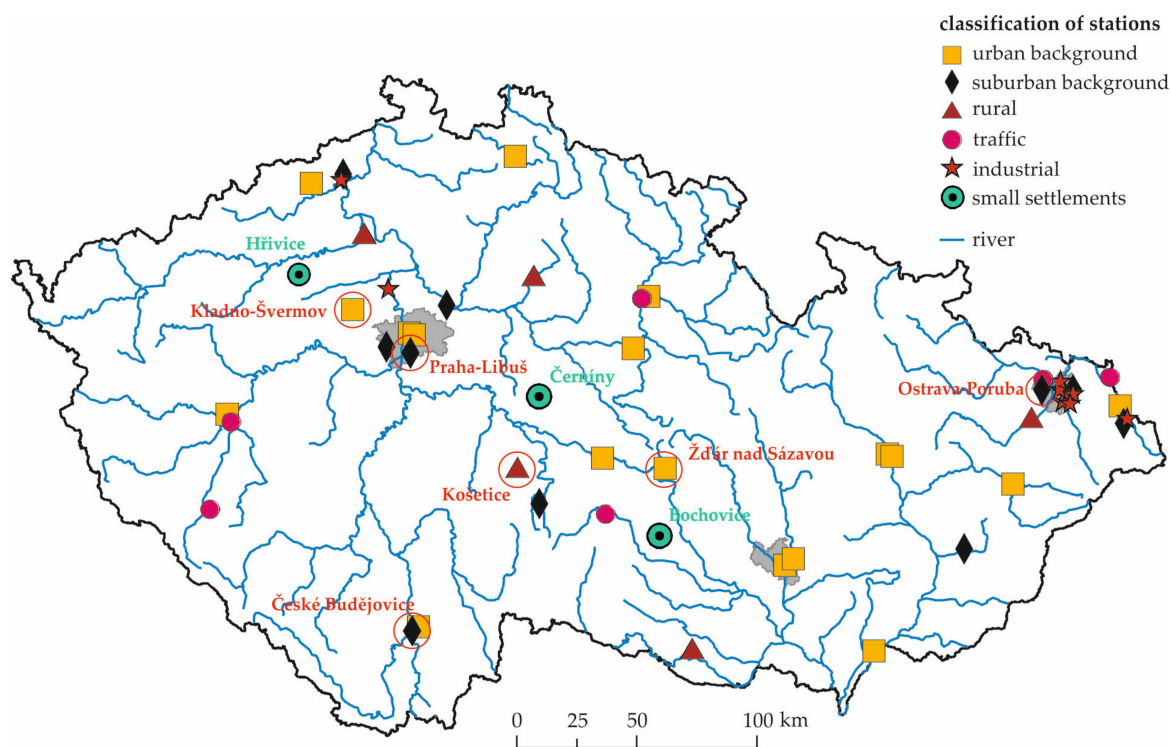


**Figure 1.** Monitoring stations of benzo(a)pyrene in the Czech Republic in 2018.

Short-term monitoring of BaP concentrations in small settlements has been made in campaigns within the Czech national project TITSMZP704—Measurement and Analysis of Air Pollution with Emphasis on the Evaluation of the Share of Individual Groups of Sources. These are case studies that monitor the variability of short-term BaP concentrations during the heating season under the specific conditions of particular small settlements. As this is an ongoing project finishing in 2021, here we will present only a sample of data from 3 small settlements (Figure 1)—Bochovice, Černíny and Hřivice—to show the level of BaP concentrations in villages where they are not regularly monitored and where solid fuel heating is predominant. Bochovice is a small village with 143 inhabitants with 58 houses, which are heated by solid fuels. In Černíny there are 370 permanent residents and 140 houses out of 167 are heated by coal or wood. Hřivice is a village with 631 inhabitants, with 251 houses heated by coal or wood. We also present the Kladno-Švermov locality as an example of an area surrounding a current monitoring station measuring very high levels of air pollution caused by local heating. Kladno-Švermov is a district to the north of Kladno city situated in a shallow valley, where almost 5000 people live. It has a high building density with both central and local heating.

### 2.3. Emission Calculation

BaP is mainly a product of incomplete combustion of organic substances at temperatures between 300 and 600 °C. Unsurprisingly, the main contribution to total BaP emission in the Czech Republic is from combustion of solid fuels in low-capacity boilers. This is mainly household fuel combustion for heating, cooking and water heating (residential sector).

BaP emissions from the residential sector are calculated on the basis of emission factors for various combinations of fuel type and installed combustion plant (see Tables A2–A5 in Appendix B). The combinations used are set from the annually updated distribution of solid fuel and type of heating equipment (Table A5 in Appendix B), resulting in country specific emission factors which reflect the particular circumstances for a given year. For the purpose of national emission inventory, the total fuel consumption in households is determined by the Czech statistical office [13]. The emissions in this

model are calculated as a sum for the whole country and comprise local heating, cooking and water heating. This national model uses emission factors at nominal heat output.

For territorial distribution of residential heating emissions, a bottom-up approach is used. The emissions are calculated for each basic territorial unit—municipalities and city districts—and comprise only the local heating from permanently occupied households. The fuel consumption at a basic territorial unit is calculated based on the average annual heating amount and specific fuel type consumption per average housing type. The base data are obtained from the 2011 Population Census (number of households, their type of heating and average floor area) and the results of the ENERGO 2015 statistical survey (share of given fuel burned in a particular installation type, share of insulated/noninsulated flats). The year-by-year changes in fuel consumption are mostly influenced by the characteristics of the heating period, which is expressed as the number of heating degree days (the sum of the differences between the reference indoor temperature and the average daily outdoor temperature on heating days). Other regional annually updated parameters are the number of households and their type of heating. Solid fuel parameters and the share of solid fuel consumption according to the installation type of the combustion plant are annually updated at a national level, based on the statistics of boiler sales ascertained by the Ministry of Industry and Trade and data from the subsidy program for the boiler replacements. Solid fuel parameters are updated according to the results of the survey on supplies and quality of solid fuels in the Czech Republic carried out by the TEKO company [15]. The regional calculation model uses a 15/85 boiler operating mode, i.e., 15% of time at nominal heat output and 85% at lower heat output. This assumption is in accordance with the Ecodesign Directive 2009/125/EC. Calculation model for the territorial distribution of emissions is more sensitive to climatic conditions in a given year than model for the national emission inventory. The highest emission difference between these two models is in 2014 and 2018, when the heating period was mild and short (see Table A6 in Appendix B).

Emission factors of solid fuels for local heating were obtained from measurement results of the most common fuel and boiler type combinations used for household heating in the Czech Republic. These measurements were carried out at the Energy Research Center of VSB-TUO [16] during the years 2008–2016. Emission factors for liquid and gas fuel were taken from the Emission inventory guidebook [17].

The transport sector comprises emissions from road transport, railways, air and water transport, off-road transport used in agriculture, forestry, building construction and area transport within large industrial enterprises. Emissions are calculated at the Transport Research Center [18] in an up-to-date version of the COPERT program [19] based on nationwide fuel consumption.

BaP emissions from combustion in nonresidential stationary sources such as power and heat generation, combustion processes in industry and manufacturing, institutions and services and waste incineration are calculated from activity data and given emission factors; national emission factors are estimated for a particular sector or taken from the Guidebook [17]. Emissions from industrial sources are either reported by the operator or calculated from activity data and emission factors.

#### 2.4. Spatial Mapping and Population Exposure

The methodology used for the creation of the BaP concentration maps is a linear regression model followed by an interpolation of its residuals; rural and urban areas are mapped separately and then merged by population density [20]. The methodology is referred to as the Regression—Interpolation—Merging Mapping (RIMM) method and is used for air quality mapping in the Czech Republic and elsewhere in Europe as well [11,21,22]. The estimate of concentrations is calculated using the relationship:

$$\hat{Z}(s_0) = c + a_1 \cdot X_1(s_0) + a_2 \cdot X_2(s_0) + \dots + a_p \cdot X_p(s_0) + \hat{R}(s_0), \quad (1)$$

where  $\hat{Z}$  is the estimated concentration value at point  $s_0$ ,  $X_i$  are the various supplementary data,  $c$  and  $a_i$  are the parameters of the linear regression model and  $\hat{R}$  is the spatial interpolation of the residuals of the linear regression model at point  $s_0$ , calculated on the basis of the residuals at the points of measurement.

The primary data for creating air pollution maps of BaP are concentrations measured at individual monitoring stations. Since there are only a limited number of monitoring stations and their spatial representativeness is variable, various supplementary (secondary) data are also used. These secondary data both provide comprehensive information about the entire territory and also exhibit regression dependence on the measured data. The main secondary sources of information are outputs of dispersion models, which combine data from emission inventories and meteorological data. In the Czech Republic, the secondary data mainly used are annual mean concentrations provided by EMEP/MSC-E [23] together with annual mean concentrations from the Czech Gaussian model SYMOS. Other supplementary data can be provided by maps of annual mean PM<sub>10</sub> and PM<sub>2.5</sub> concentrations.

The kriging and Inverse Distance Weighting (IDW) techniques are used as interpolation methods [24]. Interpolation of residuals using IDW is calculated using the relationship:

$$\hat{R}(s_0) = \frac{\sum_{i=1}^N \frac{R(s_i)}{d_{0i}^\beta}}{\sum_{i=1}^N \frac{1}{d_{0i}^\beta}}, \tag{2}$$

where  $\hat{R}$  is the estimate of the field of residuals at point  $s_0$ ,  $R(s_i)$  is the residual of the linear regression model at the measuring site  $s_i$ ,  $N$  is the number of surrounding stations used in the interpolation,  $d_{0i}$  is the distance between points  $s_0$  and  $s_i$ , and  $\beta$  is the weight.

In case of ordinary kriging, the interpolation of the residuals is calculated using the relationship:

$$\hat{R}(s_0) = \sum_{i=1}^N \lambda_i \cdot R(s_i), \text{ with } \sum_{i=1}^N \lambda_i = 1, \tag{3}$$

where  $R(s_i)$  is the residual of the linear regression model at the measuring site  $s_i$  and  $\lambda_i$  are estimated weights based on the theory of spatial statistics [24] derived from a variogram fitted to an empirical variogram  $2\gamma_v(h)$  of the field of residuals. The variogram expresses the dependence of the variability between points on the mutual distance between the points and the empirical variogram is calculated as follows:

$$2\gamma_v(h) = \frac{1}{n} \sum_{i,j; d_{ij}=h \pm \delta} (R(s_i) - R(s_j))^2, \tag{4}$$

where  $R$  are the residuals at measuring points  $s_i$  and  $s_j$ ,  $d_{ij}$  is the distance between points  $s_i$  and  $s_j$ ,  $n$  is the number of pairs of stations  $s_i$  and  $s_j$  whose mutual distance is  $h \pm \delta$ , and  $\delta$  is the tolerance.

The calculated urban and rural map layers are subsequently merged by a layer of population density  $\alpha$ :

$$\hat{Z}(s_0) = \begin{cases} \hat{Z}_r(s_0), & \text{for } \alpha(s_0) \leq \alpha_1 \\ \frac{\alpha_2 - \alpha(s_0)}{\alpha_2 - \alpha_1} \cdot \hat{Z}_r(s_0) + \frac{\alpha(s_0) - \alpha_1}{\alpha_2 - \alpha_1} \cdot \hat{Z}_u(s_0), & \text{for } \alpha_1 < \alpha(s_0) < \alpha_2 \\ \hat{Z}_u(s_0), & \text{for } \alpha(s_0) \geq \alpha_2 \end{cases}, \tag{5}$$

where  $\hat{Z}$  is the final estimate of the concentration at point  $s_0$ ,  $\hat{Z}_r$ ,  $\hat{Z}_u$  is the concentration for the rural or urban map layer, and  $\alpha_1$ ,  $\alpha_2$  are the classification intervals corresponding to the population density. For the BaP concentration maps  $\alpha_1$  was set to 200 inhabitants per km<sup>2</sup> and  $\alpha_2$  was set to 1000 inhabitants per km<sup>2</sup>.

The entire concept of separate mapping of rural and urban pollution is based on the assumption that  $\hat{Z}_r(s_0) \leq \hat{Z}_u(s_0)$  for BaP. For areas where this assumption is not fulfilled, a third layer created in a similar fashion to the urban and rural layers is used; this third layer is created using all the background stations without distinguishing between urban and rural stations.

The maps are constructed with a spatial resolution of  $1 \times 1 \text{ km}^2$ . The uncertainty of the map was assessed using the cross-validation method: concentration at the location of a measuring site is always estimated from other station data only, thus providing an objective estimate of the map quality away from measurement site locations. In this article, the uncertainty of the maps is expressed by the relative root-mean-square error (RRMSE):

$$\text{RRMSE} = \frac{\sqrt{\frac{1}{N} \sum_{i=1}^N (\hat{Z}(s_i) - Z(s_i))^2} \text{RMSE}}{\frac{1}{N} \sum_{i=1}^N Z(s_i)} \cdot 100, \quad (6)$$

where  $Z$  is the measured value of the concentration at point  $s_i$ ,  $\hat{Z}$  is its estimate using cross-validation and  $N$  is the number of measuring stations. The spatial distribution of the uncertainty was not estimated. It should be noted that the cross-validation is applied only during the interpolation of residuals; parameters of linear regression are always estimated using all the stations. Therefore, the overall uncertainty of the maps is somewhat underestimated. The uncertainties (RRMSE) were calculated for each map layer separately and were up to 30% for urban and over 60% for rural areas. The higher uncertainty of rural areas is due to lack of measurements at rural regional stations and the absence of more extensive measurements in smaller settlements in the Czech Republic.

The annual mean BaP concentration maps 2012–2018 were prepared at CHMI during the annual air quality assessments. Estimation of population exposure to above-target BaP concentrations were calculated based on maps of BaP and population density data with resolution  $1 \times 1 \text{ km}$  [13].

## 2.5. Trend Analysis

Trends of annual average BaP concentrations were analyzed at six selected monitoring stations in the Czech Republic (Figure 1). Five stations were classified as urban or suburban, the remaining station was classified as a rural regional station. Station selection was based on their classification and the quantity of data availability for trend analysis. We focus on data from urban and suburban monitoring sites since one of the aims of this study is to assess human exposure to BaP concentrations. For a comprehensive overview, the data from the Košetice rural regional site are also presented.

Trends for annual, winter (October–March) and summer (April–September) average concentrations are analyzed. The authors annually prepare average monthly concentrations of BaP for the “Air Pollution in the Czech Republic” yearbooks [22] (the newest report) and have partitioned this data into winter and summer periods. From April to September, average monthly BaP concentrations are usually below or just above the target value while for the rest of the year they very often exceed the target value.

Temporal trends, i.e., annual averages of BaP concentrations and emission, were analyzed using the nonparametric Mann-Kendall trend test with a level of significance of 0.05 [25,26]. This test is among the most widely used statistical methods for this kind of data [27–31] and is particularly useful since it tolerates missing values and the data need not conform to any particular distribution. Moreover, as only relative rather than absolute magnitudes of the data are used, this test is less sensitive towards incomplete data capture and special meteorological conditions leading to extreme values [32] that often affect air quality data.

If a linear trend is significant, the slope and severity of the trend is estimated by Sen’s test [32]. For all stations, annual average concentration and emission were analyzed for the same 2008–2018 time period. There were no missing averaged annual data.

We used R-Studio software for statistical analyses [33]. The maps were created using the geographic information system ArcGIS by ESRI [34].

## 2.6. Source Apportionment

During the update of the National air quality plans (NAQP) in 2018, a transboundary contribution to annual mean concentrations of BaP in 2015 had to be quantified. It is known that polycyclic aromatic hydrocarbons including BaP undergo gas-particle partitioning and degradation in the atmosphere, but these processes are not fully understood and other processes, e.g., secondary organic aerosol coating can protect PAHs from ozone degradation during long range transport [35]. Due to the limited time for the update of NAQP and unavailability of ready-to-use models for PAHs long-range transport, a chemical transport model CAMx v5.41 [36] was adopted to account for BaP as a passive tracer. The limitations of this approach are discussed further in the text.

The CAMx model was run in two nested domains d01 and d02 with 14.1-km and 4.7-km resolution respectively (Figure 2). The transboundary contribution was estimated with a brute-force method. Sources outside the Czech Republic were set to zero. The spatial distribution of concentrations originating from Czech sources within the 4.7-km CAMx grid was determined by the Gaussian model SYMOS [37] at 0.5-km resolution:

$$C_{CZ\_scaled}(i) = C_{CZ} \cdot \frac{S(i)}{\sum_{j=1}^n S(j)/n}, \quad (7)$$

where  $C_{CZ}$  is the contribution of Czech sources calculated by the CAMx model in a 4.7-km grid,  $S(i)$  is total contribution of Czech sources in subgrid point  $i$  calculated by the SYMOS model and  $n$  is number of subgrid points. Next, a relative contribution of sector  $C$  of Czech sources was determined:

$$P_C(i) = \frac{S_c(i)}{S(i)} \cdot \frac{C_{CZ\_scaled}(i)}{C_{nonCZ} + C_{CZ\_scaled}(i)} \cdot 100, \quad (8)$$

where  $C_{nonCZ}$  is the contribution of sources outside of the Czech Republic calculated by the CAMx model in a 4.7-km grid, and  $S_c(i)$  is the contribution of the Czech sources (sector  $C$  only) in subgrid point  $i$  calculated by the SYMOS model.

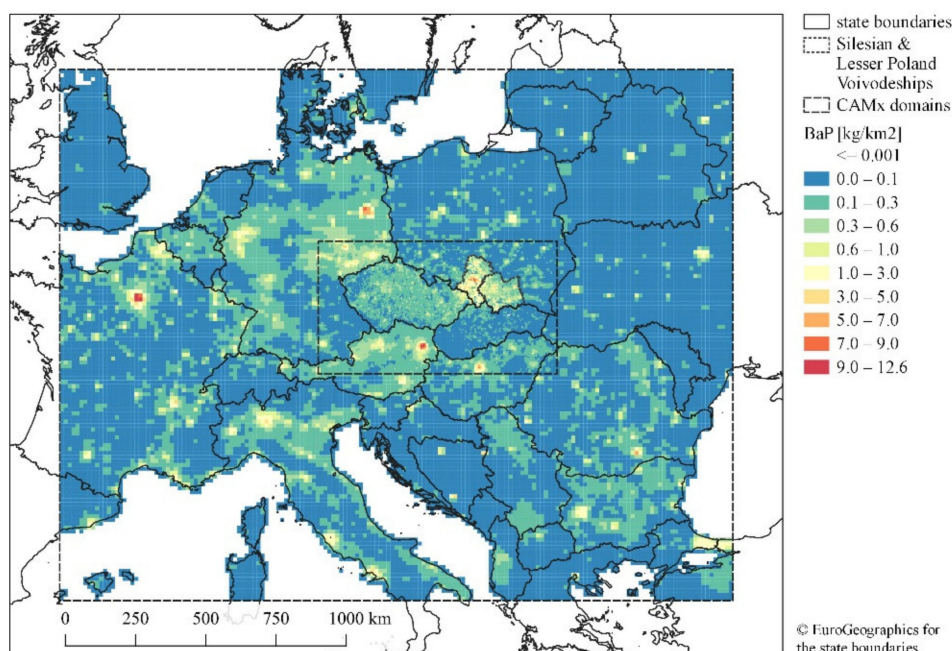


**Figure 2.** Annual benzo[a]pyrene (BaP) emissions for 2015 [ $\text{kg}\cdot\text{km}^2$ ] used in the CAMx model.

Meteorological inputs with a 1-h time step were derived from the assimilation cycle of the numerical weather prediction model ALADIN/CE version ALARO [38] operated at the CHMI at

4.7-km resolution and with 87 vertical levels. In the assimilation cycle, the analysis at 0, 6, 12 and 18 UTC was followed by a 6-h forecast. Analysis of upper-air parameters combines the driving model ARPEGE with mesoscale structures of the ALADIN model through DFI blending complemented by 3DVAR assimilation of observations [39]. Analysis of surface temperature and relative humidity is based on optimal interpolation and serves as an input to the Interaction Soil Biosphere Atmosphere (ISBA) scheme describing exchanges between the atmosphere and the land surface [40]. The 68 lowest ALADIN levels were aggregated into 26 CAMx levels, with the top of the lowest level at approximately 50 m and the highest level at approx. 10 km above ground.

High-resolution BaP emissions for the Czech Republic were taken from the calculation model for territorial distribution. For the Polish Silesian and Lesser Poland Vovoidships, BaP emissions were estimated by the ATMOTERM company within the LIFE-IP MAŁOPOLSKA project (LIFE14 IPE/PL/000021). For Slovakia, emissions from the SNAP 2 sector were taken from the national emission inventory. For other sectors in Slovakia and the rest of the modeling domain, a top-down emission inventory based on the TNO emission inventory [41] was used: emissions for the year 2015 were estimated by linear interpolation and then distributed to ten sectors following the SNAP nomenclature. Industrial emissions were allocated to sources registered in the European point source emission register E-PRTR [42] and remaining industrial emissions as well as emissions from area sources were distributed using the “industrial area” land cover class from the Corine Land Classification (CLC) database [43]. For the spatial distribution of residential heating, a combination of population density and urban area was used, assuming different fuel mixes in metropolitan and rural areas. Typically, rural areas exhibit a larger per capita emission of BaP due to the increased usage of coal and wood. A map of annual emissions used is shown in Figure 2.

The time distribution of the residential heating emissions in the Czech Republic and Silesian and Lesser Poland Vovoidships was based on temperature profiles, otherwise factors for month, day of the week and hour of the day were used [44,45]. For the vertical distribution of point source emissions from top-down inventory, typical point source parameters based on the analysis of the data from the Czech database were used for each SNAP category.

### 3. Results

#### 3.1. Emissions of Benzo(a)pyrene

In 2018, the residential sector accounted for more than 98.8% of total Czech BaP emissions (15.56 t out of total 15.74 t). The remaining percentage was produced mainly by the transport sector (0.78%, 122 kg), especially passenger cars (0.48%, 76 kg). The industrial share of total BaP emissions was 0.27% (43 kg) and the share of institutions and services 0.10% (16 kg). The emissions from industrial sources are year-round, in contrast with local heating, especially in the Moravian-Silesian region. There is also a higher proportion of coal combustion in households in this region, which is reflected in a higher BaP emission load. The contributions from the different sources of BaP emissions have not changed significantly in the last 10 years. Almost 58% of BaP emissions from the residential sector are produced by combustion of fuel wood, and the consumption of wood is still increasing (Table A2 in Appendix B). In contrast, coal consumption is decreasing in recent years, which is reflected in its decreasing share of emissions (Figure 3). In 2018, approximately 15% of households were using solid fuels for local heating, and these households are responsible for more than 98% of total BaP emissions in the Czech Republic.

Figure 4 presents BaP emissions from combustion of solid fuel in the residential sector in 2018 sorted by combustion installation and fuel type. More than 50% of total BaP emissions from the residential sector are estimated to be from fuel combustion in over-fire boilers and about 30% from fuel combustion in fireplaces and stoves.

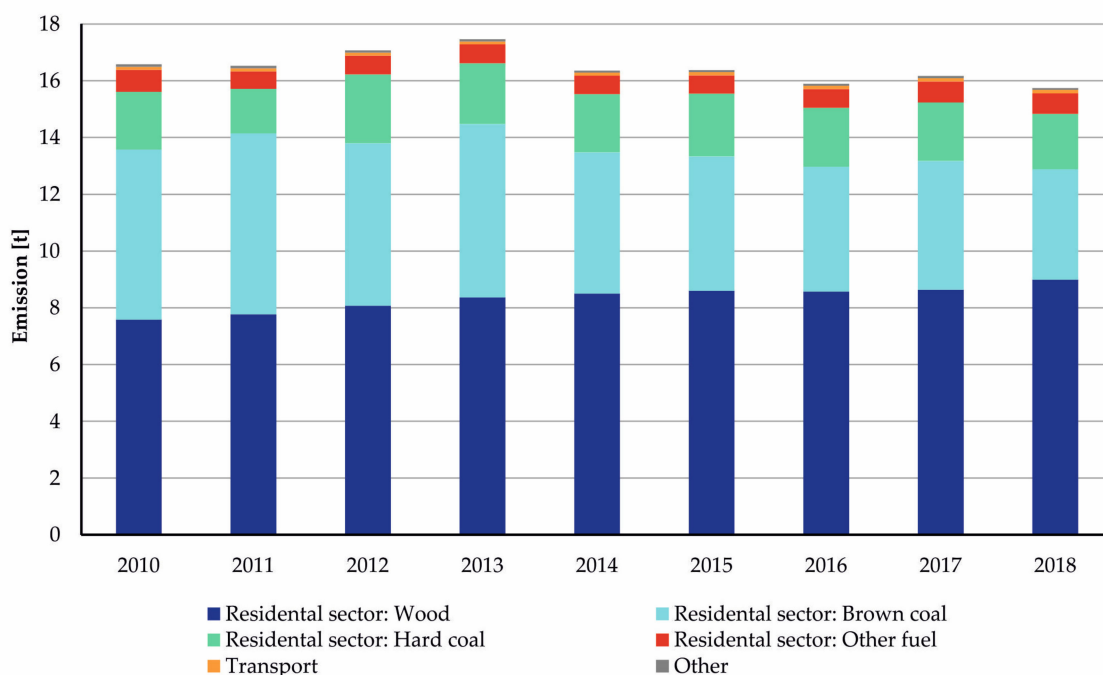


Figure 3. The development of total BaP emissions and source share, 2010–2018.

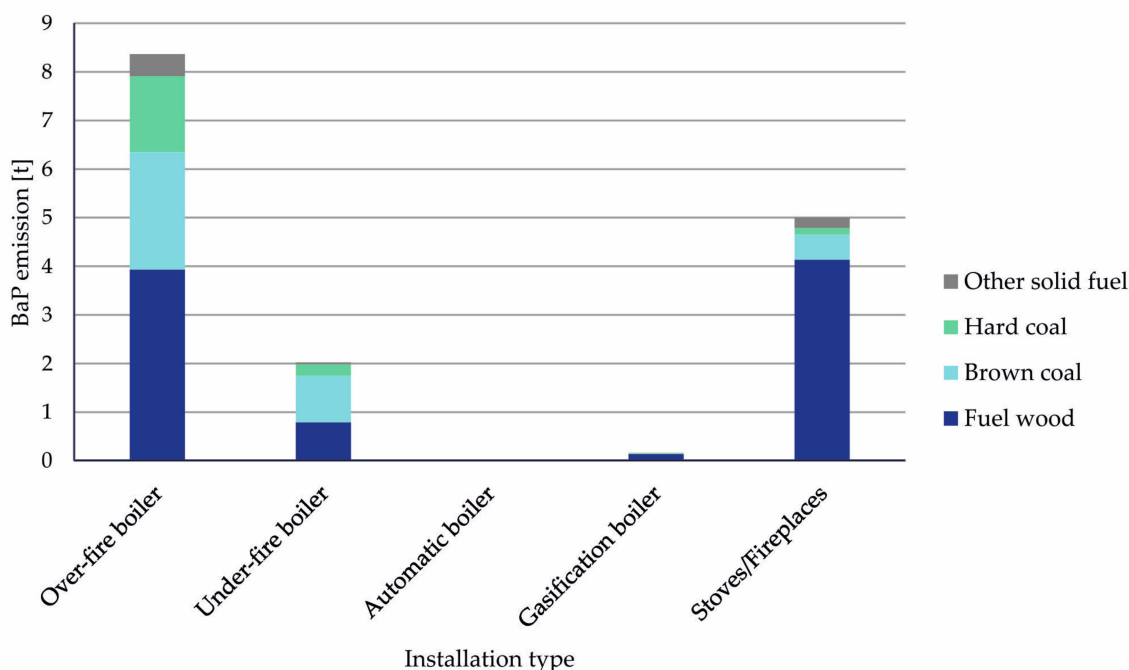
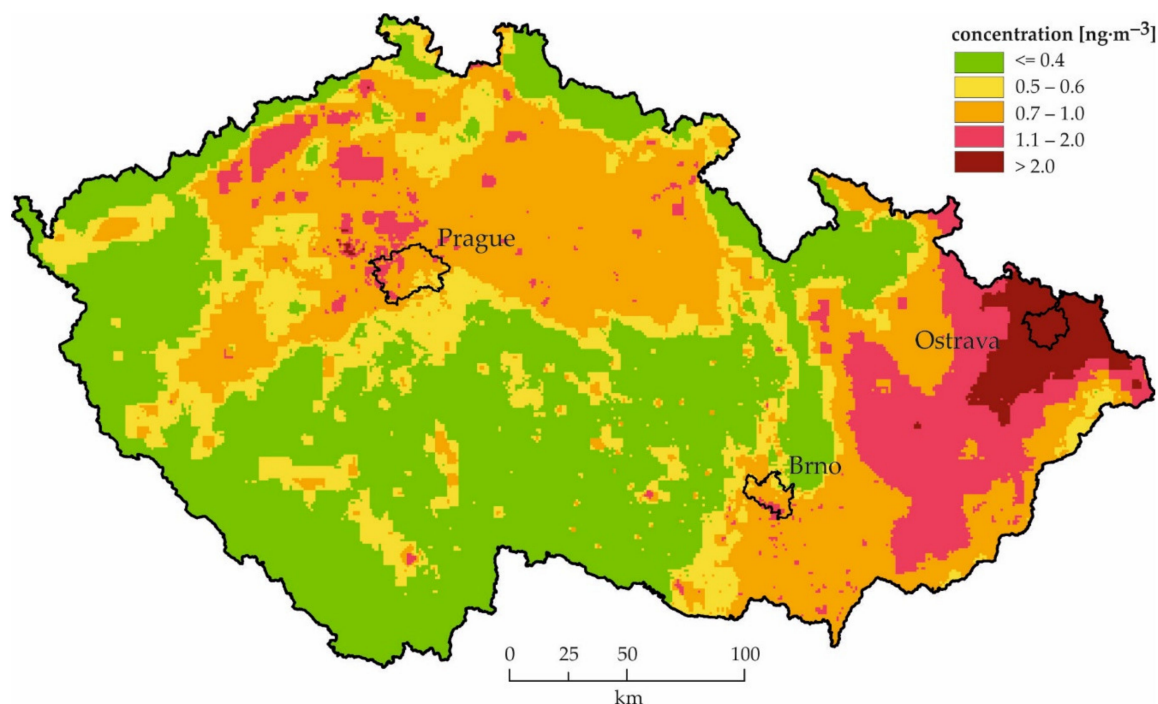


Figure 4. BaP emissions from combustion of solid fuel in residential sector in 2018 sorted by combustion installation and fuel type.

### 3.2. Ambient Air Concentrations of BaP and Population Exposure

The map of annual average concentration of BaP in 2018 is shown in Figure 5. Areas where BaP concentrations were higher than the target value of  $1 \text{ ng} \cdot \text{m}^{-3}$  (above-target) are indicated in red or brown in the figure. The thresholds correspond to the upper and lower assessment thresholds of  $0.6 \text{ ng} \cdot \text{m}^{-3}$  and  $0.4 \text{ ng} \cdot \text{m}^{-3}$ , the target value of  $1.0 \text{ ng} \cdot \text{m}^{-3}$  set by EU legislation [8], and to  $2.0 \text{ ng} \cdot \text{m}^{-3}$  to distinguish the most polluted areas in the Czech Republic. High values of BaP concentrations were estimated in the North East of the Czech Republic, referred to as the Ostrava region. Other

contaminated areas include the Kladno district (West of Prague), areas of Prague and a number of smaller towns. Areas with above-target concentrations comprised 12.6% of the Czech territory in 2018. The lowest annual average concentrations of BaP were estimated to be in locations distant from emission sources and therefore free from direct exposure (i.e., natural mountain areas). The range of measured concentration of BaP in 2018 was from  $0.4 \text{ ng}\cdot\text{m}^{-3}$  at the Košetice rural station to  $7.7 \text{ ng}\cdot\text{m}^{-3}$  at the Ostrava-Radvanice industrial station.



**Figure 5.** Field of annual average concentration of benzo[a]pyrene in the Czech Republic, 2018.

Further annual mean BaP concentration maps from 2012 to 2017, which were used in the population exposure estimation, are listed in Appendix C. Based on comparison of population numbers living in areas with the different BaP concentrations, it can be stated that there is no marked trend in the period between 2012 and 2018 (Figure 6). The average value of the percentage of the population living in the above-target areas was 49.6% during the years 2012 to 2018. The lowest number of inhabitants living in the above-target areas was estimated in 2018 (35.5%). The highest number of inhabitants (57.9%) exposed to above-target concentrations of BaP was estimated for the years 2012 and 2017. Thirty-three percent of inhabitants on average in 2012 to 2018 lived in places with concentrations of  $0.7\text{--}1.0 \text{ ng}\cdot\text{m}^{-3}$ . On average, between 2012 and 2018, 7.4% of the population lived in areas with BaP concentration lower than  $0.4 \text{ ng}\cdot\text{m}^{-3}$ , with values ranging from 3.5% in 2013 to 11% in 2014.

Figure 7 shows selected measured daily concentrations of BaP in the winter seasons of 2017 and 2018 at three project locations (Bochovice, Černíny and Hřivice) together with the data from the CHMI Kladno-Švermov station. In Kladno-Švermov, Bochovice, Černíny and Hřivice, the average concentrations of BaP were  $8.0 \pm 5.7$ ,  $2.1 \pm 2.1 \text{ ng}\cdot\text{m}^{-3}$ ,  $2.2 \pm 2.0 \text{ ng}\cdot\text{m}^{-3}$  and  $5.4 \pm 3.2 \text{ ng}\cdot\text{m}^{-3}$  respectively. The highest daily average concentration of BaP over the sampling campaign— $24.5 \text{ ng}\cdot\text{m}^{-3}$ —was observed in the Kladno-Švermov station whereas the lowest daily average concentration of BaP ( $0.1 \text{ ng}\cdot\text{m}^{-3}$ ) was recorded in Černíny. The limited amount data obtained by these campaign measurements, which were only obtained in winter, does not allow for calculation of annual average concentrations. Nevertheless, in Bochovice and Černíny the target limit value ( $1 \text{ ng}\cdot\text{m}^{-3}$ ) established by European legislation was exceeded on 59% and 54% of measurement days, respectively. In contrast, the average daily BaP concentrations monitored in Hřivice and Kladno-Švermov were below the target limit in only one case.

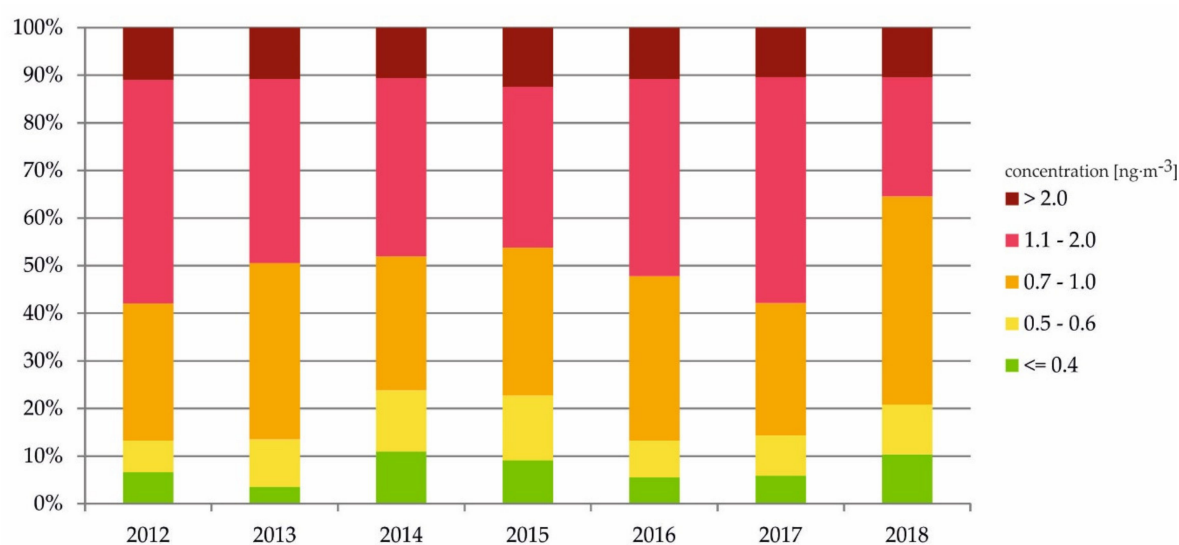


Figure 6. Population exposure to benzo[a]pyrene in the Czech Republic, 2012–2018.

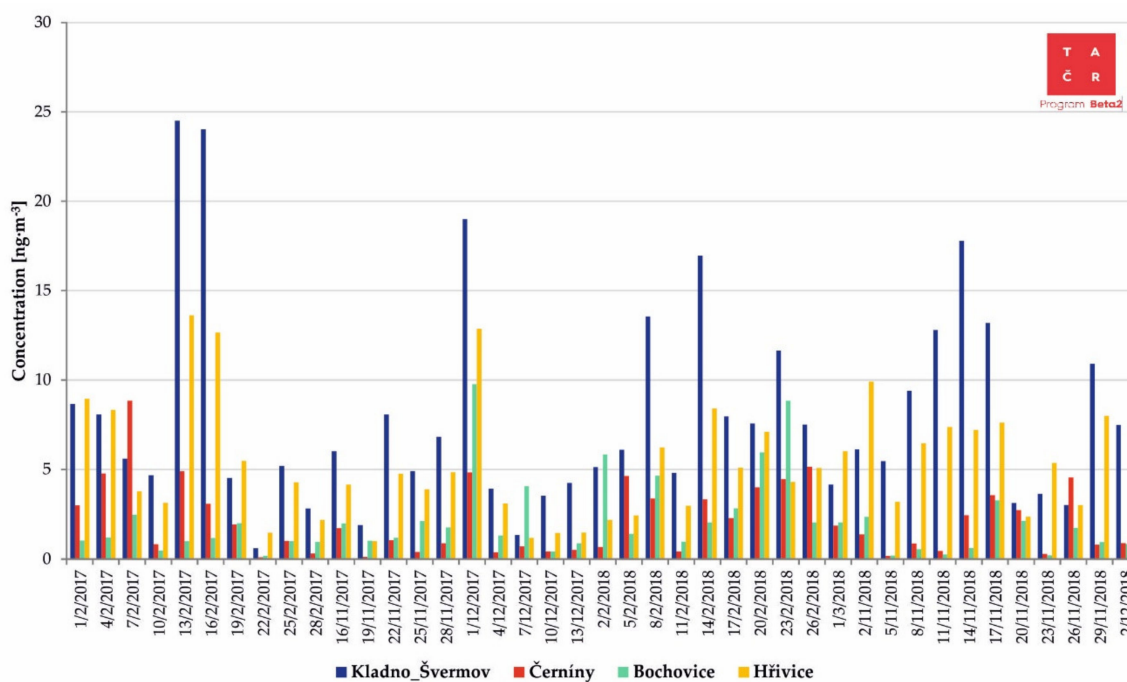


Figure 7. Daily average BaP concentration in small settlements Černíny, Bochovice and Hřivice and in the town of Kladno-Švermov in the Czech Republic, 2017–2018.

### 3.3. BaP Concentration and Emission Trends

Table 1 presents the BaP annual average concentrations during the study period 2008–2018. Annual average concentrations from 2008 to 2018 were analyzed at six selected sites (five urban and suburban stations, one rural regional station). The highest annual average value from all stations, which was  $2.1 \text{ ng}\cdot\text{m}^{-3}$ , was from 2008, with a range between  $0.4$  and  $6 \text{ ng}\cdot\text{m}^{-3}$ . When including only the five urban and suburban stations, the highest annual average value of  $2.5 \text{ ng}\cdot\text{m}^{-3}$ , with the same range, was also seen in 2008. The years with the lowest average BaP concentration of  $1.6 \text{ ng}\cdot\text{m}^{-3}$  were 2014–2018; the widest range was between  $0.4$  and  $3.9 \text{ ng}\cdot\text{m}^{-3}$  in 2015. When including only urban and suburban stations, the lowest annual average value of  $1.8 \text{ ng}\cdot\text{m}^{-3}$  was detected in 2016, 2017 and 2018; the widest range was between  $0.7$  and  $3.7 \text{ ng}\cdot\text{m}^{-3}$  in 2017. The average and median value for

all stations for the entire study period are 1.8 ng·m<sup>-3</sup> and 1.2 ng·m<sup>-3</sup> respectively. The average and median value for urban and suburban stations is 2 ng·m<sup>-3</sup> and 1.4 ng·m<sup>-3</sup>, respectively.

**Table 1.** Station characteristics, average concentrations of BaP (ng·m<sup>-3</sup>) and emission of BaP for 2008–2018.

| Station  | Character  | 2008 | 2009 | 2010 | 2011 | 2012 | 2013 | 2014 | 2015 | 2016 | 2017 | 2018 |
|--|------------|------|------|------|------|------|------|------|------|------|------|------|
| <b>Concentrations of BaP (ng·m<sup>-3</sup>)</b> |            |      |      |      |      |      |      |      |      |      |      |      |
| Kladno-Švermov                                   | urban      | 6.0  | 4.5  | 4.3  | 3.9  | 4.7  | 4.1  | 3.4  | 3.9  | 3.4  | 3.7  | 3.5  |
| Ostrava-Poruba                                   | suburban   | 3.5  | 3.3  | 3.8  | 3.4  | 3.3  | 2.9  | 2.9  | 2.6  | 2.2  | 2.5  | 2.9  |
| České Budějovice                                 | suburban   | 1.4  | 1.4  | 1.5  | 1.3  | 1.7  | 1.5  | 1.2  | 1.4  | 1.5  | 1.3  | 1.1  |
| Prague-Libuš                                     | suburban   | 1.0  | 0.9  | 0.9  | 0.9  | 1.1  | 1.2  | 1.1  | 0.9  | 0.8  | 0.9  | 0.8  |
| Ždár nad Sázavou                                 | urban      | 0.4  | 0.7  | 0.6  | 0.6  | 0.5  | 0.7  | 0.8  | 0.6  | 1.0  | 0.7  | 0.6  |
| Košetice   | rural reg. | 0.4  | 0.5  | 0.6  | 0.4  | 0.6  | 0.7  | 0.4  | 0.4  | 0.4  | 0.5  | 0.4  |
| average  |            | 2.1  | 1.9  | 2.0  | 1.8  | 2.0  | 1.9  | 1.6  | 1.6  | 1.6  | 1.6  | 1.6  |
| <b>Summer (April–September)</b>                  |            |      |      |      |      |      |      |      |      |      |      |      |
| Kladno-Švermov                                   | urban      | 1.4  | 0.7  | 0.9  | 0.7  | 1.4  | 1.0  | 0.9  | 0.5  | 0.8  | 0.8  | 0.7  |
| Ostrava-Poruba                                   | suburban   | 1.1  | 0.7  | 0.6  | 0.6  | 0.6  | 1.0  | 0.6  | 0.7  | 0.7  | 0.5  | 0.6  |
| České Budějovice                                 | suburban   | 0.3  | 0.3  | 0.3  | 0.3  | 0.3  | 0.4  | 0.3  | 0.3  | 0.3  | 0.3  | 0.1  |
| Prague-Libuš                                     | suburban   | 0.2  | 0.2  | 0.3  | 0.2  | 0.3  | 0.3  | 0.2  | 0.2  | 0.2  | 0.2  | 0.1  |
| Ždár nad Sázavou                                 | urban      | 0.2  | 0.1  | 0.1  | 0.1  | 0.2  | 0.3  | 0.3  | 0.1  | 0.2  | 0.1  | 0.1  |
| Košetice   | rural reg. | 0.2  | 0.1  | 0.1  | 0.1  | 0.1  | 0.1  | 0.1  | 0.1  | 0.1  | 0.2  | 0.1  |
| summer average                                   |            | 0.6  | 0.3  | 0.4  | 0.3  | 0.5  | 0.5  | 0.4  | 0.3  | 0.4  | 0.3  | 0.3  |
| <b>Winter (October–March)</b>                    |            |      |      |      |      |      |      |      |      |      |      |      |
| Kladno-Švermov                                   | urban      | 10.9 | 8.4  | 7.7  | 7.2  | 8.1  | 7.1  | 6.6  | 7.0  | 6.0  | 6.6  | 6.5  |
| Ostrava-Poruba                                   | suburban   | 5.9  | 5.9  | 7.0  | 6.3  | 6.1  | 4.8  | 5.3  | 4.5  | 3.8  | 4.6  | 5.3  |
| České Budějovice                                 | suburban   | 2.5  | 2.5  | 2.7  | 2.5  | 3.1  | 2.7  | 2.1  | 2.4  | 2.6  | 2.3  | 2.1  |
| Prague-Libuš                                     | suburban   | 1.8  | 1.6  | 1.5  | 1.6  | 2.0  | 2.1  | 2.0  | 1.5  | 1.4  | 1.7  | 1.4  |
| Ždár nad Sázavou                                 | urban      | 0.8  | 1.1  | 1.1  | 1.1  | 0.9  | 1.2  | 1.3  | 1.1  | 1.8  | 1.4  | 1.1  |
| Košetice   | rural reg. | 0.6  | 0.9  | 1.0  | 0.8  | 0.8  | 1.2  | 0.7  | 0.7  | 0.8  | 0.9  | 0.6  |
| winter average                                   |            | 3.7  | 3.4  | 3.5  | 3.2  | 3.5  | 3.2  | 3.0  | 2.8  | 2.7  | 2.9  | 2.8  |
| <b>Emission of BaP (t·year<sup>-1</sup>)</b>     |            |      |      |      |      |      |      |      |      |      |      |      |
| Czech Republic                                   |            | 14.0 | 14.8 | 16.6 | 16.5 | 17.1 | 17.5 | 16.4 | 16.4 | 15.9 | 16.2 | 15.7 |

In contrast, the highest annual average value of 0.7 ng·m<sup>-3</sup> at the Košetice rural regional site, representing the wider area without the local emission, was measured in 2013. The lowest annual average value and the median of 0.4 ng·m<sup>-3</sup> was recorded for six years (2008, 2011, 2014–2016, 2018). The median value for the Košetice site is 0.5 ng·m<sup>-3</sup>.

With respect to the main emission source of BaP (Figure 3), i.e., local heating causing higher levels of BaP in ambient air, we assessed concentration trends specified for the winter (October–March) and summer (April–September) period and for the year as a whole (Figures 8–10). More detailed graphs presenting the course of annual, winter and summer concentrations using boxplots at each measuring station can be found in Appendix D, Figure A2.

Around 65% of annual average concentrations from suburban and urban stations during the study period were higher than the target value of 1 ng·m<sup>-3</sup> [8]. For the sake of completeness, this figure was around 96% for the winter periods and 7% for the summer period, respectively. Only one rural regional site registered no above-target concentration during the entire study period.

Comparing the annual average values for all stations between 2008 and 2018, there is a decrease of 27% in the BaP annual average concentration and a 24% decrease for winter and 50% decrease for summer average concentrations (Figures 8–10). For urban and suburban stations, the situation is very similar with a 28%, 25% and 49% decrease for the annual, winter and summer periods respectively (Figures 8–10).

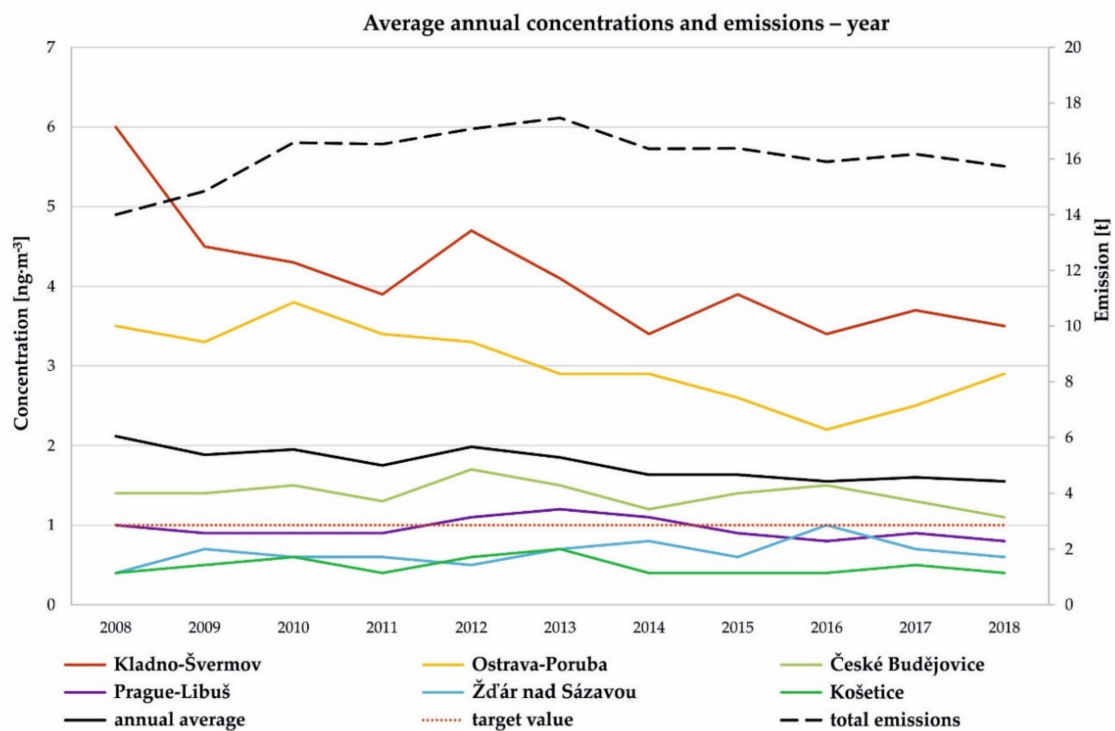


**Figure 8.** Annual average concentrations of BaP at selected monitoring sites and emissions in the Czech Republic, 2008–2018.

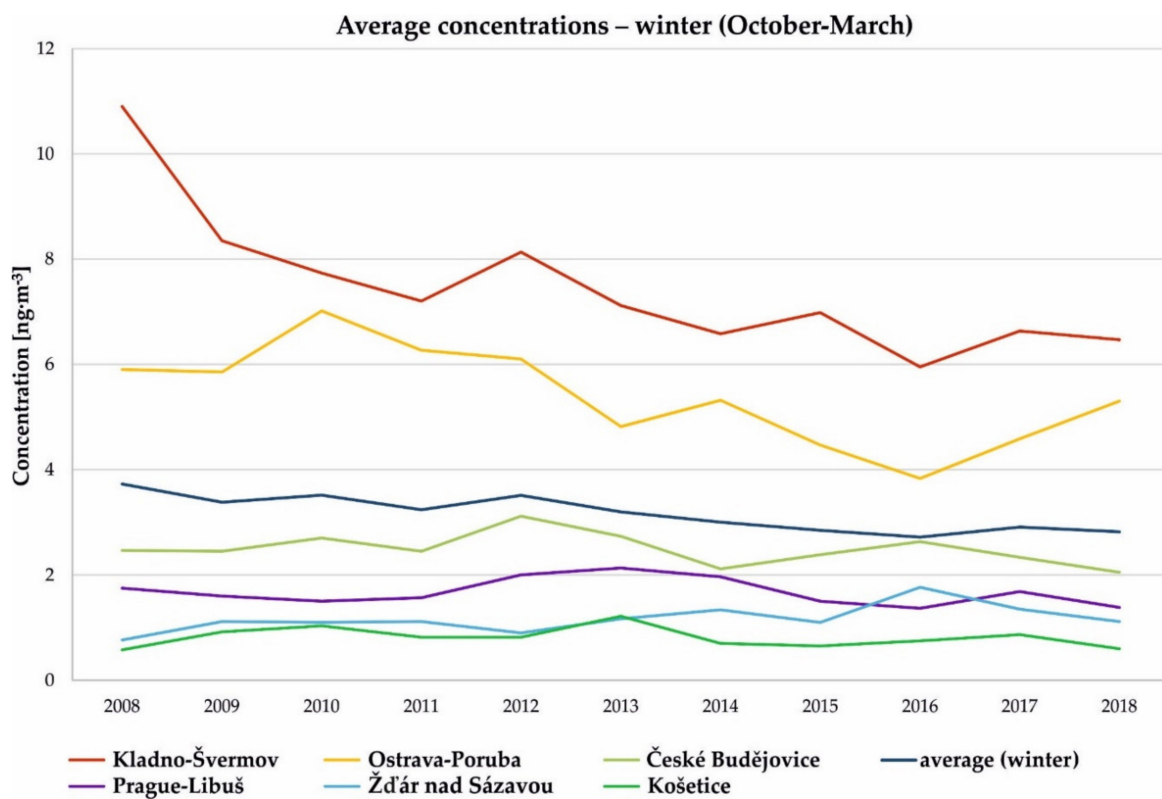


**Figure 9.** Winter average concentrations of BaP at selected monitoring sites and emissions in the Czech Republic, 2008–2018.

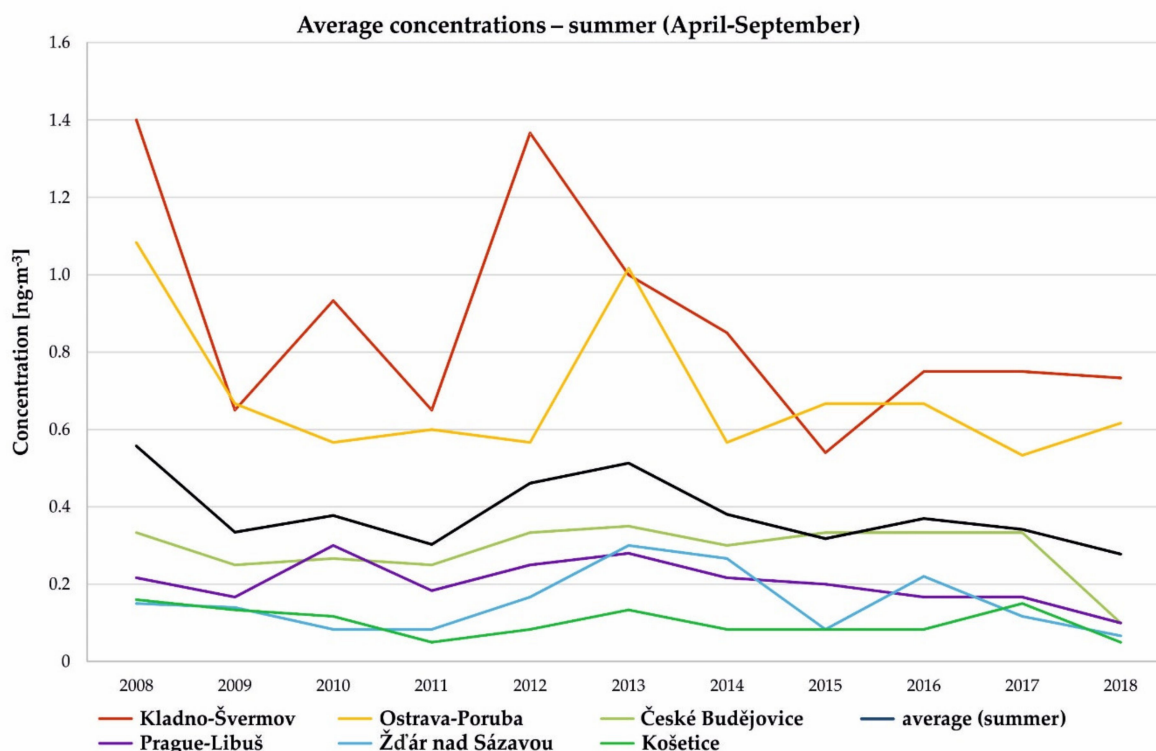


**Figure 10.** Summer average concentrations of BaP at selected monitoring sites in the Czech Republic, 2008–2018.

The Mann–Kendall test was used to assess the monotonic trend of BaP at selected monitoring sites (Table 2). Concerning annual averages, significant decreasing trends were detected at two stations (Kladno-Švermov with  $p$  value = 0.01 and Sen's slope of  $-0.15 \text{ ng}\cdot\text{m}^{-3}\cdot\text{year}^{-1}$  and Ostrava-Poruba with  $p$  value < 0.005 and Sen's slope of  $-0.12 \text{ ng}\cdot\text{m}^{-3}\cdot\text{year}^{-1}$ ). Concerning winter averages, the significant decreasing trend was detected at the same stations—Kladno-Švermov with  $p$ -Value < 0.005 and Sen's slope of  $-0.28 \text{ ng}\cdot\text{m}^{-3}\cdot\text{year}^{-1}$ , Ostrava-Poruba with  $p$ -Value = 0.03 and Sen's slope of  $-0.21 \text{ ng}\cdot\text{m}^{-3}\cdot\text{year}^{-1}$ .

The average annual and average winter concentrations overall for all stations exhibited a significant decreasing trend. The decrease per year in the BaP concentration was equal to  $0.05 \text{ ng}\cdot\text{m}^{-3}$  for annual averages and  $0.09 \text{ ng}\cdot\text{m}^{-3}$  for winter averages, respectively. For urban and suburban stations, the annual and average winter concentrations showed a similar significant decrease is similar— $0.06 \text{ ng}\cdot\text{m}^{-3}$  for annual averages and  $0.11 \text{ ng}\cdot\text{m}^{-3}$  for winter averages, respectively. No clear trend was found for BaP summer concentrations.

In terms of total BaP emission for the Czech Republic, 2013 was the year with the highest annual mean value, which was 17.5 t. BaP emissions increased by more than 11% between 2009 and 2010. This increase was due to the implementation of new statistical data for hard coal consumption from 2010. In addition, the years 2010 and 2013 were characterized by long and cold heating season compared to other years. After 2013, BaP emissions had a decreasing trend supported by milder winter seasons (especially 2014 and 2018) but also by decreasing coal consumption and especially the replacement of high-emission boilers. Consequently, no significant trend ( $p$ -Value = 0.88) was found for BaP emission development (for more details, see Section 3.1). Moreover, no correlation ( $p$ -Value = 0.054) was found between emission and the concentrations from the Košetice rural regional site representing background levels in the Czech Republic.

**Table 2.** The Mann–Kendall test to assess the monotonic trend and Sen’s slope assessment for BaP during 2008–2018.

| Station              | Mann-Kendall (tau) | Sen’s Slope<br>(ng·m <sup>-3</sup> ·year <sup>-1</sup> ) | p-Value  |
|----------------------|--------------------|--|----------|
| <b>YEAR</b>          |                    |  |          |
| Kladno-Švermov       | −0.65              | −0.15  | 0.01 *   |
| Ostrava-Poruba       | −0.70              | −0.12  | <0.005 * |
| České Budějovice     | −0.27              |  | 0.30     |
| Prague-Libuš         | 0.31               |  | 0.25     |
| Ždár nad Sázavou     | 0.32               |  | 0.22     |
| Košetice             | −0.13              |  | 0.67     |
| Average all stations | −0.76              | −0.05  | <0.005 * |
| Average UB/SUB st.   | −0.76              | −0.06  | <0.005 * |
| <b>WINTER</b>        |                    |  |          |
| Kladno-Švermov       | −0.78              | −0.28  | <0.005 * |
| Ostrava-Poruba       | −0.53              | −0.21  | 0.03 *   |
| České Budějovice     | −0.37              |  | 0.14     |
| Prague-Libuš         | −0.26              |  | 0.31     |
| Ždár nad Sázavou     | 0.47               |  | 0.06     |
| Košetice             | −0.18              |  | 0.48     |
| Average all stations | −0.78              | −0.09  | <0.005 * |
| Average UB/SUB st.   | −0.75              | −0.11  | <0.005 * |
| <b>SUMMER</b>        |                    |  |          |
| Kladno-Švermov       | −0.32              |  | 0.21     |
| Ostrava-Poruba       | −0.25              |  | 0.34     |
| České Budějovice     | 0.08               |  | 0.80     |
| Prague-Libuš         | −0.43              |  | 0.08     |
| Ždár nad Sázavou     | −0.11              |  | 0.69     |
| Košetice             | −0.33              |  | 0.20     |
| Average all stations | −0.35              |  | 0.16     |
| Average UB/SUB st.   | −0.35              |  | 0.16     |

\* Significant trend.

### 3.4. Source Apportionment

The transboundary contribution to annual average concentration, as estimated by the CAMx model in its 4.7-km resolution grid mode, is 46–70% for most (80%) of the territory of the Czech Republic, with a median value of 57% (Figure 11). The highest transboundary contribution is modeled in the relatively clean Western and Southern parts of the country and in the North-Eastern mountain regions (cf. Figure 5). When subgrid scaling is applied, the contribution of Czech sources can exceed 80% in residential heating hot spots (Figure 12). Three categories of Czech sources with a relative contribution to annual average concentration exceeding 10% were identified: residential heating—the absolutely dominant Czech source on most of the Czech territory; road transport—only in large cities Prague and Brno and in vicinity of major roads; and coke oven plants in the Ostrava agglomeration.

When mapped annual average BaP concentration is multiplied by the relative contribution of transboundary sources, regions in the North-East parts of the Czech Republic are still above 1 ng·m<sup>-3</sup>, which indicates that the target value cannot be reached without significant reduction of BaP emissions in Poland in hand with measures to mitigate Czech sources.

The reliability of source apportionment results depends of course heavily on the emission inventory and dispersion model used. As stated above, BaP was treated as passive pollutant in CAMx, which can probably lead to overestimation of long range transport due to neglect of its degradation. Nevertheless, emission inventory plays probably the more important role. At the beginning of our modeling effort in 2017, there was only a limited amount of European-scale BaP emission inventory available that could

be used in air quality models (authors were aware of [46]; gridded BaP emissions for 2015 were made available by EMEP in December 2017 and marked as unofficial data evaluation purposes only [47]). For this reason we used a top-down inventory based on [41].

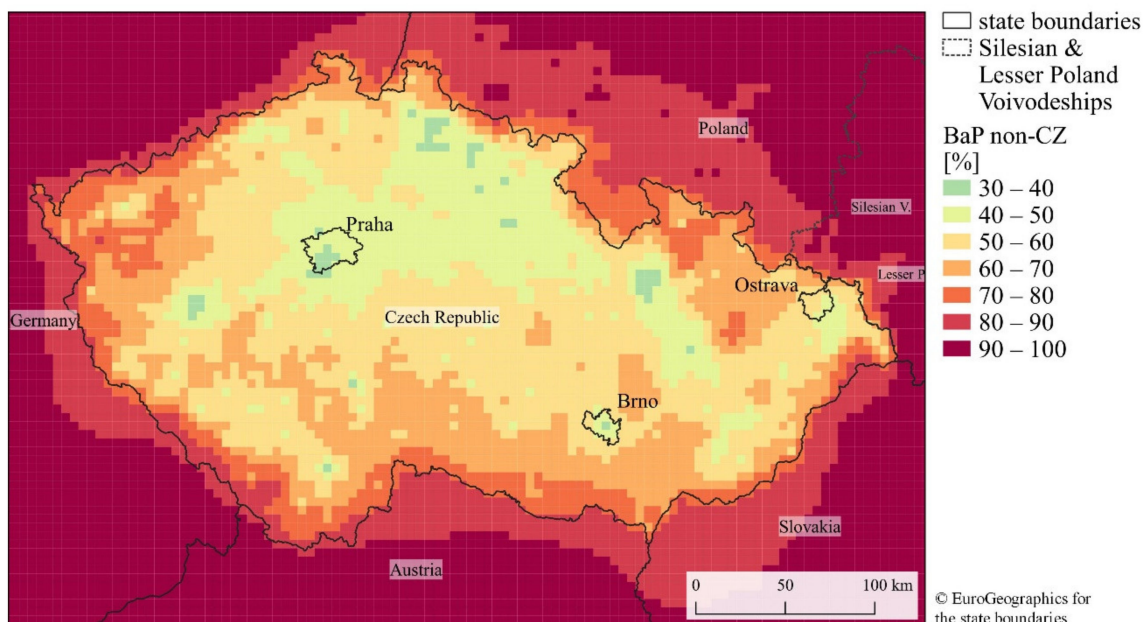


**Figure 11.** Relative contribution of transboundary sources to annual average BaP concentration in 2015 (CAMx model, 4.7-km grid).

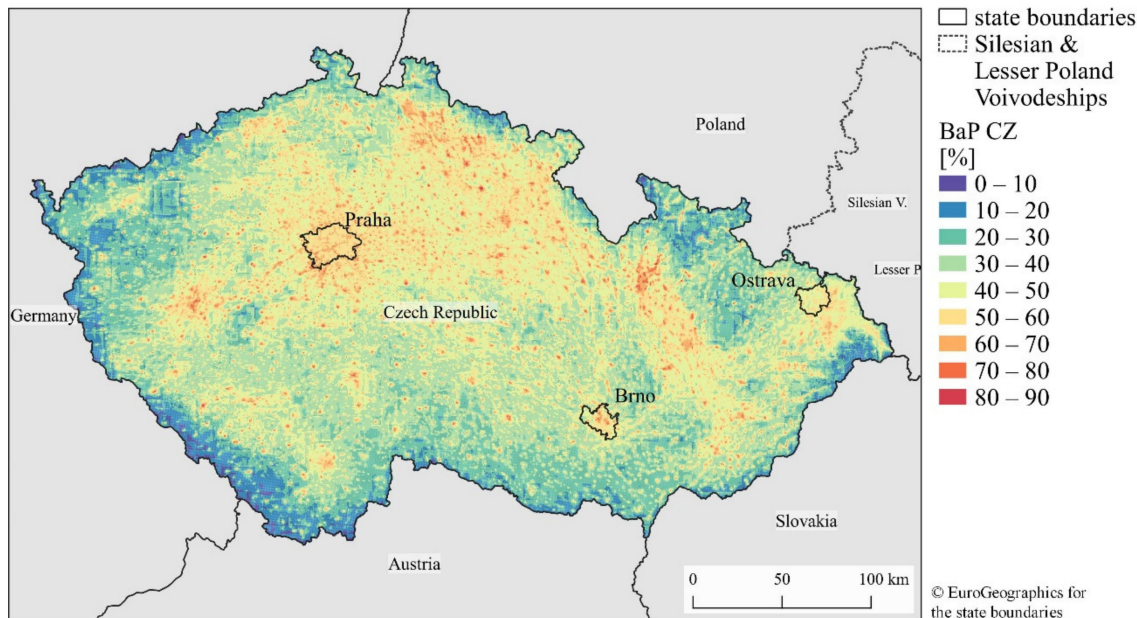


**Figure 12.** Relative contribution of Czech sources to annual average benzo[a]pyrene concentration in 2015 (CAMx model rescaled by the SYMOS model to 0.5-km grid).

Annual average BaP concentration modeled by the CAMx domain d02 was compared with measurements. Annual statistics at station locations were taken from Air Quality e-Reporting [48]. Statistics for the Czech stations were taken from the CHMI’s Air Quality Information System, since there was an error in data provided to the AQ e-Reporting. Since annual statistic in AQ e-Reporting do not include information on station classification, all available data marked as valid and verified were used.

As can be seen from Figures A3 and A4 and Table A7 in Appendix E, we get the best agreement with observations for the Czech stations (model/observation 0.3–3.6 with median 1.5). For Poland, values are generally underestimated (model/observation 0.1–1.5 with median 0.4), while for Germany and Austria the model largely overestimates measured values (model/observation 4–17.7 with median 5 for Germany and 1.9–26.1 with median 7.8 for Austria). This results in a clear South-West to North-East gradient in model bias. It seems reasonable to expect that the model bias will lead to overestimation of the transboundary contribution in the Southern part of the Czech Republic and to its underestimation in Northern parts (especially in the Ostrava agglomeration). To confirm this assumption, the transboundary contribution to annual average BaP concentrations was compared with data provided by EMEP/MSCE-E [23] (transboundary contribution to annual mean concentration provided via personal communication with A. Gusev). For this purpose, CAMx results were aggregated to the EMEP 50-km grid. From Figure A5 we can see that over approximately one third of the Czech Republic the transboundary contribution estimated by this study and by EMEP does not differ by more than 5% (absolute difference). Compared to the EMEP results, the transboundary contribution in the South-central part of the Czech Republic is 10–20% higher, while in the Ostrava agglomeration it is 5–7% lower. Nevertheless it must be noted that EMEP results are based on EMEP/CEIP gridded emission for 2015 [47], where the total BaP emissions for the Czech Republic were estimated to be 8 t based on the Czech 2017 submission. This number was corrected to 16 t in resubmission in 2019. Therefore, the contribution of Czech sources must be underestimated approximately by a factor of two in EMEP results leading to overestimation of relative transboundary contributions by a factor of 1.1–1.6. From the text above it seems likely that modeling only the dispersion of BaP can lead to an overestimation of the transboundary contribution of BaP in the Czech Republic by factor of 1.5.

#### 4. Discussion

Transport, industry and services combined do not contribute more than 2% to BaP emissions. The main source of BaP emissions in the Czech Republic is overwhelmingly local heating, especially the combustion of solid fuels in older types of boiler constructions with over-fire and under-fire type of burners (Figures 3 and 4). Compared to other European countries, the Czech Republic has the second highest average BaP emission per capita from the residential sector (1.5 g/(person-year)). The highest average emission is in Poland (1.6 g/(person-year)) whereas the EU average is 0.4 g/(person-year) [49].

The main reason for a high share of BaP emissions from local heating in the Czech Republic is specifically the combustion of solid fuel in older type of boilers (over-fire and under-fire). However, these types of boilers are being gradually replaced by low-emission boilers or by other types of heating. In 2018, the share of over-fire and under-fire boilers was estimated to be around 69%. These replacements are being accelerated by the legislative requirements of Act 201/2012 Coll. [50] that stipulates that after September 2022 only low-emission boilers meeting the parameters of at least 3rd boiler class (as defined in the EN 303-5:2012 [51]) can be in operation for solid fuel combustion in households. The replacement of old boilers was supported by a subsidy program between 2015 and 2019, with the aim of replacing up to 100,000 high-emission boilers. However, replacement of the boiler itself is not a guarantee of efficient emission reduction if the boiler is not operated properly in accordance with operating instructions.

The range of measured concentration of BaP was from  $0.4 \text{ ng}\cdot\text{m}^{-3}$  at a rural regional station to  $7.7 \text{ ng}\cdot\text{m}^{-3}$  at an industrial station in 2018. The area where BaP concentrations exceeded the target value was 12.6% in 2018 (Figure 5). The highest annual average concentrations of BaP have long been recorded throughout the entire Ostrava Region. In this region, there is the highest emission load due to a combination of local heating and the largest share of heavy industry in the Czech Republic. The transboundary contribution in the Ostrava region was estimated to be 40–60% but may be in fact somewhat lower due to model limitations. High BaP concentration values due to the effect of local heating systems have also been monitored in Kladno for a long time. Concentrations exceeding the target value for BaP also occur in Central Bohemia and in a number of municipalities. The values of

BaP concentration show that the ambient air concentrations of BaP are high in the Czech Republic in general, which is consistent with the model study of Europe [11], where the authors pointed out the ambient air concentrations of BaP to be substantially high in Central and Central Eastern Europe but also in some other European regions.

Relatively low levels of BaP have been recorded in large cities, like in the center of Helsinki [52] and in Porto [28]. In Porto, transport was identified as the main source of PAHs based on diagnostic ratios. In street canyons in Helsinki, the measured concentrations of BaP were at the same level as those in the urban background and clearly lower than those in suburban detached-house areas. These results indicate that local traffic has only a minor effect on BaP concentrations, compared with the corresponding effect of small-scale combustion. In the Czech Republic, transport is also a minor emission source of BaP (0.8%); nevertheless, levels of BaP concentrations in Prague were higher than in Porto and in street canyons in Helsinki. The higher BaP concentrations in Prague (Table 1) were caused by regional and long-range transport, especially in the center of the city in areas with a high proportion of remote central heating, where the main emission source of BaP is traffic. In suburban Prague, local heating was as important as it was in suburban Helsinki [52].

The lowest average annual concentrations are estimated at places distant from direct exposure to emission sources (natural mountain areas). The lowest measured BaP concentrations, ranging from 0.3 to 0.7 ng·m<sup>-3</sup>, have been recorded at the Košetice regional station. Nevertheless, these values are still relatively high (Table 1) and are above the WHO reference value (0.12 ng·m<sup>-3</sup>). These relative high values of BaP concentrations at a regional background station pointed out the important role of regional and long range transport in the Czech Republic. The importance of regional transport is related to the high contribution of coal combustion to BaP emissions (about 30–40%) and the long lifetime of BaP derived from coal combustion in the atmosphere as found in this study [35].

Moreover, no correlation between background BaP concentration at Košetice and emission was found. The same (lowest) value of background BaP concentration in 2008, 2011, 2014 and 2016–2018 supports our conclusion on the combined effects of emission, meteorological and dispersion conditions and transboundary contributions. Based on the CHMI data, the last four years 2015–2018 of the study period are also years with the highest ratio of good meteorological and dispersion conditions and with BaP emissions decreasing after their peak in 2013. The year 2014 can be characterized by a milder winter season and the shortest heating season for many years [22]. In contrast, the beginning of the study period could be characterized by the greater presence of moderately poor and poor dispersion conditions [53] and the lowest BaP emissions in the study period (Table 1).

Since the higher BaP concentrations are a problem in urban and suburban areas due to local heating, we chose five urban and suburban sites in the Czech Republic for the current concentration level and trend assessment. The sixth rural regional site represents the background ambient air concentration in the Czech Republic.

The highest annual average value in urban and suburban sites was detected in 2008, the lowest annual average value of 1.8 ng·m<sup>-3</sup> was detected in 2016, 2017 and 2018 with the widest range, from 0.7 to 3.7 ng·m<sup>-3</sup> in 2017. Nevertheless, the lack of correlation of BaP concentration in the five urban and suburban sites and emissions for the whole Czech Republic (mainly from local heating, Figure 8) highlights the possible domination of local influences and the influence of meteorological and dispersion conditions.

We found a significant decreasing trend for average concentrations and winter average concentrations. The development of concentrations from selected stations in the Czech Republic between 2008 and 2014 is comparable to the development of PAHs and BaP concentrations presented in the study of [28] who analyzed data from two suburban sites in Porto between 2004 and 2014. A significant decreasing trend in the framework of their study was also found. A downward trend for all types of stations and at two thirds of total stations over the period 2007–2014 was also presented by EEA [54]. A significant decreasing trend was found at 22% of European rural and urban stations [54].

The decrease in concentrations in the Czech Republic is especially noticeable since 2014 highlighting the influence of milder winter seasons in 2014 and 2018, the prevailing good dispersion conditions in 2015–2018 and decreasing coal consumption in the last few years. The significant decrease at two particular stations (Ostrava-Poruba and Kladno-Švermov) that are among those with the highest concentrations in the Czech Republic (and of course those above target value BaP concentration for the whole study period) point also to the effect of improvements in local heating.

Similarly to other studies [26,55–57], the typical seasonal variation for the BaP concentration has been shown. The BaP concentrations for October–March are more than eight times higher than for April–September. For instance, Albuquerque et al. (2016) [28] found a December–January/June–August ratio of 5 for PAHs for the eleven year study in Porto. The reasons for this are generally known—i.e., seasonal sources as local heating, higher emissions from motor vehicles and less mixing in the atmosphere due to inversions [28,57,58]. During the warmer season, on the other hand, concentrations decrease due to unstable atmospheric conditions favorable towards dispersion, increased chemical and photochemical decomposition of PAHs due to higher levels of solar radiation and higher temperatures and of course also due to decreased emissions from anthropogenic sources [59–61].

High values of daily BaP concentrations in winter months associated with local household heating were also recorded during the 2017–2018 campaign measurements in the small settlements of Bochovice, Černíny and Hřivice (Figure 7), where concentrations of BaP are not regularly monitored and where solid fuel heating predominates. The range of measured BaP concentrations was 0.1–8.0 ng·m<sup>-3</sup> in Černíny, 0.2–9.8 ng·m<sup>-3</sup> in Bochovice, and 1.0–13.6 ng·m<sup>-3</sup> in Hřivice. In particular, measured BaP concentrations in the small settlement of Hřivice were as high as and on some days even higher than in Kladno-Švermov, where some of the highest concentrations of BaP in the Czech Republic were recorded. Every year, concentrations there reach high values and exceed the target value by almost four times. Such high levels of BaP concentrations are caused on the one hand by an extremely high density of buildings, which leads to a higher BaP emission density near the surface, and on the other hand by the fact that the town is located in a shallow valley, which leads to a reduction in dispersion of pollutants during cold days. The limited amount of winter season data obtained by the campaign measurements does not allow for a calculation of annual average concentrations. The target limit value of 1 ng·m<sup>-3</sup> established by European legislation was exceeded in Bochovice, Černíny and Hřivice on 59%, 54% and almost 100% of measurement days, respectively. The measurements in these three small settlements with low-density population clearly indicates that emissions of BaP by local heating influence the short-term BaP concentration in the surroundings. Local meteorological conditions, orography of the populated area and regional and transboundary long-range transport are further factors which influence the ambient air concentration of BaP. In the Czech Republic, due to the rugged terrain, a number of settlements are located in valleys, where there may be a frequent deterioration of dispersion conditions and thus an increase in pollutant concentrations.

The reference level established for BaP by the WHO of 0.12 ng·m<sup>-3</sup> was exceeded at all monitoring sites each year. The target value of 1 ng·m<sup>-3</sup> is set by a European directive (EU, 2004) with the aim of avoiding, preventing, or reducing harmful effects on human health and/or the environment as a whole. During the period of 2012–2018, 35–58% of the urban population in the Czech Republic was found to be exposed to BaP concentrations exceeding the above mentioned target value. The lowest number of inhabitants living in the above-target areas was estimated to be in 2018. The highest number of inhabitants (58%) exposed to above-target concentrations of BaP was estimated for the years 2012 and 2017. On average, only 7% of the population lived in the areas with the lowest concentration of BaP between 2012 and 2018. BaP is carcinogenic to humans and has been considered a good indicator for the assessment of risk to human health associated with exposure from PAHs found in the environment. The individual carcinogenic potencies of PAH in relation to BaP can be expressed through the BaP equivalent concentrations (BaP eq.) and evaluation of BaP alone will probably underestimate the carcinogenic potential of the PAHs mixtures [28,62]. The uncertainty of the map is a result of the inadequate number of measurements at rural regional stations and the absence of more

extensive measurements in smaller settlements in the Czech Republic, where the air pollution by BaP would demonstrate the fundamental effect of local heating units. In addition, the maps are prepared with a resolution of  $1 \times 1$  km and therefore cannot take into account the local fragmentation of the terrain, which in the case of settlements located in valleys affects the levels of pollutants [63]. Thus, assessment of the interannual changes in the territory affected and population exposed to above-limit concentrations of BaP will also be accompanied by a greater margin of error.

## **5. Conclusions**

A complex analysis of air pollution from BaP in the Czech Republic was carried out. Ambient air BaP concentrations and their long-term trends were studied to assess the level of BaP in the Czech Republic. The calculated emissions of BaP and modeling of the transboundary contribution to the annual mean concentrations of BaP were quantified to present the causes of BaP air pollution.

The measured concentrations of BaP are high due to high emission load from the combination of local heating and heavy industry in the Czech Republic. The residential sector is responsible for more than 98.8% of BaP emissions.

Many people (50% on average) in the Czech Republic live in the area where the BaP concentrations are above the target value set by a European directive with the aim of avoiding, preventing, or reducing harmful effects on human health and/or the environment as a whole.

On the basis of the observations in small settlements described above, where BaP concentrations are not regularly monitored and where solid fuel heating predominates, it can be assumed that in small settlements, carcinogenic BaP levels may reach high levels in the short-term. Above-target values where BaP is not routinely measured can also be expected in similar municipalities with a high proportion of local heating using solid fuels. Consequently, the fraction of people living in the above-target value areas will be higher than presented.

Due to the high number of small municipalities and particularly due to the high costs for laboratory analyses and limited capacity of the laboratories, the number of measurement locations will always be limited, and therefore it is desirable to specify in more detail data on emissions and to provide substantial support to modeling.

The transboundary contribution to annual average concentration was estimated to be between 46% and 70% for most (80%) of the territory of the Czech Republic. The contribution of Czech sources can exceed 80% in residential heating hot spots. Results are nevertheless subject to limitations of the modeling approach used—it is likely that the transboundary contribution to BaP concentrations in the Czech Republic was overestimated by a factor of 1.5. Apart from residential heating, two other categories of Czech sources with relative contribution to annual local average concentration exceeding 10% were identified: road transport (large cities and vicinity of major roads) and coke oven plants in the Ostrava agglomeration.

The typical seasonal variation for the BaP concentrations has been shown. The BaP concentrations for selected air quality monitoring stations for October–March were more than eight times higher than for April–September. This is in line with the composition of emission sources in the Czech Republic, with the dominance of the local heating sector and with the different influence of meteorological and dispersion conditions in the colder and warmer parts of the year connected with the atmospheric stability and chemical properties of BaP.

We found significant decreasing trends for average concentrations and winter average concentrations. No correlation between background BaP concentration and emission was found. BaP concentration development in the Czech Republic has been influenced by the combined effect of total emission, meteorological and dispersion conditions and transboundary contributions.

The significant decrease at two particular stations belonging to those with the highest concentrations in the Czech Republic also point out the effect of improvements in local heating infrastructure. To conclude, even assuming generally good dispersion conditions and milder winter

seasons in future, a significant reduction of BaP emissions is needed to reach the target value for BaP in the Czech Republic.

**Author Contributions:** Conceptualization, M.S. and L.V.; formal analysis, M.S., L.V., O.V. and J.Š.; writing—original draft preparation, M.S., L.V., O.V. and J.Š.; writing—review and editing M.S., L.V., O.V., J.Š., J.H., J.B.; visualization, M.S., L.V., O.V. and J.Š.; supervision, M.S. All authors have read and agreed to the published version of the manuscript.

**Funding:** The presented BaP concentrations in small settlements Bochovice, Černíny and Hřivice were measured within the project “TITSMZP704—Measurement and Analysis of Air Pollution with Emphasis on the Evaluation of the Share of Individual Groups of Sources” funded with the state support of the Technology Agency of the Czech Republic under the BETA2 Programme. BaP emissions for regions outside the Czech Republic used for dispersion modeling were prepared within the project LIFE-IP MAŁOPOLSKA—Implementation of Air Quality Plan for Małopolska Region—Małopolska in Healthy Atmosphere (LIFE14 IPE/PL/000021).

**Acknowledgments:** The authors want to thank all colleagues from CHMI who participate in the measurement and processing of air quality data. We would also like to thank Alexey Gusev and Victor Shatalov from EMEP/MSC-E for providing BaP modeling results and for commenting on the text.

**Conflicts of Interest:** The authors declare that there is no conflict of interest regarding the publication of this paper.

## Appendix A

**Table A1.** Specification of monitoring stations of BaP with annual average concentration in 2018.

| Name Station                    | Classification | Longitude | Latitude  | Altitude | Average [ng·m <sup>-3</sup> ] |
|---------------------------------|----------------|-----------|-----------|----------|-------------------------------|
| Brandýs n. Labem                | B/S/R          | 14.660455 | 50.189799 | 179      | 1.6                           |
| Brno-Líšeň                      | B/U/R          | 16.678025 | 49.213212 | 340      | 0.6                           |
| Brno-Masná                      | B/U/CR         | 16.627    | 49.188833 | 214      | 0.5                           |
| Č.Budějovice-Antala Staška      | B/S/R          | 14.469916 | 48.951901 | 386      | 1.1                           |
| Čes. Budějovice-Třešň.          | B/U/R          | 14.508792 | 48.965906 | 410      | NA                            |
| Český Těšín                     | B/U/R          | 18.609726 | 49.748958 | 285      | 3.9                           |
| Doksany                         | B/R/NA-NCI     | 14.170162 | 50.458853 | 158      | 1.3                           |
| Havl.Brod-Smetan.nám.           | B/U/R          | 15.577389 | 49.606417 | 413      | NA                            |
| Hodonín                         | B/U/R          | 17.131389 | 48.857278 | 170      | 0.8                           |
| Hr.Král.-Sukovy sady            | T/U/RCI        | 15.814149 | 50.211702 | 233      | NA                            |
| Hradec Králové - tř. SNP        | B/U/R          | 15.857006 | 50.218533 | 232      | 1                             |
| Jihlava-Znojemská               | T/U/R          | 15.591278 | 49.392444 | 500      | 0.6                           |
| Karviná-ZÚ                      | T/U/R          | 18.557778 | 49.858891 | 251      | 3                             |
| Kladno-Švermov                  | B/U/RI         | 14.106048 | 50.167412 | 219      | 3.5                           |
| Klatovy soud                    | T/U/R          | 13.286923 | 49.400608 | 394      | NA                            |
| Košetice                        | B/R/AN-REG     | 15.080278 | 49.573394 | 535      | 0.4                           |
| Kralupy nad Vltavou-sportoviště | I/U/RCI        | 14.316583 | 50.251417 | 175      | NA                            |
| Kuchařovice                     | B/R/A-NCI      | 16.085817 | 48.881355 | 334      | 0.5                           |
| Liberec Rochlice                | B/U/R          | 15.069967 | 50.7551   | 422      | 1                             |
| Olomouc-Hejčín                  | B/U/R          | 17.238073 | 49.601462 | 224      | 1.3                           |
| Olomouc-Šmeralova               | B/U/R          | 17.266167 | 49.592917 | 220      | 1                             |
| Ostrava-Hrabová                 | I/S/RI         | 18.278806 | 49.778611 | 233      | 3.7                           |
| Ostrava-Kunčičky                | I/S/RI         | 18.2925   | 49.809694 | 212      | 3.4                           |
| Ostrava-Mariánské Hory          | I/U/IR         | 18.263655 | 49.82486  | 225      | 2                             |
| Ostrava-Poruba, DD              | T/U/R          | 18.165222 | 49.835472 | 282      | 2.3                           |
| Ostrava-Poruba/ČHMÚ             | B/S/R          | 18.159276 | 49.825295 | 242      | 2.9                           |
| Ostrava-Přívoz                  | I/U/IR         | 18.269741 | 49.856259 | 207      | 4.7                           |
| Ostrava-Radvanice OZO           | B/S/R          | 18.340389 | 49.818556 | 258      | 4.7                           |
| Ostrava-Radvanice ZÚ            | I/S/IR         | 18.339139 | 49.807057 | 250      | 7.7                           |
| Pardubice Dukla                 | B/U/R          | 15.763549 | 50.024038 | 239      | 0.9                           |
| Pelhřimov                       | B/S/R          | 15.208333 | 49.435    | 528      | NA                            |
| Plzeň-Roudná                    | B/U/R          | 13.381614 | 49.761788 | 337      | NA                            |
| Plzeň-Slovany                   | T/U/RC         | 13.402313 | 49.732443 | 340      | 1.1                           |
| Praha 10-Šrobárova              | B/U/RC         | 14.472661 | 50.07515  | 238      | 0.7                           |

Table A1. Cont.

| Name Station              | Classification | Longitude | Latitude  | Altitude | Average [ng·m <sup>-3</sup> ] |
|---------------------------|----------------|-----------|-----------|----------|-------------------------------|
| Praha 2-Riegrovy sady     | B/U/NR         | 14.442692 | 50.081483 | 256      | 0.7                           |
| Praha 4-Libuš             | B/S/R          | 14.445933 | 50.007304 | 301      | 0.8                           |
| Praha 5-Řeporyje          | B/S/RA         | 14.309517 | 50.030419 | 321      | NA                            |
| Rožd'alovice-Ruská        | B/R/A-NCI      | 15.178303 | 50.301984 | 198      | 1                             |
| Studénka                  | B/R/A-NCI      | 18.089306 | 49.720936 | 231      | 2.8                           |
| Teplíce                   | B/U/R          | 13.85125  | 50.645278 | 257      | 0.9                           |
| Třinec-Konská             | I/S/IRA        | 18.650061 | 49.702427 | 318      | 3.1                           |
| Třinec-Nebory             | B/S/RNI        | 18.628415 | 49.683714 | 331      | 2.4                           |
| Ústí n. L.-Prokopa Diviše | I/U/RCI        | 14.031243 | 50.662979 | 155      | NA                            |
| Ústí n.L.-Kočkov          | B/S/RN         | 14.041195 | 50.683524 | 367      | 0.5                           |
| Valašské Meziříčí         | B/U/R          | 17.966976 | 49.472059 | 290      | 2.2                           |
| Vratimov                  | I/S/RI         | 18.318472 | 49.769806 | 261      | 4                             |
| Zlín                      | B/S/RN         | 17.667175 | 49.232905 | 258      | 1.2                           |
| Ždár nad Sázavou          | B/U/RC         | 15.941    | 49.564556 | 569      | 0.6                           |

NA—not available data for annual average calculation.

## Appendix B

Table A2. Fuel consumption in residential sector 2008–2018.

| Fuel Type       | Fuel Consumption [TJ/year] |         |         |         |         |         |         |         |         |         |         |
|-----------------|----------------------------|---------|---------|---------|---------|---------|---------|---------|---------|---------|---------|
|                 | 2008                       | 2009    | 2010    | 2011    | 2012    | 2013    | 2014    | 2015    | 2016    | 2017    | 2018    |
| Brown coal      | 27,707                     | 28,967  | 30,756  | 33,466  | 30,516  | 33,209  | 27,822  | 27,216  | 26,794  | 28,724  | 25,043  |
| Briquetness     | 3307                       | 4245    | 4121    | 2628    | 2924    | 2944    | 2470    | 2411    | 2371    | 3062    | 3241    |
| Hard coal       | 2275                       | 2659    | 7961    | 6212    | 9748    | 8692    | 8515    | 9332    | 9147    | 9318    | 8985    |
| Coke            | 676                        | 1102    | 1018    | 872     | 916     | 870     | 873     | 882     | 865     | 889     | 825     |
| Wood—dry        | 30,614                     | 32,438  | 33,335  | 34,320  | 35,756  | 37,140  | 37,872  | 38,425  | 38,746  | 39,336  | 41,039  |
| Wood—wet        | 25,615                     | 27,141  | 27,891  | 28,716  | 29,918  | 31,076  | 31,688  | 32,151  | 32,419  | 32,912  | 34,338  |
| Bio-briquetness | 476                        | 857     | 1156    | 1197    | 1333    | 1469    | 1700    | 1700    | 2040    | 2210    | 1918    |
| Pellets         | 391                        | 476     | 799     | 850     | 850     | 935     | 1020    | 1122    | 1190    | 1360    | 1530    |
| Natural gas     | 85,789                     | 86,803  | 99,745  | 83,837  | 84,713  | 84,990  | 68,873  | 74,919  | 83,471  | 83,924  | 78,663  |
| LPG             | 1424                       | 1195    | 1057    | 1378    | 1930    | 1700    | 1976    | 1976    | 1976    | 1976    | 2205    |
| Total           | 178,273                    | 185,883 | 207,837 | 193,475 | 198,604 | 203,026 | 182,809 | 190,133 | 199,019 | 203,710 | 197,787 |

Source: CZSO [13].

Table A3. Emission factors of BaP for local heating at nominal heat output.

| Fuel Type       | Over-Fire Boilers [mg/GJ] | Under-Fire Boilers [mg/GJ] | Automatic Boilers [mg/GJ] | Gasification Boilers [mg/GJ] | Stoves [mg/GJ] | –[mg/GJ] | Reference |
|-----------------|---------------------------|----------------------------|---------------------------|------------------------------|----------------|----------|-----------|
| Brown coal      | 384.6                     | 124.4                      | 0.1                       | 0.7                          | 384.6          |          | [64]      |
| Briquetness     | 106.6                     | 21.8                       | 0.1                       | 0.7                          | 106.6          |          | [64]      |
| Hard coal       | 316.2                     | 186.0                      | 0.1                       | 39.2                         | 316.2          |          | [64]      |
| Coke            | 316.2                     | 186.0                      | 0.1                       | 39.2                         | 316.2          |          | [64]      |
| Wood—dry        | 92.1                      | 68.0                       | 0.2                       | 17.5                         | 92.1           |          | [64]      |
| Wood—wet        | 230.6                     | 68.0                       | 0.2                       | 2.9                          | 230.6          |          | [64]      |
| Bio-briquetness | 92.1                      | 68.0                       | 0.2                       | 17.5                         | 92.1           |          | [64]      |
| Pellets         | 92.1                      | 68.0                       | 0.2                       | 17.5                         | 92.1           |          | [64]      |
| Natural gas     |                           |                            |                           |                              |                | 0.00056  | [17]      |
| Fuel oil        |                           |                            |                           |                              |                | 0.08     | [17]      |

**Table A4.** Emission factors of BaP for local heating at lower heat output.

| Fuel Type       | Over-Fire Boilers [mg/GJ] | Under-Fire Boilers [mg/GJ] | Automatic Boilers [mg/GJ] | Gasification Boilers [mg/GJ] | Stoves [mg/GJ] | –[mg/GJ] | Reference |
|-----------------|---------------------------|----------------------------|---------------------------|------------------------------|----------------|----------|-----------|
| Brown coal      | 276.0                     | 134.4                      | 4.8                       | 7.3                          | 276.0          |          | [64]      |
| Briquettest     | 106.6                     | 21.8                       | 4.8                       | 7.3                          | 106.6          |          | [64]      |
| Hard coal       | 504.8                     | 29.5                       | 2.7                       | 39.2                         | 504.8          |          | [64]      |
| Coke            | 504.8                     | 29.5                       | 2.7                       | 39.2                         | 504.8          |          | [64]      |
| Wood—dry        | 253.7                     | 97.8                       | 1.4                       | 9.0                          | 253.7          |          | [64]      |
| Wood—wet        | 191.3                     | 75.0                       | 1.4                       | 52.5                         | 191.3          |          | [64]      |
| Bio-briquettest | 253.7                     | 97.8                       | 1.4                       | 9.0                          | 253.7          |          | [64]      |
| Pellets         | 253.7                     | 97.8                       | 1.4                       | 9.0                          | 253.7          |          | [64]      |
| Natural gas     |                           |                            |                           |                              |                | 0.00056  | [17]      |
| Fuel oil        |                           |                            |                           |                              |                | 0.08     | [17]      |

**Table A5.** Distribution of solid fuel consumption according to the type of heating equipment in 2018.

| Fuel Type       | Over-Fire Boilers [%] | Under-Fire Boilers [%] | Automatic Boilers [%] | Gasification Boilers [%] | Stoves [%] |
|-----------------|-----------------------|------------------------|-----------------------|--------------------------|------------|
| Brown coal      | 25                    | 31                     | 31                    | 8                        | 5          |
| Briquettest     | 55                    | 21                     | 6                     | 4                        | 14         |
| Hard coal       | 55                    | 14                     | 21                    | 5                        | 5          |
| Coke            | 89                    | 8                      | 1                     | 0                        | 2          |
| Wood—dry        | 32                    | 17                     | 4                     | 17                       | 30         |
| Wood—wet        | 33                    | 14                     | 3                     | 12                       | 38         |
| Bio-briquettest | 17                    | 9                      | 5                     | 10                       | 59         |
| Pellets         | 0.5                   | 0.5                    | 54                    | 0                        | 45         |

**Table A6.** Comparison of BaP emissions from residential sector calculated in top-down and bottom-up model 2008–2018.

| Reporting Year | BaP Emissions [t]    |                      | Emission Difference (Bottom-Up/Top-Down) |      | Number of Heating Degree Days |
|----------------|----------------------|----------------------|--|------|-------------------------------|
|                | Top-Down (Reporting) | Bottom-Up (Modeling) | [t]                                      | [%]  |                               |
| 2018           | 15.6                 | 14.1                 | –1.5                                     | –10% | 3684                          |
| 2017           | 16.0                 | 16.1                 | 0.2                                      | 1%   | 4138                          |
| 2016           | 15.7                 | 16.0                 | 0.3                                      | 2%   | 4053                          |
| 2015           | 16.2                 | 15.6                 | –0.6                                     | –4%  | 3892                          |
| 2014           | 16.2                 | 14.5                 | –1.6                                     | –11% | 3611                          |
| 2013           | 17.3                 | 17.5                 | 0.2                                      | 1%   | 4310                          |
| 2012           | 16.9                 | 17.1                 | 0.2                                      | 1%   | 4208                          |
| 2011           | 16.3                 | 16.1                 | –0.2                                     | –1%  | 3970                          |
| 2010           | 16.4                 | 17.1                 | 0.7                                      | 4%   | 4567                          |
| 2009           | 14.6                 | 14.3                 | –0.3                                     | –2%  | 3952                          |
| 2008           | 13.8                 | 14.4                 | 0.6                                      | 4%   | 3973                          |

Appendix C

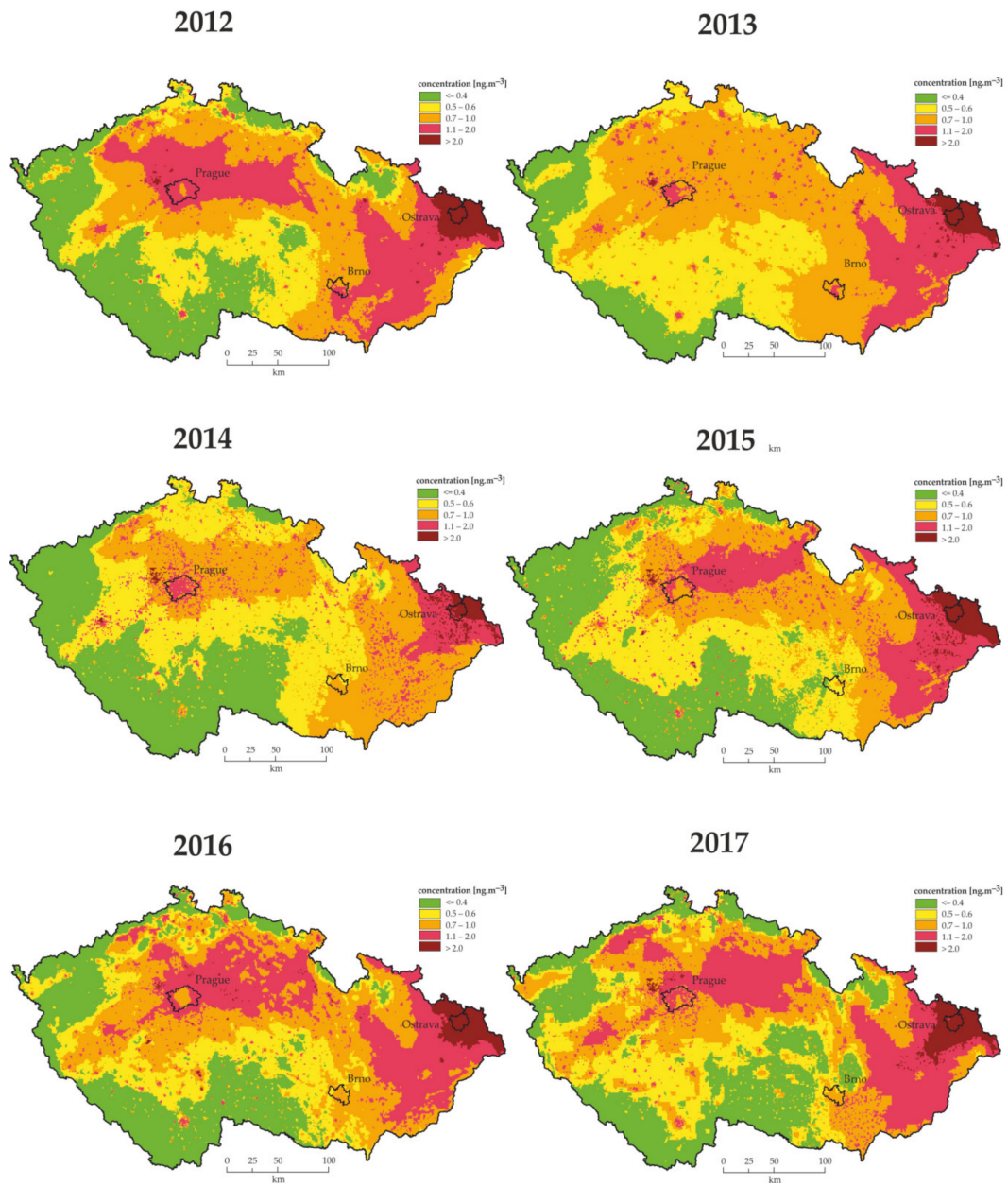


Figure A1. Field of annual average concentration of benzo[a]pyrene in the Czech Republic, 2012–2017.

Appendix D

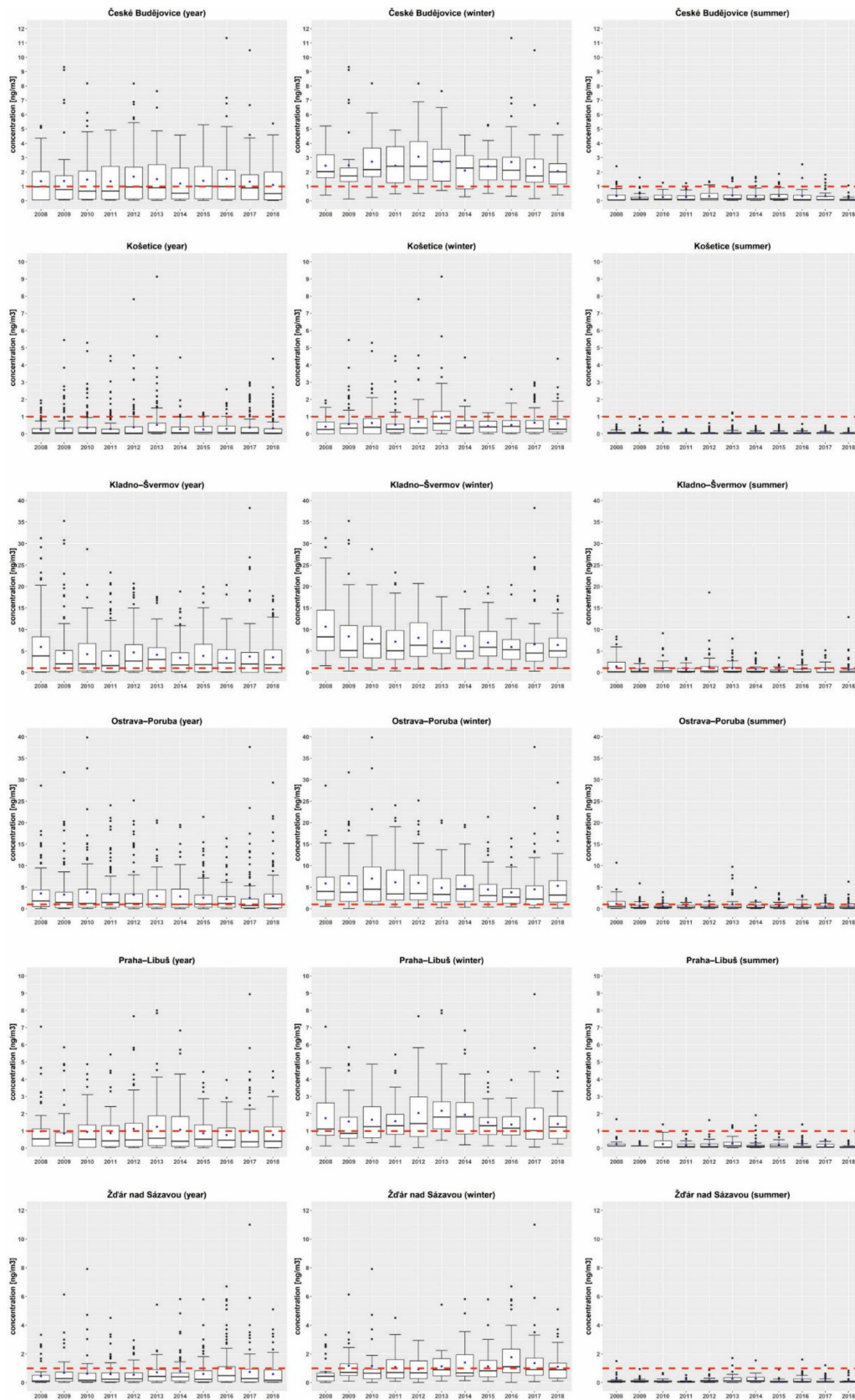
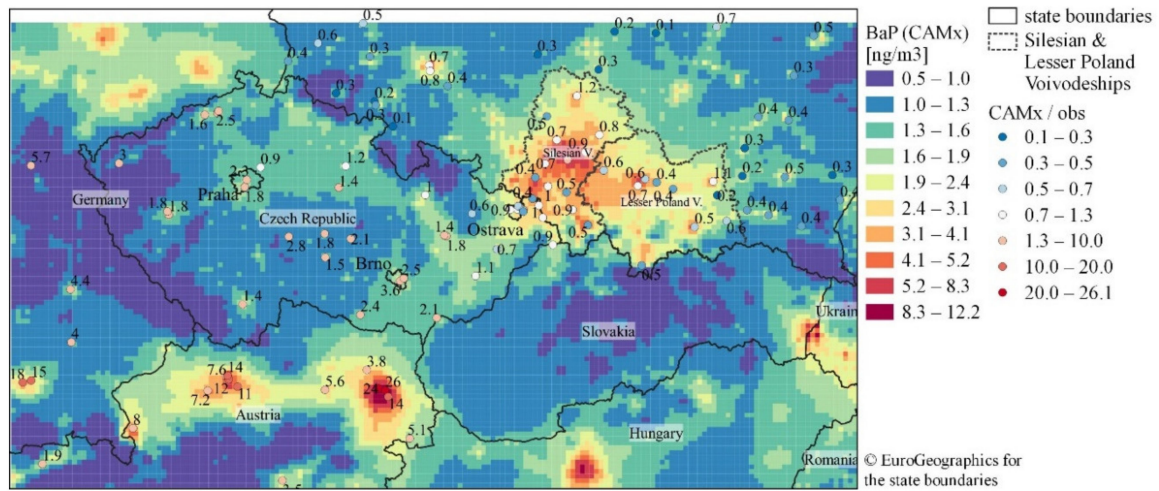
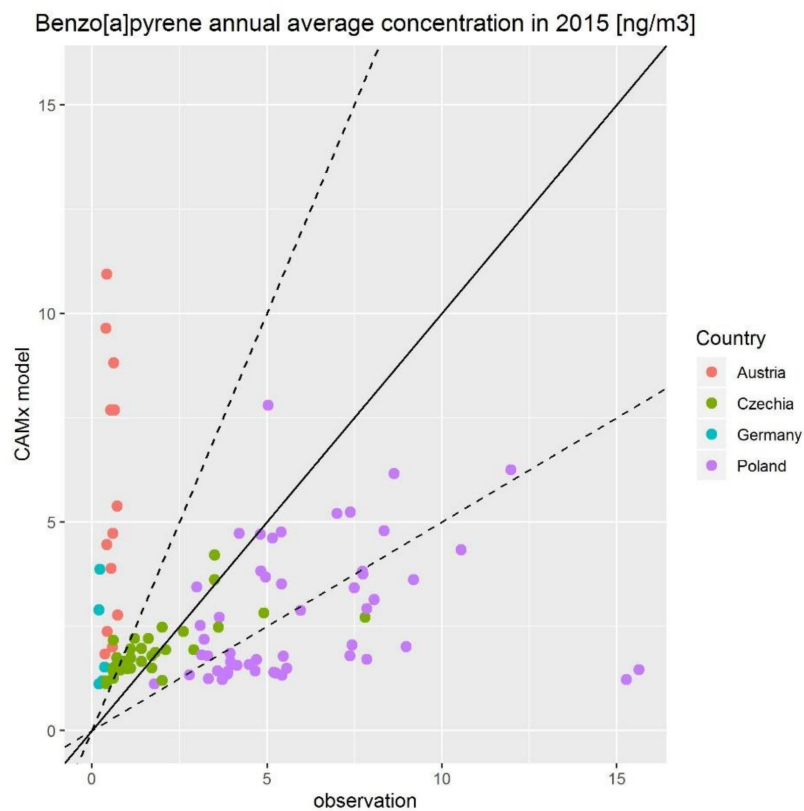


Figure A2. Boxplots of BaP concentrations at selected monitoring sites, 2008–2018.

Appendix E



**Figure A3.** Annual average benzo[a]pyrene concentration in 2015 (CAMx model) and ratio of measured and modeled concentration at station locations.



**Figure A4.** Scatter plot of modeled and measured annual average benzo[a]pyrene concentrations in 2015 for CAMx domain d02. Solid line denotes ideal model equal to observation, dashed lines mark area, where model values are within a factor of two from observations.

**Table A7.** Ratio of modeled and measured annual average benzo[a]pyrene concentration.

| Country        | Number of Stations | CAMx/Measurement |         |        |      |         |      |
|----------------|--------------------|------------------|---------|--------|------|---------|------|
|                |                    | Min              | 1st Qu. | Median | Mean | 3rd Qu. | Max  |
| Germany        | 5                  | 4.0              | 4.4     | 5.7    | 9.4  | 15.4    | 17.7 |
| Austria        | 14                 | 1.9              | 5.2     | 7.8    | 10.4 | 13.8    | 26.1 |
| Czech Republic | 34                 | 0.3              | 1.0     | 1.5    | 1.6  | 2.0     | 3.6  |
| Poland         | 52                 | 0.1              | 0.3     | 0.4    | 0.5  | 0.7     | 1.5  |

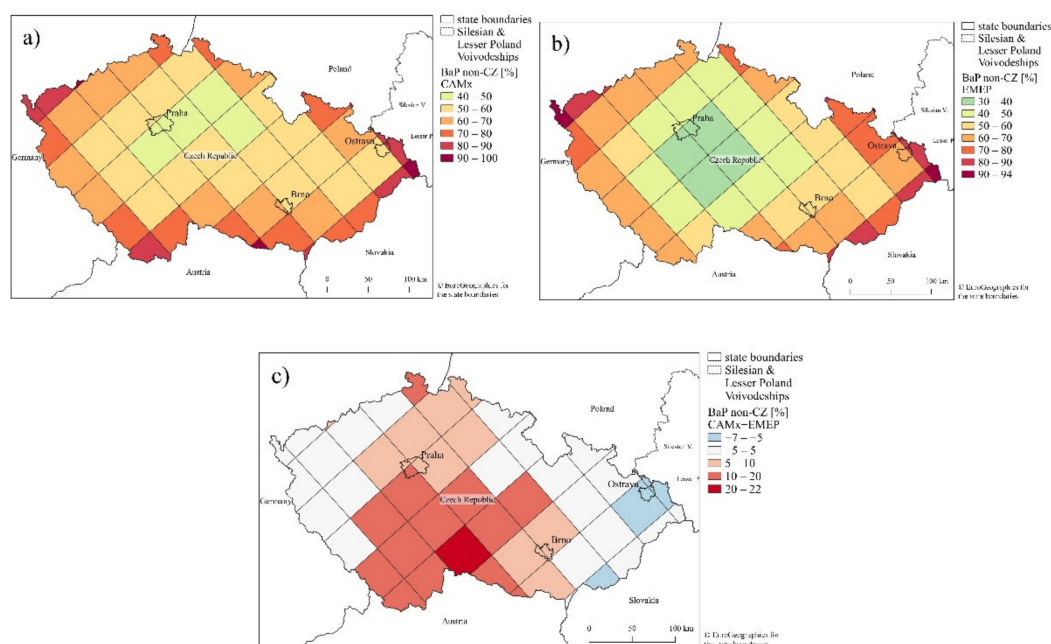


**Figure A5.** Relative contribution of transboundary sources to annual average benzo[a]pyrene concentration in 2015: (a) CAMx model averaged on EMEP grid, (b) EMEP model, and (c) difference CAMx–EMEP.

**References**

1. Abdel-Shafy, H.I.; Mansour, M.S.M. A review on polycyclic aromatic hydrocarbons: Source, environmental impact, effect on human health and remediation. *Egypt. J. Pet.* **2016**, *25*, 107–123. [CrossRef]
2. Choi, H.; Jedrychowski, W.; Spengler, J.; Camann, D.E.; Whyatt, R.M.; Rauh, V.; Tsai, W.Y.; Perera, F.P. International Studies of Prenatal Exposure to Polycyclic Aromatic Hydrocarbons and Fetal Growth. *Environ. Health Perspect.* **2006**, *114*, 1744–1750. [CrossRef]
3. WHO. *Air Quality Guidelines for Europe*, 2nd ed.; WHO Regional Office for Europe: Copenhagen, Denmark, 2000; pp. 92–97.
4. Edwards, S.C.; Jedrychowski, W.; Butscher, M.; Camann, D.; Kieltyka, A.; Mroz, E.; Flak, E.; Li, Z.; Wang, S.; Rauh, V. Prenatal exposure to airborne polycyclic aromatic hydrocarbons and children’s intelligence at 5 years of age in a prospective cohort study in Poland. *Environ. Health Perspect.* **2010**, *118*, 1326–1331. [CrossRef] [PubMed]
5. Daly, G.; Wania, F. Organic Contaminants in Mountains. *Environ. Sci. Technol.* **2005**, *39*, 385–398. [CrossRef] [PubMed]
6. Sofowote, U.M.; Hung, H.; Rastogi, A.K.; Westgate, J.N.; Deluca, P.F.; Su, Y.; McCarry, B.E. Assessing the long-range transport of PAH to a sub-Arctic site using positive matrix factorization and potential source contribution function. *Atmos. Environ.* **2001**, *45*, 967–976. [CrossRef]
7. Tamamura, S.; Sato, T.; Ota, Y.; Wang, X.; Tang, N.; Hayakawa, K. Long-range transport of polycyclic aromatic hydrocarbons (PAHs) from the eastern Asian continent to Kanazawa, Japan with Asian dust. *Atmos. Environ.* **2007**, *41*, 2580–2593. [CrossRef]

8. EU. Directive 2004/107/EC of the European Parliament and of the Council of 15 December 2004 Relating to Arsenic, Cadmium, Mercury, Nickel and Polycyclic Aromatic Hydrocarbons in Ambient Air. OJ L 23, 26.1; European Environment Agency: Copenhagen, Denmark, 2005; pp. 3–16.
9. WHO. WHO Guidelines for Indoor Air Quality: Selected Pollutants, 1st ed.; World Health Organization, European Centre for Environment and Health: Bonn, Germany, 2010; pp. 289–347.
10. ETC/ACM. Evaluation of Current Limit and Target Values as Set in the EU Air Quality Directive, Technical Paper 2011/3; The European Topic Centre on Air Pollution and Climate Change Mitigation: Bilthoven, The Netherlands, 2011; pp. 25–26.
11. Guerreiro, C.B.B.; Horálek, J.; de Leeuw, F.; Couvidat, F. Benzo(a)pyrene in Europe: Ambient air concentrations, population exposure and health effects. *Environ. Pollut.* **2016**, *214*, 657–667. [CrossRef] [PubMed]
12. EEA. Air Quality in Europe—2019 Report; EEA Report No. 10/2019; European Environment Agency: Copenhagen, Denmark, 2019.
13. Available online: <https://www.czso.cz/csu/czso/home> (accessed on 3 July 2020).
14. Available online: <http://portal.chmi.cz/> (accessed on 3 July 2020).
15. Tyle, P. Přehled o Dodávkách a Jakosti Tuhých Paliv na Uzemí ČR v Roce 2018 Pro Učely Registrů Emisních Zdrojů. (An Overview of the Supply and Quality of Solid Fuels in the Czech Republic in 2018 for the purpose Registers Emission Sources); TEK0: Prague, Czech Republic, 2019.
16. Available online: <https://vec.vsb.cz/cs/pracoviste/zkusebna-kotlu/> (accessed on 3 July 2020).
17. EEA. EMEP/EEA Air Pollutant Emission Inventory Guidebook 2019; European Environment Agency: Luxembourg, 2020.
18. Available online: <https://www.cdv.cz/en/> (accessed on 3 July 2020).
19. Available online: <https://www.emisia.com/utilities/copert/> (accessed on 3 July 2020).
20. ETC/ACC. Spatial Mapping of Air Quality for European Scale Assessment. ETC/ACC Technical Paper 2006/6. 2007. Available online: [https://www.eionet.europa.eu/etcs/etc-atni/products/etc-atni-reports/etcacc\\_techpaper\\_2006\\_6\\_spat\\_aq](https://www.eionet.europa.eu/etcs/etc-atni/products/etc-atni-reports/etcacc_techpaper_2006_6_spat_aq) (accessed on 19 May 2020).
21. ETC/ACM. European Air Quality Maps for 2015; ETC/ACM Technical Paper 2017/7; The European Topic Centre on Air Pollution and Climate Change Mitigation: Bilthoven, The Netherlands, 2018.
22. CHMI. Air Pollution in the Czech Republic in 2018, Graphical Yearbook (Czech/English); Czech Hydrometeorological Institute: Prague, Czech Republic, 2019.
23. EMEP/MSCE-E: Database on Modelling Results of HMs and POPs (1990–2017). Available online: <http://en.msceast.org/index.php/pollution-assessment/emep-domain-menu?id=119> (accessed on 3 July 2020).
24. Cressie, N. *Statistics for Spatial Data*; Wiley: New York, NY, USA, 1993.
25. Mann, H.B. Nonparametric tests against trend. *Econometrica* **1945**, *13*, 245–259. [CrossRef]
26. Kendall, M.G. *Rank Correlation Methods*; Charles Graffin: London, UK, 1955.
27. Garrido, A.; Jimenez-Guerrero, P.; Ratola, N. Levels, trends and health concerns of atmospheric PAHs in Europe. *Atmos. Environ.* **2014**, *99*, 474–484. [CrossRef]
28. Albuquerque, M.; Coutinho, M.; Borrego, C. Long-term monitoring and seasonal analysis of polycyclic aromatic hydrocarbons (PAHs) measured over a decade in the ambient air of Porto, Portugal. *Sci. Total Environ.* **2016**, *543*, 439–448. [CrossRef]
29. Barzeghara, V.; Sarbakhshc, P.; Hassanvandd, M.S.; Faridie, S.; Gholampoura, A. Long-term trend of ambient air PM<sub>10</sub>, PM<sub>2.5</sub>, and O<sub>3</sub> and their health effects in Tabriz city, Iran, during 2006–2017. *Sustain. Cities Soc.* **2020**, *54*, 1–12. [CrossRef]
30. Hůnová, I.; Baumelt, V.; Modlík, M. Long-term trends in nitrogen oxides at different types of monitoring stations in the Czech Republic. *Sci. Total Environ.* **2020**, *699*, 134378. [CrossRef] [PubMed]
31. De Leeuw, F.A.A.M. Trends in ground level ozone concentrations in the European Union. *Environ. Sci. Policy* **2000**, *3*, 189–199. [CrossRef]
32. Gilbert, R.O. *Statistical Methods for Environmental Pollution Monitoring*; Van Nostrand Reinhold: New York, NY, USA, 1987.
33. R Core Team. *R: A Language and Environment for Statistical Computing*; R Foundation for Statistical Computing: Vienna, Austria, 2019. Available online: [www.R-project.org](http://www.R-project.org) (accessed on 5 March 2020).
34. Available online: [www.esri.com](http://www.esri.com) (accessed on 3 July 2020).

35. Shimada, K.; Nohchib, M.; Yangc, X.; Sugiyamad, T.; Miurae, K.; Takamif, A.; Satof, K.; Chenc, X.; Katog, S.; Kajjih, Y.; et al. Degradation of PAHs during long range transport based on simultaneous measurements at Tuoji Island, China, and at Fukue Island and Cape Hedo, Japan. *Environ. Pollut* **2020**, *260*, 113906. [[CrossRef](#)] [[PubMed](#)]
36. ENVIRON. User's Guide to the Comprehensive Air Quality Model with Extensions (CAMx) Version 5.40. 2011. Available online: <http://www.camx.com> (accessed on 30 April 2020).
37. CHMI. Czech Reference Dispersion Model SYMOS'97 (in Czech Only). 2020. Available online: <http://portal.chmi.cz/aktualni-situace/stav-ovzdusi/modelovani-kvality-ovzdusi/model-symos> (accessed on 30 April 2020).
38. Termonia, P.; Fisher, C.; Bazile, E.; Bouyssel, F.; Brožková, R.; Bénard, P.; Bochenek, B.; Degrauwe, D.; Derková, M.; El Khatib, R.; et al. The ALADIN System and its canonical model configurations AROME CY41T1 and ALARO CY40T1. *Geosci. Model Dev.* **2018**, *11*, 257–281. [[CrossRef](#)]
39. Bučánek, A.; Brožková, R.; Trojáková, A. Asimilační schéma BlendVar v ČHMÚ. *Meteorol. Zprávy* **2015**, *68*, 180–185.
40. Giard, D.; Bazile, E. Implementation of a New Assimilation Scheme for Soil and Surface Variables in a Global NWP Model. *Mon. Weather Rev.* **2000**, *128*, 997–1015. [[CrossRef](#)]
41. Van der Denier Gon, H.; van het Bolscher, M.; Visschedijk, A.; Zandveld, P. Emissions of persistent organic pollutants and eight candidate POPs from UNECE–Europe in 2000, 2010 and 2020 and the emission reduction resulting from the implementation of the UNECE POP protocol. *Atmos. Environ.* **2007**, *41*, 9245–9261. [[CrossRef](#)]
42. European Commission. Guidance Document for the implementation of the European PRTR. 2006. Available online: [https://ec.europa.eu/environment/industry/stationary/e-prtr/pdf/en\\_prtr.pdf](https://ec.europa.eu/environment/industry/stationary/e-prtr/pdf/en_prtr.pdf) (accessed on 30 April 2020).
43. Copernicus. Corine Land Cover Classification Spatial Data Set. 2018. Available online: <https://land.copernicus.eu/pan-european/corine-land-cover/clc2018> (accessed on 30 April 2020).
44. Bultjes, P.J.H.; van Loon, M.; Schaap, M.; Teeuwse, S.; Visschedijk AJ, H.; Bloos, J.P. *Project on the Modelling and Verification of Ozone Reduction Strategies: Contribution of TNO-MEP, TNO-Report, MEP-R2003/166*; TNO: Apeldoorn, The Netherlands, 2003.
45. Dernier van der Gon, H.; Hendriks, C.; Kuenen, J.; Segers, A.; Visschedijk, A. *A Description of Current Temporal Emission Patterns and Sensitivity of Predicted AQ for Temporal Emission Patterns*; EU FP7 MACC Deliverable Report D\_D-EMIS\_1.3; TNO: Utrecht, The Netherlands, 2011; Available online: [https://atmosphere.copernicus.eu/sites/default/files/2019-07/MACC\\_TNO\\_del\\_1\\_3\\_v2.pdf](https://atmosphere.copernicus.eu/sites/default/files/2019-07/MACC_TNO_del_1_3_v2.pdf) (accessed on 30 April 2020).
46. Berdowski, J.J.M.; Baas, J.; Bloos, J.P.J.; Visschedijk, A.J.H.; Zandveld, P.Y.J. *The European Emission Inventory of Heavy Metals and Persistent Organic Pollutants for 1990*; TIB: Hannover, Germany, 1997.
47. EMEP/CEIP: Spatially Distributed Emission Data as Used in EMEP Models. 2019. Available online: [https://www.ceip.at/new\\_emep-grid/01\\_grid\\_data](https://www.ceip.at/new_emep-grid/01_grid_data) (accessed on 3 July 2020).
48. EEA. Air Quality e-Reporting—Air Quality Annual Statistics Calculated by the EEA. 2020. Available online: <http://aidef.apps.eea.europa.eu/> (accessed on 20 February 2020).
49. Inventory Files NFR. Submissions 2020 (Reporting Year 2018). ANNEX 1: National Sector Emissions: Main Pollutants, Particulate Matter, Heavy Metals and Persistent Organic Pollutants. Available online: [https://ceip.at/ms/ceip\\_home1/ceip\\_home/status\\_reporting/2020\\_submissions](https://ceip.at/ms/ceip_home1/ceip_home/status_reporting/2020_submissions) (accessed on 18 May 2020).
50. Act No 201/2012 Coll. On the Protection of Air. In *Collection of Law*; MVCR: Prague, Czech Republic, 13 June 2012; Available online: <https://www.psp.cz/sqw/sbirka.sqw?cz=201&r=2012> (accessed on 18 May 2020).
51. EN 303-5:2012. In *Heating Boilers—Part 5: Heating Boilers for Solid Fuels, Manually and Automatically Stoked, Nominal Heat Output of Up to 500 kW—Terminology, Requirements, Testing and Marking*; Comité Européen de Normalisation: Brussels, Belgium, 2012.
52. Hellén, H.; Kangas, L.; Kousa, A.; Vestenius, M.; Teinilä, K.; Karppinen, A.; Kukkonen, J.; Niemi, J.V. Evaluation of the impact of wood combustion on benzo[a]pyrene (BaP) concentrations; ambient measurements and dispersion modeling in Helsinki, Finland. *Atmos. Chem. Phys.* **2017**, *17*, 3475–3487. [[CrossRef](#)]
53. CHMI. *Air Pollution in the Czech Republic in Current Year. Graphical Yearbook (Czech/English)*; Czech Hydrometeorological Institute: Prague, Czech Republic, 2009–2019; Available online: [http://portal.chmi.cz/files/portal/docs/uoco/isko/grafroc/grafroc\\_GB.html](http://portal.chmi.cz/files/portal/docs/uoco/isko/grafroc/grafroc_GB.html) (accessed on 30 April 2020).

54. EEA. *Air Quality in Europe—2016 Report*; EEA Report No. 28/2016; European Environment Agency: Luxembourg, 2016.
55. Tham, Y.W.F.; Takeda, K.; Sakugawa, H. Polycyclic aromatic hydrocarbons (PAHs) associated with atmospheric particles in Higashi Hiroshima, Japan: Influence of meteorological conditions and seasonal variations. *Atmos. Res. Vol.* **2008**, *88*, 224–233. [[CrossRef](#)]
56. Masiol, M.; Hofer, A.; Squizzato, S.; Piazza, R.; Rampazzo, G.; Pavoni, B. Carcinogenic and mutagenic risk associated to airborne particle-phase polycyclic aromatic hydrocarbons: A source apportionment. *Atmos. Environ.* **2012**, *60*, 375–382. [[CrossRef](#)]
57. Gianelle, V.; Colombi, C.; Caserini, S.; Ozgen, S.; Galante, S.; Marongiu, A.; Lanzani, G. Benzo(a)pyrene air concentrations and emission inventory in Lombardy region, Italy. *Atmos. Pollut. Res.* **2013**, *4*, 257–266. [[CrossRef](#)]
58. Liu, Y.; Tao, S.; Yang, Y.; Dou, H.; Yang, Y.; Coveney, R.M. Inhalation exposure of traffic police officers to polycyclic aromatic hydrocarbons (PAHs) during the winter in Beijing, China. *Sci. Total Environ.* **2007**, *383*, 98–105. [[CrossRef](#)] [[PubMed](#)]
59. Li, Z.; Porter, E.N.; Sjodin, A.; Larry, L.; Need-Ham, L. Characterization of PM<sub>2.5</sub> bound polycyclic aromatic hydrocarbons in Atlanta. Seasonal variations at urban, suburban, and rural ambient air monitoring sites. *Atmos. Environ.* **2009**, *49*, 4187–4193. [[CrossRef](#)]
60. Ludykar, D.; Westerholm, R.; Almen, J. Cold start emissions at +22, −7 and −20 degrees C ambient temperatures from a three-way catalyst (TWC) car: Regulated and unregulated exhaust components. *Sci. Total Environ.* **1999**, *235*, 65–69. [[CrossRef](#)]
61. Teixeira, E.C.; Agudelo-Castañeda, D.M.; Fachel, J.M.G.; Leal, K.A.; de Oliveira Garcia, K.; Wiegand, F. Source identification and seasonal variation of polycyclic aromatic hydrocarbons associated with atmospheric fine and coarse particles in the Metropolitan Area of Porto Alegre, RS, Brazil. *Atmos. Res.* **2012**, *118*, 390–403. [[CrossRef](#)]
62. Ma, W.L.; Zhu, F.J.; Liu, L.Y.; Jia, H.L.; Yang, M.; Li, Y.F. PAHs in Chinese atmosphere Part II: Health risk assessment. *Ecotoxicol. Environ. Saf.* **2020**, *200*, 110774. [[CrossRef](#)]
63. Giovannini, L.; Ferrero, E.; Karl, T.; Rotach, M.W.; Staquet, C.; Trini Castelli, S.; Zardi, D. Atmospheric Pollutant Dispersion over Complex Terrain: Challenges and Needs for Improving Air Quality Measurements and Modeling. *Atmosphere* **2020**, *11*, 646. [[CrossRef](#)]
64. Hopan, F.; Horák, J. *Výpočet Emisních Faktorů Znečišťujících Látek Pro Léta 2001 až 2012 a Tři Varianty Pro Rok 2022 na Základě Experimentálních a Statistických Dat. (Calculation of Emission Factors of Pollutants for Years 2001–2012 and Three Scenarios for 2022 Based on Experimental and Statistic Data)*; Energy Research Center VSB: Ostrava, Czech Republic, 2014; p. 13.



© 2020 by the authors. Licensee MDPI, Basel, Switzerland. This article is an open access article distributed under the terms and conditions of the Creative Commons Attribution (CC BY) license (<http://creativecommons.org/licenses/by/4.0/>).

## Article

# High NO<sub>2</sub> Concentrations Measured by Passive Samplers in Czech Cities: Unresolved Aftermath of Dieselgate?

Michal Vojtisek-Lom <sup>1,2,\*</sup> , Miroslav Suta <sup>3</sup>, Jitka Sikorova <sup>1</sup> and Radim J. Sram <sup>1</sup> 

<sup>1</sup> Department of Genetic Toxicology and Epigenetics, Institute of Experimental Medicine AS CR, Videnska 1083, 142 20 Prague, Czech Republic; jitka.sikorova@iem.cas.cz (J.S.); radim.sram@iem.cas.cz (R.J.S.)

<sup>2</sup> Department of Automotive, Combustion Engine and Railway Engineering, Faculty of Mechanical Engineering, Czech Technical University of Prague, Technicka 4, 166 07 Prague, Czech Republic

<sup>3</sup> Center for Environment and Health, Thámova 1275/21, 301 00 Plzeň, Czech Republic; miroslav.suta@centrum.cz

\* Correspondence: michal.vojtisek@fs.cvut.cz or michal.vojtisek@tul.cz; Tel.: +420-774-262-854

**Abstract:** This work examines the effects of two problematic trends in diesel passenger car emissions—increasing NO<sub>2</sub>/NO<sub>x</sub> ratio by conversion of NO into NO<sub>2</sub> in catalysts and a disparity between the emission limit and the actual emissions in everyday driving—on ambient air quality in Prague. NO<sub>2</sub> concentrations were measured by 104 membrane-closed Palmes passive samplers at 65 locations in Prague in March–April and September–October of 2019. NO<sub>2</sub> concentrations measured by city stations during those periods were comparable with the average values during 2016–2019. The average measured NO<sub>2</sub> concentrations at the selected locations, after correcting for the 18.5% positive bias of samplers co-located with a monitoring station, were 36 µg/m<sup>3</sup> (range 16–69 µg/m<sup>3</sup>, median 35 µg/m<sup>3</sup>), with the EU annual limit of 40 µg/m<sup>3</sup> exceeded at 32% of locations. The NO<sub>2</sub> concentrations have correlated well (R<sup>2</sup> = 0.76) with the 2019 average daily vehicle counts, corrected for additional emissions due to uphill travel and intersections. In addition to expected “hot-spots” at busy intersections in the city center, new ones were identified, i.e., along a six-lane road V Holešovičkách. Comparison of data from six monitoring stations during 15 March–30 April 2020 travel restrictions with the same period in 2016–2019 revealed an overall reduction of NO<sub>2</sub> and even a larger reduction of NO. The spatial analysis of data from passive samplers and time analysis of data during the travel restrictions both demonstrate a consistent positive correlation between traffic intensity and NO<sub>2</sub> concentrations along/near the travel path. The slow pace of NO<sub>2</sub> reductions in Prague suggests that stricter vehicle NO<sub>x</sub> emission limits, introduced in the last decade or two, have so far failed to sufficiently reduce the ambient NO<sub>2</sub> concentrations, and there is no clear sign of remedy of Dieselgate NO<sub>x</sub> excess emissions.

**Keywords:** NO<sub>2</sub>; passive sampler; Dieselgate; Prague; traffic volume; citizen science; air quality; public policy; health effects



**Citation:** Vojtisek-Lom, M.; Suta, M.; Sikorova, J.; Sram, R.J. High NO<sub>2</sub> Concentrations Measured by Passive Samplers in Czech Cities: Unresolved Aftermath of Dieselgate? *Atmosphere* **2021**, *12*, 649. <https://doi.org/10.3390/atmos12050649>

Academic Editor: Iva Hünová

Received: 1 April 2021

Accepted: 16 May 2021

Published: 19 May 2021

**Publisher's Note:** MDPI stays neutral with regard to jurisdictional claims in published maps and institutional affiliations.



**Copyright:** © 2021 by the authors. Licensee MDPI, Basel, Switzerland. This article is an open access article distributed under the terms and conditions of the Creative Commons Attribution (CC BY) license (<https://creativecommons.org/licenses/by/4.0/>).

## Highlights

- NO<sub>2</sub> measured by 104 passive samplers at 65 places in Prague, corrected mean 36 µg/m<sup>3</sup>
- NO<sub>2</sub> increases with traffic intensity corrected for intersections and hills
- High NO<sub>2</sub>/NO<sub>x</sub> ratios and excess NO<sub>x</sub> emissions from diesel cars a culprit
- Not much improvement after “Dieselgate”
- Reductions below 40 µg/m<sup>3</sup> suggested based on health evidence literature review

## 1. Introduction

Mobile sources, including on-road vehicles, remain to be one of the largest contributors to the air pollution in most metropolitan areas in Europe, with particulate matter and

nitrogen oxides ( $\text{NO}_x$ , defined as a sum of nitric oxide NO and nitrogen dioxide  $\text{NO}_2$ ) being of highest concern. Outdoor air pollution is now being considered one of the leading causes of premature death [1], with estimated tolls of approximately half a million premature deaths annually in the EU [2], and associated economic damage around 5% of GDP in Central Europe [3]. At the same time, the state-of-the-art technology of the internal combustion engine has improved considerably over the last decades. Very low levels of sulfur and metals in the fuel have allowed the introduction of three-way catalysts on spark ignition engines, a common technology used throughout the U.S. over the last four decades with a somewhat delayed deployment in Europe, and the introduction of diesel particle filters on virtually all on-road diesel engines manufactured in the last decade. The emissions of nitrogen oxides, primarily NO, on engines operating with excess air remained a challenge, being ultimately resolved about a decade ago with selective catalytic reduction (SCR) systems on heavy-duty vehicles [4] and more recently also on light-duty vehicles.

In the EU, the concentrations of  $\text{NO}_2$ , deemed to be more detrimental to human health than NO, are limited and monitored in the ambient air. Overall, the concentrations of  $\text{NO}_2$  have not been decreasing as fast as those of other key pollutants. In the Czech Republic, the concentrations of  $\text{NO}_2$  at most air quality monitoring stations have been, according to the data in [5], decreasing by on the order of 1% a year over the last two decades. A gradual decrease of  $\text{NO}_2$  concentrations in the overall atmosphere above the Czech Republic over the last decade has been also reported from remote sensing satellite measurements [6].

$\text{NO}_2$  in ambient air originates both from direct (primary) emissions and from gradual conversion of NO into  $\text{NO}_2$  [7]. While the total emissions of  $\text{NO}_x$  have been gradually decreasing, there is no apparent trend of a decrease in  $\text{NO}_2$  primary emissions over the last 15 years [6]. One of the culprits of high primary  $\text{NO}_2$  emissions are diesel vehicles, which have been, over the last two decades, equipped with oxidation catalysts, which convert a considerable portion of NO into  $\text{NO}_2$ . In the U.S., average  $\text{NO}_2/\text{NO}_x$  ratio in vehicle exhaust (all vehicles, including predominantly gasoline cars and light trucks and predominantly diesel heavy trucks) was 5.3% [8], compared to approximately 15% in Europe [9].

This paper explores a hypothesis that the observed decrease in  $\text{NO}_2$  concentrations falls short of that expected based on order-of-magnitude decrease in vehicle  $\text{NO}_x$  emissions limits and that non-compliant diesel cars could substantially contribute to this shortfall. The underlying aspects of  $\text{NO}_x$  emissions and the adverse health effects of  $\text{NO}_2$  are summarized. The results of a monitoring  $\text{NO}_2$  with passive samplers are reported and discussed in light of these findings. As an additional insight, the effects of coronavirus related restrictions on NO and  $\text{NO}_2$  concentrations in Prague are reported and discussed.

## 2. Review of Trends and Shortcomings in $\text{NO}_2$ and $\text{NO}_x$ Emissions from Vehicles

Nitrogen oxide (NO) is formed in combustion processes from atmospheric nitrogen and oxygen at high temperatures [10,11], which are generally associated both with efficient combustion and with high thermal efficiency of the engine. Subsequent oxidation of NO in the atmosphere yields primarily nitrogen dioxide ( $\text{NO}_2$ ), a brownish irritant gas. Other oxides of nitrogen— $\text{N}_2\text{O}_2$ ,  $\text{N}_2\text{O}_3$ ,  $\text{N}_2\text{O}_4$ ,  $\text{N}_2\text{O}_5$ —are generated in small concentrations, are unstable and short-lived in the atmosphere. The oxides of nitrogen are summarily referred to as  $\text{NO}_x$ , although there is no precise definition. Often,  $\text{NO}_x$  is evaluated as the sum of NO and  $\text{NO}_2$ . Technically, the sum of  $\text{NO}_x$  also includes nitrous oxide ( $\text{N}_2\text{O}$ ), which is, however, not hazardous to human health, but is a potent greenhouse.  $\text{NO}_x$  leads to the formation of nitrous acid ( $\text{HNO}_2$ ) [12,13], nitric acid ( $\text{HNO}_3$ ) and a variety of salts such as ammonium nitrate, present in the atmosphere as particulate matter [14]. Photodissociation of  $\text{NO}_2$  under the presence of sunlight produces NO and atomic oxygen, which reacts with molecular oxygen to form ozone [15], a highly reactive compound generally harmful to human health, organisms and plants.  $\text{NO}_x$  and ground-level (tropospheric) ozone are, together with particulate matter, the principal part of urban air pollution.

On spark ignition engines, CO and VOC, principally a product of incomplete oxidation of fuel and to a lesser extent engine lubricating oil, and NO<sub>x</sub> have been successfully abated by the combination of three-way catalysts [16] and by maintaining stoichiometric air–fuel ratio through closed-loop control of the quantity of fuel injected [17]. This technology has proven to be remarkably efficient.

On diesel engines, the emissions of NO<sub>x</sub> have been, at first, controlled through delayed combustion timing and exhaust gas recirculation, both associated with a slight fuel penalty, and at a later time, with NO<sub>x</sub> storage and reduction catalysts and selective reduction catalysts (SCR). The reduction of NO<sub>x</sub> has historically come at an expense of both capital and operating costs, with operating costs including either fuel (notably on older vehicles using delayed combustion, exhaust gas recirculation, NO<sub>x</sub> storage and reduction catalysts) or a reducing agent used in SCR (mostly aqueous solution of urea, known as diesel exhaust fluid or “AdBlue”). These costs have motivated, over the last few decades, many manufacturers and vehicle users to circumvent NO<sub>x</sub> reduction efforts, as the savings were realized by them directly, while considerably larger overall damage to human health was born by the society, a problem known as the Tragedy of the Commons [18]. A widespread practice of dual engine mapping in the U.S. in the 1990s [19,20] has led to the gradual extension of vehicle emissions limits to ordinary on-road operation first of heavy-duty and later of light-duty vehicles [21–23]. In the heavy-duty vehicle engine sector, many recent studies now show that on-road NO<sub>x</sub> emissions of newer heavy-duty vehicles have been successfully reduced by an order of magnitude except for low-load operation typical for congested urban areas. Quiros et al. [24] reports NO<sub>x</sub> emissions of 2013 and 2014 model year heavy trucks of 0.36 g/km during motorway operation in California. Jiang et al. [25] reports, for similar conditions, 0.3 g/km NO<sub>x</sub> during extraurban and motorway operation. Grigoratos et al. [26] reports NO<sub>x</sub> emissions during motorway operation in Europe of 0.07, 0.08, 0.17 and 0.24 g/kWh for four trucks and 0.80 g/kWh for a bus. Giechaskiel et al. [22] reports NO<sub>x</sub> emissions of a garbage collection truck of less than 0.4 g/kWh during extraurban operation (note: for heavy vehicles, emissions per kWh roughly correspond to emissions per km).

Unfortunately, this has not been the case with light-duty vehicles with diesel engines, highly prevalent in Europe, where they account for several tens of percent of vehicle registration and in Prague, for about two thirds of vehicles counted on the road [27]. Large portion of European automobile diesel engines produced over the last one to two decades have been reported to emit substantially, often by an order of magnitude, more NO<sub>x</sub> on the road than during the type approval test [28–32]. Weiss et al. [29] reports on-road NO<sub>x</sub> emissions factors  $0.76 \pm 0.12$  g/km for Euro 4,  $0.71 \pm 0.30$  g/km for Euro 5 and  $0.21 \pm 0.09$  for Euro 6. In a more recent study by Suarez-Bertoa et al. [23], NO<sub>x</sub> emissions from Euro 6 diesel cars varied substantially from mid tens to mid hundreds of milligrams of NO<sub>x</sub> per kilometer, with a median value of about 0.2 g/km NO<sub>x</sub> during the city-motorway test.

At the same time, on nearly all light-vehicle diesel engines of the last decade or so, oxidation catalysts are used to convert NO into NO<sub>2</sub>, as higher concentrations of NO<sub>2</sub>, around 10%, are beneficial both for the combustion of soot in DPF and for the “fast” reduction of NO<sub>x</sub> in SCR catalysts. As a result, NO<sub>2</sub> from newer engines accounts for 10% of NO<sub>x</sub> [33,34]. On passenger cars and light-duty trucks, NO<sub>2</sub>/NO<sub>x</sub> ratios of around 10–15% up to Euro 3 and 25–30% for Euro 4 and 5 were found in a London remote sensing study [35]. In the U.S., NO<sub>2</sub>/NO<sub>x</sub> ratio from heavy duty diesel trucks have doubled from around 7% in 2010 (average of trucks passing on the road in a given year, not a model year of the vehicles) to around 15% in 2018 [36]. This increase, however, did not result in an absolute increase in NO<sub>2</sub> emissions, as total NO<sub>x</sub> emissions have decreased dramatically due to the widespread use of SCR catalysts. According to Preble [36], “Fleet-average NO<sub>2</sub> emission rates remained about the same, despite the intentional oxidation of engine-out NO to NO<sub>2</sub> in DPF systems, due to the effectiveness of SCR systems in reducing NO<sub>x</sub> emissions and mitigating the DPF-related increase in primary NO<sub>2</sub> emissions”.

In Europe, NO<sub>x</sub> emissions from diesel cars have not, however, decreased in proportion to the decreasing emissions limits. A recent on-road study in Prague reports the mean emissions of Euro 5 and 6 diesel cars and vans of over 0.1 g/km NO<sub>2</sub> and over 0.5 g/km NO<sub>x</sub> [37], while a recent study of one of the most common diesel cars (Euro 6) reported about 0.15 g/km over WLTC cycle, and about 0.4 g/km over the Artemis driving cycle [38], which is more than the 0.08 g/km Euro 6 limit for total NO<sub>x</sub> (with which the vehicle reasonably complied over the NEDC cycle).

The presumption of the regulators that increased the NO<sub>2</sub>/NO<sub>x</sub> ratio after the oxidation catalyst and before the DPF, highly beneficial both for DPF and SCR operation, will be mitigated by the rather high efficiency of the NO<sub>x</sub> aftertreatment, envisioned in both U.S. EPA and EU emissions standards, which has been compromised by intentional acts resulting in diminished, or even zero, efficiency of the NO<sub>x</sub> aftertreatment. Examples of such acts include dual-mapping of the engines by the manufacturers (a prime example of which is “Dieselgate”) and disabling of the SCR (and emulating its proper functioning to the on-board diagnostics by “SCR emulators”) by vehicle operators. Under such conditions, relatively high amounts of NO<sub>2</sub>, intended to be reduced in NO<sub>x</sub> aftertreatment, are emitted out of the tailpipe. Logically, this results in very high, and much higher than intended, primary emissions of NO<sub>2</sub> in the streets. This finding is consistent with the rather slow decrease in NO<sub>2</sub> concentrations.

### 3. Review of the Impact of NO<sub>2</sub> to Central Nervous System in Children and Adults

The first experimental data were obtained several decades ago, indicating that air pollution may induce behavioral changes. Singh [39] studied the effect of NO<sub>2</sub> exposure on pregnant mice, exposed during gestation day 7–18. Prenatal exposure significantly altered the righting reflex and aerial righting score. These results suggest that maternal NO<sub>2</sub> exposure produce deficits in the functional capability of the offspring.

Wang et al. [40] was the first one, who studied the impact of NO<sub>2</sub> exposure to children’s neurobehavioral changes. They studied this effect in the year 2005 on two groups of children (A  $N = 431$ , B  $N = 430$ ) in the age of 8–10 years using neurobehavioral testing. Group A was exposed to 7  $\mu\text{g NO}_2/\text{m}^3$ , group B to 36  $\mu\text{g NO}_2/\text{m}^3$ . Children from the polluted area showed poor performance in all tests: visual simple reaction time, continuous performance, digit symbol, pursuit aiming and sign register. This study found a significant relationship between chronic low-level traffic related air pollution and neurobehavioral function in exposed children.

Guxens et al. [41] analyzed the association between prenatal exposure, diet and infant mental development in four regions in Spain, in 1889 children, who were exposed to  $29.0 \pm 11.2 \mu\text{g NO}_2/\text{m}^3$  (20.1–36.8). Infant mental development was evaluated at 14 months by Bailey Scales of Mental Development. Exposure to NO<sub>2</sub> did not show a significant association with mental development. Inverse association was observed in infants whose mothers reported low intake of fruit/vegetables during pregnancy ( $-4.13$  ( $-7.06, -1.21$ )). This study suggests that antioxidants in fruits and vegetables during pregnancy may modulate an adverse effect of NO<sub>2</sub> on infants’ mental development.

Kim et al. [42] investigated the association between maternal exposure to NO<sub>2</sub> of 49.4  $\mu\text{g}/\text{m}^3$  (25.9–84.8) and neurodevelopment in children in Korea (mental development index (MDI) and the psychomotor development index (PDI) by Bailey scales of mental development) at ages 6, 12 and 24 months. This study used 455–371 children. NO<sub>2</sub> exposure impaired psychomotor development ( $\beta = -1.30$ ;  $p = 0.05$ ). At 6 months NO<sub>2</sub> affected MDI ( $\beta = -3.12$ ;  $p < 0.001$ ) and PDI ( $\beta = -3.01$ ;  $p < 0.001$ ). These data suggest that exposure to NO<sub>2</sub> may delay neurodevelopment in early childhood.

A similar study was organized in Spain on 438 mother-child pairs by Lertxundi et al. [43] at 15 months of age, using the Bailey scales of mental development. A 1  $\mu\text{g NO}_2/\text{m}^3$  increase during pregnancy decreased the mental score ( $\beta = -0.29$ ; 90% CI:  $-0.47; -0.11$ ). Prenatal residential exposure to NO<sub>2</sub> adversely affects infant motor and cognitive development.

A prospective cohort study was conducted with 2715 children aged 7–10 years in Barcelona, Spain, as a part of the BREATHE project (brain development and air pollution ultrafine particles in school children [44]). Children were tested every 3 months with a computerized test. Cognitive development was assessed with the n-back and the attentional network test as working memory and inattentiveness. NO<sub>2</sub> exposure was completed in the outdoors in a low traffic region  $40.5 \pm 9.6 \mu\text{g}/\text{m}^3$  and high traffic region  $56.1 \pm 11.5 \mu\text{g}/\text{m}^3$ . Children attending schools with higher NO<sub>2</sub> pollution had an 11.5% (95% CI 8.9%–12.5%) slower working memory and slower growth in all cognitive measurements, which means a smaller improvement in cognitive development.

Pujol et al. [45] selected from this cohort 263 children, aged 8–12 years, for magnetic resonance investigation (MRI) to analyze brain volumes, tissue composition, myelination, cortical thickness, neural tract architecture, membrane metabolites and functional connectivity. Outdoor NO<sub>2</sub> exposure was  $46.8 \pm 12.0 \mu\text{g}/\text{m}^3/\text{year}$  and indoor NO<sub>2</sub> exposure was  $29.4 \pm 11.7 \mu\text{g}/\text{m}^3/\text{year}$ . Higher NO<sub>2</sub> exposure was associated with slower brain maturation with changes specifically concerning the functional domain.

Forns et al. [46] evaluated 2897 children from the Barcelona cohort within the BREATHE project. NO<sub>2</sub> exposure in schools was  $29.82 \mu\text{g}/\text{m}^3$  (11.47–65.65) and outdoor was  $48.46 \mu\text{g}/\text{m}^3$  (25.92–84.55). Behavioral development was assessed using the strengths and difficulties questionnaire (SDQ), which was filled out by parents. NO<sub>2</sub> exposure was positively associated with SDQ total difficulties scores, suggesting more frequent behavioral problems. This study was understood as the first one to evaluate the impact of air pollution on behavioral development in schoolchildren using both indoor and outdoor air pollution levels measured at schools. NO<sub>2</sub> outdoor levels (IQR =  $22.26 \mu\text{g}/\text{m}^3$ ) significantly increased total difficulties score (1.07, 95% CI: 1.01, 1.14,  $p < 0.05$ ). NO<sub>2</sub> exposure at school is associated with worse general behavioral development in schoolchildren.

Min and Min [47] studied in Korea 8936 children born in the year 2002 and followed them for the next 10 years, investigating the relationship between exposure to NO<sub>2</sub> and attention-deficit hyperactive disorder (ADHD). They diagnosed 313 children with ADHD. The hazard ratio (HR) associated with the increase in  $1 \mu\text{g}$  of the NO<sub>2</sub>/m<sup>3</sup> was 1.03 (95% CI: 1.02–1.04). Comparing infants with lowest tertile of NO<sub>2</sub> exposure with the highest tertile of NO<sub>2</sub>, HR = 2.10 (95% CI: 1.54–2.85), exposure had a 2 fold increased risk of ADHD. The study showed a significant association between exposure to NO<sub>2</sub> and the incidence of ADHD in children.

Sentis et al. [48] evaluated prenatal and postnatal exposure to NO<sub>2</sub> and attentional function in children at 4–5 years of age in four regions of Spain ( $N = 1298$ ). The attentional function was evaluated by the Conners kiddie continuous performance test (K-CPT). The prenatal NO<sub>2</sub> level was  $31.1 \mu\text{g}/\text{m}^3$  (18.4–37.9). Higher exposure to prenatal levels of NO<sub>2</sub> was associated with a 1.12 ms (95% CI; 0.22, 2.02) increase in hit reaction time and 6% increase in the number of emission errors (95% CI: 1.01, 1.11) per  $10 \mu\text{g}/\text{m}^3$  increase in prenatal NO<sub>2</sub>. Higher exposure to NO<sub>2</sub> during pregnancy is associated with impaired attentional function, especially increased inattentiveness in children aged 4–5 years. This reduced attentional function in population could lead to poor educational indicators. It seems to be important that this effect was observed with NO<sub>2</sub> concentrations lower than EU standard  $40 \mu\text{g}/\text{m}^3$ .

Sunyer et al. [49] followed in 2012–2013 2687 school children from Barcelona, assessing children's attention process 4 times every three months, using the attention network test (ANT). NO<sub>2</sub> indoor pollution was  $30.09 \pm 9.51 \mu\text{g}/\text{m}^3$  and ambient air pollution was  $37.75 \pm 18.41 \mu\text{g}/\text{m}^3$ . Daily ambient levels were negatively associated with all attention processes (children in the bottom quartile of daily exposure to NO<sub>2</sub> had a 14.8 ms (95% CI: 11.2, 18.4) faster response time than those in the top quartile, which corresponds to a 1.1 month delay (95% CI: 0.84, 1.37) in natural development). Short-term exposure to NO<sub>2</sub> is associated with potential harmful effects on neurodevelopment.

Forns et al. [50] examined after 3.5 years the cohort of children from Barcelona ( $N = 1439$ ), whose cognitive development was evaluated 4 times in the years 2012/2013 [43].

Working memory was estimated by a computerized n-back test. Exposure to NO<sub>2</sub> was related to the slower development of working memory ( $\beta = -4.22$ , 95% CI:  $-6.22, -2.22$ ). These reductions corresponded to a  $-20\%$  (95% CI:  $-30.1, -10.7$ ) change in annual working memory development associated with one interquartile range increase in outdoor NO<sub>2</sub>. Forns et al. [50] observed a persistent negative association between NO<sub>2</sub> levels at school and cognitive development over a course of 3.5 years. Therefore, they suggested that highly exposed children might face obstacles to fully achieve their academic goals.

Vert et al. [51] analyzed association between exposure to NO<sub>2</sub> and mental disorders on 958 residents from Barcelona (45–74 years old). Long-term residential exposure (period 2009–2014) was related to patients' self-reported history of anxiety and depression disorders. NO<sub>2</sub> exposure corresponded to  $57.3 \mu\text{g}/\text{m}^3$  (50.7–62.7). NO<sub>2</sub> increased the odd ratio for depression of 2.00 (95% CI: 1.37, 2.93) for each  $10 \mu\text{g NO}_2/\text{m}^3$  increase. The study shows that long-term exposure to NO<sub>2</sub> may increase the incidence of depression.

Aleman et al. [52] analyzed on the group of children from the BREATHE project ( $N = 1667$  at the age of 11 years), if there is any association between traffic-related air pollution and the  $\epsilon 4$  allele of the apolipoprotein E gene, which is understood as a genetic risk factor for Alzheimer's disease. NO<sub>2</sub> exposure at the home address was  $54.25 \pm 18.40 \mu\text{g}/\text{m}^3$  and at schools was  $47.74 \pm 12.95 \mu\text{g}/\text{m}^3$ . NO<sub>2</sub> exposure increased behavioral problems scores (characterized by SDQ) in  $\epsilon 4$  carriers ( $N = 366$ ) vs. non-carriers ( $N = 1223$ ) 1.14 (95% CI: 1.04, 1.26) vs. 1.02 (95% CI: 0.95, 1.10,  $p = 0.04$ ) and was associated with smaller caudate volume in  $\epsilon 4$  carriers ( $N = 37$ ) vs. non-carriers ( $N = 126$ )  $-737.9$  (95% CI:  $-1201.3, -274.5$ ) vs.  $-157.6$  (95% CI:  $-388.8, 73.6$ ,  $p = 0.03$ ). Annual average NO<sub>2</sub> concentrations in children's schools were associated with smaller caudate volume and higher behavior problem scores among APOE  $\epsilon 4$  allele carriers. It is possible that  $\epsilon 4$  carriers are more vulnerable to neuroinflammatory and oxidative stress induced by air pollution exposure.

Carey et al. [53] investigated the incidence of dementia to residential level of NO<sub>2</sub> in London. Among 130,978 adults aged 50–79 years was, in the period 2005–2013, 2181 subjects diagnosed with dementia (39% Alzheimer's disease and 29% vascular dementia). The average annual concentration of NO<sub>2</sub> was  $37.1 \pm 5.7 \mu\text{g}/\text{m}^3$ . Higher risk of Alzheimer's disease was observed in subjects exposed to the highest concentrations of NO<sub>2</sub> ( $>41.5 \mu\text{g}/\text{m}^3$ ) vs. subjects with the lowest concentrations of NO<sub>2</sub> ( $<31.9 \mu\text{g}/\text{m}^3$ ) (HR = 1.40, 95% CI 1.12–1.74). These associations were more consistent for Alzheimer's disease than vascular dementia. Study found evidence of a positive association between residential level of NO<sub>2</sub> across London and being diagnosed with dementia.

Roberts et al. [54] explored the effect of NO<sub>2</sub> exposure to mental health problems in children in London, U.K. ( $N = 284$ ). Symptoms of anxiety, depression, conduct disorder and ADHD were assessed at ages 12 and 18. NO<sub>2</sub> concentration in the year 2007 was  $37.9 \pm 5.5 \mu\text{g}/\text{m}^3$  (IQR 34.1–41.7). They did not observe any association between NO<sub>2</sub> exposure in childhood and mental health problems at age 12. However, they detected association between NO<sub>2</sub> exposure and subsequent development of symptoms and clinically diagnosable depression and conduct disorders at age 18. They demonstrated that NO<sub>2</sub> exposure at age 12 years was significantly associated with major depressive disorder at age 18.

Prenatal exposure to NO<sub>2</sub> and sex dependent infant cognitive and motor development was analyzed by Lertxundi et al. [55] in children at 4–6 years of age, in four regions in Spain ( $N = 1119$ ). Infant neuropsychological development was assessed by McCarthy scales: verbal, perceptive-manipulative, numeric, general cognitive, memory and motor. NO<sub>2</sub> exposure during pregnancy was from  $18.7 \pm 6.1$  to  $41.8 \pm 10.7 \mu\text{g}/\text{m}^3$ . The majority of cognitive domains were negative for NO<sub>2</sub>, associations were more negative for boys, statistically significant for memory, global cognition and verbal. These findings indicate a greater vulnerability of boys in domains related to memory, verbal and general cognition.

Jorcano et al. [56] assessed association between NO<sub>2</sub> and depressive and anxiety symptoms, and aggressive symptoms in children of 7–11 years, related to their prenatal

and postnatal exposure. Data were analyzed in 13,182 children from eight European population-based cohorts. Prenatal NO<sub>2</sub> levels ranged from 15.9 to 43.5 µg/m<sup>3</sup>, postnatal levels ranged from 14.0 to 43.5 µg/m<sup>3</sup>. A total of 1108 (8.4%) and 870 (6.6%) children were classified as having depressive and anxiety symptoms, and with aggressive symptoms. Obtained results suggest that prenatal and postnatal exposure to NO<sub>2</sub> is not associated with depressive and anxiety symptoms or aggressive symptoms in children of 7–11 years old.

Loftus et al. [57] used the mother–child cohort from the CANDLE study and analyzed the impact of prenatal NO<sub>2</sub> exposure ( $22.3 \pm 7.1$  µg/m<sup>3</sup>) and postnatal exposure ( $16.2 \pm 4.7$  µg/m<sup>3</sup>) on childhood behavior ( $N = 975$ ). In the sample 64% were African American, 53% had a household annual income below USD 35,000 and the child's age was 4.3 years. Mothers completed the child behavior checklist, a measure of problem behaviors in the past two weeks. The 4 µg/m<sup>3</sup> higher prenatal NO<sub>2</sub> was positively associated with externalizing behavior (6%, 95% CI: 1, 11%) and the effect of postnatal exposure was stronger (8%, 95% CI: 0, 16%). Prenatal NO<sub>2</sub> exposure was also associated with significant internalizing and externalizing behaviors. NO<sub>2</sub> exposure is positively associated with child behavior problems and African American and low SES children may be more susceptible.

Kulick et al. [58] examined in 5330 participants from the Northern Manhattan area of New York City the effect of long-term exposure to NO<sub>2</sub> (annual estimates  $57.4 \pm 22.1$  µg/m<sup>3</sup>) and PM<sub>2.5</sub> (annual estimates  $13.1 \pm 4.8$  µg/m<sup>3</sup>), predominantly in women, with a median age of 75.2 ( $\pm 6.46$ ) years. A + IQR increase of residential NO<sub>2</sub> was predictive of a 22.SD (95% CI, 0.30,  $-0.14$ ) low global cognitive score at baseline and a more rapid decline ( $-0.06$  SD; 95% CI  $-0.08$ ,  $-0.04$ ) in global cognitive function between biennial visits.

Erikson et al. [59] studied the association between NO<sub>2</sub> exposure and total gray matter and total white matter volumes in adults, using sample from UK Biobank. Participants were recruited from 2006 to 2010, a subset with magnetic-resonance brain imaging (MRI) included 18,292 participants, with an average age of 62 (44–80) and NO<sub>2</sub> levels were  $25.61 \pm 6.86$  µg/m<sup>3</sup>. The mean total gray-matter volume was 708,111 mm<sup>3</sup> ( $\pm 47,940$ ), the mean total white-matter volume was 708,111 mm<sup>3</sup> ( $\pm 40,696$ ). The total gray-matter volume was inversely associated with NO<sub>2</sub> ( $b = -103$ ,  $p < 0.01$ ). The effect of NO<sub>2</sub> on gray-matter volume was more pronounced in females ( $b = 161$ ,  $p < 0.05$ ). Obtained findings suggest that NO<sub>2</sub> concentrations lower than EU standard could be associated with reduced total gray-matter.

All reviewed studies indicate a significant health risk of NO<sub>2</sub> exposure at concentrations lower than the EU annual limit of 40 µg/m<sup>3</sup>:

- Prenatal exposure impaired attentional function at the age of 4–5 years;
- Induce neurobehavioral changes in children at the age of 8–10 years;
- Affect attention process in children aged 8–12 years and induced changes are persistent for another 3.5 years;
- Increase major depressive disorder at age 18;
- Increase the incidence of dementia;
- Exposure to NO<sub>2</sub> is associated with reduced total gray-matter.

The overall evidence presented in the mentioned studies suggests that attainment of the current EU annual limit for NO<sub>2</sub> of 40 µg/m<sup>3</sup> may not be sufficient for the protection of human health and further reductions of NO<sub>2</sub> concentrations would be beneficial and should be considered. In Switzerland, the current limit for the annual average of NO<sub>2</sub> is 30 µg/m<sup>3</sup>.

#### 4. Measurement of NO<sub>2</sub> in Prague by Passive Samplers

To build up on this hypothesis, the measurements of NO<sub>2</sub> concentrations at various locations by passive samplers are examined. Some of the results were presented by Deutsche Umwelthilfe [60] as preliminary data; in this study, the results from Prague were examined in a greater detail.

For passive monitoring, membrane-closed Palmes tube [61] passive samplers (Passam, Switzerland [62]) were used. Several hundreds of samplers were placed at selected locations

in the Czech Republic, out of which 65 were in Prague, during spring and fall of 2019 (46 and 58 samplers, respectively, a total of 104 samplers), each time for a period of approximately one month. The placement of the tubes generally followed the requirements set in the EU air quality directive (2008/50)—placement away from buildings at a breathing height 1.5–4 m, away from larger obstructions, and for traffic sites, within 10 m of curbside and, in most cases, over 25 m from intersections. In some cases, the samplers were placed closer to intersections, and in some cases, the samplers were placed in less conspicuous places such as behind a traffic sign (see photo in Figure 1), to reduce the chances of tampering. The expanded uncertainty (95% confidence) of the measurement given by the manufacturer is 18.3% for a concentration range 20–40  $\mu\text{g}/\text{m}^3$  [62]. The location of samplers is shown on an overview map in Figure 1. The same map also shows the locations of the national air quality monitoring stations referred to in this study.

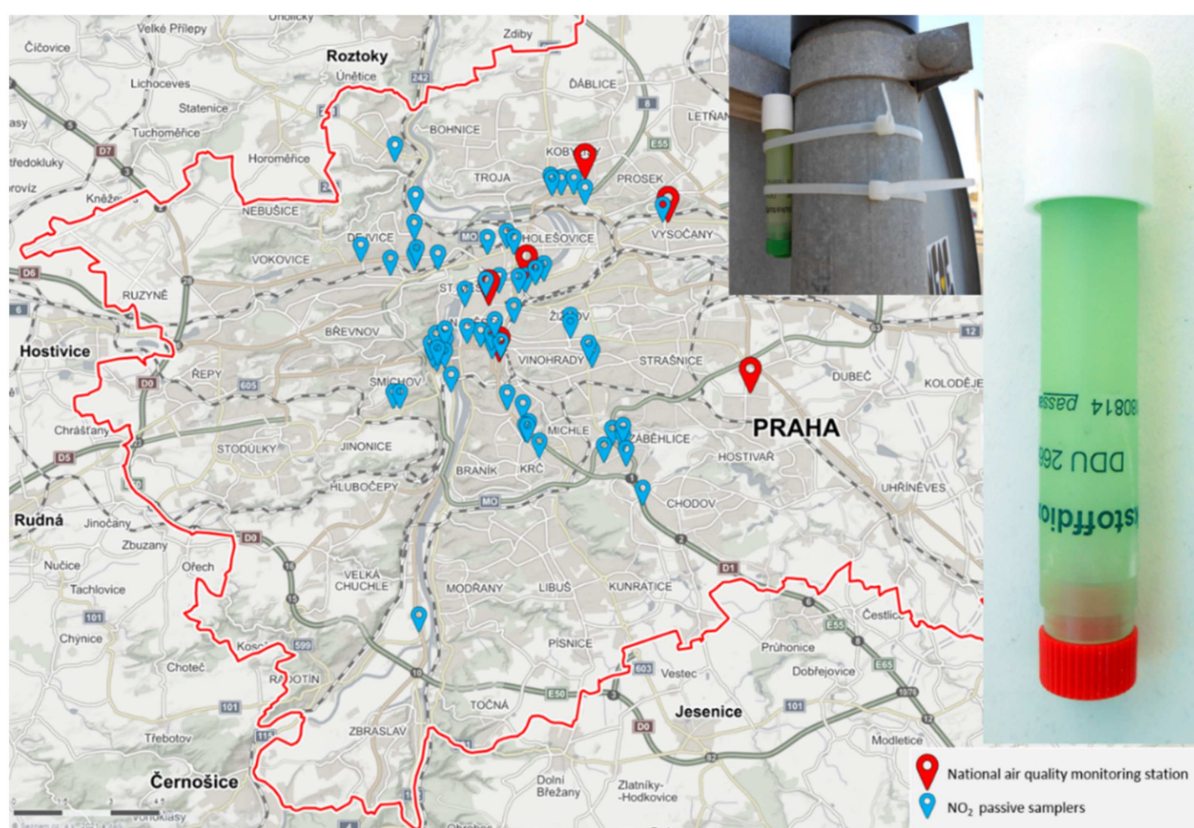


**Figure 1.** Locations of the passive samplers and air quality monitoring stations used for comparison in this study. Photo of a sampler is shown in the upper right corner. (Map source: [www.mapy.cz](http://www.mapy.cz) (accessed on 18 May 2021), © Seznam.cz, a.s., used with permission).

The measured concentrations are given in Table 1. For the spring campaign, the dates of the sampling are listed in the “spring measurement period” column, while for the fall campaign, a value is given when a measurement has taken place during the three sampling periods, as some locations were sampled twice. The spring, fall and overall average concentrations, divided by a correction factor of 1.185 (will be explained later in the manuscript) are given. For each location, the average daily vehicle traffic counts reported by the City of Prague Highway Department for 2019 [63] are reported. This table also reports vehicle counts adjusted for additional emissions due to inclines and intersections, these adjustments are discussed later in the manuscript.

Table 1. Measured NO<sub>2</sub> concentrations and average daily vehicle counts.

| NO <sub>2</sub> Measurements by Passive Samplers | Spring Measurement Period | Concentration as Analyzed [ $\mu\text{g}/\text{m}^3$ ] |                        |                        |                         | Adjusted (div 1.185) Concentrations |      |         | Traffic Vehicles/Day |                |          | Hill Climb | Inter-Section | >6 tons Excl. Zone |  |   |
|--|---------------------------|--|------------------------|------------------------|-------------------------|-------------------------------------|------|---------|----------------------|----------------|----------|------------|---------------|--------------------|--|---|
|  |                           | March–April  | 30 August–29 September | 7 September–30 October | 29 September–30 October | Spring                              | Fall | Average | Total Vehicles       | Heavy Vehicles | Adjusted |            |               |                    |  |   |
| 31 Budějovická                                   | 9 March–6 April           | 34   |                        |                        |                         | 28                                  |      | 28      |                      |                |          |            |               |                    |  | 1 |
| 32 třída 5. května 39                            | 9 March–6 April           | 43   |                        |                        | 41                      | 36                                  | 35   | 35      | 73,818               | 2200           | 110,727  | 50%        |               |                    |  | 1 |
| 33 Na Veselí                                     | 9 March–6 April           | 49   |                        |                        | 41                      | 41                                  | 35   | 38      | 15,500               | 400            | 31,000   | 100%       |               |                    |  | 1 |
| 34 Sokolská/Ječná                                | 9 March–6 April           | 78   | 70                     |                        | 63                      | 66                                  | 56   | 61      | 56,000               | 1700           | 280,000  | 100%       | 100%          |                    |  | 1 |
| 35 Ječná/Štěpánská                               | 9 March–6 April           | 64   |                        | 63                     |                         | 54                                  | 53   | 53      | 27,600               | 700            | 138,000  | 100%       | 100%          |                    |  | 1 |
| 36 Jugoslávských partyzánů 27                    | 9 March–6 April           | 35   |                        |                        |                         | 29                                  |      | 29      | 16,723               | 800            | 16,723   |            |               |                    |  |   |
| 37 Na pískách/Evropská                           | 9 March–6 April           | 52   |                        | 56                     |                         | 44                                  | 48   | 46      | 40,600               | 1700           | 162,400  |            |               | 100%               |  |   |
| 38 Kafkova/Svatovítská                           | 9 March–6 April           | 46   |                        | 46                     |                         | 39                                  | 39   | 39      | 26,101               | 1000           | 104,404  |            |               | 100%               |  |   |
| 39 Svatovítská/tunel                             | 9 March–6 April           | 31   |                        | 34                     |                         | 26                                  | 29   | 27      | 36,901               | 1000           | 36,901   |            |               |                    |  |   |
| 40 Na Ořechovce                                  | 9 March–6 April           | 45   |                        |                        |                         | 38                                  |      | 38      | 12,800               | 400            | 12,800   |            |               |                    |  |   |
| 41 Dejvice train station                         | 9 March–6 April           | 73   |                        | 59                     |                         | 62                                  | 50   | 56      | 29,200               | 1400           | 131,400  | 50%        | 100%          |                    |  | 1 |
| 42 Hradčanská (metro station)                    | 9 March–6 April           | 34   |                        | 36                     |                         | 29                                  | 30   | 30      | 18,409               | 1100           | 18,409   |            |               |                    |  | 1 |
| 43 Veletržní/Sochařská                           | 9 March–6 April           | 50   |                        | 47                     |                         | 43                                  | 40   | 41      | 22,100               | 600            | 99,450   | 50%        | 100%          |                    |  | 1 |
| 44 Janovského/Veletržní                          | 9 March–6 April           | 41   |                        | 34                     |                         | 34                                  | 29   | 31      | 19,400               | 400            | 77,600   |            |               | 100%               |  | 1 |
| 45 Křížovnická                                   | 9 March–6 April           | 40   |                        |                        |                         | 34                                  |      | 34      | 21,000               | 500            | 21,000   |            |               |                    |  | 1 |
| 46 Vinohradská/Flora                             | 9 March–6 April           | 34   |                        |                        | 37                      | 29                                  | 31   | 30      | 26,400               | 600            | 26,400   |            |               |                    |  |   |
| 47 Flora-mall (bus stop)                         | 9 March–6 April           | 43   |                        |                        | 35                      | 36                                  | 30   | 33      | 11,312               | 200            | 45,248   |            |               | 100%               |  |   |
| 48 Bělocerkevská (bus stup)                      | 9 March–6 April           | 51   |                        |                        | 46                      | 43                                  | 39   | 41      | 26,500               | 1000           | 132,500  | 100%       | 100%          |                    |  |   |
| 49 Vršovická (Slavia tram stop)                  | 9 March–6 April           | 33   |                        |                        | 36                      | 28                                  | 31   | 29      | 13,900               | 600            | 55,600   |            |               | 100%               |  |   |
| 52 Rumunská/Sokolská                             | 9 March–6 April           | 53   |                        |                        |                         | 45                                  |      | 45      | 43,100               | 1300           | 129,300  | 50%        | 50%           |                    |  | 1 |
| 120 Severní Spořilov podchod                     | 13 March–24 April         | 45   |                        |                        |                         | 38                                  |      | 38      | 48,900               | 7200           | 73,350   | 50%        |               |                    |  |   |
| 121 Chodov/Dálnice                               | 13 March–24 April         | 55   |                        |                        |                         | 46                                  |      | 46      | 118,100              | 15,600         | 177,150  | 50%        |               |                    |  |   |
| 122 Zenklova/Na Korábě                           | 13 March–24 April         | 39   |                        |                        | 30                      | 33                                  | 25   | 29      | 13,000               | 400            | 13,000   |            |               |                    |  |   |
| 123 Vychovatelna (bus)                           | 13 March–24 April         | 67   |                        |                        | 49                      | 57                                  | 41   | 49      | 109,300              | 4700           | 163,950  | 50%        |               |                    |  |   |
| 124 Rokoska (podchod)                            | 13 March–24 April         | 64   |                        |                        | 53                      | 54                                  | 45   | 49      | 88,561               | 4200           | 132,842  | 50%        |               |                    |  |   |
| 125 V Holešovičkách 8/10                         | 13 March–24 April         | 51   |                        |                        | 45                      | 43                                  | 38   | 40      | 88,561               | 4200           | 132,842  | 50%        |               |                    |  |   |
| 126 Hotel Pawllovia                              | 13 March–24 April         | 40   |                        |                        | 43                      | 34                                  | 36   | 35      | 88,561               | 4200           | 88,561   |            |               |                    |  |   |
| 127 main train station                           | 13 March–24 April         | 42   | 51                     |                        |                         | 35                                  | 43   | 39      | 85,053               | 200            | 85,053   |            |               |                    |  | 1 |
| 128 Hrusická 6 (balcony)                         | 13 March–24 April         | 21   |                        |                        |                         | 18                                  |      | 18      | 0                    | 0              | 0        |            |               |                    |  |   |

Table 1. Cont.

| NO <sub>2</sub> Measurements by Passive Samplers | Spring Measurement Period | Concentration as Analyzed [ $\mu\text{g}/\text{m}^3$ ] |                        |                        |                         | Adjusted (div 1.185) Concentrations |      |         | Traffic Vehicles/Day |                |          | Hill Climb | Inter-Section | >6 tons Excl. Zone |   |
|--|---------------------------|--|------------------------|------------------------|-------------------------|-------------------------------------|------|---------|----------------------|----------------|----------|------------|---------------|--------------------|---|
|  |                           | March–April  | 30 August–29 September | 7 September–30 October | 29 September–30 October | Spring                              | Fall | Average | Total Vehicles       | Heavy Vehicles | Adjusted |            |               |                    |   |
| 129 hlavní 25 (balcony)                          | 13 March–24 April         | 29   |                        |                        |                         | 25                                  |      | 25      | 8000                 | 200            | 8,000    |            |               |                    |   |
| 130 Havni/most                                   | 13 March–24 April         | 37   |                        |                        |                         | 31                                  |      | 31      | 50,487               | 7400           | 75,731   | 50%        |               |                    |   |
| 181 Kotevní 2                                    | 19 March–24 April         | 32   |                        |                        |                         | 27                                  |      | 27      | 26,500               | 600            | 26,500   |            |               |                    | 1 |
| 182 Strakonická 21/23                            | 19 March–24 April         | 41   |                        |                        |                         | 35                                  |      | 35      | 54,753               | 3300           | 54,753   |            |               |                    | 1 |
| 183 Svornosti 19a                                | 19 March–24 April         | 48   |                        |                        |                         | 41                                  |      | 41      | 11,800               | 300            | 11,800   |            |               |                    | 1 |
| 184 Zborovská 3                                  | 19 March–24 April         | 48   | 44                     |                        | 44                      | 41                                  | 37   | 39      | 14,500               | 300            | 58,000   |            | 100%          |                    | 1 |
| 185 V Botanice 4 (regional government)           | 19 March–24 April         | 56   | 49                     |                        | 63                      | 47                                  | 47   | 47      | 25,028               | 500            | 100,112  |            | 100%          |                    | 1 |
| 186 V Botanice (bank)                            | 19 March–24 April         | 43   |                        |                        | 44                      | 37                                  | 37   | 37      | 22,000               | 500            | 88,000   |            | 100%          |                    | 1 |
| 187 Plzeňská 14, Hotel IBIS                      | 19 March–24 April         | 49   |                        |                        | 42                      | 41                                  | 35   | 38      | 32,700               | 700            | 130,800  |            | 100%          |                    |   |
| 188 Radlická 14/Anděl                            | 19 March–24 April         | 48   |                        |                        | 48                      | 40                                  | 41   | 41      | 25,030               | 600            | 100,120  |            | 100%          |                    |   |
| 189 Ostrovskeho                                  | 19 March–24 April         | 43   | 41                     |                        |                         | 36                                  | 34   | 35      | 23,191               | 500            | 92,762   |            | 100%          |                    |   |
| 190 Billa Karlin                                 | 19 March–24 April         | 32   |                        | 28                     |                         | 27                                  | 24   | 25      |                      |                |          |            |               |                    |   |
| 191 Pobřežní (bussiness center)                  | 19 March–24 April         | 43   |                        | 40                     |                         | 37                                  | 33   | 35      | 31,200               | 1200           | 31,200   |            |               |                    |   |
| 192 Pobřežní (monitoring stattion)               | 19 March–24 April         | 38   |                        | 30                     |                         | 32                                  | 26   | 29      | 31,200               | 1200           | 31,200   |            |               |                    |   |
| 193 Negreliho viadukt                            | 19 March–24 April         | 33   |                        | 39                     |                         | 28                                  | 33   | 30      | 13,335               | 800            | 13,335   |            |               |                    |   |
| 194 Florenc (bus stop)                           | 19 March–24 April         | 46   |                        | 42                     |                         | 39                                  | 36   | 37      | 14,612               | 800            | 58,448   |            | 100%          |                    |   |
| 195 Nám. Republiky (Kotva)                       | 19 March–24 April         | 47   |                        |                        |                         | 40                                  |      | 40      | 8300                 | 300            | 33,200   |            | 100%          |                    | 1 |
| Mezibranská 3                                    | none                      |  | 84                     |                        | 79                      |                                     | 69   | 69      | 59,645               | 1800           | 298,225  | 100%       | 100%          |                    | 1 |
| Sokolská/Ječná, Prague                           | none                      |  | 74                     |                        | 63                      |                                     | 58   | 58      | 55,445               | 1700           | 277,225  | 100%       | 100%          |                    | 1 |
| Rumunská/Legerova, Prague                        | none                      |  | 62                     |                        | 52                      |                                     | 48   | 48      | 45,452               | 1300           | 181,808  |            | 100%          |                    | 1 |
| Bubenská, Prague                                 | none                      |  |                        | 48                     |                         |                                     | 40   | 40      | 28,300               | 800            | 113,200  |            | 100%          |                    |   |
| Vysočanská, Prague                               | none                      |  |                        | 26                     |                         |                                     | 22   | 22      | 15,700               | 400            | 15,700   |            |               |                    |   |
| Vysočanská (CHMÚ), Prague                        | none                      |  |                        | 37                     |                         |                                     | 31   | 31      | 37,035               | 1600           | 148,140  |            | 100%          |                    |   |

Table 1. Cont.

| NO <sub>2</sub> Measurements by Passive Samplers | Spring Measurement Period | Concentration as Analyzed [ $\mu\text{g}/\text{m}^3$ ] |                        |                        |                         | Adjusted (div 1.185) Concentrations |      |         | Traffic Vehicles/Day |                |          | Hill Climb | Inter-Section | >6 tons Excl. Zone |  |
|--|---------------------------|--|------------------------|------------------------|-------------------------|-------------------------------------|------|---------|----------------------|----------------|----------|------------|---------------|--------------------|--|
|  |                           | March–April  | 30 August–29 September | 7 September–30 October | 29 September–30 October | Spring                              | Fall | Average | Total Vehicles       | Heavy Vehicles | Adjusted |            |               |                    |  |
| Thámová/Sokolovská, Prague                       | none                      |  |                        | 28                     |                         |                                     | 24   | 24      |                      |                |          |            |               |                    |  |
| Radlická (ČSOB), Prague                          | none                      |  |                        | 38                     |                         |                                     | 32   | 32      |                      |                |          |            |               |                    |  |
| Radlická (Kotelna Park), Prague                  | none                      |  |                        | 33                     |                         |                                     | 28   | 28      |                      |                |          |            |               |                    |  |
| Resslova 1/3, Prague                             | none                      |  |                        | 52                     |                         |                                     | 44   | 44      | 33,027               | 700            | 148,622  | 50%        |               | 100%               |  |
| Spořilov 1, Prague                               | none                      |  |                        |                        | 51                      |                                     | 43   | 43      |                      |                |          |            |               |                    |  |
| Spořilov 2, Prague                               | none                      |  |                        |                        | 34                      |                                     | 28   | 28      |                      |                |          |            |               |                    |  |
| Boční/Jihovýchodní VII, Prague                   | none                      |  |                        |                        | 28                      |                                     | 24   | 24      |                      |                |          |            |               |                    |  |
| Pankrác 1 BAUHAUS, Prague                        | none                      |  |                        |                        | 37                      |                                     | 31   | 31      |                      |                |          |            |               | 100%               |  |
| Pankrác 2 Doudlebská, Prague                     | none                      |  |                        |                        | 29                      |                                     | 25   | 25      |                      |                |          |            |               | 100%               |  |
| Pankrác 3 viadukt, Prague                        | none                      |  |                        |                        | 32                      |                                     | 27   | 27      |                      |                |          |            |               | 100%               |  |
| Pankrác 4 Hvězdova 35, Prague                    | none                      |  |                        |                        | 31                      |                                     | 26   | 26      |                      |                |          |            |               | 100%               |  |
| Radlická/Klicperova, Prague                      | none                      |  |                        |                        | 48                      |                                     | 41   | 41      | 25,030               | 500            | 100,120  |            |               | 100%               |  |
| Suchdol AV ČR, Prague                            | none                      |  |                        |                        | 20                      |                                     | 17   | 17      | 0                    | 0              | 0        |            |               |                    |  |
| Suchdol AV ČR, Prague                            | none                      |  |                        |                        | 19                      |                                     | 16   | 16      | 0                    | 0              | 0        |            |               |                    |  |

#### 4.1. Validation by Comparison with the Air Quality Monitoring Network

According to [64], passive diffusion tubes for measuring NO<sub>2</sub> concentrations in air were originally developed in the late 1970s for personal monitoring. They have been widely used in Europe for spatial and temporal measurement of NO<sub>2</sub> concentrations. The method has been found to be cheap, simple, and “provides concentration data in most circumstances that are sufficiently accurate for assessing exposure and compliance with Air Quality criteria” [64]. Reporting on a series of comparison tests, Buzica et al. [65] have concluded that “In the case of NO<sub>2</sub>, all the results of the laboratory and field experiments respected the requirements necessary for the demonstration of equivalence” and that the MCPT are equivalent to the reference methods for assessment of NO<sub>2</sub>. Passive diffusion tubes were reported to show a positive bias when sampling close to sources of NO, such as roadside or street canyons [64]. At the same time, prolonged (several weeks) sampling periods were reported to lead to negative bias [64]. A review done by the Joint Research Center of the European Commission [66], done in part to assess the feasibility of using the samplers for the long-term monitoring of nitrogen dioxide, with the particular aim of checking compliance with the European Union annual limit value of 40 µg/m<sup>3</sup>, citing a range of previous studies, reports that the “precision of the sampler showed that it is usually better than 5% when using a barrier or shelter to reduce effects of wind-induced turbulence” and that “the relative expanded uncertainty of individual results was estimated to be 32% for worst-case conditions”, with lower values, generally <25%, obtained, for example, by parallel measurements with a reference method, by direct approaches, concluding that overall, “the Palmes tube is at least suitable for performing long-term measurements of NO<sub>2</sub> for indicative purposes, and possibly even for fixed measurements”. Recent review of biases associated with Palmes tube type passive samplers by Heal et al. [67] suggests that “The effect of net bias can be reduced by application of a local “bias adjustment” factor derived from collocations of PDTs with a chemiluminescence analyzer. When this is carried out, the PDT is suitable as an indicative measure of NO<sub>2</sub> for air quality assessments”.

To evaluate the bias, the data from passive samplers were compared to the data from selected relevant stations of the national air quality monitoring network, listed in Table 2. The national network uses chemiluminescence analyzers capable of measuring both NO and total NO<sub>x</sub>, with NO<sub>2</sub> calculated as the difference of total NO<sub>x</sub> and NO. The uncertainty of the measurements is periodically determined through analysis of reference samples, repeated measurements of the same sample, interlaboratory exercises, and for 2019, was reported to be a combination of absolute uncertainty of 2.3 µg/m<sup>3</sup> and a relative uncertainty of 12.3% [68].

The results of this comparison are given in Figure 2. In each case, the value reported by the passive sampler was compared to the average of hourly values from the monitoring station over the period during which the sampler was exposed. The three larger points (in red/orange) represent two samplers collocated with the Karlín monitoring station over two separate one-month periods and one sampler collocated with the Vysočanská monitoring station, show a linear correlation with a slope of 1.185 (at zero intercept; standard error of slope 0.008; differences passive sampler vs. monitoring station of +20%, +17% and +18%). While it can be argued that a regression of three points has a limited meaning, in this case, it shows that three different samplers, each used in a different time period, has produced readings that are a consistent multiple of the monitoring station data. Additionally, two samplers placed at the city urban background reference station for particulate matter (Suchdol campus of the Czech Academy of Sciences, last two lines in Table 1) during the same time period show a relative difference of 6%. These findings are in line with the 5% precision of the Palmes tube samples reported in [66].

**Table 2.** Measured NO<sub>2</sub> concentrations and average daily vehicle counts—monitoring network.

| NO <sub>2</sub><br>Measurements<br>by the National<br>Air Quality<br>Monitoring<br>Network | Average of 1-h Concentrations [µg/m <sup>3</sup> ] |                    |                      |                           |                         | Average Concentrations  |        |      | Traffic Vehicles/Day |        | Hill<br>Climb | Inter-<br>Section | >6 tons<br>Excl.<br>Zone |          |
|--|--|--------------------|----------------------|---------------------------|-------------------------|-------------------------|--------|------|----------------------|--------|---------------|-------------------|--------------------------|----------|
|  | Station  | 9 March–6<br>April | 19 March–21<br>April | 30 August–29<br>September | 7                       | 29                      | Spring | Fall | 2016–2019            | Actual |               |                   |                          | Adjusted |
|  |  |                    |                      |                           | September–30<br>October | September–30<br>October |        |      |                      |        |               |                   |                          |          |
| Legerova   | 46   | 62                 | 45                   |                           | 45                      | 54                      | 45     | 51   | 46,300               | 1300   | 185,200       |                   | 100%                     | 1        |
| Namesti<br>Republiky   | 29   | 35                 | 26                   |                           | 36                      | 32                      | 31     | 30   | 10,400               | 300    | 41,600        |                   | 100%                     | 1        |
| Kobylisy   | 20   | 21                 |                      |                           | 26                      | 20                      | 26     | 20   | 0                    | 0      | 0             |                   |                          |          |
| Průmyslová   | 31   | 32                 |                      |                           | 30                      | 32                      | 30     | 31   | 35,000               | 2000   | 35,000        |                   |                          |          |
| Vysočanská   | 29   | 37                 |                      | 31                        |                         | 33                      | 31     | 35   | 37,035               | 3500   | 37,035        |                   |                          |          |
| Karlín   |  | 32                 |                      | 26                        |                         | 32                      | 26     | 29   | 31,200               | 1200   | 31,200        |                   |                          |          |

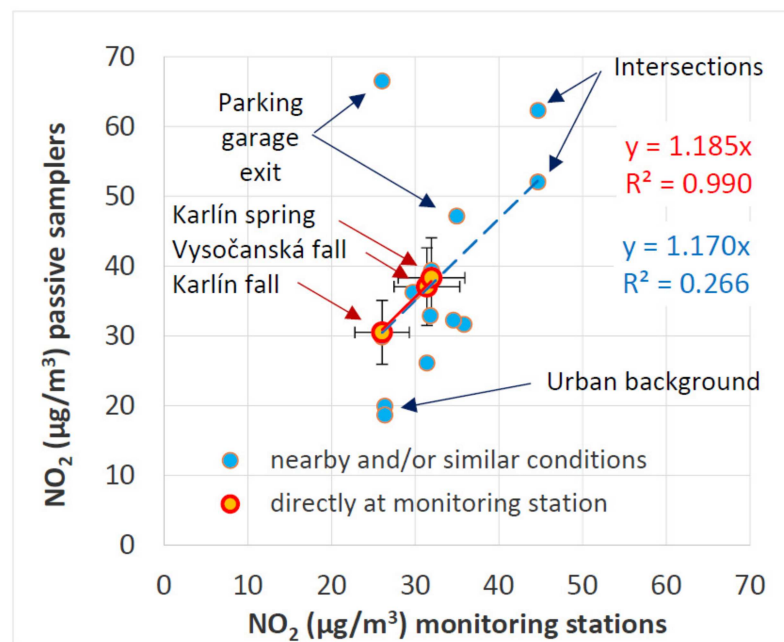


**Figure 2.** Comparison of passive sampler reported NO<sub>2</sub> concentrations to the corresponding average values from corresponding monitoring stations. Larger points circled in red denote the collocation of the sampler at the monitoring station.

Smaller blue points in Figure 2 show additional locations. Two samplers were placed at an urban background monitoring station Suchdol, however, data from this station was not available, and the readings are compared with another background monitoring station in Kobylisy. Two samplers were placed near Náměstí Republiky monitoring station, but a few dozen meters away and near an exit/entrance ramp to a large shopping center underground parking garage. Two samplers were placed on the corner of Legerova and Rumunská, near the monitoring station but at an intersection controlled by a traffic light. The readings from these four samplers were higher than from the monitoring station, which can be reasonably expected as they were near stopped and accelerating vehicles. The slope for the additional samplers was 1.17 with a standard error of 0.09; it should be noted that differences between actual NO<sub>2</sub> concentrations at the sampler and at the monitoring station are most likely the largest source of uncertainty.

Additional samplers close to the Legerova station (about 150 m from a large intersection) were closer to intersections and therefore exposed to additional cross-traffic, in addition to the increase in emissions rates in the vicinity of intersections. Two samplers were also placed at the Legerova monitoring station (urban hotspot) in the spring of 2019, but both were stolen. Additional samplers were placed near the Karlín monitoring station and near the Náměstí Republiky monitoring stations, and in the general vicinity of the Legerova station. The NO<sub>2</sub> concentrations reported for the samplers were compared with the average NO<sub>2</sub> concentrations measured by the monitoring station, obtained by averaging data over the time the samplers were exposed on the site.

Additional samplers used in the comparison were at reasonably close locations with not overly dissimilar traffic, and were not too far from the 15% tolerance reported by the Defra report [64]. It should be noted that the tolerance is applicable to the deviation of the sampler-reported and reference value, and not to the differences due to the samplers being at different locations with different emissions characteristics.

For all subsequent data analysis, the concentrations from the passive samplers were divided by the regression slope of 1.185. It should be noted that while this correction represents the best judgment by the authors, it is based on limited data and could be viewed as arbitrary, as the difference could arise out of the 12.3% uncertainty of the reference measurement the manufacturer-reported 18% expanded uncertainty of the passive sampler.

#### 4.2. Comparison of NO<sub>2</sub> during Passive Samplers Deployment with Long-Term Averages

The variation of climatic and weather conditions is an additional source of bias to consider when comparing passive samplers to annual mean values. Figure 3 shows that the average values of NO<sub>2</sub> recorded at the monitoring stations over sampling periods of individual samplers (different four-week periods in March–April 2019) did not dramatically differ from annual means during the last four years (2016–2019), although differences in trends were observed among the stations. For example, the Legerova urban hotspot station exhibited an annual average of 51 µg/m<sup>3</sup> (2016–2019), compared to 46 µg/m<sup>3</sup> during the period of 9 March–April 6 and 62 µg/m<sup>3</sup> during 19 March–24 April. The Náměstí Republiky urban background station had a 2016–2019 average of 30 µg/m<sup>3</sup>, compared to 29 µg/m<sup>3</sup> during 9 March–6 April and 35 µg/m<sup>3</sup> during 19 March–24 April. It should be noted that the NO<sub>2</sub> concentrations were generally lower during mid-March and higher during mid-April. Overall, the NO<sub>2</sub> concentrations during the sampling periods are believed to be representative of the annual average concentrations.

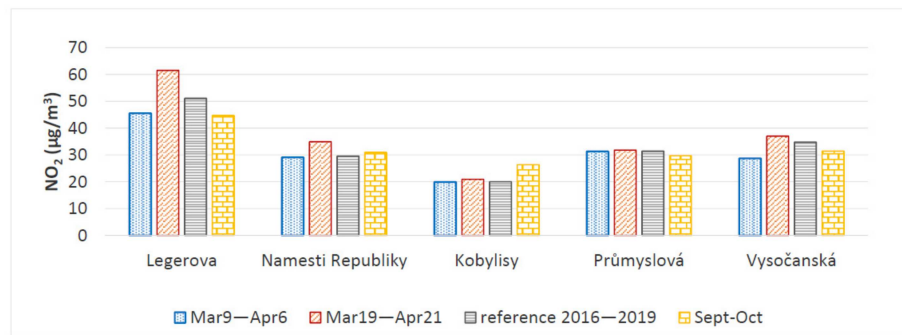


**Figure 3.** Comparison of monitoring station NO<sub>2</sub> averages during sampling periods with four-year average.

The consistency of the measurement by passive samplers during spring and fall periods is shown, along with data from the reference monitoring stations, in Figure 4. The slope of regression (with intercept forced through zero) was  $0.91 \pm 0.05$  for the monitoring stations and  $0.92 \pm 0.02$  for the passive samplers, showing that the monitoring stations and the passive samplers reported the same overall trends in NO<sub>2</sub> concentrations.

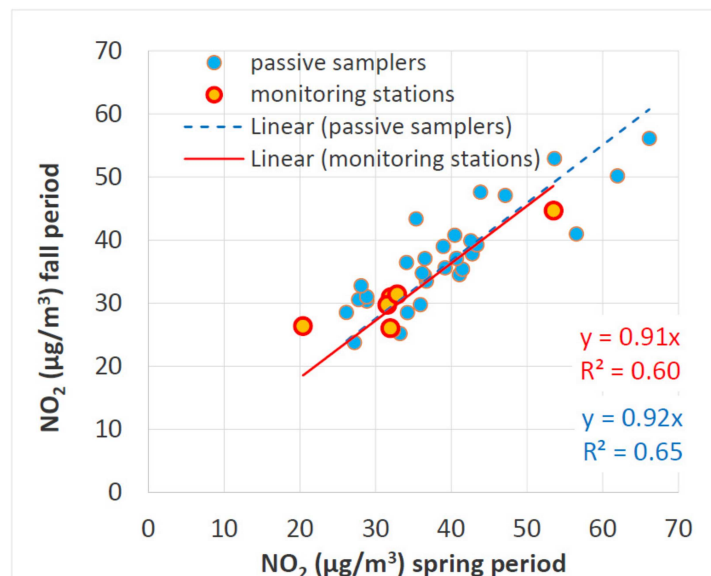


**Figure 4.** Comparison of spring and fall NO<sub>2</sub> concentrations.

#### 4.3. Effects of Traffic

For further analysis, all passive sampler measurements were divided by a factor of 1.185 (the slope of regression of passive sampler vs. reference  $\text{NO}_2$ , see Figure 1).

The relationship between the vehicular traffic intensity and the  $\text{NO}_2$  concentrations measured by the passive samplers is given in Figure 5. As samplers were used over two different periods, they are plotted separately in two series, one for each period, along with the average values from Legerova and Náměstí Republiky monitoring stations. It appears that there is a moderate positive trend of  $\text{NO}_2$  increasing with traffic. Additionally, samplers located next to an uphill section of a divided highway (or a one-way street with the traffic going in the uphill direction) and next to an intersection tend to exhibit higher  $\text{NO}_2$  concentrations. It also appears that the  $\text{NO}_2$  concentrations are higher in urban canyons and congested streets of the city center and near intersections.

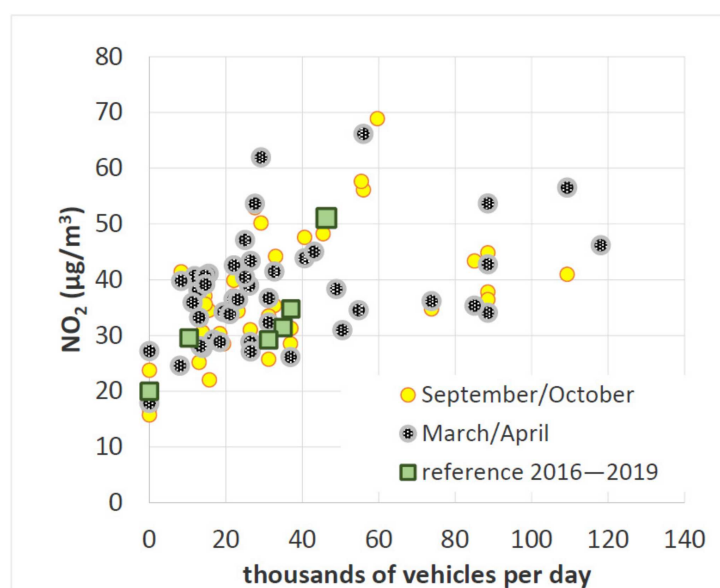


**Figure 5.** Relationship between traffic intensity and  $\text{NO}_2$  concentrations measured by passive samplers in spring and fall of 2019 and by the national monitoring network (average of 2016–2019).

To assess whether high  $\text{NO}_2$  are associated with truck traffic, samplers located in the area with limited access of vehicles over 6 tons gross weight (entry by permit only, restricted to local traffic) are plotted separately in Figure 6 (for locations where multiple samplers were used, average values are plotted). It is clear from the figure that the highest  $\text{NO}_2$  were measured in areas where trucks over 6 tons are mostly excluded.

To account for additional emissions due to hills and intersections, the intensity of traffic traveling uphill was increased by 100% to account for additional fuel consumption, and for samplers located at intersections, the intensity of traffic was increased by 300% to account for fuel consumed at idle and when accelerating (where the intersection was without a major delay, such as time-synchronized signals at intersections of a larger one-way street with a side street or pedestrian crossing, the factor was reduced by one half). These adjustment factors were arbitrarily selected based on experience with vehicle emissions behavior (additional emissions due to climbing a hill, additional emissions due to idling at intersections and acceleration from intersections) and were independent of each other. (Note: as an example of rough calculation for a passenger car diesel engine, the acceleration of a 1500 kg car from 0 to 50 km/h requires a gain of kinetic energy of 145 kJ or 40 Wh, corresponding, at 250 g/kWh engine fuel consumption, to 10 g of fuel. The fuel consumption at idle is about 5 g/min. A one-minute stop and acceleration consumes 15 g of fuel. Driving at steady speed requires about 30 g of fuel per km, or 3 g per 100 m. If half of the cars stop and wait, the emissions in a 100 m segment around the intersection

are 9 g, compared to 3 g in the case of free-flowing traffic. For simplicity, NO<sub>x</sub> emissions are assumed to be proportional to the fuel consumption.) The relationship between the adjusted vehicle volume and NO<sub>2</sub> concentrations is plotted in Figure 7.

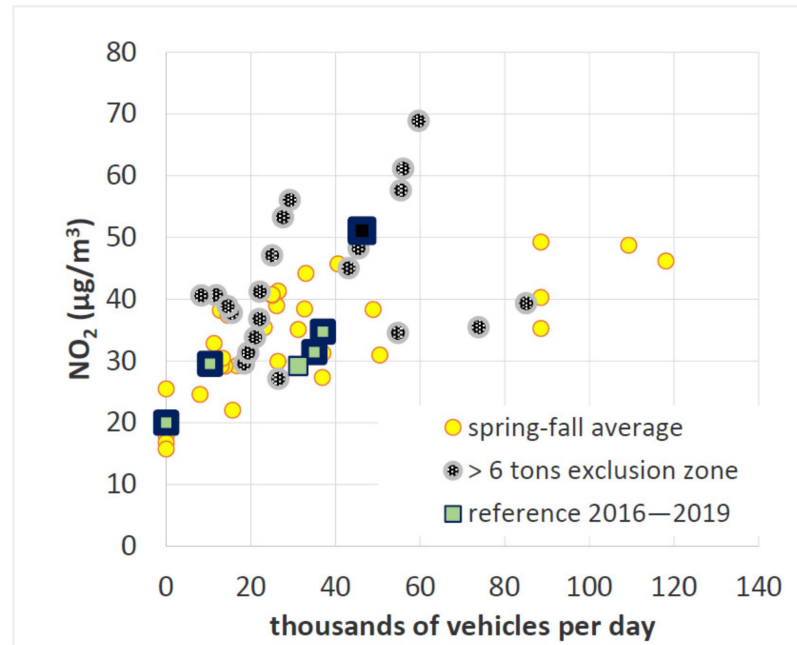


**Figure 6.** Relationship between traffic intensity and NO<sub>2</sub> concentrations measured by passive samplers (average of all measurement periods) and by the national monitoring network (average of 2016–2019).

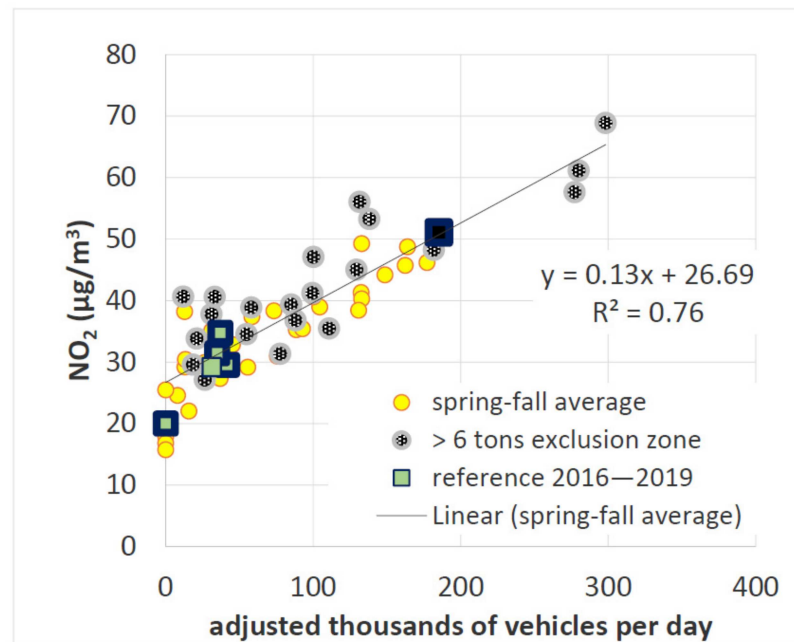


**Figure 7.** Relationship between adjusted traffic intensity (traffic count × (1 + fraction of vehicles travelling uphill + 3 × fraction of vehicles stopping at an intersection)) and NO<sub>2</sub> concentrations measured by passive samplers (average of all measurement periods) and by the national monitoring network (average of 2016–2019).

The relatively strong correlation between the adjusted traffic volumes and  $\text{NO}_2$  concentrations ( $R^2 = 0.78$  for September–October data and  $0.76$  for spring–fall averages; slope  $0.13 \pm 0.01$ ; intercept  $27 \pm 1 \mu\text{g}/\text{m}^3$ ) suggests that “local”  $\text{NO}_2$ , comprising of primary  $\text{NO}_2$  emitted from the tailpipe and  $\text{NO}_2$  formed locally from  $\text{NO}$  by reaction with ozone (i.e., [69]), is a considerable and in many locations dominant source of  $\text{NO}_2$ . There is no observable difference between the sampling locations where truck traffic over 6 tons was excluded and the locations where it was not excluded. Overall, there seems to be a very strong correlation between the estimated relative intensity of mobile source emissions and the measured  $\text{NO}_2$  concentrations. It is likely that the correlation could be further improved by taking into the account distance from the traffic, traffic on adjacent streets, tunnel exits and other compounding factors.

A similar plot of the regression of the dependency of  $\text{NO}_2$  on adjusted traffic volumes is plotted separately for the spring and fall campaigns in Figure 8, with red line denoting the legal annual  $\text{NO}_2$  limit of  $40 \mu\text{g}/\text{m}^3$  and green line the Swiss federal limit of  $30 \mu\text{g}/\text{m}^3$  (shown for illustration in support of the health review). The regression shows that  $\text{NO}_2$  concentrations, in all cases, increased by  $0.13 \mu\text{g}/\text{m}^3$  per 1000 vehicles daily traffic volume, adjusted for uphill and intersections, where adjusted traffic count is traffic count multiplied by a factor of  $(1 + \text{fraction of vehicles travelling uphill} + 3 \times \text{fraction of vehicles stopping at an intersection})$ . It should be noted that the intercept of the regression ( $25\text{--}28 \mu\text{g}/\text{m}^3$  in Figures 7 and 8; (standard error of slope is  $0.01$ ; standard error of intercept is  $1 \mu\text{g}/\text{m}^3$ ) is higher than the “urban background” concentrations of  $15\text{--}20 \mu\text{g}/\text{m}^3$ , most likely due to accounting only for traffic on major roads and not for parking garages, taxi waiting areas, and similar locations. Even the urban background concentrations cannot be considered as  $\text{NO}_2$  concentrations that would be theoretically be expected if no motor vehicles were operated in Prague, due to the dispersion and transport of the pollutants.

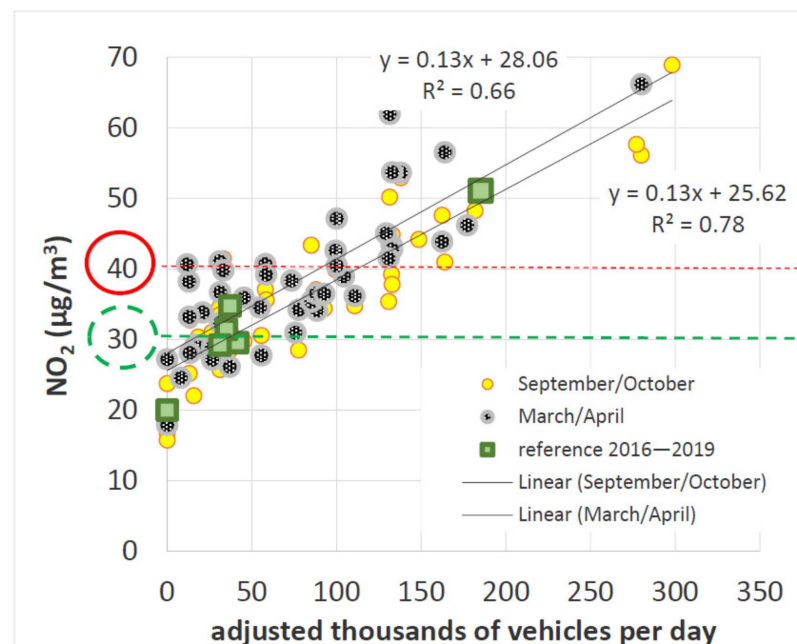


**Figure 8.** Relationship between adjusted traffic intensity (traffic count  $\times (1 + \text{fraction of vehicles travelling uphill} + 3 \times \text{fraction of vehicles stopping at an intersection})$ ) and  $\text{NO}_2$  concentrations measured by passive samplers (average of all measurement periods) and by the national monitoring network (average of 2016–2019). EU annual limit of  $40 \mu\text{g}/\text{m}^3$   $\text{NO}_2$  shown as a red line, Swiss federal limit of  $30 \mu\text{g}/\text{m}^3$   $\text{NO}_2$  shown as a dotted green line.

Even at a rather conservative adjustment of the passive sampler readings (according to the regression, the sampler readings were 18% higher, however, this was, to a large extent, due to many samplers being at locations where the concentrations would reasonably be

expected to be higher than at the corresponding monitoring station), it is clear from Figure 7 that the annual average limit of  $40 \mu\text{g}/\text{m}^3$   $\text{NO}_2$  is likely to be exceeded at numerous locations throughout Prague, generally, where the adjusted traffic volumes exceed the equivalent of 100 thousands of vehicles per day. This is, for example, the north-south passageway through the center city (Wilsonova, Sokolská and Legerova street) with many intersections, but also roads like V Holešovičkách (a six-lane road with 85–90 thousand vehicles per day, with a gradient of approximately 3%), a possible new hot-spot in Prague. In the worst case (intersection of two one-way streets with all vehicles traveling uphill), this limit could be reached already at 20 thousand vehicles per day, as also apparent from Figure 6.

### 5. Effects of Travel Restrictions on Ambient NO and $\text{NO}_2$ Concentrations

In order to assess the contribution of light and heavy vehicles to NO and  $\text{NO}_2$  concentrations, hour-by-hour NO and  $\text{NO}_2$  ambient air quality data from the national air quality monitoring network was analyzed for a period of 14 March–30 April 2020, during which travel restrictions were imposed, including the prohibition of all non-cargo international travel (truck traffic was exempted). For reference, the same period was assessed for four previous years.

A total of five stations in Prague were selected:

- a. Legerova street, considered an urban hotspot, with about 45 thousand vehicles traveling daily in one direction (with similar traffic volumes in the opposite direction on a parallel street), primarily (97–98%) light-duty vehicles (trucks over 12 tons are restricted from entering inner Prague and trucks over 6 tons are restricted in the Prague historical district);
- b. Vysočanská street and Průmyslová street, two traffic stations located on heavily traveled main roads used by local and transit truck traffic;
- c. Náměstí Republiky, urban background station in a historical city center, on the border of pedestrian area
- d. Kobylišy, a station in a suburban residential neighborhood
- e. For comparison, a rural background station in Košetice, serving as the Czech national reference station, was used as a reference.

Arithmetic and geometric means and the  $\text{NO}_2/\text{NO}_x$  ratios are plotted, for each station and all years, in Table 3. A single-factor analysis of variance (ANOVA) was performed to compare the variances among the five data sets (one for the year 2020, four for each of the reference years 2016–2019) with the differences within the sets. The associated  $p$ -value ( $p_1$ ) was compared to the  $p$ -value ( $p_2$ ) associated with the difference between mean for the year 2020 and the grand mean for all five years. The higher of the  $p_2/p_1$  ratio and the  $p_2$  (ensuring that the significance of the difference of the year 2020 is much higher than the difference among the years) is then considered the resulting  $p$ -value of the test.

As an alternative analysis, the statistical difference of data from each year from the combined data set for all five years was evaluated using a  $t$ -test, and the  $p$ -value associated with the test for the year 2020 was divided by the average of the four  $p$ -values associated with each of the four reference years.

It is apparent from the Table 2 that NO concentrations significantly decreased at all three traffic stations, with a highest mean decrease of 46% at Legerova and at the Košetice rural background station. The decrease in  $\text{NO}_2$  concentrations was lower than for NO at all Prague stations, highest at Legerova (20%), and even higher (40%) at the Košetice rural background station. As vehicles emit primarily NO, the  $\text{NO}_2/\text{NO}_x$  ratio tends to increase with the age of the emissions, being lowest (around 60%) at Legerova street, 65–70% at Vysočanská, Průmyslová and Náměstí Republiky, 80% at the Kobylišy residential background station and around 90% at the rural station in Košetice. One possible interpretation of the increase in the  $\text{NO}_2/\text{NO}_x$  ratio at Legerova could be that the primary emissions of both NO and  $\text{NO}_2$  were reduced, with lower reduction in “background”  $\text{NO}_2$  originating from  $\text{NO}_x$  emitted elsewhere. Another possible explanation is the reaction

of NO with ozone, yielding NO<sub>2</sub> [70]. Both March and April of 2020 were substantially sunnier than average—4 sunny days and 180 h of sunshine in March and 13 sunny days and 290 h of sunshine in April, compared to 1981–2010 average of about 3 sunny days and 120 h of sunshine for March and 3–4 sunny days and 180 h of sunshine for April [71].

**Table 3.** Comparison of NO and NO<sub>2</sub> concentrations at six monitoring stations during March–April 2020 travel restrictions with the same period during the prior four years.

| Station   | 14 March–30 April  | µg/m <sup>3</sup> , Arithmetic Mean |                 |                 | µg/m <sup>3</sup> , Geometric Mean |                 |                 | Ratio                            |
|---|--------------------|-------------------------------------|-----------------|-----------------|------------------------------------|-----------------|-----------------|----------------------------------|
|   | Year               | NO                                  | NO <sub>2</sub> | NO <sub>x</sub> | NO                                 | NO <sub>2</sub> | NO <sub>x</sub> | NO <sub>2</sub> /NO <sub>x</sub> |
| Legerova<br>type: traffic<br>predominantly<br>light-duty < 3.5 tons | 2016               | 43.5 ± 47.2                         | 55.2 ± 27.4     | 122.0 ± 95.1    | 24.8 ± 3.1                         | 48.4 ± 1.7      | 91.7 ± 2.2      | 55% ± 16%                        |
|   | 2017               | 35.4 ± 38.6                         | 46.5 ± 28.3     | 100.8 ± 84.7    | 17.1 ± 4.0                         | 36.8 ± 2.1      | 67.4 ± 2.7      | 57% ± 16%                        |
|   | 2018               | 44.7 ± 46.2                         | 59.3 ± 29.0     | 128.0 ± 94.3    | 24.6 ± 3.4                         | 51.4 ± 1.8      | 95.5 ± 2.3      | 57% ± 17%                        |
|   | 2019               | 36.9 ± 38.2                         | 55.0 ± 27.2     | 111.7 ± 81.2    | 21.6 ± 3.1                         | 46.8 ± 1.9      | 83.9 ± 2.3      | 58% ± 14%                        |
|   | 2020               | 21.6 ± 27.7                         | 43.2 ± 21.0     | 76.5 ± 59.3     | 12.2 ± 2.9                         | 38.4 ± 1.6      | 60.5 ± 2.0      | 66% ± 15%                        |
|   | 2020 vs. 2016–2019 | −46% ****                           | −20% ****       | −34% ****       | −44% ****                          | −16% ****       | −28% ****       | +23% ****                        |
| Průmyslová<br>type: traffic<br>all types, truck transit             | 2016               | 24.8 ± 40.1                         | 34.6 ± 19.8     | 72.8 ± 77.2     | 9.1 ± 4.8                          | 29.3 ± 1.8      | 48.7 ± 2.4      | 64% ± 20%                        |
|   | 2017               | 21.9 ± 33.2                         | 33.4 ± 20.2     | 67.0 ± 67.9     | 8.1 ± 4.8                          | 27.3 ± 1.9      | 44.3 ± 2.5      | 65% ± 19%                        |
|   | 2018               | 21.4 ± 35.8                         | 31.8 ± 22.0     | 64.7 ± 72.4     | 6.5 ± 5.5                          | 24.1 ± 2.2      | 38.1 ± 2.9      | 67% ± 20%                        |
|   | 2019               | 19.7 ± 39.0                         | 30.6 ± 21.3     | 60.8 ± 77.3     | 5.8 ± 5.2                          | 24.3 ± 2.0      | 37.1 ± 2.6      | 69% ± 19%                        |
|   | 2020               | 16.0 ± 29.0                         | 27.5 ± 19.4     | 52.0 ± 60.1     | 5.5 ± 4.3                          | 21.0 ± 2.2      | 31.8 ± 2.7      | 69% ± 17%                        |
|   | 2020 vs. 2016–2019 | −27% **                             | −15% *          | −22% ***        | −24% ****                          | −20% ****       | −24% ****       | 6%                               |
| Vysočanská<br>type: traffic<br>all types, truck transit             | 2016               | 22.7 ± 29.5                         | 38.0 ± 18.9     | 72.9 ± 60.4     | 12.0 ± 3.3                         | 33.5 ± 1.7      | 55.7 ± 2.1      | 63% ± 16%                        |
|   | 2017               | 18.4 ± 26.6                         | 35.1 ± 19.1     | 63.5 ± 56.5     | 8.2 ± 3.9                          | 30.3 ± 1.7      | 46.6 ± 2.2      | 68% ± 17%                        |
|   | 2018               | 18.8 ± 25.1                         | 36.0 ± 19.9     | 64.9 ± 54.7     | 7.8 ± 4.3                          | 30.5 ± 1.8      | 46.9 ± 2.3      | 68% ± 18%                        |
|   | 2019               | 17.4 ± 22.3                         | 34.1 ± 19.1     | 60.8 ± 49.9     | 8.7 ± 3.5                          | 28.9 ± 1.8      | 45.5 ± 2.2      | 66% ± 16%                        |
|   | 2020               | 14.2 ± 19.9                         | 33.2 ± 18.9     | 55.1 ± 45.0     | 7.0 ± 3.3                          | 28.1 ± 1.8      | 41.8 ± 2.1      | 70% ± 16%                        |
|   | 2020 vs. 2016–2019 | −27% ***                            | −7% ****        | −16% ****       | −23% ****                          | −9% ****        | −14% ****       | 8%                               |
| Náměstí Republiky<br>type: urban<br>background                      | 2016               | 12.0 ± 14.0                         | 20.2 ± 7.1      | 38.8 ± 26.4     | 6.9 ± 3.2                          | 19.2 ± 1.4      | 33.3 ± 1.7      | 59% ± 26%                        |
|   | 2017               | 12.1 ± 12.5                         | 33.1 ± 14.6     | 51.7 ± 30.8     | 9.4 ± 1.9                          | 30.4 ± 1.5      | 46.0 ± 1.6      | 66% ± 15%                        |
|   | 2018               | 15.6 ± 19.5                         | 35.2 ± 17.7     | 59.1 ± 43.7     | 9.8 ± 2.6                          | 31.5 ± 1.6      | 49.1 ± 1.8      | 65% ± 18%                        |
|   | 2019               | 10.9 ± 14.2                         | 31.9 ± 15.2     | 48.7 ± 33.5     | 7.5 ± 2.1                          | 28.9 ± 1.5      | 41.9 ± 1.7      | 70% ± 13%                        |
|   | 2020               | 10.8 ± 10.6                         | 27.8 ± 14.5     | 44.6 ± 28.2     | 8.0 ± 2.1                          | 24.9 ± 1.6      | 38.4 ± 1.7      | 66% ± 12%                        |
|   | 2020 vs. 2016–2019 | −14%                                | −7%             | −10%            | −3%                                | −8%             | −9%             | 2%                               |
| Kobylisy<br>type: residential<br>background                         | 2016               | 3.8 ± 9.3                           | 10.4 ± 6.3      | 16.3 ± 19.0     | 1.2 ± 3.4                          | 9.1 ± 1.7       | 11.9 ± 2.0      | 80% ± 16%                        |
|   | 2017               | 3.7 ± 9.4                           | 14.5 ± 8.7      | 19.7 ± 19.9     | 1.5 ± 3.1                          | 12.7 ± 1.7      | 15.4 ± 1.9      | 80% ± 16%                        |
|   | 2018               | 3.7 ± 8.8                           | 21.7 ± 15.9     | 27.5 ± 26.0     | 1.4 ± 3.2                          | 17.2 ± 1.9      | 20.4 ± 2.1      | 86% ± 11%                        |
|   | 2019               | 3.4 ± 8.8                           | 19.6 ± 15.7     | 25.0 ± 27.1     | 1.1 ± 3.2                          | 15.8 ± 1.9      | 18.4 ± 2.0      | 87% ± 14%                        |
|   | 2020               | 2.8 ± 5.9                           | 17.3 ± 14.1     | 21.0 ± 20.8     | 1.5 ± 2.3                          | 13.0 ± 2.1      | 14.8 ± 2.2      | 81% ± 14%                        |
|   | 2020 vs. 2016–2019 | −22%                                | 4%              | −5%             | 14%                                | −2%             | −8%             | −6%                              |
| Košetice<br>national reference<br>background<br>outside of Prague   | 2016               | 0.5 ± 0.6                           | 6.0 ± 2.6       | 6.8 ± 3.1       | 0.3 ± 2.0                          | 5.4 ± 1.6       | 6.2 ± 1.6       | 90% ± 7%                         |
|   | 2017               | 0.3 ± 0.4                           | 7.3 ± 3.0       | 7.8 ± 3.2       | 0.3 ± 1.8                          | 6.7 ± 1.5       | 7.2 ± 1.5       | 93% ± 5%                         |
|   | 2018               | 0.3 ± 0.4                           | 3.9 ± 2.7       | 4.3 ± 3.0       | 0.2 ± 2.6                          | 3.1 ± 2.0       | 3.5 ± 1.9       | 90% ± 9%                         |
|   | 2019               | 0.2 ± 0.3                           | 3.6 ± 1.9       | 4.0 ± 2.1       | 0.1 ± 2.9                          | 3.1 ± 1.8       | 3.5 ± 1.7       | 91% ± 9%                         |
|   | 2020               | 0.2 ± 0.3                           | 3.1 ± 1.7       | 3.5 ± 1.9       | 0.1 ± 2.8                          | 2.7 ± 1.8       | 3.0 ± 1.8       | 90% ± 9%                         |
|   | 2020 vs. 2016–2019 | −27% ***                            | −7% **          | −16% ***        | −23% **                            | −9%             | −14% *          | +8% ***                          |

\*  $p < 0.05$ , \*\*  $p < 0.01$ , \*\*\*  $p < 0.001$ , \*\*\*\*  $p < 0.0001$ .

It should be noted, however, that the interplay of different factors is rather complex. For example, diminished traffic volumes result in lower frequency of low-speed driving in congested areas, during which the efficiency of exhaust aftertreatment is reduced, resulting in higher overall exhaust temperatures (and thus higher production of NO<sub>2</sub> in oxidation catalysts), but also higher probability of SCR functionality (and thus lower NO<sub>x</sub> emissions)—however, due to Dieselgate, the reality of NO<sub>x</sub> aftertreatment efficiency is likely to be variable, questionable and poorly known.

Additionally, according to [72], it appears that on-road oxidation of NO by ambient O<sub>3</sub> is a significant, but so far ignored, contributor to curbside and near-road NO<sub>2</sub>. This is in agreement with on-road NO<sub>2</sub>/NO<sub>x</sub> ratios in U.S. being reported to be 25–35% and substantially higher than anticipated tailpipe emissions rates [73].

## 6. Discussion

A detailed analysis of NO<sub>2</sub> concentrations measured by the passive samplers shows a clear correlation of NO<sub>2</sub> concentrations with daily traffic counts, adjusted for additional emissions due to uphill travel and stopping at intersections. This finding is in good agreement with the data from the monitoring stations, which, by themselves, are too sparse to make such inference. The correlation of NO<sub>2</sub> concentrations with vehicular traffic intensity is also apparent from the comparison of the data from state air quality monitoring stations during the period of 14 March–30 April 2020, during which travel restrictions were imposed, including the prohibition of all non-cargo international travel, with comparable periods of four previous years. Overall, the findings confirm that vehicular traffic, through primary NO<sub>2</sub> emissions (and possibly through fast reaction of primary NO with ozone), directly affects the NO<sub>2</sub> concentrations in the immediate vicinity.

This correlation, along with correlation of passive sampler readings and air quality monitoring stations, and good consistency of reported NO<sub>2</sub> concentrations among samplers used within the same location at different time periods, all suggest that passive samplers appear to provide, at a reasonable cost and effort, a fairly good image of the distribution of NO<sub>2</sub> concentrations. Judging from limited data, the passive samplers were found to measure about 18.5% higher values than the monitoring stations. Repeated—and most likely deliberate—removals of passive samplers from the immediate vicinity of the monitoring stations have prevented a more quantitative comparison. A comparison of a broader set of data reveals a slightly smaller bias, contributed to, in several cases, by the passive samplers being at more exposed locations (i.e., near the exit of a large underground parking garage) than the monitoring stations. The true bias could therefore be possibly even lower.

Since the trends are comparable within and outside the heavy truck exclusion area, this seems to be primarily an effect of cars and other lighter vehicles (per city statistics, about 90% of traffic is passenger cars [63]). Additionally, there is no correlation between the measured NO<sub>2</sub> concentrations and the heavy vehicle traffic count or between the measured NO<sub>2</sub> concentration and the fraction of heavy vehicles. This is in line with the findings that truck NO<sub>x</sub> emissions have decreased to a considerably higher extent than those of diesel cars in Europe.

The samplers at the locations with highest fraction of heavy vehicles (10–15%, vs. average for all locations 4%) and with the highest absolute heavy vehicle counts (7–16 thousands/day, vs. average 1.7 thousands/day) have measured 25–35 µg/m<sup>3</sup> NO<sub>2</sub>, which is in the second lowest quartile (median concentration is 35 µg/m<sup>3</sup>). This may also be, in part, due to a dependent factor that heavy vehicle traffic is limited in the high population density city center.

The monitoring station at Legerova street is most likely not the absolute hot-spot—it is expected that the emissions of NO<sub>x</sub> would be higher on the parallel street where the vehicles travel uphill (Legerova is one-way street downhill) and at nearby intersections. The street V Holešovičkách, a six-lane road, which is, unlike most other roads of similar size, immediately bordered by residential neighborhoods, with a traffic intensity approaching 100 thousand vehicles per day, a major increase after the opening of a new complex of tunnels providing an alternative route through congested areas, further complicated by a 3% grade, could easily be the next traffic hot-spot.

Considering the finding that about half of the vehicles traveling on the road are not older than 7 years [27], and the several-fold decrease in NO<sub>x</sub> emissions standards over the last decade and half, a much sharper decrease of NO<sub>2</sub> concentrations would be expected than the approximately 1% annually reported by Hůnová [5]; a higher reduction of about 2.5% annually was observed in Western Europe, and about 4.7% annually in United States and Canada [74]. Given the decrease in the limit values of roughly two thirds from Euro 3 (0.50 g/km NO<sub>x</sub>, 2000) to Euro 5 (0.18 g/km, 2009–2010) and from Euro 4 (0.25 g/km NO<sub>x</sub>, 2005) to Euro 6 (0.08 g/km, 2014–2015), the introduction of Euro 5 in late 2009 and Euro 6 in late 2014 should have resulted in about a two thirds NO<sub>x</sub> reduction in at least

half of the vehicles, or about one third reduction in  $\text{NO}_x$  emissions in general. As learned from the analysis of the effects of traffic restrictions, the effect on  $\text{NO}_2$  concentrations may be different, and possibly somewhat smaller than the reduction in  $\text{NO}_x$  emissions, due to atmospheric chemistry. The effects of such a decrease could also have been diminished by an increase in traffic, however, in the center city, the intensity of automobile traffic has been stagnating, or even slightly decreasing.

The mediocre decrease in  $\text{NO}_2$  concentrations, despite more dramatic reduction being expected from improving vehicle technology, is in line with earlier findings that the real  $\text{NO}_x$  emissions of diesel vehicles did not decrease despite the decreasing emissions limits. The situation should have been, however, substantially remedied by “post-Dieselgate” vehicles and by repairs of vehicles affected by Dieselgate. Since it was not, a question therefore arises as to the possibility that Dieselgate relevant repairs were not done on a sufficient number of vehicles and/or were not sufficiently effective and/or were reversed to the “original factory conditions” by the vehicle owners. The authors do not have any reliable statistics on this matter. Furthermore, considering that all three mentioned situations could be associated with criminal offenses and/or considerable civil penalties, detailed investigation of the matter is likely to be considerably difficult.

If there is no assurance that the  $\text{NO}_2$  concentrations will decrease dramatically due to a radical improvement in primary  $\text{NO}_x$  emissions, the only other suitable strategy to improve the air quality is to reduce, to the extent required, the intensity of vehicular traffic. Contrary to the remote regions where automobiles are, in most cases, the only practical means of travel, Prague has an extensive network of public transit. According to the City of Prague statistics [63], only 29% of trips in Prague are done by automobile, 26% of trips are by walking and 42% of trips by public transit. Of the public transit, slightly over one third is done by subway, and another third by trams and commuter rail, which are, with the exception of a rather small number of diesel rail cars used on sparsely traveled rail lines, run on electric power, and therefore with very small effect on  $\text{NO}_2$  emissions. The remaining third of trips is by diesel buses, the majority of which are equipped with SCR catalysts, and potentially reaching  $\text{NO}_x$  emissions not much larger (and according to measurements possibly even smaller) levels, per kilometer and vehicle, than an average diesel car. It is therefore readily apparent that shifting from an average automobile to any other means of transport is likely to reduce the  $\text{NO}_2$  concentrations. (Shift to electric power, compressed natural gas, or other “clean” propulsion is a gradual process and is unlikely to be done, within a few years, on a sufficiently large number of vehicles to make a difference throughout the city).

## 7. Summary and Conclusions

Despite massive reductions in diesel cars  $\text{NO}_x$  emission limits, of about two thirds from Euro 3 to Euro 5 and from Euro 4 to Euro 6,  $\text{NO}_2$  concentrations throughout the Czech Republic have been decreasing at a mediocre rate of 1% annually.

A review of the underlying engine emissions trends shows that the conversion of NO into  $\text{NO}_2$  in diesel oxidation catalysts, beneficial for regeneration of diesel particle filters and for the functioning of the SCR systems for  $\text{NO}_x$  reduction, did not, contrary to the intentions of the legislation, go hand in hand with a major reduction of  $\text{NO}_x$  emissions in subsequent (downstream)  $\text{NO}_x$  aftertreatment devices. As a result, primary  $\text{NO}_2$  emissions from light duty diesel vehicles are in most cases considerably higher than intended in the emissions legislation due to non-adherence of many manufacturers to the primary intent of the legislation.

A review of the health effects on  $\text{NO}_2$  on children shows that all reviewed studies indicate a significant effect of prenatal  $\text{NO}_2$  exposure to children’s neurobehavioral development, in adults to dementia at concentrations lower than EU standards of  $40 \mu\text{g}/\text{m}^3/\text{year}$ . These results should be understood as a strong recommendation to reduce the  $\text{NO}_2$  concentrations below the current EU standard. All presented studies prove that  $\text{NO}_2$  can

significantly deteriorate CNS and therefore this knowledge should be used to improve the quality of our lives.

To elucidate the effects of motorized traffic on NO<sub>2</sub> concentrations, data from 104 passive NO<sub>2</sub> samplers deployed at 65 locations in Prague during March–April and September–October of 2019 were examined. Comparisons with the national monitoring network show a positive bias of 18.5% for colocated samplers and 17% for samplers nearby (or in similar settings as) the monitoring stations. There was a good correlation among repeated measurements at the same locations. The data from the national air quality monitoring network show that the average concentrations in both spring and fall sampling periods were consistent with 2016–2019 averages.

The average measured NO<sub>2</sub> concentrations at the selected locations, after correcting for the 18.5% bias, were in the range of 16–69 µg/m<sup>3</sup>, with a mean of 36 µg/m<sup>3</sup> and a median of 35 µg/m<sup>3</sup>, and were higher than the EU and national limit (annual average) of 40 µg/m<sup>3</sup> at 32% of locations. The NO<sub>2</sub> concentrations have correlated well with the intensity of traffic (average daily vehicle counts), corrected for additional emissions due to uphill travel and due to idling at, and accelerating from, intersections. Several additional “hot-spots” were identified, in addition to the “hot-spot” monitoring station at Legerova street (2016–2019 NO<sub>2</sub> average of 51 µg/m<sup>3</sup>), where the vehicles travel on a slight decline on a one-way street: several intersections at Sokolská street, parallel with Legerova with uphill direction of travel, and emerging hot-spots along V Holešovičkách street, where the traffic intensity increased due to the opening of a new series of tunnels. Analysis of the effect of coronavirus related travel restrictions were evaluated by comparing the data from six monitoring stations (15 March–30 April 2020, relative to the same period during 2016–2019) reveal a reduction of NO, NO<sub>2</sub> and NO<sub>x</sub> (except for a small increase of NO<sub>2</sub> at one of the background stations), with NO reduction being, at high traffic locations, higher than that of NO<sub>2</sub>. The spatial analysis of data from passive samplers and time analysis of data during the travel restrictions both demonstrate a consistent positive correlation between traffic intensity and NO<sub>2</sub> concentrations along/near the travel path.

It appears that decreases in vehicle NO<sub>x</sub> emission limits, introduced in the last decade or two, have failed to sufficiently reduce the ambient NO<sub>2</sub> concentrations in exposed locations in Prague. This is in part due to increased fraction of NO<sub>2</sub> in NO<sub>x</sub> in newer vehicles, and in part due to “a major disparity between the numerical value of the emission limit and the actual emissions in everyday driving”. Further, there is no apparent sign of, and it is far from clear that, the “excess emissions” of NO<sub>x</sub>, a problem known as Dieselgate, have been efficiently remedied.

**Author Contributions:** M.S. has organized the passive sampling campaign, selected locations, placed and removed samplers, and secured funding. R.J.S. has compiled the review of health effects. J.S. has participated in data analysis. M.V.-L. reviewed the engine emissions and did a large share of data analysis and manuscript writing. All authors have read and agreed to the published version of the manuscript.

**Funding:** The acquisition and analysis of the passive samplers was funded by Deutsche Umwelthilfe (Environmental Action Germany), Hackescher Markt 4, 10178 Berlin, Germany, [www.duh.de](http://www.duh.de) (accessed on 18 May 2021). Evaluation of the passive samplers and some of the background research on emissions was done (M.V.) within the H2020 project no. 851002 uCARE. You can also reduce emissions. Review of the health effects and remaining work has been supported by the European Regional Development Fund under Grant Healthy Aging in Industrial Environment HAIE (CZ.02.1.01/0.0/0.0/16\_019/0000798).

**Institutional Review Board Statement:** Not applicable.

**Informed Consent Statement:** Not applicable.

**Data Availability Statement:** Most of the relevant data is contained in the manuscript. Sampling and analytical protocols associated with passive samplers are available from Miroslav Šuta. Traffic volume data are publicly available, see the link in the reference list. Data from the national air

quality monitoring network are a third-party data and must be requested directly from the Czech Hydrometeorological Institute.

**Acknowledgments:** The data from the national air quality monitoring network was provided by the Czech Hydrometeorological Institute. The authors thank Václav Novák, the Head of the Air Quality Information System Department, for providing the data and for helpful advice.

**Conflicts of Interest:** The authors declare no conflict of interest.

## References

1. Health Effect Institute. State of Global Air Report. 2018. Available online: <https://www.stateofglobalair.org/sites/default/files/soga-2018-report.pdf> (accessed on 8 February 2021).
2. European Environment Agency (EEA). *Air Quality in Europe*; European Environment Agency: Copenhagen, Denmark, 2020. Available online: <https://www.eea.europa.eu/publications/air-quality-in-europe-2020-report> (accessed on 8 February 2021).
3. World Bank. *The Cost of Pollution: Strengthening the Economic Case for Action*; World Bank: Washington, DC, USA, 2016. Available online: <https://openknowledge.worldbank.org/bitstream/handle/10986/25013/108141.pdf?sequence=4&isAllowed=y> (accessed on 8 February 2021).
4. Hesterberg, T.W.; Long, C.M.; Sax, S.N.; Lapin, C.A.; McClellan, R.O.; Bunn, W.B.; Valberg, P.A. Particulate matter in new technology diesel exhaust (NTDE) is quantitatively and qualitatively very different from that found in traditional diesel exhaust (TDE). *J. Air Waste Manag. Assoc.* **2011**, *61*, 894–913. [CrossRef] [PubMed]
5. Hunova, I.; Baumelt, V.; Modlik, M. Long-term trends in nitrogen oxides at different types of monitoring stations in the Czech Republic. *Sci. Total Environ.* **2020**, *699*, 134378. [CrossRef]
6. Georgoulas, A.K.; van der, A.J.R.; Stammes, P.; Boersma, K.F.; Eskes, H.J. Trends and trend reversal detection in 2 decades of tropospheric NO<sub>2</sub> satellite observations. *Atmos. Chem. Phys.* **2019**, *19*, 6269–6294. [CrossRef]
7. Casquero-Vera, J.A.; Lyamani, H.; Titos, G.; Borrás, E.; Olmo, F.J.; Alados-Arboledas, L. Impact of primary NO<sub>2</sub> emissions at different urban sites exceeding the European NO<sub>2</sub> standard limit. *Sci. Total Environ.* **2019**, *646*, 1117–1125. [CrossRef] [PubMed]
8. Wild, R.J.; Dubé, W.P.; Aikin, K.C.; Eilerman, S.J.; Neuman, J.A.; Peischl, J.; Ryerson, T.B.; Brown, S.S. On-road measurements of vehicle NO<sub>2</sub>/NO<sub>x</sub> emission ratios in Denver, Colorado, USA. *Atmos. Environ.* **2017**, *148*, 182–189. [CrossRef]
9. Grange, S.K.; Lewis, A.C.; Moller, S.J.; Carslaw, D.C. Lower vehicular primary emissions of NO<sub>2</sub> in Europe than assumed in policy projections. *Nat. Geosci.* **2017**, *10*, 914–918. [CrossRef]
10. Zeldovich, Y.B. The Oxidation of Nitrogen in Combustion Explosions. *Acta Physicochim.* **1946**, *21*, 577–628.
11. Lavoie, G.A.; Heywood, J.B.; Keck, J.C. Experimental and Theoretical Study of Nitric Oxide Formation in Internal Combustion Engines. *Combust. Sci. Technol.* **1970**, *1*, 313–326. [CrossRef]
12. Gutzwiller, L.; Arens, F.; Baltensperger, U.; Gaggeler, H.W.; Ammann, M. Significance of Semivolatile Diesel Exhaust Organics for Secondary HONO Formation. *Environ. Sci. Technol.* **2002**, *36*, 677–682. [CrossRef]
13. Kurtenbach, R.; Becker, K.H.; Gomes, J.A.G.; Kleffmann, J.; Lorzer, J.C.; Spittler, M.; Wiesen, P.; Ackermann, R.; Geyer, A.; Platt, U. Investigations of emissions and heterogeneous formation of HONO in a road traffic tunnel. *Atmos. Environ.* **2001**, *35*, 3385–3394. [CrossRef]
14. Heeb, N.V.; Zimmerli, Y.; Czerwinski, J.; Schmid, P.; Zennegg, M.; Haag, R.; Seiler, C.; Wichser, A.; Ulrich, A.; Honegger, P.; et al. Reactive nitrogen compounds (RNCs) in exhaust of advanced PM–NO<sub>x</sub> abatement technologies for future diesel applications. *Atmos. Environ.* **2011**, *45*, 3203–3209. [CrossRef]
15. Seinfeld, J.H.; Pandis, S.N. *Atmospheric Chemistry and Physics: From Air Pollution to Climate Change*; John Wiley and Sons: Hoboken, NJ, USA, 1998.
16. Mooney, J.J.; Thompson, C.E.; Dettling, J.C. Three-Way Conversion Catalysts Part of the New Emission Control System. *SAE Trans.* **1977**, *86*, 1553–1562.
17. Falk, C.D.; Mooney, J.J. Three—Way Conversion Catalysts: Effect of Closed—Loop Feed—Back Control and Other Parameters on Catalyst Efficiency. *SAE Trans.* **1980**, *89*, 1822–1832.
18. Hardin, G. The tragedy of the commons. *Science* **1968**, *162*, 1243–1248. [CrossRef]
19. Thompson, G.; Carder, D.; Clark, N.; Gautam, M. Summary of In-use NO<sub>x</sub> Emissions from Heavy-Duty Diesel Engines. *SAE Int. J. Commer. Veh.* **2009**, *1*, 162–184. [CrossRef]
20. United States Department of Justice (USDOJ). Clean Air Act Diesel Engine Cases. 2015. Available online: <https://www.justice.gov/enrd/diesel-engines> (accessed on 2 February 2021).
21. United States Code of Federal Regulations (US CFR). Volume 40, Part § 86.1370: Not-To-Exceed Test Procedures. 2000. As Amended by Subsequent Regulations. Available online: <https://www.law.cornell.edu/cfr/text/40/86.1370> (accessed on 18 May 2021).
22. Gieshaskiel, B.; Gioria, R.; Carriero, M.; Lahde, T.; Forloni, F.; Perujo Mateos del Parque, A.; Martini, G.; Bissi, L.M.; Terenghi, R. Emission Factors of a Euro VI Heavy-duty Diesel Refuse Collection Vehicle. *Sustainability* **2019**, *11*, 1067. [CrossRef]
23. Suarez-Bertoa, R.; Valverde, V.; Clairotte, M.; Pavlovic, J.; Giechaskiel, B.; Franco, V.; Kregar, Z.; Astorga-Llorens, M. On-road emissions of passenger cars beyond the boundary conditions of the real-driving emissions test. *Environ. Res.* **2019**, *176*, 108572. [CrossRef]

24. Quiros, D.C.; Thiruvengadam, A.; Pradhan, S.; Besch, M.; Thiruvengadam, P.; Demirgok, B.; Carder, D.; Oshinuga, A.; Huai, T.; Hu, S. Real-world emissions from modern heavy-duty diesel, natural gas, and hybrid diesel trucks operating along major California freight corridors. *Emiss. Control Sci. Technol.* **2016**, *2*, 156–172. [[CrossRef](#)]
25. Jiang, Y.; Yang, J.; Cocker, D., 3rd; Karavalakis, G.; Johnson, K.C.; Durbin, T.D. Characterizing emission rates of regulated pollutants from model year 2012 + heavy-duty diesel vehicles equipped with DPF and SCR systems. *Sci. Total Environ.* **2018**, *619–620*, 765–771. [[CrossRef](#)]
26. Grigoratos, T.; Fontaras, G.; Giechaskiel, B.; Zacharof, N. Real world emissions performance of heavy-duty Euro VI diesel vehicles. *Atmos. Environ.* **2019**, *201*, 348–359. [[CrossRef](#)]
27. Skacel, J.; Vojtisek, M.; Beranek, V.; Pechout, M. Black Sheep—Detecting Polluting Vehicles on the Road Using Roadside Particle Measurement. In Proceedings of the ETH Conference on Combustion Generated Nanoparticles, Zurich, Switzerland, 18–21 June 2018. Available online: [https://nanoparticles.ch/archive/2018\\_Skacel\\_PO.pdf](https://nanoparticles.ch/archive/2018_Skacel_PO.pdf) (accessed on 2 February 2021).
28. Vojtisek-Lom, M.; Fenkl, M.; Dufek, M.; Mares, J. *Off-Cycle, Real-World Emissions of Modern Light Duty Diesel Vehicles*; SAE International: Warrendale, PA, USA, 2009. [[CrossRef](#)]
29. Weiss, M.; Bonnel, P.; Kuhlwein, J.; Provenza, A.; Lambrecht, U.; Alessandrini, S.; Carriero, M.; Colombo, R.; Forni, F.; Lanappe, G.; et al. Will Euro 6 reduce the NO<sub>x</sub> emissions of new diesel cars?—Insights from on-road tests with Portable Emissions Measurement Systems (PEMS). *Atmos. Environ.* **2012**, *62*, 657–665. [[CrossRef](#)]
30. Ligterink, N.; Kadijk, G.; Mensch, P.; van Hausberger, S.; Rexeis, M. *Investigations and Real World Emission Performance of Euro 6 Light-Duty Vehicles*; Report TNO 2013 R11891; TNO: The Hague, The Netherlands, 2013; p. 53.
31. Franco, V.; Sanchez, F.P.; German, J.; Mock, P. *Real-World Exhaust Emissions from Modern Diesel Cars a Meta-Analysis of PEMS Emissions Data from EU (EURO 6) and US (TIER 2 BIN 5/ULEV II) Diesel Passenger Cars*; White Paper; International Council Clean on Transportation (ICCT): Berlin, Germany, 2014.
32. Yang, L.; Franco, V.; Mock, P.; Kolke, R.; Zhang, S.; Wu, Y.; German, J. Experimental Assessment of NO<sub>x</sub> Emissions from 73 Euro 6 Diesel Passenger Cars. *Environ. Sci. Technol.* **2015**, *49*, 14409–14415. [[CrossRef](#)]
33. Olsen, D.B.; Kohls, M.; Arney, G. Impact of oxidation catalysts on exhaust NO<sub>2</sub>/NO<sub>x</sub> ratio from lean-burn natural gas engines. *J. Air Waste Manag. Assoc.* **2010**, *60*, 867–874. [[CrossRef](#)] [[PubMed](#)]
34. Carslaw, D.C. Evidence of an increasing NO<sub>2</sub>/NO<sub>x</sub> emissions ratio from road traffic emissions. *Atmos. Environ.* **2005**, *39*, 4793–4802. [[CrossRef](#)]
35. Carslaw, D.; Rhys-Tyler, G. *Remote Sensing of NO<sub>2</sub> Exhaust Emissions from Road Vehicles: A Report to the City of London Corporation and London Borough of Ealing*; DEFRA: London, UK, 2013.
36. Preble, C.V.; Harley, R.A.; Kirchstetter, T.W. *Measuring Real-World Emissions from the On-Road Heavy-Duty Truck Fleet*; University of California: Berkeley, CA, USA, 2019.
37. Vojtisek-Lom, M.; Beranek, V.; Klir, V.; Jindra, P.; Pechout, M.; Vorisek, T. On-road and laboratory emissions of NO, NO<sub>2</sub>, NH<sub>3</sub>, N<sub>2</sub>O and CH<sub>4</sub> from late-model EU light utility vehicles: Comparison of diesel and CNG. *Sci. Total Environ.* **2018**, *616–617*, 774–784. [[CrossRef](#)]
38. Pechout, M.; Kotek, M.; Jindra, P.; Macoun, D.; Hart, J.; Vojtisek-Lom, M. Comparison of hydrogenated vegetable oil and biodiesel effects on combustion, unregulated and regulated gaseous pollutants and DPF regeneration procedure in a Euro6 car. *Sci. Total Environ.* **2019**, *696*, 133748. [[CrossRef](#)]
39. Singh, J. Nitrogen dioxide exposure alters neonatal development. *Neurotoxicology* **1988**, *9*, 545–549.
40. Wang, S.Q.; Zhang, J.L.; Zeng, X.D.; Zeng, Y.M.; Wang, S.C.; Chen, S.Y. Association of traffic-related air pollution with children’s neurobehavioral functions in Quanzhou, China. *Environ. Health Perspect.* **2009**, *117*, 1612–1618. [[CrossRef](#)] [[PubMed](#)]
41. Guxens, M.; Aguilera, I.; Ballester, E.; Estarlich, M.; Fernandez-Somoano, A.; Lertxundi, A.; Lertxundi, N.; Mendez, M.A.; Tardon, A.; Vrijheid, M.; et al. Prenatal exposure to residential air pollution and infant mental development: Modulation by antioxidants and detoxification factors. *Environ. Health Perspect.* **2012**, *120*, 144–149. [[CrossRef](#)] [[PubMed](#)]
42. Kim, E.; Park, H.; Hong, Y.-C.; Ha, M.; Kim, Y.; Kim, B.N.; Kim, Y.; Roh, Y.M.; Lee, B.E.; Ryu, J.M.; et al. Prenatal exposure to PM<sub>10</sub> and NO<sub>2</sub> and children’s neurodevelopment from birth to 24 months of age: Mothers and Children Environmental Health (MOCEH) study. *Sci. Total Environ.* **2014**, *481*, 439–445. [[CrossRef](#)]
43. Lertxundi, A.; Baccini, M.; Letxundi, N.; Fano, E.; Aranbarri, A.; Martinez, M.D.; Ayerdi, M.; Alvarez, J.; Santa-Marina, L.; Dorronsoro, M.; et al. Exposure to fine particle matter, nitrogen dioxide and benzene during pregnancy and cognitive and psychomotor developments in children at 15 months of age. *Environ. Int.* **2015**, *80*, 33–40. [[CrossRef](#)]
44. Sunyer, J.; Esnaola, M.; Alvarez-Pedrerol, M.; Forn, J.; Rivas, I.; Lopez-Vicente, M.; Suades-Gonzalez, E.; Foraster, M.; Garcia-Esteban, R.; Basagana, X.; et al. Association between traffic-related air pollution in schools and cognitive development in primary school children: A prospective cohort study. *PLoS Med.* **2015**, *12*, e1001792. [[CrossRef](#)] [[PubMed](#)]
45. Pujol, J.; Martinez-Vilavella, G.; Macia, D.; Fenoll, R.; Alvarez-Pedrerol, M.; Rivas, I.; Forn, J.; Blanco-Hinojo, L.; Capellades, J.; Querol, X.; et al. Traffic pollution exposure is associated with altered brain connectivity in school children. *Neuroimage* **2016**, *129*, 175–184. [[CrossRef](#)] [[PubMed](#)]
46. Forn, J.; Dadvand, P.; Foraster, M.; Alvarez-Pedrerol, M.; Rivas, I.; Lopez-Vicente, M.; Suades-Gonzalez, E.; Garcia-Esteban, R.; Esnaola, M.; Cirach, M. Traffic-related air pollution, noise at school, and behavioral problems in Barcelona schoolchildren: A cross-sectional study. *Environ. Health Perspect.* **2016**, *124*, 529–535. [[CrossRef](#)] [[PubMed](#)]

47. Min, J.; Min, K. Exposure to ambient PM<sub>10</sub> and NO<sub>2</sub> and the incidence of attention-deficit hyperactivity disorder in childhood. *Environ. Int.* **2017**, *99*, 221–227. [[CrossRef](#)] [[PubMed](#)]
48. Sentis, A.; Sunyer, J.; Dalmau-Bueno, A.; Andiarrena, A.; Ballester, F.; Ciracha, M.; Estarlich, M.; Fernandez-Somoano, A.; Ibarluzea, J.; Iniguez, C.; et al. Prenatal and postnatal exposure to NO<sub>2</sub> and child attentional function at 4–5 years of age. *Environ. Int.* **2017**, *106*, 170–177. [[CrossRef](#)]
49. Sunyer, J.; Suades-Gonzales, E.; Garcia-Esteban, R.; Rivas, I.; Pujol, J.; Alvarez-Pedrerol, M.; Forns, J.; Querol, X.; Basagana, X. Traffic-related air pollution and attention in primary school children. Short-term association. *Epidemiology* **2017**, *28*, 181–189. [[CrossRef](#)]
50. Forns, J.; Dadvand, P.; Esnaola, M.; Alvarez-Pedrerol, M.; Lopez-Vicente, M.; Garcia-Esteban, R.; Cirach, M.; Basagana, X.; Guxens, M.; Sunyer, J. Longitudinal association between air pollution exposure at school and cognitive development in school children over a period of 3.5 years. *Environ. Res.* **2017**, *159*, 416–421. [[CrossRef](#)]
51. Vert, C.; Sanchez-Benavides, G.; Martinez, D.; Gotsens, X.; Gramunt, N.; Cirach, M.; Molinuevo, J.L.; Sunyer, J.; Nieuwenhuisen, M.J.; Crous-Bou, M.; et al. Effect of long-term exposure to air pollution on anxiety and depression in adults: A cross-sectional study. *Int. J. Hyg. Environ. Health* **2017**, *220*, 1074–1080. [[CrossRef](#)]
52. Alemany, S.; Vilor-Tejedor, N.; Garcia-Esteban, R.; Bustamante, M.; Dadvand, P.; Esnaola, M.; Mortamais, M.; Forns, J.; van Drooge, B.L.; Alvarez-Pedrerol, M.; et al. Traffic-related air pollution, APOE  $\epsilon$ 4 status, and neurodevelopmental outcomes among school children enrolled in the BREATHE project (Catalonia, Spain). *Environ. Health Perspect.* **2018**, *126*, 087001. [[CrossRef](#)]
53. Carey, I.M.; Anderson, H.R.; Atkinson, R.W.; Beevers, S.; Cook, D.G.; Strachan, D.P.; Dajnak, D.; Gulliver, J.; Kelly, F.J. Are noise and air pollution related to the incidence of dementia? A cohort study in London, England. *BMJ Open* **2018**, *8*, e022404. [[CrossRef](#)]
54. Roberts, S.; Arseneault, L.; Barratt, B.; Danese, A.; Odgers, C.L.; Moffitt, T.E.; Reuben, A.; Kelly, F.J.; Fisher, H.L. Exploration of NO<sub>2</sub> and PM<sub>2.5</sub> air pollution and mental health problems using high-resolution data in London-based children from a UK longitudinal cohort study. *Psychiatry Res.* **2019**, *272*, 8–17. [[CrossRef](#)] [[PubMed](#)]
55. Lertxundi, A.; Andiarrena, A.; Martinez, M.D.; Ayerdi, M.; Murcia, M.; Estarlich, M.; Guxens, M.; Sunyer, J.; Julvez, J.; Ibarluzea, J. Prenatal exposure to PM<sub>2.5</sub> and NO<sub>2</sub> and sex-dependent infant cognitive and motor development. *Environ. Res.* **2019**, *174*, 114–121. [[CrossRef](#)]
56. Jorcano, A.; Lubczynska, M.J.; Pierotti, L.; Altung, H.; Ballester, F.; Cesaroni, G.; El Marroun, H.; Fernandez-Somoano, A.; Freire, C.; Hanke, W.; et al. Prenatal and postnatal exposure to air pollution and emotional and aggressive symptoms in children from 8 European birth cohorts. *Environ. Int.* **2017**, *131*, 104927. [[CrossRef](#)] [[PubMed](#)]
57. Loftus, C.T.; Ni, Y.; Szpiro, A.A.; Hazlehurst, M.F.; Tylavsky, F.A.; Bush, N.R.; Sathyanarayana, S.; Carroll, K.N.; Young, M.; Karr, C.J.; et al. Exposure to ambient air pollution and early childhood behavior: A longitudinal cohort study. *Environ. Res.* **2020**, *183*, 109075. [[CrossRef](#)] [[PubMed](#)]
58. Kulick, E.R.; Wellenius, G.A.; Boehma, A.K.; Joyce, N.R.; Schupf, N.; Kaufman, J.D.; Mayeux, R.; Sacco, R.L.; Manly, J.J.; Elkind, M.S.V. Long-term exposure to air pollution and trajectories of cognitive decline among older adults. *Neurology* **2020**, *94*, e1782–e1792. [[CrossRef](#)] [[PubMed](#)]
59. Erickson, L.D.; Gale, S.D.; Anderson, J.E.; Brown, B.L.; Hedges, D.W. Association between exposure to air pollution and total gray matter and total white matter volumes in adults: A cross-sectional study. *Brain Sci.* **2020**, *10*, 164. [[CrossRef](#)] [[PubMed](#)]
60. Deutsche Umwelthilfe e.V. (DUH). NO<sub>2</sub> Report Hotspots in Germany, Czech Republic, Slovenia, Bulgaria and Serbia. October 2019. Available online: [https://www.duh.de/fileadmin/user\\_upload/download/Projektinformation/Verkehr/Abgasalarm/NO2\\_Report\\_17\\_10\\_19.pdf](https://www.duh.de/fileadmin/user_upload/download/Projektinformation/Verkehr/Abgasalarm/NO2_Report_17_10_19.pdf) (accessed on 3 May 2021).
61. Palmes, E.D.; Gunnison, A.F.; DiMattio, J.; Tomczyk, C. Personal Sampler for Nitrogen Dioxide. *Am. Ind. Hyg. Assoc. J.* **1976**, *37*, 570–577. [[CrossRef](#)]
62. Passam. NO<sub>2</sub> Passive Sampler Data Sheet and Specifications, Switzerland. Available online: [https://www.passam.ch/wp-content/uploads/2020/01/en\\_NO2lt.pdf](https://www.passam.ch/wp-content/uploads/2020/01/en_NO2lt.pdf) (accessed on 2 February 2021).
63. Technická Správa Komunikací hl. m. Prahy (TSK City of Prague Highway Department). Prague Transportation Yearbook. 2019. Available online: <http://www.tsk-praha.cz/static/udi-rocenka-2019-en.pdf> (accessed on 7 February 2021).
64. Cape, J.N. *Review of the Use of Passive Diffusion Tubes for Measuring Concentrations of Nitrogen Dioxide in Air*; DEFRA: London, UK, 2005.
65. Buzica, D.; Gerboles, M.; Plaisance, H. The equivalence of diffusive samplers to reference methods for monitoring O<sub>3</sub>, benzene and NO<sub>2</sub> in ambient air. *J. Environ. Monit.* **2008**, *10*, 1052–1059. [[CrossRef](#)]
66. Hafkenschied, T.; Fromage-Marriette, A.; Goelen, E.; Hangartner, M.; Pfeffer, U.; Plaisance, H.; de Santis, F.; Saunders, K.; Swaans, W.; Tang, S.; et al. *Review of the Application of Diffusive Samplers for the Measurement of Nitrogen Dioxide in Ambient Air in the European Union*; EUR 23793 EN; OPOCE: Luxembourg, 2009. Available online: <https://publications.jrc.ec.europa.eu/repository/handle/JRC51106> (accessed on 2 May 2021).
67. Heal, M.R.; Laxen, D.P.H.; Marner, B.B. Biases in the Measurement of Ambient Nitrogen Dioxide (NO<sub>2</sub>) by Palmes Passive Diffusion Tube: A Review of Current Understanding. *Atmosphere* **2019**, *10*, 357. [[CrossRef](#)]
68. Czech Hydrometeorological Institute (CHMI)—Air Quality Division. Air Pollution and Atmospheric Deposition in Data, The Czech Republic: Annual Tabular Overview 2019: Commentary on the Summary Annual Tabular Survey. Available online: [https://www.chmi.cz/files/portal/docs/uoco/isko/tab\\_roc/2019\\_enh/pdf/kom.pdf](https://www.chmi.cz/files/portal/docs/uoco/isko/tab_roc/2019_enh/pdf/kom.pdf) (accessed on 2 May 2021).

69. Altshuller, A.P. Thermodynamic considerations in the interactions of nitrogen oxides and oxy-acids in the atmosphere. *J. Air Pollut. Control. Assoc.* **1956**, *6*, 97–100. [[CrossRef](#)]
70. Finlayson-Pitts, B.J.; Pitts, J.N. *Chemistry of the Upper and Lower Atmosphere: Theory, Experiments, and Applications*; Academic Press: London, UK, 2000; p. 266. ISBN 9780122570605.
71. Czech Hydrometeorological Institute (CHMI). Historical Data—Meteorology and Climatology: Monthly Observation REPORTS—Weather Records for Prague. Available online: <https://www.chmi.cz/historicka-data/pocasi/mesicni-data/mesicni-prehledy-pozorovani#> (accessed on 2 May 2021).
72. Yang, B.; Zhang, K.M.; Xu, W.D.; Zhang, S.; Batterman, S.; Baldauf, R.W.; Deshmukh, P.; Snow, R.; Wu, Y.; Zhang, Q.; et al. On-Road Chemical Transformation as an Important Mechanism of NO<sub>2</sub> Formation. *Environ. Sci. Technol.* **2018**, *58*, 4574–4582. [[CrossRef](#)] [[PubMed](#)]
73. Richmond-Bryant, J.; Owen, R.C.; Graham, S.; Snyder, M.; McDow, S.; Oakes, M.; Kimbrough, S. Estimation of on-road NO<sub>2</sub> concentrations, NO<sub>2</sub>/NO<sub>x</sub> ratios, and related roadway gradients from near-road monitoring data. *Air Qual. Atmos. Health* **2017**, *10*, 611–625. [[CrossRef](#)]
74. Geddes, J.A.; Martin, R.V.; Boys, B.L.; van Donkelaar, A. Long-term trends worldwide in ambient NO<sub>2</sub> concentrations inferred from satellite observations. *Environ. Health Perspect.* **2016**, *124*, 281–289. [[CrossRef](#)] [[PubMed](#)]



Article

# Low-Cost Air Quality Sensors: One-Year Field Comparative Measurement of Different Gas Sensors and Particle Counters with Reference Monitors at Tušimice Observatory

Petra Bauerová <sup>1,\*</sup>, Adriana Šindelářová <sup>1</sup>, Štěpán Rychlík <sup>2</sup>, Zbyněk Novák <sup>3</sup> and Josef Keder <sup>1</sup>

<sup>1</sup> Czech Hydrometeorological Institute, Tušimice Observatory, Tušimice 6, 432 01 Kadaň, Czech Republic; adriana.sindelarova@chmi.cz (A.Š.); josef.keder@chmi.cz (J.K.)

<sup>2</sup> Czech Hydrometeorological Institute, Central Ambient Air Quality Laboratories, Generála Šišky 942, 142 00 Prague, Czech Republic; stepan.rychlik@chmi.cz

<sup>3</sup> Envitech Bohemia s.r.o., Ovocná 34/1021, 161 00 Prague, Czech Republic; novak@envitech-bohemia.cz

\* Correspondence: petra.bauerova@chmi.cz; Tel.: +420-474-332-668

Received: 20 April 2020; Accepted: 9 May 2020; Published: 11 May 2020



**Abstract:** With attention increasing regarding the level of air pollution in different metropolitan and industrial areas worldwide, interest in expanding the monitoring networks by low-cost air quality sensors is also increasing. Although the role of these small and affordable sensors is rather supplementary, determination of the measurement uncertainty is one of the main questions of their applicability because there is no certificate for quality assurance of these non-reference technologies. This paper presents the results of almost one-year field testing measurements, when the data from different low-cost sensors (for SO<sub>2</sub>, NO<sub>2</sub>, O<sub>3</sub>, and CO: Cairclip, Envea, FR; for PM<sub>1</sub>, PM<sub>2.5</sub>, and PM<sub>10</sub>: PMS7003, Plantower, CHN, and OPC-N2, Alphasense, UK) were compared with co-located reference monitors used within the Czech national ambient air quality monitoring network. The results showed that in addition to the given reduced measurement accuracy of the sensors, the data quality depends on the early detection of defective units and changes caused by the effect of meteorological conditions (effect of air temperature and humidity on gas sensors and effect of air humidity with condensation conditions on particle counters), or by the interference of different pollutants (especially in gas sensors). Comparative measurement is necessary prior to each sensor's field applications.

**Keywords:** microsensors; particle counter; gas analyzers; relative humidity; air pollution

## 1. Introduction

Similarly to other countries, in the Czech Republic, the public's interest in the current state of ambient air quality is increasing, especially in cities and locations exposed to industrial sources of pollution. Although the national air quality network is representatively deployed over the entire territory, covering all types of monitoring sites (urban, industrial, and background) and potential air pollution sources (traffic, agricultural, and industrial), requests to widen the spatial resolution of the measurement network (to almost personal exposure) are still increasing in the public sector [1–3].

During the last three years, the Czech Hydrometeorological Institute (CHMI) has recorded several requests for assistance in processing data from public projects that applied sensors in cities or other places of interest. Most of these projects suffered from severe shortcomings in the following points:

1. Clearly defined sensor application targets;
2. Appropriate sensor placement (study design) to monitor the given target;

3. Selection of suitable sensor types;
4. Initial and continuous verification of sensor measurement quality;
5. Sensor data control and processing;
6. Appropriate use and interpretation of results.

The indicated order of these points is very important because effective and successful sensor application depends mainly on the first four points. Unfortunately, most of the applicants for assistance turn to the experts only at points five or six, but it should be emphasized that even professionally processed data cannot save a poorly designed project. This paper deals with the two main points highlighted in bold above (sensor type selection and measurement quality control).

Among all the issues, the selection of appropriate and reliable sensors is always a challenging goal [4]. There is a wide range of air quality sensors available on the market, which grows every year, while no regulatory legislation or standards for quality control exist yet. Although some activities in creating international standards for air quality sensors evaluation have been already started (e.g., the European Committee for Standardization [5]), in the meantime, different specialized institutions are trying to objectively evaluate and show the measurement quality of recently produced sensor units (by performing standard statistical procedures including descriptive statistics, calculation of correlation coefficients, coefficients of determination, or measurement errors [4,6–9]). A common summary of all these independent evaluations is that this miniaturized technology has some limits, manifested primarily by different performance in real outdoor (uncontrolled) conditions than in laboratory evaluations under controlled conditions (e.g., [4,10]). The measurement quality of electrochemical gas sensors is usually susceptible to changes in ambient air temperature (T) and relative humidity (RH) [4] (for the effect of increasing sensor unit temperature on sensor sensitivity or zero offset, see Mead et al. [11]), and to cross-interference of various gases (especially between O<sub>3</sub> and NO<sub>2</sub>; [11,12]), which often leads to the overestimation of the real concentrations [7,13]. Miniaturized optical particle counters are susceptible especially to high RH conditions (close to water condensing conditions), which may lead to erroneous estimation of particle size and mass concentration due to potential particle hygroscopic growth (particles' ability to bind water) [14].

All of the above-mentioned negative effects on sensor measurement quality can be filtered out of the measured datasets using different correction procedures (e.g., [7,9,13,14]) if they are clearly defined at least at the beginning of the measurement (or also during the comparative measurement; ideally applied on a daily correction routine [15]). Some sensor manufacturers state that they have already implemented certain correction algorithms (for the elimination of cross-sensitivity or T and RH effects) in the sensors' processing units. However, the algorithms used are usually not published, so the verification of the effectiveness of applied methods is again impossible without performing comparative control measurement of the given sensor unit.

Under the circumstances that measurement quality of both gas and aerosol sensors can be affected by changes in ambient meteorological conditions (T, RH) is evident, that the effect of seasonality (the effect of particular months) plays an important role [4,13,16]. The different timing of short-term comparative measurement tests (within days) may, therefore, be one of the main reasons that mixed information about the performance quality of particular sensor types is reported across literature [4,6,9,14]. Although this is known as one of the shortcomings of this topic [14], there are (so far) only very few studies providing results from long-term field comparisons (lasting at least three months or more) of different types of air quality sensors [13,16–18].

The aim of this study is to show the performance of different Cairpol gas sensor pairs (Cairclip for SO<sub>2</sub>, NO<sub>2</sub>, O<sub>3</sub>, and CO) and miniature Plantower (PMS7003) and Alphasense (OPC-N2) particle counter pairs (for PM<sub>1</sub>, PM<sub>2.5</sub>, and PM<sub>10</sub> mass concentration) within almost one year of continuous field comparative measurement with the corresponding reference monitors and equivalent optical particle monitor used in the CHMI ambient air quality network (all data used are available in Supplement 2). This paper follows up on recently published studies [13,17] and complements and extends the results obtained.

## 2. Experimental Methodology

### 2.1. Study Area and Experimental Design

Field-testing measurement of different kinds of air quality sensors took place at Tušimice Observatory (the northwest area of the Czech Republic; GPS: 50°22'35.59" N, 13°19'39.76" E), a professional station of the CHMI focused on the integration of ground-based and remote sensing methods in meteorology and air quality measurement. The station is located in a semi-agricultural and semi-industrial background, surrounded by three brown coal-fired power plants and a spacious open-pit brown coal mine. All the sensor types were tested in pairs (to control intra-sensors variability) and installed in the appropriate housings (ventilated boxes; Figure 1) on the roof of the automatic ambient air quality monitoring reference station. Comparative testing measurement was carried out continuously between the end of 2017 and the beginning of 2019 (Cairpol gas sensors measured from November 2017 until September 2018, Plantower particle counters from March 2018 until December 2018, and Alphasense from September 2018 until January 2019).

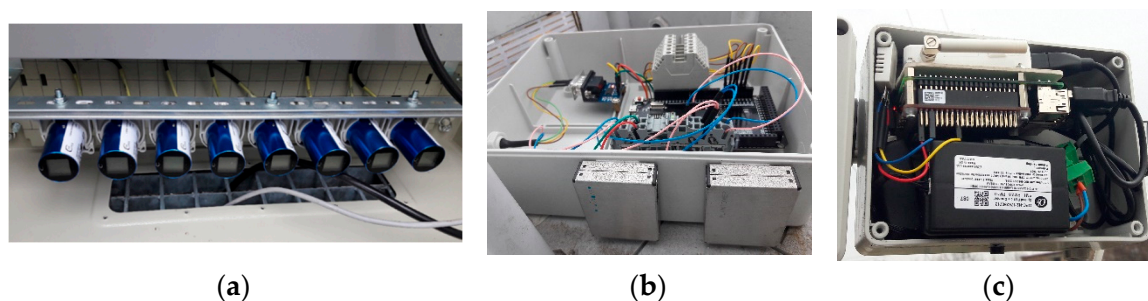


**Figure 1.** Tested pairs of sensor units installed on the roof of the reference monitoring station within the ventilated boxes: (a) pairs of Cairclip sensors for SO<sub>2</sub>, NO<sub>2</sub>, O<sub>3</sub>, and CO (Cairpol, FR); (b) pairs of PMS7003 particle counters (Plantower, CHN) and (c) OPC-N2 particle counters (Alphasense, UK) for PM<sub>1</sub>, PM<sub>2.5</sub>, and PM<sub>10</sub> [13,17].

### 2.2. Technical Specification of Tested Sensors and Reference (or Equivalent to Reference) Monitors

#### 2.2.1. Cairpol Gas Sensors

The detailed specifications of Cairclip SO<sub>2</sub>, NO<sub>2</sub>, O<sub>3</sub>, and CO electrochemical sensors (Cairpol, Envea, France (FR); Figure 1a) have been described in our previous study [13], so here we cover them only briefly. Cairclip sensors are small, tube-shaped, autonomous measuring units (weight 55 g). Each sensor unit has its own battery with an operating time from 24 to 36 h (or it can be connected directly to a 5V DC power supply with a current demand of 500 mA) and a small screen, where the measured values and device status are displayed. The fundamental technical parameters of the particular sensors are listed in Table 1. All the units have an optionally adjustable measuring period from 1 min to 15 or 60 min. The operating conditions stated by the manufacturer are in temperatures (Ts) from −20 °C to 50 °C and relative humidity (RH) from 15% to 90% (non-condensing conditions). Special attention can be given to the O<sub>3</sub> Cairpol sensor, which is actually a combined type of sensor for O<sub>3</sub>/NO<sub>2</sub>. It has the same limit of detection, range of measurement, uncertainty, and admitted effect of temperature on zero value drift as the NO<sub>2</sub> Cairclip sensor itself [19,20]. Although the exact algorithm for sensor response on O<sub>3</sub> separately is not known [19,21,22], given the strong positive correlation of concentrations measured by the combined O<sub>3</sub> sensor with concentrations measured by the Cairpol sensor for SO<sub>2</sub>, NO<sub>2</sub>, or CO (see the Results section (Section 3.1)), we assume that it indicates a modified sum of O<sub>3</sub>, NO<sub>2</sub>, and possibly other oxidants' values [11–13,22,23].

**Table 1.** Technical parameters of different Cairpol gas sensors specified by the manufacturer [19,20,24,25].<sup>1</sup>

| Gas Sensor Type   | Measurement Range | Limit of Detection | Uncertainty | Interference Effect  | Temperature Effect on Zero Value |
|---|-------------------|--------------------|-------------|--|----------------------------------|
| Cairclip SO <sub>2</sub> (ppb)  | 0–1000            | 50                 | <25%        | NO <sub>2</sub> , O <sub>3</sub> : ~–125%<br>H <sub>2</sub> S: ~5%<br>CO, H <sub>2</sub> : <1%   | Not detected                     |
| Cairclip NO <sub>2</sub> (ppb)  | 0–250             | 20                 | <30%        | Cl <sub>2</sub> : ~80%<br>sulfur compounds: negative interference<br>O <sub>3</sub> : ~80%   | ±50 ppb                          |
| Cairclip O <sub>3</sub> (ppb, also O <sub>3</sub> /NO <sub>2</sub> ppb) | 0–250             | 20                 | <30%        | Cl <sub>2</sub> : ~80%<br>sulfur compounds: negative interference  | ±50 ppb                          |
| Cairclip CO (ppm)   | 0–20              | 0.05               | <25%        | H <sub>2</sub> < 60%<br>Long-term high concentrations of H <sub>2</sub> S, NO <sub>x</sub> , SO <sub>2</sub> may interfere with the signal | ±1 ppm                           |

<sup>1</sup> All the mentioned technical specifications were based on laboratory testing under standard operating conditions at T = 20 °C (±2 °C), RH = 50% (±10%), and p = 1013 hPa (±5%).

### 2.2.2. Plantower and Alphasense Miniature Particle Counters

The PMS7003 optical particle counters (Plantower, China (CHN); Figure 1b) for measuring mass concentrations of PM<sub>1</sub>, PM<sub>2.5</sub>, and PM<sub>10</sub> (by converting the particle number concentration in an air volume of 0.1 L) are small boxes with dimensions of 48 × 37 × 12 mm. This particle analyzer is not a fully autonomous measurement unit because it is powered externally (power supply 4.5–5.5 V DC, current demand 100 mA) and needs to be connected to a processing unit (Figure 1b). The fundamental technical parameters of PMS7003 analyzers are listed in Table 2. The sampling frequency is 1 s. The operating conditions stated by the manufacturer are in Ts from –10 °C to 60 °C and RH from 0% to 99% [26].

The OPC-N2 (Alphasense, United Kingdom (UK); Figure 1c) optical particle counters for measuring particle number concentration and mass concentrations of PM<sub>1</sub>, PM<sub>2.5</sub>, and PM<sub>10</sub> (conversion to air volume 1.2 L) are small measuring units with dimensions of 75 × 60 × 65 mm. Similarly to the previous analyzers (PMS7003 from Plantower), even these units need to be powered externally (power supply 4.8–5.2 V DC, current demand 175 mA) and connected to a processing unit (Figure 1c). For technical specifications, see Table 2 again. The sampling interval is optional, from 1 to 10 s. The operating conditions are stated in Ts from –20 °C to 50 °C and RH from 0% to 95% (under non-condensing conditions) [27].

**Table 2.** Technical parameters of Plantower and Alphasense optical particle counters specified by the manufacturers [26,27].

| Particle Counter Type | Measured Fractions                                       | Detection Range (µm) | Measurement Range          | Maximum Consistency Error/Coincidence Probability   | Standard Volume |
|-----------------------|--|----------------------|----------------------------|---|-----------------|
| Plantower PMS7003     | PM <sub>1</sub><br>PM <sub>2.5</sub><br>PM <sub>10</sub> | 0.30–10.00           | 0–500 (µg/m <sup>3</sup> ) | ±10% at conc. 100–500 µg/m <sup>3</sup><br>±10 µg/m <sup>3</sup> at conc. 0–100 µg/m <sup>3</sup> | 0.1 L           |
| Alphasense OPC-N2     | PM <sub>1</sub><br>PM <sub>2.5</sub><br>PM <sub>10</sub> | 0.38–17.00           | 0–10,000 (particles/s)     | 0.84% at 10 <sup>6</sup> particles/L  | 1.2 L           |

### 2.2.3. Reference Monitors and Other Equivalent Methods

During the testing measurement, all the above-mentioned sensors were compared to the appropriate reference monitors (RMs) or to other equivalent analyzers (Fidas200 particle analyzer) currently used in the CHMI ambient air quality monitoring network. For monitoring gaseous pollutants, RMs from Teledyne API company (San Diego, CA, USA) were used: the SO<sub>2</sub> analyzer T100 (UV fluorescence method with minimum measurement range 0–50 ppb, maximum range 0–20 ppm, and limit of detection 0.4 ppb), the NO<sub>2</sub> analyzer T200 (chemiluminescence detection method with the same measurement ranges and limit of detection as the aforementioned T100), and the O<sub>3</sub> analyzer

T400 (UV absorption method with minimum range 0–100 ppb, maximum range 0–10 ppm, and limit of detection <0.4 ppb) [28].

For monitoring aerosol concentrations in fractions PM<sub>2.5</sub> and PM<sub>10</sub>, reference monitors MP101M (Environment SA, Envea, FR) based on radiometry (beta ray absorption) were used (measurement range 0–10,000 µg/m<sup>3</sup>, limit of detection 0.5 µg/m<sup>3</sup>) [29]. Given the similarity of measurement technology, we have also used for sensor comparison the Fidas200 (Palas, Germany (DE)) optical particle counter for PM<sub>1</sub>, PM<sub>2.5</sub>, and PM<sub>10</sub> (measuring particle number concentration of up to 64 size channels with a range of 1–20,000 particles/cm<sup>3</sup> and mass concentrations with a range of 0–1500 µg/m<sup>3</sup>) [30]. The Fidas200 optical counter is equipped with an Intelligent Aerosol Drying System (IADS), which ensures water removal before particle measurement. During the last year, the Fidas200 was found to be a suitable equivalent monitor to an RM for the determination of PM mass concentrations in ambient air quality in the Czech Republic (according to successful tests of equivalence; published only within the CHMI [31]).

#### 2.2.4. Data Analysis and Data Control

The measured data from all tested sensors were cleaned of any outages and negative values (treated as missing values; mentioned further as not available (NA)) before processing. However, to show the real sensor performance, all the other measured values (even the possible outliers) were left in the dataset for basic statistical processing in the first stage. The hourly averages of all measured concentrations were calculated from 10 min of data (gas pollutants in ppb or ppm, aerosol particles in µg/m<sup>3</sup>). In the event that more than 40% of the values were missing in any particular hour, the whole hourly average was considered to be NA.

Firstly, summary statistics of all measured values during the field-testing period were performed (mean values and standard deviations (SDs) of concentrations measured by sensor pairs and by RMs), including the intra-sensors correlation within pairs of similar sensor types. Given the non-normal distribution of most of the measured values (Figures S1–S4 in the Supplement 1), non-parametric Spearman's rank correlation coefficients ( $r_s$ ) were used in this study (similarly as in Bauerová et al. [13] and Fishbain et al. [32]). Further summary statistics of different sensors' performance were calculated, including the presence (indicating the sensors' availability over time in percentage [32]), correlation with RMs and other equivalent monitors ( $r_s$ ), and measurement errors for indicating the differences between the sensor and RM measurements (calculated as mean bias error (MBE), mean absolute error (MAE) and root mean square error (RMSE); see e.g., Feenstra et al. [6]).

Finally, in the second stage, an identification of significant outliers (defined as higher than  $3 \times \max$  of the hourly average RM concentration reached during the testing period; [13,33]) was performed and their representation in the dataset was expressed in percentage. In the case of suitable sensors (with correlation coefficients  $r_s$  resulting from comparison with RMs at least  $>0.50$ ), the coefficients of determination ( $R^2$ ) were determined according to the best-fitting regression equation in comparison with the RM (not only linear relationships). In addition, the potential effect of ambient T or RH on the sensors' measurement quality was assessed according to the values of  $r_s$  and  $R^2$ .

### 3. Results

#### 3.1. Cairpol Gas Sensors

The summary statistic of concentrations measured by different Cairclip gas sensors and by corresponding RMs is listed in Table 3 (except RM for CO, which is not available at the testing station). The results showed that despite the significant strong correlations (for all sensor types  $r_s > 0.80$ ) of the measured concentrations within the pairs of particular sensors (intra-sensors correlation), significant data drifts were also found within the pairs of SO<sub>2</sub> and CO sensors (in the case of the SO<sub>2</sub> sensors, a difference in mean concentration values of about 60 ppb from the beginning of the measurement, i.e., in 100% of the data; in the case of the CO sensors, a difference of about 10 ppm after three months of measurement, i.e., in 75.2% of the data; see Figure 2 or Figures S1 and S4 in

Supplement 1). In the case of the NO<sub>2</sub> and O<sub>3</sub> sensors, such data drifts within the pairs did not appear during the entire testing measurement (only for a selected time period; see Figure 2). The percentage of valid data (hourly average concentrations of different gases) measured by Cairclip sensors in particular months of the testing period is shown in Table S1 in Supplement 1.

**Table 3.** Summary statistics of gaseous pollutant concentrations (SO<sub>2</sub>, NO<sub>2</sub>, O<sub>3</sub>, and CO) measured by pairs of Cairpol (Cairclip) sensors (ID 1 and 2) and by corresponding reference monitors.

| Type of Sensor                 | Sensor ID              |               | Intra-Sensors<br>Correlation (r <sub>s</sub> ) <sup>2</sup> | Reference Monitor      |
|--------------------------------|------------------------|---------------|---|------------------------|
|                                | Mean ± SD <sup>1</sup> |               |   | Mean ± SD <sup>1</sup> |
|                                | 1                      | 2             |   |                        |
| Cairclip SO <sub>2</sub> (ppb) | 97.68 ± 53.45          | 31.01 ± 30.16 | 0.99  | 1.67 ± 1.69            |
| Cairclip NO <sub>2</sub> (ppb) | 30.54 ± 13.63          | 29.61 ± 13.49 | 1.00  | 6.31 ± 4.20            |
| Cairclip O <sub>3</sub> (ppb)  | 22.53 ± 12.50          | 23.68 ± 12.83 | 1.00  | 32.57 ± 17.42          |
| Cairclip CO (ppm)              | 1.81 ± 0.97            | 12.26 ± 7.49  | 0.81  | - <sup>3</sup>         |

<sup>1</sup> SD = standard deviation. <sup>2</sup> r<sub>s</sub> = Spearman’s rank correlation coefficient. <sup>3</sup> There is no reference monitor available for CO at the Tušimice station.

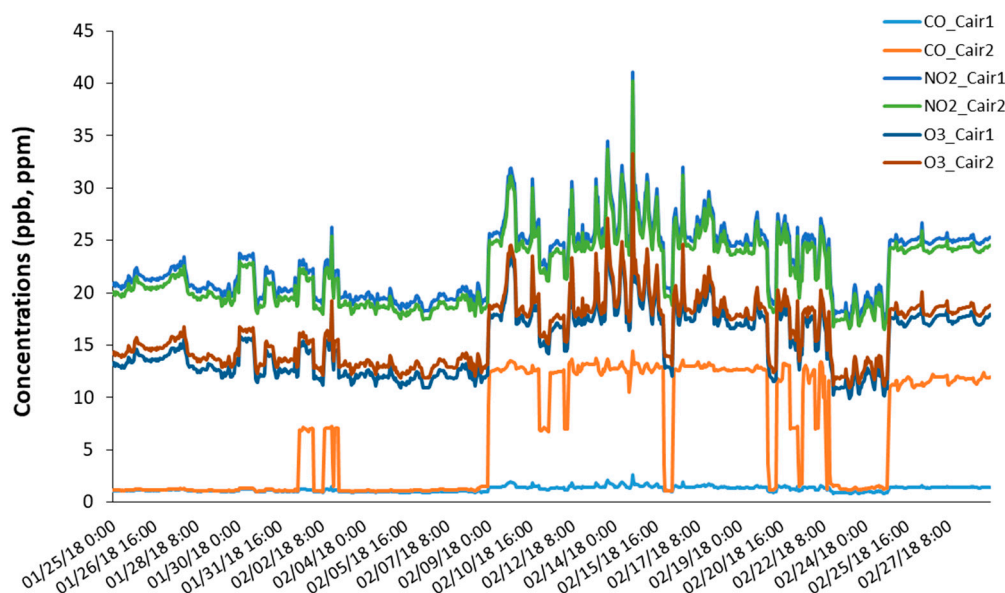


**Figure 2.** The course of CO, NO<sub>2</sub>, and O<sub>3</sub> hourly concentrations (in ppb, only CO in ppm) measured by Cairclip gas sensors during the selected part of the testing period (from 25 January until 28 February 2018).

The comparison with the RMs showed very weak measurement quality in the case of the SO<sub>2</sub> and NO<sub>2</sub> sensors. There were high differences in the measured concentrations (Table 3, Figures S1 and S2 in Supplement 1), and the calculated measurement errors were very high (Table 4). In the case of the SO<sub>2</sub> Cairclip sensors, no correlation with the RM was detected (r<sub>s</sub> around zero; Figure S5), in the case of the NO<sub>2</sub> sensors the correlation with the RM was significant but negative (r<sub>s</sub> = −0.26 in both tested units; Table 4, Figure S6). The strongest correlations (r<sub>s</sub> = 0.68 for both units) and the lowest measurement errors occurred during the inter-comparison with the RM detected in the combined O<sub>3</sub> Cairclip sensors (Table 4, Figures S3 and S7; compared with the concentrations measured by the O<sub>3</sub> RM). The concentrations measured by these combined sensors were, however, also significantly positively inter-correlated with the concentrations measured by all other types of Cairclip gas sensors (SO<sub>2</sub> sensors r<sub>s</sub> > 0.98, NO<sub>2</sub> sensors r<sub>s</sub> = 1.00, CO sensors r<sub>s</sub> > 0.79; see Table S2 in Supplement 1 and Figure 2).

**Table 4.** Summary of Cairpol (Cairclip) gas sensor performance statistics in comparison with the corresponding reference monitors (RMs).

| Type of Sensor                 | Sensor ID | Presence <sup>1</sup> (%) | Correlation with RM<br>$r_s$ <sup>2</sup> | Measurement Error <sup>3</sup> |        |        |
|--------------------------------|-----------|---------------------------|---|--------------------------------|--------|--------|
|                                |           |                           |   | MBE                            | MAE    | RMSE   |
| Cairclip SO <sub>2</sub> (ppb) | 1         | 94.8                      | <i>0.02</i>                               | -110.11                        | 110.11 | 119.89 |
|                                | 2         | 72.6                      | <i>0.00</i>                               | -30.35                         | 30.52  | 44.46  |
| Cairclip NO <sub>2</sub> (ppb) | 1         | 94.8                      | -0.26                                     | -27.99                         | 27.99  | 30.54  |
|                                | 2         | 94.8                      | -0.26                                     | -27.13                         | 27.13  | 29.75  |
| Cairclip O <sub>3</sub> (ppb)  | 1         | 94.8                      | 0.68                                      | 11.13                          | 13.31  | 15.03  |
|                                | 2         | 94.8                      | 0.68                                      | 9.94                           | 12.47  | 14.16  |
| Cairclip CO (ppm)              | 1         | 94.8                      | -   | -                              | -      | -      |
|                                | 2         | 94.8                      | -   | -                              | -      | -      |

<sup>1</sup> Presence is indicating the sensors' availability over the time of the whole testing period in percentage. <sup>2</sup>  $r_s$  = Spearman's rank correlation coefficient. Coefficients highlighted in italics are statistically non-significant ( $p > 0.05$ ). <sup>3</sup> Measurement error calculated as: MBE = mean bias error, MAE = mean absolute error, RMSE = root mean square error.

In all the Cairclip sensors, significant correlations of measured gas concentrations with the ambient air T ( $r_s > 0.79$ ) and RH ( $r_s < -0.50$ ) were found (Table S2 in Supplement 1). Even in the case of the best-performing combined O<sub>3</sub> sensors, the measurement quality changed significantly during the testing period (see the differences between the cold period from November to March and the warm period from April to September in Figure 3). The better sensor performance was reached during the warmer months when the real O<sub>3</sub> concentrations reached the values over 40 ppb (Figure S8). The presence of significant outliers (values  $> 3 \times$  max RM one hourly average concentration) was 51% and 10% in the case of SO<sub>2</sub> Cairclip sensors (SO<sub>2</sub>\_Cair1 and SO<sub>2</sub>\_Cair2, respectively), and 0.01% in the case of NO<sub>2</sub> Cairclip sensors (both units). In combined O<sub>3</sub> Cairclip sensors, no significant outliers were detected during the testing period.

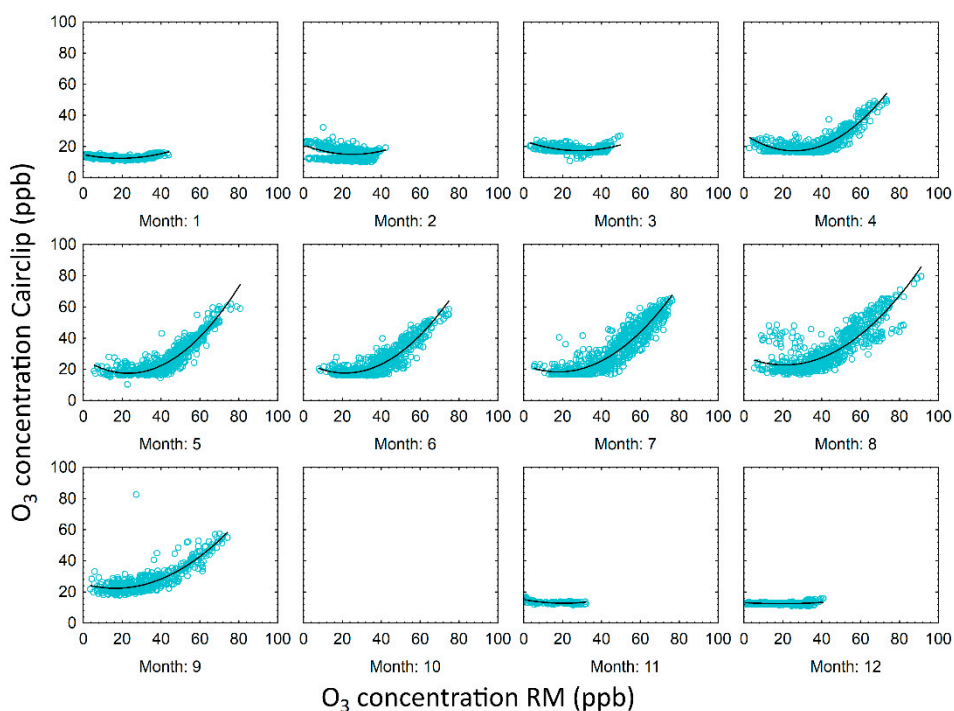


**Figure 3.** The relationship between O<sub>3</sub> concentrations measured by Cairpol Cairclip sensors and by the RM (both in ppb) with differentiation into particular months of the testing period (lasting from November 2017 until September 2018). The black line presents the polynomial best-fit regression line (degree = 2).

### 3.2. Plantower and Alphasense Particle Counters

The summary statistic of PM<sub>1</sub>, PM<sub>2.5</sub>, and PM<sub>10</sub> mass concentrations measured by two tested types of particle counters—PMS7003 Plantower and OPC-N2 Alphasense—and by RMs or a Fidas200 monitor is listed in Table 5 (in the case of an RM, no PM<sub>1</sub> mass concentrations are available). The intra-sensors comparison within pairs showed highly significant correlations in the measured PM concentrations in both the Plantower and Alphasense sensors (both types  $r_s > 0.95$  in all PM fractions; see Table 5). In both sensor types, no significant data drifts were found within the sensor pairs, although the OPC-N2 sensors had a tendency to differ in mean and standard deviation (SD) concentration values (especially in the case of PM<sub>2.5</sub> and PM<sub>10</sub> fractions, which had a higher occurrence of outlying values; see Table 5). The percentage of valid data (hourly average PM concentrations) measured by Plantower and Alphasense particle counters in particular months of the testing period is shown in Tables S3 and S4, respectively, in Supplement 1.

The comparison with the RMs and equivalent Fidas200 showed a very good measurement quality of the PMS7003 Plantower particle counters. The means and SDs of all measured PM fraction concentrations corresponded very well with both control monitors, and no significant outliers appeared (Table 5, Figures S9–S11 in Supplement 1). This also resulted in a significant positive correlation of the measured data (with optical Fidas200  $r_s > 0.70$  for all fractions measured within a sensor pair, with radiometric RM  $r_s > 0.62$  for PM<sub>2.5</sub> and PM<sub>10</sub> fractions; Table 6, Figure 4 and Figure S12), and low measurement error of these sensing units (Table 6).

In the case of the OPC-N2 Alphasense particle counters, the measurement quality was considerably weaker in comparison with the Fidas200 or RM. The mean values and SDs of the concentrations measured by the sensors and by the control monitors differed significantly in all PM fractions (Table 5, Figures S13–S15). Despite a strong positive correlation with both control monitors (with Fidas200  $r_s > 0.75$  for all fractions, with RM  $r_s > 0.63$  for PM<sub>2.5</sub> and PM<sub>10</sub>; Table 6, Figure 5, and Figure S16 in Supplement 1), the high values of the measurement errors showed the presence of extreme outliers in all PM fractions analyzed by OPC-N2 sensors (Table 6; the maximum PM<sub>1</sub> concentration measured by the OPC-N2 was 256.6 µg/m<sup>3</sup>, the maximum PM<sub>2.5</sub> concentration was 569.8 µg/m<sup>3</sup>, and the maximum PM<sub>10</sub> concentration was 9036.7 µg/m<sup>3</sup>).

In both tested particle counter types, the concentrations of all measured fractions correlated weakly negatively (yet statistically significantly) with ambient T (Plantower sensors  $r_s < -0.24$ , Alphasense sensors  $r_s < -0.16$ ) and significantly positively with RH (Plantower sensors  $r_s > 0.46$ , Alphasense sensors  $r_s > 0.57$ ; see Tables S5 and S6 in Supplement 1). In the case of the PMS7003 particle counters, there were no extreme outliers in the measured concentrations detected in relation to the effect of changing T and RH. Conversely, in the OPC-N2 particle counters, 5.4% of the PM<sub>2.5</sub> data and 6.2% of the PM<sub>10</sub> data were determined as extreme outliers (>3× max RM one hourly average concentration); most of them were detected at the time with high ambient RH (RH > 90%; see Figure 6).

**Table 5.** Summary statistics of particulate matter (PM<sub>1</sub>, PM<sub>2.5</sub>, and PM<sub>10</sub>) concentrations (µg/m<sup>3</sup>) measured by pairs of Plantower (PMS7003) and Alphasense (OPC-N2) particle counters (ID 1 and 2) and by a corresponding Fidas200 optical particle counter and reference monitors (RMs).

| Type of Sensor            | Sensor ID       |                 | Intra-Sensors Correl.<br>$r_s$ <sup>2</sup> | Fidas200      | RM                     |
|---------------------------|-----------------|-----------------|---|---------------|------------------------|
|                           | 1               | 2               |   | Mean ± SD     | Mean ± SD <sup>1</sup> |
| PMS7003 PM <sub>1</sub>   | 15.14 ± 12.37   | 13.38 ± 10.95   | 0.95  | 12.67 ± 10.26 | - <sup>3</sup>         |
| PMS7003 PM <sub>2.5</sub> | 22.14 ± 19.33   | 20.67 ± 17.17   | 0.96  | 14.63 ± 11.00 | 17.39 ± 12.21          |
| PMS7003 PM <sub>10</sub>  | 24.34 ± 21.92   | 22.56 ± 18.69   | 0.96  | 22.19 ± 14.76 | 24.46 ± 16.85          |
| OPC-N2 PM <sub>1</sub>    | 39.59 ± 43.72   | 43.95 ± 47.82   | 0.99  | 15.17 ± 12.53 | - <sup>3</sup>         |
| OPC-N2 PM <sub>2.5</sub>  | 56.86 ± 72.36   | 67.87 ± 85.24   | 0.99  | 17.05 ± 13.72 | 17.93 ± 14.25          |
| OPC-N2 PM <sub>10</sub>   | 149.40 ± 536.43 | 196.00 ± 661.98 | 0.99  | 22.63 ± 17.39 | 25.14 ± 19.56          |

<sup>1</sup> SD = standard deviation. <sup>2</sup>  $r_s$  = Spearman’s rank correlation coefficient. <sup>3</sup> There is no reference monitor available for PM<sub>1</sub>.

**Table 6.** Summary of Plantower (PMS7003) and Alphasense (OPC-N2) particle counters’ performance statistics in comparison with a Fidas200 optical particle counter and the reference monitors (RMs).

| Type of Sensor            | Sensor ID | Presence (%) <sup>1</sup> | Correlation with Fidas200 <sup>1</sup> , RM <sup>2</sup> |                             | Measurement Error |                  |                   |                  |                  |                   |
|---------------------------|-----------|---------------------------|--|-----------------------------|-------------------|------------------|-------------------|------------------|------------------|-------------------|
|                           |           |                           | r <sub>S</sub> <sup>2</sup>                              | r <sub>S</sub> <sup>3</sup> | MBE <sup>4</sup>  | MAE <sup>4</sup> | RMSE <sup>4</sup> | MBE <sup>5</sup> | MAE <sup>5</sup> | RMSE <sup>5</sup> |
| PMS7003 PM <sub>1</sub>   | 1         | 93.3                      | 0.88   | -                           | -2.70             | 4.08             | 6.86              | -                | -                | -                 |
|                           | 2         | 94.9                      | 0.91   | -                           | -1.08             | 3.24             | 4.74              | -                | -                | -                 |
| PMS7003 PM <sub>2.5</sub> | 1         | 94.8                      | 0.87   | 0.63                        | -7.94             | 8.92             | 13.53             | -4.93            | 10.61            | 14.99             |
|                           | 2         | 93.0                      | 0.90   | 0.66                        | -6.08             | 7.13             | 10.58             | -3.07            | 9.10             | 12.56             |
| PMS7003 PM <sub>10</sub>  | 1         | 95.9                      | 0.70   | 0.62                        | -2.51             | 11.05            | 15.93             | -0.31            | 12.05            | 16.63             |
|                           | 2         | 95.9                      | 0.73   | 0.63                        | -0.82             | 9.70             | 13.82             | 1.39             | 11.01            | 15.16             |
| OPC-N2 PM <sub>1</sub>    | 1         | 86.5                      | 0.85   | -                           | -26.27            | 27.52            | 45.43             | -                | -                | -                 |
|                           | 2         | 78.3                      | 0.83   | -                           | -28.91            | 30.47            | 50.51             | -                | -                | -                 |
| OPC-N2 PM <sub>2.5</sub>  | 1         | 86.5                      | 0.83   | 0.66                        | -43.27            | 44.59            | 81.71             | -42.68           | 46.07            | 84.58             |
|                           | 2         | 78.3                      | 0.81   | 0.63                        | -51.38            | 52.97            | 97.64             | -50.79           | 54.30            | 100.52            |
| OPC-N2 PM <sub>10</sub>   | 1         | 86.5                      | 0.77   | 0.68                        | -140.12           | 143.56           | 620.93            | -137.11          | 142.96           | 621.47            |
|                           | 2         | 78.3                      | 0.75   | 0.66                        | -174.61           | 178.06           | 766.85            | -171.60          | 177.21           | 767.39            |

<sup>1</sup> Presence is indicating the sensors’ availability over the time of the whole testing period in percentage. <sup>2</sup> Correlations with Fidas200 optical particle counter tested by: r<sub>S</sub> = Spearman’s rank correlation coefficient. <sup>3</sup> Correlations with RM tested by: r<sub>S</sub> = Spearman’s rank correlation coefficient. <sup>4</sup> Measurement error calculated as: MBE = mean bias error, MAE = mean absolute error, RMSE = root mean square error, where the modeled concentrations were given by the Fidas200 optical particle counter (in µg/m<sup>3</sup>). <sup>5</sup> Measurement error calculated as: MBE = mean bias error, MAE = mean absolute error, RMSE = root mean square error, where the modeled concentrations were given by the corresponding RM (in µg/m<sup>3</sup>).

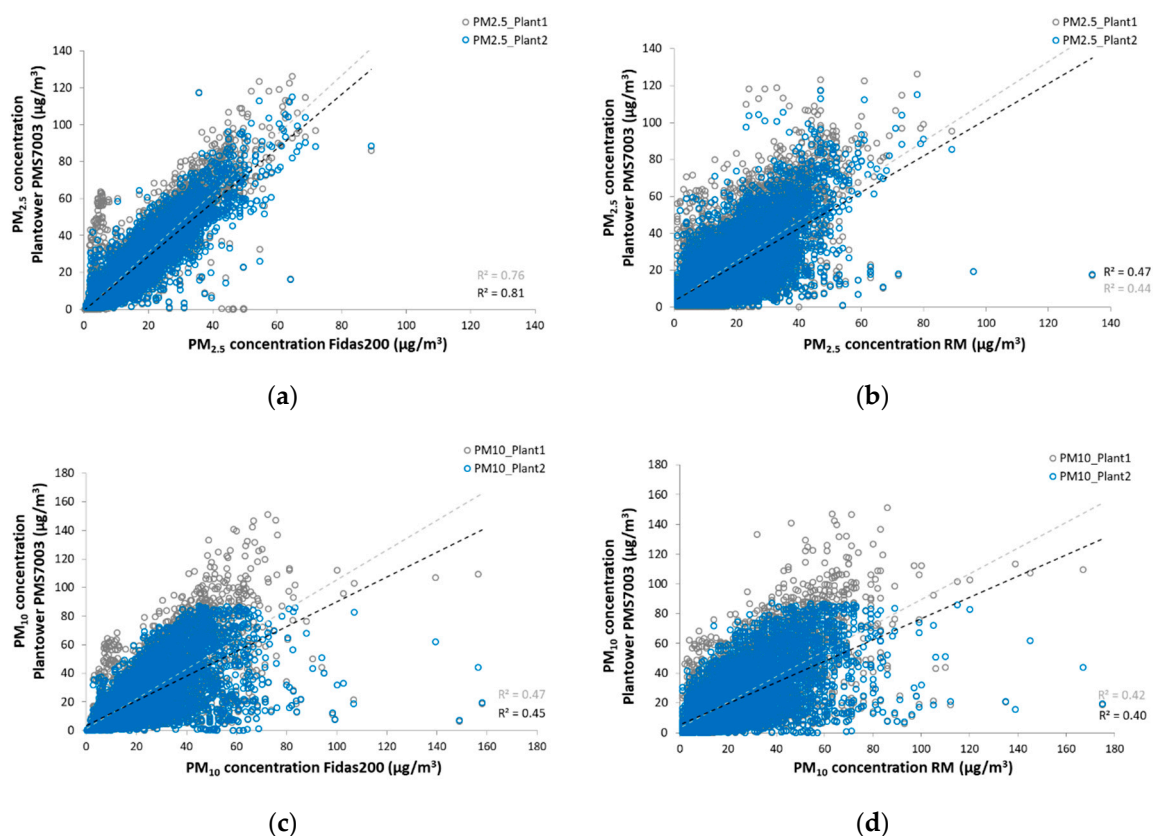


**Figure 4.** The relationship between the PM<sub>2.5</sub> and PM<sub>10</sub> concentrations (µg/m<sup>3</sup>) measured by Plantower PMS7003 particle counters (Plant1 in gray, Plant2 in blue) and by control monitors: (a) PM<sub>2.5</sub> concentration comparison with equivalent optical Fidas200 monitor; (b) PM<sub>2.5</sub> concentration comparison with radiometric RM; (c) PM<sub>10</sub> concentration comparison with equivalent optical Fidas200 monitor; (d) PM<sub>10</sub> concentration comparison with radiometric RM. The coefficients of determination (R<sup>2</sup>) were estimated from the linear best-fit regression lines.

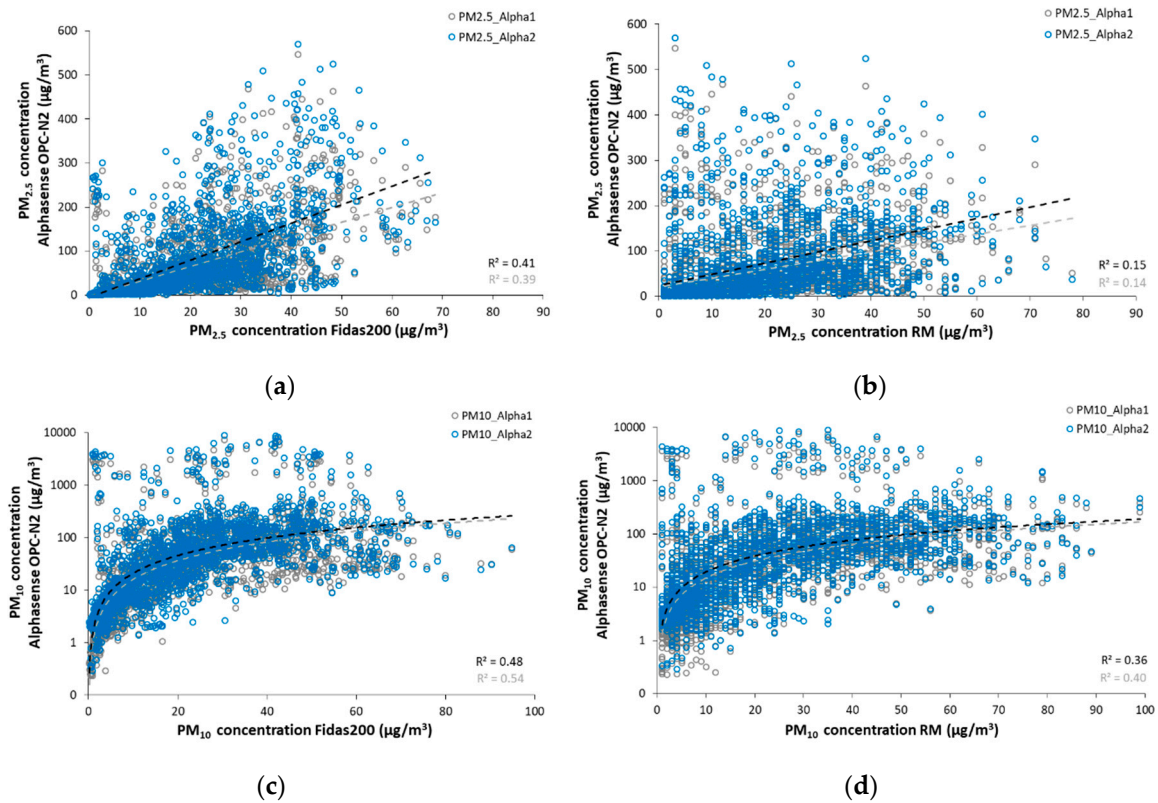


**Figure 5.** The relationship between the PM<sub>2.5</sub> and PM<sub>10</sub> concentrations (μg/m<sup>3</sup>) measured by Alphasense OPC-N2 particle counters (Alpha1 in gray, Alpha2 in blue; including outliers) and by control monitors: (a) PM<sub>2.5</sub> concentration comparison with equivalent optical Fidas200 monitor; (b) PM<sub>2.5</sub> concentration comparison with radiometric RM; (c) PM<sub>10</sub> concentration comparison with equivalent optical Fidas200 monitor; (d) PM<sub>10</sub> concentration comparison with radiometric RM. In the case of PM<sub>2.5</sub>, the coefficients of determination (R<sup>2</sup>) were estimated from the linear best-fit regression lines. In the case of PM<sub>10</sub>, the y-axis is converted to a logarithmic scale and the R<sup>2</sup> values were estimated from the power best-fit regression lines.

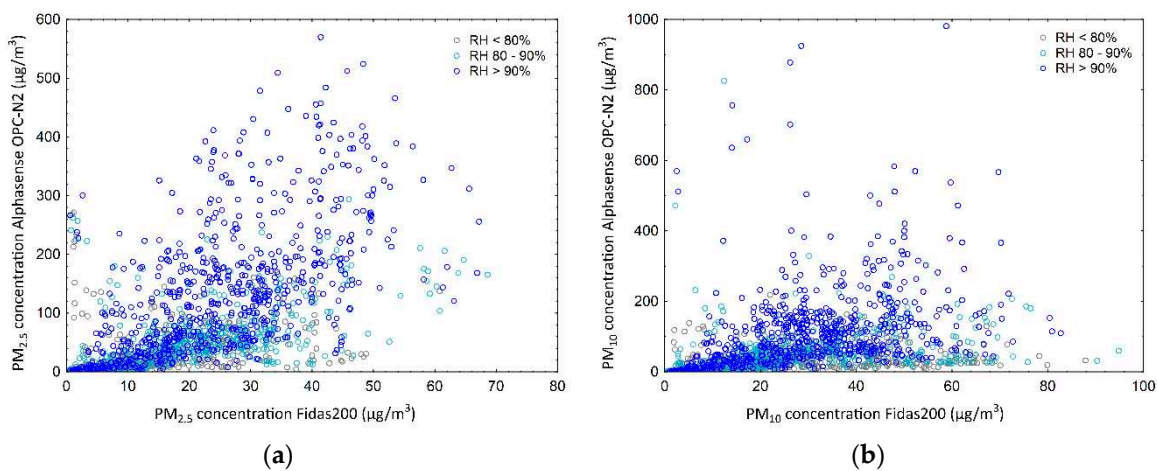


**Figure 6.** The relationship between PM concentrations (μg/m<sup>3</sup>) measured by OPC-N2 Alphasense particle counters and by an optical Fidas200 monitor: (a) comparison of PM<sub>2.5</sub> concentrations; (b) comparison of PM<sub>10</sub> concentrations (only concentrations <1000 μg/m<sup>3</sup> are shown), both colored according to the ambient relative humidity (RH).

## 4. Discussion

Small sensors can undoubtedly serve as an affordable and easy-to-use complementary solution for further development of the ambient air quality monitoring network. Nevertheless, due to the limits of this miniaturized technology, special attention should be given to the selection of suitable sensor types during the planning of specific intent and to the subsequent data control and verification before and continuously during each application. This study was performed to show the individual measurement quality of different gas sensors and particle counters and the possible changes during long-lasting outdoor measurement while compared to corresponding reference monitors.

### 4.1. Cairpol Gas Sensors

The results of the Cairpol Cairclip gas sensors showed a highly unsatisfactory performance of the SO<sub>2</sub>, NO<sub>2</sub>, and CO sensor units. The measured SO<sub>2</sub> and CO concentrations drifted significantly within pairs of identical sensor types. Such data drifts arising in electrochemical gas sensors can be caused by several reasons [34]; one which is often discussed is the aging of the sensor unit [35–37]. In our case, the data drift of SO<sub>2</sub> concentrations was observed in the first sensor (SO<sub>2</sub>\_Cair1) right from the beginning of the testing measurement (see Figure S1 in Supplement 1). Therefore, we assumed the presence of a defective or poorly calibrated unit (from the manufacturer). Conversely, in the case of CO, the data drift appeared in the second sensor unit (CO\_Cair2) after three months of measurements. Given that it occurred exactly at the same time that there was also a certain increase in other concentrations measured by the NO<sub>2</sub> and O<sub>3</sub> sensors (Figure 2), an erroneous measurement caused by sudden interference with other gases cannot be ruled out. Furthermore, the comparison of the Cairpol gas sensors with the corresponding RMs showed very weak measurement quality in the case of the SO<sub>2</sub> and NO<sub>2</sub> Cairclip sensors (no relationship and a significantly negative relationship with RM concentrations; respectively). Although we have found no other study describing the field performance of SO<sub>2</sub> Cairclip sensors (except our previous study [13]), the weak results in SO<sub>2</sub> measurement were also recorded in other sensors from different manufacturers [9,22]. In the case of the NO<sub>2</sub> Cairclip sensors, some comparative field studies are available, but the information about measurement quality varies widely [7,18,22]. Our results showed that, in both cases, the concentrations measured by the Cairclip sensors were inappropriately overestimated against the real SO<sub>2</sub> and NO<sub>2</sub> concentrations, and, therefore, these sensor units were again evaluated as non-compliant and probably defective.

The best performance was observed in the combined O<sub>3</sub> Cairclip sensors, where both the intra-sensors comparison in pairs and the comparison with the RM achieved very satisfactory results (similarly as in Jiao et al. [22]). However, it should be pointed out here that the quality of the O<sub>3</sub> sensor measurement changed significantly during the year, when in the warmer months (from April to September) the sensors' performance was significantly better ( $R^2$  up to 0.79), than in the colder months (where almost no relationship with the RM was observed,  $R^2 < 0.34$  [13]; Figure 3). This can be explained by the lowered reactivity of this sensor on low ambient O<sub>3</sub> concentrations (during the colder months) and on the other hand better reactivity during the warmer months, when the O<sub>3</sub> concentrations are naturally higher. With respect to the improvement of the mutual relationship between the sensor and RM O<sub>3</sub> measurement under the real concentrations over 40 ppb (see Figure S8 in Supplement 1), we assume that the effective limit of detection of the combined O<sub>3</sub> Cairclip sensor may be actually at least a half more than the value of 20 ppb stated by the manufacturer. At the same time, given the strong correlation of the combined O<sub>3</sub> sensors with all the other Cairpol sensors (Figure 2), we cannot rule out even a certain effect of interference with other gases. Continuous data control and post-measurement data validation (by the application of some correction indices [7,9,13,14]) should, therefore, always be considered here.

It should also be mentioned that, during our long-term field testing, we reached the maximum lifetime of electrochemical Cairclip sensors after 11 months of continuous measurement. After this period, all gas concentrations measured by all sensor units drifted significantly to unreal stable values

and, therefore, the sensors were dismantled. To our knowledge, there is no other study for the comparison of the operational lifetime duration of these sensors.

#### 4.2. Plantower and Alphasense Particle Counters

Similarly to some other studies focused on field comparative measurement of Plantower and Alphasense miniature particle counters [14,16,38], we found very good results in the intra-sensors comparison of measured concentrations within pairs of identical sensor types. In both cases, no significant data drifts appeared during the testing period, although for the Alphasense OPC-N2 particle counters, a higher variability in PM concentrations measured within the sensor pair was recorded (especially in maximum concentrations; see also Feenstra et al. [6] or Bulot et al. [16]). The comparison with the RMs and Fidas200 monitor showed very satisfactory results in the case of the Plantower PMS7003 sensors (see also the course of hourly concentrations in Figure S17 in Supplement 1). In all PM fractions, the concentrations measured by the Plantower sensors were systematically lightly overestimated against the concentrations measured by both control monitors (similarly as in the studies by Zheng et al. [38] and Bulot et al. [16]). Naturally, better performance was found when compared to the optical Fidas200 monitor (given the similarity of the measuring method), than to radiometric RMs. Unlike with the Alphasense, we did not detect any extreme outliers for Plantower sensors during the entire testing period (lasting 10 months). With regard to the very good performance of the Plantower sensors, we assume that the manufacturer may have applied a very effective correction algorithm in the sensor processing unit.

In the case of the Alphasense OPC-N2 sensors we found, similarly to Crilley et al. [14] and Feinberg et al. [18], data artifacts (outliers in the form of extremely high concentrations) in all of the aerosol fractions ( $PM_{10}$ ,  $PM_{2.5}$ , and  $PM_{10}$ ) under high ambient relative humidity conditions ( $RH > 80\%$ ; Figure 6). The most noticeable effect of high air humidity on measurement error occasion was seen in the case of  $PM_{10}$  fraction, where the maximum hourly average concentrations even reached above  $9000 \mu\text{g}/\text{m}^3$ . We assume that such extreme measurement errors were caused by the high particle hygroscopicity under the condensation conditions (increased particle water content), which resulted in wrong particle size detection and its mass concentration [14]. Overall, the OPC-N2 counters tended to significantly overestimate the real PM concentrations (Figure S17 in Supplement 1), which is reflected by weaker and not always linear relationships with the control monitors (Figure 5; similarly as in other studies [6,14,18]). Therefore, we join in the recommendation for continuous data control and post-measurement data validation while using Alphasense particle counters for ambient air monitoring [14].

The maximum limit was not reached in any of the tested particle counters before completion of the comparative measurement (Plantower sensors tested within a 10-month period, Alphasense sensors tested only for five months).

## 5. Conclusions

Four miniaturized Cairpol gas sensors and two different miniaturized particle counters (Plantower and Alphasense) were tested in duplicates against collocated reference and other control monitors in a long-lasting comparative measurement at the Tušimice Observatory. The  $\text{SO}_2$ ,  $\text{NO}_2$ , and CO Cairclip sensors were identified as inappropriate due to their weak measurement quality or data inconsistency within sensor pairs. The combined  $\text{O}_3$  Cairpol sensor achieved satisfactory results, but interference with meteorological conditions and other gases definitely needs to be considered during data processing and interpretation. Among the particle counters, the Plantower PMS7003 definitely showed a higher measurement quality than the Alphasense OPC-N2 counters, which were more likely to be affected by high relative humidity and had a higher occurrence of measurement outliers.

We believe that this paper can help to clarify the real (outdoor) sensor performance and possible tendency to change the measurement quality over time. The results of this study show that long-term comparison studies are of great importance and should be further supported and developed by

scientists. They can serve the general public, as an important material for decision making when purchasing suitable sensor types and for the suppression of common mistakes during their application, or the manufacturers, for identifying main issues and for further product development. Finally, we still believe that comparative measurements with RMs have to be necessarily implemented at least before each field application (ideally also during the measurement at given intervals), because it is the only way to detect possible sensor failures or systematic and random measurement deviations of sensors.

**Supplementary Materials:** The following are available online at <http://www.mdpi.com/2073-4433/11/5/492/s1>. Electronic Supplementary Material 1 (Supplement 1) contains all supplementary tables and figures (10 pages, 6 tables, 17 figures). Supplementary material 2 (Supplement 2) is containing the complete dataset used for preparation of this article.

**Author Contributions:** Technical concept and measurement preparation, Z.N., J.K., Š.R. and P.B.; Software for data collection, Z.N.; Data control and processing, P.B., A.Š.; writing—original draft preparation, P.B.; writing—review and editing, J.K., A.Š., Š.R.; supervision, J.K.; All authors have read and agreed to the published version of the manuscript.

**Funding:** This research received no external funding.

**Acknowledgments:** We are grateful to the leadership of the CHMI and Envitech Bohemia for enabling the realization of this study, to all the technicians who participated in commissioning the tested instruments, to Erin Naillon for proofreading the manuscript, and to four anonymous reviewers for their comments to earlier version of the manuscript.

**Conflicts of Interest:** The authors declare no conflicts of interest.

## References

1. Kumar, P.; Morawska, L.; Martani, C.; Biskos, G.; Neophytou, M.; Di Sabatino, S.; Bell, M.; Norford, L.; Britter, R. The rise of low-cost sensing for managing air pollution in cities. *Environ. Int.* **2015**, *75*, 199–205. [[CrossRef](#)]
2. McKercher, G.R.; Salmond, J.A.; Vanos, J.K. Characteristics and applications of small, portable gaseous air pollution monitors. *Environ. Pollut.* **2017**, *223*, 102–110. [[CrossRef](#)]
3. Languille, B.; Gros, V.; Bonnaire, N.; Pommier, C.; Honoré, C.; Debert, C.; Gauvin, L.; Srairi, S.; Annesi-Maesano, I.; Chaix, B.; et al. A methodology for the characterization of portable sensors for air quality measure with the goal of deployment in citizen science. *Sci. Total Environ.* **2020**, *708*, 134698. [[CrossRef](#)]
4. Collier-Oxandale, A.; Feenstra, B.; Papapostolou, V.; Zhang, H.; Kuang, M.; Boghossian, B.D.; Polidori, A. Field and laboratory performance evaluations of 28 gas-phase air quality sensors by the AQ-SPEC program. *Atmos. Environ.* **2020**, *220*, 117092. [[CrossRef](#)]
5. Gerboles, M. European Committee for Standardization: CEN/TC 264/WG 42—Ambient Air—Air Quality Sensors. Available online: [https://standards.cen.eu/dyn/www/f?p=204:22:0:::FSP\\_ORG\\_ID,FSP\\_LANG\\_ID:2012773,25&cs=13EA71B95E446E4F77D5EEB632F4BF317](https://standards.cen.eu/dyn/www/f?p=204:22:0:::FSP_ORG_ID,FSP_LANG_ID:2012773,25&cs=13EA71B95E446E4F77D5EEB632F4BF317) (accessed on 5 May 2020).
6. Feenstra, B.; Papapostolou, V.; Hasheminassab, S.; Zhang, H.; Der Boghossian, B.; Cocker, D.; Polidori, A. Performance evaluation of twelve low-cost PM<sub>2.5</sub> sensors at an ambient air monitoring site. *Atmos. Environ.* **2019**, *216*, 116946. [[CrossRef](#)]
7. Spinelle, L.; Gerboles, M.; Villani, M.G.; Aleixandre, M.; Bonavitacola, F. Field calibration of a cluster of low-cost available sensors for air quality monitoring. Part A: Ozone and nitrogen dioxide. *Sens. Actuators B Chem.* **2015**, *215*, 249–257. [[CrossRef](#)]
8. Spinelle, L.; Gerboles, M.; Villani, M.G.; Aleixandre, M.; Bonavitacola, F. Field calibration of a cluster of low-cost commercially available sensors for air quality monitoring. Part B: NO, CO and CO<sub>2</sub>. *Sens. Actuators B Chem.* **2017**, *238*, 706–715. [[CrossRef](#)]
9. Borrego, C.; Costa, A.M.; Ginja, J.; Amorim, M.; Coutinho, M.; Karatzas, K.; Sioumis, T.; Katsifarakis, N.; Konstantinidis, K.; De Vito, S.; et al. Assessment of air quality microsensors versus reference methods: The EuNetAir joint exercise. *Atmos. Environ.* **2016**, *147*, 246–263. [[CrossRef](#)]
10. Castell, N.; Dauge, F.R.; Schneider, P.; Vogt, M.; Lerner, U.; Fishbain, B.; Broday, D.; Bartonova, A. Can commercial low-cost sensor platforms contribute to air quality monitoring and exposure estimates? *Environ. Int.* **2017**, *99*, 293–302. [[CrossRef](#)]

11. Mead, M.I.; Popoola, O.A.M.; Stewart, G.B.; Landshoff, P.; Calleja, M.; Hayes, M.; Baldovi, J.J.; McLeod, M.W.; Hodgson, T.F.; Dicks, J.; et al. The use of electrochemical sensors for monitoring urban air quality in low-cost, high-density networks. *Atmos. Environ.* **2013**, *70*, 186–203. [[CrossRef](#)]
12. Wei, P.; Ning, Z.; Ye, S.; Sun, L.; Yang, F.; Wong, K.C.; Westerdahl, D.; Louie, P.K.K. Impact analysis of temperature and humidity conditions on electrochemical sensor response in ambient air quality monitoring. *Sensors* **2018**, *18*, 59. [[CrossRef](#)] [[PubMed](#)]
13. Bauerová, P.; Novák, Z.; Rychlík, Š.; Keder, J. Small air quality sensors: In vivo testing of electrochemical Cairpol sensors in comparison to reference measurement. *WIT Trans. Ecol. Environ.* **2018**, *230*, 343–354.
14. Crilley, L.R.; Shaw, M.; Pound, R.; Kramer, L.J.; Price, R.; Young, S.; Lewis, A.C.; Pope, F.D. Evaluation of a low-cost optical particle counter (Alphasense OPC-N2) for ambient air monitoring. *Atmos. Meas. Tech.* **2018**, *11*, 709–720. [[CrossRef](#)]
15. Zoest, V.; Van Osei, F.B.; Stein, A.; Hoek, G. Calibration of low-cost NO<sub>2</sub> sensors in an urban air quality network. *Atmos. Environ.* **2019**, *210*, 66–75. [[CrossRef](#)]
16. Bulot, F.M.J.; Johnston, S.J.; Basford, P.J.; Easton, N.H.C.; Apetroaie-Cristea, M.; Foster, G.L.; Morris, A.K.R.; Cox, S.J.; Loxham, M. Long-term field comparison of multiple low-cost particulate matter sensors in an outdoor urban environment. *Sci. Rep.* **2019**, *9*, 7497. [[CrossRef](#)] [[PubMed](#)]
17. Bauerová, P.; Keder, J. *Hodnocení Testovacího Měření Různých Typů Malých Senzorů Kvality O vzduší na Observatoři Tušimice: Cairclip (Cairpol, FR), PMS7003 (Plantower, CHN)*; Czech Hydrometeorological Institute: Prague, Czech Republic, 2019.
18. Feinberg, S.; Williams, R.; Hagler, G.S.W.; Rickard, J.; Brown, R.; Garver, D.; Harshfield, G.; Stauffer, P.; Mattson, E.; Judge, R.; et al. Long-term evaluation of air sensor technology under ambient conditions in Denver, Colorado. *Atmos. Meas. Tech.* **2018**, *11*, 4605–4615. [[CrossRef](#)]
19. Cairpol. *Technical Datasheet Cairsens O<sub>3</sub>/NO<sub>2</sub>*; Cairpol Environment S.A.: Poissy, France, 2016.
20. Cairpol. *Technical Datasheet Cairsens NO<sub>2</sub>*; Cairpol Environment S.A.: Poissy, France, 2016.
21. Spinelle, L.; Gerboles, M.; Aleixandre, M. *Report of Laboratory and in-Situ in situ Validation of Micro-Sensor Sensor for Monitoring Ambient air Pollution. O12: CairClip O<sub>3</sub>/NO<sub>2</sub> of Cairpol (F)*; Publications Office of the European Union: Luxembourg, 2013.
22. Jiao, W.; Hagler, G.; Williams, R.; Sharpe, R.; Brown, R.; Garver, D.; Judge, R.; Caudill, M.; Rickard, J.; Davis, M.; et al. Community Air Sensor Network (CAIRSENSE) project: Evaluation of low-cost sensor performance in a suburban environment in the southeastern United States. *Atmos. Meas. Tech.* **2016**, *9*, 5281–5292. [[CrossRef](#)]
23. Notario, A.; Bravo, I.; Adame, J.A.; Díaz-de-Mera, Y.; Aranda, A.; Rodríguez, A.; Rodríguez, D. Behaviour and variability of local and regional oxidant levels (OX = O<sub>3</sub> + NO<sub>2</sub>) measured in a polluted area in central-southern of Iberian Peninsula. *Environ. Sci. Pollut. Res.* **2013**, *20*, 188–200. [[CrossRef](#)]
24. Cairpol. *Technical Datasheet Cairsens SO<sub>2</sub>*; Cairpol Environment S.A.: Poissy, France, 2016.
25. Cairpol. *Technical Datasheet Cairsens CO*; Cairpol Environment S.A.: Poissy, France, 2016.
26. Yong, Z.; Haoxin, Z. *Digital Universal Particle Concentration Sensor: PMS7003 Series Data Manual*; Plantower: Beijing, China, 2016.
27. Alphasense. *Alphasense User Manual OPC-N2 Optical Particle Counter*; Sensor Technology House: Essex, UK, 2015.
28. Teledyne API. Available online: <http://www.teledyne-api.com/> (accessed on 5 March 2018).
29. Environment, SA. Available online: <http://www.environnement-sa.com/> (accessed on 14 January 2019).
30. Palas, Fidas200. Available online: <https://www.palas.de/en/product/fidas200> (accessed on 20 November 2018).
31. Smolík, P.; Rychlík, Š. *Validační Zpráva Pro Metodu T 22 AA-005*; Czech Hydrometeorological Institute: Prague, Czech Republic, 2019.
32. Fishbain, B.; Lerner, U.; Castell, N.; Cole-Hunter, T.; Popoola, O.; Broday, D.M.; Martinez Iniguez, T.; Nieuwenhuisen, M.; Jovasevic-Stojanovic, M.; Topalovic, D.; et al. An evaluation tool kit of air quality micro-sensing units. *Sci. Total Environ.* **2017**, *575*, 639–648. [[CrossRef](#)]
33. van Zoest, V.M.; Stein, A.; Hoek, G. Outlier Detection in Urban Air Quality Sensor Networks. *Water Air Soil Pollut.* **2018**, *229*, 1–13. [[CrossRef](#)]
34. Weissert, L.F.; Alberti, K.; Miskell, G.; Pattison, W.; Salmond, J.A.; Henshaw, G.; Williams, D.E. Low-cost sensors and microscale land use regression: Data fusion to resolve air quality variations with high spatial and temporal resolution. *Atmos. Environ.* **2019**, *213*, 285–295. [[CrossRef](#)]

35. Clements, A.L.; Griswold, W.G.; RS, A.; Johnston, J.E.; Herting, M.M.; Thorson, J.; Collier-Oxandale, A.; Hannigan, M. Low-Cost Air Quality Monitoring Tools: From Research to Practice (A Workshop Summary). *Sensors* **2017**, *17*, 2478. [[CrossRef](#)] [[PubMed](#)]
36. Clements, A.L.; Reece, S.; Conner, T.; Williams, R. Observed data quality concerns involving low-cost air sensors. *Atmos. Environ. X* **2019**, *3*, 100034. [[CrossRef](#)]
37. Lewis, A.C.; Von Schneidmesser, E.; Peltier, R.E. *Low-Cost Sensors for the Measurement of Atmospheric Composition: Overview of Topic and Future Applications*; WMO-No.121.; World Meteorological Organization: Geneva, Switzerland, 2018.
38. Zheng, T.; Bergin, M.H.; Johnson, K.K.; Tripathi, S.N.; Shirodkar, S.; Landis, M.S.; Sutaria, R.; Carlson, D.E. Field evaluation of low-cost particulate matter sensors in high-and low-concentration environments. *Atmos. Meas. Tech.* **2018**, *11*, 4823–4846. [[CrossRef](#)]



© 2020 by the authors. Licensee MDPI, Basel, Switzerland. This article is an open access article distributed under the terms and conditions of the Creative Commons Attribution (CC BY) license (<http://creativecommons.org/licenses/by/4.0/>).



Article

# Long-Term Trends of Air Pollution at National Atmospheric Observatory Košetice (ACTRIS, EMEP, GAW)

Milan Váňa <sup>1,\*</sup>, Adéla Holubová Smejkalová <sup>1,2</sup>, Jaroslava Svobodová <sup>1</sup> and Pavel Machálek <sup>3</sup>

<sup>1</sup> Czech Hydrometeorological Institute, Košetice Observatory, 394 22 Košetice, Czech Republic; adela.holubova@chmi.cz (A.H.S.); jaroslava.svobodova@chmi.cz (J.S.)

<sup>2</sup> Institute for Environmental Studies, Faculty of Science, Charles University, 128 01 Prague, Czech Republic

<sup>3</sup> Czech Hydrometeorological Institute, 143 06 Prague, Czech Republic; pavel.machalek@chmi.cz

\* Correspondence: milan.vana@chmi.cz; Tel.: +420-725-895-574

Received: 30 March 2020; Accepted: 19 May 2020; Published: 21 May 2020



**Abstract:** The National Atmospheric Observatory Košetice operated by the Czech Hydrometeorological Institute was established in 1988 as a station specializing in air quality monitoring at the background scale. The observatory is located in the free area outside of the settlement and represents the Czech Republic in various international projects. The objective of the present study is to detect the long-term trends of air quality at the background scale of the Czech Republic. The statistical method used for trend analysis is based on the nonparametric Mann–Kendall test. Generally, the results show that the fundamental drop in emission of basic air pollutants was reflected in the significant decrease in pollution levels. A most significant drop was detected for sulphur. No trend was found for NO<sub>2</sub> in 1990–2012, but a visibly decreasing tendency was registered in the last 7 years. A slightly decreasing trend was registered for O<sub>3</sub> in the whole period, but a slightly increasing tendency was found after 2006. More importantly, the number of episodes exceeding the target value for human health dropped significantly. The reduction of volatile organic compounds (VOCs) emissions was reflected in a statistically significant decrease of concentrations. Only isoprene, which is of natural origin, displays an inverse trend. Concentrations of elemental carbon (EC) and organic carbon (OC) dropped since 2010, but only for EC is the trend statistically significant.

**Keywords:** long-term trends; background scale; air quality; Czech Republic

## 1. Introduction

The danger caused by large-scale, global and regional pollution started to be recognised in the 1960s. Such pollution might end up resulting in irreversible changes in both terrestrial and ocean ecosystems and global climate change. The research and monitoring efforts required to detect the changes in the atmosphere at global and regional scales must be based on broad-ranging international cooperation. It was, first of all, international institutions (World Meteorological Organization, United Nations Economic Commission for Europe ECE, United Nations Environment Programme) that initiated, in the 1960s and 1970s, the first international monitoring programmes [1].

To support the above-mentioned programmes, Czech Hydrometeorological Institute (CHMI) established the National Atmospheric Observatory Košetice (NAOK), specialized in monitoring and research of air quality at the background scale of Czech Republic.

After the political changes in 1989, the air quality control and protection became one of the most important political priorities in the Czech Republic. Immense funds were invested in emission reductions (mainly from large power plants) in the Czech Republic during the 1990s, resulting in a

marked improvement in the air quality, the levels of which in some regions had previously ranked among the worst in the world. Nevertheless, the growing industry and traffic after 2000 have caused the air quality in the Czech Republic to begin to deteriorate again. Irresponsible conduct of individuals who use low-quality fuels or even municipal waste in household heating systems, emitting hazardous chemicals to the air, is a contributing factor that cannot be neglected. Fine dust is the most serious problem at the moment. The Ministry of the Environment developed a National Emission Reduction Programme of the Czech Republic in 2007, and it has been approved by the government. The document comprises several key measures to contribute to an improvement in the current state of the environment and environmental and health protection.

The objective of the study is to detect the long-term trends of air quality at the background scale of the Czech Republic. Thirty-year data series is sufficient for detection of long-term trends of air quality. The study is based on the data generated within the National Air Pollution Monitoring Network, stored in Air Quality Information System and annually published e.g., [2]. Generally, the development of air quality in the last three decades was affected by various circumstances: the essential political changes in Central and Eastern Europe in the end of the 1980s brought a substantial decrease in emissions in the Czech Republic and more widely in the Central European region thanks to international conventions and also economic and political development. The meteorological conditions for long-range transport in Europe were changed as well, and the question of global climate change assumed importance. Measurement techniques showed significant improvement, as did our knowledge concerning the behaviour of air pollutants in the atmosphere. All these aspects influenced the long-term trends at the background scale of the Czech Republic very significantly.

## **2. Materials and Methods**

### *2.1. Site Description and Overall Context*

NAOK is located in the agricultural countryside outside of settlements in the southern part of the Czech Republic, district of Pelhřimov (49°35' N, 15°05', 534 E m asl, Figure 1). More detailed description of physical-geographical conditions is available in [3]. The operation of NAOK started in 1988, but some basic air quality measurements were implemented since the middle of the 1980s in the vicinity of the observatory. The main task of NAOK throughout its history was to detect the long-term trends of air quality at the background scale of the Czech Republic and Central Europe and to represent the Czech Republic in the long-term programmes of air quality monitoring and research GAW/WMO (Global Atmosphere Watch), EMEP (Co-operative Programme for Monitoring and Evaluation of Long-range Transmission of Air Pollutants in Europe) and ICP-IM (International Co-operative Programme on Integrated Monitoring).

After 2004, when Czech Republic joined the EU, NAOK, thanks to its excellent location and long-term homogeneous data series, has been participating in several EU projects. The first was EUSAAR (European Supersites for Atmospheric Aerosol Research), focused on the research of atmospheric aerosols. The essential importance for the advancement of NAOK in the last decade brought participation in ACTRIS RI (Aerosol, Clouds and Trace gases Research Infrastructure). NAOK is a core of Large Research Infrastructure (LRI) ACTRIS Czech Republic (ACTRIS-CZ), a unique platform for the long-term background air quality monitoring and research closely related to climate, environmental and health issues qualified as societal challenges. ACTRIS-CZ represents a national node of the existing European ACTRIS Research Infrastructure (RI) established with the support of the EU 7th Framework Programme INFRA-2010-1-1.1.16 (EU FP7) and ACTRIS-2 project of EU Horizon 2020 (H2020-INFRAIA-2014-2015: Integrating and Opening Existing National and Regional Research Infrastructures of European Interest). In December 2015, ACTRIS was adopted on the ESFRI roadmap 2016 for Research Infrastructures. LRI ACTRIS-CZ RI is based on the long-term collaboration of 4 research partners: Czech Hydrometeorological Institute (CHMI), The Institute of Chemical Process Fundamentals of the CAS (ICPF), Global Change Research Institute of the CAS (GCRI) and Masaryk University (MU) at the research facility of NAOK.



**Figure 1.** Location of National Atmospheric Observatory Košetice (NAOK) in the European, Czech and local context.

### 2.2. Measurement Methods

NAOK is a part of the National Air Pollution Monitoring Network (operated by CHMI). All measurements are carried out according to the quality-controlled procedures. This network operates online (automatic analyzers) and offline (samplers) instruments. Filter analyses are done mainly in the central laboratory of immissions in Prague. The data validation procedure is in line with the EC directive 2008/50/EC. An overview of methods of measured components used in this study are listed in Table 1. A detailed description of each method is available in [4].

**Table 1.** Used sampling methods—year of start, type of measurement, method of determination.

| Component          | Start of Measurement | Type of Measurement | Method                            |
|--------------------|----------------------|---------------------|-----------------------------------|
| CO                 | 1996                 | online              | IR corel. absorption spectrometry |
| EC/OC              | 2009                 | offline             | heat decomposition_FID            |
| NO <sub>x</sub>    | 1994                 | online              | chemiluminescence                 |
| O <sub>3</sub>     | 1992                 | online              | UV-absorption                     |
| PM <sub>10</sub>   | 1996                 | online              | radiometry                        |
| PM <sub>2.5</sub>  | 2004                 | offline             | gravimetry                        |
| SO <sub>2</sub>    | 1992                 | online              | UV-fluorescence                   |
| SO <sub>4</sub>    | 1988                 | offline             | ion chromatography                |
| VOCs               | 1995                 | offline             | gas chromatography                |
| ΣNH <sub>4</sub> * | 2002                 | offline             | spectrophotometry                 |
| ΣNO <sub>3</sub> * | 2002                 | offline             | ion chromatography                |

\* The sum consists of gaseous and particulate matter.

### 2.3. Statistical Evaluation

The statistical method used for the evaluation of long-term trends is based on the nonparametric Mann–Kendall test for the trend and the nonparametric Sen’s method for the magnitude of the trend. Mann–Kendall test is used since missing values are allowed and the data need not conform to any particular distribution. Sen’s method is not greatly affected by gross data errors or outliers, and it can also be computed when data are missing. Sen’s estimator is closely related to the Mann–Kendall test. Mann–Kendall test is recommended and plentifully used for long-term trend evaluation in air quality because it enables one to evaluate non-complete data series and does not require specific distribution of measured values. On the other hand, it is not possible to use it for assessment of short-term variability and annual variation. Due to its properties, the Mann–Kendall test was used to analyze long-term trends of air pollution measurements data in a harmonized way for EMEP Assessment report [5].

The presence of trend is evaluated using Z value. A positive and negative value of Z indicates an upward and downward trend, respectively. The statistics Z has a normal distribution.

The existence and significance of trend is tested by using four different  $\alpha$  levels of significance. The different  $\alpha$  levels used are  $\alpha = 0.1$ ,  $\alpha = 0.05$ ,  $\alpha = 0.01$  and  $\alpha = 0.001$ .

Trend statistics it is given as a result of the significance level of that trend, marked by

- + if there is a trend at the  $\alpha = 0.1$  level,
- \* if there is a trend at the  $\alpha = 0.05$  level,
- \*\* if there is a trend at the  $\alpha = 0.01$  level and
- \*\*\* if there is a trend at  $\alpha = 0.001$  level.

This means that when the mark is “\*\*\*”, the trend is very significant, and when the mark is “+”, the significance of the trend is fairly poor, only 10%. If the mark is missing, then there is no trend at significance level  $\alpha = 0.1$  [6].

### 3. Results

Political and economic changes after the fall of the iron curtain brought a general drop in industrial production and later significant changes in the structure of the industry. These changes were reflected in the reduction of sulphur emissions in the Czech Republic by almost 90% in the period of 1990–2000 (Figure 2). The results of long-term monitoring show that the emission decrease was reflected in reduced pollution levels. Sulphur dioxide concentrations in the atmosphere declined nearly by the same order of magnitude as the emissions (Figure 3c). The steep drop of  $\text{SO}_2$  concentrations was more pronounced in the 1990s. The frequency of episodes with extremely high concentrations decreased rapidly (Figure 3e). In the new millennium, the mean annual concentrations dropped below  $5 \mu\text{g}\cdot\text{m}^{-3}$ , but a slightly decreasing trend was found also in the period 2001–2019 (Figure 3f). In the EMEP domain,  $\text{SO}_2$  emission reductions started in the 1980s–1990s; therefore, changes in concentrations will have occurred earlier than 1990. However, concentrations have continued to decrease continuously during the period under review. The timing of concentration decreases varies between countries according to national implementation of emission reduction strategies, but on average, the decrease was larger in the early 1990s and levelled off since then [5].

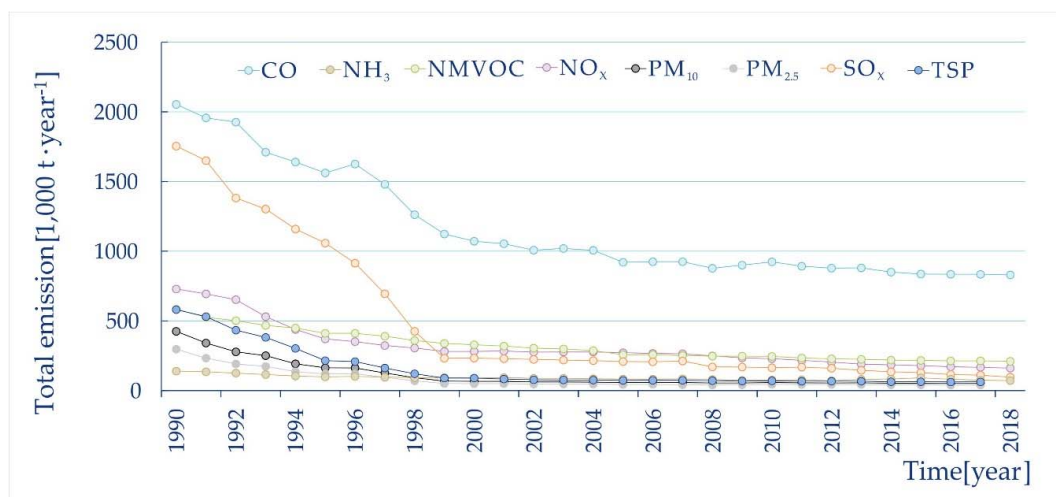


**Figure 2.** Total emissions of basic pollutants in the Czech Republic in the period 1990–2018. Results are based on emission inventories outcomes, regularly evaluated and published in air pollution reports in the Czech republic (e.g., [2]).

In the period of 1994–2012, no trend of nitrogen oxides concentration was found, in spite of the fact that the nitrogen emissions declined by 54% during the period under review (Figure 3b). In the period of 1990–2012, the emissions dropped by 72% and in the EU by 55% [6]. Mean annual concentrations varied around  $10 \mu\text{g}\cdot\text{m}^{-3}$ . These results were in very good correspondence with the trends at the

background level in the neighbouring countries (Austria, Germany) [5]. The reasons are uncertain. One of the explanations could be the significant changes in the structure of nitrogen emissions. In the last 7 years, a visibly decreasing tendency of  $\text{NO}_2$  concentrations was found and the mean annual concentrations dropped continuously to  $4 \mu\text{g}\cdot\text{m}^{-3}$ . The evaluation of the data from the EMEP network shows that for the period of 1990–2001, the fraction of sites where significant negative trends were observed was high (58%), but it slowed down after 2002.

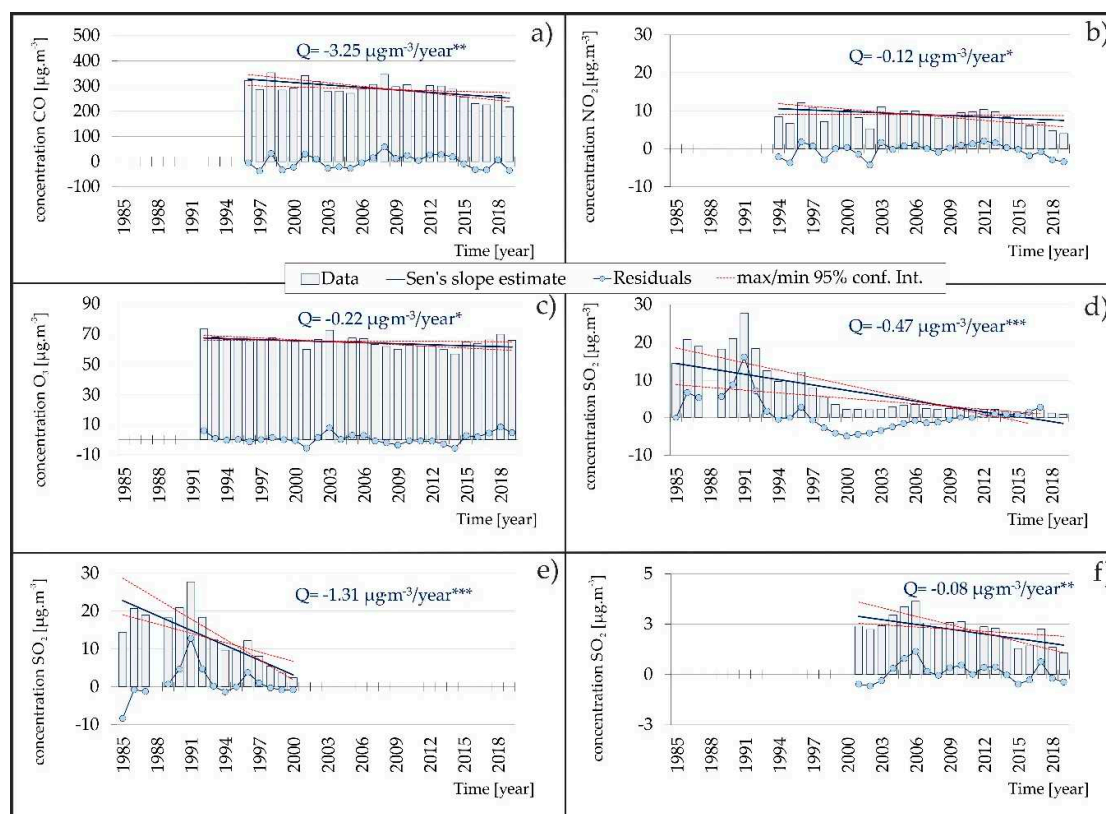


**Figure 3.** Results of Mann–Kendal test for gaseous pollutants; (a) CO, (b)  $\text{NO}_2$ , (c)  $\text{O}_3$ , (d)  $\text{SO}_2$  1985–2018, (e)  $\text{SO}_2$  1985–2000, (f)  $\text{SO}_2$  2001–2018.

$\text{NO}$  concentration at the background scale is quite low, and mean annual concentrations varied around  $1 \mu\text{g}\cdot\text{m}^{-3}$ . The long-term trend describes similar patterns for  $\text{NO}_2$ : no trend in the period 1994–2012 and decreasing tendency after 2012.

A slightly decreasing trend was found in mean annual concentrations of tropospheric ozone in the whole period and also in the first part of the period under review (Figure 3c). On the contrary, a slightly increasing tendency was found after 2006. It is caused probably by increasing temperature during the last two decades. A warm period displays similar patterns as the whole year. On the contrary, no trend was found in the cold period [7]. More importantly, the number of episodes exceeding the target value for human health dropped significantly during the period (Figure 4), and interannual variations can be explained by meteorological conditions. The target value of tropospheric ozone for the protection of human health is exceeded when the eight-hour running mean is higher than  $120 \mu\text{g}\cdot\text{m}^{-3}$  25 times on average for 3 years. Visibly higher values were recorded in the years with extreme summer temperatures over long periods and well-established heat waves over continental Europe (2003, 2015, 2017).

A statistically significant trend was found for carbon dioxide. Mean annual concentrations decreased continuously during the whole period (Figure 3a).

Most non-methane volatile organic compounds (VOCs) follow an annual course that reflects their emission levels, i.e., with maximums in winter and minimums in summer. Isoprene is an exception.

In general, the reduction of VOCs emissions in the last two decades was reflected in a decrease of concentrations at the regional scale of the Czech Republic [8]. A statistically significant downward trend was found for almost all of measured VOCs, and only the ethane trend was less significant (Table 2). The trend of isoprene concentrations is controlled first of all by natural conditions and shows different patterns from other VOCs. We detected a statistically very significant upward trend of isoprene concentration in the period under review. Favourable conditions for isoprene emissions are in hot summer periods. An increasing tendency was visible especially in the last decade. This is in good correlation with increasing mean annual temperature in the current period of changing climate conditions (hot summers, long periods with high temperatures). It follows from the current report on VOC measurements in the context of EMEP [9] that the VOC concentrations continuously decrease on a regional scale and thus reflect the decreasing trend in emissions. The concentration level at NAO Koštice is comparable with those at the German, Swiss and French stations. The Czech station has long been characterised by lower annual average ethane concentrations. For most VOCs, the concentrations measured in the winter are usually similar to those at German stations, while the values at NAOK are slightly lower in the summer.

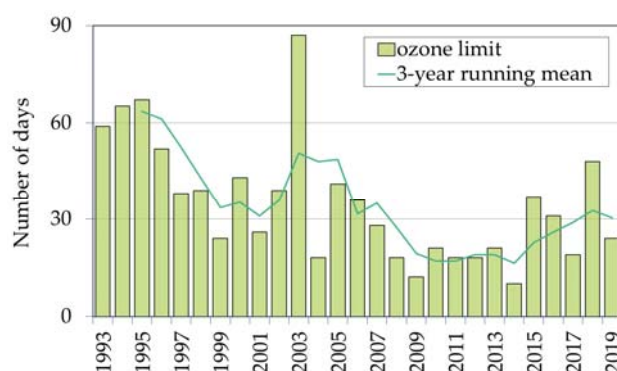


Figure 4. Number of days with target limit for surface ozone exceedances (1993–2019).

Table 2. Trend significance of measured VOCs.

| Time Series       | First Year | Last Year | n  | Test Z | Signific. | Q      |
|-------------------|------------|-----------|----|--------|-----------|--------|
| Acetylene         | 1993       | 2018      | 26 | -5.16  | ***       | -46.91 |
| Benzene           | 1993       | 2018      | 26 | -3.92  | ***       | -8.11  |
| Butenes           | 1993       | 2018      | 25 | -2.06  | *         | -2.93  |
| Cyklohexane       | 1996       | 2018      | 23 | -2.85  | **        | -1.13  |
| Cyklopentane      | 1995       | 2018      | 22 | -3.13  | **        | -0.69  |
| Ethane            | 1993       | 2018      | 26 | -1.94  | +         | -12.71 |
| Ethene            | 1993       | 2018      | 26 | -4.89  | ***       | -28.23 |
| Ethylbenzene      | 1993       | 2018      | 25 | -0.86  |           | -0.68  |
| i-Butane          | 1993       | 2018      | 26 | -5.73  | ***       | -6.56  |
| i-Octane          | 1997       | 2018      | 21 | 1.60   |           | 0.24   |
| i-Pentane         | 1993       | 2018      | 25 | -5.63  | ***       | -9.92  |
| Isopren           | 1993       | 2018      | 26 | 3.66   | ***       | 1.95   |
| m,p-Xylene        | 1993       | 2018      | 25 | -0.30  |           | -0.18  |
| Metylcyklopentane | 1996       | 2018      | 22 | -3.70  | ***       | -1.26  |
| n-Butane          | 1993       | 2018      | 26 | -4.94  | ***       | -11.28 |
| n-Hexane          | 1993       | 2018      | 25 | -3.95  | ***       | -3.15  |
| n-Octane          | 1997       | 2018      | 22 | 0.57   |           | 0.22   |
| Nonane            | 1996       | 2018      | 22 | -0.73  |           | -0.21  |
| n-Pentane         | 1993       | 2018      | 25 | -5.11  | ***       | -5.88  |
| o-Xylene          | 1993       | 2018      | 25 | 0.21   |           | 0.22   |
| Pentenes          | 1996       | 2018      | 23 | -2.03  | *         | -0.67  |
| Propane           | 1993       | 2018      | 26 | -4.74  | ***       | -14.20 |
| Propene           | 1993       | 2018      | 26 | -4.79  | ***       | -4.73  |
| Toluene           | 1993       | 2018      | 26 | -4.63  | ***       | -8.28  |

“\*\*\*”—the trend is very significant; “+”—the significance of the trend is fairly poor, only 10%. If the mark is missing, then there is no trend at significance level  $\alpha = 0.1$ .

The measurement of aerosol particles covers periods of different duration. The longest records are available for sulphate in aerosol and PM<sub>10</sub>. Table 3 shows that the concentrations were changed significantly during the period under review. Changes in concentration levels reflect the development of emission (Figure 2), which is in line with both national and international environmental measures.

Outcomes of sulphur and PM<sub>10</sub> show the highest level of trend significance (Figure 5c,d). Sulphur concentration continuously decreased during the whole period. On the other hand, the evaluation of PM<sub>10</sub> data shows that the mean annual concentrations in the period of 2001–2006 reached a similar level as in 1996 (29.8 µg·m<sup>-3</sup>) (Figure 5c). The same patterns were observed across the Czech Republic at different types of stations. After 2001, the drop of emission was slower compared to the previous period. The increase of PM<sub>10</sub> concentrations was probably influenced by meteorological and dispersion conditions [10]. A higher level of trend significance is observed for PM<sub>2,5</sub> concentrations. After 2005, when a level over 18 µg·m<sup>-3</sup> was recorded, the linear decreasing trend is observed. These outcomes are analogous for PM<sub>10</sub>.

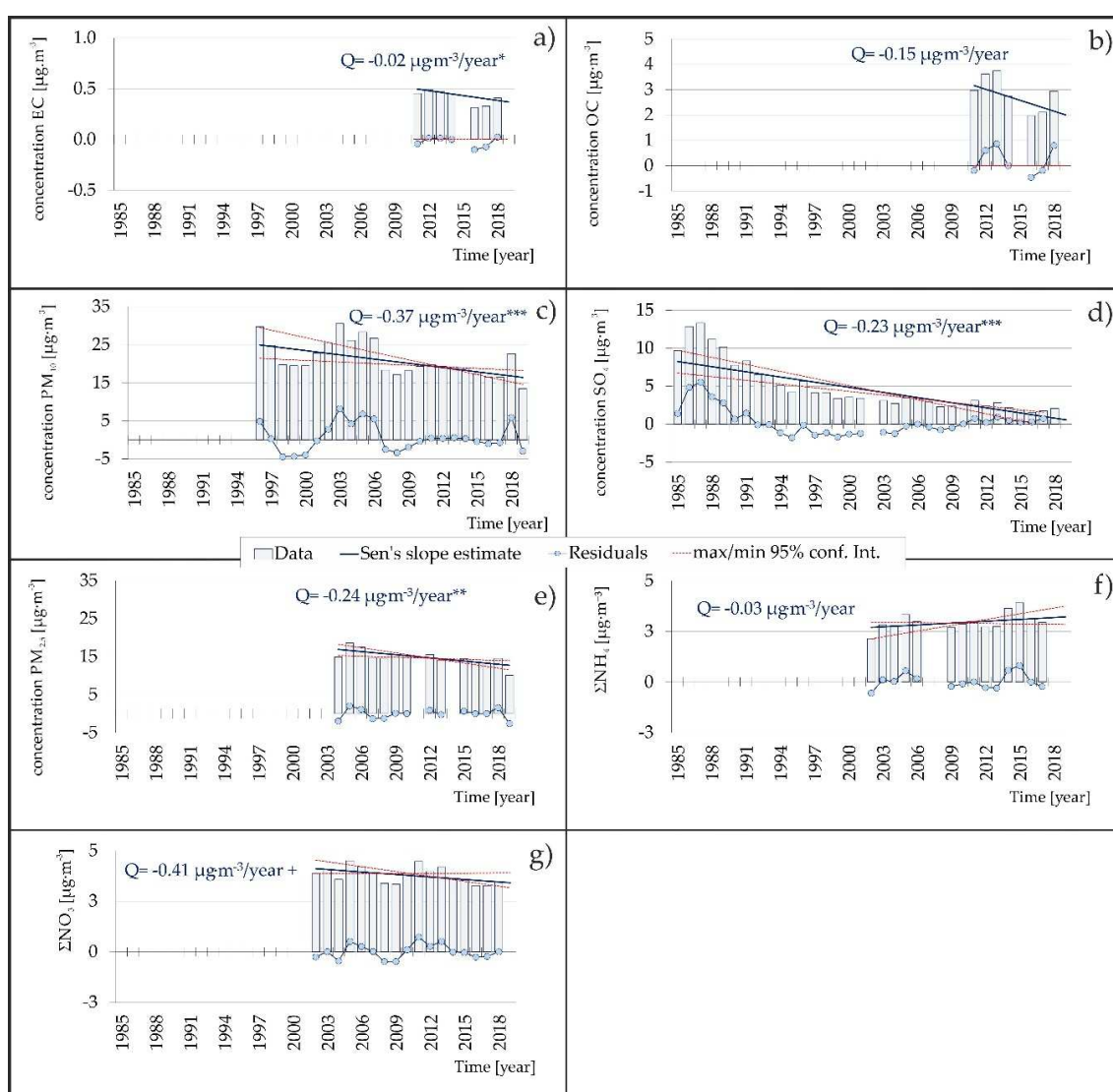


**Figure 5.** Results of Mann–Kendall test for aerosol particles; (a) EC, (b) OC, (c) PM<sub>10</sub>, (d) SO<sub>4</sub>, (e) PM<sub>2,5</sub>, (f) ΣNH<sub>4</sub>, (g) ΣNO<sub>3</sub>.

An insignificant trend is visible for the sums of ammonium and nitrates (Figure 5f,g) that are measured from 2002. This is in line with the fact that the emission development is more or less at the same level (Figure 2). No visible annual variation was found (Table 3). Concentrations of elemental

(EC) and organic carbon (OC) dropped from 2010 (Table 3), but only for EC is the trend statistically significant (Figure 5a,b).

**Table 3.** Changes in annual aerosol concentrations at the beginning and the end of the evaluated period.

| Component           | EC  | OC  | PM <sub>10</sub> | SO <sub>4</sub> | PM <sub>2.5</sub> | ΣNH <sub>4</sub> | ΣNO <sub>3</sub> |
|---------------------|---|-----|------------------|-----------------|-------------------|------------------|------------------|
|                     | concentration [ $\mu\text{g}\cdot\text{m}^{-3}$ ] |     |                  |                 |                   |                  |                  |
| Beginning of period | 0.5   | 3.3 | 29.8             | 9.6             | 14.9              | 2.1              | 3.9              |
| End of period       | 0.4   | 2.9 | 13.4             | 2.1             | 10.1              | 2.9              | 3.5              |

#### 4. Summary

Generally, the results show that the fundamental drop in emission of basic air pollutants in the Czech Republic and widely in the Central European region in the period under review was reflected in the significant decrease of air pollution levels at the background scale of the Czech Republic. A statistically very significant drop in mean annual concentrations of sulphur dioxide was detected in the period of 1990–2000. After 2000, the mean annual concentrations dropped below  $5 \mu\text{g}\cdot\text{m}^{-3}$ , but a slightly decreasing trend was found also in the period of 2001–2019.

No trend was found by the evaluation of nitrogen dioxide in the atmosphere in the period of 1990–2012, in spite of the fact that the nitrogen emissions declined by half during the period under review. In the last 7 years, a visibly decreasing tendency of NO<sub>2</sub> concentrations was registered, and the mean annual concentrations dropped continuously to  $4 \mu\text{g}\cdot\text{m}^{-3}$ .

A slightly decreasing trend was found in mean annual concentrations of tropospheric ozone in the whole period and also in the first part of the period under review. On the contrary, a slightly increasing tendency was found after 2006. It is caused probably by increasing temperature during the last two decades. More importantly, the number of episodes with the target value for human health exceedances dropped significantly during the period.

The reduction of VOCs emissions in Central Europe was reflected in a statistically significant decrease of concentrations at the regional level of the Czech Republic. Only isoprene, which is of natural origin, displays an inverse trend.

Sulphur concentration in aerosol continuously decreased during the whole period. The evaluation of PM<sub>10</sub> data shows that the mean annual concentrations in the period of 2001–2006 reached a similar level as in 1996. The higher level of trend significance is observed for PM<sub>2.5</sub> concentrations, but the general outcomes are analogous as for PM<sub>10</sub>. Concentrations of EC and OC dropped from 2010, but only for EC is the trend statistically significant.

**Author Contributions:** Conceptualization, M.V.; methodology, A.H.S.; validation, M.V., A.H.S., J.S.; formal analysis, M.V., A.H.S.; investigation, M.V., A.H.S.; resources, M.V.; data curation, J.S., P.M.; writing—original draft preparation, M.V.; writing—review and editing, M.V.; visualization, A.H.S.; supervision, M.V.; project administration, M.V.; funding acquisition, M.V. All authors have read and agreed to the published version of the manuscript.

**Funding:** This research was funded by the project for support of national research infrastructure ACTRIS—participation of the Czech Republic (ACTRIS-CZ - LM2015037)—Ministry of Education, Youth and Sports of the Czech Republic.

**Acknowledgments:** The research leading to these results has received funding from the project for support of national research infrastructure ACTRIS—participation of the Czech Republic (ACTRIS-CZ - LM2015037)—Ministry of Education, Youth and Sports of the Czech Republic.

**Conflicts of Interest:** The authors declare no conflict of interest.

#### References

- Váňa, M.; Holoubek, I. *Quality of the Natural Environment in the Czech Republic at the Regional Level (Results of the Košetice Observatory)*; ČHMÚ: Praha, Czech Republic, 2001.
- CHMI. *Air Pollution in the Czech Republic in 2018*; ČHMÚ: Praha, Czech Republic, 2019; ISBN 978-80-87577-95-0.

3. Váňa, M.; Dvorská, A. *Košetice Observatory 25 Years*; ČHMÚ: Praha, Czech Republic, 2014; ISBN 978-80-87577-40-0.
4. Summary Tabular Survey. Available online: [http://portal.chmi.cz/files/portal/docs/uoco/isko/tab\\_roc/2018\\_enh/index\\_GB.html](http://portal.chmi.cz/files/portal/docs/uoco/isko/tab_roc/2018_enh/index_GB.html) (accessed on 3 March 2020).
5. Colette, A.; Aas, W.; Banin, L.; Braban, C.F.; Ferm, M.; González Ortiz, A.; Ilyin, I.; Mar, K.; Pandolfi, M.; Putaud, J.-P.; et al. *Air Pollution Trends in the EMEP Region between 1990 and 2012. Joint Report of the EMEP Task Force on Measurements and Modelling (TFMM), Chemical Co-Ordinating Centre (CCC), Meteorological Synthesizing Centre-East (MSC-E), Meteorological Synthesizing Centre-West (MSC-W)*; NILU: Kjeller, Norway, 2016; ISBN 978-82-425-2833-9.
6. EEA. *European Union Emission Inventory Report 1990–2014 under the UNECE Convention on Long-Range Transboundary Air Pollution (LRTAP)*; EEA Report No 16/2016; European Environment Agency: Copenhagen, Denmark, 2016; ISBN 978-92-9213-748-9.
7. Váňa, M.; Pekárek, J. *Long Term Trends of Tropospheric Ozone in the Czech Republic 1992–2018. WIT Transactions on Ecology and the Environment; Air Pollution XXVII*; WIT Press: Southampton, UK, 2019; Volume 236, pp. 21–33.
8. Váňa, M.; Pekárek, J. Trendy znečištění ovzduší a srážek na Observatoři Košetice. *Ochrana ovzduší* **2013**, *25*, 15–19.
9. Solberg, S.; Claude, A.; Reimann, S. *VOC Measurements 2016. EMEP/CCC-Report 4/2018*; NILU: Kjeller, Norway, 2018; ISBN 978-82-425-2946-6.
10. CHMI. *Air Pollution in the Czech Republic in 2016*; ČHMÚ: Praha, Czech Republic, 2017; ISBN 978-80-87577-72-1.



© 2020 by the authors. Licensee MDPI, Basel, Switzerland. This article is an open access article distributed under the terms and conditions of the Creative Commons Attribution (CC BY) license (<http://creativecommons.org/licenses/by/4.0/>).



Article

# Air Quality in Brno City Parks

Jiří Huzlík<sup>1,\*</sup>, Jitka Hegrová<sup>1</sup>, Karel Effenberger<sup>1</sup>, Roman Ličbínský<sup>1</sup> and Martin Brtnický<sup>2,3</sup>

<sup>1</sup> Transport Research Centre, Lisenska 33a, 636 00 Brno, Czech Republic; jitka.hegrova@cdv.cz (J.H.); karel.effenberger@cdv.cz (K.E.); roman.licbinsky@cdv.cz (R.L.)

<sup>2</sup> Department of Agrochemistry, Soil Science, Microbiology and Plant Nutrition, Faculty of AgriSciences, Mendel University in Brno, Zemedelska 1, 613 00 Brno, Czech Republic; martin.brtnicky@mendelu.cz

<sup>3</sup> Institute of Chemistry and Technology of Environmental Protection, Brno University of Technology, Faculty of Chemistry, Purkynova 118, 621 00 Brno, Czech Republic

\* Correspondence: jiri.huzlik@cdv.cz

Received: 30 March 2020; Accepted: 12 May 2020; Published: 15 May 2020



**Abstract:** Parks embody an important element of urban infrastructure and a basic type of public space that shapes the overall character of a city. They form a counterweight to built-up areas and public spaces with paved surfaces. In this context, parks compensate for the lack of natural, open landscapes in cities and thus have a fundamental impact on the quality of life of their inhabitants. For this reason, it is important to consider the quality of the environment in urban parks, air quality in particular. Concentrations of gaseous pollutants, namely, nitric oxide (NO), nitrogen dioxide (NO<sub>2</sub>), and ozone (O<sub>3</sub>), were measured in parks of Brno, the second-largest city in the Czech Republic. Relevant concentration values of PM<sub>10</sub> solids were determined continuously via the nephelometric method, followed by gravimetric method-based validation. The results obtained through the measurement of wind direction, wind speed, temperature, and relative humidity were used to identify potential sources of air pollution in parks. The “openair” and “openairmaps” packages from the OpenSource software R v. 3.6.2 were employed to analyze the effect of meteorological conditions on air pollution. Local polar concentration maps found use in localizing the most serious sources of air pollution within urban parks. The outcomes of the analyses show that the prevailing amount of the pollution determined at the measuring point most likely originates from the crossroads near the sampled localities. At the monitored spots, the maximum concentrations of pollutants are reached especially during the morning rush hour. The detailed time and spatial course of air pollution in the urban parks were indicated in the respective concentration maps capturing individual pollutants. Significantly increased concentrations of nitrogen oxides were established in a locality situated near a busy road (with the traffic intensity of 33,000 vehicles/d); this scenario generally applied to colder weather. The highest PM<sub>10</sub> concentrations were measured at the same location and at an average temperature that proved to be the lowest within the entire set of measurements. In the main city park, unlike other localities, higher concentrations of PM<sub>10</sub> were measured in warmer weather; such an effect was probably caused by the park being used to host barbecue parties.

**Keywords:** air pollution; urban parks; particulate matter; nitrogen oxides; ozone

## 1. Introduction

Urban green spaces, namely, city parks, are very often considered localities providing the best air quality in a city, and thus they become frequently targeted by citizens seeking relaxation and active recreation. However, there are very few studies supporting this generally accepted claim.

Xing et al. [1–3] noticed improved air quality in small urban parks within a distance from surrounding streets due to the dispersion of air pollutants within park areas. Importantly in this

context, trees can reduce wind speed and potentially trap pollutants. Most available studies point to a reduction of PM concentration levels inside city parks. Von Schneidmesser [4] stated that suitably distributed greenery can decrease the concentration of PMs by 20%, down to relative ambient average concentrations. Ou et al. [5] monitored PM<sub>2.5</sub> and PM<sub>10</sub> mass concentrations during the fall of 2018, identifying a significant drop in both PM<sub>10</sub> and PM<sub>2.5</sub> levels close to parks. A decrease of 23% in the total mass of PM<sub>2.5</sub> in a national park compared to an urban area is presented in paper [6]. Zhu et al. [7] analyzed the impact exerted by different types of plant communities on ambient PM<sub>10</sub> and PM<sub>2.5</sub> concentrations by using a spatial model. The results showed that differences in the levels of ambient PM concentrations among plant communities resulted from their composition and also other factors, including height (significantly lower ambient PM concentrations were recorded near small plants, namely, ones of less than 1 m), leaf area, or distance from the pollution source or edge of the park. Greenery increases the efficiency of reduction in ambient PM concentrations; however, this capability markedly depends on the season of the year. A significant decrease of PM<sub>2.5</sub> concentrations in La Carolina, a large city park in Ecuador, was described in [8]. Otosen et al. [9] measured differences in PM<sub>1.0</sub>, PM<sub>2.5</sub>, PM<sub>10</sub>, NO<sub>2</sub>, and CO concentrations in front of and behind vegetation barriers along roads (hedges during dormancy and the vegetative period). This type of greenery can mitigate the effects of air pollution generated by traffic, and, truly, a decrease in PM concentrations was measured. Contrariwise, no impact on the concentration of gasses was determined. In a relevant study by Abhijith and Kumar [10], the concentrations of PM<sub>10</sub>, PM<sub>2.5</sub>, PM<sub>1.0</sub>, and black carbon were established in close vicinity of the three types of green infrastructure. The influence of separate hedges or shrubs, separate trees, and a mixture of trees and hedges/shrubs was assessed when located at different distances from a road, namely, at very close (<1 m from the road) and more remote (>2 m from the road) spots. The most prominent reductions were recorded in a mixture of trees and hedges under close distance conditions and in separate hedges positioned more remotely. An assessment of various PM fractions showed that separate hedges and a combination of trees and hedges decrease fine particle concentrations behind the green barrier. Relevant analyses then indicated a reduction of vehicle-related particles (i.e., those containing iron and its oxides, Ba, Cr, Mn) in the background of the green infrastructure, as compared to the front area. A similar paper on green infrastructure barriers, Mori et al. [11], characterized measurements of PMs sized between 0.2 µm and 100 µm. The authors described a reduction in PM particles at different distances from the road (measured by passive samplers), proposing that the actual results are influenced by different planting densities in two different green vegetation types of two heights.

Air pollution and human health, as well as green infrastructure and human health, are often studied together. Linking green infrastructure with air quality and human health is an aspect of interest for Kumar et al., who, in a corresponding review [12], concluded that although urban vegetation can bring health benefits, the knowledge of its wider applicability in efforts to reduce air pollution remains overly insufficient and must be further refined. Almedia et al. [13] discussed differences in pollutant concentrations (PM<sub>10</sub>, NO<sub>2</sub>, and O<sub>3</sub>) between schools near roads in urban areas and schools adjacent to forests and roads in the same environment. The results correlate with respiratory problems exhibited by children within all areas of interest. The PM<sub>10</sub> and NO<sub>2</sub> concentrations proved to be higher at points closer to roads with intense traffic flows and lower at spots near parks with dense vegetation. Sheridan et al. [14] focused on NO<sub>x</sub> concentrations in the city of London, especially in parks and playgrounds, finding dangerously high levels of NO<sub>2</sub> at all places of interest (playgrounds, parks, and gardens), those open to the influx of the pollutant in particular. Lingberg et al. [15] described a reduction of air pollution in parks within the city of Gothenburg, Sweden; they emphasized the “park effect”, namely, the assumption that parks embody a considerably cleaner local environment thanks to an interaction of two effects: dilution (the distance effect) and deposition. Trees and other vegetation can absorb and capture air pollutants, thus improving the air quality in cities. Due to a lack of local-scale information, the impact of urban parks and forest vegetation on the levels of nitrogen dioxide (NO<sub>2</sub>) and ground-level ozone (O<sub>3</sub>) were studied in Baltimore, USA. Yli-Pelkonen et al. [16]

concluded that O<sub>3</sub> concentrations were significantly lower in tree-covered habitats than in open ones. Conversely, NO<sub>2</sub> concentrations did not differ significantly between tree-covered and open habitats, meaning that it is again necessary to stress the choice and variability of greenery. Hewitt et al. [17] discussed several options of how to improve air quality by using different types of green infrastructure, introducing a novel conceptual framework as policy guidance; the authors' interpretation of the problem includes a flow chart to aid decision-making as regards the "green infrastructure to improve urban air quality".

Air pollution poses a major risk to human health, causing premature deaths and potentially reducing the quality of life. Quantifying the role of vegetation in curbing air pollution concentrations is an important step. Most current methods to calculate pollution cutback procedures are static and thus represent neither atmospheric transport of pollutants nor pollutants and meteorology interaction. The focus on urban parks as a tool to facilitate air purification and climate regulation embodies the basis of articles by Vieira et al. [18] and Mexia et al. [19]. These authors concluded that ecosystem service strongly depends on the vegetation type; thus, for example, air purification is more pronounced in mixed forest, and carbon reduction is influenced by tree density. Further, Jones et al. [20] developed a method to calculate health benefits directly from changes in pollutant (including PM<sub>2.5</sub>, NO<sub>2</sub>, SO<sub>2</sub>, and O<sub>3</sub>) concentrations, exploiting an atmospheric chemistry transport model.

In our paper, the concentrations of PM<sub>10</sub> solids were determined continuously, by utilizing the nephelometric method followed by gravimetric method-based validation. To identify potential sources of air pollution in parks, we evaluated the air quality within the local environment via correlation with measurements of wind direction, wind speed, temperature, and relative humidity. The "openair" and "openairmaps" packages from the OpenSource software R were employed to analyze the effects of wind on air pollution. Local polar concentration maps found application in locating the directions of wind coming from the most serious air pollution sources. Sampling and analyses were performed to confirm the assumption that the main sources of the pollution at the measuring point are most likely the roads and/or crossroads near the sampled localities.

Due to the information gap concerning air quality in city parks, the goal of our study was to obtain data on air pollution in urban parks and associated details relevant to the relationship between this pollution and meteorological parameters, prominently including temperature, wind speed, and wind direction; in this context, our efforts also involved comparing these data with pollution around the parks. Based on the findings, we then aimed to estimate the sources of air pollution in the monitored parks.

## **2. Method**

### *2.1. Sampling*

The sampling was carried out in three pre-selected city parks in Brno, the Czech Republic; two of the parks are located in areas with a high traffic impact (near main roads), while one is found in a low traffic load environment (a small park inside a courtyard). The main city park of Lužánky exhibits the largest surface area of all the monitored parks, and it is located near the city center, surrounded by roads with heavy traffic. Two air quality monitoring spots were positioned in the park: one place in the middle of the area, and the other on the edge of the park, near a playground and the traffic-laden roads. This park is frequently visited and used for sports and leisure activities, including picnics.

The Koliště park is adjacent to a road with heavy traffic (33,000 cars/d). It occupies a large walking-friendly area, and there is a very popular restaurant in the middle of the park. However, due to the traffic-laden road, the location is not a popular target for sports, children's activities, or picnics. The air quality was measured near a junction of two main roads.

Tyršův sad is a very small park in the city center, situated inside a courtyard. This park is mostly used only for short walks, especially with dogs. The air quality measurement was performed in the middle of the area.

The devices were installed together at the place of interest.

## 2.2. Instrumentation

The NO, NO<sub>2</sub>, O<sub>3</sub>, and PM<sub>10</sub> concentrations were determined by using two Airpointer units (Recordum Messtechnik GmbH, Austria). These devices measure pollutant concentrations via separate modules utilizing type-approved reference methods (NO<sub>2</sub>/NO<sub>x</sub>, O<sub>3</sub>) classified as relevant by the EU, WHO, US-EPA, and other competent responsible organizations worldwide.

The measurement principle to define the levels of NO<sub>2</sub>/NO<sub>x</sub> is chemiluminescence (EN14211). The Airpointer NO<sub>x</sub> module was equipped with a delay loop to measure NO and NO<sub>2</sub> from the same sample. An external calibration gas with a concentration of 425 ppb NO in N<sub>2</sub> (SIAD, Italy) was employed to periodically check the span point.

The O<sub>3</sub> measurement principally exploits UV absorption (EN 14625); for the given purpose, an internal ozone generator to allow regular span point checking was applied.

The parameters are calibrated annually by the Slovak Hydrometeorological Institute.

The Airpointer PM<sub>10</sub> module utilizes nephelometry for measuring solid particles' concentrations. Gravimetric measurements of PM<sub>10</sub> concentrations executed within 24 h intervals were carried out to calibrate the nephelometric method. Sequential samplers SVEN LECKEL SEQ 47/50-CD (Sven Leckel Ingenieurbüro GmbH, Germany) were employed for the calibration. The particles were collected on cellulose nitrate filters with the porosity of 1.2 µm (Merck, Germany) and weighed on a Mettler Toledo MX/A microbalance.

The meteorological parameters (air temperature, relative humidity, air pressure, wind speed, and wind direction) were measured by using a compact meteorological station integrated with the Airpointer. These parameters are regularly calibrated by the Czech Metrology Institute.

The data from the Airpointer were downloaded as CSV files and saved in the form of Microsoft Excel files (XLSX). The concentrations measured in ppb were converted to concentrations in µg m<sup>-3</sup>. The medians, upper and lower quartiles, and other percentiles for the monitored pollutants, temperature, relative humidity, and wind speed were calculated in MS Excel. The results were then processed by the Origin program (OriginLab, USA) to yield graphs. The dependencies of and relationships between the pollutant concentrations on the wind speed and direction were processed via the "openair" and "openairmaps" packages of OpenSource program R [21,22]. The package "openairmaps" supports "openair" for plotting on various maps. The maps include those available via the "ggmap" package, e.g., Google Maps, and leaflet ones to facilitate plotting bivariate polar plots. Our research utilized the "Esri.WorldImagery" map source and the "Non-parametric Wind Regression" (NWR) technique to display the concentration maps as bivariate polar plots.

## 2.3. Measurement Conditions and Positioning of Instruments

The concentrations of PM<sub>10</sub> and also those of the gaseous pollutants NO, NO<sub>2</sub>, and O<sub>3</sub> in three parks within the city of Brno, the Czech Republic, were measured in one-minute intervals. The same scenario was applied to the meteorological conditions, namely, air temperature (T), relative humidity (RH), air pressure (p), wind speed (WS), and wind direction (WD). The NO<sub>2</sub> and PM<sub>10</sub> measurements at automated air pollution monitoring stations operated by the Czech Hydrometeorological Institute were employed for comparing the measurement results with those acquired at a heavy traffic locality (Údolní, the Hot Spot) and background localities (Arboretum—the natural city background station, and Dětská nemocnice—the commercial city background station). Tables 1 and 2 show the geographic coordinates of the localities and display the time intervals of the measurement.

**Table 1.** The geographic coordinates of the measured localities.

| Sampling Locality         | Latitude ° N | Longitude ° E |
|---------------------------|--------------|---------------|
| Tyršův sad                | 49.2027128   | 16.6023589    |
| Lužánky SS <sup>1</sup>   | 49.2083389   | 16.6077778    |
| Lužánky SVC <sup>2</sup>  | 49.2065792   | 16.6069417    |
| Koliště                   | 49.1966892   | 16.6145658    |
| Koliště road <sup>3</sup> | 49.1970100   | 16.6147853    |
| Úvoz Hot Spot             | 49.1980897   | 16.5936431    |
| Arboretum                 | 49.2160872   | 16.6138364    |
| Dětská nemocnice          | 49.2027244   | 16.6162872    |

<sup>1</sup> Site Svojsík’s Cabin. <sup>2</sup> Site Leisure Centre. <sup>3</sup> Site alongside an adjacent roadway.

**Table 2.** The measurement times related to the localities.

| Campaign Start  | Campaign End     | Lužánky SS <sup>1</sup> | Lužánky SVC <sup>2</sup> | Tyršův Sad | Koliště | Úvoz | Dětská n. | Arboretum | Koliště Road <sup>3</sup> |
|-----------------|------------------|-------------------------|--------------------------|------------|---------|------|-----------|-----------|---------------------------|
| 12.9.2018 12:00 | 26.9.2018 11:59  |                         | x                        |            |         |      |           |           |                           |
| 18.1.2019 7:00  | 1.2.2019 6:59    |                         |                          |            | x       | x    | x         | x         |                           |
| 8.2.2019 7:00   | 22.2.2019 6:59   |                         |                          | x          |         | x    | x         | x         |                           |
| 6.3.2019 7:00   | 20.3.2019 6:59   | x                       | x                        |            |         | x    | x         | x         |                           |
| 7.6.2019 7:00   | 21.6.2019 6:59   |                         |                          |            | x       | x    | x         | x         |                           |
| 2.8.2019 7:00   | 16.8.2019 6:59   |                         |                          | x          |         |      |           |           |                           |
| 22.8.2019 7:00  | 5.9.2019 6:59    | x                       | x                        |            |         |      |           |           |                           |
| 8.11.2019 0:00  | 25.11.2019 23:59 |                         |                          |            |         |      |           |           | x                         |

<sup>1</sup> Site Svojsík’s Cabin. <sup>2</sup> Site Leisure Centre. <sup>3</sup> Site alongside an adjacent roadway.

Figures 1–3 show the positions of the measurement devices at the sampling sites. The devices were secured against theft with chains and connected to a power supply with a cable. The progress of the measurement was checked via an Internet connection through a SIM card.



**Figure 1.** The devices at Tyršův sad.



**Figure 2.** The devices at Lužánky: (a) Svojsík's Cabin; (b) Leisure Centre.



**Figure 3.** The devices at Koliště: (a) Inside the park; (b) at the adjacent roadway.

Figure 4 shows the location of the sampling sites on a map of Brno.

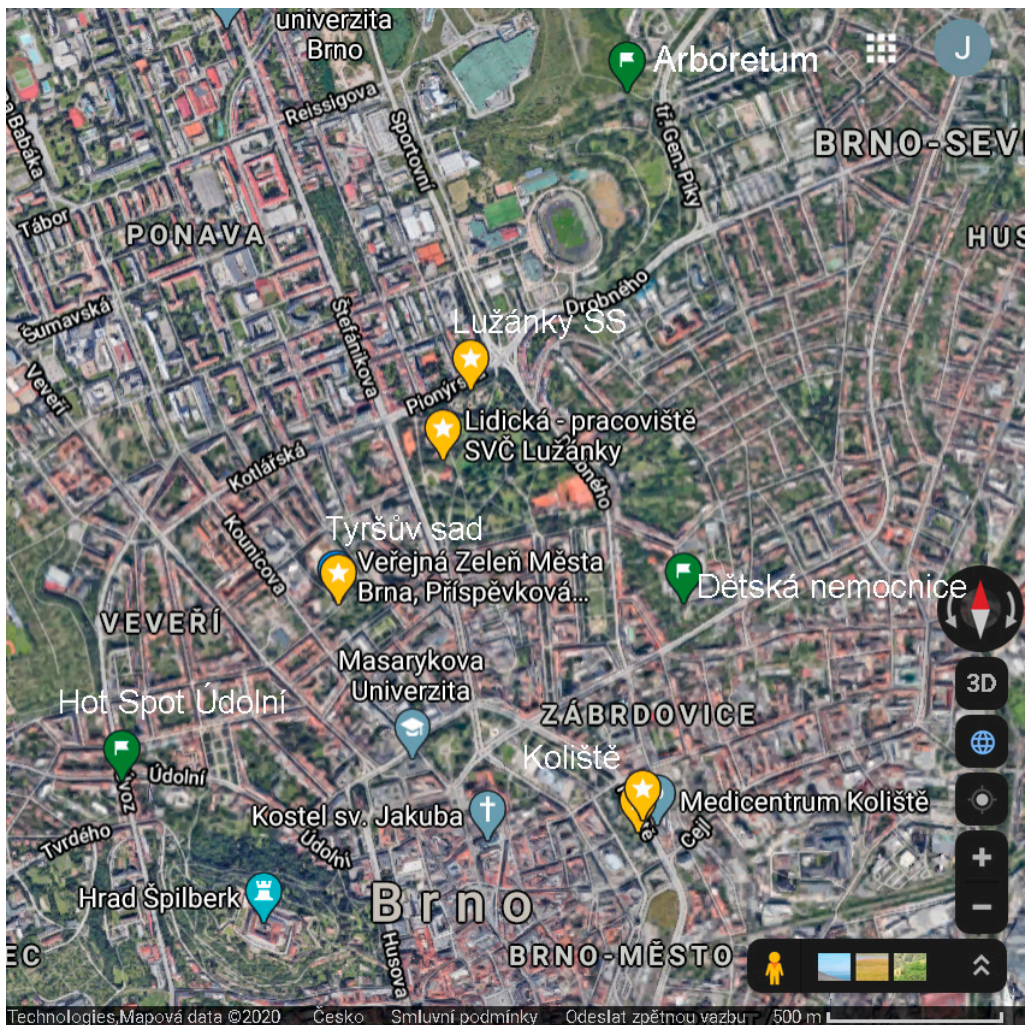


Figure 4. The sampling (yellow marks) and reference (green marks) localities.

#### 2.4. $PM_{10}$ Calibration

As nephelometric measurements are performed in one-minute intervals, the conversion factor was calculated for each 24 h measurement interval according to the formula

$$f = \frac{PM_{10}^{grav}}{PM_{10}^{neph}} \quad (1)$$

where

$PM_{10}^{grav}$  is the gravimetric  $PM_{10}$  concentration over 24 h ( $\mu\text{g}/\text{m}^3$ ), and  $PM_{10}^{neph}$  is the average nephelometric  $PM_{10}$  concentration over 24 h ( $\mu\text{g}/\text{m}^3$ )

The calculated emission factor is discontinuous, and was thus smoothed by the function

$$Factor = f_i + \frac{f_{i+1} - f_i}{2} \times \left( tgh \left[ p \times \left( t - t_{day} \times floor \left( \frac{t + \frac{t_{day}}{2}}{t_{day}} \right) \right) \right] + 1 \right), \quad (2)$$

where

*Factor* is the smoothed conversion factor in time *t*

$f_i$  is the conversion factor for the  $i$ th day  
 $f_{i+1}$  is the conversion factor for the  $(i + 1)$ th day  
 $p$  is the smoothing parameter ( $p = 0.004$ )  
 $t$  is the time from the start of the measurement (minutes)  
 $t_{day}$  is the length of the day (minutes)  
 $floor()$  is the rounding down function  
 $tgh[]$  is the hyperbolic tangent function

The  $PM_{10}$  concentration was calculated for every minute by the function

$$PM_{10} = Factor \times PM_{10}^{neph} \tag{3}$$

An example of the factors' calculation for the site Tyršův sad is shown in Figure 5.

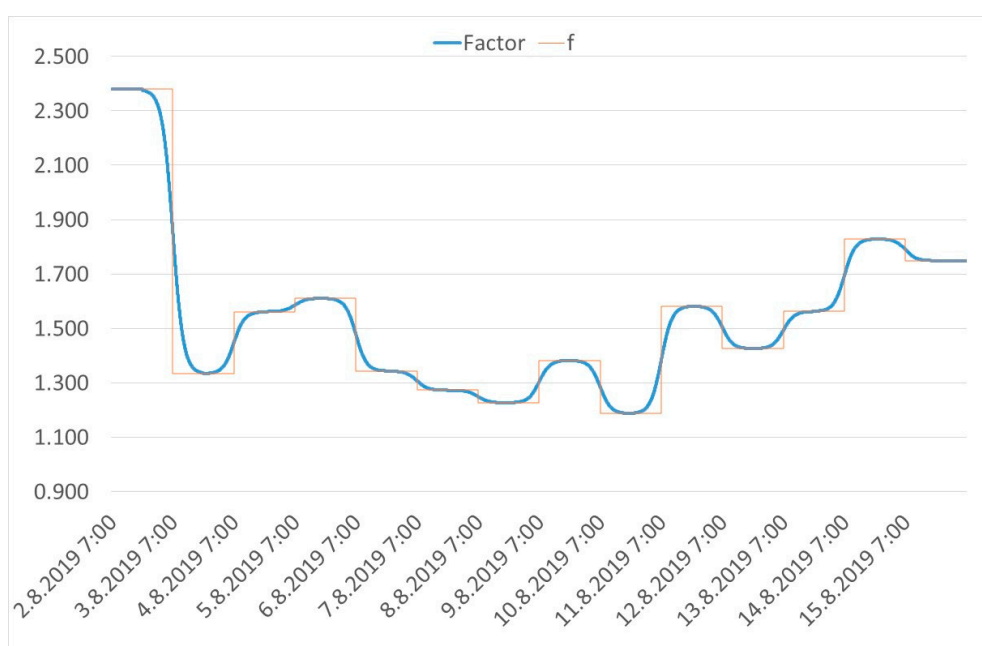


Figure 5. A comparison of the factors for the locality Tyršův sad from 2.8.2019 7:00:00 to 16.8.2019 6:59:00.

### 3. Results and Discussion

Each measurement at a park is represented by a dataset with 20,160 observations, and the measurement at the Koliště road locality is represented by a dataset with 25,920 observations. Therefore, the results were summarized as percentiles and mean values to be calculated in MS Excel. Table 3 shows the intervals in which 90% of the measured values are considered for each parameter.

Table 3. The measurement results: the 0.05 and 0.95 percentiles of the measured parameters.

| Site        | Start           | Percentile | NO<br>μg/m <sup>3</sup> | NO <sub>2</sub><br>μg/m <sup>3</sup> | NO <sub>x</sub><br>μg/m <sup>3</sup> | PM <sub>10</sub><br>μg/m <sup>3</sup> | O <sub>3</sub><br>μg/m <sup>3</sup> | T<br>°C | RH<br>% | WS<br>m/s |
|-------------|-----------------|------------|-------------------------|--------------------------------------|--------------------------------------|---------------------------------------|-------------------------------------|---------|---------|-----------|
| Tyršův sad  | 8.2.2019 7:00   | 0.05       | 0.92                    | 8.90                                 | 10.89                                | 4.05                                  | 3.42                                | -1.16   | 55.50   | 0.00      |
|             |                 | 0.95       | 133.54                  | 76.87                                | 286.17                               | 75.44                                 | 116.78                              | 9.56    | 92.33   | 0.90      |
| Tyršův sad  | 2.8.2019 7:00   | 0.05       | 0.50                    | 2.77                                 | 3.99                                 | 6.05                                  | 17.43                               | 13.96   | 40.54   | 0.00      |
|             |                 | 0.95       | 4.80                    | 18.66                                | 25.09                                | 17.05                                 | 102.21                              | 28.22   | 94.27   | 0.80      |
| Lužánky SVC | 12.9.2018 12:00 | 0.05       | 1.23                    | 4.10                                 | 6.67                                 | 3.10                                  | 1.01                                | 5.52    | 44.48   | 0.00      |
|             |                 | 0.95       | 40.74                   | 54.41                                | 114.90                               | 29.45                                 | 100.47                              | 25.91   | 100.00  | 1.52      |

Table 3. Cont.

| Site         | Start          | Percentile | NO<br>µg/m <sup>3</sup> | NO <sub>2</sub><br>µg/m <sup>3</sup> | NO <sub>x</sub><br>µg/m <sup>3</sup> | PM <sub>10</sub><br>µg/m <sup>3</sup> | O <sub>3</sub><br>µg/m <sup>3</sup> | T<br>°C | RH<br>% | WS<br>m/s |
|--------------|----------------|------------|-------------------------|--------------------------------------|--------------------------------------|---------------------------------------|-------------------------------------|---------|---------|-----------|
| Lužánky SVC  | 6.3.2019 7:00  | 0.05       | 2.13                    | 3.43                                 | 6.95                                 | 7.65                                  | 5.48                                | 0.53    | 42.93   | 0.00      |
|              |                | 0.95       | 21.71                   | 50.43                                | 86.07                                | 33.21                                 | 112.67                              | 12.90   | 100.00  | 1.61      |
| Lužánky SVC  | 22.8.2019 7:00 | 0.05       | 0.74                    | 4.42                                 | 6.03                                 | 11.28                                 | 5.49                                | 11.41   | 41.59   | 0.00      |
|              |                | 0.95       | 18.23                   | 39.68                                | 67.52                                | 53.80                                 | 116.80                              | 29.28   | 93.92   | 1.14      |
| Lužánky SS   | 6.3.2019 7:00  | 0.05       | 1.18                    | 4.67                                 | 6.84                                 | 4.64                                  | 2.75                                | −0.15   | 43.38   | 0.00      |
|              |                | 0.95       | 38.42                   | 55.78                                | 115.50                               | 35.88                                 | 130.53                              | 12.90   | 93.55   | 1.15      |
| Lužánky SS   | 22.8.2019 7:00 | 0.05       | 1.55                    | 6.52                                 | 9.56                                 | 16.27                                 | 1.77                                | 11.76   | 41.54   | 0.00      |
|              |                | 0.95       | 29.27                   | 40.73                                | 86.31                                | 78.20                                 | 112.04                              | 29.62   | 100.00  | 0.82      |
| Koliště      | 18.1.2019 7:00 | 0.05       | 1.22                    | 17.67                                | 20.26                                | 24.19                                 | 4.46                                | −8.68   | 58.53   | 0.00      |
|              |                | 0.95       | 136.72                  | 87.80                                | 291.13                               | 134.13                                | 81.96                               | 1.58    | 92.78   | 1.38      |
| Koliště      | 7.6.2019 7:00  | 0.05       | 0.92                    | 7.06                                 | 9.85                                 | 6.06                                  | 19.39                               | 16.37   | 43.15   | 0.00      |
|              |                | 0.95       | 8.12                    | 36.20                                | 48.46                                | 55.14                                 | 122.94                              | 30.44   | 99.10   | 1.25      |
| Koliště road | 8.11.2019 0:00 | 0.05       | 1.85                    | 11.34                                | 15.00                                | 21.61                                 | 2.96                                | 2.34    | 73.24   | 0.00      |
|              |                | 0.95       | 153.88                  | 61.53                                | 288.60                               | 93.26                                 | 34.30                               | 12.36   | 94.73   | 1.74      |

The results of the measurements at the automatic air pollution monitoring stations were used to compare the air pollution concentrations in the parks and their vicinity. The hourly averages of the NO<sub>2</sub> and PM<sub>10</sub> concentrations were compared, as the data are measured in hourly intervals. The results are shown in Table 4.

Table 4. The results of the measurement at the Automated Air Pollution Monitoring Stations—the 0.05 and 0.95 percentiles of the measured concentrations.

| Automated Air Pollution Monitoring Station | Start          | Percentile | NO <sub>2</sub><br>µg/m <sup>3</sup> | PM <sub>10</sub><br>µg/m <sup>3</sup> |
|--|----------------|------------|--------------------------------------|---------------------------------------|
| Úvoz                                       | 18.1.2019 7:00 | 0.05       | 23.01                                | 24.75                                 |
|  |                | 0.95       | 86.46                                | 119.25                                |
| Arboretum                                  | 18.1.2019 7:00 | 0.05       | 13.60                                | 13.55                                 |
|  |                | 0.95       | 60.65                                | 101.23                                |
| Dětská nemocnice                           | 18.1.2019 7:00 | 0.05       | 13.60                                | 13.75                                 |
|  |                | 0.95       | 79.80                                | 108.00                                |
| Úvoz                                       | 8.2.2019 7:00  | 0.05       | 19.17                                | 8.75                                  |
|  |                | 0.95       | 82.08                                | 91.75                                 |
| Arboretum                                  | 8.2.2019 7:00  | 0.05       | 12.95                                | 8.20                                  |
|  |                | 0.95       | 53.23                                | 76.00                                 |
| Dětská nemocnice                           | 8.2.2019 7:00  | 0.05       | 10.90                                | 8.00                                  |
|  |                | 0.95       | 80.90                                | 76.50                                 |
| Úvoz                                       | 6.3.2019 7:00  | 0.05       | 8.43                                 | 2.00                                  |
|  |                | 0.95       | 67.29                                | 67.25                                 |
| Arboretum                                  | 6.3.2019 7:00  | 0.05       | 6.04                                 | 2.50                                  |
|  |                | 0.95       | 40.88                                | 27.65                                 |
| Dětská nemocnice                           | 6.3.2019 7:00  | 0.05       | 3.39                                 | 3.00                                  |
|  |                | 0.95       | 54.72                                | 28.00                                 |
| Úvoz                                       | 7.6.2019 7:00  | 0.05       | 9.84                                 | 10.00                                 |
|  |                | 0.95       | 75.16                                | 44.00                                 |
| Arboretum                                  | 7.6.2019 7:00  | 0.05       | 4.80                                 | 8.58                                  |
|  |                | 0.95       | 26.67                                | 36.90                                 |
| Dětská nemocnice                           | 7.6.2019 7:00  | 0.05       | 3.40                                 | 8.00                                  |
|  |                | 0.95       | 46.70                                | 40.25                                 |

Figure 6 compares the individual mean values (medians) of the measured pollutant concentrations and meteorological parameters. The dispersions of these values are represented through the upper and lower quartiles, an interpretation that is more plausible than that rendered via the mean and standard deviations because the data have an asymmetric statistical distribution. This is also clearly seen in Figure 6: the vertical lines, whose length represents the size of the first and the third quartiles, are not identically long.

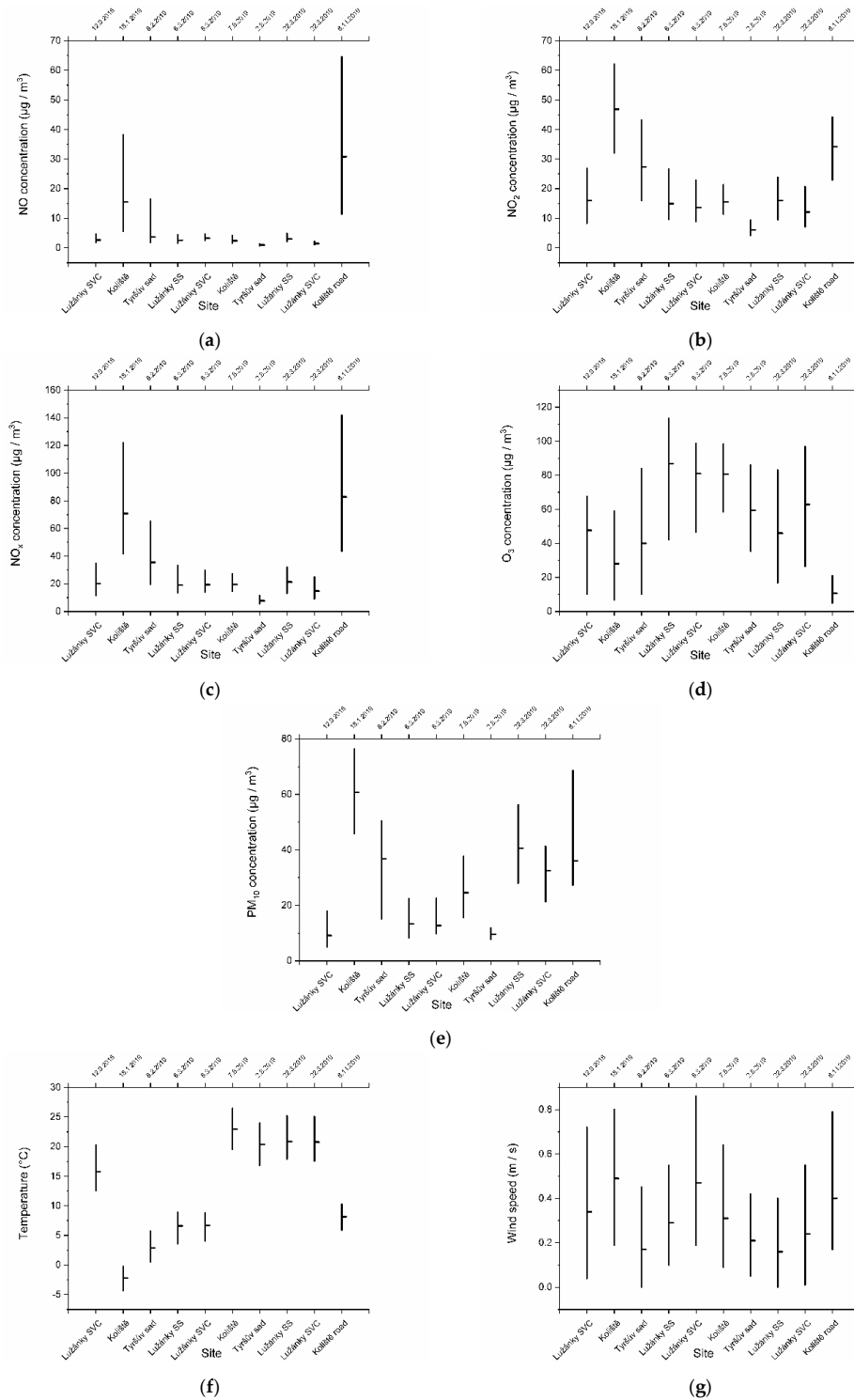
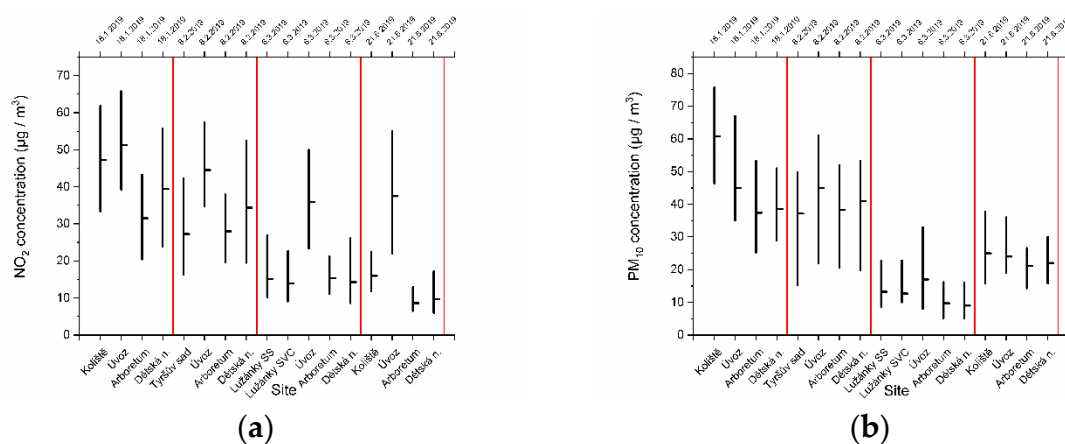


Figure 6. The NO (a), NO<sub>2</sub> (b), NO<sub>x</sub> (c), O<sub>3</sub> (d), and PM<sub>10</sub> (e) concentrations and temperature (f) plus wind speed (g) measured in the parks: the medians and quartiles.

The highest NO concentrations were measured in the immediate vicinity of the road adjacent to the Koliště park and then directly in the park; in both cases, the measurement was performed during a cold season (January, November). Similarly, the highest NO<sub>2</sub> concentrations were determined next to the road adjacent to the Koliště park and directly in the park (but also in Tyršův sad); in all of the cases, the measurement was carried out during a cold season (January, November, February). The highest total concentrations of nitrogen oxides (NO<sub>x</sub>) were acquired, as in the NO, in the immediate vicinity of the road adjacent to the Koliště park and directly in the park, during a cold season (January, November). The highest O<sub>3</sub> concentrations were measured in springtime, the lowest one in winter. The solid particles detected at Lužánky SVC and Lužánky SS exhibited a higher concentration in August than in the colder months (March, September), which is not a normal effect. This deviation arises from the fact that, in these localities, people often gather for barbecue parties and use the parks' public cooking facilities during the summer months, whereas the other parks are not frequented for this purpose.

Figure 6f,g shows also the differences between the speeds and variations between the temperatures at the sampling sites, respectively. The March, February, and January temperatures reached significantly lower than the September, August, and June ones.

Figure 7a compares graphically the NO<sub>2</sub> air pollution in the parks, with the pollution measured at the reference stations, while Figure 7b displays, in the same manner, the air pollution caused by PM<sub>10</sub>. The individual measurement campaigns are separated by the red lines. As can be seen, the air pollution in the parks, with the exception of the Koliště park for PM<sub>10</sub>, was lower than that at the traffic locality, and the pollution at the background localities approached the value. The exception concerning the Koliště park was probably due to the fact that this area is relatively narrow compared to Lužánky; thus, in wintertime, when the vegetation is leafless, it provides less from the dust generated on the nearby busy roads. Moreover, it is obvious from the representation that the parks ensure better air protection from nitrogen oxides than against dust.



**Figure 7.** The NO<sub>2</sub> (a) and PM<sub>10</sub> (b) concentrations in the parks and at the automated air pollution monitoring sites.

The average concentrations of the measured pollutants were compared with the legal limits [23,24], Table 5. The excess values are marked in pink.

**Table 5.** The average concentrations from the measured localities as compared with the legal limits.

| Site                               | Measurement Start | NO <sub>2</sub><br>μg·m <sup>-3</sup> | NO <sub>x</sub><br>μg·m <sup>-3</sup> | PM <sub>10</sub><br>μg·m <sup>-3</sup> | O <sub>3</sub><br>mg·m <sup>-3</sup> | NO <sub>2</sub> | PM <sub>10</sub><br>Count <sup>4</sup> | O <sub>3</sub> |
|------------------------------------|-------------------|---------------------------------------|---------------------------------------|--|--------------------------------------|-----------------|--|----------------|
| Lužánky SVC                        | 12.9.2018 12:00   | 20.52                                 | 32.74                                 | 12.01                                  | 44.95                                | 0               | 0                                      | 0              |
| Lužánky SVC                        | 6.3.2019 7:00     | 18.41                                 | 28.96                                 | 16.60                                  | 71.44                                | 0               | 0                                      | 0              |
| Lužánky SVC                        | 22.8.2019 7:00    | 16.01                                 | 22.22                                 | 33.57                                  | 61.48                                | 0               | 2                                      | 3              |
| Lužánky SS                         | 6.3.2019 7:00     | 20.46                                 | 33.65                                 | 16.16                                  | 77.10                                | 0               | 0                                      | 20             |
| Lužánky SS                         | 22.8.2019 7:00    | 18.53                                 | 30.31                                 | 43.46                                  | 50.46                                | 0               | 4                                      | 0              |
| Koliště                            | 18.1.2019 7:00    | 48.89                                 | 100.97                                | 66.60                                  | 34.47                                | 0               | 11                                     | 0              |
| Koliště                            | 7.6.2019 7:00     | 17.66                                 | 22.94                                 | 27.16                                  | 77.51                                | 0               | 0                                      | 14             |
| Koliště road                       | 8.11.2019 0:00    | 34.67                                 | 108.83                                | 47.72                                  | 14.13                                | 0               | 4                                      | 0              |
| Tyršův sad                         | 8.2.2019 7:00     | 32.95                                 | 67.61                                 | 36.20                                  | 48.78                                | 0               | 4                                      | 0              |
| Tyršův sad                         | 2.8.2019 7:00     | 7.86                                  | 10.18                                 | 10.20                                  | 59.95                                | 0               | 0                                      | 0              |
| <b>Legal limits</b>                |                   |                                       |                                       |  |                                      |                 |  |                |
| Annual average limit               |                   | 40 <sup>1</sup>                       | 30 <sup>2</sup>                       | 40 <sup>1</sup>                        |                                      |                 |  |                |
| Day average limit <sup>1</sup>     |                   |                                       |                                       |  |                                      |                 | 50                                     |                |
| Day average count <sup>1</sup>     |                   |                                       |                                       |  |                                      |                 | 35                                     |                |
| Hourly average limit <sup>2</sup>  |                   |                                       |                                       |  |                                      | 200             |  |                |
| Hourly average count <sup>2</sup>  |                   |                                       |                                       |  |                                      | 18              |  |                |
| Max 8 h average limit <sup>3</sup> |                   |                                       |                                       |  |                                      |                 |  | 120            |
| Max 8 h average count <sup>3</sup> |                   |                                       |                                       |  |                                      |                 |  | 25             |

<sup>1</sup> Human health protection. <sup>2</sup> Ecosystems and vegetation protection. <sup>3</sup> Limit for tropospheric ozone. <sup>4</sup> Count of legal limit excess instances.

It is possible to claim that in most localities the NO<sub>x</sub> limit for ecosystems and vegetation protection was exceeded, except for Lužánky SVC in March and August 2019, Tyršův sad in August 2019, and Koliště in June 2019. The NO<sub>2</sub> concentration reached beyond the human health protection limit only in January 2019, when the lowest average temperature of all measurement campaigns was recorded. The PM<sub>10</sub> concentrations exceeded the same limit only at Koliště in January 2019, Koliště road in November 2019, and Lužánky SS in August 2019.

The analysis of the relationship between the individual pollutants' concentrations, wind speed, and wind direction was utilized to identify the places from which the highest pollutant concentrations reached the sampling site. The concentration scale of the measured pollutants is shown in Figure 12.

The color scale shown in Figure 8 expresses concentrations depending on wind direction (angle coordinate) and wind speed (radius coordinate). Figure 9, Figure 10, Figure 11, Figure 12, Figure 13, Figure 14, Figure 15, Figure 16, Figure 17, Figure 18 introduce the concentration polar maps of the measured pollutants at all of the localities.



**Figure 8.** The concentration scale for the “openmaps” graphs.

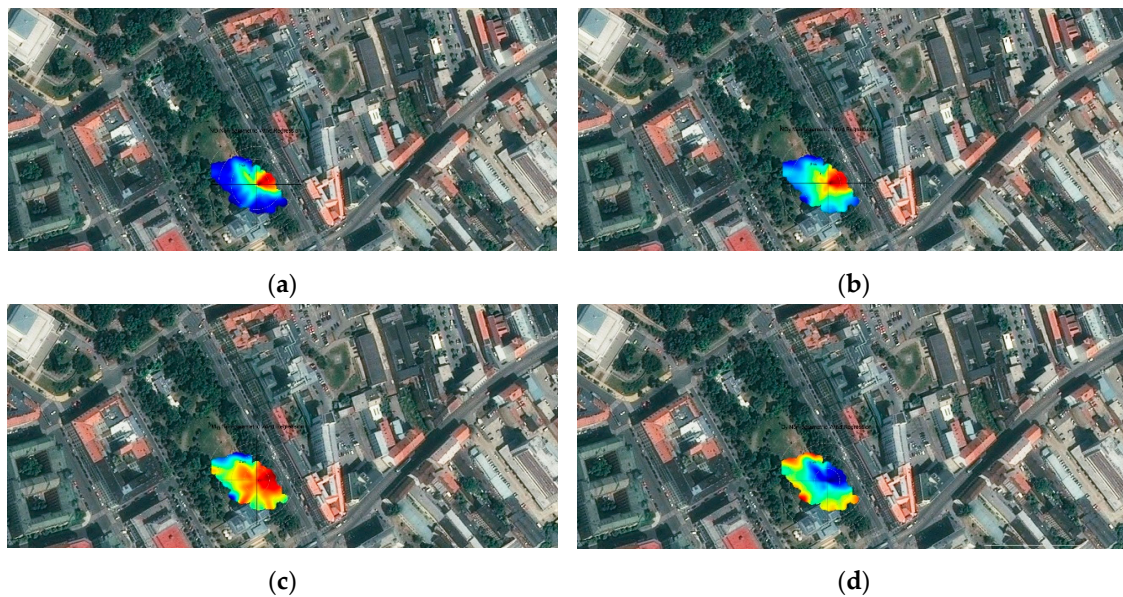


**Figure 9.** The NO (a), NO<sub>2</sub> (b), PM<sub>10</sub> (c), and O<sub>3</sub> (d) concentration relationships to the wind speed and direction at Koliště; sampling started on 18.1.2019 7:00.

Figure 9a,b shows that the highest concentrations of nitrogen oxides were measured with an east wind blowing from the adjacent road. Under the east to northwest wind direction, the lowest ozone concentrations were measured (Figure 9d). The lowest PM<sub>10</sub> concentration was obtained in north and south winds, meaning that transport embodies the most likely source of the nitrogen oxides; there is a larger amount of PM<sub>10</sub> sources; and, probably, the activities pursued within the area contribute to the dust circulation in the park (Figure 9c).



**Figure 10.** The NO (a), NO<sub>2</sub> (b), PM<sub>10</sub> (c), and O<sub>3</sub> (d) concentration relationships to the wind speed and direction at Koliště; sampling started on 7.6.2019 7:00.

Figure 10a,b shows that the highest concentrations of nitrogen oxides were measured with east and west winds blowing from the adjacent road and the opposite side. The impact of traffic on the road west of the park, which had not manifested itself in January, probably shows here. From the

south through the east to the northwest, the lowest ozone concentrations were measured (Figure 10d). The highest PM<sub>10</sub> concentrations were acquired in calm weather.

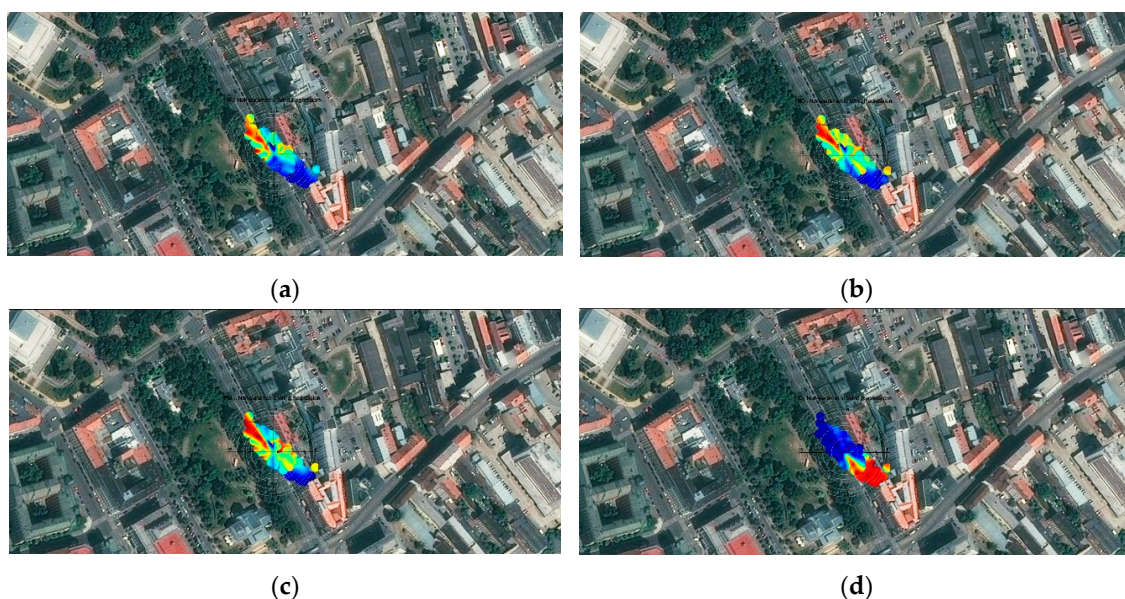


**Figure 11.** The NO (a), NO<sub>2</sub> (b), PM<sub>10</sub> (c), and O<sub>3</sub> (d) concentration relationships to the wind speed and direction at Koliště road; sampling started on 8.11.2019 0:00.

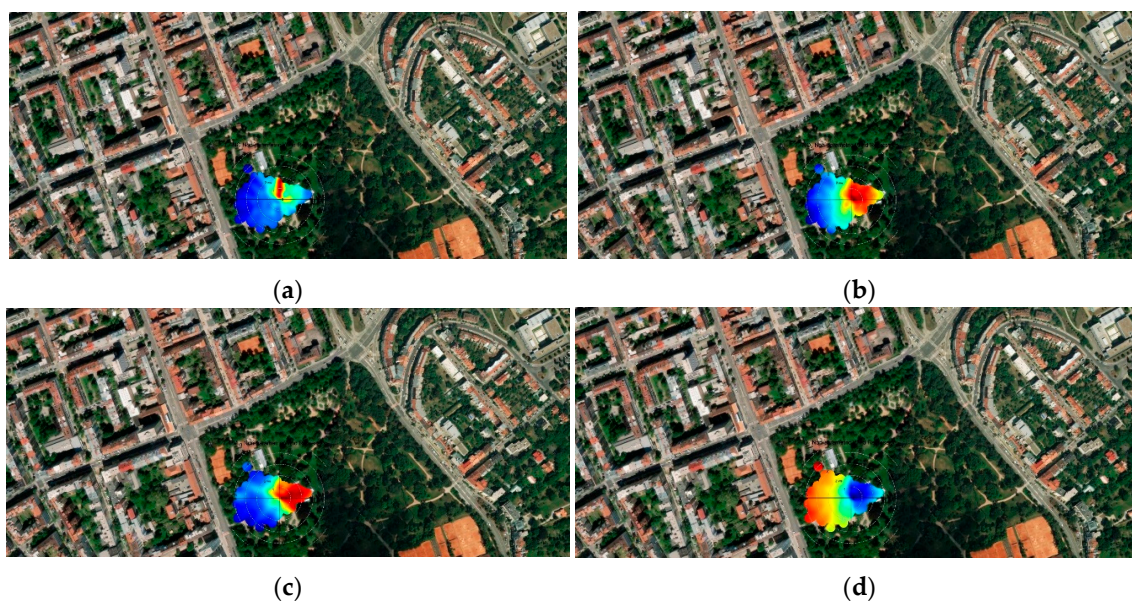
Figure 11a–c shows that the highest concentrations of nitrogen oxides and PM<sub>10</sub> were measured with northwest wind blowing in the direction of the vehicles traveling towards the Airpointer along the near lane of the road. At the same wind direction, we measured the lowest concentrations of O<sub>3</sub> (Figure 11d), meaning that both the oxides of nitrogen and the PM<sub>10</sub> had most likely originated from traffic in this case.



**Figure 12.** The NO (a), NO<sub>2</sub> (b), PM<sub>10</sub> (c), and O<sub>3</sub> (d) concentration relationships to the wind speed and direction at Lužánky SVC; sampling started on 12.9.2018 12:00.

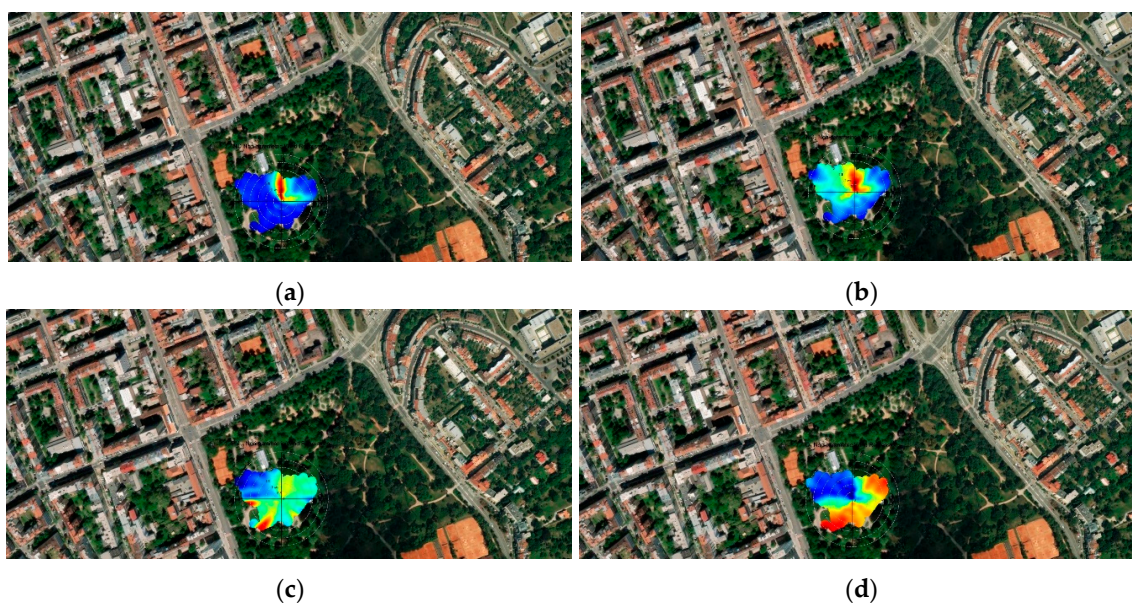
Figure 12a indicates that the highest NO concentrations were measured with a east wind. The highest NO<sub>2</sub> concentrations were determined in eastern wind directions, namely, from the south to the north, similarly to PM<sub>10</sub> (Figure 12b,c). At low wind speeds, we acquired the lowest O<sub>3</sub>

concentrations of the (Figure 12d), meaning that both the  $\text{NO}_2$  and the  $\text{PM}_{10}$  had probably been generated by similar sources. The  $\text{NO}$  had most likely originated from the traffic on the road east of the park.



**Figure 13.** The  $\text{NO}$  (a),  $\text{NO}_2$  (b),  $\text{PM}_{10}$  (c), and  $\text{O}_3$  (d) concentration relationships to the wind speed and direction at Lužánky SVC; sampling started on 6.3.2019 7:00.

Figure 13a indicates that the highest  $\text{NO}$  concentrations were measured with a north wind, similarly to the situation in Figure 14. The highest  $\text{NO}_2$  concentrations were acquired under eastern wind directions, namely, from the south to the north, similarly to  $\text{PM}_{10}$  (Figure 13b,c). This scenario resembles that represented in Figure 16. In eastern wind directions, we measured the lowest  $\text{O}_3$  concentrations (Figure 13d). The  $\text{NO}$  had probably originated from the traffic on the road north of the park.



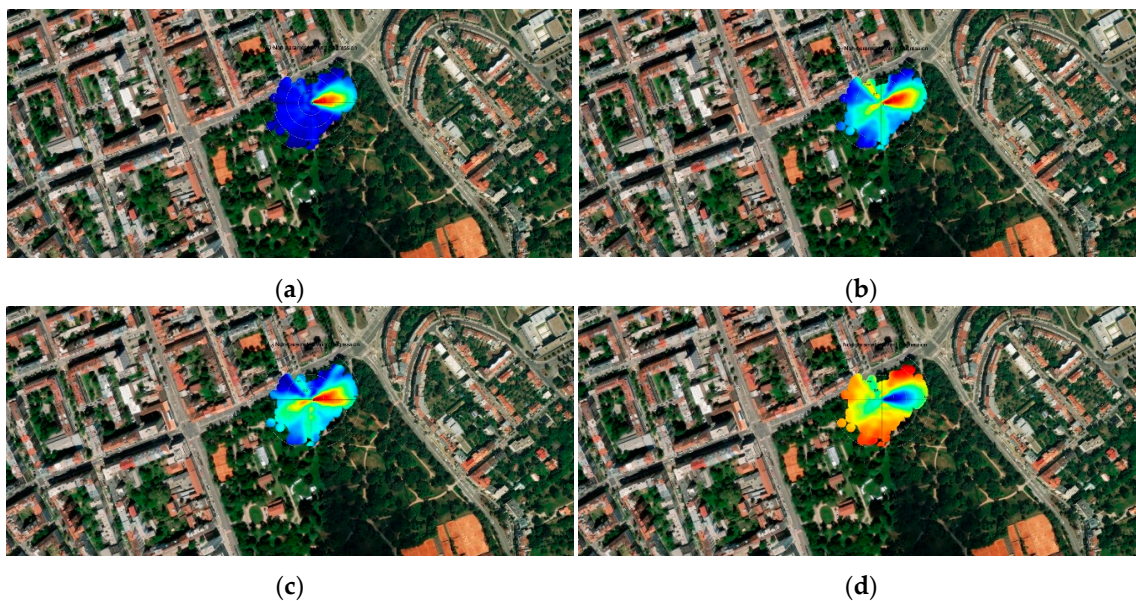
**Figure 14.** The  $\text{NO}$  (a),  $\text{NO}_2$  (b),  $\text{PM}_{10}$  (c), and  $\text{O}_3$  (d) concentration relationships to the wind speed and direction at Lužánky SVC; sampling started on 22.8.2019 7:00.

Figure 14b shows that the highest NO<sub>2</sub> concentrations were measured under northern wind directions (Figure 14b). In western to northern wind directions, we established the lowest concentrations of O<sub>3</sub> (Figure 14d). The nitrogen oxides had probably originated from the traffic on the road north of the park. The PM<sub>10</sub> concentrations did not exhibit any significant relationship to the wind direction in this case.



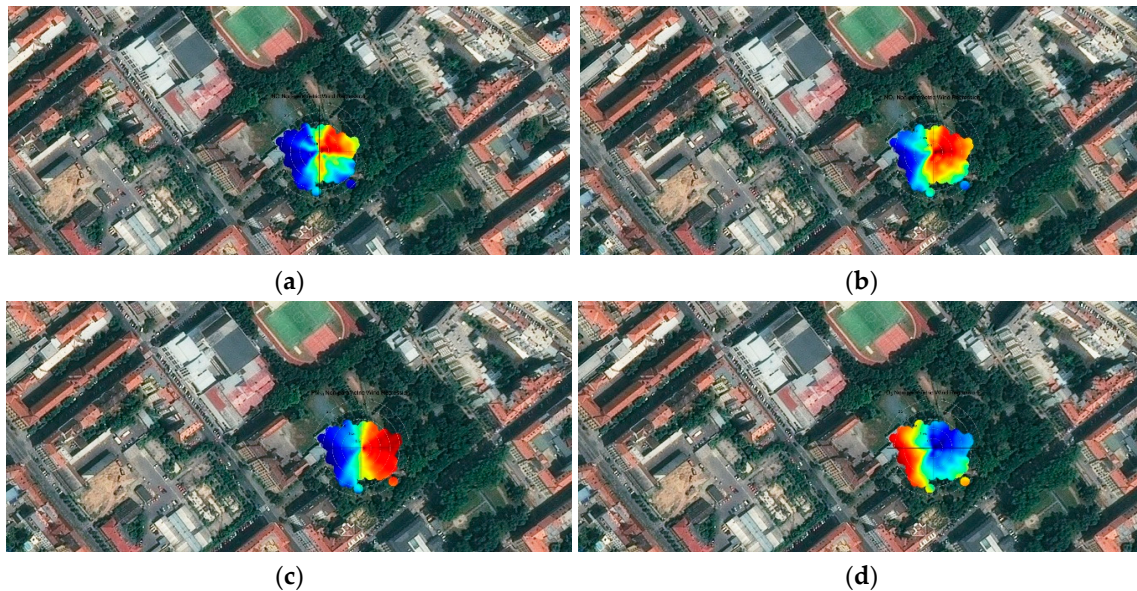
**Figure 15.** The NO (a), NO<sub>2</sub> (b), PM<sub>10</sub> (c), and O<sub>3</sub> (d) concentration relationships to the wind speed and direction at Lužánky SS; sampling started on 6.3.2019 7:00.

Figure 15a–c indicates that the highest NO, NO<sub>2</sub>, and PM<sub>10</sub> concentrations were measured under a northeastern wind direction. In the same wind directions, we acquired the lowest concentrations of O<sub>3</sub> (Figure 15d). Both the nitrogen oxides and the PM<sub>10</sub> had probably been generated by the traffic on the crossroads to the northeast of the park.



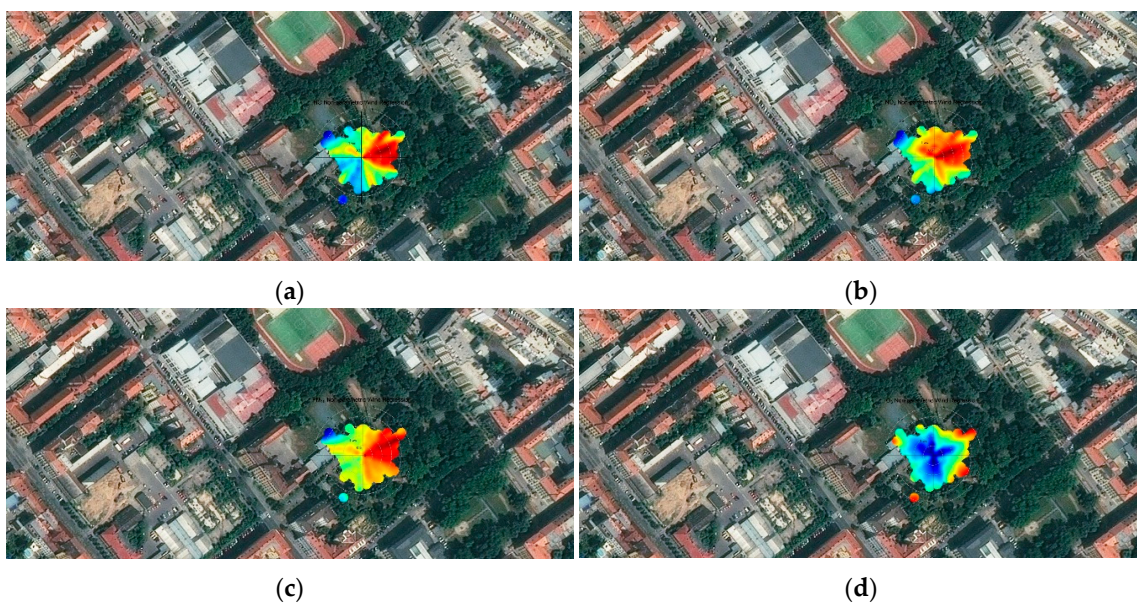
**Figure 16.** The NO (a), NO<sub>2</sub> (b), PM<sub>10</sub> (c), and O<sub>3</sub> (d) concentration relationships to the wind speed and direction at Lužánky SS; sampling started on 22.8.2019 7:00.

Figure 16 displays a situation similar to that shown in Figure 15. It clearly follows from the images in both of the figures that, at the Lužánky SS locality, the traffic pollution (NO) is contained by the Svojsík srub building. At the Lužánky SVC site (Figures 12–14), conversely, the NO source is blocked by the Leisure Center from the west.



**Figure 17.** The NO (a), NO<sub>2</sub> (b), PM<sub>10</sub> (c), and O<sub>3</sub> (d) concentration relationships to the wind speed and direction at Tyršův sad; sampling started on 8.2.2019 7:00.

There are no significant transport-based air pollution sources near Tyršův sad; the air pollution at this location can be rather generated by long-distance transfer or, especially in wintertime, PM<sub>10</sub> from local heating. Figure 17 shows the pollution from eastern directions, and Figure 18 displays the ambiguous situation at the site.



**Figure 18.** The NO (a), NO<sub>2</sub> (b), PM<sub>10</sub> (c), and O<sub>3</sub> (d) concentration relationships to the wind speed and direction at Tyršův sad; sampling started on 2.8.2019 7:00.

As outlined above, the problem of reducing PM concentrations in urban parks has been discussed in diverse papers, e.g., [4–6]. Other articles analyzed the impact of urban greenery on NO<sub>x</sub>, NO<sub>2</sub> [14], and O<sub>3</sub> [16]. In this study, the outcomes presented within the referenced research reports are followed and developed through such procedural approaches as monitoring the influence of wind and air temperature on pollutant concentrations. The measurements have shown that, in addition to vegetation, seasonal changes of meteorological conditions and human activities in parks embody a substantial aspect modifying the local situation, as observed at Lužánky park in August 2019. The obtained results have confirmed the conclusions proposed by Kumar et al. [12], namely, that progressive steps need to be taken to bring further knowledge in the field. The relationships between O<sub>3</sub>, NO, and NO<sub>2</sub> were studied by Han et al. [25]; interestingly, the outcomes of our research resemble Han et al.'s findings in suggesting that, as regards the study area(s), the daily NO cycle initiated by flue gas emissions from motor vehicles and continued by the related conversion of the pollutant into NO<sub>2</sub>, had a major impact on the regular ozone process. The daily course of concentrations in these pollutants was similar, too.

#### 4. Conclusions

In four 14-day campaigns, concentrations of NO, NO<sub>2</sub>, PM<sub>10</sub>, and O<sub>3</sub> were measured at five diverse locations, of which four were enclosed within Brno parks and one set at a road adjacent to a park. Compared to the average values, significantly higher nitrogen oxide concentrations were determined at the monitored spots of Koliště and Koliště-road in colder weather. Both of the locations are situated near a busy road exhibiting a traffic intensity of 33,000 vehicles/d. In terms of PM<sub>10</sub>, the highest concentrations were obtained at Koliště park, with an average air temperature that proved to be the lowest among the values adopted for the other measurements. At Lužánky park, the PM<sub>10</sub> concentrations measured in warmer weather reached higher than those acquired during colder periods—an effect probably caused by the park being a popular public barbecue place. Using the “openairmaps” software package, we determined the directions pointing to the main sources of pollution at the individual spots. Based on this procedure, it was estimated that the main air pollution sources affecting the parks lie in the adjacent roads and crossroads. In some cases, however, human activities of people in the parks (barbecue) can also be regarded as important or semi-critical. By extension, we established that the overall surface layout, prominently including buildings in the park, can locally shield the impact of traffic on the air quality. Interestingly, the air quality in the parks approached that of the urban background locations, except for Koliště park, which, due to its shape and proximity to a very busy road, showed the characteristics of a regular traffic location.

**Author Contributions:** Conceptualization, J.H. (Jiří Huzlík); Data curation, J.H. (Jitka Hegrová) and K.E.; Formal analysis, J.H. (Jiří Huzlík), J.H. (Jitka Hegrová) and K.E.; Funding acquisition, J.H. (Jitka Hegrová) and M.B.; Investigation, J.H. (Jiří Huzlík) and R.L.; Methodology, J.H. (Jiří Huzlík), J.H. (Jitka Hegrová), R.L. and M.B.; Project administration, J.H. (Jitka Hegrová), R.L. and M.B.; Resources, J.H. (Jiří Huzlík), J.H. (Jitka Hegrová) and K.E.; Supervision, J.H. (Jitka Hegrová), R.L. and M.B.; Validation, J.H. (Jiří Huzlík), J.H. (Jitka Hegrová) and R.L.; Visualization, J.H. (Jiří Huzlík) and R.L.; Writing—original draft, J.H. (Jiří Huzlík) and R.L.; Writing—review & editing, J.H. (Jiří Huzlík), J.H. (Jitka Hegrová), K.E. and R.L. All authors have read and agreed to the published version of the manuscript.

**Funding:** This article was produced under support from the Technology Agency of the Czech Republic within the ÉTA framework, project TL01000286, on the research infrastructure acquired from the Operational Programme Research and Development for Innovations (CZ.1.05/2.1.00/03.0064).

**Conflicts of Interest:** The authors declare no conflicts of interest. The funders had no role in the designing of the study; in the collection, analyses, or interpretation of the data; in the writing of the manuscript; or in the decision to publish the results.

#### References and Note

1. Xing, Y.; Brimblecombe, P. Urban park layout and exposure to traffic-derived air pollutants. *Landsc. Urban Plan.* **2020**, *194*, 103682. [[CrossRef](#)]
2. Xing, Y.; Brimblecombe, P. Trees and parks as, the lungs of cities. *Urban For. Urban Green.* **2020**, *48*, 126552. [[CrossRef](#)]

3. Xing, Y.; Brimblecombe, P. Role of vegetation in deposition and dispersion of air pollution in urban parks. *Atmos. Environ.* **2019**, *201*, 73–83. [CrossRef]
4. Von Schneidemesser, E.; Steinmar, K.; Weatherhead, E.C.; Bonn, B.; Gerwig, H.; Quedenau, J. Air pollution at human scales in an urban environment: Impact of local environment and vehicles on particle number concentrations. *Sci. Total Environ.* **2019**, *688*, 691–700. [CrossRef]
5. Qu, H.; Lu, X.; Liu, L.; Ye, Y. Effects of traffic and urban parks on PM10 and PM2.5 mass concentrations. *Energy Sour. Part A Recover. Util. Environ. Eff.* **2019**, 1–13. [CrossRef]
6. Kang, S.; Kang, T.; Park, T.; Park, G.; Lee, J.; Hong, J.-W.; Hong, J.; Lee, J.; Lee, T. Characterization of Aerosol Composition, Concentration, and Sources in Bukhansan National Park, Korea. *J. Korean Soc. Atmos. Environ.* **2018**, *34*, 457–468. [CrossRef]
7. Zhu, C.; Przybysz, A.; Chen, Y.; Guo, H.; Chen, Y.; Zeng, Y. Effect of spatial heterogeneity of plant communities on air PM10 and PM2.5 in an urban forest park in Wuhan, China. *Urban For. Urban Green.* **2019**, *46*, 126487. [CrossRef]
8. Hernandez, W.; Mendez, A.; Diaz-Marquez, A.M.; Zalakeviciute, R.; Zalakeviciute, R.; Marquez, D. Robust Analysis of PM2.5 Concentration Measurements in the Ecuadorian Park La Carolina. *Sensors* **2019**, *19*, 4648. [CrossRef]
9. Ottosen, T.-B.; Kumar, P. The influence of the vegetation cycle on the mitigation of air pollution by a deciduous roadside hedge. *Sustain. Cities Soc.* **2020**, *53*, 101919. [CrossRef]
10. Abhijith, K.; Kumar, P. Field investigations for evaluating green infrastructure effects on air quality in open-road conditions. *Atmos. Environ.* **2019**, *201*, 132–147. [CrossRef]
11. Mori, J.; Fini, A.; Galimberti, M.; Ginepro, M.; Burchi, G.; Massa, D.; Ferrini, F. Air pollution deposition on a roadside vegetation barrier in a Mediterranean environment: Combined effect of evergreen shrub species and planting density. *Sci. Total Environ.* **2018**, *643*, 725–737. [CrossRef] [PubMed]
12. Kumar, P.; Druckman, A.; Gallagher, J.; Gatersleben, B.; Allison, S.; Eisenman, T.S.; Hoang, U.; Hama, S.; Tiwari, A.; Sharma, A.; et al. The nexus between air pollution, green infrastructure and human health. *Environ. Int.* **2019**, *133*, 105181. [CrossRef] [PubMed]
13. Almeida, L.D.O.E.; Favaro, A.; Raimundo-Costa, W.; Anhê, A.C.B.M.; Ferreira, D.C.; Blanes-Vidal, V.; Senhuk, A.P.M.D.S. Influence of urban forest on traffic air pollution and children respiratory health. *Environ. Monit. Assess.* **2020**, *192*, 175. [CrossRef] [PubMed]
14. Sheridan, C.E.; Roscoe, C.J.; Gulliver, J.; De Preux, L.; Fecht, D. Inequalities in Exposure to Nitrogen Dioxide in Parks and Playgrounds in Greater London. *Int. J. Environ. Res. Public Health* **2019**, *16*, 3194. [CrossRef] [PubMed]
15. Klingberg, J.; Broberg, M.C.; Strandberg, B.; Thorsson, P.; Pleijel, H. Influence of urban vegetation on air pollution and noise exposure—A case study in Gothenburg, Sweden. *Sci. Total Environ.* **2017**, *599*, 1728–1739. [CrossRef]
16. Yli-Pelkonen, V.; Scott, A.A.; Viippola, V.; Setälä, H.M. Trees in urban parks and forests reduce O<sub>3</sub>, but not NO<sub>2</sub> concentrations in Baltimore, MD, USA. *Atmos. Environ.* **2017**, *167*, 73–80. [CrossRef]
17. Hewitt, C.N.; Ashworth, K.; MacKenzie, R. Using green infrastructure to improve urban air quality (GI4AQ). *Ambio* **2019**, *49*, 62–73. [CrossRef] [PubMed]
18. Vieira, J.; Matos, P.; Mexia, T.; Silva, P.; Lopes, N.; Freitas, C.; Correia, O.; Santos-Reis, M.; Branquinho, C.; Pinho, P. Green spaces are not all the same for the provision of air purification and climate regulation services: The case of urban parks. *Environ. Res.* **2018**, *160*, 306–313. [CrossRef]
19. Mexia, T.; Vieira, J.; Príncipe, A.; Anjos, A.; Silva, P.; Lopes, N.; Freitas, C.; Santos-Reis, M.; Correia, O.; Branquinho, C.; et al. Ecosystem services: Urban parks under a magnifying glass. *Environ. Res.* **2018**, *160*, 469–478. [CrossRef]
20. Jones, L.; Vieno, M.; Fitch, A.; Carnell, E.J.; Steadman, C.; Cryle, P.; Holland, M.; Nemitz, E.; Morton, D.; Hall, J.; et al. Urban natural capital accounts: Developing a novel approach to quantify air pollution removal by vegetation. *J. Environ. Econ. Policy* **2019**, *8*, 413–428. [CrossRef]
21. Anonymous. The R Project for Statistical Computing. Available online: <http://www.r-project.org/> (accessed on 13 February 2012).
22. Carslaw, D.; Ropkins, K. Openair—An R package for air quality data analysis. *Environ. Model. Softw.* **2012**, *27*, 52–61. [CrossRef]

23. Directive 2008/50/EC of the European Parliament and of the Council of 21 May 2008 on ambient air quality and cleaner air for Europe. Available online: <https://eur-lex.europa.eu/legal-content/en/ALL/?uri=CELEX%3A32008L0050> (accessed on 12 May 2020).
24. Act 201/2012 Coll. Of the Czech Republic of 2 May 2012 on Air Protection.
25. Han, S.; Bian, H.; Feng, Y.; Liu, A.; Li, X.; Zeng, F.; Zhang, X. Analysis of the Relationship between O<sub>3</sub>, NO and NO<sub>2</sub> in Tianjin, China. *Aerosol Air Qual. Res.* **2011**, *11*, 128–139. [[CrossRef](#)]



© 2020 by the authors. Licensee MDPI, Basel, Switzerland. This article is an open access article distributed under the terms and conditions of the Creative Commons Attribution (CC BY) license (<http://creativecommons.org/licenses/by/4.0/>).

Article

# F-Gases: Trends, Applications and Newly Applied Gases in the Czech Republic

Markéta Müllerová <sup>1</sup>, Eva Krtková <sup>1,\*</sup> and Zuzana Rošková <sup>1,2</sup>

<sup>1</sup> National Inventory System for GHG Emissions, Air Quality Protection Division, Czech Hydrometeorological Institute, Na Šabatce 2050/17, 143 06 Praha, Czech Republic; marketa.mullerova@chmi.cz (M.M.); zuzana.roskova@chmi.cz (Z.R.)

<sup>2</sup> Department of Environmental Chemistry, Faculty of Environmental Technology, University of Chemistry & Technology in Prague, Technická 5, 166 28 Praha, Czech Republic

\* Correspondence: eva.krtkova@chmi.cz; Tel.: +420-244-032-422

Received: 24 March 2020; Accepted: 24 April 2020; Published: 30 April 2020



**Abstract:** Emissions of fluorinated greenhouse gases (F-gases), which are used as replacements for ozone-depleting substances, have risen sharply since 1995. The rapid increase in F-gas emissions coupled with their global warming potential (GWP) has led to increased worldwide attention to monitoring emission levels and subsequently regulating the use of F-gases. These restrictions apply in particular to applications for which alternative technologies are available that are more economically efficient and have minor or no impact on the Earth's climate system. This paper brings new information about changes in composition of consumed F-gases in the Czech Republic. Since no F-gases are produced in the country, data about F-gas consumption are obtained from three resources which give information about import and export. The paper also describes implementation of newly used F-gases, which are used as replacements for specific F-gases, into emission calculation models. Emissions are estimated according to the methodology developed by the Intergovernmental Panel on Climate Change (IPCC). Although consumption of F-gases with high GWP has already started decreasing, it will have no effect on F-gas emissions for several years.

**Keywords:** F-gases; greenhouse gases; global warming potential; substitutes for ozone depleting substances; Czech Republic

## 1. Introduction

Fluorinated greenhouse gases (F-gases) are anthropogenic gases used mainly as substitutes for ozone-depleting substances. Although F-gases do not damage the atmospheric ozone layer, they contribute significantly to the global greenhouse effect [1]. Two main groups of F-gases can be distinguished; hydrofluorocarbons (HFCs) and perfluorocarbons (PFCs) [2]. The difference between the HFCs and PFCs groups is in the degree of fluorination. The first group consists in partly fluorinated F-gases, whereas the second group contains fully fluorinated molecules [3]. There is an important difference between these two groups, especially in terms of the greenhouse effect, i.e., their lifetimes in the atmosphere. While the lifetime of HFCs varies between a few days and 250 years, most PFCs can remain in the atmosphere for thousands of years [4]. F-gases are used, for instance, as fire suppressors, aerosols, refrigerants in refrigerators, in air conditioning systems, etc.

Since global warming potential (GWP) of F-gases is many times greater than that of carbon dioxide (CO<sub>2</sub>), the EU is taking regulatory action to control them [4]. GWP measures how much energy 1 ton of a gas will absorb over a certain time period, relative to 1 ton of CO<sub>2</sub> [5]. Regulation (EU) 517/2014 outlines guidelines and information about reporting by companies. Directive 2006/40/EC (and also the MAC (mobile air conditioning) Directive) is focused on prohibition of using F-gases in mobile

air conditioning. But it does not suggest any way to accomplish this goal [6]. F-gases are subject to a reporting duty. Facilities that produce, import or export 1 metric ton or 100 tonnes CO<sub>2</sub> eq. and more F-gases must report such information [7].

In the following chapters, European legislative measures are described in more detail, it is shown how they affect composition of consumed F-gases in the Czech Republic, and information about newly used F-gases is added in the same way as information about their integration into the F-gas emission calculation model PHOENIX, which is a country specific estimation model for F-gas emissions. Newly applied F-gases change the results of the F-gas emissions in the Czech Republic and affect in this way also the total emission from greenhouse gases. The PHOENIX model is continuously improved to provide accurate and transparent results.

The paper provides an overview of the trends of F-gases used in the Czech Republic including recent updates and changes following application of the newly developed F-gases with low GWP.

## **2. Regulation (European Union, EU) No 517/2014 and Mobile Air Conditioning (MAC) Directive**

This regulation was published after approval by the European Parliament (EP) and the Council in April 2014. The Regulation is based on Regulation (EC) No 842/2006 on certain fluorinated greenhouse gases. The aim of the Regulation is to reduce emissions of F-gases, which have to be decreased by 72–73% by 2030 against the reference year of 1990. The regulation therefore provides rules on containment, use, recovery and destruction of F-gases and conditions on the placing on the market complemented by quantitative limits [8].

The objective of the regulation could be achieved, e.g., by replacing current gases with high GWP to gases with lower impact or, preferably, with no impact on the climate. In this context, the regulation also provides rules for training responsible persons for the safe-handling of alternative refrigerants, because some alternatives to F-gases have undesirable properties, such as lower flash point and toxicity [8].

The measures which entered into force on 1 January 2020 affect a wide range of equipment. From this date, it is prohibited to place on the market:

- Mobile room air-conditioning equipment that contains HFCs with GWP of 150 or more;
- Refrigerators and freezers for commercial use that contain HFCs with GWP of 2 500 or more (starting 2022, limit of GWP will be 150);
- Stationary refrigeration equipment that contains HFCs with GWP of 2500 or more.

These measures have an impact on the use of the mixtures R-404a (GWP 3943 [4]) and R-507a (GWP 3985 [4]), which are mainly used in stationary commercial refrigeration [9].

The subject of the MAC Directive is to lay down the requirements for air-conditioning systems fitted into vehicles. The directive applies to passenger cars comprising no more than eight seats in addition to the driver's seat and vehicles designed and constructed for the carriage of goods and having a maximum mass not exceeding 1305 kilograms. Since 1 January 2017, mobile air-conditioning systems in new vehicles, which are brought into service in the EU, must not contain gases with GWP of 150 and more [6].

## **3. Trends and Applications in the Czech Republic**

The base year for reporting obligation of F-gases in the Czech Republic is 1995. F-gases are not produced in this country and all of them are imported. Data about direct import/export, use and destruction are obtained from ISPOP (Integrated system of reporting obligations), the F-gas register (Questionnaire on production, import, export, feedstock use and destruction of the substances listed in Annexes I or II of the F-gas regulation) and the Customs Administration of the Czech Republic [10].

The major share of F-gases (about 99%) is used for refrigeration and air conditioning systems, approximately 75% of F-gases is used for refrigeration and stationary air conditioning and 25% is used

in mobile air conditioning. Manufacturers use a wide range of mixtures containing HFCs. In the past, mixtures containing PFCs were also used, but these mixtures has not been used since 2010 [10].

### 3.1. Refrigeration and Stationary Air-Conditioning Systems

ISPOP provides information about import, export, regeneration, destruction and the first placing on the market of F-gases. The ISPOP database contains the EU market data. The threshold for submitting data to ISPOP by importers, exporters and users is 0.1 metric tonne of F-gases. The F-gas register provides data about the imported, exported and disposed amounts of F-gases and also contains information about the average specific charge of equipment, amount of imported, exported or disposed equipment and information about specific use of the equipment. Information in the F-gas register is related to the trade between EU countries and non-EU countries and the threshold for submitting data to the F-gas register is more than 1 metric tonne of F-gases. The threshold refers to the sum of F-gases, not each imported/exported gas separately. Customs data provide information about trading between the Czech Republic and the global market. These data provide information about imported/exported products and containers of fluorinated greenhouse gases; information is classified according to the combined nomenclature, which is regularly updated [10].

The global market is covered in the inventory since the data sources cover trade between the Czech Republic and EU countries and also non-EU countries. Verification of the data by each importer/exporter/user of F-gases in all the data sources is a very important step in the process of inventory preparation, because it is necessary to avoid double counting [10].

The main type of mixture used in the Czech Republic for stationary air conditioning/refrigeration is R-410a [9] (GWP 1924 [4]), a mixture of HFC-32 and HFC-125 in a ratio of 50:50. Mixtures R-407c, R-507a and R-404a are used in smaller amounts. R-407c (GWP 1624 [4]) is a mixture of HFC-32, HFC-125 and HFC-134a in a ratio of 23:25:52 and it is used mainly in stationary air conditioning. R-507a is a mixture of HFC-125 and HFC-143a in a ratio of 50:50. R-404a contains HFC-125, HFC-143a and HFC-134a gases in a ratio of 44:52:4 [10].

In the national inventory, mixtures are compartmentalized into individual gases. The trend of use of particular F-gases is depicted in Figure 1. As can be seen, there was a significant decrease in the use of HFC-125, and HFC-143a even did not appear in the market in 2018. These two gases have high GWP, and their decrease is based on the fact that manufacturers are preparing for limitation of these gases and their mixtures. As can be seen on the second graph in Figure 1a,b, although the amount of F-gases used in 2018 is similar to in 2017, the used gases have a smaller impact on global warming.

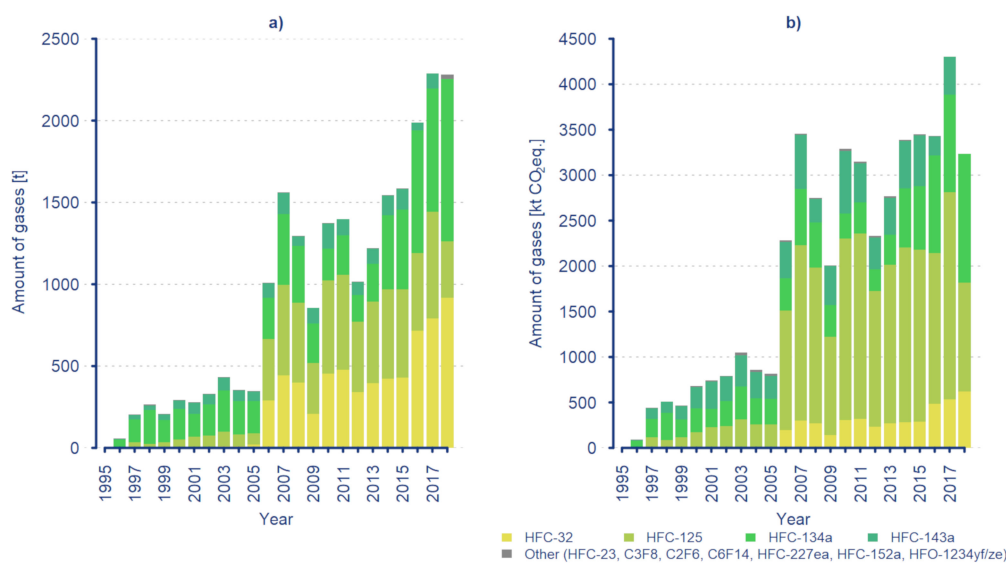


**Figure 1.** Trend in F-gases used for refrigerants and air conditioning in the Czech Republic in tonnes (a) compared to the trend in F-gases recalculated to kt CO<sub>2</sub> eq (b).

The EU regulations force manufacturers to find alternatives to F-gases with high GWP. One option for them is to develop new mixtures with lower GWP. Another option is to use natural refrigerants, such as ammonia, isobutene, propane and CO<sub>2</sub>, which have already been used in the past [11]. The coming years will show which option is more convenient for manufacturers; nevertheless, we can expect a gradual decrease in the use of F-gases in this field.

### 3.2. Mobile Air Conditioning

A different approach than for refrigeration and stationary air conditioning is used for estimation of the amount of F-gases employed in mobile air conditioning. The data collection is based on knowledge of the number of vehicles, percentage of vehicles with air conditioning and average amount of refrigerants in these vehicles. Data about production are obtained from the Automotive Industry Association. These data contain the production figures for the Czech automobile industry since 1995. Three car producers (ŠKODA AUTO Inc., Hyundai Motor Manufacturing Czech Ltd. and TPCA), bus producers (SOR Libchavy Ltd., Iveco Czech Republic Inc. and others) and one truck producer (TATRA TRUCKS Inc.) are currently operating in the Czech Republic. More detailed data about production (e.g., production of particular models) are obtained directly from ŠKODA AUTO Inc. and TPCA, whose production covers approximately 85% of all new passenger cars produced in the Czech Republic. Knowledge of the production of particular models makes determination of the average initial charge more accurate. The initial charge of passenger cars decreased over the years from 750 g per unit to 500 g per unit [10].

The only refrigerant used for mobile air conditioning from 1995 to 2015 was HFC-134a (GWP 1300 [4]). Since 2015, it has been prohibited to use this gas in mobile air conditioning and manufacturers have started filling cars for the EU market with hydrofluoroolefin (HFO)-1234yf and this gas has been the main refrigerator in mobile air conditioning since then. This change is the result of implementation of the MAC Directive. It is assumed that HFO-1234yf will not be replaced by some other refrigerant in next few years, so its consumption will depend solely on the number of cars produced. As can be seen from the second graph in Figure 2a,b, the impact of HFO-1234yf on global warming is more than thousand times smaller than the impact of HFC-134a. More detailed comparison of these two gases is presented in the following section.



**Figure 2.** The trend in gases filled into new vehicles in the Czech Republic in tonnes (a) compared to the trend in F-gases recalculated into kt CO<sub>2</sub> eq (b).

#### 4. Newly Employed F-Gases in the Czech Republic

HFO-1234yf and HFO-1234ze are newly used as alternatives to HFC-134a. Both new HFCs have an olefinic structure and low GWP. Because of their structure they are called hydrofluoroolefins (HFOs) [12].

There are apparent some similarities between HFO-1234ze(E), HFO-1234yf and the older F-gas HFC-134a summarized in Table 1. Their chemical structures are also similar. A slight difference is caused by the position of the F atom in the olefinic part of the molecule (which is shown in Figure 3). Because of their harmful potential, the American Industrial Hygiene Association (AIHA) set workplace environmental exposure levels (WEEL), for HFO-1234ze equal to 800 ml.m<sup>-3</sup> and, for HFO-1234yf, 500 ml.m<sup>-3</sup> per 8 hours shift [13]. Other thermodynamic properties of mentioned F-gases are captured in the Table 1 [14–17].

**Table 1.** Thermodynamic properties of hydrofluoroolefins (HFOs) compared to hydrofluorocarbon HFC-134a.

| Properties              | Units | HFO-1234ze(E) | HFO-1234ze(Z) | HFO-1234yf | HFC-134a |
|-------------------------|-------|---------------|---------------|------------|----------|
| CAS <sup>1</sup>        |       | 29118-24-9    | 29118-25-0    | 754-12-1   | 811-97-2 |
| Boiling point           | °C    | −19           | 10            | −29        | −26      |
| Critical point          | °C    | 109           | 150           | 95         | 102      |
| Vapour pressure (25 °C) | kPa   | 500           | 184           | 677        | 665      |
| Source                  |       | [14]          | [15,16]       | [17]       |          |
| GWP [4]                 |       | <1            |               | <1         | 1300     |

<sup>1</sup> CAS number is a registry number characteristic for each chemical. It was classified by Chemical Abstract Service (CAS). The number is divided into three parts. First part is the most variable, it could contain from 2 to 7 digits, second part contains only two and last just one digit. Those three parts are separated by a dash. Every chemical has its own CAS number which is specific for one substance.

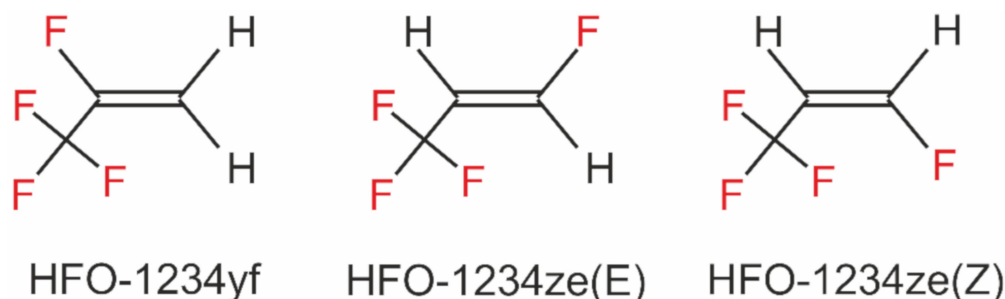


**Figure 3.** This figure shows the chemical structures of HFO-1234yf and two isomers of HFO-1234ze [15].

##### 4.1. Hydrofluoroolefin (HFO)-1234yf

A newly employed F-gas has the official designation HFO-1234yf (also R-1234yf or HFC-1234yf). The systematic chemical name for HFO-1234yf is 2, 3, 3, 3-tetrafluoroprop-1-ene.

HFO-1234yf belongs to third-generation refrigerants. Its GWP value is smaller than 1 [4] which is very low compared, e.g., with HFC-134a, whose GWP is 1300 [4]. Both these F-gases have quite similar vapour pressures under laboratory conditions and also similar boiling points and critical points. HFO-1234yf is poorly combustible but is slightly flammable. The flammability of the gas is a reason for concern. This behaviour of HFO-1234yf is the reason why greater specialisation is required for employees working with it, like safety training and how to handle flammable things, etc. [18]. HFO-1234yf shows slight activity in the Ames test, which is used for the testing mutagenic and carcinogenic activity of the tested substances. Further investigations did not find any mutagenic activity. Thus, HFO-1234yf does not cause any genetic changes and the doses are low for all the tests performed in the study by [19].

#### 4.2. HFO-1234ze

HFO-1234ze has two isomeric structures: trans-1, 3, 3, 3-tetrafluoroprop-1-ene with suffix (E) or cis-1, 3, 3, 3-tetrafluoroprop-1-ene with suffix (Z) [20]. The suffixes are abbreviations of the German words *Entgegen* (E, opposite) and *Zusammen* (Z, together) [21]. HFO-1234ze(E) is used more often because of its similarity to its predecessor HFC-134a.

It has very low GWP and consequently it is used more often, as it has only small or no impact on the planet Earth. HFO-1234ze has been tested for its toxic and harmful potential for humans. The research of Rusch and his colleagues (2012) [22] was related to the inhalation toxicity of HFO-1234ze, showing that the effective dose is very high, i.e., HFO-1234ze has very low toxic potential. Nonetheless, they found that its target organs are the liver and kidneys. Some histopathological changes were found in these organs.

#### 4.3. Mixtures

At the present time, manufactures can choose between mixtures which were used less often in the past, or mixtures with new gases. R-407 represents mixtures which have long been available but were of little interest to manufactures until the present time. Its GWP is still rather large; however, this mixture has a broad range of applications. It is used in commercial, industrial and transport refrigeration. R-449a, which includes HFO-1234yf, is used in the same area. Mixture R-452a, also with HFO-1234yf, is used chiefly in transport refrigeration.

Mixtures that replace HFC-134a still contain this gas to which new kinds of gases are added. These include HFO-1234yf for R-513a and HFO-1234ze for R-450a. These mixtures are used in medium- and high-temperature commercial and industry refrigeration, air conditioning and heat pumps. Table 2 shows overview of mostly widely used replacement mixtures in the Czech Republic.

**Table 2.** Overview of mostly widely used replacement mixtures in the Czech Republic [23].

| Gas    | Substitute of: | Constituents |         |        |            |            | GWP 100-Year <sup>1</sup> |
|--------|----------------|--------------|---------|--------|------------|------------|---------------------------|
|        |                | HFC-134a     | HFC-125 | HFC-32 | HFO-1234yf | HFO-1234ze |                           |
| R-407a | R-404a/R-507a  | 40%          | 40%     | 20%    |            |            | 1923                      |
| R-449a | R-404a/R-507a  | 25.7%        | 24.7%   | 24.3%  | 25.3%      |            | 1282                      |
| R-452a | R-404a/R-507a  |              | 59%     | 11%    | 30%        |            | 1945                      |
| R-513a | HFC-134a       | 44%          |         |        | 56%        |            | 573                       |
| R-450a | HFC-134a       | 42%          |         |        |            | 58%        | 547                       |

<sup>1</sup> Calculated according 5th Intergovernmental Panel on Climate Change (IPCC) Assessment Report, no climate feedbacks are included.

Other newly developed mixtures, which haven't been introduced on the market yet, commonly combine formerly used HFCs with new HFOs in various ratios.

## 5. Calculation of Emissions from Refrigeration and Stationary Air Conditioning in the Czech Republic

Emissions from refrigeration and stationary air-conditioning systems are estimated with the national PHOENIX calculation model defined according to the methodology developed by the Intergovernmental Panel on Climate Change (IPCC). In the inventory, five sub-applications are defined: commercial, domestic, industrial, and transport refrigeration and stationary air conditioning [24].

When calculating emissions of F-gases, time lag between consumption and emissions is taken in account. Time lag results from the fact that a chemical placed into a new product may only slowly leak out over time, not being released until end-of-life. Thanks to this and according to data availability, emissions can be estimated in a various ways with varying degrees of complexity and data intensity [24]. In the Czech Republic, Tier 2a, called the Emission-factor approach, is used. It takes in account the national and regional regulations governing the use of F-gases, defines the emission factors for refrigerant charge, during operation, at servicing and at equipment end of life [24].

The calculation model is divided into four main parts: input, divider, emission estimates and output. In input, there are emission factors, legislative measures and annual data about consumption of F-gases for the initial filling of new equipment and for servicing equipment in use. Collecting of the data from annual consumption is described in Section 3.1 and legislative measures are described in Section 2. Emission factors are defined for each sub-application and life-cycle stage of gas. Emission factors used for emission estimates are shown in Table 3. Their selection should be based on the national information provided by manufacturers, service providers, disposal companies and other organizations. However, obtaining such detailed information is very difficult under the current state of administration in the Czech Republic and thus the emission factors are based on the expert judgement in the default ranges proposed by IPCC 2006 Gl., Table 7.9 [24].

**Table 3.** Emission factors used for emission estimates in 2018.

| Source<br>Sub-Application   | Lifetimes<br>[Years] | Emission Factors<br>[% of Initial Charge/Year] |                     | End-of-Life Emissions [%] |                          |
|-----------------------------|----------------------|--|---------------------|---------------------------|--------------------------|
|                             |                      | (d)  | (k)                 | (x)                       | ( $\eta_{rec,d}$ )       |
| Factor in Equation          |                      | Initial Emissions                              | Operation Emissions | Recovery Efficiency       | Initial Charge Remaining |
| Commercial Refrigeration    | 10.50                | 3.00   | 13.00               | 55.00                     | 70.00                    |
| Domestic Refrigeration      | 13.50                | 0.50   | 3.50                | 55.00                     | 70.00                    |
| Industrial Refrigeration    | 17.00                | 3.00   | 13.00               | 55.00                     | 70.00                    |
| Transport Refrigeration     | 8.50                 | 0.50   | 20.00               | 55.00                     | 30.00                    |
| Stationary Air Conditioning | 13.50                | 0.50   | 6.50                | 55.00                     | 70.00                    |

Each gas is divided into six groups according its area of application. The percentage share of each gas in the area of application, as can be seen in Table 4, is currently based on sectoral expert judgement, which is supported by the data obtained from the Association of Refrigeration and Air Conditioning. As we can see, F-gases are mostly used for commercial refrigeration and have not been used for domestic refrigeration since 2015. For 2018 emission estimates, two new gases were included into calculation model: HFO-1234yf and HFO-1234ze. Their distribution by application area is based on information about distribution of gases and mixtures which these two gases replace.

**Table 4.** Distribution of HFCs use by application area used for emission calculations in 2018.

| Reported F-Gases | Commercial Refrigeration | Domestic Refrigeration | Industrial Refrigeration | Transport Refrigeration | Stationary Air Conditioning |
|------------------|--------------------------|------------------------|--------------------------|-------------------------|-----------------------------|
| HFC-125          | 40%                      | x                      | 15%                      | 5%                      | 40%                         |
| HFC-143a         | 60%                      | x                      | 15%                      | 5%                      | 20%                         |
| HFC-23           | 100%                     | x                      | x                        | x                       | x                           |
| HFC-134a         | 60%                      | x                      | 15%                      | 5%                      | 20%                         |
| HFC-227ea        | 100%                     | x                      | x                        | x                       | x                           |
| HFC-32           | 40%                      | x                      | 15%                      | 5%                      | 40%                         |
| HFC-152a         | 100%                     | x                      | x                        | x                       | x                           |
| HFO-1234yf       | 30%                      | x                      | 8%                       | 53%                     | 10%                         |
| HFO-1234ze       | 53%                      | x                      | 5%                       | 15%                     | 27%                         |

Using the symbol x indicates, that the gas is not applied in the area.

Emission estimates of individual gases are calculated separately for each area of application. Calculations of emission estimates are identical for all the F-gases and all sub-applications; however, the difference is in use of specific emission factors for each area of application. Total emissions for individual F-gas in individual area of application are calculated as the sum of emissions from filling new equipment  $E_{charge}$ , emissions during the equipment lifetime  $E_{lifetime}$  and emissions at the system end of life  $E_{end\ of\ life}$ .

Emissions from filling  $E_{charge}$  for year  $t$  are calculated according to the equation:

$$E_{charge, t} = M_t \frac{k}{100} \tag{1}$$

where  $M_t$  is the amount of chemical used for the first fill and  $k$  is the emission factor for assembly losses charged into new equipment (see Table 3).

Emissions during the lifetime  $E_{lifetime, t}$  are calculated according to the equation:

$$E_{charge, t} = B_t \frac{x}{100} \tag{2}$$

where  $B_t$  is the amount of chemical banked in the system and  $x$  represents the annual emission rate (see Table 3).  $B_t$  is calculated as:

$$B_t = S_t - E_{charge, t} - E_{end\ of\ life, t} + B_{t-1} - E_{lifetime, t-1} \tag{3}$$

where  $S_t$  is the amount of chemical charged into equipment (amount of gas consumed in year  $t$ ).

Emissions at the end of life  $E_{end\ of\ life, t}$  are calculated according to the equation:

$$E_{end\ of\ life, t} = H_t \left( 1 - \frac{\eta_{rec, d}}{100} \right) \tag{4}$$

where  $\eta_{rec, d}$  is recovery efficiency at disposal (see Table 3).  $H_t$  is the amount of chemical remaining in the system at decommissioning and is calculated by using a Gaussian model with mean at the lifetime expectancy [25].

As can be seen in Figure 4, although the trend in F-gas consumption varies, emissions are consistently increasing, which is caused by the time lag mentioned above. In the coming years, we can expect no change in the increasing trend since the effect of reducing F-gas consumption will appear with delay.

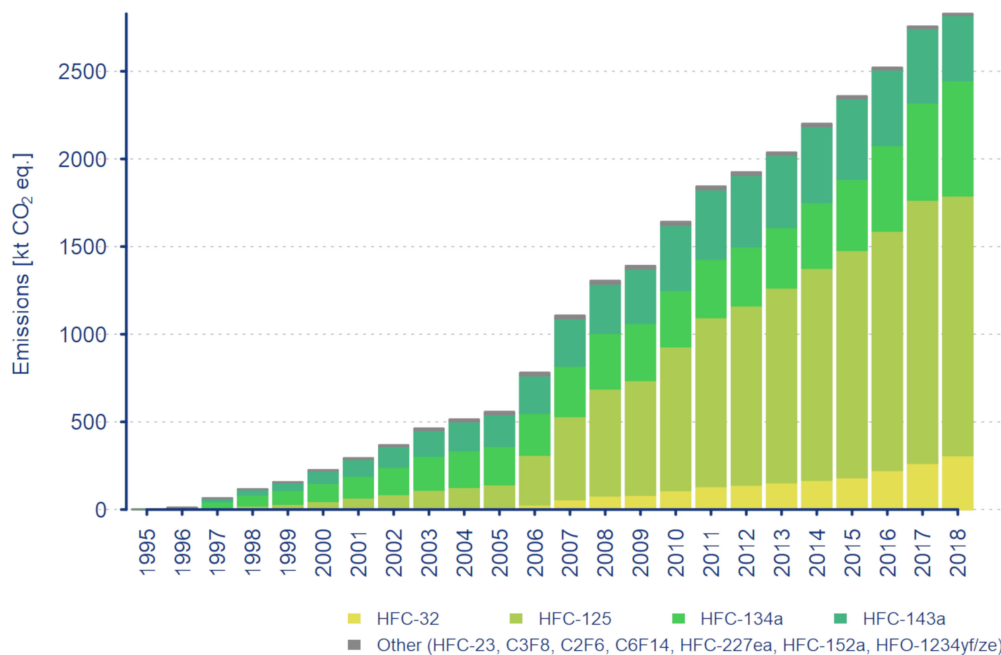


Figure 4. The trend in emissions from refrigeration and stationary air conditioning in the Czech Republic.

## 6. Concluding Remarks

Because F-gases have been used as substitutes for ozone-depleting substances, their consumption has been increasing strongly since 1995. The main sector where F-gases are employed is in refrigeration and air-conditioning systems. Because of the large global warming potential of F-gases, the EU has adopted legislative measures to prevent a further increase in their emissions. Alternative solutions to F-gases are already on the market. On the basis of the collected data, it can be seen that consumption of F-gases stopped increasing even before main part of EU legislative measures came into force. Therefore, in the coming years, especially from 2020, we expect a gradual decrease in the consumption of F-gases in refrigeration and stationary air-conditioning systems. No decrease is expected in mobile air-conditioning systems.

A more important factor than consumption itself is the composition of the consumed F-gases, because there can be big differences in the impact on global warming between individual gases. There, we can see great progress. In recent years, manufacturers started using new gases, especially HFO-1234yf with very low global warming potential, which is the main refrigerant in mobile air conditioning at the present time and we can expect that it will also be used more widely in other sectors in the coming years. Currently, HFO-1234yf is mainly used in transport refrigeration (except mobile air conditioning), whereas HFO-1234ze is mainly used in commercial refrigeration.

Since HFO-1234yf and HFO-1234ze will certainly become an integral part of the refrigeration industry, these two gases were implemented into the PHOENIX model, the country-specific estimation model for F-gas emissions. The base year of their use in refrigeration and stationary air conditioning is 2018. Newly applied F-gases changes the results of the F-gas emissions in the Czech Republic and affects in this way also the total emission from green-house gases. However, since time lag between consumption and emissions is taken in account, changes in emission trend will appear with delay.

The new F-gases have lower global warming potential than those used earlier, which is a great benefit. But they are also subject to some scepticism since their characteristics have not been examined in sufficient detail yet. One already known problem is their flammability, which ranks them in category A2L. Category A2L compounds are slightly flammable and exhibit low toxicity. Their low toxicity has been demonstrated by their high effective doses in toxicological experiments conducted on mammals (mice, dogs, etc.). This toxicological information was also employed for adjustment of WEEL values, which are higher than  $400 \text{ ml.m}^{-3}$  for the newly employed F-gases [26]. Despite their low toxic potential, they should not be taken lightly. Their harmful effect could be hidden in the future and better information will be gained from future epidemiologic studies.

**Author Contributions:** M.M.: Data curation, Methodology, Writing—original draft; E.K.: Methodology, Supervision, Writing—review & editing, Z.R.: Methodology, Writing—original draft. All authors have read and agree to the published version of the manuscript.

**Funding:** This research received no external funding.

**Conflicts of Interest:** The authors declare no conflict of interest.

## References

1. EU Legislation to Control F-Gases Climate Action. Available online: [https://ec.europa.eu/clima/policies/f-gas/legislation\\_en#tab-0-0](https://ec.europa.eu/clima/policies/f-gas/legislation_en#tab-0-0) (accessed on 14 January 2020).
2. Fluorinated Greenhouse Gas. Available online: <https://dcaae.gov.ie/en-ie/environment/topics/air-quality/fluorinated-greenhouse-gas/Pages/default.aspx> (accessed on 14 January 2020).
3. Fluorované Skleníkové Plyny-Ministerstvo Životního Prostředí. Available online: [https://www.mzp.cz/fluorovane\\_sklenikove\\_plyny](https://www.mzp.cz/fluorovane_sklenikove_plyny) (accessed on 11 February 2020).
4. Myhre, G.; Shindell, D. (Eds.) Anthropogenic and Natural Radiative Forcing. In *Climate Change 2013: The Physical Science Basis. Contribution of Working Group I to the Fifth Assessment Report of the Intergovernmental Panel on Climate Change*; Cambridge University Press: Cambridge, UK; New York, NY, USA, 2013; pp. 659–740.

5. US EPA. Understanding Global Warming Potentials Greenhouse Gas (GHG) Emissions. Available online: <https://www.epa.gov/ghgemissions/understanding-global-warming-potentials> (accessed on 18 February 2020).
6. Directive 2006/40/EC of the European Parliament and of the Council of 17 May 2006 Relating to Emissions from Air Conditioning Systems in Motor Vehicles and Amending Council Directive 70/156/EEC (Text with EEA Relevance). Official Journal of the European Union: Brussels, Belgium, 2006; pp. 12–18.
7. Quota Allocation, the HFC Registry and Data Reporting. Available online: [https://ec.europa.eu/clima/policies/f-gas/reporting\\_en](https://ec.europa.eu/clima/policies/f-gas/reporting_en) (accessed on 18 February 2020).
8. Regulation (EU) No 517/2014 of the European Parliament and of the Council of 16 April 2014 on Fluorinated Greenhouse Gases and Repealing Regulation (EC) No 842/2006 Text with EEA Relevance. Official Journal of the European Union: Brussels, Belgium, 2014; pp. 195–230.
9. Řeháček, V. Antropogenní emise fluoridu sírového, fluoridu dusitého, částečně fluorovaných uhlovodíků a zcelafluorovaných uhlovodíků v roce 2015 v České republice, Praha, 2016.
10. CHMI. *National Inventory Report*; Czech Hydrometeorological Institute: Praha, Czech Republic, 2020.
11. Cavallini, A.; Zilio, C. Carbon dioxide as a natural refrigerant. *Int. J. Low Carbon Technol.* **2007**, *2*, 225–249. [CrossRef]
12. Low GWP Synthetic Refrigerants. Available online: <https://www.danfoss.com/en/about-danfoss/our-businesses/cooling/refrigerants-and-energy-efficiency/refrigerants-for-lowering-the-gwp/low-gwp-synthetic-refrigerants/> (accessed on 11 February 2020).
13. Occupational Alliance for Risk Science-Workplace Environmental Exposure Levels (WEEL). Available online: <https://www.tera.org/OARS/OARS%20WEELS%20Jan%202014.pdf> (accessed on 9 March 2020).
14. Solstice™ ze (HFO-1234ze) Refrigerant. Available online: <https://www.climalife.co.uk/docs/Solstice%201234ze%20brochure.pdf> (accessed on 9 March 2020).
15. Gil, B.; Kasperski, J. Efficiency Evaluation of the Ejector Cooling Cycle using a New Generation of HFO/HCFO Refrigerant as a R134a Replacement. *Energies* **2018**, *11*, 2136. [CrossRef]
16. Fedele, L.; Di Nicola, G.; Brown, J.S. Measurements and Correlations of cis-1,3,3,3-Tetrafluoroprop-1-ene (R1234ze(Z)) Saturation Pressure. *Int. J. Thermophys.* **2014**, *35*, 1–12. [CrossRef]
17. Daviran, S. A comparative study on the performance of HFO-1234yf and HFC-134aas an alternative in automotive air conditioning systems. *Appl. Therm. Eng.* **2017**, *110*, 1091–1100. [CrossRef]
18. Brož, J. Nové Chladivo HFO 1234yf–Budoucnost Již Začala. Available online: <http://portal.sda-cia.cz/clanky/download/2012-07-Chladivo-HFO.pdf> (accessed on 9 March 2020).
19. Minor, B.; Spatz, M. HFO-1234yf Low GWP Refrigerant Update. In Proceedings of the International Refrigeration and Air Conditioning Conference, Purdue, IN, USA, 14–17 July 2008; p. 937.
20. Honeywell Solstice®ze Refrigerant (HFO-1234ze): The Environmental Alternative to Traditional Refrigerants. Available online: <https://www.honeywell-refrigerants.com/india/?document=solstice-ze-hfo-1234ze-brochure-2012&download=1.%20FPR-003/2015-01> (accessed on 11 February 2020).
21. Khandelwal, P. E/Z System of Nomenclature of Geometrical Isomers. Available online: <https://biyanicolleges.org/ez-system-of-nomenclature-of-geometrical-isomers/> (accessed on 11 February 2020).
22. Rusch, G. The acute, genetic, developmental and inhalation toxicology of trans-1,3,3,3-tetrafluoropropene (HFO-1234ze). *Drug Chem. Toxicol.* **2012**, *36*, 170–180. [CrossRef] [PubMed]
23. Westfalen. Available online: [http://www.westfalen.cz/fileadmin/user\\_uploads/Westfalen\\_Tschechien/Prospekte/IP5\\_CZ\\_verze\\_pro\\_Web.pdf](http://www.westfalen.cz/fileadmin/user_uploads/Westfalen_Tschechien/Prospekte/IP5_CZ_verze_pro_Web.pdf) (accessed on 11 March 2020).
24. IPCC. *IPCC Guidelines for National Greenhouse Gas Inventories*; Institute for Global Environmental Strategies (IGES) for the IPCC: Kanagawa, Japan, 2006; ISBN 4-88788-032-4.
25. Ondrušová, B.; Krtková, E. The Phoenix calculation model for emission estimates of F-gases used in refrigeration and air conditioning. *Meteorol. Zprávy* **2018**, *1*, 24–29.
26. SAFTENG. Available online: <https://www.safteng.net/index.php/free-section/safety-info-posts/chemical-process-safety-psmmp/3946-refrigerant-hfo-1234yf-and-flame-retardant-clothing-part-5> (accessed on 11 March 2020).



MDPI  
St. Alban-Anlage 66  
4052 Basel  
Switzerland  
Tel. +41 61 683 77 34  
Fax +41 61 302 89 18  
[www.mdpi.com](http://www.mdpi.com)

*Atmosphere* Editorial Office  
E-mail: [atmosphere@mdpi.com](mailto:atmosphere@mdpi.com)  
[www.mdpi.com/journal/atmosphere](http://www.mdpi.com/journal/atmosphere)





MDPI  
St. Alban-Anlage 66  
4052 Basel  
Switzerland

Tel: +41 61 683 77 34  
Fax: +41 61 302 89 18

[www.mdpi.com](http://www.mdpi.com)



ISBN 978-3-0365-1761-2